Universiteit
Leiden
The Netherlands

Upconverting nanovesicles for the activation of ruthenium anti-cancer prodrugs with red light

Askes, S.H.C.

Citation
Askes, S. H. C. (2016, November 24). *Upconverting nanovesicles for the activation of ruthenium anti-cancer prodrugs with red light*. Retrieved from https://hdl.handle.net/1887/44378

Version:	Not Applicable (or Unknown)
License:	Licence agreement concerning inclusion of doctoral thesis in the Institutional Repository of the University of Leiden
Downloaded from:	https://hdl.handle.net/1887/44378

Note: To cite this publication please use the final published version (if applicable).

Cover Page

Universiteit Leiden

The handle http://hdl.handle.net/1887/44378 holds various files of this Leiden University dissertation.

Author: Askes, S.H.C.
Title: Converting nanovesicles for the activation of ruthenium anti-cancer prodrugs with red light
Issue Date: 2016-11-24

UPCONVERTING NANOVESICLES FOR THE ACTIVATION OF RUTHENIUM ANTI-CANCER PRODRUGS WITH RED LIGHT

PROEFSCHRIFT

Ter verkrijging van

de graad van Doctor aan de Universiteit Leiden,

op gezag van Rector Magnificus Prof. mr. C. J. J. M. Stolker,

volgens besluit van het College voor Promoties

te verdedigen op donderdag 24 november 2016

klokke 10:00 uur

Sven Holger Christiaan Askes

geboren te Culemborg, Nederland, 1989

Samenstelling Promotiecommissie

Promotor

Prof. dr. E. Bouwman

Copromotor

Dr. S. Bonnet

Overige Leden

Prof. dr. J. Brouwer

Prof. dr. A. Kros

Prof. dr. S. Baluschev
Verbonden aan Sofia University "St. Kliment Ochridski" (Bulgarije) en Max Planck Institute for Polymer Research (Mainz, Germany)

Dr. F. C. Grozema
Verbonden aan Technische Universiteit Delft

Dr. L. Salassa
Verbonden aan Centre for Cooperative Research in Biomaterials "CIC biomaGUNE" (San Sebastián, Spain)

This work has been financially supported by Nederlandse Organisatie voor Wetenschappelijk Onderzoek (NWO).

Printing was financially supported by Avantes BV.

"Just remember, you can't climb the ladder of success with your hands in your pockets"

Arnold Schwarzenegger

"Those worlds in space are as countless as all the grains of sand on all the beaches of the Earth. Each of those worlds is as real as ours. In every one of them, there's a succession of incidences, events, occurrences which influence its future. Countless worlds, numberless moments, an immensity of space and time. And our small planet, at this moment, here we face a critical branch-point in the history. What we do with our world, right now, will propagate down through the centuries and powerfully affect the destiny of our descendants. It is well within our power to destroy our civilization, and perhaps our species as well. If we capitulate to superstition, or greed, or stupidity we can plunge our world into a darkness deeper than the time between the collapse of classical civilization and the Italian Renaissance. But we are also capable of using our compassion and our intelligence, our technology and our wealth to make an abundant and meaningful life for every inhabitant of this planet. To enhance enormously our understanding of the Universe, and to carry us to the stars."

Carl Sagan

Dedicated to all great minds of past and present,
on whose shoulders we may stand.

Table of Contents

Chapter 1 7

Introduction I: Ruthenium polypyridyl complexes as potential anticancer prodrugs in photoactivated chemotherapy

Chapter 2 21

Introduction II: Light upconversion using triplet-triplet annihilation

Chapter 3 43

Activation of a photodissociative ruthenium complex by triplet-triplet annihilation upconversion in liposomes

Chapter 4 59

Triplet-triplet annihilation upconversion followed by FRET for the red light activation of a photodissociative ruthenium complex in liposomes

Chapter 5 81

Imaging the lipid bilayer of giant unilamellar vesicles using red-to-blue light upconversion

Chapter 6 95

Temperature dependence of triplet-triplet annihilation upconversion in phospholipid membranes

Chapter 7 109

Synthesis and in-vitro application of upconverting silica-coated liposomes

Chapter 8 135

Activation of liposome-bound Ru(II) prodrugs using red-to-blue triplet-triplet annihilation upconversion in a biological context

Chapter 9 179

Imaging upconverting polymersomes in cancer cells: biocompatible anti-oxidants brighten triplet-triplet annihilation upconversion

Chapter 10 203

Summary, conclusions, and outlook

Appendix I : Determination of quantum yield of upconversion 215

Appendix II : Supporting information for Chapter 3 221

Appendix III : Supporting information for Chapter 4 223

Appendix IV : Supporting information for Chapter 5 245

Appendix V : Supporting information for Chapter 6 251

Appendix VI : Supporting information for Chapter 7 253

Appendix VII : Supporting information for Chapter 8 257

Appendix VIII : Supporting information for Chapter 9 267

Samenvatting in het Nederlands 285

Curriculum Vitae 293

List of publications 295

Acknowledgements 297

CHAPTER 1

Introduction I: Ruthenium polypyridyl complexes as potential anticancer prodrugs in photoactivated chemotherapy

Light-sensitive ruthenium(II) polypyridyl complexes are classical tools in photochemistry that have recently been proposed as prodrugs for photoactivated chemotherapy (PACT). The use of light allows for excellent spatial and temporal control over prodrug activation so that the harmful systemic side-effects of chemotherapy are prevented. In this chapter, the topics of ruthenium anti-cancer drugs and photoactivated chemotherapy are introduced. Special attention is given to the mechanism of photosubstitution in ruthenium complexes, and examples are highlighted of ruthenium photosubstitution that are activated with visible light. Finally, it is addressed how the activation wavelength of PACT prodrugs can be shifted to the phototherapeutic window, in order to achieve a better therapeutic efficacy.

1.1 Anticancer transition metal complexes

After the serendipitous discovery of cisplatin in 1969 and its clinical introduction in 1978 as the world's first platinum anticancer drug, the scientific community was convinced that heavy metal coordination compounds, in particular based on platinum, could have potent anti-tumor activity.[1] The excitement of a new form of cancer therapy soon motivated researchers to look for similar compounds with enhanced toxicity against tumors and reduced side-effects.[2] The era of platinum-based chemotherapy began, in which thousands of cisplatin-analogues were tested *in vitro* and in animals, and nearly 40 of them were tested in clinical trials.[3] Although the exact mechanism of action of cisplatin remains elusive even today, it is generally accepted that the cytotoxic activity of platinum compounds is due to binding with the DNA, which prevents cell replication.[4] Despite the tremendous research efforts only two other compounds were ultimately approved for use in clinics worldwide: carboplatin and oxaliplatin (Figure 1.1). It seemed that the discovery of cisplatin had been indeed a lucky shot, and it was realized that it had been a misconception that only compounds analogous to cisplatin are promising clinical anticancer candidates.[3] To break free from this "cisplatin-paradigm", significant efforts have been undertaken towards the development of non-classical platinum complexes. Promising routes are targeted delivery, prodrug activation by light, intracellular prodrug reduction, among others.[4b, 5]

Initially, research on coordination compounds with transition metals such as Ru, Au, Co, Fe, and Ni could not compete with the enormous enthusiasm for platinum chemistry. However, they have received increasing recognition as potent anticancer complexes in the last three decades.[2-3, 5] The leap from platinum to other metals is appealing: a wide variety in coordination geometry, binding preferences, oxidation states, redox activity, and ligand exchange kinetics may lead to a controlled mechanism of cytotoxicity that was previously unattainable with platinum compounds.[3] Of these metals, ruthenium appears to be one of the most promising.[2] As the research described in this thesis concerns the development of ruthenium-based anticancer drugs, this metal will be the focus of this introduction chapter.

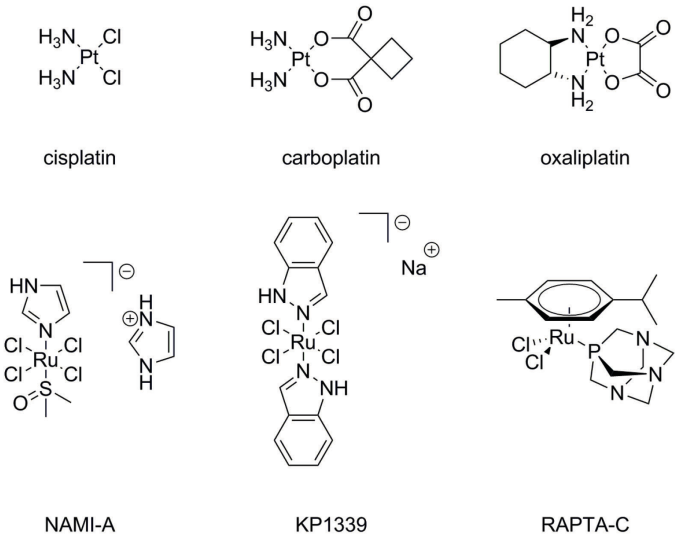

Figure 1.1. Chemical structures of cisplatin, carboplatin, oxaliplatin, NAMI-A, KP1339, and RAPTA-C.

1.2 Ruthenium anticancer drugs

Ruthenium is one of the transition metals most studied for the synthesis of anticancer coordination compounds, and is only surpassed in the number of reported studies by platinum.[6] The advantages of ruthenium complexes include:

i. The preparative coordination chemistry is well-developed, reliable, and the chemical structures are predictable.[3, 7] The usual hexacoordinate octahedral geometry implies a very different reactivity compared to square-planar platinum(II) compounds.[3]

ii. The ligand exchange rates are in the order of minutes to days and can be tuned so that the complexes are relatively kinetically inert under physiological conditions or can interact with physiological processes occurring on the same timescale.[2-3, 8]

iii. The 2+, 3+, and 4+ oxidation states are accessible under physiological conditions,[2-3, 7] which allows the possibility of *in situ* redox-activation of substitutionally inert Ru(III) complexes to active Ru(II) complexes in the highly reductive environment of tumors.[2]

iv. The photophysics and photochemistry of ruthenium complexes is well described and understood,[9] allowing for the smart design of *in situ* light-activatable anticancer compounds.

In the last decade, three major ruthenium-based anticancer drugs have been tested in (pre)clinical trials: KP1339, NAMI-A, and RAPTA-C, see Figure 1.1.[10] In preclinical studies, ruthenium chemotherapeutic drugs were shown to have better selectivity towards tumors and exhibit fewer side-effects than platinum drugs.[2] The activity of ruthenium anticancer drugs are still compared to that of cisplatin, even though they have little in common and each ruthenium compound appears to have a very distinct mode of action.[2-3, 7, 10-11] The cytotoxic effects of KP1339, NAMI-A, and RAPTA-C are mainly attributed to interactions with other biomolecules than nuclear DNA. Regardless, the binding of ruthenium anticancer drugs to DNA is a well-studied subject that is preferred over interaction studies with different biological targets.[12] Ru(II) and Ru(III) coordination compounds interact with DNA due to the relative softness of these ions, which lead to high binding affinities for nitrogen-rich DNA bases.[7] DNA intercalation, groove-bending, and other non-covalent interactions are also possible when the ruthenium compounds contain large planar aromatic ligands.[13] Upon interaction, the complex can either stay covalently or non-covalently bound and disrupt cell proliferation, or induce DNA damage.[7] However, it is important to realize that many Ru complexes do not end up in the nucleus and assert their toxicity through other interactions that are not yet well-explored.

Ruthenium anticancer drugs can be roughly divided into five categories:

i. Active Ru(II) complexes that easily hydrolyze and coordinate to their target biomolecule.
ii. Ru(III) complexes that are activated upon reduction to the Ru(II) complex.
iii. Substitutionally inert Ru(II) complexes that bind non-covalently to DNA or proteins by groove binding or intercalation.[14]
iv. Complexes targeted to unconventional biomolecular targets, *e.g.* specific enzyme inhibitors.[2]
v. Photoactivatable complexes that become toxic or have a toxic effect upon light irradiation

The research described in this thesis focusses on the last category of compounds. They are potential compounds for photoactivated chemotherapy (PACT) and photodynamic therapy (PDT). These topics are introduced in the following sections.

1.3 Photoactivated chemotherapy

Photoactivated chemotherapy (PACT) is a form of anticancer chemotherapy in which a non-toxic prodrug is systemically or dermally administered, and activated selectively at the tumor site by irradiation with visible light. This promising technique provides accurate spatial and temporal control over drug activation that may lead to selective tumor treatment with less side-effects.[9-10, 15] The mechanisms of photoactivated chemotherapy fall into four broad categories: (i) photosensitization or singlet oxygen generation, also known as photodynamic therapy (PDT), (ii) photothermal reaction, (iii) photoinduced redox reactions, and (iv) photosubstitution.[9] In practice, it is difficult to distinguish the different pathways in the complex confinement of a cell. The different photoactivation pathways are often in competition with each other, and depend on solvent, oxygen level, possible reactants present, and the excitation wavelength.[9] The following sections focus on PDT and photosubstitution mechanisms.

1.4 The phototherapeutic window

The organic and metal-organic molecules used in PACT often only absorb considerably in the ultraviolet and blue wavelength region. Light with these wavelengths does not penetrate the body very well due to significant absorption by biomolecules such as melanin and hemoglobin (see Figure 1.2).[16] Furthermore, spatial variations in refractive index within human tissue result in substantial scattering of light: higher energy light (blue region) is scattered more than low energy light (red region).[16] As a result of light scattering and absorption, wavelengths between 700 – 800 nm penetrate human tissue to about 1 cm, while wavelengths near 600 nm penetrate to only 0.5 cm.[17] For blue and ultraviolet light, the penetration depth is a millimeter or less. Wavelengths above 950 nm are absorbed by the molecular vibrations of water. For these reasons, the wavelength domain between about 600 and 950 nm has the optimum transmittance of light, and is therefore called the "phototherapeutic window".[7, 10, 17-18] Moreover, a high dose of blue light itself is toxic for certain tissue types,[19] while red light does not damage tissues at light intensities relevant to PACT.[I] Overall, using red to near-infrared light

[I] Superficial PDT is usually executed with light intensities of 50 – 100 $mW.cm^{-2}$.[20] In the case of internal irradiation using diffuser-tipped light-fibers, the intensity is expressed in terms of $mW.cm^{-1}$ diffuser length. For example, the 630 nm light dose for photodynamic therapy with the clinically approved drug "photofrin" is prescribed as 270 $mW.cm^{-1}$ for < 15 minutes.[21]

would lead to the simultaneous irradiation of a greater tumor volume, while not harming the healthy tissue around it.

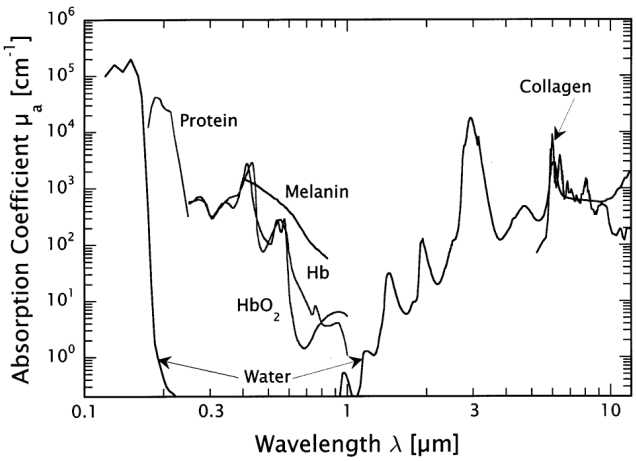

Figure 1.2: Optical absorption coefficients of the major human body chromophores. The phototherapeutic window in which light penetrates the body the deepest, lies between 600 and 950 nm. Reprinted with permission from Vogel et al. [16] © (2003) American Chemical Society.

1.5 Photodynamic therapy

Photodynamic therapy (PDT) was developed as early as the 1900s, but was popularized in clinical therapy by Dougherty in the late 1970s and early 1980s.[18c] Two types of PDT are known that both include strongly absorbing photosensitizer molecules such as porphyrins and phthalocyanins.[18c] In PDT type 1, the photosensitizer absorbs light and then reacts with biomolecules by means of an electron-transfer mechanism.[7] In PDT type 2, which is by far the most common, the photosensitizer is used to generate reactive oxygen species (ROS). Figure 1.3 schematically shows the most important photophysical pathways that are involved in this mechanism. Upon absorption of light the photosensitizer molecule reaches an excited singlet state, which is immediately followed by intersystem crossing (ISC) to a triplet state. Upon collision with ground-state molecular oxygen ($^3\Sigma_g$ state), which is also a triplet state, triplet-triplet annihilation (TTA) may occur. TTA causes the photosensitizer to relax to the singlet ground state, while dioxygen is promoted to a higher-energy singlet state ($^1\Sigma_g$). After internal conversion to the $^1\Delta_g$ state, singlet dioxygen may either chemically react with other molecules, or relax back to the ground state non-radiatively or by emission of a 1270 nm photon. Reaction of singlet oxygen with cell constituents leads to the irreversible oxidation of DNA, lipids, amino-acids, cofactors, and proteins.

This damage triggers pathways towards programmed cell death (apoptosis), or cause instant cell death (necrosis).

Although PDT is a promising and increasingly accepted therapy, a few issues need to be addressed.[18a] Firstly, many photosensitizers do not absorb strongly in the phototherapeutic window and rely on blue to green light for activation, leading to poor therapeutic efficiency. Furthermore, many photosensitizers suffer from photobleaching during treatment and poor water solubility, and are often retained in tissues which causes prolonged light-sensitivity for the patient. Most importantly, many tumor tissues are poorly oxygenated ("hypoxic") because of lack of angiogenesis, while the functioning of PDT relies on the presence of dioxygen.[22] It would therefore be beneficial to use PACT drugs that are activated by light but are toxic *via* an oxygen-independent mechanism.

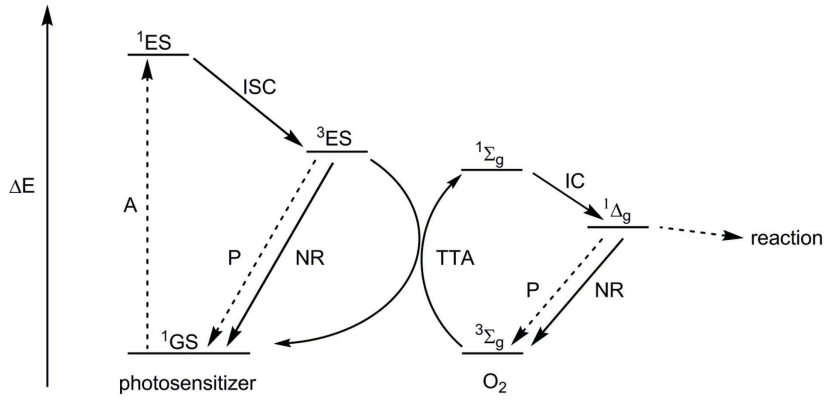

Figure 1.3. Jablonski diagram of the foremost photophysical pathways in photodynamic therapy (type 2), involving a photosensitizer drug and molecular oxygen. Dashed arrows represent transitions in which photons are involved. Abbreviations: GS (ground state), A (Absorption), ES (excited state), ISC (intersystem crossing), P (phosphorescence), NR (non-radiative decay), TTA (triplet-triplet annihilation), IC (internal conversion).

1.6 Photosubstitution

A different PACT mechanism is based on photosubstitution, which relies on caging of a drug with a light-cleavable protective ligand. Upon light activation, the protective ligand dissociates and the active compound is released. Such a strategy does not rely on the presence of dioxygen and is therefore appealing for treatment of hypoxic tumors. Especially ruthenium complexes with heterocyclic N-donor ligands have been widely recognized as particularly attractive candidates for PACT, because of the near-unity intersystem crossing

efficiency to the triplet Metal-to-Ligand Charge Transfer state (^{3}MLCT) state, long-lived excited states, highly tunable photochemical properties, and intensively studied properties in general.[7, 18a] The desirable features for such ruthenium photosubstitution anticancer drugs include: (i) solubility and stability in aqueous biological media, (ii) high cell uptake, (iii) negligible cytotoxicity in the dark and acute anticancer activity when irradiated, (iv) high quantum yield for photosubstitution, and (v) low influence of oxygen on the photophysical and photochemical properties.[9]

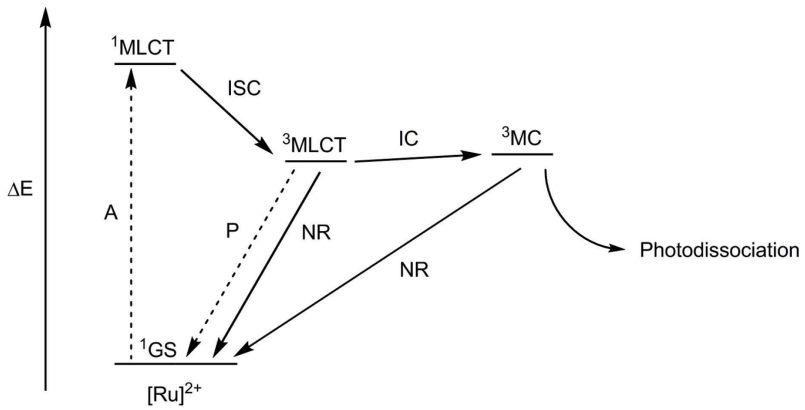

Figure 1.4. Jablonski diagram of the foremost photophysical pathways of a typical photosubstitution Ru polypyridyl complex. Dashed arrows represent transitions in which photons are involved. Abbreviations: GS (ground state), A (Absorption), ISC (intersystem crossing), P (phosphorescence), NR (non-radiative decay), IC (internal conversion), MC (metal centered). Adapted from Göttle et al. [23]

The mechanism of photosubstitution is well understood for ruthenium bipyridine and terpyridine complexes.[23-24] Figure 1.4 illustrates the photosubstitution mechanism for a typical Ru(II) complex with a photolabile ligand. After excitation to the singlet Metal-to-Ligand Charge Transfer state (^{1}MLCT) state and intersystem crossing to the ^{3}MLCT state, a dissociative triplet metal-centered state (^{3}MC) is within reach of (thermal) internal conversion. This ^{3}MC state has dissociative character because the antibonding dσ* orbitals of the metal center become partially occupied, which weakens and elongates a metal-ligand bond. This weakening allows one of the ligands to be substituted by water, thereby giving rise to the potentially cytotoxic aqua derivative. In a biological setting, it is proposed that the aquated coordination site can be used for interactions with biomolecules.[18a, 25]

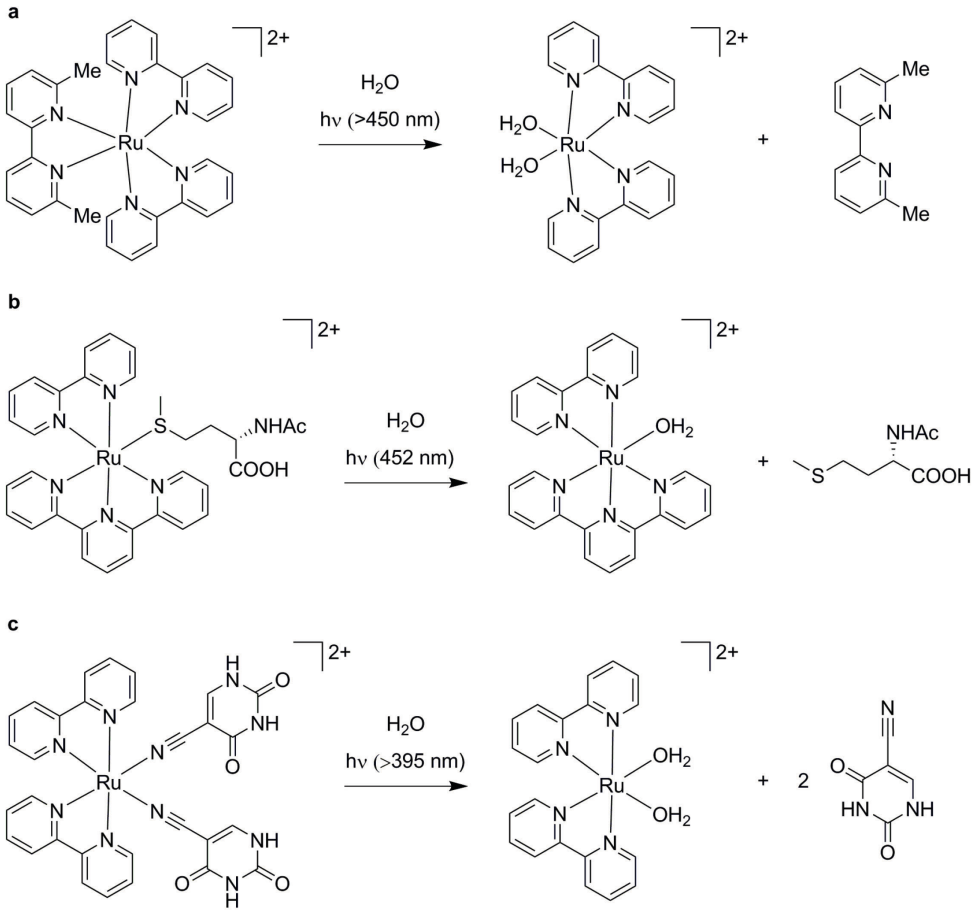

Figure 1.5. Representative examples of photosubstitution ruthenium polypyridyl complexes from the groups of Glazer (a),[26] Bonnet (b),[25d] and Turro (d).[27]

Most Ru(II) polypyridyl complexes are actually quite photostable and the photosubstitution pathway is in competition with other processes such as phosphorescence and non-radiative relaxation.[9, 23a] The mechanism of photosubstitution is strongly dependent on the energy, shape, and position of the potential energy surfaces of the ^{3}MLCT and ^{3}MC states, which determine the accessibility of the ^{3}MC state and hence the dissociation rate.[23a] Meanwhile, the energy gap between ground state and the ^{1}MLCT state determines the maximum absorption wavelength. This means that, ideally, the ^{1}MLCT and ^{3}MC states are both low in energy, so that the complex absorbs in the phototherapeutic window and the photosubstitution takes place efficiently.[23a, 28] In practice, a good trade-off between these two parameters is difficult to achieve.

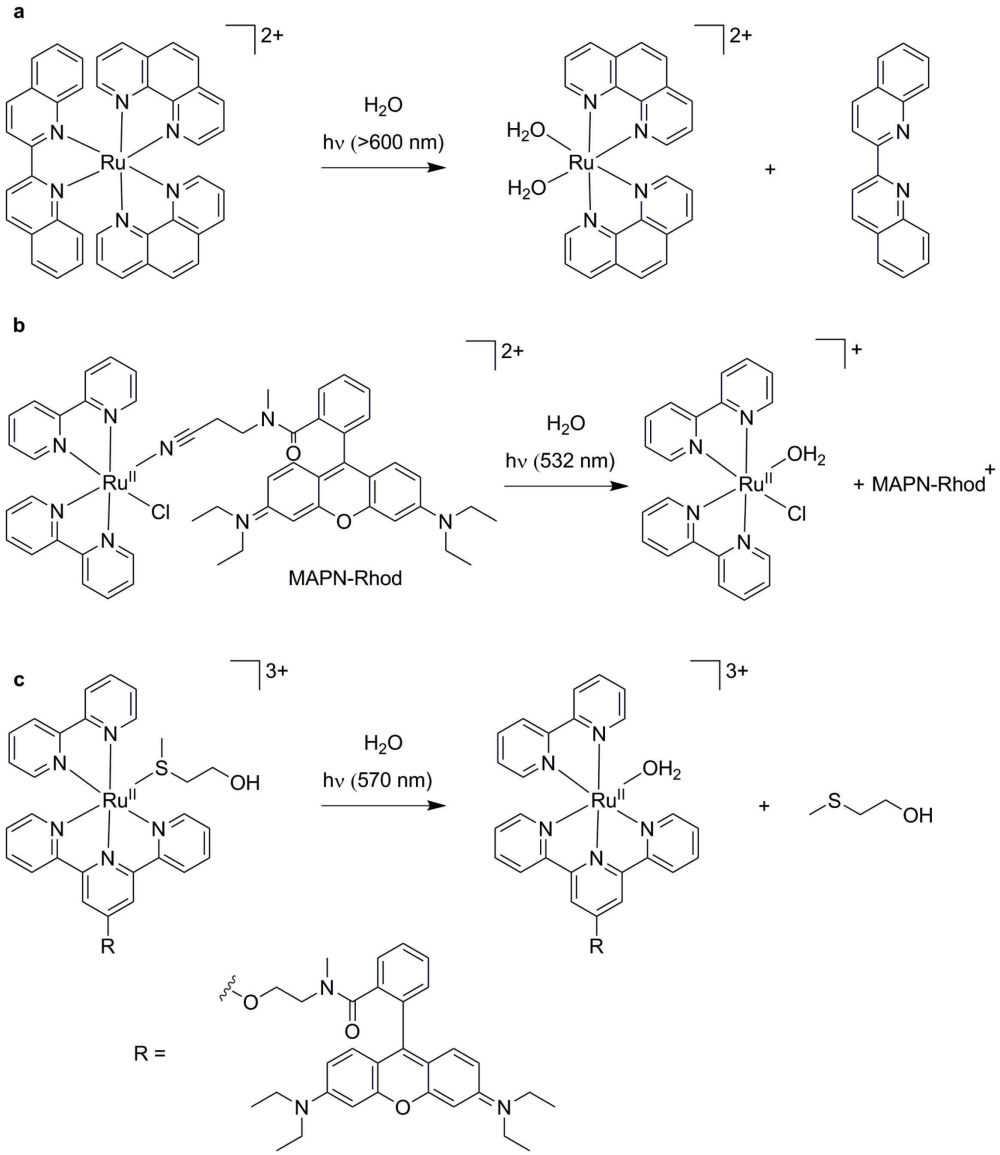

Figure 1.6. Representative examples of photosubstitutionally active ruthenium polypyridyl complexes that are activated with red, green, or yellow light from the groups of Glazer (a),[18a] Etchenique (b),[28] and Bonnet (c), respectively.[29]

A viable strategy to optimize photochemical access to the ^{3}MC state is to induce distortion of the octahedral symmetry around the Ru(II) center. Such distortion leads to smaller overlap between the nitrogen lone pairs and the orbitals of the ruthenium center, and consequently to a smaller ligand field splitting and lower energy of the dissociative triplet Metal-Centered state (^{3}MC) state.[18a, 23b, 26] This makes the ^{3}MC state more accessible from the

photochemically generated ^{3}MLCT state. Popular strategies to induce such distortion include the use of bulky polypyridyl ligands that induce steric hindrance or use of the terpyridine ligand, which coordinates in a strained manner. However, lowering the ^{3}MC state too much is known to cause complex instability in the dark, which is highly undesirable for phototherapeutic purposes.

Some noteworthy examples of blue-light responsive photosubstitutionally active Ru(II) polypyridyl complexes as PACT compounds are given in Figure 1.5. The group of Glazer reported that the strained complex $[Ru(bpy)_2(dmbpy)]^{2+}$ (bpy = bipyridine, dmbpy = 6,6'-dimethylbipyridine) ejects the dmbpy ligand upon >450 nm irradiation which causes a 2 order of magnitude increase in cytotoxicity.[26] The group of Turro reported the complex *cis*-$[Ru(bpy)_2(CNU)_2]^{2+}$ (CNU = 5-cyanouracil) that ejects two equivalents of CNU upon >395 nm irradiation.[27] Both the resulting ruthenium aqua species and the CNU potentially have a biological effect, but photocytotoxicity data on this complex have not been yet published. In recent years, our own research group has mainly focused on analogues of $[Ru(tpy)(bpy)(SRR')]^{2+}$ (tpy = terpyridine, SRR' = thioether ligand) such as $[Ru(tpy)(bpy)(N\text{-acetyl-L-methionine})]^{2+}$, which selectively photoejects the thioether ligand upon 452 nm light irradiation.[23b, 25a, 25d]

Examples of ruthenium complex activation with green or red light are much more rare. An interesting approach to achieve green light activation is demonstrated by the group of Etchenique with the complex $[Ru(bpy)_2(MAPN\text{-}Rhod)Cl]^+$ (MAPN-Rhod = N-methylaminopropionitrile-rhodamine), see Figure 1.6b.[28] The MAPN-Rhod ligand absorbs strongly around 532 nm, and is able to sensitize the GS→^{1}MLCT transition of the ruthenium complex, which normally is not very sensitive for green light, by an intramolecular FRET mechanism (Förster Resonance Energy Transfer). Formally, this was designated to be a "reverse-FRET" mechanism, because in contrast to normal FRET, the maximum emission wavelength of the energy donor is lower in energy than the maximum absorption of the energy acceptor. Photosubstitution is then achieved by the same mechanism as explained above. A similar reverse-FRET strategy was pursued within our group with the complex $[Ru(tpy\text{-}Rhod)(bpy)(2\text{-methylthioethanol})]^{3+}$, see Figure 1.6c.[29] Due to the presence of the rhodamine ligand, it was found that the complex absorbed yellow light very strongly (ε_{570nm} = 44 000 $M^{-1}.cm^{-1}$), while surprisingly, the photodissociation reaction was equally efficient with yellow

(570 nm) and blue light (452 nm). The group of Glazer prepared the strained complex $[Ru(phen)_2(biq)]^{2+}$ (phen = 1,10-phenanthroline, biq = 2,2'-biquinoline), which ejects the biq ligand after light irradiation (Figure 1.6a).[18a] Interestingly, this compound could be photoactivated with red and near-infrared light, which represents the first example of ruthenium based PACT in the phototherapeutic window. The phototoxicity index (PI, *i.e.* the EC_{50} in dark conditions divided by the EC_{50} in light conditions) with blue and infra-red light (both at a dose of 7 $J.cm^{-2}$) was determined to have values of 44 and 3, respectively, while the PI for the well-known PDT drug aminolevulinic acid was determined to be >18. The substantial absorbance up to 700 nm (ε at 650 nm = 500 $M^{-1}.cm^{-1}$) was attributed to direct ^{1}GS to ^{3}MLCT absorption.[30]

1.7 Photosubstitution in the phototherapeutic window

Although some examples exist of photosubstitution ruthenium complexes that are activated with green to near-infrared light (see section 1.6), it remains challenging to realize high photosubstitution efficiency in the phototherapeutic window. Apart from molecular design and modification, other photochemical and photophysical strategies are under development to red-shift the activation wavelength. First of all, two-photon absorption (TPA) can be used, which is the quasi-simultaneous absorption of two photons of low energy to match the ^{1}GS→^{1}MLCT transition energy. Although this technique is effective in shifting the wavelength of activation, and has been used before for ruthenium polypyridyl complexes,[31] it requires high photon density light sources, and it is technically challenging to realize the irradiation of large volumes (*e.g.* a tumor). Secondly, photon upconversion can be used to combine multiple low energy photons into one higher energy photon. The most popular techniques to achieve photon upconversion *in vitro* are by use of lanthanoid-based upconverting nanoparticles (UCNP) and triplet-triplet annihilation upconversion (TTA-UC). The focus of the research described in this thesis is using TTA-UC for the activation of Ru polypyridyl compounds, and is further introduced in Chapter 2.

1.8 References

[1] B. Rosenberg, L. Vancamp, J. E. Trosko, V. H. Mansour, *Nature* **1969**, *222*, 385-386.
[2] E. Antonarakis, A. Emadi, *Cancer Chemother. Pharmacol.* **2010**, *66*, 1-9.
[3] M. A. Jakupec, M. Galanski, V. B. Arion, C. G. Hartinger, B. K. Keppler, *Dalton Trans.* **2008**, 183-194.
[4] a) J. Reedijk, *Chem. Rev.* **1999**, *99*, 2499-2510; b) K. S. Lovejoy, S. J. Lippard, *Dalton Trans.* **2009**, 10651-10659.
[5] P. C. A. Bruijnincx, P. J. Sadler, *Curr. Opin. Chem. Biol.* **2008**, *12*, 197-206.

[6] U. Schatzschneider, J. Niesel, I. Ott, R. Gust, H. Alborzinia, S. Wölfl, *Chem. Med. Chem.* **2008**, *3*, 1104-1109.
[7] M. J. Clarke, *Coord. Chem. Rev.* **2003**, *236*, 209-233.
[8] H. Yamada, T. Koike, J. K. Hurst, *J. Am. Chem. Soc.* **2001**, *123*, 12775-12780.
[9] N. J. Farrer, L. Salassa, P. J. Sadler, *Dalton Trans.* **2009**, 10690-10701.
[10] T. Gianferrara, A. Bergamo, I. Bratsos, B. Milani, C. Spagnul, G. Sava, E. Alessio, *J. Med. Chem.* **2010**, *53*, 4678-4690.
[11] M. Pongratz, P. Schluga, M. A. Jakupec, V. B. Arion, C. G. Hartinger, G. Allmaier, B. K. Keppler, *J. Anal. At. Spectrom.* **2004**, *19*, 46-51.
[12] M. G. Walker, V. Gonzalez, E. Chekmeneva, J. A. Thomas, *Angew. Chem. Int. Ed.* **2012**, *51*, 12107-12110.
[13] S. Schäfer, I. Ott, R. Gust, W. S. Sheldrick, *Eur. J. Inorg. Chem.* **2007**, *2007*, 3034-3046.
[14] G. Gasser, I. Ott, N. Metzler-Nolte, *J. Med. Chem.* **2011**, *54*, 3-25.
[15] M. M. Lerch, M. J. Hansen, G. M. van Dam, W. Szymanski, B. L. Feringa, *Angew. Chem., Int. Ed.* **2016**, *55*, 10978-10999.
[16] A. Vogel, V. Venugopalan, *Chem. Rev.* **2003**, *103*, 577-644.
[17] K. Plaetzer, B. Krammer, J. Berlanda, F. Berr, T. Kiesslich, *Lasers in Medical Science* **2009**, *24*, 259-268.
[18] a) E. Wachter, D. K. Heidary, B. S. Howerton, S. Parkin, E. C. Glazer, *Chem. Commun.* **2012**, *48*, 9649-9651; b) K. Szaciłowski, W. Macyk, A. Drzewiecka-Matuszek, M. Brindell, G. Stochel, *Chem. Rev.* **2005**, *105*, 2647-2694; c) R. R. Allison, C. H. Sibata, *Photodiagnosis. Photodyn. Ther.* **2010**, *7*, 61-75; d) K. R. Byrnes, R. W. Waynant, I. K. Ilev, X. Wu, L. Barna, K. Smith, R. Heckert, H. Gerst, J. J. Anders, *Lasers in Surgery and Medicine* **2005**, *36*, 171-185.
[19] S. L. H. Hopkins, B. Siewert, S. H. C. Askes, P. van Veldhuizen, R. Zwier, M. Heger, S. Bonnet, *Photochem. Photobiol. Sci.* **2016**, *15*, 644-653.
[20] H. Moseley, J. W. Allen, S. Ibbotson, A. Lesar, A. McNeill, M. A. Camacho-Lopez, I. D. W. Samuel, W. Sibbett, J. Ferguson, *British Journal of Dermatology* **2006**, *154*, 747-750.
[21] Photofrin, *http://www.photofrin.com/*, accessed on **17 May 2016**
[22] a) H. J. Feldmann, M. Molls, P. Vaupel, *Strahlenther. Onkol.* **1999**, *175*, 1-9; b) P. Vaupel, F. Kallinowski, P. Okunieff, *Cancer Res.* **1989**, *49*, 6449-6465.
[23] a) P. S. Wagenknecht, P. C. Ford, *Coord. Chem. Rev.* **2011**, *255*, 591-616; b) A. J. Göttle, F. Alary, M. Boggio-Pasqua, I. M. Dixon, J.-L. Heully, A. Bahreman, S. H. C. Askes, S. Bonnet, *Inorg. Chem.* **2016**, *55*, 4448-4456.
[24] a) A.-C. Laemmel, J.-P. Collin, J.-P. Sauvage, *Eur. J. Inorg. Chem.* **1999**, *1999*, 383-386; b) P. C. Ford, *Chem. Sci.* **2016**, *7*, 2964-2986.
[25] a) S. Bonnet, B. Limburg, J. D. Meeldijk, R. J. M. Klein Gebbink, J. A. Killian, *J. Am. Chem. Soc.* **2010**, *133*, 252-261; b) M. A. Sgambellone, A. David, R. N. Garner, K. R. Dunbar, C. Turro, *J. Am. Chem. Soc.* **2013**, *135*, 11274-11282; c) U. Schatzschneider, *Eur. J. Inorg. Chem.* **2010**, *2010*, 1451-1467; d) R. E. Goldbach, I. Rodriguez-Garcia, J. H. van Lenthe, M. A. Siegler, S. Bonnet, *Chem. Eur. J.* **2011**, *17*, 9924-9929.
[26] B. S. Howerton, D. K. Heidary, E. C. Glazer, *J. Am. Chem. Soc.* **2012**, *134*, 8324-8327.
[27] R. N. Garner, J. C. Gallucci, K. R. Dunbar, C. Turro, *Inorg. Chem.* **2011**, *50*, 9213-9215.
[28] O. Filevich, B. Garcia-Acosta, R. Etchenique, *Photochem. Photobiol. Sci.* **2012**, *11*, 843-847.
[29] A. Bahreman, J.-A. Cuello-Garibo, S. Bonnet, *Dalton Trans.* **2014**, *43*, 4494-4505.
[30] S. L. H. Higgins, K. J. Brewer, *Angew. Chem., Int. Ed.* **2012**, *51*, 11420–11422.
[31] M. Salierno, E. Marceca, D. S. Peterka, R. Yuste, R. Etchenique, *J. Inorg. Biochem.* **2010**, *104*, 418-422.

CHAPTER 2

Introduction II: Light upconversion using triplet-triplet annihilation

Light upconversion is the conversion of low-energy light to high-energy light, which can be exploited in applications such as bio-imaging and photoactivated chemotherapy. Among the various principles of light upconversion, triplet-triplet annihilation upconversion (TTA-UC) holds great promise because it can be realized at low excitation intensities and with high efficiency. In this chapter, the TTA-UC mechanism is outlined in detail and nanoparticle systems are discussed with which TTA-UC can be achieved in biological systems. Furthermore, one of the fundamental issues of the TTA-UC mechanism is the inherent oxygen sensitivity. Because solving this issue is of critical importance for the advancement of biological TTA-UC applications, this chapter also discusses in detail how the oxygen sensitivity can be overcome in biological systems. Finally, an outline is given for this thesis.

Sven H.C. Askes and Sylvestre Bonnet. Manuscript in preparation

2.1 The principle of light upconversion

Light upconversion is the photophysical process in which light is converted from low energy (high wavelength, such as red light) to higher energy (low wavelength, such as blue light) by combining the energy of multiple photons. Light upconversion has been recognized to have great potential in biological applications such as bio-imaging and photoactivated chemotherapy (PACT). The advantages of upconversion bio-imaging are evident: first of all, *in vitro* upconversion bio-imaging with red to near-infrared excitation wavelengths reduces irradiation damage and allows a longer or more frequent observation. Secondly, because the emitted light has more energy than the excitation light, upconverted emission can be readily distinguished from autofluorescence so that an excellent imaging contrast can be achieved. Thirdly, red to near-infrared excitation light is able to penetrate deeper *in vivo* so that deeper imaging can be performed.

Besides bio-imaging, light upconversion can be used to activate PACT drugs, that are often only sensitive for UV to green light, with wavelengths in the phototherapeutic window (600 – 950 nm). This strategy is particularly suited for promising PACT drug classes such as blue-light sensitive ruthenium polypyridyl complexes (Chapter 1), Pt(IV) complexes that are activatable with UV to blue light,[1] light-cleavable organic moieties such as *o*-nitrobenzyl groups and coumarin derivatives that are activatable up to the green wavelength range,[2] and photo-isomerizing molecules such as azobenzenes.[3] Practically, this strategy involves red to near-infrared light being upconverted inside the tumor to blue light, which can then be used to activate a prodrug. Using red to near-infrared light instead of UV to green light would lead to a tumor treatment at greater tissue depth. Moreover, in contrast to UV to blue light, red to near-infrared light does not cause any tissue ablation at doses relevant to PACT (see Section 1.4).

The three most relevant forms of light upconversion in combination with PACT are two-photon absorption (TPA), lanthanoid-based upconverting nanoparticles (UCNPs), and triplet-triplet annihilation upconversion (TTA-UC). TPA relies on the simultaneous absorption of two low-energy photons by chromophores with high two-photon absorption cross sections, after which the combined energy of both photons can be used to trigger high-energy requiring photochemistry.[4] For example, this strategy has been explored with two-photon responsive Ru complexes[5] and for drug release from

photocleavable coumarin-derivatized vesicles.[6] Although appealing, the requirement that two photons must be simultaneously absorbed invokes the cumbersome and expensive use of high-power pulsed lasers. Moreover, the required high photon density (MW.cm^{-2} to GW.cm^{-2} irradiances)[7] are only obtained when the laser is focused to a microscopic irradiation volume. Obviously, treatment of a large tumor would be tedious and time-consuming. The alternative UCNPs are crystalline nano-sized particles that are made of low-phonon energy matrices, such as β-$NaYF_4$, that can be advantageously used as upconversion platform and drug carrier in one.[8] The upconverting properties rely on the sequential absorption of infrared photons (808 or 980 nm) by sensitizer lanthanoid ions such as Nd^{3+} or Yb^{3+} that transfer this energy multiple times to emitter ions such as Er^{3+}, Tm^{3+}, or Ho^{3+}.[8e] The combined energy is ultimately released in the form of UV, blue, green, and/or red photons.[8e] UCNPs are enormously popular for bio-imaging and drug activation purposes,[9] despite that they suffer from low quantum yields of upconversion (typically << 0.5% in aqueous solution), low absorbance coefficients, and the need for high power excitation (> 1 W.cm^{-2}) to achieve decent levels of prodrug activation.[10] Even in the NIR domain, high laser intensities (especially at 980 nm) leads to undesired tissue ablation.[11] In contrast, TTA-UC features much higher upconversion quantum yields (~5% in aqueous solution)[12] at much lower excitation intensities (typically < 0.2 W.cm^{-2}),[13] and features molecular chromophores with high molar absorption coefficients. Because of these advantages, the research described in this thesis explored the potential of combining TTA-UC and bio-imaging or PACT.

2.2 Triplet-triplet annihilation upconversion

TTA-UC was already demonstrated several times by Parker and Hatchard in the 1960s,[14] but in those days this phenomenon merely received recognition as photophysical curiosity. It was only in the 21st century that the principle was rediscovered and research on TTA-UC has since then received an exponentially growing amount of scientific interest.[15] Now, TTA-UC has become a powerful photophysical trick with promising applications such as oxygen sensing,[16] extending the action spectrum of photosynthetic organisms,[17] photocatalysis,[18] solar energy harvesting,[19] bio-imaging,[12, 20] and drug delivery and activation (*e.g.* PACT).[21]

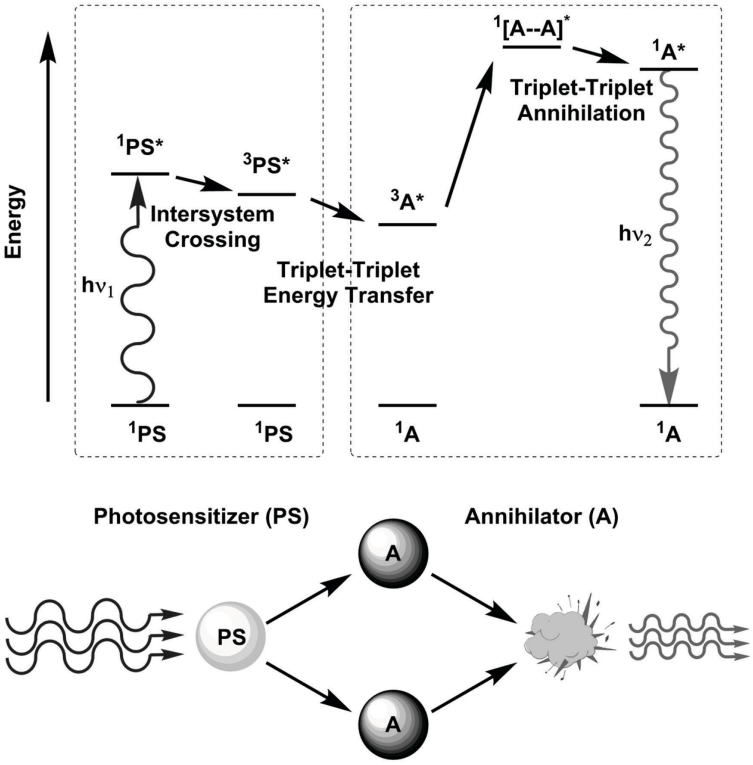

Figure 2.1. Jablonski diagram of the photophysical processes involved in TTA-UC.

TTA-UC is based on the photophysical interplay of photosensitizer (**PS**) and annihilator chromophores (**A**), see Figure 2.1.[4, 9f, 15a, 22] The photosensitizer absorbs low energy light ($h\nu_1$), after which intersystem crossing (ISC) leads to a long-lived triplet state (Equation 2.1):

$$^1\boldsymbol{PS} + h\nu_1 \xrightarrow{r_{abs}} {}^1\boldsymbol{PS}^* \xrightarrow{k_{ISC}} {}^3\boldsymbol{PS}^* \qquad \textit{Equation 2.1}$$

where r_{abs} is the rate of light absorption by the photosensitizer (in mol.L^{-1}.s^{-1}), and k_{ISC} is the rate constant of ISC (in s^{-1}). The triplet state energy of ^{3}**PS*** is transferred to the annihilator by a Dexter-type energy transfer upon diffusional collision, called triplet-triplet energy transfer (TTET); a succession of TTET leads to a buildup of triplet state annihilator molecules due to a generally very long triplet state annihilator lifetime (Equation 2.2):

$$^3\boldsymbol{PS}^* + {}^1\boldsymbol{A} \xrightarrow{k_{TTET}} {}^1\boldsymbol{PS} + {}^3\boldsymbol{A}^* \qquad \textit{Equation 2.2}$$

where k_{TTET} is the second-order rate constant of TTET (in $M^{-1}.s^{-1}$). At this stage, triplet back transfer from annihilator to sensitizer is usually eliminated by keeping the sensitizer to annihilator molar ratio very low (typically 1:10 to 1:200).[23] Then, two excited state triplet annihilator molecules produce an encounter-pair upon diffusional collision. The encounter-pair has either singlet, triplet, or quintet multiplicity, with 1/9, 3/9, and 5/9 chance of formation, respectively (discussed in more detail later). The singlet-state encounter-pair will result in triplet-triplet annihilation (TTA), where one molecule departs in a higher-energy singlet excited state while the other converts to the ground state (Equation 2.3):

$$^3\boldsymbol{A}^* + {}^3\boldsymbol{A}^* \rightarrow {}^1(\boldsymbol{A}-\boldsymbol{A})^* \rightarrow {}^1\boldsymbol{A}^* + {}^1\boldsymbol{A} \qquad \textit{Equation 2.3}$$

where this overall TTA step is a bimolecular process and thus has a second-order rate constant, k_{TTA} (in $M^{-1}.s^{-1}$). Note that TTA is only possible if the energy of the encounter pair exceeds the energy of the singlet excited annihilator. Finally, the singlet excited state returns to the ground state by fluorescent emission of a high energy photon ($h\nu_2$), realizing light upconversion (Equation 2.4):

$$^1\boldsymbol{A}^* \xrightarrow{k_F} {}^1\boldsymbol{A} + h\nu_2 \qquad \textit{Equation 2.4}$$

where k_F is the rate constant of annihilator fluorescence (in s^{-1}). Due to the dependence on molecular contact in the TTET and TTA steps, the overall process heavily relies on the diffusion of sensitizer and/or annihilator chromophores. In case molecular diffusion is restricted, it may rely on diffusion of the triplet excitons through the material.[23] In systems that rely on molecular diffusion, it is often found that the TTA step is rate-limiting, *i.e.* the TTA-rate has values comparable to the rate of molecular diffusion.[23] In such systems, the TTA-UC mechanism is therefore very dependent on the viscosity of the host material or solution.[15a, 23-24]

The anti-stokes shift, *i.e.* the wavelength difference between excitation source and the lowest emission maximum, determines the maximum upconversion energy gain of TTA-UC (ΔE_{UC}, in eV) that can be achieved. ΔE_{UC} is limited to twice the energy of the incident photon, because TTA-UC is a two-photon process. However, this limit is in practice never reached, because of inevitable enthalpic energy losses during ISC (ΔH_1 in eV), TTET (ΔH_2 in eV), and TTA (ΔH_3 in eV). ΔE_{UC} is therefore constrained by the sum of enthalpic losses, as described by Equation 2.5:[25]

$$\Delta E_{UC} = 2(h\nu_1 - \Delta H_1 - \Delta H_2) - \Delta H_3 \qquad \textit{Equation 2.5}$$

where $h\upsilon_1$ is the energy of the absorbed photons (in eV). Of these energy losses, ΔH_2 is most easily reduced by carefully aligning sensitizer and annihilator excited state triplet levels. The highest ΔE_{UC} thus far achieved is 0.94 eV for a couple that is excited at 670 nm ($h\upsilon_1$ = 1.85 eV) and emits at 445 nm ($h\upsilon_2$ = 2.79 eV). [25]

The evolutions in time of the excited states in the TTA-UC scheme are governed by the following set of rate equations (Equation 2.6 to Equation 2.9):

$$\frac{d[^1\boldsymbol{PS}^*]}{dt} = r_{abs} = \frac{\varphi_{exc}\left(1 - 10^{-A_{\lambda_{exc}}}\right)}{V} \qquad \textit{Equation 2.6}$$

$$\frac{d[^3\boldsymbol{PS}^*]}{dt} = k_{ISC}[^1\boldsymbol{PS}^*] - k_p[^3\boldsymbol{PS}^*] - k_{^3PS}[^3\boldsymbol{PS}^*] - k_{TTET}[^3\boldsymbol{PS}^*][^1\boldsymbol{A}] \qquad \textit{Equation 2.7}$$

$$\frac{d[^3\boldsymbol{A}^*]}{dt} = k_{TTET}[^3\boldsymbol{PS}^*][^1\boldsymbol{A}] - k_{^3A}[^3\boldsymbol{A}^*] - k_{TTA}[^3\boldsymbol{A}^*]^2 \qquad \textit{Equation 2.8}$$

$$\frac{d[^1\boldsymbol{A}^*]}{dt} = k_{TTA}[^3\boldsymbol{A}^*]^2 - k_F[^1\boldsymbol{A}^*] - k_{^1A}[^1\boldsymbol{A}^*] \qquad \textit{Equation 2.9}$$

where φ_{exc} is the photon flux at the excitation wavelength (mol photons.s^{-1}), $A_{\lambda_{exc}}$ is the absorbance at the excitation wavelength (assuming only **PS** absorbs at this wavelength), V is the irradiation volume (in L), k_p is the rate

constant of sensitizer phosphorescence (in s^{-1}), $k_{^3PS}$ is the non-radiative decay rate constant of ^{3}**PS*** (in s^{-1}), $k_{^3A}$ is the decay rate constant of ^{3}**A*** when no TTA occurs (in s^{-1}; usually only non-radiative decay), , and $k_{^1A}$ is the non-radiative decay rate constant of $^1\boldsymbol{A}^*$. Finally, note that the set of rate equations listed above described a rather simplified TTA-UC scheme: it does not account for (i) triplet back-transfer from ^{3}**A*** to ^{1}**PS**, (ii) hetero TTA between ^{3}**PS*** and ^{3}**A***, and (iii) homo TTA between pairs of ^{3}**PS***, which may become relevant at high [**PS**] and high excitation intensity.[7b, 22]

From Equation 2.6 to Equation 2.9, the overall efficiency of TTA-UC (Φ_{UC}) under stead-state conditions, defined as the number of upconverted photons per number of excited state photosensitizers upon illumination, is expressed by Equation 2.10:[23]

$$\Phi_{UC} = \frac{number\ of\ upconverted\ photons}{number\ of\ excited\ state\ PS} = \frac{1}{2}\Phi_{ISC}\Phi_{TTET}\Phi_{TTA}\Phi_F \qquad \textit{Equation 2.10}$$

in which Φ_{ISC} is the quantum yield of intersystem crossing, Φ_{TTET} the quantum yield of TTET, Φ_{TTA} the quantum yield of triplet-triplet annihilation, and Φ_F the quantum yield of fluorescence of the annihilator. The factor ½ accounts for the fact that two excited state photosensitizers maximally produce one excited singlet-state annihilator, *i.e.* the intrinsic maximum Φ_{UC} is 50%. Overall, Equation 2.10 underlines that each step needs to be optimized for a high Φ_{UC}. Usually, **PS** and **A** are chosen so that Φ_{ISC} and Φ_F have values close to unity, and k_{ISC} and k_F are generally very fast and thus not rate-limiting. Therefore, the overall efficiency is mainly governed by Φ_{TTET} and Φ_{TTA}. In the steady state (continuous wave excitation) Φ_{TTET} is expressed as the ratio of the quenching rate of ^{3}**PS*** ($k_{TTET}[^1\mathbf{A}][^3\mathbf{PS}^*]$, in $mol.L^{-1}.s^{-1}$) and the total decay rate of ^{3}**PS*** in presence of annihilator (Equation 2.11):[22]

$$\Phi_{TTET} = \frac{k_{TTET}[^1\boldsymbol{A}][^3\boldsymbol{PS}^*]}{k_p[^3\boldsymbol{PS}^*] + k_{^3PS}[^3\boldsymbol{PS}^*] + k_{TTET}[^1\boldsymbol{A}][^3\boldsymbol{PS}^*]} = \frac{k_{TTET}[^1\boldsymbol{A}]}{k_p + k_{^3PS} + k_{TTET}[^1\boldsymbol{A}]} \qquad \textit{Equation 2.11}$$

This expression states that higher annihilator concentrations lead to higher TTET efficiencies. For example, for a TTA-UC system in organic solution with a **PS** lifetime of 300 µs (*i.e.* $k_p + k_{^3PS} = 3 \times 10^4$ s^{-1}), 10 mM **A**, and realizing that triplet energy transfer in solution is usually diffusion limited (*i.e.* $k_{TTET} \approx 1 \times 10^9$ M^{-1}.s^{-1}),[22] the triplet quenching rate has a value of 10^7 s^{-1} and thus near unity energy transfer efficiencies are obtained. Next, Φ_{TTA} can be expressed in the steady state (continuous wave excitation) as the ratio of the triplet-triplet annihilation rate ($k_{TTA}[^3\mathbf{A}^*]^2$, in mol.L^{-1}.s^{-1}) and the total decay rate of the annihilator triplets (Equation 2.12):[22]

$$\Phi_{TTA} = f \times \frac{k_{TTA}[^3\boldsymbol{A}^*]^2}{k_{^3A}[^3\boldsymbol{A}^*] + k_{TTA}[^3\boldsymbol{A}^*]^2} = f \times \frac{k_{TTA}[^3\boldsymbol{A}^*]}{k_{^3A} + k_{TTA}[^3\boldsymbol{A}^*]} \qquad \textit{Equation 2.12}$$

where f is the spin statistical factor. This factor f takes into account that the encounter-pair of the two triplet state annihilator molecules has either singlet, triplet, or quintet multiplicity, with 1/9, 3/9, or 5/9 probability, respectively; only the singlet state multiplicity leads to the desired high-energy excited singlet state. However, because quintet states are not energetically accessible and triplet state encounter-pairs are partially recycled into triplet excited state annihilator molecules, the probability can be increased to 40% (i.e. f = 0.4).[15a, 23, 26] In some systems, f can be even further increased to approach unity.[7b] Furthermore, Equation 2.12 underlines that the TTA efficiency is directly dependent on the production of $^3\mathbf{A}^*$ and approaches unity when $k_{^3A} << k_{TTA}[^3\mathbf{A}^*]$, also known as the "strong annihilation regime". Usually, annihilators are chosen with metastable triplet states that feature lifetimes in the millisecond range (*i.e.* $k_{^3A} \approx 1 \times 10^3$).[22, 27] For instance, at a diffusion-limited TTA rate (*i.e.* $k_{TTA} \approx 1 \times 10^9$ M^{-1}.s^{-1}) this means that a triplet concentration of about 1×10^{-6} M would lead to a 50% TTA efficiency. Furthermore, it is important to realize that in the strong annihilation regime, Φ_{TTA} becomes a constant and the overall TTA-UC process becomes only dependent on the rate of triplet production, *i.e.* light absorption, as described in more detail in recent kinetic treatments.[26] In other words: in the strong annihilation regime, the triplet state manifold is so well-populated that TTA is the predominant photophysical route and competing quenching processes are negligible.[23, 26c] This has the immediate consequence that in the "weak annihilation regime" (*i.e.* when $k_{^3A} >> k_{TTA}[^3\mathbf{A}^*]$) , the intensity variation of TTA-UC is quadratically dependent on the excitation intensity variation – as

would be expected for a two-photon process –, while in the strong annihilation regime this dependence becomes linear. Indeed, this phenomenon is systematically observed for TTA-UC systems, see Figure 2.2. The transition point at which this excitation intensity dependency shifts from quadratic to linear is called the intensity threshold (I_{th}), and is strictly defined as the intensity at which the value of Φ_{UC} is half of the maximum.[7b] Monguzzi *et al.* have demonstrated that the value of I_{th} is proportional to $(k_{3_A})^2$ and is inversely proportional to k_{TTA}, Φ_{TTET}, and $A_{\lambda_{exc}}$.[7b] Thus, in order to obtain high Φ_{UC} at low excitation intensity, (i) annihilators with long lived triplet states are required, (ii) the absorbance of **PS** needs to be high (due to high [**PS**], high molar extinction coefficient, or both), (iii) the TTET step should occur with near-unity yield, and (iv) the TTA rate should be maximized. Typically, I_{th} has a value below 0.2 W.cm^{-2}, while the lowest reported value thus far is 6 μW.cm^{-2}.[28] To put these values in perspective, the solar radiance at the earth surface (AM1.5) is about 0.1 W.cm^{-2} and the linear power regime for lanthanoid-based upconverting nanoparticles is only reached at excitation intensities above 150 W.cm^{-2}.[10]

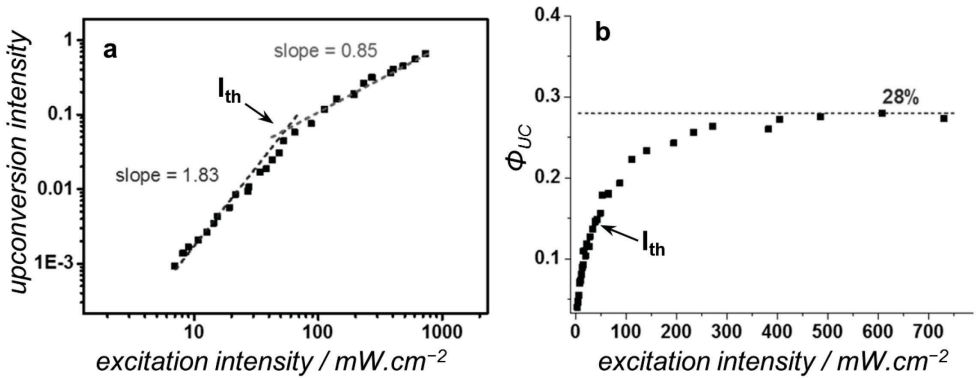

Figure 2.2. Typical power dependency of upconversion emission in a TTA-UC scheme. As an example, data of a green-to-blue upconverting system is shown with an I_{th} of 0.05 W.cm^{-2} and a maximum Φ_{UC} of 28%. (a) Upconversion emission intensity as a function of excitation intensity. The indicated slopes are obtained when the data is plotted on a double logarithmic scale. (b) Upconversion quantum yield (Φ_{UC}) as a function of excitation intensity. Reprinted (adapted) with permission from Duan et al.[29] © American Chemical Society.

The combined photophysical properties of photosensitizer and annihilator greatly influence Φ_{UC} and ΔE_{UC}, and only well-chosen combinations of photosensitizer and annihilator will lead to TTA-UC. The most important requirement for TTA-UC is the energy match between the triplet state energy levels of both molecules: ideally, the triplet energy level of the annihilator is

slightly lower in energy than the triplet energy level of the photosensitizer to accommodate favorable TTET. Besides this, the desirable characteristics of the photosensitizer include (i) high molar extinction coefficient, (ii) high ISC efficiency (Φ_{ISC}), (iii) long triplet lifetime (τ_T), and (iv) small singlet-triplet energy gap.[15a, 23, 30] These criteria are very well satisfied by palladium or platinum porphyrin complexes, which therefore have become benchmark photosensitizers in TTA-UC schemes. Typical examples are palladium tetra-(di-*tert*-butyl)phenyltetraquinoxalino porphyrin (PdTPTQP), palladium tetraphenyltetrabenzoporphyrin (PdTPTBP), and platinum octaethylporphyrin (PtOEP), see Figure 2.3. Moreover, metalloporphyrins usually feature a large absorption gap between Q-bands and Soret bands, so that re-absorption of the upconverted light is mostly eliminated. For the annihilator the most important requirements are (i) high fluorescence quantum yield (Φ_F), (ii) long triplet lifetime (τ_T), (iii) an excited singlet state with slightly less than twice the energy of the excited triplet state, and (iv) an excited singlet state with higher energy than the wavelength used to excite the photosensitizer.[15a, 23] Suitable annihilator molecules include anthracene, pyrene, perylene, rubrene, and diphenyl anthracene (DPA), see Figure 2.3.

A few early examples of well-matching photosensitizer-annihilator combinations are given in Table 2.1; numerous other examples have been reviewed elsewhere.[4, 9f, 15a] All of these sensitizer-annihilator pairs exhibit very large anti-stokes shift from green/red to blue (0.72-0.94 eV shift), and their relevant energy levels satisfy the requirements discussed earlier. It is worthwhile to note that these early results have been acquired in deoxygenated apolar organic solvents to dissolve the highly lipophilic molecules and to prevent quenching by molecular oxygen, which is the most predominant quenching pathway in TTA-UC schemes. Since these early examples in organic solution, TTA-UC has been demonstrated in rubbery and glassy polymers,[15a, 23-24, 31] hydro-, organo- and ionogels,[32] and a variety of nano- and micro-sized particle systems.[12-13, 18b, 20, 28, 33]

Table 2.1: Examples of photosensitizer-annihilator combination and their main TTA-UC properties.

Photosensitizer	**Annihilator**	λ_{exc} **(nm)**	λ_{em} **(nm)**	ΔE_{UC} **(eV)**	Φ_{UC} **(%)**	**Ref.**
PdTPTQP	perylene	670	445	0.94	0.6	[25]
PdTPTBP	3-(4-tert-butylphenyl)perylene	635	450	0.81	6.6	[34]
PtOEP	DPA	536	410	0.72	19	[35]
$[Ru(dmbpy)_3]^{2+}$ [a]	anthracene	514.5	375	0.90	-	[36]

[a] dmbpy = 4,4′-dimethyl-2,2′-bipyridine

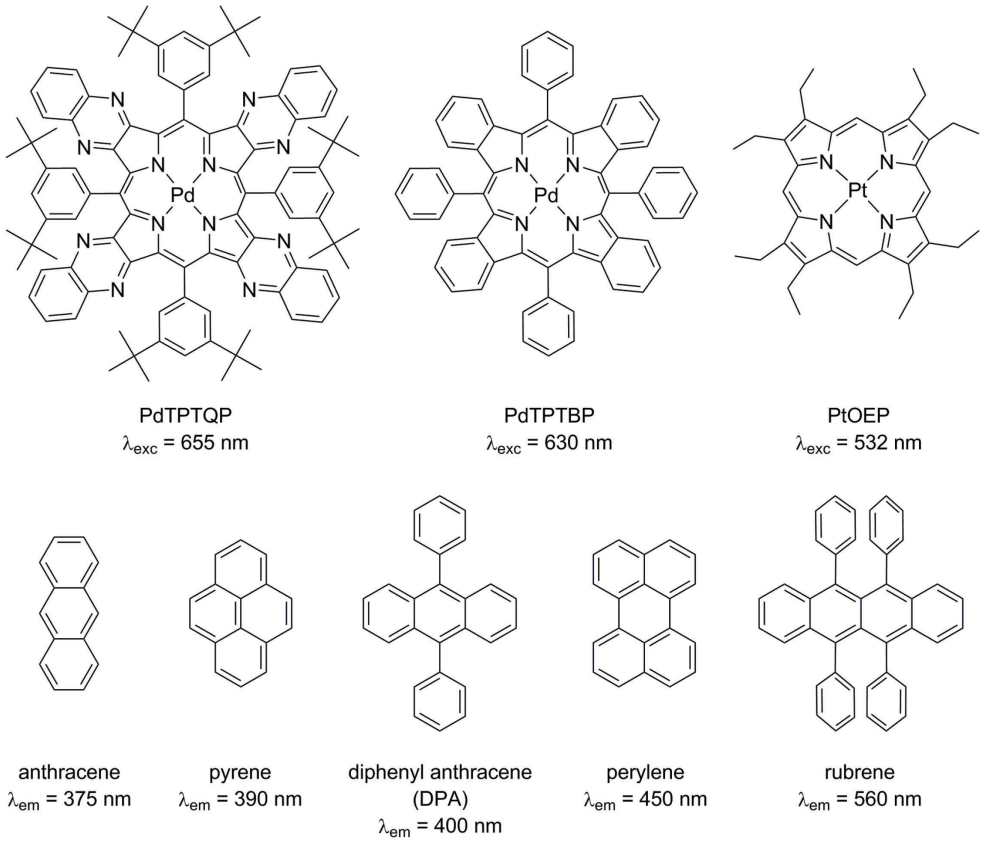

Figure 2.3. Chemical structures of frequently-used photosensitizers (top row) and annihilators (bottom row) in TTA-UC schemes. Approximate values for the highest absorption bands of photosensitizers and lowest emission peaks of annihilators are mentioned.[15a, 25]

2.3 Overcoming the oxygen sensitivity of TTA-UC

Whereas for some applications the oxygen sensitivity of TTA-UC can be exploited, for example to build an oxygen sensor,[16] for most other applications oxygen quenching leads to dysfunctional systems in which (i) upconversion does not work in air, and (ii) the highly reactive singlet oxygen that is generated by this quenching process leads to photodamage of the chromophores and the matrix (Figure 2.4). To counter these issues, several approaches have been developed in recent years. First of all, it has been shown that TTA-UC systems with very high TTET and TTA rates are less sensitive, because upconversion then successfully competes with the diffusion of oxygen. Especially promising are systems that feature supramolecular annihilator networks that support facile migration of triplet excitons. For example, the work of Kimizuka and coworkers shows that organogels or nano-

MOFs are excellent host systems for TTA-UC: densely-packed annihilator networks resulted in triplet exciton diffusion rates that by far exceed the molecular diffusion rate of molecules in organic solvents.[28-29, 32b, 32c, 37] The second strategy involves using matrices that obstruct the diffusion of molecular oxygen, which has been exemplified with polymers that were covalently or non-covalently functionalized with sensitizer and annihilator.[31b, 31h, 31i, 38] However, the low diffusion rate in these materials generally caused the upconversion efficiency to be low. An interesting solution to this problem was presented by Baluschev and Landfester *et al.*, who encapsulated micron-sized red-to-green upconverting oil-core nanocapsules in a cellulose matrix.[39] The cellulose acted as an oxygen barrier, so that TTA-UC was allowed to be efficient (Φ_{UC} = 4.1%) and long lasting in air. In other work by the same authors in collaboration with Turshatov, similar nanocapsules of 100 – 140 nm in diameter were embedded in electrospun polyvinyl alcohol (PVA) nanofibers with a diameter of 270 – 480 nm.[40] This nm-thick PVA wrapping successfully blocked diffusion of oxygen to the nanocapsules. These results show that it is possible to block oxygen with a nm-scale coating of an oxygen impermeable material.

Finally, it has been realized that oxygen sensitivity can be eliminated by the use of (singlet) oxygen scavengers. The idea of ground-state oxygen scavenging is self-evident: a reducing agent is added to remove dissolved oxygen so that the solution is deoxygenated until depletion of the scavenger. For instance, sodium sulfite has been used to deoxygenate a green-to-blue upconverting oil-in-water micro-emulsion.[33i] In the case of singlet oxygen scavenging, oxygen is consumed only upon irradiation of the sensitizer (Figure 2.4). Upon irradiation, singlet oxygen is produced which then reacts with the scavenger, causing a locally deoxygenated environment around the photosensitizer (micro-)environment. Once the oxygen concentration is low enough, TTA-UC is no longer restricted and upconverted light effectively appears upon further irradiation. Suitable scavengers that have been used for TTA-UC are alkene-terminated polyisobutylene, oleic acid, linoleic acid, and hyper-branched unsaturated polyphosphates.[12b, 12c, 13a, 31e, 33b, 33f] The former three examples rely on the reaction of the unsaturated bond with singlet oxygen to make peroxide derivatives.

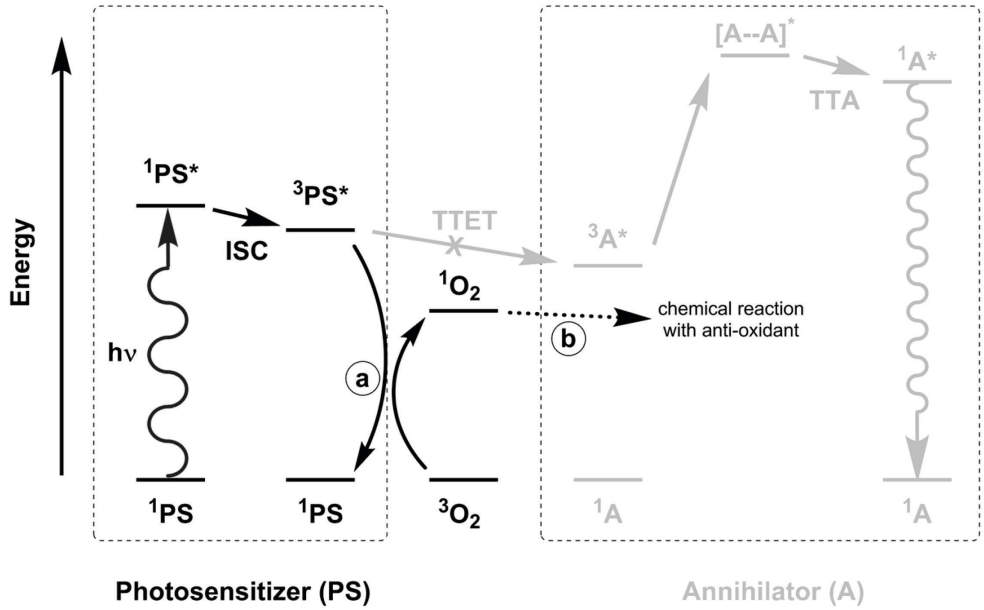

Figure 2.4. Oxygen sensitivity of the TTA-UC mechanism: After the photosensitizer reaches the triplet excited state, instead of engaging in triplet-triplet energy transfer (TTET) to the annihilator, it is quenched by ground state molecular oxygen to produce singlet oxygen (a). Quenching of the triplet state annihilator by oxygen can also occur (not shown). To overcome this issue, sacrificial anti-oxidants can be added to the mixture which chemically react with singlet oxygen (b). Then, TTA-UC is no longer restricted when the oxygen concentration is (nearly) depleted.

With biological TTA-UC applications in mind, quenching by molecular oxygen is also an especially important issue. For instance, using an oxygen-sensitive device for tumor imaging or treatment would surely lead to unreliable results, because oxygen concentrations vary drastically in the complex microenvironment of a tumor.[41] In the remaining sections of this chapter TTA-UC nanoparticles are described that have been used in bio-imaging or for PACT, and strategies to reduce the *in vitro* oxygen sensitivity are discussed.

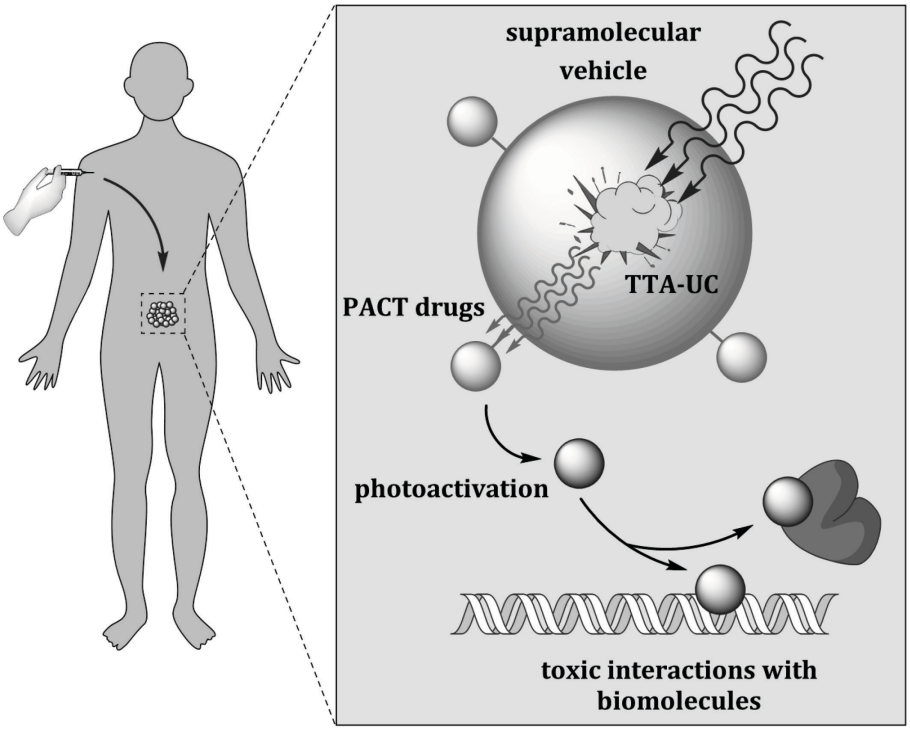

Figure 2.5. Schematic representation of the combination of a supramolecular vehicle, TTA-UC, and PACT drugs for in vivo tumor treatment. The device is injected in the body, after which it accumulates at the tumor site and the tumor is irradiated with red light. The red light is then locally upconverted to blue light, which activates the PACT prodrug (blue) anchored to the vehicle's surface or kept inside the vehicle. After irradiation the activated drug (red) dissociates from the vehicle and causes toxic interactions with biomolecules.

2.4 TTA-UC in bio-imaging and PACT

For biological TTA-UC applications, it is essential to combine sensitizer and annihilator in a supramolecular manner, so that they colocalize at the required site, and to facilitate molecular contact and migration of triplet states. Additionally, for PACT it is highly desirable to compartmentalize the light-activatable prodrug together with the upconversion dye-pair, in order to utilize the upconverted light effectively (Figure 2.5). Meanwhile, supramolecular vehicles such as nanoparticles have emerged as extremely versatile tools in biomedical applications.[2, 42] Because the TTA-UC dye pairs are usually very lipophilic, supramolecular systems are preferred with very lipophilic compartments. So far, six systems have emerged in which water-soluble nano-systems are combined with TTA-UC in a biological setting: silica-coated Pluronic F127 micelles,[12a, 20b] polylactic acid-block-polyethylene glycol

(PLA-b-PEG) micelles,[33j] dye-modified cellulose templates,[20c] and a variety of oil-core nanocapsules,[12b, 12c, 20a, 20d] see Table 2.2. These systems will be further detailed in this section. Furthermore, in Chapter 8 and Chapter 9 we report the imaging of upconversion luminescence in cancer cells using liposomes and polymersomes as carrier systems.

Green-to-blue upconverting silica-coated Pluronic F127 micelles were prepared in the group of Li.[12a] It was demonstrated that these micelles were non-toxic, had a high upconversion quantum yield, and could be used for *in vitro* upconversion imaging of cells and *in vivo* upconversion imaging of mouse lymph nodes. In a later publication,[12b] it was reported that particles created with this experimental procedure, but functionalized with a red-to-green or red-to-yellow upconverting pair instead only resulted in very weak upconversion emission. In a similar strategy, polylactic acid-block-polyethylene glycol was used to self-assemble green-to-blue upconverting micelles.[33j] The authors hypothesized that the upconverted blue emission was transferred *via* FRET to a blue-light responsive coumarin derivative, which induced photo-uncaging of a cell-binding peptide. However, control experiments in which the annihilator or sensitizer was omitted from the micelle formulation were not considered, so that it cannot be confirmed that uncaging of the peptide was indeed caused by TTA-UC. Regardless, after irradiation *ex vivo* with green light, and adding the nanoparticle suspension to cells, the nanoparticles showed a large increase in cell-binding. The functioning of this strategy in more biologically relevant conditions has yet to be demonstrated. The group of Siegwart prepared 350 nm sized cellulose aggregates that were functionalized with an infrared-to-yellow upconverting TTA-UC pair.[20c] The aggregates were taken up by HeLa cells in 2D culture and after intratumoral injection in a xenograft mouse model. The topics of oxygen sensitivity, upconversion efficiency, particle morphology, and biocompatibility of the approach were unfortunately not addressed.

Four types of oil-core nanocapsules with average hydrodynamic sizes from 100 - 200 nm have been demonstrated to be excellent hosts for TTA-UC, and were successfully imaged *in vitro* and *in vivo*.[12b, 12c, 20a, 20d] The oily interior favors molecular diffusion and effectively dissolves large amounts of hydrophobic compounds in a small particle volume. The exact chemical composition of both core and shell greatly affected the upconverting capabilities of the particles in presence of oxygen. First of all, the group of Landfester and Turshatov demonstrated green-to-blue upconversion with

hexadecane-core PSAA-shell (PSAA = polystyrene-polyacrylic acid copolymer) nanocapsules.[20d] These particles only produced upconversion after deoxygenation, and only "*in vitro"* after fixation and sealing of the sample in a glove box. In a next paper, red-to-green upconverting 1-phenylhexadecane-core PMMA-shell (PMMA = polymethyl methacrylate) were reported.[20a] Likewise, no upconversion in air could be established, which suggests that a nano-scale polymeric shell cannot safeguard the dyes inside the particles from quenching by oxygen. However, in living HeLa cells, some upconversion emission was in fact observed. Interestingly, upconversion brightened when the cells were treated with valinomycin, which stimulates mitochondria to enhance their oxygen consumption. This example demonstrates that *ex vitro* air stability is no definite prerequisite for obtaining upconversion *in vitro*. It is unclear why TTA-UC systems that do not work in air are capable of upconversion in living cells. We speculate that the presence of endogenous anti-oxidants are responsible for scavenging ground-state or singlet oxygen (see Section 2.3). Differences in oxygen concentration within each cell and differences between cells may also modify the ability of particles to perform TTA-UC.

The group of Li prepared red-to-green and red-to-yellow upconverting soy bean oil-core BSA-dextran-shell nanocapsules (BSA = bovine serum albumin).[12b] This system was able to perform upconversion in air. It was for the first time realized that reductive compounds can facilitate TTA-UC: soy bean oil contains oleic acid and linoleic acid, which both are unsaturated fatty acids that react with singlet oxygen, see Section 2.3. As mentioned before, the underlying rationale is that in an oxygen-rich environment, the photosensitizer produces singlet oxygen that can react with a scavenger, resulting in a locally deoxygenated micro-environment. Apart from the "reducing oil core", it was proposed that the BSA-shell participated in singlet oxygen scavenging, because BSA contains many tryptophan residues that are capable of reacting with singlet oxygen as well. Although the performance of the particles in 2D cell cultures was not established, the particles were successfully used for lymphatic imaging of living mice. Finally, the group of Kim prepared red-to-blue and red-to-green upconverting oleic acid-core silica shell nanocapsules.[12c] Here, pure oleic acid was chosen as scavenger to allow the particles to upconvert in air. From the article, it was not clear whether the particles were functional in 2D cell cultures, as the data showed fixated cells to which a commercial anti-fading reagent was added. Regardless, the particles

were successfully used in imaging of tumors *in vivo* with upconversion luminescence. Overall, from reviewing these published TTA-UC particle systems, it becomes clear that acquiring upconversion *in vitro* and *in vivo* has been a poorly explored subject so far.

2.5 Emission stability of TTA-UC in a biological context

A poorly addressed research topic is the emission stability in time of TTA-UC nanoparticles in a biological context. To the best of our knowledge, the emission stability has only been briefly discussed in the work of Li *et al.*, who show that green-to-blue upconversion of silica-coated Pluronic F127 micelles in HeLa cells was completely stable for at least 10 minutes under continuous illumination (no exact excitation intensity given);[12a, 20b] no further explanation is given why the emission is so stable. Of course, the stability requirements depend greatly on the application. Long-term bio-imaging methods require stable emission for seconds to minutes under continuous irradiation, but for short-term experiments, the emission stability is not especially critical. For the combination of TTA-UC and PACT, high stabilities are required up to hours of irradiation time at high irradiances (up to ~1 $W.cm^{-2}$) in order to release enough biologically active species. For instance, in comparable work that combines lanthanoid-based upconverting nanoparticles and PACT/PDT, typical treatment durations vary from 20 min up to more than 5 h.[43] Two critical questions are therefore: (i) how long-lasting is the upconversion emission in a biological context with current nanoparticle systems and (ii) how can the emission stability be improved? For instance, as mentioned before, many TTA-UC nanoparticles rely on the presence of endogenous or supplemental anti-oxidants in order to function *in vitro* or *in vivo*. However, after a certain time, the anti-oxidants may be depleted and oxygen can quench the TTA-UC process once again. Overall, the temporal stability of TTA-UC emission in a biological context, and the enhancement of this stability with for example anti-oxidants, are important aspects that need to be considered in future work. We argue that it is simply not enough to only demonstrate that a given TTA-UC system functions in air-equilibrated solutions: it is of utmost importance to show the temporal stability at a given excitation intensity and a given oxygenation level in order to conclude on the usability of a system for each specific application.

Table 2.2. Summary of known TTA-UC nanoparticle systems that have been developed for bio-imaging and PACT purposes, and their most important (photo)physical properties.

	Vesicle		**Micelle**		**Nanocapsule**				**Cellulose aggre-gates**
Inner material	H_2O	H_2O	Pluronic F127	PLA-PEG	HD	1-PHD	oleic acid	soy bean oil	cellulose
Shell material	Phospho-lipid mixtures	PiB-PEG-Me	Silica		PSAA	PMMA	Silica	BSA-dextran conjugate	Tween 20
λ_{exc} / λ_{em} (nm)	532/400 630/450	630/450	532/430	532/430	514/450	633/550 708/555	635/470 635/505	635/525 635/550	850/595
Φ_{UC} (%) at 20 °C	2.3 0.3 – 2.4	0.2	2.2[a]	1.9[a]	N/A	N/A	3.3[b] 4.3[b]	1.7[b] 4.8[b]	N/A
I_{th} (mW.cm^{-2})	50 – 60	220 – 260	>360[a]	~100[a]	N/A	N/A	>>300[b]	50[b] 75[b]	N/A
Hydro-dynamic size (nm)	130 – 170	80 or 150	22	37	200	225	217	116 95	350
Reference	This thesis[21]	This thesis	[12a, 20b]	[33]	[20d]	[20a]	[12c]	[12b]	[20c]

[a] Influence of oxygen not reported. [b] Values obtained in air. PLA-PEG = polylactic acid-polyethylene glycol block copolymer, HD = hexadecane, 1-PHD = 1-phenylhexadecane, PiB-PEG-Me = polyisobutylene-polyethylene glycol block copolymer, PSAA = polystyrene-polyacrylic acid copolymer, PMMA = polymethyl methacrylate, BSA = bovine serum albumin

2.6 Thesis goal and outline

In the research described in this thesis, the goal was to prepare an upconverting nano-device that is able to generate blue light inside living cancer cells with which a light-sensitive ruthenium anticancer prodrug can be activated in order to kill the cells. The device should only become toxic upon light irradiation in the phototherapeutic window. To achieve this goal, it is likely that the following requirements need to be met:

i. high upconversion efficiency (Φ_{UC}) at human body temperature (37 °C)
ii. upconversion at low excitation intensity (*i.e.* a low I_{th}) so that use of high power lasers is prevented
iii. a large upconversion energy gain (ΔE_{UC}) to shift the activation wavelength to the phototherapeutic window (preferably red to near-infrared light)
iv. efficient energy transfer to the ruthenium prodrug
v. low oxygen sensitivity
vi. high temporal emission stability
vii. low cytotoxicity of the nano-device in the dark
viii. high cytotoxicity of the nano-device upon red to near-infrared light irradiation within a clinically relevant time span

In Chapter 3, I will describe how efficient red-to-blue and green-to-blue upconversion can be obtained in a liposome drug carrier. The red-to-blue upconversion is used to trigger the photodissociation of a ruthenium polypyridyl complex that is anchored to another liposome. In Chapter 4, the ruthenium complex is this time attached to the same liposome as that containing photosensitizer and annihilator molecules, and it is shown that the upconversion energy is transferred non-radiatively from the annihilator to the ruthenium complex *via* Förster resonance energy transfer (FRET). In Chapter 5 it is shown that red-to-blue upconversion is located in the lipid bilayer of the liposomes and that TTA-UC can be used to image the membrane of giant vesicles. Chapter 6 describes results of the investigation whether red-to-blue TTA-UC in liposomes is also efficient at human body temperature; I will describe how the upconversion efficiency is dependent on temperature in a variety of liposome compositions. Chapter 7 describes research that investigated whether a silica coating around the liposomes can protect the TTA-UC process from quenching by molecular oxygen. In Chapter 8 the *in vitro* applicability is addressed of liposomes that are functionalized with a red-to-

blue upconverting dye couple and ruthenium polypyridyl complexes, and whether it is possible to trigger a cytotoxic effect upon red light irradiation. Furthermore, the effect is of supplemental anti-oxidants on the performance of this system is reported. In Chapter 9 I will describe how red-to-blue upconversion can be obtained in polymersomes, and that the upconversion luminescence can be imaged in living cancer cells. Furthermore, I will address whether anti-oxidants increase the upconversion luminescence *in vitro*. Finally, in Chapter 10 the thesis is concluded by summing up the advantages and limits of TTA-UC for pro-drug activation, and future research directions are proposed.

2.7 References

[1] a) F. S. Mackay, J. A. Woods, H. Moseley, J. Ferguson, A. Dawson, S. Parsons, P. J. Sadler, *Chem. Eur. J.* **2006**, *12*, 3155-3161; b) A. F. Westendorf, J. A. Woods, K. Korpis, N. J. Farrer, L. Salassa, K. Robinson, V. Appleyard, K. Murray, R. Grünert, A. M. Thompson, P. J. Sadler, P. J. Bednarski, *Mol. Cancer Ther.* **2012**, *11*, 1894-1904; c) S. Perfahl, M. M. Natile, H. S. Mohamad, C. A. Helm, C. Schulzke, G. Natile, P. J. Bednarski, *Mol. Pharm.* **2016**.

[2] A. Y. Rwei, W. Wang, D. S. Kohane, *Nano Today* **2015**, *10*, 451-467.

[3] M. Schönberger, D. Trauner, *Angew. Chem., Int. Ed.* **2014**, *53*, 3264-3267.

[4] C. Ye, L. Zhou, X. Wang, Z. Liang, *Phys. Chem. Chem. Phys.* **2016**.

[5] M. Salierno, E. Marceca, D. S. Peterka, R. Yuste, R. Etchenique, *J. Inorg. Biochem.* **2010**, *104*, 418-422.

[6] J. Dong, Z. Xun, Y. Zeng, T. Yu, Y. Han, J. Chen, Y.-Y. Li, G. Yang, Y. Li, *Chem. Eur. J.* **2013**, *19*, 7931-7936.

[7] a) V. Nikolenko, R. Yuste, L. Zayat, L. M. Baraldo, R. Etchenique, *Chem. Commun.* **2005**, 1752-1754; b) A. Monguzzi, R. Tubino, S. Hoseinkhani, M. Campione, F. Meinardi, *Phys. Chem. Chem. Phys.* **2012**, *14*, 4322-4332.

[8] a) D. K. Chatterjee, M. K. Gnanasammandhan, Y. Zhang, *Small* **2010**, *6*, 2781-2795; b) C. Li, J. Lin, *J. Mater. Chem.* **2010**, *20*, 6831-6847; c) J. Shen, L. Zhao, G. Han, *Adv. Drug Delivery Rev.* **2012**; d) D. K. Chatterjee, L. S. Fong, Y. Zhang, *Adv. Drug Delivery Rev.* **2008**, *60*, 1627-1637; e) M. Lin, Y. Zhao, S. Wang, M. Liu, Z. Duan, Y. Chen, F. Li, F. Xu, T. Lu, *Biotechnol. Adv.* **2012**, *30*, 1551-1561.

[9] a) P. Zhang, W. Steelant, M. Kumar, M. Scholfield, *J. Am. Chem. Soc.* **2007**, *129*, 4526-4527; b) C. Wang, H. Tao, L. Cheng, Z. Liu, *Biomaterials* **2011**, *32*, 6145-6154; c) E. Ruggiero, J. Hernandez-Gil, J. C. Mareque-Rivas, L. Salassa, *Chem. Commun.* **2015**; d) W. Lv, T. S. Yang, Q. Yu, Q. Zhao, K. Y. Zhang, H. Liang, S. J. Liu, F. Y. Li, W. Huang, *Adv. Sci.* **2015**, *2*, 1500107; e) S. S. Lucky, K. C. Soo, Y. Zhang, *Chem. Rev.* **2015**; f) J. Zhou, Q. Liu, W. Feng, Y. Sun, F. Li, *Chem. Rev.* **2014**, *115*, 395-465; g) J. Liu, Y. Liu, W. Bu, J. Bu, Y. Sun, J. Du, J. Shi, *J. Am. Chem. Soc.* **2014**, *136*, 9701-9709.

[10] J.-C. Boyer, F. C. J. M. van Veggel, *Nanoscale* **2010**, *2*, 1417-1419.

[11] Z. Chen, W. Sun, H.-J. Butt, S. Wu, *Chem. Eur. J.* **2015**, *21*, 9165-9170.

[12] a) Q. Liu, T. Yang, W. Feng, F. Li, *J. Am. Chem. Soc.* **2012**, *134*, 5390-5397; b) Q. Liu, B. Yin, T. Yang, Y. Yang, Z. Shen, P. Yao, F. Li, *J. Am. Chem. Soc.* **2013**, *135*, 5029-5037; c) O. S. Kwon, H. S. Song, J. Conde, H.-i. Kim, N. Artzi, J.-H. Kim, *ACS Nano* **2016**, *10*, 1512-1521.

[13] a) J.-H. Kim, J.-H. Kim, *ACS Photonics* **2015**, *2*, 633-638; b) S. Baluschev, V. Yakutkin, G. Wegner, T. Miteva, G. Nelles, A. Yasuda, S. Chernov, S. Aleshchenkov, A. Cheprakov,

Appl. Phys. Lett. **2007**, *90*, 181103-181103; c) P. Mahato, A. Monguzzi, N. Yanai, T. Yamada, N. Kimizuka, *Nat. Mater.* **2015**, *14*, 924-930.
[14] a) C. A. Parker, C. G. Hatchard, *Proc. Chem. Soc.* **1962**, 386; b) C. A. Parker, C. G. Hatchard, T. A. Joyce, *Nature* **1965**, *205*, 1282-1284.
[15] a) T. N. Singh-Rachford, F. N. Castellano, *Coord. Chem. Rev.* **2010**, *254*, 2560-2573; b) J. Zhao, S. Ji, H. Guo, *RSC Adv.* **2011**, *1*, 937-950.
[16] S. M. Borisov, C. Larndorfer, I. Klimant, *Adv. Funct. Mater.* **2012**, *22*, 4360-4368.
[17] a) M. Filatov, S. Ritz, I. Ilieva, V. Mailänder, K. Landfester, S. Baluschev, *SPIE Newsroom* **2014**, *DOI: 10.1117/2.1201403.005378*; b) K. R. Menon, S. Jose, G. K. Suraishkumar, *Biotechnol. J.* **2014**, *9*, 1547-1553.
[18] a) M. Majek, U. Faltermeier, B. Dick, R. Pérez-Ruiz, A. Jacobi von Wangelin, *Chem. Eur. J.* **2015**, *21*, 15496-15501; b) O. S. Kwon, J. H. Kim, J. K. Cho, J. H. Kim, *ACS Appl. Mater. Interfaces* **2015**, *7*, 318-325.
[19] a) A. Monguzzi, S. M. Borisov, J. Pedrini, I. Klimant, M. Salvalaggio, P. Biagini, F. Melchiorre, C. Lelii, F. Meinardi, *Adv. Funct. Mater.* **2015**, *25*, 5617-5624; b) A. Nattestad, C. Simpson, T. Clarke, R. W. MacQueen, Y. Y. Cheng, A. Trevitt, A. J. Mozer, P. Wagner, T. W. Schmidt, *Phys. Chem. Chem. Phys.* **2015**; c) S. P. Hill, T. Banerjee, T. Dilbeck, K. Hanson, *J. Phys. Chem. Lett.* **2015**, *6*, 4510-4517; d) A. Nattestad, Y. Y. Cheng, R. W. MacQueen, T. F. Schulze, F. W. Thompson, A. J. Mozer, B. Fückel, T. Khoury, M. J. Crossley, K. Lips, G. G. Wallace, T. W. Schmidt, *J. Phys. Chem. Lett.* **2013**, *4*, 2073-2078.
[20] a) C. Wohnhaas, V. Mailänder, M. Dröge, M. A. Filatov, D. Busko, Y. Avlasevich, S. Baluschev, T. Miteva, K. Landfester, A. Turshatov, *Macromol. Biosci.* **2013**, *13*, 1422–1430; b) Q. Liu, W. Feng, T. Yang, T. Yi, F. Li, *Nat. Protocols* **2013**, *8*, 2033-2044; c) A. Nagai, J. B. Miller, P. Kos, S. Elkassih, H. Xiong, D. J. Siegwart, *ACS Biomater. Sci. Eng.* **2015**, *1*, 1206-1210; d) C. Wohnhaas, A. Turshatov, V. Mailänder, S. Lorenz, S. Baluschev, T. Miteva, K. Landfester, *Macromol. Biosci.* **2011**, *11*, 772-778.
[21] a) S. H. C. Askes, M. Kloz, G. Bruylants, J. T. Kennis, S. Bonnet, *Phys. Chem. Chem. Phys.* **2015**, *17*, 27380-27390; b) S. H. C. Askes, A. Bahreman, S. Bonnet, *Angew. Chem., Int. Ed.* **2014**, *53*, 1029-1033.
[22] T. W. Schmidt, F. N. Castellano, *J. Phys. Chem. Lett.* **2014**, *5*, 4062-4072.
[23] Y. C. Simon, C. Weder, *J. Mater. Chem.* **2012**, *22*, 20817-20830.
[24] T. N. Singh-Rachford, J. Lott, C. Weder, F. N. Castellano, *J. Am. Chem. Soc.* **2009**, *131*, 12007-12014.
[25] Y. Y. Cheng, B. Fückel, T. Khoury, R. l. G. C. R. Clady, N. J. Ekins-Daukes, M. J. Crossley, T. W. Schmidt, *J. Phys. Chem. A* **2011**, *115*, 1047-1053.
[26] a) Y. Y. Cheng, B. Fückel, T. Khoury, R. l. G. C. R. Clady, M. J. Y. Tayebjee, N. J. Ekins-Daukes, M. J. Crossley, T. W. Schmidt, *J. Phys. Chem. Lett.* **2010**, *1*, 1795-1799; b) Y. Y. Cheng, T. Khoury, R. G. C. R. Clady, M. J. Y. Tayebjee, N. J. Ekins-Daukes, M. J. Crossley, T. W. Schmidt, *Phys. Chem. Chem. Phys.* **2010**, *12*, 66-71; c) A. Haefele, J. Blumhoff, R. S. Khnayzer, F. N. Castellano, *J. Phys. Chem. Lett.* **2012**, *3*, 299-303.
[27] C. A. Parker, T. A. Joyce, *Chem. Commun.* **1966**, 108b-109.
[28] P. Mahato, N. Yanai, M. Sindoro, S. Granick, N. Kimizuka, *J. Am. Chem. Soc.* **2016**.
[29] P. Duan, N. Yanai, N. Kimizuka, *J. Am. Chem. Soc.* **2013**, *135*, 19056–19059.
[30] W. Wu, J. Sun, S. Ji, W. Wu, J. Zhao, H. Guo, *Dalton Trans.* **2011**, *40*, 11550-11561.
[31] a) R. R. Islangulov, J. Lott, C. Weder, F. N. Castellano, *J. Am. Chem. Soc.* **2007**, *129*, 12652-12653; b) A. Monguzzi, R. Tubino, F. Meinardi, *J. Phys. Chem. A* **2009**, *113*, 1171-1174; c) P. B. Merkel, J. P. Dinnocenzo, *J. Lumin.* **2009**, *129*, 303-306; d) X. Cui, J. Zhao, Y. Zhou, J. Ma, Y. Zhao, *J. Am. Chem. Soc.* **2014**, *136*, 9256-9259; e) F. Marsico, A. Turshatov, R. Peköz, Y. Avlasevich, M. Wagner, K. Weber, D. Donadio, K. Landfester, S. Baluschev, F. R. Wurm, *J. Am. Chem. Soc.* **2014**; f) A. J. Tilley, B. E. Robotham, R. P. Steer, K. P. Ghiggino, *Chem. Phys. Lett*; g) X. Jiang, X. Guo, J. Peng, D. Zhao, Y. Ma, *ACS Appl. Mater. Interfaces* **2016**; h) S. H. Lee, J. R. Lott, Y. C. Simon, C. Weder, *J. Mater. Chem. C* **2013**, *1*, 5142-5148; i) S.-H. Lee, Á. Sonseca, R. Vadrucci, E. Giménez, E. J. Foster, Y.

Simon, *J. Inorg. Organomet. Polym. Mater.* **2014**, *24*, 898-903; j) S. H. Lee, D. C. Thévenaz, C. Weder, Y. C. Simon, *J. Polym. Sci., Part A: Polym. Chem.* **2015**, *53*, 1629-1639.

[32] a) R. Vadrucci, C. Weder, Y. C. Simon, *Mater. Horiz.* **2015**, *2*, 120-124; b) P. Duan, N. Yanai, H. Nagatomi, N. Kimizuka, *J. Am. Chem. Soc.* **2015**, *137*, 1887-1894; c) T. Ogawa, N. Yanai, A. Monguzzi, N. Kimizuka, *Sci. Rep.* **2015**, *5*, 10882; d) Y. Murakami, Y. Himuro, T. Ito, R. Morita, K. Niimi, N. Kiyoyanagi, *J. Phys. Chem. B* **2016**, *120*, 748-755; e) R. Vadrucci, C. Weder, Y. C. Simon, *J. Mater. Chem. C* **2014**, *2*, 2837-2841.

[33] a) Z. Huang, X. Li, M. Mahboub, K. Hanson, V. Nichols, H. Le, M. L. Tang, C. J. Bardeen, *Nano Lett.* **2015**, *15*, 5552-5557; b) J.-H. Kim, F. Deng, F. N. Castellano, J.-H. Kim, *ACS Photonics* **2014**, *1*, 382-388; c) Y. C. Simon, S. Bai, M. K. Sing, H. Dietsch, M. Achermann, C. Weder, *Macromol. Rapid Commun.* **2012**, *33*, 498-502; d) K. Tanaka, H. Okada, W. Ohashi, J.-H. Jeon, K. Inafuku, Y. Chujo, *Bioorg. Med. Chem.* **2013**, *21*, 2678-2681; e) A. Turshatov, D. Busko, S. Baluschev, T. Miteva, K. Landfester, *New J. Phys.* **2011**, *13*, 083035; f) J.-H. Kim, J.-H. Kim, *J. Am. Chem. Soc.* **2012**, *134*, 17478-17481; g) C. Ye, B. Wang, R. Hao, X. Wang, P. Ding, X. Tao, Z. Chen, Z. Liang, Y. Zhou, *J. Mater. Chem. C* **2014**, *2*, 8507-8514; h) X. Cao, B. Hu, R. Ding, P. Zhang, *Phys. Chem. Chem. Phys.* **2015**; i) M. Penconi, P. L. Gentili, G. Massaro, F. Elisei, F. Ortica, *Photochem. Photobiol. Sci.* **2014**, *13*, 48-61; j) W. Wang, Q. Liu, C. Zhan, A. Barhoumi, T. Yang, R. G. Wylie, P. A. Armstrong, D. S. Kohane, *Nano Lett.* **2015**, *15*, 6332-6338; k) S. Mutsamwira, E. W. Ainscough, A. C. Partridge, P. J. Derrick, V. V. Filichev, *J. Phys. Chem. B* **2015**, *119*, 14045-14052; l) Z. Huang, X. Li, B. D. Yip, J. M. Rubalcava, C. J. Bardeen, M. L. Tang, *Chem. Mater.* **2015**, *27*, 7503-7507; m) C. Zhang, J. Y. Zheng, Y. S. Zhao, J. Yao, *Chem. Commun.* **2010**, *46*, 4959-4961; n) S. P. Hill, T. Dilbeck, E. Baduell, K. Hanson, *ACS Energy Lett.* **2016**, 3-8; o) D. C. Thévenaz, S. H. Lee, F. Guignard, S. Balog, M. Lattuada, C. Weder, Y. C. Simon, *Macromol. Rapid Commun.* **2016**; p) M. Poznik, U. Faltermeier, B. Dick, B. Konig, *RSC Adv.* **2016**, *6*, 41947-41950.

[34] A. Turshatov, D. Busko, Y. Avlasevich, T. Miteva, K. Landfester, S. Baluschev, *Chem. Phys. Chem.* **2012**, *13*, 3112-3115.

[35] a) M. Penconi, F. Ortica, F. Elisei, P. L. Gentili, *J. Lumin.* **2012**; b) A. Monguzzi, R. Tubino, F. Meinardi, *Phys. Rev. B* **2008**, *77*, 155122.

[36] R. R. Islangulov, D. V. Kozlov, F. N. Castellano, *Chem. Commun.* **2005**, 3776-3778.

[37] S. Hisamitsu, N. Yanai, N. Kimizuka, *Angew. Chem. Int. Ed.* **2015**, *54*, 11550-11554.

[38] a) P. C. Boutin, K. P. Ghiggino, T. L. Kelly, R. P. Steer, *J. Phys. Chem. Lett.* **2013**, 4113-4118; b) M. Tzenka, Y. Vladimir, N. Gabriele, B. Stanislav, *New J. Phys.* **2008**, *10*, 103002.

[39] A. J. Svagan, D. Busko, Y. Avlasevich, G. Glasser, S. Baluschev, K. Landfester, *ACS Nano* **2014**, *8*, 8198-8207.

[40] C. Wohnhaas, K. Friedemann, D. Busko, K. Landfester, S. Baluschev, D. Crespy, A. Turshatov, *ACS Macro Lett.* **2013**, *2*, 446-450.

[41] a) H. J. Feldmann, M. Molls, P. Vaupel, *Strahlenther. Onkol.* **1999**, *175*, 1-9; b) P. Vaupel, F. Kallinowski, P. Okunieff, *Cancer Res.* **1989**, *49*, 6449-6465; c) E. E. Graves, M. Vilalta, I. K. Cecic, J. T. Erler, P. T. Tran, D. Felsher, L. Sayles, A. Sweet-Cordero, Q.-T. Le, A. J. Giaccia, *Clin. Cancer Res.* **2010**, *16*, 4843-4852.

[42] a) I. Brigger, C. Dubernet, P. Couvreur, *Adv. Drug Delivery Rev*; b) J. Nam, N. Won, J. Bang, H. Jin, J. Park, S. Jung, S. Jung, Y. Park, S. Kim, *Adv. Drug Delivery Rev.* **2012**; c) C. Sanchez-Cano, M. J. Hannon, *Dalton Trans.* **2009**, 10702-10711; d) S. Svenson, *Mol. Pharm.* **2013**; e) A. Bansal, Y. Zhang, *Acc. Chem. Res.* **2014**.

[43] a) J. Liu, W. Bu, L. Pan, J. Shi, *Angew. Chem., Int. Ed.* **2013**, *52*, 4375-4379; b) L. Zhao, J. Peng, Q. Huang, C. Li, M. Chen, Y. Sun, Q. Lin, L. Zhu, F. Li, *Adv. Funct. Mater.* **2014**, *24*, 363-371; c) S. Cui, D. Yin, Y. Chen, Y. Di, H. Chen, Y. Ma, S. Achilefu, Y. Gu, *ACS Nano* **2012**.

CHAPTER 3

Activation of a photodissociative ruthenium complex by triplet-triplet annihilation upconversion in liposomes

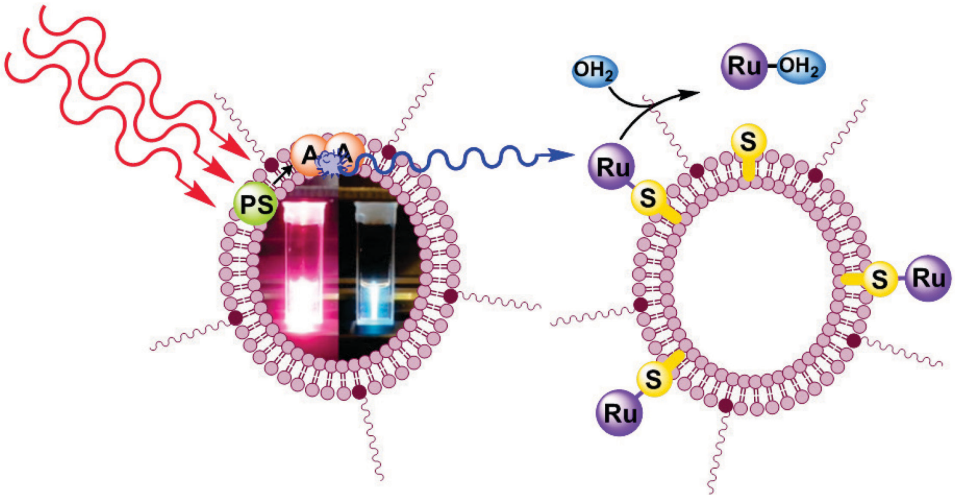

Liposomes capable of generating blue photons in situ by triplet-triplet annihilation upconversion of either green or red light, were prepared. The red-to-blue upconverting liposomes were capable of triggering the photodissociation of ruthenium polypyridyl complexes from PEGylated liposomes using a clinical grade PDT laser source (630 nm).

This chapter was published as a communication: S. H. C. Askes, A. Bahreman, S. Bonnet, *Angew. Chem., Int. Ed.* **2014**, *53*, 1029-1033.

3.1 Introduction

Light-sensitive ruthenium(II) polypyridyl compounds are classical tools in photochemistry that have recently been proposed as prodrugs for photoactivatable anticancer therapy (PACT).[1] As shown in classical photodynamic therapy (PDT), the use of light to treat cancer allows for spatially and temporally controlling the toxicity of an anticancer drug, which lowers side effects for cancer patients. Meanwhile, loading anticancer drugs into drug carriers such as liposomes helps targeting the compounds to tumor tissues. Especially sterically hindered liposomes, *i.e.*, those grafted with polyethylene glycol chains, have been recognized as versatile and biocompatible drug carriers for the treatment of various diseases because of their long lifetime in the blood circulation. With such PEGylated liposomes uptake in tumors is enhanced due to the so-called enhanced permeability and retention (EPR) effect.[2] In PACT, activation of for example ruthenium-functionalized liposomes could be realized after cell uptake using visible light. However, most ruthenium(II) polypyridyl compounds require activation with blue light (400 – 500 nm), *i.e.*, outside the phototherapeutic window (600 – 1000 nm), in which light permeates mammalian tissues optimally. In this work, *in situ* upconversion of red to blue light is realized using triplet-triplet annihilation upconversion (TTA-UC), and combined with ruthenium-functionalized liposomes to trigger the activation of the ruthenium complex using a clinical grade PDT laser source.

In TTA-UC, low energy photons are converted into higher energy photons by means of a bimolecular mechanism involving a sensitizer and two annihilator molecules.[3] The sensitizer absorbs the low-energy light, undergoes intersystem crossing (ISC) to a triplet state, and transfers its energy to an annihilator molecule *via* triplet-triplet energy transfer (TTET). Collision of two triplet annihilator molecules leads to triplet-triplet annihilation (TTA), whereby one molecule is promoted to the excited singlet state, while the other one falls back to the ground state. The singlet annihilator returns to the ground state by emission of a high-energy photon, thus realizing upconversion. TTA-UC with a range of molecule pairs has been realized in organic solvent,[3a, 3b, 3d] ionic liquid,[4] polymers,[3a, 3c, 5] and various water-soluble nanoparticles.[6] In this communication, we demonstrate the first examples of TTA-UC in the lipid bilayer of neutral liposomes.

3.2 Results and discussion

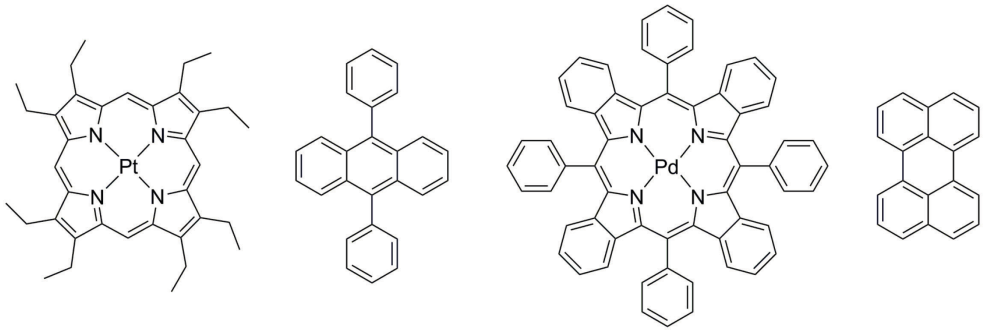

*Figure 3.1. Chemical structures of platinum octaethylporphyrin (**1**), 9,10-diphenylanthracene (**2**), palladium tetraphenyltetrabenzoporphyrin (**3**), and perylene (**4**).*

Two well-investigated TTA-UC couples were considered for incorporation in liposomes: platinum octaethylporphyrin (**1**) and 9,10-diphenylanthracene (**2**) on the one hand, and palladium tetraphenyltetrabenzoporphyrin (**3**) and perylene (**4**) on the other hand (Figure 3.1). Obviously, when included in liposomes these highly apolar molecules favor the lipophilic interior of the lipid bilayer. Liposomes made of 1,2-dimyristoyl-*sn*-glycero-3-phosphocholine (DMPC) and containing 4 mol% of sodium N-(carbonyl-methoxypolyethylene glycol-2000)-1,2-distearoyl-*sn*-glycero-3-phosphoethanolamine (DSPE-MPEG-2000), the sensitizer **1** or **3**, and/or the annihilator **2** or **4**, were prepared by extrusion in DPBS buffer solution (Table 3.1). The diameters of the liposomes (130 – 170 nm) were measured by dynamic light scattering. UV-VIS absorption and luminescence spectra of liposomes containing either the sensitizer or the annihilator, *i.e.*, of samples **L1**, **L2**, **L3**, and **L4**, were comparable to that of the corresponding compounds in toluene solution (Figure S.II.1). Thus, incorporation of any of the four molecules shown in Figure 3.1 into the DMPC bilayers did not change their spectroscopic properties.

Although in liposome samples **L1-2** and **L3-4** both molecules of each upconverting couple were successfully inserted into the bilayer, it was initially uncertain whether their diffusion in the two-dimensions of the bilayer would be sufficient to allow TTA-UC to occur.[3a] After deoxygenation these samples were excited at either 532 nm or 630 nm, respectively, near the absorption maximum of the highest Q-band of **1** (λ_{max} = 536 nm) or **3** (λ_{max} = 628 nm),

respectively. A bright blue luminescence was observed in both cases (Figure 3.2) after suppressing the scattered excitation light with notch and/or short pass filters. Under the same experimental conditions, no blue emission was observed for **L1**, **L2**, **L3**, or **L4**, thus proving that both components of each upconverting couple are necessary for the upconversion to occur. To the best of our knowledge, **L1-2** and **L3-4** are the first examples showing TTA-UC in liposomes. As both green-to-blue and red-to-blue upconversion was obtained, the use of liposomes appears to be a straightforward manner to solubilize TTA-UC couples in aqueous solution.

*Table 3.1. Overview of liposomal formulations used in this work. [DMPC], [PEG], [**1**], [**2**], [**3**], [**4**] and [**5**] represent the bulk concentrations in DMPC, DSPE-MPEG-2000, **1**, **2**, **3**, **4** and $\mathbf{5}^{2+}$, respectively, in DPBS buffer.*

Code	[DMPC] (mM)	[DSPE-mPEG-2000] (mM)	[1] (μM)	[2] (μM)	[3] (μM)	[4] (μM)	[5] (mM)
L1-2	20	0.80	3.5	100	-	-	-
L1	20	0.80	3.5	-	-	-	-
L2	20	0.80	-	100	-	-	-
L3-4	20	0.80	-	-	2.5	50	-
L3	20	0.80	-	-	2.5	-	-
L4	20	0.80	-	-	-	50	-
L5	5.0	0.20	-	-	-	-	0.20

The luminescence spectra of **L1-2** and **L3-4** were measured at 298 K under argon (Figure 3.3). Upon excitation at 532 nm, **L1-2** shows a structured upconversion band at 433 nm, corresponding to emission of **2** in toluene (Figure S.II.1b). A second band was present as well; its emission maximum (646 nm) was consistent with the phosphorescence of **1** in toluene (Figure S.II.1a). Similarly, for **L3-4** excitation at 630 nm leads to an upconversion band at 473 nm, and a second band at 800 nm (Figure 3.3). The upconversion emission corresponds to emission of **4** in toluene (Figure S.II.1d), apart from the first peak at 447 nm that was filtered by the 633 nm notch filter used for rejecting the scattered excitation (Figure S.II.2). The peak at 800 nm in the emission spectrum of **L3-4** corresponds to the phosphorescence of **3**, as observed in toluene (Figure S.II.1c). In both samples, the phosphorescence band corresponds to a unimolecular event, *i.e.*, emission from a photosensitizer molecule in the triplet state, whereas the upconversion band derives from bimolecular events leading to emission from an annihilator in the singlet state.

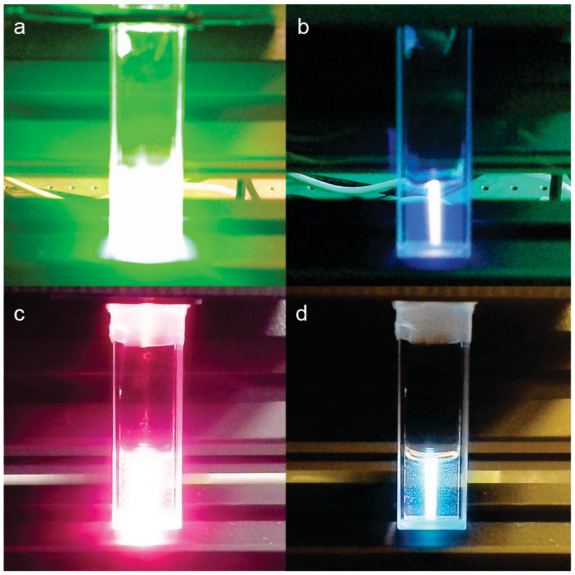

*Figure 3.2. Digital photographs of **L1-2** and **L3-4** under irradiation at 532 nm and 630 nm, respectively, with 27 mW excitation power (for both systems) in a 2.6 mm diameter beam (intensity: 0.51 W.cm⁻²). (a) **L1-2** without filter. (b) **L1-2** with 533 nm notch filter and <575 nm short pass filter. (c) **L3-4** without filter. (d) **L3-4** with 633 nm notch filter. Samples were deoxygenated and maintained at 298 K.*

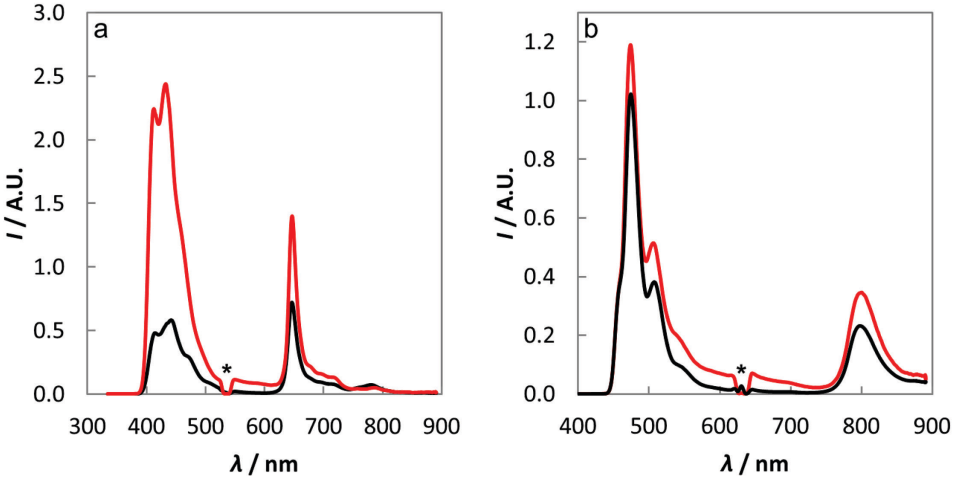

*Figure 3.3. (a) Emission spectra of liposome sample **L1-2** (black) and of a toluene solution containing **1** and **2** at the same bulk concentrations (red, [**1**] = 3.5 μM and [**2**] = 100 μM). (b) Emission spectra of the liposome sample **L3-4** (black) and of a toluene solution containing **3** and **4** at the same bulk concentrations (red, [**3**] = 2.5 μM and [**4**] = 50 μM). Asterisks indicate excitation (532 nm for **L1-2** and 630 nm for **L3-4**). The samples were deoxygenated before measurement. Spectra acquired at 298 K, excitation power for both samples 27 mW, 2.6 mm diameter beam, intensity 0.51 W.cm⁻².*

The luminescence spectra of both upconverting couples were measured in toluene using the same bulk concentrations for the sensitizer and annihilator as for **L1-2** and **L3-4**. The upconversion intensity for couple **1**-**2** was found to be four times weaker in liposomes than in toluene at 298 K, and for couple **3**-**4** it was comparable for both sample types (Figure 3.3). Upon inserting the sensitizer and annihilator in the lipid bilayer two phenomena take place simultaneously. On the one hand, compartmentalization of the lipophilic molecules in the bilayer increases their local concentrations, which increases the probability of intermolecular collisions and therefore the rates of TTET and TTA. On the other hand, two-dimensional diffusion in a lipid bilayer is somewhat slower than in a non-viscous isotropic toluene solution, which may decrease TTA-UC efficiency in liposomes. Overall, our data show that the trade-off is excellent and that efficient TTA-UC occurs in PEGylated DMPC liposomes (at 298 K).

Table 3.2. Upconversion quantum yield (Φ_{uc}) in liposomes and toluene at 293 K.

	Φ_{uc} (%)	
TTA-UC Couple	**in PEGylated DMPC liposomes**	**in toluene**
1-2[a]	2.3 (**L1-2**)	5.1[b]
3-4[c]	0.5 (**L3-4**)	1.2[d]

*[a] 532 nm, 10 mW excitation power, 1.5 mm diameter beam (intensity 0.57 W.cm^{-2}). [b] [**1**] = 3.5 μM, [**2**] = 100 μM. [c] 630 nm, 10 mW excitation power, 2.5 mm diameter beam (intensity 0.20 W.cm^{-2}). [d] [**3**] = 2.5 μM, [**4**] = 50 μM.*

Measurements of upconversion quantum yields (Φ_{uc}) are usually done by relative actinometry.[3a] However, intense scattering in liposome samples would make any comparison with a reference compound in homogeneous solution challenging. For this reason, the upconversion quantum yields of **L1-2** and **L3-4** were measured using an absolute method, *i.e.* with an integrating sphere and a calibrated spectrometer (Appendix I). The setup was similar to that used by Boyer *et al.* for determining the upconversion quantum yield of lanthanoid-based nanoparticles.[7] For **L1-2**, **L3-4**, and for their toluene analogues, Φ_{uc} was determined upon irradiation using a 10 mW continuous beam (Table 3.2). At 293 K Φ_{uc} in PEGylated DMPC liposomes was found roughly half of that in toluene for both couples, with values of 2.3% and 0.5% for **L1-2** and **L3-4**, respectively, *versus* 5.1% and 1.2% in toluene. To the best of our knowledge, this is the first time that the quantum yield of TTA-UC has been determined using an absolute method.

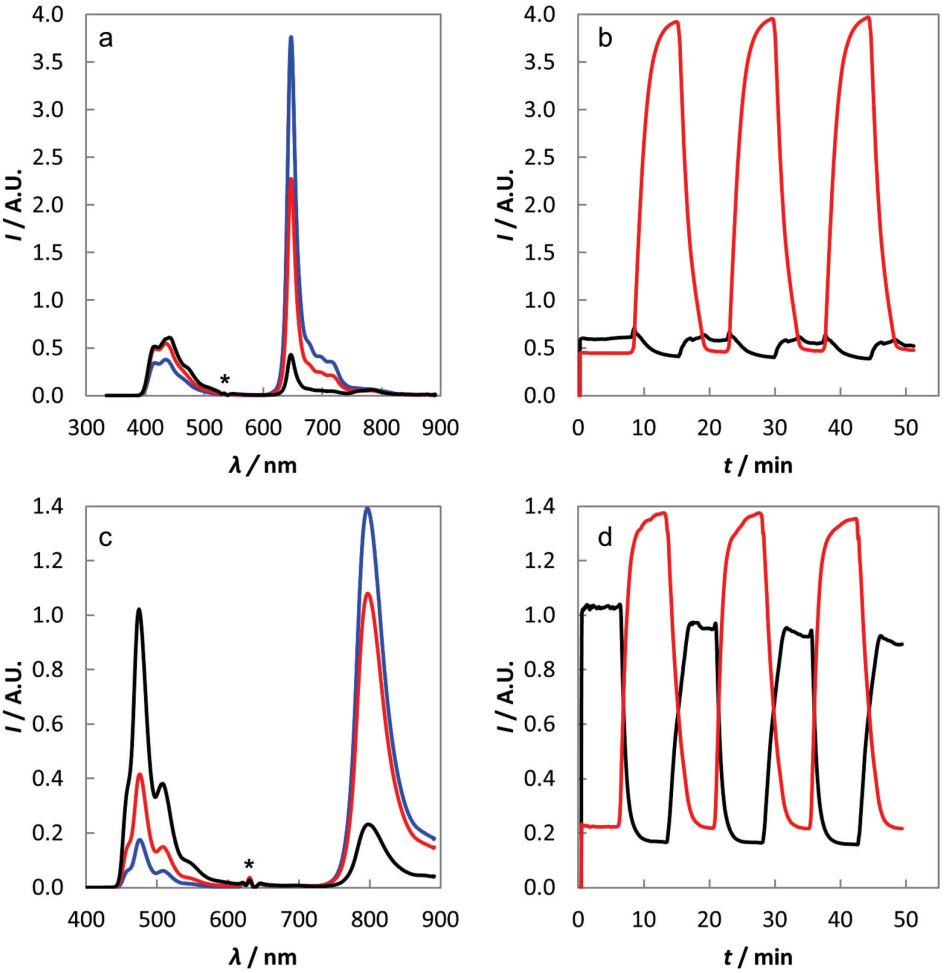

*Figure 3.4. (a) Luminescence spectrum of **L1-2** at 288 K (blue), 293 K (red) and at 298 K (black). (b) Time dependency of the upconversion at 436 nm (black) and of the phosphorescence at 646 nm (red) of **L1-2** during three warming and cooling cycles from 288 to 298 K and from 298 to 288 K. (c) Luminescence spectrum of **L3-4** at 288 K (blue), 293 K (red) and 298 K (black). (d) Time dependency of the upconversion at 473 nm (black) and of the phosphorescence at 800 nm (red) of **L3-4** during three warming and cooling cycles from 288 to 298 K and from 298 to 288 K. Asterisks indicate excitation wavelengths (532 nm for **L1-2** and 630 nm for **L3-4**. Samples were deoxygenated before measurement. Excitation power for both samples: 27 mW, 2.6 mm diameter beam, intensity 0.51 W.cm^{-2}.*

The TTA-UC process is diffusion controlled, and therefore depends on temperature. For this reason, luminescence spectra were measured for **L1-2** and **L3-4** at 288, 293, and 298 K (Figure 3.4a and Figure 3.4c). Upon warming, the sensitizer phosphorescence decreased for both samples, while the upconversion emission increased markedly. In contrast, for toluene samples at

the same bulk concentrations both the upconversion and phosphorescence intensities slightly decreased with increasing temperatures (Figure S.II.3) as a result of faster non-radiative decay. The liposome samples were subjected to three warming-cooling cycles while continuously monitoring their luminescence (Figure 3.4b and Figure 3.4d). The temperature dependence of the upconversion was found to be reversible, which advocates for a reversible, physical cause rather than an irreversible chemical evolution (such as aggregation or photoreactions of the chromophores). As the change of the upconversion *vs.* phosphorescence ratio occurs at a temperature that fits the gel-to-fluid phase transition temperature (T_m) of DMPC membranes (296.9 K), we interpret this change as a consequence of the much increased translational diffusion coefficient (D_T) of membrane-embedded molecules above T_m, compared to that at temperatures below T_m.[8] TTET and TTA are both expected to occur much more frequent in the liquid phase of the membrane, *i.e.*, above T_m, which would lead to an increase in the probability of upconversion (an intermolecular process) at the cost of phosphorescence (a monomolecular process). Similar observations were made for TTA-UC in rubbery polymer matrixes by Sing-Rachford and co-workers.[5e]

In order to prove that *in situ* upconverted blue photons may be used to activate light-activatable prodrugs using red light, ruthenium-functionalized liposomes were mixed with the upconverting liposomes **L3-4** (Figure 3.5b). The ruthenium complex [Ru(tpy)(bpy)(SRR')]$^{2+}$ (**5**$^{2+}$, see Figure 3.5a and experimental section) was selected because it has a single light-sensitive Ru-S bond. This kind of photoactivatable ruthenium compound shows stability in the dark but hydrolyzes to the aqua species [Ru(tpy)(bpy)(H_2O)]$^{2+}$ (**6**$^{2+}$) upon irradiation with blue light into its Metal-to-Ligand Charge Transfer state.[9] A thioether-cholesterol ligand (SRR') can be used to anchor the complex to lipid bilayers, as has been demonstrated in our group.[9a, 9c] PEGylated DMPC liposomes bearing 3.7 mol% of complex **5**$^{2+}$ were prepared (sample **L5**,Table 3.1) and added in 1:1 volumetric ratio to the red-to-blue upconverting liposome sample **L3-4**. Both types of liposomes being grafted with sterically hindering polyethylene glycol (PEG) tails, fusion of the liposomes does not occur, and only radiative energy transfer between the upconverting liposomes and the ruthenium-functionalized liposomes should take place (Figure 3.5b).[10]

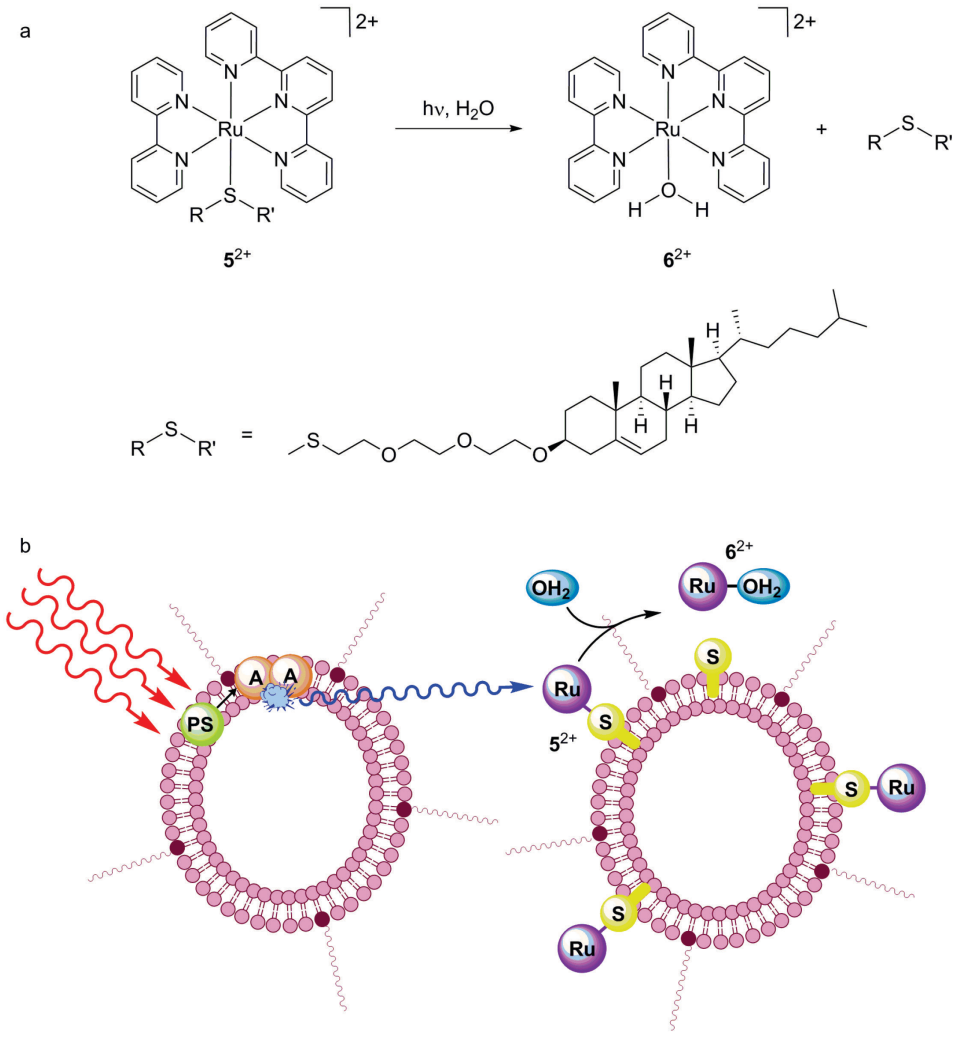

Figure 3.5. (a) Chemical structures of $\mathbf{5}^{2+}$ *and* $\mathbf{6}^{2+}$ *and the conversion of* $\mathbf{5}^{2+}$ *into* $\mathbf{6}^{2+}$*. (b) Cartoon illustrating the TTA-UC process in the lipid bilayer, using a photosensitizer (PS) and an annihilator (A). Radiative energy transfer from the annihilator to complex* $\mathbf{5}^{2+}$*, indicated with a blue arrow, triggers light-induced hydrolysis of* $\mathbf{5}^{2+}$ *to release* $\mathbf{6}^{2+}$ *in solution.*

The liposome mixture was deoxygenated and irradiated at 298 K for 2 hours with a 120 mW 630 nm laser light beam from a clinical grade Diomed PDT laser. The photoreaction was monitored by UV-vis spectroscopy at fixed intervals during irradiation (Figure 3.6). Although the absorbance of **4** dominates the spectrum, the characteristic band of the hydrolyzed photoproduct ($\mathbf{6}^{2+}$) could clearly be seen, rising between 450 and 550 nm as a

function of irradiation time. The isosbestic point at 457 nm showed that a single photochemical process was taking place. Monitoring the absorbance at 490 nm allowed for quantitatively measuring the build-up of $\mathbf{6}^{2+}$ as a function of irradiation time, which reached a plateau after 3 hours irradiation (Figure 3.6b). As a control experiment, a mixture of liposomes **L4** and **L5** was irradiated under the same experimental conditions as above. In liposomes **L4** the absence of sensitizer prevents upconversion from occurring, and the red photons can only excite the ruthenium complex by direct absorption in the tail of the ^{1}MLCT band. The extinction coefficient of $\mathbf{5}^{2+}$ being very low at 630 nm ($\varepsilon \leq 100$ M^{-1}.cm^{-1}), even under a strong photon flux the photoconversion to $\mathbf{6}^{2+}$ was much slower than in presence of **L3-4** (Figure 3.6b), *i.e.*, the upconverting liposomes achieve efficient sensitization of the photosubstitution reaction. A second control experiment showed that no photodissociation occurred in absence of light. Overall, these data are the first evidence that blue photons produced *in situ* by upconversion of PDT-compatible red photons, can be used to enhance the photodissociation rate of polypyridyl ruthenium complexes.

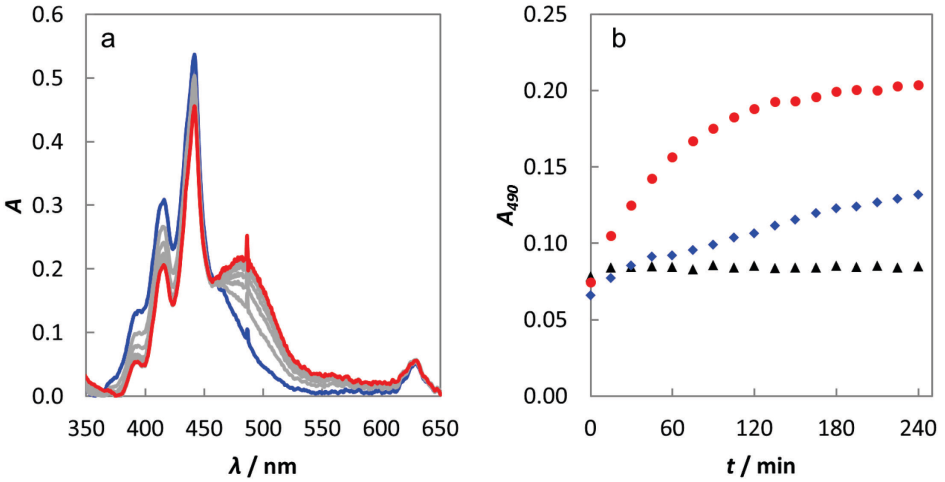

*Figure 3.6. (a) Absorption spectra, after baseline correction, of a 1:1 vol% mixture of liposome samples **L3-4** and **L5** (Table 3.1) during red light irradiation (630 nm). Blue line: spectrum at t = 0; red line: spectrum at t = 240 min; grey lines: spectra measured every 30 min. (b) Plot of the absorbance at 490 nm during red light irradiation (630 nm) of a 1:1 vol% mixture of **L3-4** and **L5** (red dots), of a 1:1 vol% mixture of **L4** and **L5** (blue diamonds), and absorbance at 490 nm of a 1:1 vol% mixture of **L4** and **L5** left in the dark (black triangles). Irradiation conditions: power 120 mW, beam diameter 2.6 mm, intensity 2.3 W.cm^{-2}, T = 298 K, sample volume 1 mL.*

3.3 Conclusion

In conclusion, triplet-triplet annihilation upconversion was for the first time realized in PEGylated liposomes and characterized by absolute quantum yield

measurement. Red-to-blue upconverting liposomes **L3-4**, when mixed with ruthenium-functionalized, PEGylated liposomes **L5** and irradiated with a clinical grade PDT laser at 630 nm, were able to trigger *via* radiative energy transfer the hydrolysis of the Ru-S bond and to release complex $\mathbf{6}^{2+}$. The upconverting liposomes transform two low-energy photons, which penetrate far in biological tissues but are poorly absorbed by the ruthenium complex, into one blue photon that does not need to travel into tissues and can directly promote the complex into its photoreactive excited state. Metal-ligand photodissociation mediated by upconverted light represents exciting perspectives for photoactivatable chemotherapy in oxygen-poor tissues such as hypoxic tumors. Obviously, the oxygen sensitivity of TTA-UC in liposomes needs to be addressed before concluding on the practical application of such systems *in vivo*. However, the high quantum yield of TTA-UC in liposomes and the excellent molar absorptivity of porphyrin sensitizers, for example compared to lanthanoid-based upconverting nanoparticles, may offer fascinating applications in bio-imaging, photoactivatable chemotherapy, and other applications where the *in situ* generation of blue light is required.

3.4 Experimental section

3.4.1 General

Platinum octaethylporphyrin (**1**) and palladium tetraphenyl tetrabenzoporphyrin (**3**) were purchased from Frontier Scientific, Inc. (Logan, Utah, USA). Diphenyl anthracene (**2**) was purchased from Alfa Aesar GmbH & Co KG (Karlsruhe, Germany). Perylene (**4**) was purchased from Sigma-Aldrich Chemie BV (Zwijndrecht, The Netherlands). Sodium N-(carbonyl-methoxypolyethylene glycol-2000)-1,2-distearoyl-sn-glycero-3-phosphoethanolamine (DSPE-MPEG-2000) and 1,2-dimyristoyl-*sn*-glycero-3-phosphocholine (DMPC) were purchased from Lipoid GmbH (Ludwigshafen, Germany) and stored at −18 °C. Dulbecco's phosphate buffered saline (DPBS) was purchased from Sigma Aldrich and had a formulation of 8 $g.L^{-1}$ NaCl, 0.2 $g.L^{-1}$ KCl, 0.2 $g.L^{-1}$ KH_2PO_4, and 1.15 $g.L^{-1}$ K_2HPO_4 with a *pH* of 7.1-7.5. All chemicals were used as received. The syntheses of the thioether-cholesterol conjugate SRR' and [Ru(terpy)(bpy)(Cl)](Cl) are described elsewhere.[9c, 11]

Regular UV-Vis absorption spectra were taken on a Varian Cary 50 UV-Vis spectrometer. Emission spectra with excitation wavelengths 416 and 378 nm were taken on a Shimadzu RF-5301PC spectrofluorimeter at ambient atmosphere. Emission spectra with excitation wavelengths 532 nm and 630 nm were measured in the same setup as for upconversion emission spectrometry, detailed below, and were always collected from deoxygenated samples that had been thoroughly bubbled with argon (Argon 4.6, LindeGas) for at least 30 minutes with a rate of ~2 bubbles per second.

3.4.2 Synthesis of $5(PF_6)_2$

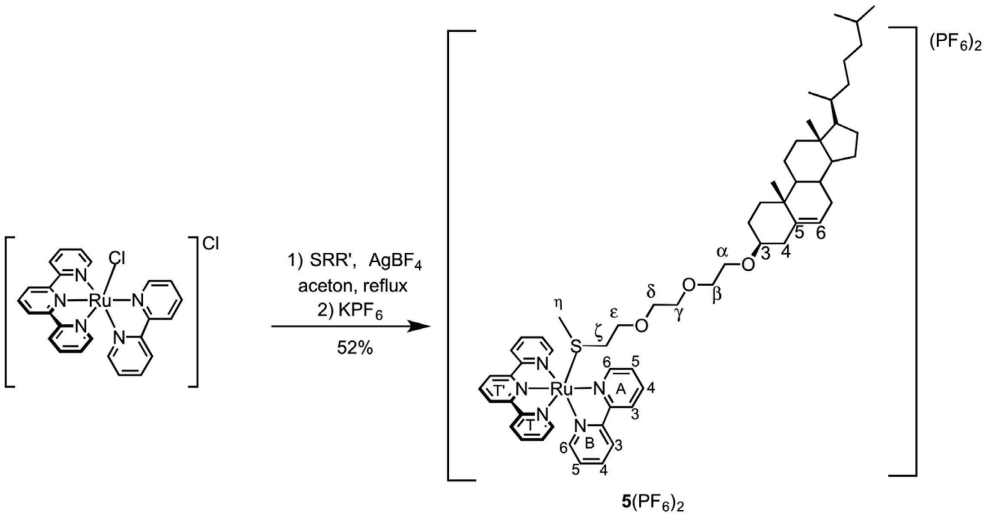

Scheme 3.1. Synthesis of ***5****$(PF_6)_2$*

[Ru(tpy)(bpy)(Cl)](Cl) (100 mg, 0.18 mmol), ligand SRR' (117 mg, 0.21 mmol), and $AgBF_4$ (73 mg, 0.37 mmol) were dissolved in acetone (30 mL). The reaction mixture was refluxed for 20 h in the dark. After cooling to room temperature it was filtered hot over Celite, and the solvent was removed by rotary evaporator under reduced pressure. The product was purified by column chromatography on silica gel (acetone/H_2O/sat. aq. KPF_6 100:10:1.5, R_f = 0.35). Acetone was evaporated under vacuum, upon which the product precipitated as an orange solid. **5**$(PF_6)_2$ was filtered, washed with water and dried under vacuum for 4 h. (124 mg, 52%). ^{1}H NMR (300 MHz, δ in $CDCl_3$) 9.72 (d, J = 5.3 Hz, 1H, A6), 8.55 (m, J = 8.2 Hz, 3H, A3 + T3'), 8.41 (d, J = 7.9 Hz, 2H, T3), 8.34 (d, J = 8.0 Hz, 1H, B3), 8.27 − 8.14 (m, 2H, A4 + T4'), 8.03 − 7.85 (m, 3H, A5 + T4), 7.74 (t, 1H, B4), 7.68 (d, J = 5.0 Hz, 2H, T6), 7.36 (m, 2H, B5 + B6), 7.16 (m, 2H, T5), 5.30 (d, J = 4.8 Hz, 1H, 6), 3.75 (t, J = 6.6 Hz, 2H, ζ), 3.64 − 3.37 (m, 10H, α + β + γ + δ + ε), 3.13 (s, 1H, 3), 2.40 − 0.75 (m, 47H), 0.67 (s, 3H). ^{13}C NMR (75 MHz, δ in $CDCl_3$) 157.67 + 157.01 + 156.31 + 156.29 (B2+ A2 + T2 + T2'), 153.18 (T6), 151.95 (A6), 149.80 (B6) , 140.86 (5),139.09 (T4), 138.56 +138.37 (B4 + A4), 137.56 (T4'), 128.91 (T5), 128.35 (A5), 127.87 (B5), 125.16 (T3), 124.85 (A3), 124.48 (T3'), 124.03 (B3), 121.86 (6), 79.56 (3), 70.88 + 70.35 + 70.30 + 67.52 + 67.30 (α + β + γ + δ + ε), 56.86, 56.28, 50.26, 42.44, 39.88, 39.64, 39.22, 37.28, 36.97, 36.31, 35.91, 34.47, 32.06, 32.01, 29.82, 28.35, 28.13, 24.42, 23.97, 22.95, 22.69, 21.19, 19.53, 18.85, 15.04, 12.00. UV-Vis: λ_{max} (ε in L.mol^{-1}.cm^{-1}) in $CHCl_3$: 457 nm (6090). ES MS m/z exp. (calc.): 519.7 (519.4, $[M-2PF_6]^{2+}$). Elemental analysis for $C_{59}H_{79}F_{12}N_5O_3P_2RuS$: (calc.); C, 53.31; H, 5.99; N, 5.27; S, 2.41. (Found); C, 53.34; H, 6.22; N, 5.15; S 2.41.

3.4.3 Liposome preparation

All liposome formulations were prepared by the classical hydration-extrusion method. As an example, the preparation of **L1-2** is described here. Aliquots of chloroform stock solutions containing the liposome constituents were added together in a flask to obtain a solution with 20 μmol DMPC, 0.8 μmol DSPE-MPEG-2000, 100 nmol **2**, and 3.5 nmol **1**. The organic solvent was removed by rotary evaporation and subsequently under high vacuum for at least 30 minutes to

create a lipid film. 1.0 mL DPBS buffer was added and the lipid film was hydrated by 5 cycles of freezing the flask in liquid nitrogen and thawing in warm water (50 °C). The resulting dispersion was extruded through a Whatman Nuclepore 0.2 μm polycarbonate filter at 40-50 °C at least 11 times using a mini-extruder from Avanti Polar Lipids, Inc. (Alabaster, Alabama, USA). The number of extrusions was always odd to prevent any unextruded material ending up in the final liposome sample. The extrusion filter remained colorless after extrusion, suggesting complete inclusion of the TTA-UC compounds in the lipid bilayer. Liposomes were stored in the dark at 4 °C and used within 7 days. The average liposome size and polydispersity index were measured with a Malvern Instruments Zetasizer Nano-S machine, operating with a wavelength of 632 nm.

3.4.4 Setup for upconversion emission spectroscopy

Upconversion emission spectra were measured with a custom-built setup, see Figure 3.7. All optical parts were connected with FC-UVxxx-2 (xxx = 200, 400, 600) optical fibers from Avantes (Apeldoorn, The Netherlands), with a diameter of 200-600 μm, respectively, and that were suitable for the UV-Vis range (200 – 800 nm). The excitation source was either a continuous wave Aries 150 532 nm portable DPSS laser from LaserGlow (Toronto, ON, Canada), or a clinical grade Diomed 630 nm PDT laser. The 630 nm light was filtered through a FB630-10, 630 nm band pass filter (Thorlabs, Dachau/Munich, Germany) put between the laser and the sample. The excitation power was controlled using a NDL-25C-4 variable neutral density filter (Thorlabs), and measured using either a PM20 optical power meter or a S310C thermal sensor connected to a PM100USB power meter (Thorlabs). Sample deoxygenation was performed in an external ice-cooled pear-shaped flask by bubbling argon for 30 minutes with a rate of 2 bubbles per second, after which the sample was transferred to the cuvette by cannulation under argon. The sample was held under argon in a 104F-QS or 104F-OS semi-micro fluorescence cuvette from Hellma GmbH & Co. KG (Müllheim, Germany) in a CUV-UV/VIS-TC temperature-controlled cuvette holder (Avantes), and was irradiated from the top with a collimated 2.6 mm diameter beam. Emission measurement was performed by means of a 2048L StarLine CCD spectrometer from Avantes under a 90° angle with respect to excitation. The excitation light was rejected using either a NF533-17 533 nm or NF633-25 633 nm notch filter from Thorlabs.

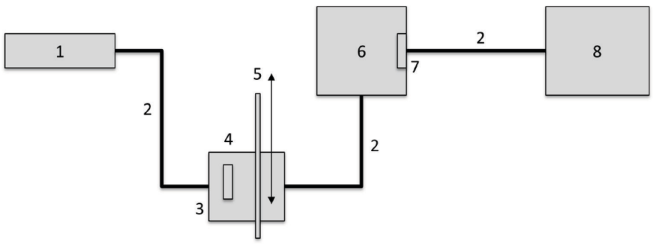

Figure 3.7. Setup used for upconversion emission spectroscopy. Legend: (1) laser source, (2) optical fibers, (3) filter holder, (4) band pass filter that can be installed or removed, (5) variable neutral density filter that can be installed or removed, (6) temperature-controlled cuvette holder, (7) notch filter, (8) CCD spectrometer.

3.4.5 Photosubstitution experiments using red light

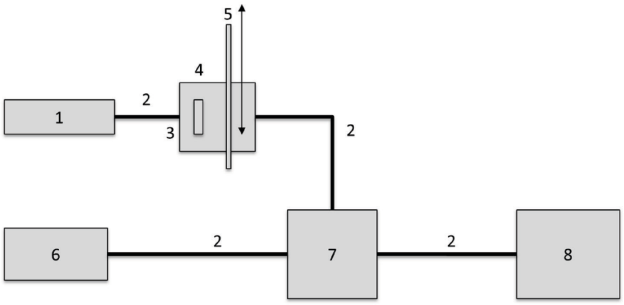

Figure 3.8. Setup used for photosubstitution experiments using red light. Legend: (1) 630 nm laser source, (2) optical fibers, (3) filter holder, (4) 630 nm band pass filter, (5) variable neutral density filter that can be installed or removed, (6) halogen-deuterium light source for absorption measurements, (7) temperature controlled cuvette holder, (8) CCD spectrometer.

Photosubstitution experiments using red light were performed with a custom build setup, see Figure 3.8. 1 mL of the liposome mixture, prepared as described in the main text, was deoxygenated by bubbling argon through the sample with a rate of ~2 bubbles per second for at least 30 minutes in an external ice-cooled pear-shaped flask, after which the sample was transferred by means of cannulation under argon to a 104F-QS or 104F-OS semi-micro fluorescence cuvette from Hellma GmbH & Co. KG (Müllheim, Germany) in a CUV-UV/VIS-TC temperature-controlled cuvette holder from Avantes. The sample was held under argon atmosphere at a constant temperature of 298 K and irradiated for 4 hours from the top with a 120 mW 630 nm laser light beam from a clinical grade Diomed 630 nm PDT laser. The laser was collimated to a beam of 2.6 mm diameter to reach an intensity of 2.3 $W.cm^{-2}$; in such conditions, a cylinder of approximately 0.13 cm^3 was simultaneously excited by the laser. UV-Vis absorption spectra were measured using an Avalight DH-S-BAL halogen-deuterium lamp (Avantes) as light source and an 2048L StarLine spectrometer (Avantes) as detector, both connected to the cuvette holder at a 180° angle. A UV-Vis absorption spectrum was measured every 15 min; each time the laser was switched off, the halogen-deuterium lamp was turned on, a spectrum was recorded, the halogen-deuterium lamp was switched off, and the laser was switched on again. Each UV-Vis measurement took approximately 10 seconds in total. The baseline of each spectrum was corrected for Tyndall and Rayleigh scattering and drift of the halogen-deuterium light source, using Microsoft Excel 2010 and Origin 8.5 software.

3.4.6 Beam profiling

A beam profiler was used for measuring the beam diameters of the laser beams in the aforementioned setups. It consisted of a Trust Webcam Spotlight Pro, of which the front lens was pried off and replaced by NE510A (OD = 1) and NE520A (OD = 2) absorptive neutral density filters (Thorlabs). The laser beam was pointed directly on the photovoltaic chip of the webcam (4.8 mm wide and 3.6 mm high). Then, $1/e^2$ laser beam diameters in pixels were determined by Beams, an open source beam profiling software downloadable from http://ptomato.name/opensource/beams/beams.html. The beam diameter in millimeters was calculated by dividing the average beam diameter in pixels by the total number of horizontal pixels and multiplying this with the chip width in millimeters. For example, the diameter of the beam in Figure 3.9 was determined to be $\frac{339\text{ px}}{640\text{ px}} \times 4.8\text{ mm} = 2.5\text{ mm}$.

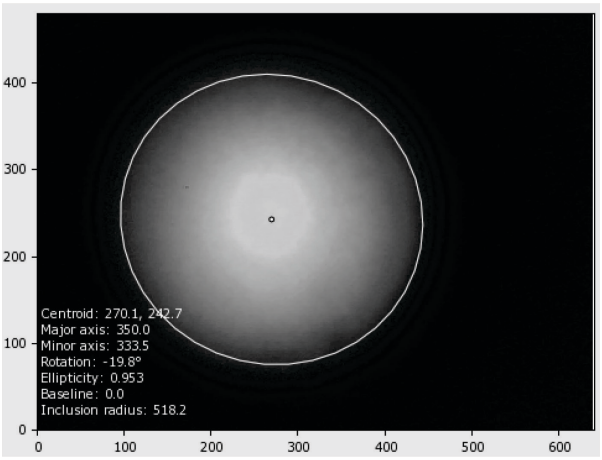

Figure 3.9. Example output generated by the beam profiling setup in combination with the Beams software package. Axes represent chip width and height in pixels.

3.5 References

[1] a) L. Zayat, C. Calero, P. Alborés, L. Baraldo, R. Etchenique, *J. Am. Chem. Soc.* **2003**, *125*, 882-883; b) P. J. Bednarski, F. S. Mackay, P. J. Sadler, *Anticancer Agents Med Chem* **2007**, *7*, 75-93; c) N. J. Farrer, L. Salassa, P. J. Sadler, *Dalton Trans.* **2009**, 10690-10701; d) U. Schatzschneider, *Eur. J. Inorg. Chem.* **2010**, *2010*, 1451-1467; e) S. L. H. Higgins, K. J. Brewer, *Angew. Chem., Int. Ed.* **2012**, *51*, 11420–11422; f) B. S. Howerton, D. K. Heidary, E. C. Glazer, *J. Am. Chem. Soc.* **2012**, *134*, 8324-8327; g) M. A. Sgambellone, A. David, R. N. Garner, K. R. Dunbar, C. Turro, *J. Am. Chem. Soc.* **2013**, *135*, 11274-11282.

[2] a) M. Ferrari, *Nat. Rev. Cancer* **2005**, *5*, 161-171; b) Y. Matsumura, H. Maeda, *Cancer Res.* **1986**, *46*, 6387-6392.

[3] a) T. N. Singh-Rachford, F. N. Castellano, *Coord. Chem. Rev.* **2010**, *254*, 2560-2573; b) J. Zhao, S. Ji, H. Guo, *RSC Adv.* **2011**, *1*, 937-950; c) Y. C. Simon, C. Weder, *J. Mater. Chem.* **2012**, *22*, 20817-20830; d) Y. Y. Cheng, B. Fückel, T. Khoury, R. l. G. C. R. Clady, N. J. Ekins-Daukes, M. J. Crossley, T. W. Schmidt, *J. Phys. Chem. A* **2011**, *115*, 1047-1053.

[4] Y. Murakami, H. Kikuchi, A. Kawai, *J. Phys. Chem. B* **2013**, *117*, 2487-2494.

[5] a) C. Wohnhaas, K. Friedemann, D. Busko, K. Landfester, S. Baluschev, D. Crespy, A. Turshatov, *ACS Macro Lett.* **2013**, *2*, 446-450; b) R. R. Islangulov, J. Lott, C. Weder, F. N. Castellano, *J. Am. Chem. Soc.* **2007**, *129*, 12652-12653; c) P. B. Merkel, J. P. Dinnocenzo, *J. Lumin.* **2009**, *129*, 303-306; d) A. Monguzzi, R. Tubino, F. Meinardi, *J. Phys. Chem. A* **2009**, *113*, 1171-1174; e) T. N. Singh-Rachford, J. Lott, C. Weder, F. N. Castellano, *J. Am. Chem. Soc.* **2009**, *131*, 12007-12014.

[6] a) A. Turshatov, D. Busko, S. Baluschev, T. Miteva, K. Landfester, *New J. Phys.* **2011**, *13*, 083035; b) J.-H. Kang, E. Reichmanis, *Angew. Chem., Int. Ed.* **2012**, *51*, 11841-11844; c) J.-H. Kim, J.-H. Kim, *J. Am. Chem. Soc.* **2012**, *134*, 17478-17481; d) Q. Liu, B. Yin, T. Yang, Y. Yang, Z. Shen, P. Yao, F. Li, *J. Am. Chem. Soc.* **2013**, *135*, 5029-5037; e) K. Tanaka, H. Okada, W. Ohashi, J.-H. Jeon, K. Inafuku, Y. Chujo, *Bioorg. Med. Chem.* **2013**, *21*, 2678-2681; f) C. Wohnhaas, V. Mailänder, M. Dröge, M. A. Filatov, D. Busko, Y. Avlasevich, S. Baluschev, T. Miteva, K. Landfester, A. Turshatov, *Macromol. Biosci.* **2013**, *13*, 1422–1430; g) Y. C. Simon, S. Bai, M. K. Sing, H. Dietsch, M. Achermann, C. Weder, *Macromol. Rapid Commun.* **2012**, *33*, 498-502.

[7] J.-C. Boyer, F. C. J. M. van Veggel, *Nanoscale* **2010**, *2*, 1417-1419.

[8] a) R. N. A. H. Lewis, N. Mak, R. N. McElhaney, *Biochemistry* **1987**, *26*, 6118-6126; b) C.-H. Chang, H. Takeuchi, T. Ito, K. Machida, S.-i. Ohnishi, *J. Biochem.* **1981**, *90*, 997-1004; c) D. Marsh, *Handbook of Lipid Bilayers*, 2nd ed., Taylor & Francis Group, LLC, Boca Raton, FL, USA, **2013**.

[9] a) S. Bonnet, B. Limburg, J. D. Meeldijk, R. J. M. Klein Gebbink, J. A. Killian, *J. Am. Chem. Soc.* **2010**, *133*, 252-261; b) R. E. Goldbach, I. Rodriguez-Garcia, J. H. van Lenthe, M. A. Siegler, S. Bonnet, *Chem. Eur. J.* **2011**, *17*, 9924-9929; c) A. Bahreman, B. Limburg, M. A. Siegler, R. Koning, A. J. Koster, S. Bonnet, *Chem. Eur. J.* **2012**, *18*, 10271-10280.

[10] D. Needham, T. J. McIntosh, D. D. Lasic, *Biochim. Biophys. Acta, Biomembr.* **1992**, *1108*, 40-48.

[11] K. J. Takeuchi, M. S. Thompson, D. W. Pipes, T. J. Meyer, *Inorg. Chem.* **1984**, *23*, 1845-1851.

CHAPTER 4

Triplet-triplet annihilation upconversion followed by FRET for the red light activation of a photodissociative ruthenium complex in liposomes

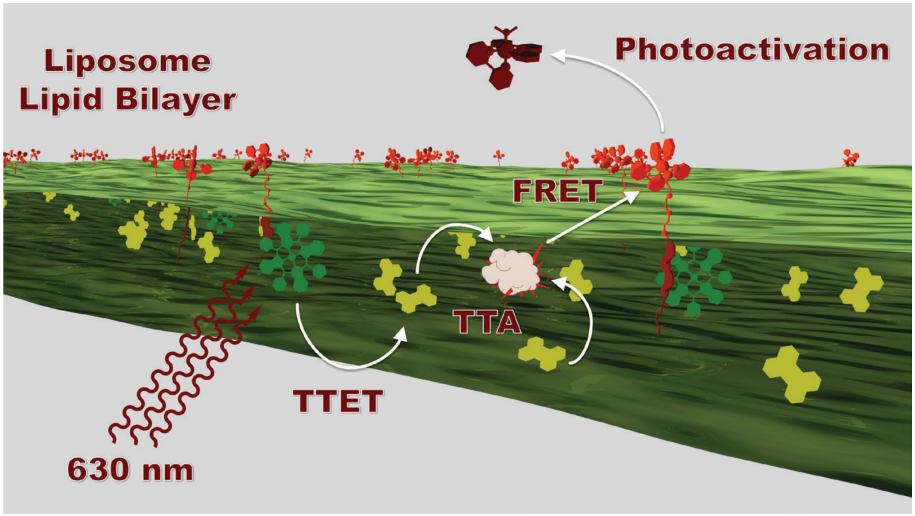

Upconversion is a promising way to trigger high-energy photochemistry with low-energy photons. However, combining upconversion schemes with non-radiative energy transfer is challenging because bringing several photochemically active components in close proximity results in complex multi-component systems where quenching processes may deactivate the whole assembly. In this work, PEGylated liposomes were prepared that contained three photoactive components: a porphyrin dye absorbing red light, a perylene moiety emitting in the blue, and a light-activatable ruthenium prodrug sensitive to blue light. Time-dependent spectroscopic studies demonstrate that singlet perylene excited states are non-radiatively transferred to the nearby ruthenium complex by Förster Resonance Energy Transfer (FRET). Under red-light irradiation of the three-component membranes, triplet-triplet annihilation upconversion (TTA-UC) occurs followed by FRET, which results in a more efficient activation of the ruthenium prodrug compared to a physical mixture of two-component upconverting liposomes and liposomes containing only the ruthenium complex. This work represents a rare example where TTA-UC and FRET are combined to achieve prodrug activation in the phototherapeutic window.

This chapter was published as a full article: S. H. C. Askes, M. Kloz, G. Bruylants, J. T. Kennis, S. Bonnet, *Phys. Chem. Chem. Phys.* **2015**, *17*, 27380-27390

4.1 Introduction

Light-sensitive ruthenium(II) polypyridyl compounds are classical tools in photochemistry that have been recently proposed as prodrugs in photoactivatable anticancer therapy (PACT).[1] As shown in classical photodynamic therapy (PDT), the use of light to treat cancer allows for spatially and temporally controlling the release of a toxic species, which lowers side effects for cancer patients.[2] Whereas PDT drugs rely on the photocatalytic generation of singlet oxygen to kill cancer cells, PACT exerts cytotoxic activity mainly *via* an oxygen-independent mechanism, which makes them suitable for hypoxic tumors.[1c, 1d, 1g, 3] Meanwhile, loading anticancer drugs into drug carriers such as liposomes helps targeting the compounds to tumor tissues.[2a, 4] Especially sterically hindered liposomes, *i.e.*, those grafted with polyethylene glycol chains, have been recognized as versatile and biocompatible drug carriers for the treatment of various diseases because of their long lifetime in the blood circulation. With such PEGylated liposomes tumor uptake is increased because of the so-called enhanced permeability and retention (EPR) effect.[5] In PACT, activation of, for example, ruthenium-functionalized liposomes could be realized using visible light.[6] However, most ruthenium(II) polypyridyl compounds require activation with blue light (400 – 500 nm), which is outside the so-called "phototherapeutic window", a range of wavelengths (600 – 1000 nm) that permeate mammalian tissues optimally. This drawback can be circumvented by using upconverting drug carriers: once in a tumor they locally convert red photons into blue photons that subsequently activate the phototherapeutic drug without having to travel over long distances in the tissue.

Triplet-triplet annihilation upconversion (TTA-UC), a photophysical interplay of light and molecular dyes, is very promising for upconversion because it features strong red light absorption and high upconversion quantum yields at low irradiation power. In TTA-UC, low-energy photons are converted into higher-energy photons by means of a bimolecular mechanism involving a sensitizer and two annihilator molecules (Figure 4.1).[7] The sensitizer absorbs the low-energy light to generate a triplet state, which is transferred to an annihilator molecule by collisions. Further collision of two triplet annihilator molecules leads to triplet–triplet annihilation (TTA), whereby one annihilator molecule is promoted to the high energy-emitting singlet excited state, while the other falls back to the ground state. TTA-UC has been demonstrated in organic solvent,[7a, 7b, 7d] ionic liquid,[8] polymer matrix,[7a, 7c, 9] functionalized

polymer,[10] various water-soluble nanodevices,[1h, 11] and in a solvent-free liquid.[12] In all these systems further use of the upconverted light, for example to activate a prodrug,[1h] excite a quantum dot,[11h] control a soft actuator,[13], or power photoelectrochemistry,[14] relied exclusively on radiative energy transfer, because the molecule sensitive to high-energy light lies too far, at the nanoscale (>10 nm), from the annihilator. For example, Kwon *et al.* showed that TTA-UC in the core of oleic acid nanoparticles, encapsulated by a 12 nm thick silica layer, could trigger a photocatalytic reaction on CdS nanoparticles grafted on the silica shell, but that the shell was too thick to allow non-radiative energy transfer.[11h] Non-radiative energy transfer would be by far preferable as it is more efficient; however, it also requires a close contact, at the nanoscale, between the annihilator molecule and the functional molecule to be photoactivated.

In this work PEGylated liposomes were used as a supramolecular scaffold to put palladium tetraphenyltetrabenzoporphyrin (**1**) and perylene (**2**) in close proximity to the cytotoxic ruthenium complex $[Ru(tpy)(bpy)(SRR'))]^{2+}$ ($\mathbf{3}^{2+}$, see Figure 4.1a). When put together the red photosensitizer **1** and the blue emitter **2** are capable of red-to-blue TTA upconversion. On the other hand, $\mathbf{3}^{2+}$ dissociates, upon blue light irradiation, into the aqua species $[Ru(tpy)(bpy)(H_2O)]^{2+}$ ($\mathbf{4}^{2+}$) and the free thioether ligand (Figure 4.1a).[1h, 6, 15] The cytotoxicity of $\mathbf{3}^{2+}$ and its modification by blue light irradiation is a complex matter that will be reported in a separate paper.[16] Here we realized that the Metal-to-Ligand Charge Transfer (MLCT) absorption band of $\mathbf{3}^{2+}$ ideally overlaps with the emission spectrum of **2** (Figure 4.2), a feature which maximizes the distance at which non-radiative energy transfer from **2** to $\mathbf{3}^{2+}$ may take place. In liposomes containing all three components **1**, **2**, and $\mathbf{3}^{2+}$, the average distance between photochemically active components becomes shorter than 5 − 8 nm, for which non-radiative energy transfer may take place (see Figure 4.1b).[17] However, such proximity might also open unwanted quenching routes, such as energy back-transfer from the complex to either photosensitizer or annihilator, hetero triplet-triplet annihilation between any pair of triplets present in the membrane, or phase separation of one of the molecules. In this chapter it is explored *via* steady-state and time-dependent spectroscopic studies how efficient non-radiative energy transfer from perylene to the ruthenium complex is, and whether the red-light triggered photosubstitution reaction in the three-component liposomes is more or less efficient than the (known) physical mixture of upconverting liposomes

(containing only **1** and **2**) and ruthenium-functionalized liposomes (containing only $\mathbf{3}^{2+}$).[9h]

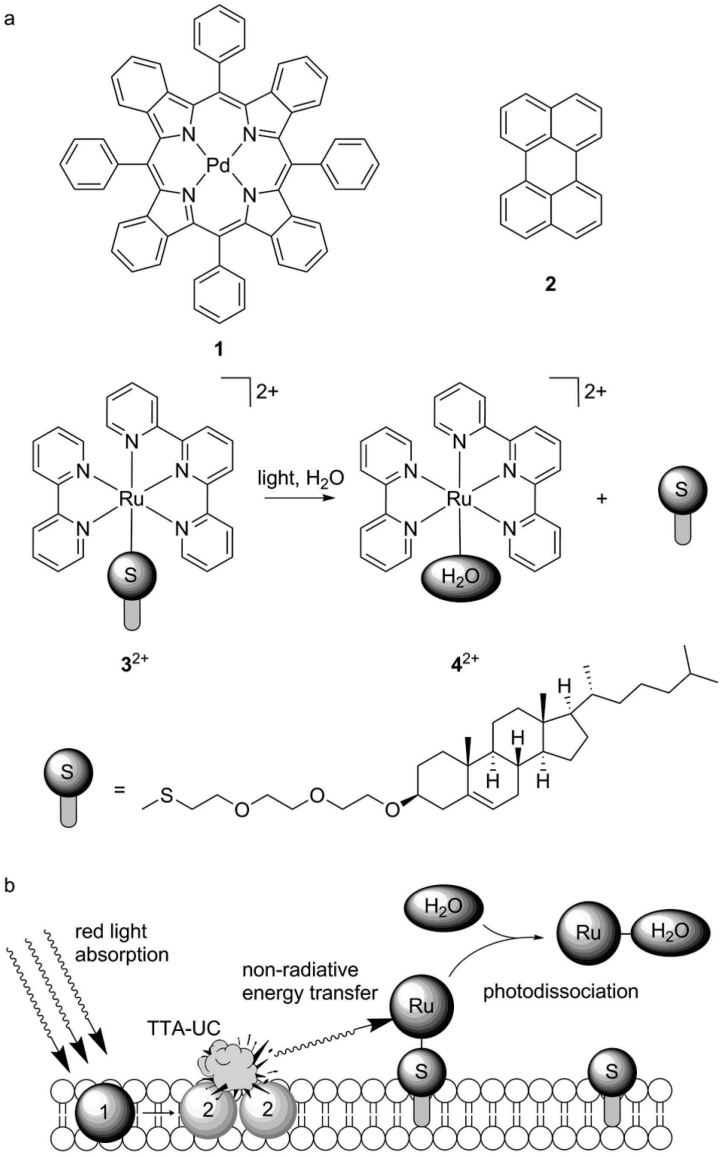

*Figure 4.1. a) Chemical structures of palladium tetraphenyltetrabenzoporphyrin (**1**), perylene (**2**), $[Ru(tpy)(bpy)(SRR')]^{2+}$ ($\mathbf{3}^{2+}$), and $[Ru(tpy)(bpy)(H_2O)]^{2+}$ ($\mathbf{4}^{2+}$), and the photochemical reaction from $\mathbf{3}^{2+}$ to $\mathbf{4}^{2+}$. b) Cartoon showing the sequence of photochemical events demonstrated in this work: red light is absorbed by compound **1**, after which triplet-triplet annihilation upconversion (TTA-UC) occurs, followed by non-radiative energy transfer from **2** to $\mathbf{3}^{2+}$, and finally the ruthenium prodrug photodissociates from the lipid bilayer.*

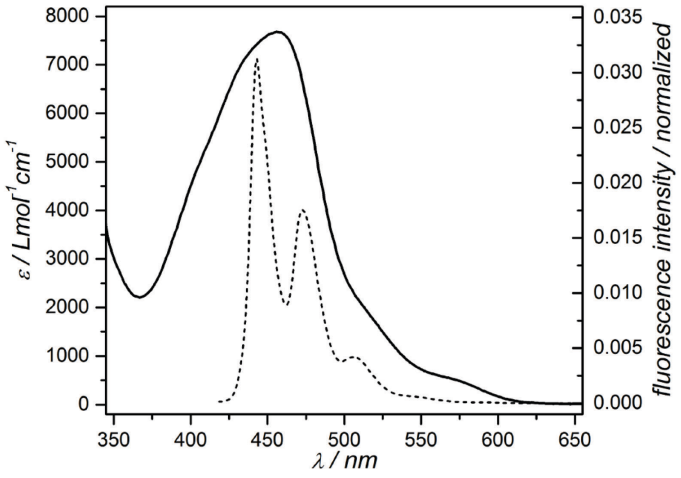

*Figure 4.2. Absorption spectrum of **3**$^{2+}$ in chloroform (solid, left axis, ε_{max} = 7700 at λ_{max} = 456 nm) and area-normalized emission spectrum of compound **2** in PEGylated DMPC liposomes (dashed, right axis, λ_{exc} = 400 nm, 0.5 mol% of compound **2** with respect to the lipids).*

4.2 Results and Discussion

4.2.1 Liposome preparation and characterization.

PEGylated liposomes were prepared as shown in Table 4.1 from a mixture of 1,2-dimyristoyl-sn-glycero-3-phosphocholine (DMPC), 4 mol% sodium N-(carbonyl-methoxypolyethylene glycol-2000)-1,2-distearoyl-sn-glycero-3-phosphoethanolamine (DSPE-MPEG-2000), and compound **1**, **2**, and/or **3**$(PF_6)_2$, using a standard hydration-extrusion protocol in Dulbecco's phosphate buffered saline (DPBS). PEGylation prevented liposomes fusion and/or aggregation that would interfere with the experiments. The true concentration of **3**$^{2+}$ in all liposome samples was determined experimentally by inductively coupled plasma optical emission spectroscopy (ICP-OES) to be on average 89% of the expected value (Figure S.III.1). The average vesicle diameter and polydispersity index were determined by dynamic light scattering (DLS); typical values were 130 – 170 nm and 0.05 – 0.20, respectively.

Table 4.1. Lipid formulations of the PEGylated DMPC liposomes used in this work.

Sample	[DMPC] (mM)	[DSPE-PEG-2000] (μM)	[1] (μM)	[2] (μM)	[3^{2+}] (μM)
L123	5.0	200	2.5	25	50 – 220[a]
L12	5.0	200	2.5	25	-
L23	5.0	200	-	25	10 – 290[a]
L2	5.0	200	-	25	-
L3	5.0	200	-	-	200
L0	5.0	200	-	-	-

*[a] The amount of **3^{2+}** used for **L123** and **L23** varied; hence a concentration range is given here. The true ruthenium concentrations were determined with ICP-OES.*

Because on the one hand, molecular diffusion plays an important role in TTA-UC, and on the other hand, phase separation of one of the dyes could impair the efficiency of the system, the gel-to-liquid phase transition temperature of a series of PEGylated DMPC liposomes was determined by Differential Scanning Calorimetry (Figure S.III.2). The transition temperature for PEGylated DMPC liposomes without any chromophores (**L0**) is 25.2 °C, with a pretransition peak at 14 °C. Functionalizing these liposomes with 0.05 mol% **1** and 0.5 mol% **2** (**L12)** caused a small decrease in the main transition peak height, but the main features of the thermogram remained, which indicates that the membrane was only slightly perturbed by the presence of the TTA-UC dyes and that the dyes are buried into the lipid bilayer. Next, a series of liposomes **L123** was measured, which in addition to 0.05 mol% **1** and 0.5 mol% **2** also contained 1 to 4 mol% of the ruthenium complex. A progressive yet small decrease in the main transition temperature was observed compared to **L12**: from 25.1 °C for 0 mol% to 23.2 °C for 4 mol% **3^{2+}**. Additionally, the main transition peak broadened and its intensity decreased upon increasing Ru concentration, while the pretransition peak disappeared already after inclusion of 1 mol% of the **3^{2+}** complex. These observations are compatible with the expected interaction of complex **3^{2+}** with the zwitterionic polar heads of the lipids. For this range of ruthenium concentrations however, no evidence was found that suggested phase separation of either **1**, **2**, or **3^{2+}**. Overall, these DSC results show that at 20 °C and at 37 °C, all liposome formulations are in the gel phase and liquid crystalline phase, respectively.

4.2.2 Photodissociation experiments using red light.

Red-light irradiation experiments were first conducted to evaluate whether **L123** liposomes, which contained both dyes for TTA-UC plus the ruthenium complex **3^{2+}**, would achieve higher photodissociation rates than a mixture of **L12** and **L3**, in which the upconversion and the photosubstitution on the

ruthenium complex are physically separated on two different liposomes.[1h] For all red light irradiation experiments the liposome samples were diluted with isotonic buffer so that the optical density due to the MLCT band of the Ru complex stayed low ($A_{450\text{-}500} \leq 0.25$ with a 10 mm path length). Under such conditions, radiative energy transfer between the blue emitting perylene and the blue absorbing ruthenium complex is minimized, while the solution absorbance remains high enough for monitoring the experiments using UV-Vis absorption spectroscopy. The bulk concentrations of **1**, of **2**, and/or $\mathbf{3}^{2+}$ were kept equal in all experiments. Red light irradiation was realized for three hours at physiological temperature (310 K) and under anoxic conditions using a 630 nm clinical grade PDT laser set at low power (30, 60, or 120 mW, for an intensity of 0.24, 0.48, or 0.95 $W.cm^{-2}$). UV-Vis absorption and luminescence emission spectra were measured during irradiation every 15 minutes.

The UV-Vis absorption spectrum of a **L123** sample containing 3.5 mol% of $\mathbf{3}^{2+}$ evolved during red light irradiation at 120 mW power as shown in Figure 4.3a. A band between 450 and 600 nm, typical of the aqua complex $\mathbf{4}^{2+}$, rises, while two isosbestic points are observed at 370 and 456 nm. The only photochemical reaction occurring in such conditions is thus the hydrolysis reaction of $\mathbf{3}^{2+}$ to $\mathbf{4}^{2+}$. The evolution of the absorbance at 490 nm (Figure 4.3c) clearly showed that the reaction was finished after two hours of irradiation. For comparison, a 1:1 volume mixture of **L12** and **L3** was irradiated under the same conditions, where only radiative energy transfer may occur. Slower photodissociation kinetics was observed (Figure 4.3c). Apparently, the optical density of the sample was high enough so that $\mathbf{3}^{2+}$ in **L3** could reabsorb a significant amount of the blue photons upconverted by **L12**. When liposomes **L23** were irradiated that contained only **2** and $\mathbf{3}^{2+}$, no TTA-UC could occur and very slow photodissociation was observed due to the low but non-zero molar absorption coefficient of $\mathbf{3}^{2+}$ at 630 nm ($\varepsilon_{630} < 100$ $M^{-1}.cm^{-1}$). Overall, our results clearly show that **L123** achieved a higher photodissociation rate than a mere physical mixture of **L12** and **L3**, and of course of **L23**.

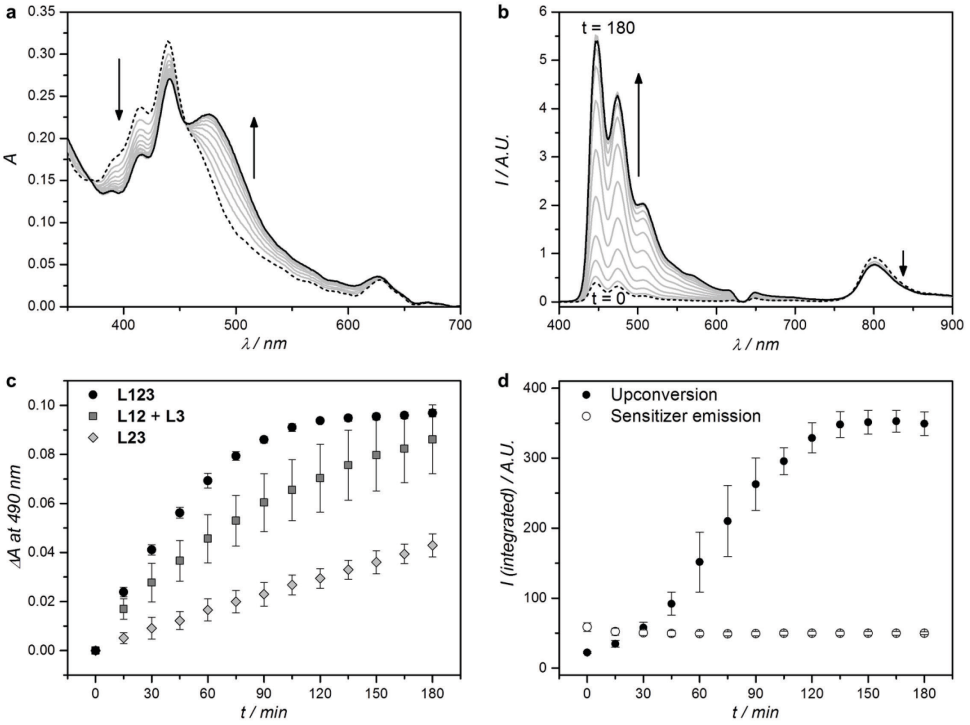

*Figure 4.3. Absorption (a) and luminescence emission (b) spectra of **L123** during red-light irradiation (630 nm) of liposomes functionalized with **3**$^{2+}$. Dashed line: spectrum at t = 0; black solid line: spectrum at t = 180 minutes; grey lines: spectra measured every 15 minutes. c) Difference in absorbance at 490 nm, after baseline correction, during red-light irradiation (630 nm) of **L123** (black filled circles), a 1:1 volume mixture of **L12** and **L3** (dark-grey filled squares), and **L23** (light-grey filled diamonds). Error bars represent standard deviation of three independent experiments. d) Integrated upconversion emission (400 - 600 nm, black filled circles) and integrated sensitizer emission (750 - 900 nm, open circles) during red-light irradiation of **L123**. Error bars represent standard deviation of three independent experiments. Irradiation conditions: power 120 mW, beam diameter 4 mm, intensity 0.95 W.cm^{-2}, T = 310 K, sample volume 1.5 ml, 8% of sample volume simultaneously irradiated. Liposome dispersions used in these experiments were prepared as in Table 4.1, and then diluted with PBS buffer prior to measurement so that every time [**1**] = 0.25 μM, and [**2**] = 2.5 μM. The bulk concentration of **3**$^{2+}$ was experimentally determined with ICP-OES and was 19 ± 1 μM, 21 ± 3 μM, and 20 ± 2 μM for **L123**, **L23**, and **L3**, respectively.*

When the red light-induced photodissociation reaction of **L123** was followed by luminescence emission spectroscopy (Figure 4.3b), a peak at 800 nm, corresponding to the phosphorescence of **1**, and a broad structured emission band ranging from 400 to 600 nm, corresponding to the upconverted emission of **2**, could clearly be identified.[1h] Interestingly, the upconverted emission intensity evolved a lot during irradiation. It was initially very weak compared to the upconversion emission of **L12** alone (Figure S.III.3), but increased

roughly 15-fold during the course of the reaction. No further evolution was observed after two hours of irradiation, which closely matches the reaction time observed by UV-Vis absorption spectroscopy. The low initial upconversion emission intensity, combined with the observation by UV-Vis spectroscopy that the photosubstitution clearly occurred, suggested that the upconverted energy may be transferred non-radiatively from **2** to $\mathbf{3}^{2+}$. As the reaction proceeded, and $\mathbf{3}^{2+}$ was progressively liberated from the membrane to diffuse in solution, non-radiative energy transfer from perylene to the ruthenium complex becomes less efficient, thus explaining the recovery of the blue emission when all ruthenium complex were detached from the membrane. To prove this hypothesis, we studied the non-radiative energy transfer between **2** and $\mathbf{3}^{2+}$ by direct excitation of perylene with violet or blue light, and studied the evolution of the system with time-dependent absorption and emission spectroscopy.

4.2.3 Is there non-radiative energy transfer from 2 to 3^{2+}?

Assuming that the same singlet excited state of **2** is reached by blue light excitation of **2** in absence of **1** and by red-light excitation of **1** in presence of **2**, a series of **L23** liposomes was prepared with a fixed amount of **2** (0.5 mol%), a varying amount (0.4 – 3.5 mol%) of $\mathbf{3}^{2+}$, but no red photosensitizer (**1**). The aim of this study was to determine with time-dependent spectroscopy whether the singlet excited state of **2** could transfer its energy non-radiatively to the ruthenium complex. Control liposomes were also prepared that contained only perylene (**L2**) or only 3.3 mol% of $\mathbf{3}^{2+}$ (**L3**). All liposomes were first studied by ultrafast transient absorption (TA) spectroscopy with 400 nm excitation (40 fs pulse duration, 20 – 60 nJ/pulse) while recording the transient absorption spectrum from 430 to 730 nm in the ps to ns range. The TA data were globally fitted using the software package Glotaran.[18] Full data set and analysis is detailed in Figure 4.4, Table 4.2, and in Appendix III. In short, the TA spectrum of **L2** 1.0 ns after a 400 nm excitation pulse (Figure S.III.4) closely matched literature reports for perylene in cyclohexane. It features negative signals from 430 to 550 nm due to ground state bleach and stimulated emission, and a strong positive band centered at 700 nm due to excited state absorption.[19] Global analysis using Glotaran gave an excited state lifetime of 6.00 ± 0.10 ns for **2** in **L2**, which also corresponds to literature values.[19-20] For **L3** the transient absorption spectrum 1.0 ps after the excitation pulse at 400 nm showed a negative band ranging from 400 to 500 nm and a weaker featureless positive band from 500 nm to 800 nm. The

former coincides with the MLCT absorption band in the steady state absorption spectrum (Figure 4.2) and can be attributed to ground state bleaching of the ruthenium complex. The latter is attributed to excited state absorption. The time evolution of the transient spectrum was best fitted with Glotaran to give an excited state lifetime of 0.52 ns for $\mathbf{3}^{2+}$. UV-VIS spectroscopy before and after the TA experiment showed that in such conditions negligible photodissociation occurred (see Appendix III).

The TA data of liposomes **L23** were qualitatively very similar to that of **L2**, and global fitting did not allow for detecting any feature reminiscent of $\mathbf{3}^{2+}$ as in **L3**. However, the average excited state lifetime (τ) of **2** decreased strongly as a function of the mol fraction of $\mathbf{3}^{2+}$ (Figure 4.4c and Table 4.2): from τ = 6.0 ns without any ruthenium complex in the membrane (**L2**) addition of up to 3.3 mol% ruthenium complex (**L23**) lowered the lifetime of **2** down to 0.3 ns, which shows non-radiative quenching of the excited state of **2** by $\mathbf{3}^{2+}$. These results were confirmed by steady state fluorescence spectroscopy and time-correlated single photon counting (TCSPC). Because $\mathbf{3}^{2+}$ is not emissive at all, **2** is observed selectively using fluorescence techniques. The steady-state fluorescence spectra of the series of liposomes **L23** clearly showed a decrease in fluorescence intensity of **2** with increasing concentration of $\mathbf{3}^{2+}$ in the membrane (Figure 4.4a). TCSPC was performed with 440 nm excitation (0.6 pJ/pulse), while monitoring the emission at 474 nm on the nanosecond scale. The TCSPC results were very similar to TA data: the singlet excited state lifetime of **2** was found to be τ = 6.2 ns in absence of $\mathbf{3}^{2+}$, and decreased to τ = 0.9 ns in presence of 3.5 mol% of $\mathbf{3}^{2+}$ (see Figure 4.4b and Table 4.2). Clearly, the singlet state of **2** is quenched by the nearby ruthenium complex. Although no rising of a Ru-based excited state could be detected by TA spectroscopy in **L23**, probably due to its low and rather broad features as observed in **L3**, the increased rate of the photosubstitution reaction in liposomes **L123** irradiated with red light, the recovery of the upconverted emission when the ruthenium aqua complex leaves the membrane, and the quenching of **2** by $\mathbf{3}^{2+}$ observed in **L23**, conclude to non-radiative energy transfer occurring from **2** to $\mathbf{3}^{2+}$ both in **L23** and in **L123**.

*Table 4.2. Best-fit average lifetimes (τ in ns) and energy transfer efficiencies (E_{ET}, calculated from Equation 4.1) at 293 K and 310 K for the excited state quenching of **2** by **3**$^{2+}$ at different **3**$^{2+}$ mol fractions in PEGylated (4 mol%) DMPC vesicles, as measured with transient absorption (TA) spectroscopy and time-correlated single photon counting (TCSPC). All liposomes had a fixed amount of compound **2** (0.5 mol%). Transient absorption spectroscopy data was globally fitted using the software package Glotaran.[18] Full datasets are given in Appendix III, as well as detailed information on data analysis.*

	molar percentage of 3^{2+} in PEGylated DMPC liposomes					
	0.0	**0.4**	**0.8**	**1.7**	**2.5**	**3.3**
TA spectroscopy at 293 K						
τ	6.00 ± 0.10	3.03 ± 0.02	1.52 ± 0.01	1.04 ± 0.01	0.40 ± 0.00	0.29 ± 0.00
E_{ET}	0%	50%	75%	83%	93%	95%
	molar percentage of 3^{2+} in PEGylated DMPC liposomes					
	0.0	**0.5**	**0.9**	**1.7**	**2.4**	**3.5**
TCSPC at 293 K						
τ	6.17 ± 0.01	4.67 ± 0.01	2.50 ± 0.05	1.29 ± 0.02	1.25 ± 0.05	0.85 ± 0.06
E_{ET}	0%	24%	60%	79%	80%	86%
TCSPC at 310 K						
τ	5.69 ± 0.01	4.00 ± 0.01	2.37 ± 0.07	1.14 ± 0.00	0.84 ± 0.00	0.45 ± 0.00
E_{ET}	0%	30%	58%	80%	85%	92%

From TA, steady-state fluorescence, and TCSPC data, the non-radiative energy transfer efficiency (E_{ET}) was calculated for each composition of the liposomes **L23** following Equation 4.1 (see also Figure 4.4d, Table 4.2, and Appendix III):

$$E_{ET} = 1 - \frac{\tau}{\tau_0} = 1 - \frac{I}{I_0} \qquad \textit{Equation 4.1}$$

where τ and τ_0 are the averaged lifetimes of **2** in presence and absence, respectively, of **3**$^{2+}$ in the membrane, and I and I_0 are the corresponding fluorescence intensities. A plot of E_{ET} as a function of the experimental mol fraction of **3**$^{2+}$ in the membrane (Figure 4.4d) shows that the energy transfer efficiency rises up to 80% or more for concentration of the ruthenium complex above 2.5 mol%. Additionally, these data could be fitted with a modified Stern-Volmer curve (see Appendix III), and the rate of quenching of the singlet state of **2** by **3**$^{2+}$ was determined to be 5.2 x 10^7 $M^{-1}.s^{-1}$. When performing TCSPC experiments at biological temperature (T = 310 K), at which the photodissociation experiments were conducted, the results were very similar (see Table 4.2): τ was found to be 5.7 ns when no ruthenium

complex was present, went down to 0.45 ns at 3.5 mol% of $\mathbf{3}^{2+}$ in the membrane, and E_{ET} increased to slightly higher values at all complex concentrations when compared to TCSPC data at 293 K. Overall, it is concluded that at human body temperature energy transfer from the singlet excited state of **2** to the ruthenium complex $\mathbf{3}^{2+}$ is very efficient above 2 - 2.5 mol% of $\mathbf{3}^{2+}$ in the membrane, and is responsible for the efficient activation of $\mathbf{3}^{2+}$ under red light irradiation of **L123** liposomes.

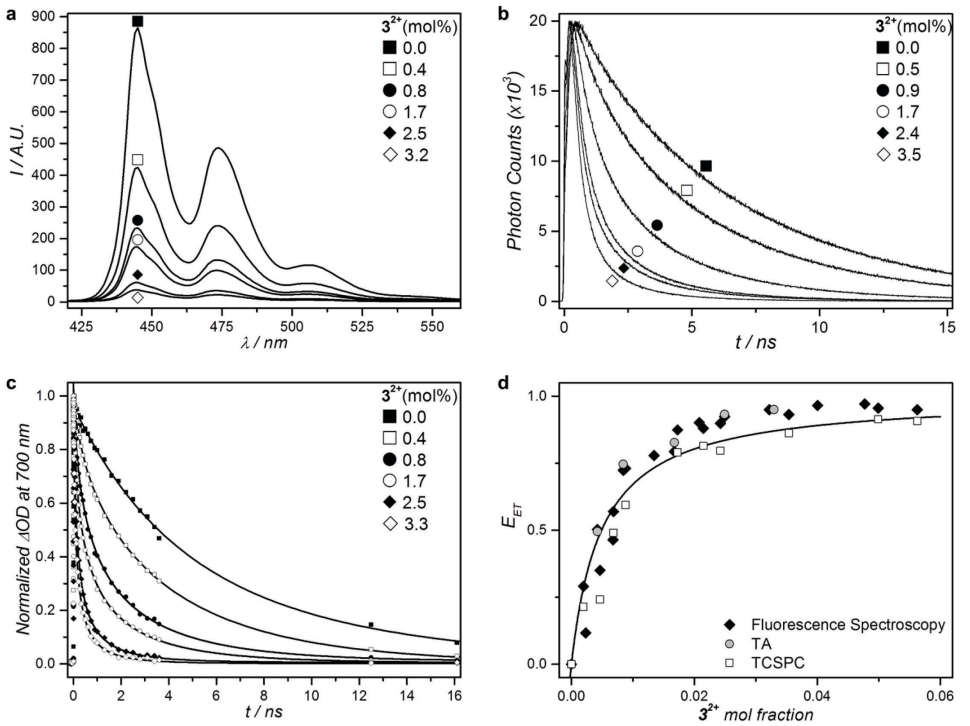

*Figure 4.4. Steady-state fluorescence spectra (a) and excited state time decays of **2** (b and c) for a series of PEGylated (4 mol%) DMPC liposomes containing a fixed amount of compound **2** (0.5 mol%) and 0 to 4 mol% of compound $\mathbf{3}^{2+}$ at 293 K. a) Steady-state fluorescence spectra (λ_{exc} = 400 nm, [**2**] = 1 μM). b) Fluorescence decay curves from time-correlated single photon counting (λ_{exc} = 440 nm, λ_{em} = 474 nm, [**2**] = 1 μM). c) Normalized transient absorption kinetic traces at 700 nm. Best-fit curves drawn as solid lines for samples with addition of $\mathbf{3}^{2+}$ according to a three-dimensional Förster decay model (see Appendix III). For the sample without addition of $\mathbf{3}^{2+}$, the fit curve represents a bi-exponential decay model. d) Energy transfer efficiency (E_{ET}) as a function of the mol fraction of $\mathbf{3}^{2+}$ at 293 K, calculated from time-correlated single photon counting data (empty squares), transient absorption data (grey filled circles), and steady state fluorescence spectroscopy (black filled diamonds). Best-fit curve according to a Stern-Volmer model (see Appendix III).*

4.2.4 Does the aqua photoproduct quench the perylene excited state as well?

Theoretically, when the ruthenium complex hydrolyses to the aqua species it is no longer attached to the cholesterol anchor and as the membrane is made of neutral lipids $\mathbf{4}^{2+}$ will diffuse away from the membrane.[6] After photodissociation **2** should thus regain its unquenched lifetime of ca. 6 ns. To probe this hypothesis, liposomes **L23** with 4 mol% of $\mathbf{3}^{2+}$ (2.5 mM DMPC bulk concentration) were irradiated with blue light (420 nm) until full conversion of $\mathbf{3}^{2+}$ to $\mathbf{4}^{2+}$ was detected by UV-vis spectroscopy. No change in size or polydispersity of the liposomes was observed as judged by dynamic light scattering, indicating that the liposomes were unaffected by the light treatment. The lifetime of **2** was then measured with TA spectroscopy again, and indeed increased from 0.3 ns prior to irradiation to 3.9 ns after irradiation, owing to the decreased concentration of the energy acceptor $\mathbf{3}^{2+}$ in the membrane. However, the lifetime did not rise to the unquenched value of 6.0 − 6.2 ns found in **L2**. To explain this observation, new **L23** samples were prepared using the same relative composition of the membrane, but with an 8 times higher lipid bulk concentration. In such concentrated liposomes the lifetime after the photoreaction rose to only 1.7 ns, which clearly demonstrated that the excited state lifetime of compound **2** depends on the bulk concentration of the aqua complex $\mathbf{4}^{2+}$. Our interpretation of this observation is that at higher concentrations the chance of finding $\mathbf{4}^{2+}$ in proximity of the membrane, and thus of **2,** increases and that non-radiative energy transfer can occur to $\mathbf{4}^{2+}$ as well. Overall, the rise in the lifetime of **2** upon blue light irradiation of the **L23** samples confirms the results from the red light photodissociation experiments on **L123**: when the energy acceptor leaves the membrane, **2** no longer performs as much non-radiative energy transfer as when the complex is bound to the membrane, but instead loses its energy radiatively, which explains the increased blue emission at the end of the photoreaction (Figure 4.3b).

4.2.5 What is the mechanism of energy transfer?

In photochemistry, non-radiative energy transfer such as that between **2** and $\mathbf{3}^{2+}$ is either described by a Dexter or to a Förster mechanism. The Förster mechanism relies on long-range dipole-dipole interactions and can be efficient up to a distance of 10 nm for spectrally well-matching donor-acceptor pairs. In the Dexter mechanism, direct orbital overlap is required between donor and acceptor, and energy transfer efficiency decays quickly beyond distances of 1

nm between the donor and the acceptor. For Dexter-type energy transfer, high mobility of both the donor and acceptor is imperative to realize energy transfer within the nanosecond timeframe in which **2** is in its singlet excited state. However, the DMPC bilayer at room temperature does not support such mobility: diffusion coefficients for fluorescent probes in DMPC membranes are typically 0.01 $\mu m^2.s^{-1}$ at 292 K,[21] which leads to a negligible displacement of 5 x 10^{-3} $Å^2$ in the 6 ns excited state lifetime of **2**. In other words, in the timeframe in which **2** is in the singlet excited state the lipid bilayer is practically frozen. Also, there is no significant difference in quenching efficiency (*vide supra*) below (293 K) and above (310 K) the phase transition temperature at which the lipid bilayer transforms from a gel-like to liquid crystalline structure, which advocates for a diffusion-independent quenching mechanism. Finally, **2** is located in the hydrophobic interior of the lipid bilayer, while the positively charged center of $\mathbf{3}^{2+}$, responsible for accepting the energy, is dangling at the bilayer-water interface.[22] Therefore, it is very unlikely that **2** and $\mathbf{3}^{2+}$ can come in close contact to realize orbital overlap. For these reasons, we conclude that the most likely mechanism of energy transfer is Förster Resonance Energy Transfer (FRET). Based on this assumption, and following the work of Holmes *et al.*,[23] the decay curves from TA and TCSPC data were satisfactorily fitted with a three-dimensional Förster decay function (see Appendix III). From the fitting parameters, the experimental Förster distance R_0, for which FRET occurs with 50% efficiency, was calculated to be 29 Å. This value fits rather well the theoretical value (41 Å) that can be calculated from the spectra overlap shown in Figure 4.2 (see Appendix III). Both values also match the thickness of a DMPC lipid bilayer (36 Å),[21] which explains why FRET between **2** and $\mathbf{3}^{2+}$ is so efficient in this system.

4.2.6 Overall efficiency of the sequential combination of TTA-UC and FRET

Based on the evidence presented above, we propose that the enhanced photosubstitution rate when the three photoactive components **1**, **2**, and $\mathbf{3}^{2+}$ are present in the same membrane (**L123**) and irradiated with red light, results from the combination of TTA-UC between **1** and **2**, and FRET from **2** to $\mathbf{3}^{2+}$. To the best of our knowledge, this is one of the rare systems in which TTA-UC and FRET are combined to activate a photosensitive molecule.[24] Figure 4.5 shows a qualitative Jablonski diagram of this system: instead of realizing upconverted blue emission, the energy that is stored in the singlet excited perylene molecule is primarily transferred to the ruthenium complex

by FRET, to generate the singlet MLCT excited state. This excited state in turn leads to the selective substitution of the thioether ligand by a water molecule *via* the classical mechanism involving intersystem crossing to the ^{3}MLCT state followed by thermal promotion of a triplet Metal-Centered state (^{3}MC). In such a sequence, the photosubstitution quantum efficiency E_{total} under red light irradiation, defined as the total number of photosubstitution reactions divided by the total number of red photons absorbed, is the product of the individual efficiencies, see Equation 4.2:

$$E_{total} = \Phi_{UC} E_{ET} \Phi_{Ru} \qquad \textit{Equation 4.2}$$

where Φ_{UC} is the upconversion quantum yield (Appendix I), also defined as the quantum yield of generation of the singlet excited state of **2**, E_{ET} is the efficiency of the non-radiative energy transfer (FRET) from **2** to $\mathbf{3}^{2+}$, and Φ_{Ru} is the quantum yield of photosubstitution under blue light irradiation. This expression is only valid at the beginning of the reaction (t = 0), *i.e.* when the influence of radiative energy transfer is low and the non-radiative energy transfer efficiency is more or less constant. Φ_{UC} was experimentally measured at 310 K in absence of $\mathbf{3}^{2+}$ and a value of 1.5% was found (see Appendix I). Note that such a measurement intrinsically takes into account any energy transfer from excited singlet **2** to ground state **1**. Φ_{Ru} has a value of 0.52%.[6] Estimating an energy transfer efficiency of 90 ± 5% at 3.5 mol% $\mathbf{3}^{2+}$, the theoretical value of E_{total} should be 0.007%. Experimentally, a value can be determined directly from the UV-Vis spectroscopy data in Figure 4.3c, by taking the slope at t = 0 of a plot of the amount of moles of $\mathbf{3}^{2+}$ as a function of the amount of photons absorbed since t = 0 (see Figure S.III.9). E_{total} was found to be 0.027%, which is in reasonable agreement with the theoretical value. The difference between theory and experiment is attributed to radiative energy transfer[1h] and direct absorption of the red light by $\mathbf{3}^{2+}$, which have both been neglected in Equation 4.2.

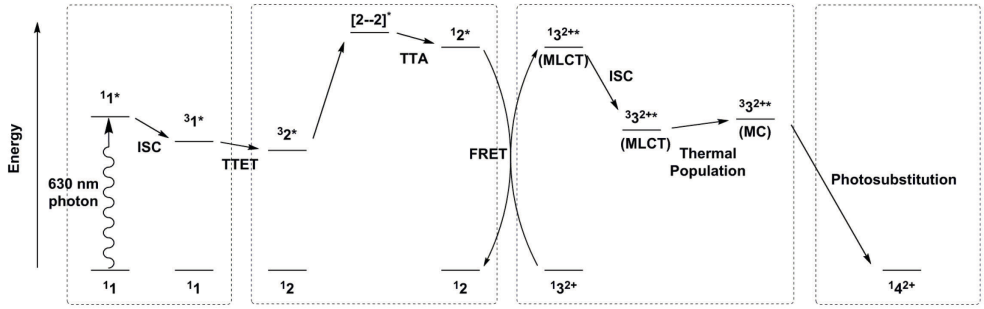

*Figure 4.5. Qualitative Jablonski diagram for a sequential combination of TTA-UC, FRET, and photosubstitution in liposomes **L123** under red light irradiation. Abbreviations: intersystem crossing (ISC), triplet-triplet energy transfer (TTET), triplet-triplet annihilation (TTA), Förster Resonance Energy Transfer (FRET), metal-to-ligand charge transfer (MLCT) state, metal-centered (MC) state.*

In principle, at such power densities (~ 1 W.cm^{-2}) the quantum efficiency of photodissociation reaction under red light irradiation should not depend on the photon flux. It was indeed shown that the TTA upconversion quantum yield does not depend on light intensity above a certain intensity threshold I_{th}.[25] For the 2-component liposomes **L12** we demonstrated recently[26] that indeed the TTA-UC intensity linearly scales with irradiation intensity above I_{th} = 0.05 W.cm^{-2}, while a quadratic dependence of the upconversion intensity on irradiation power is observed at lower intensities, *i.e.*, between 50 and 8 mW.cm^{-2} (see also Figure S.IV.4). When 3-component liposomes **L123** were irradiated with 30, 60, or 120 mW power, *i.e.*, 0.24, 0.48, and 0.95 W.cm^{-2}, respectively, the increase in photosubstitution reaction rate was found almost proportional to light intensity (Figure S.III.10). In other words, at these intensities the overall efficiency of the photosubstitution reaction was indeed found, within experimental errors, independent on the red light intensity (Figure S.III.11). Clinical PDT frequently reports the use of light intensities of 1 W.cm^{-2}, and recent work even used intensities as high as 79 W.cm^{-2},[27] which underlines the biological applicability of TTA-UC in liposomes as a prodrug activation strategy.

4.3 Conclusion

This work is one of the first demonstrations that TTA-UC can be combined with FRET.[28] By putting the three photochemically active components **1**, **2**, and **3**$^{2+}$ inside a single lipid bilayer highly efficient non-radiative energy transfer between the upconverted perylene excitation and the ground state of complex **3**$^{2+}$ occurs. Under red light excitation from a commercial PDT laser

the photosubstitution reaction of $\mathbf{3}^{2+}$ to $\mathbf{4}^{2+}$ was much faster in the combined liposomes **L123** than using radiative energy transfer, *i.e.*, in a physical mixture of **L12** and **L3**. In principle, this strategy can be generalized to any blue-light absorbing (pro)drug with good spectral overlap with the perylene emission. Light activation triggered by TTA-UC upconversion and FRET is especially attractive for the treatment of hypoxic tumors, in which classical PDT lose efficacy. For example, a system combining TTA-UC and PACT would function optimally. In the field of anticancer prodrug activation lanthanoid-doped upconverting nanoparticles have shown promising results,[3, 29] but the upconversion is poorly efficient in water and it requires laser powers in the multi-Watt regime that can be detrimental to cell viability.[30] Adding TTA-UC in the palette of the medicinal photochemist offers a significant alternative to the upconverting strategy: more light is absorbed, higher upconversion efficiencies are achieved at intensities as low as 10 $mW.cm^{-2}$, and the molecular nature of the photoactive components allows for studying the mechanism of energy transfer in great detail. Recent work from our lab has shown that the problem of the sensitivity of TTA-upconversion schemes to dioxygen can be addressed using for example sodium sulfite.[26] These approaches may be combined to achieve red-to-blue TTA-upconversion and prodrug activation *in vivo*.

4.4 Experimental section

4.4.1 General

Palladium tetraphenyltetrabenzoporphyrin (**1**) was purchased from Frontier Scientific, Inc. (Logan, Utah, USA). Perylene (**2**) was purchased from Sigma-Aldrich Chemie BV (Zwijndrecht, The Netherlands). Sodium N-(carbonyl-methoxypolyethylene glycol-2000)-1,2-distearoyl-sn-glycero-3-phospho ethanolamine (DSPE-MPEG-2000), and 1,2-dimyristoyl-sn-glycero-3-phosphocholine (DMPC) were purchased from Lipoid GmbH (Ludwigshafen, Germany) and stored at −18 °C. Dulbecco's phosphate buffered saline (DPBS) was purchased from Sigma Aldrich and had a formulation of 8 $g.L^{-1}$ NaCl, 0.2 $g.L^{-1}$ KCl, 0.2 $g.L^{-1}$ KH_2PO_4, and 1.15 $g.L^{-1}$ K_2HPO_4 with a *pH* of 7.1-7.5. All chemicals were used as received. The synthesis of $\mathbf{3[PF_6]_2}$ is described in Chapter 3.[1h] The concentration of $\mathbf{3}^{2+}$ in the liposome samples was measured with inductively coupled plasma optical emission spectroscopy (ICP-OES) after lysis of 100 − 500 µL of liposome suspension in 4 mL 65% nitric acid for 24 hours at 90 °C, and dilution to 10.0 mL. Regular UV-Vis absorption and emission spectra were recorded on a Varian Cary 50 UV-Vis spectrometer and a Shimadzu RF-5301PC spectrofluorimeter, respectively.

4.4.2 Liposome assembly

All liposome formulations were prepared by the classical hydration-extrusion method. As an example, the preparation of **L123** is described here. Aliquots of chloroform stock solutions containing the liposome constituents were added together in a flask to obtain a solution with

5.0 µmol DMPC, 0.20 µmol DSPE-MPEG-2000, 2.5 nmol **1**, 25 nmol **2**, and 0.20 µmol **3[PF$_6$]$_2$**. The organic solvent was removed by rotary evaporation and subsequently under high vacuum for at least 30 minutes to create a lipid film. 1.0 mL DPBS buffer was added and the lipid film was hydrated by 4 cycles of freezing the flask in liquid nitrogen and thawing in warm water (50 °C). The resulting dispersion was extruded through a Whatman Nuclepore 0.2 µm polycarbonate filter at 40-50 °C at least 11 times using a mini-extruder from Avanti Polar Lipids, Inc. (Alabaster, Alabama, USA). The number of extrusions was always odd to prevent any unextruded material ending up in the final liposome sample. The extrusion filter remained practically colorless after extrusion, suggesting near-complete inclusion of the chromophoric compounds in the lipid bilayer. Liposomes were stored in the dark at 4 °C and used within 7 days. The average liposome size and polydispersity index (PDI) were measured with a Malvern Instruments Zetasizer Nano-S machine, operating with a wavelength of 632 nm. The size and PDI were typically 130 – 170 nm and 0.05 – 0.20, respectively.

4.4.3 Time-Correlated Single Photon Counting (TCSPC)

For TCSPC experiments, a FluoTime 200 system from PicoQuant (Berlin, Germany) was used, operating with a PicoHarp 300 photon counting module, a PDL 800-B picosecond pulsed diode laser driver set at 10 MHz repetition rate, and a 440 nm LDH-P-C-440 laser diode. Samples were excited at 440 nm (6 µW laser power, 0.6 pJ/pulse) and detection was recorded at 474 nm. A 111-QS cuvette from Hellma GmbH & Co. KG (Müllheim, Germany) was used and was thermostated in the holder at either 293 K or 310 K with a TC 125 temperature controller from Quantum Northwest (Seattle, WA, USA). Samples were always allowed a minimum of 7 minutes of thermal equilibration before measurement. The samples were greatly diluted so that in all cases, [**2**] = 1 µM and the absorption at excitation and emission wavelengths was below 0.1 (for 10 mm path length). The data was fitted with Origin Pro 8.5 software.

4.4.4 Transient Absorption (TA) Spectroscopy

Transient absorption spectroscopy was performed on a femtosecond laser setup described in detail elsewhere.[31] A combined Libra and Legend laser system from Coherent produced pulses at 40 fs duration and 1 kHz repetition rate. Long delays were achieved by using two individual femtosecond amplifiers for pump and probe. Due to the shared source of seed pulses among the two lasers (the Legend was seeded from the Libra seed), femtosecond time resolution and arbitrary long pump probe delays were achieved. The pump laser was fed into an automated optical parametric amplifier that allowed conversion of the input pulse into any wavelength in the region 480 – 1600 nm while keeping the pulse duration. In this case, the samples were excited with 400 nm light (20 – 60 µW, 20 – 60 nJ/pulse). The laser driving the probe beam was focused on a calcium fluoride plate to generate a super continuum spanning from 360 – 1200 nm, which enabled spectrally resolved probing without the need for scanning. After passing through the sample, the probe beam was dispersed on a 256 element diode array, calculating pump-on pump-off difference signal on a shot to shot basis. The diode array was calibrated so that the spectrum was recorded from 430 to 730 nm. High concentration samples were used with [**2**] = 0.1 mM in a 110-QS cuvette from Hellma with a 1 mm optical path length so that $A_{400} \leq 0.6$ (including sample scatter). The sample volume was 200 µL and the cuvette was mounted on a shaker to ensure mixing throughout the measurement. The acquisition time per sample was approximately 2 hours. It was confirmed with UV-Vis absorption spectroscopy before and after TA spectroscopy that the blue excitation did not cause any photochemical degradation of the samples within the measurement time. In TA experiments involving blue-

light irradiated samples, 500 µl sample was irradiated with 10 mW 420 nm light (M420F2 fiber-coupled high-power LED from Thorlabs) for a minimum of 2 hours. The reaction was monitored with UV-Vis spectroscopy to control the reaction time until all $\mathbf{3}^{2+}$ had converted to $\mathbf{4}^{2+}$, at which point the spectrum no longer evolved.

4.4.5 Photodissociation experiments with red light

Photodissociation experiments were conducted in a custom-built setup (Figure S.III.8). All optical parts were connected with FC-UVxxx-2 (xxx = 200, 400, 600) optical fibers from Avantes (Apeldoorn, The Netherlands), with a diameter of 200-600 µm, respectively, and that were suitable for the UV-Vis range (200 – 800 nm). 1.5 mL of the diluted liposome sample was deoxygenated by bubbling argon through the sample with a rate of ~2 bubbles per second for at least 30 minutes in an external ice-cooled pear-shaped flask. After this period, bubbling was stopped while maintaining the argon flow, and the sample was warmed in a water bath of approximately 40 °C for 10 minutes. Then, the sample was transferred by means of cannulation with argon pressure to a 111-OS macro fluorescence cuvette from Hellma in a CUV-UV/VIS-TC temperature-controlled cuvette holder from Avantes. The sample was allowed to equilibrate at 310 K for an additional 10 minutes while stirring. The sample was held under argon atmosphere at a constant temperature of 310 K and irradiated for 4 hours from the side with a 630 nm laser light beam from a clinical grade Diomed 630 nm PDT laser, set at a power of 30, 60, or 120 mW. The 630 nm light was filtered through a FB630-10, 630 nm band pass filter (Thorlabs, Dachau/Munich, Germany) put between the laser and the sample. The excitation power was controlled using a NDL-25C-4 variable neutral density filter (Thorlabs), and measured using a S310C thermal sensor connected to a PM100USB power meter (Thorlabs). The laser was collimated to a beam of 4 mm diameter to reach an intensity of 0.24, 0.48, or 0.95 $W.cm^{-2}$; in such conditions, a cylinder of approximately 0.13 cm^3 was simultaneously excited by the laser (8% of the total sample volume). UV-Vis absorption spectra were measured using an Avalight-DHc halogen-deuterium lamp (Avantes) as light source and a 2048L StarLine spectrometer (Avantes) as detector, both connected to the cuvette holder at a 180° angle and both at a 90° angle with respect to the red laser irradiation direction. The filter holder between cuvette holder and detector was in a position without a filter (Figure S.III.8, item 8). Luminescence emission spectra were measured using the same detector but with the UV-Vis light source switched off. To visualize the spectrum from 550 nm to 900 nm, while blocking the red excitation light, a Thorlabs NF-633 notch filter was used in the variable filter holder. To visualize the spectrum from 400 nm to 550 nm, an OD4 575 nm short pass filter (Edmund Optics, York, United Kingdom, part no. 84-709) was used. A UV-Vis absorption and two emission spectra (one for each filter) were measured every 15 min; each time the emission spectra were measured first by switching the filter holder to the appropriate position, then the laser was switched off, the halogen-deuterium lamp was turned on, the filter holder was switched to an open position, a UV-Vis absorption spectrum was recorded, the halogen-deuterium lamp was switched off, and the laser was switched on again. Each UV-Vis measurement took approximately 15 seconds in total. All spectra were recorded with Avasoft software from Avantes and further processed with Microsoft Office Excel 2010 and Origin Pro software. For each UV-Vis absorption spectrum, a baseline subtraction was performed followed by an evaporation correction to account for a slight loss of solvent as a result of the constant argon flow in the cuvette during the experiment. The emission spectra obtained from the two filters were stitched together at 550 nm to obtain a continuous spectrum from 400 to 900 nm. No correction was needed to seamlessly connect the spectra.

4.4.6 Differential Scanning Calorimetry

Differential scanning calorimetry (DSC) was performed on a TA Instruments (DE, USA) nano-DSC III instrument in the range of 278 to 333 K with a scanning rate of 1 K.min^{-1} at 3 atm. The capillary cell (V = 300 µL) was filled with the liposome solution (lipid bulk concentration of 5 mM) containing different concentrations of **1**, **2** and **3**$^{2+}$. The reference cell was filled with the corresponding liposome-free buffer solution. A blank measurement was performed with PBS buffer. The liposome dispersions were degassed for 10 − 15 minutes prior to measurement on a Nalgene degassing station. For each sample, at least two cycles of heating and cooling were performed with 10 minutes of thermal equilibration between the ramps. The machine was cleaned beforehand with 50% formic acid and rinsed thoroughly with Milli-Q water. The thermograms were processed and analyzed using NanoAnalyze software from TA Instruments.

4.5 References

[1] a) L. Zayat, C. Calero, P. Alborés, L. Baraldo, R. Etchenique, *J. Am. Chem. Soc.* **2003**, *125*, 882-883; b) P. J. Bednarski, F. S. Mackay, P. J. Sadler, *Anticancer Agents Med Chem* **2007**, *7*, 75-93; c) N. J. Farrer, L. Salassa, P. J. Sadler, *Dalton Trans.* **2009**, 10690-10701; d) U. Schatzschneider, *Eur. J. Inorg. Chem.* **2010**, *2010*, 1451-1467; e) S. L. H. Higgins, K. J. Brewer, *Angew. Chem., Int. Ed.* **2012**, *51*, 11420–11422; f) B. S. Howerton, D. K. Heidary, E. C. Glazer, *J. Am. Chem. Soc.* **2012**, *134*, 8324-8327; g) M. A. Sgambellone, A. David, R. N. Garner, K. R. Dunbar, C. Turro, *J. Am. Chem. Soc.* **2013**, *135*, 11274-11282; h) S. H. C. Askes, A. Bahreman, S. Bonnet, *Angew. Chem., Int. Ed.* **2014**, *53*, 1029-1033.

[2] a) A. Master, M. Livingston, A. Sen Gupta, *J. Controlled Release* **2013**, *168*, 88-102; b) S. G. Bown, *J. Natl. Compr. Canc. Netw.* **2012**, *10 Suppl 2*, S69-74; c) A. M. Bugaj, *Photochem. Photobiol. Sci.* **2011**, *10*, 1097; d) D. W. Felsher, *Nat. Rev. Cancer* **2003**, *3*, 375-379.

[3] E. Ruggiero, A. Habtemariam, L. Yate, J. Mareque Rivas, L. Salassa, *Chem. Commun.* **2014**, *50*, 1715-1718.

[4] a) R. R. Sawant, V. P. Torchilin, *Soft Matter* **2010**, *6*, 4026-4044; b) R. Weijer, M. Broekgaarden, M. Kos, R. van Vught, E. A. J. Rauws, E. Breukink, T. M. van Gulik, G. Storm, M. Heger, *J. Photochem. Photobiol., C* **2015**, *23*, 103-131.

[5] a) M. Ferrari, *Nat. Rev. Cancer* **2005**, *5*, 161-171; b) Y. Matsumura, H. Maeda, *Cancer Res.* **1986**, *46*, 6387-6392.

[6] S. Bonnet, B. Limburg, J. D. Meeldijk, R. J. M. Klein Gebbink, J. A. Killian, *J. Am. Chem. Soc.* **2010**, *133*, 252-261.

[7] a) T. N. Singh-Rachford, F. N. Castellano, *Coord. Chem. Rev.* **2010**, *254*, 2560-2573; b) J. Zhao, S. Ji, H. Guo, *RSC Adv.* **2011**, *1*, 937-950; c) Y. C. Simon, C. Weder, *J. Mater. Chem.* **2012**, *22*, 20817-20830; d) Y. Y. Cheng, B. Fückel, T. Khoury, R. l. G. C. R. Clady, N. J. Ekins-Daukes, M. J. Crossley, T. W. Schmidt, *J. Phys. Chem. A* **2011**, *115*, 1047-1053.

[8] Y. Murakami, T. Ito, A. Kawai, *J. Phys. Chem. B* **2014**, *118*, 14442–14451.

[9] a) C. Wohnhaas, K. Friedemann, D. Busko, K. Landfester, S. Baluschev, D. Crespy, A. Turshatov, *ACS Macro Lett.* **2013**, *2*, 446-450; b) R. R. Islangulov, J. Lott, C. Weder, F. N. Castellano, *J. Am. Chem. Soc.* **2007**, *129*, 12652-12653; c) P. B. Merkel, J. P. Dinnocenzo, *J. Lumin.* **2009**, *129*, 303-306; d) A. Monguzzi, R. Tubino, F. Meinardi, *J. Phys. Chem. A* **2009**, *113*, 1171-1174; e) T. N. Singh-Rachford, J. Lott, C. Weder, F. N. Castellano, *J. Am. Chem. Soc.* **2009**, *131*, 12007-12014.

[10] a) P. C. Boutin, K. P. Ghiggino, T. L. Kelly, R. P. Steer, *J. Phys. Chem. Lett.* **2013**, *4*, 4113-4118; b) S.-H. Lee, Á. Sonseca, R. Vadrucci, E. Giménez, E. J. Foster, Y. Simon, *J. Inorg. Organomet. Polym. Mater.* **2014**, *24*, 898-903.

[11] a) A. Turshatov, D. Busko, S. Baluschev, T. Miteva, K. Landfester, *New J. Phys.* **2011**, *13*, 083035; b) J.-H. Kang, E. Reichmanis, *Angew. Chem., Int. Ed.* **2012**, *51*, 11841-11844; c)

J.-H. Kim, J.-H. Kim, *J. Am. Chem. Soc.* **2012**, *134*, 17478-17481; d) Q. Liu, B. Yin, T. Yang, Y. Yang, Z. Shen, P. Yao, F. Li, *J. Am. Chem. Soc.* **2013**, *135*, 5029-5037; e) K. Tanaka, H. Okada, W. Ohashi, J.-H. Jeon, K. Inafuku, Y. Chujo, *Bioorg. Med. Chem.* **2013**, *21*, 2678-2681; f) C. Wohnhaas, V. Mailänder, M. Dröge, M. A. Filatov, D. Busko, Y. Avlasevich, S. Baluschev, T. Miteva, K. Landfester, A. Turshatov, *Macromol. Biosci.* **2013**, *13*, 1422–1430; g) Y. C. Simon, S. Bai, M. K. Sing, H. Dietsch, M. Achermann, C. Weder, *Macromol. Rapid Commun.* **2012**, *33*, 498-502; h) O. S. Kwon, J.-H. Kim, J. K. Cho, J.-H. Kim, *ACS Appl. Mater. Interfaces* **2015**, *7*, 318-325; i) M. Penconi, P. L. Gentili, G. Massaro, F. Elisei, F. Ortica, *Photochem. Photobiol. Sci.* **2014**, *13*, 48-61; j) J.-H. Kim, J.-H. Kim, *ACS Photonics* **2015**, *2*, 633-638.

[12] P. Duan, N. Yanai, N. Kimizuka, *J. Am. Chem. Soc.* **2013**, *135*, 19056–19059.

[13] Z. Jiang, M. Xu, F. Li, Y. Yu, *J. Am. Chem. Soc.* **2013**, *135*, 16446-16453.

[14] R. S. Khnayzer, J. Blumhoff, J. A. Harrington, A. Haefele, F. Deng, F. N. Castellano, *Chem. Commun.* **2012**, *48*, 209-211.

[15] a) R. E. Goldbach, I. Rodriguez-Garcia, J. H. van Lenthe, M. A. Siegler, S. Bonnet, *Chem. Eur. J.* **2011**, *17*, 9924-9929; b) A. Bahreman, B. Limburg, M. A. Siegler, R. Koning, A. J. Koster, S. Bonnet, *Chem. Eur. J.* **2012**, *18*, 10271-10280.

[16] B. Siewert, V. H. S. v. Rixel, E. J. v. Rooden, S. L. Hopkins, M. J. B. Moester, F. Ariese, M. A. Siegler, S. Bonnet, *Eur. J. Inorg. Chem.* **2016**, Accepted Manuscript.

[17] J. R. Lakowicz, *Principles of Fluorescence Spectroscopy*, 3rd ed., Springer Science+Business Media, LLC, New York, NY, USA, **2006**.

[18] S. L. Joris J. Snellenburg, Ralf Seger, Katharine M. Mullen, Ivo H. M. van Stokkum, *J. Stat. Softw.* **2012**, *49*, 1-22.

[19] Y. H. Meyer, P. Plaza, *Chem. Phys.* **1995**, *200*, 235-243.

[20] A. S. Holmes, D. J. S. Birch, T. Salthammer, *J. Fluoresc.* **1993**, *3*, 77-84.

[21] D. Marsh, *Handbook of Lipid Bilayers*, 2nd ed., Taylor & Francis Group, LLC, Boca Raton, FL, USA, **2013**.

[22] A. Bahreman, M. Rabe, A. Kros, G. Bruylants, S. Bonnet, *Chem. Eur. J.* **2014**, *20*, 7429-7438.

[23] A. S. Holmes, K. Suhling, D. J. S. Birch, *Biophys. Chem.* **1993**, *48*, 193-204.

[24] W. Wang, Q. Liu, C. Zhan, A. Barhoumi, T. Yang, R. G. Wylie, P. A. Armstrong, D. S. Kohane, *Nano Lett.* **2015**, *15*, 6332-6338.

[25] A. Haefele, J. Blumhoff, R. S. Khnayzer, F. N. Castellano, *J. Phys. Chem. Lett.* **2012**, *3*, 299-303.

[26] S. H. C. Askes, N. L. Mora, R. Harkes, R. I. Koning, B. Koster, T. Schmidt, A. Kros, S. Bonnet, *Chem. Commun.* **2015**, 9137-9140.

[27] S. G. Bown, A. Z. Rogowska, D. E. Whitelaw, W. R. Lees, L. B. Lovat, P. Ripley, L. Jones, P. Wyld, A. Gillams, A. W. R. Hatfield, *Gut* **2002**, *50*, 549-557.

[28] W. Wang, Q. Liu, C. Zhan, A. Barhoumi, T. Yang, R. G. Wylie, P. A. Armstrong, D. S. Kohane, *Nano Lett.* **2015**, DOI: 10.1021/acs.nanolett.1025b01325.

[29] a) Y. Dai, H. Xiao, J. Liu, Q. Yuan, P. a. Ma, D. Yang, C. Li, Z. Cheng, Z. Hou, P. Yang, J. Lin, *J. Am. Chem. Soc.* **2013**, *135*, 18920-18929; b) Y. Min, J. Li, F. Liu, E. K. L. Yeow, B. Xing, *Angew. Chem., Int. Ed.* **2014**, *53*, 1012-1016; c) E. Ruggiero, J. Hernández-Gil, J. C. Mareque-Rivas, L. Salassa, *Chem. Commun.* **2015**, *51*, 2091-2094.

[30] Y.-F. Wang, G.-Y. Liu, L.-d. Sun, J.-W. Xiao, J.-C. Zhou, C.-H. Yan, *ACS Nano* **2013**, *7*, 7200-7206.

[31] a) R. Berera, R. Grondelle, J. M. Kennis, *Photosynth. Res.* **2009**, *101*, 105-118; b) J. Ravensbergen, F. F. Abdi, J. H. van Santen, R. N. Frese, B. Dam, R. van de Krol, J. T. M. Kennis, *J. Phys. Chem. C* **2014**, *118*, 27793-27800.

CHAPTER 5

Imaging the lipid bilayer of giant unilamellar vesicles using red-to-blue light upconversion

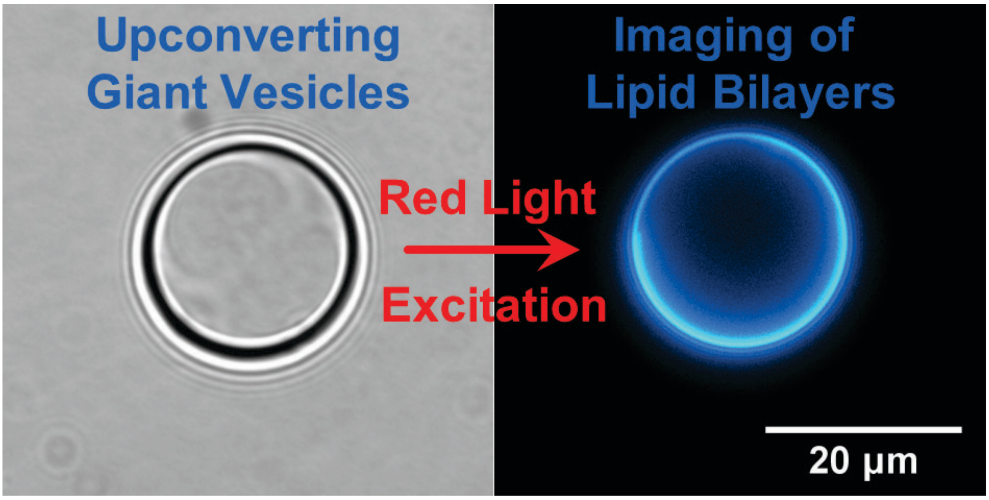

Red-to-blue triplet-triplet annihilation upconversion was obtained in giant unilamellar vesicles. The upconverted light was homogeneously distributed across the membrane and could be utilized for the imaging of individual giant vesicles in three dimensions. These results show the great potential of TTA-UC for imaging applications under anoxic conditions.

This chapter was published as a communication: S. H. C. Askes, N. Lopez Mora, R. Harkes, R. I. Koning, B. Koster, T. Schmidt, A. Kros, S. Bonnet, *Chem. Commun.* **2015**, *51*, 9137-9140.

5.1 Introduction

Upconversion luminescence (bio)imaging offers great advantages over conventional imaging. The absence of auto-fluorescence results in high contrast images, while photons of low energy, *i.e.* within the phototherapeutic window (600 – 1000 nm), afford higher tissue penetration and negligible irradiation damage. For these reasons lanthanoid-based upconverting nanoparticles (UCNPs), for example, have attracted much interest.[1] However, UCNPs suffer from several disadvantages, such as the need for high excitation power, the low absorption cross section of lanthanoid ions, and low upconversion efficiency in aqueous solution (typically ≤0.5%).[1b] In contrast, triplet-triplet annihilation upconversion (TTA-UC) requires low excitation intensity (<100 $mW.cm^{-2}$), employs sensitizers having high extinction coefficients in the phototherapeutic window, and has achieved upconversion quantum yields up to 14% in aqueous solution.[1b, 2]

In TTA-UC, low-energy photons are converted into higher-energy photons by means of a photophysical mechanism involving a couple of molecular dyes called the sensitizer and annihilator (see Chapter 2, Figure 2.1 for a qualitative Jablonski diagram).[3] The sensitizer absorbs the low-energy light, undergoes intersystem crossing (ISC) to a triplet state, and transfers its energy to the annihilator molecule by triplet–triplet energy transfer. Further collision of two triplet annihilator molecules leads to triplet–triplet annihilation (TTA), whereby one annihilator molecule is promoted to the excited singlet state, whereas the other one falls back to the ground state. The singlet annihilator returns to the ground state by emission of a high-energy photon, thus realizing upconversion. Most molecular dyes used in TTA-UC are highly lipophilic and require supramolecular strategies to be used in aqueous solution.[4] For example, sub-micrometer sized TTA-UC particles have been proposed for *in vitro* or *in vivo* imaging.[1b, 4c, 4d] We now demonstrate that TTA-UC can also be used for the imaging of lipid membranes.

Giant Unilamellar Vesicles (GUVs) are classical tools in fluorescence imaging, as their large size (1–100 μm diameter) allows for direct observation of individual vesicles by optical microscopy techniques.[5] GUVs have for example been used for visualizing lipid rafts, membrane fusion, or ion transport.[6] In this study we functionalized PEGylated GUVs with palladium tetraphenyltetrabenzoporphyrin (**1**) as photosensitizer and perylene (**2**) as the annihilator (Figure 5.1a), and studied red-to-blue TTA-UC in the

membrane of the vesicles by optical microscopy. The aim of the study was to investigate the dye distributions across the membrane, the homogeneity of upconverted emission in the lipid bilayer, and the upconversion stability under imaging conditions. The growth of high-quality giant vesicles with a well-defined shape in physiologically relevant conditions, *i.e.*, at high ionic strengths, was until recently considered as a challenge, but a new method was recently developed by some of us that is compatible with such conditions (up to 320 mOsm.kg^{-1}).[7]

5.2 Results and discussion

Upconverting giant vesicles **GUV12** were thus prepared from a lipid mixture of 95 mol% phospholipid (either 1,2-dimyristoyl-sn-glycero-3-phosphocholine, *i.e.* DMPC, or 1,2-dioleoyl-sn-glycero-3-phosphocholine, *i.e.* DOPC), 4 mol% sodium N-(carbonyl-methoxypolyethylene glycol-2000)-1,2-distearoyl-sn-glycero-3-phosphoethanolamine (DSPE-MPEG-2000), 0.5 mol% compound **2**, and 0.02 mol% compound **1**. The complete procedure is described in the experimental section. Briefly, the dye-containing lipid mixture in chloroform was deposited on a chemically cross-linked dextran–poly(ethylene glycol) hydrogel substrate, dried to form a lipid film, and then the film was re-hydrated with phosphate buffered saline (PBS) supplemented with 0.3 M sodium sulfite (Na_2SO_3) and 0.2 M sucrose at 293 – 308 K. Transferring the solution onto a microscopy slide allowed for bright field imaging on a custom-build microscope based on an inverted microscopy setup. The images (Figure 5.1c) confirmed that for both lipid compositions (DMPC or DOPC) free-floating single vesicles were obtained, together with clusters of smaller vesicles. The images also show that the self-assembled vesicles were giant (diameter 1 – 100 μm), unilamellar, and spherical. The fact that almost identical procedures can be employed for preparing GUVs from lipids having a marked difference in their gel-to-liquid transition temperature (T_m = −17.3 °C and 23.9 °C for pure DOPC and DMPC, respectively)[8], demonstrates the flexibility of the GUV preparation method. For comparison, much smaller LUVs (samples **LUV12**) with an average diameter of *ca*. 150 nm were prepared from the same lipid mixture but using a standard hydration-extrusion protocol (Figure S.IV.1).

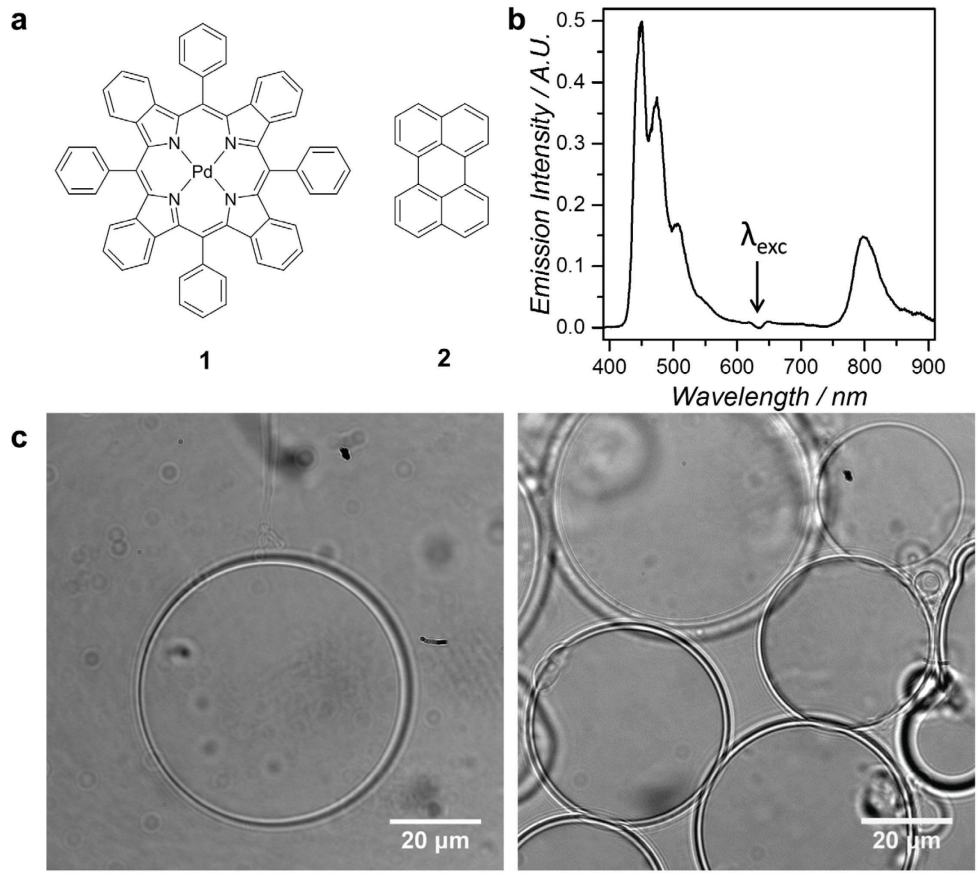

*Figure 5.1. a) Chemical structures of palladium tetraphenyltetrabenzoporphyrin (**1**) and perylene (**2**). b) Emission spectra of DOPC upconverting GUVs with 30 mW 630 nm excitation (0.24 W.cm^{-2} intensity) at 298 K in sulfite-supplemented (0.3 M) PBS buffer under air. c) Bright field micrographs of DOPC (left) and DMPC (right) upconverting giant vesicles at 298 K.*

Sodium sulfite was added in the buffer as an oxygen-scavenging agent. Since the triplet states involved in TTA-UC are readily quenched by molecular oxygen, it is common practice to deoxygenate samples before measuring upconverted emission. With LUVs de-oxygenation can be achieved by, for example, bubbling the solution with argon or N_2. In the case of GUVs imaging however, bubbling an inert gas through the solution would at least impair visualization of single GUVs during a long time period of time due to convection, or even lead to damaging of the giant vesicles, so that supplementing the buffer with an oxygen scavenger is highly preferred. In a preliminary experiment, upconversion emission spectra of **LUV12** samples deoxygenated by either argon bubbling for 30 minutes or by adding 0.3 M

sodium sulfite to the buffer, were compared (see Figure S.IV.2 and experimental section for details). When irradiated at 630 nm the emission spectrum of such LUVs at 298 K shows at 800 nm the phosphorescence band of **1**, and between 450 and 600 nm the blue singlet emission from **2** (Figure S.IV.2). The spectra from both deoxygenation methods were found to be very similar. It was thus concluded that Na_2SO_3 does not interfere with the photophysical processes at the origin of upconversion, and that sulfite might be used for scavenging dioxygen in a GUV-containing sample as well.

Indeed, even though addition of Na_2SO_3 significantly increased the ionic strength of the buffer (from 278 ± 1 mOsm.kg^{-1} for PBS buffer to 884 ± 11 mOsm.kg^{-1} when supplemented with 0.3 M sodium sulfite), as explained above sodium sulfite did not prevent the assembly of DMPC or DOPC **GUV12** using the hydrogel method. No differences in vesicle yield and morphology were observed in presence or absence of sodium sulfite in the buffer. This result demonstrates that the dextran–poly(ethylene glycol) hydrogel substrate is able to produce GUVs at high ionic strength, which is a significant advantage over alternative GUV preparation methods such as electroformation or gentle hydration, which often fail in such conditions. When irradiated at 630 nm under air, the emission spectrum of the DMPC or DOPC **GUV12** samples prepared in a sulfite-supplemented buffer was identical to the emission spectrum of the corresponding **LUV12** samples (Figure 5.1b and Figure S.IV.3), showing that the dyes **1** and **2** were indeed incorporated in the lipid bilayer.

GUV12 samples were then visualized by emission microscopy at 298 K (Figure 5.2). When the vesicles were illuminated with violet light (405 nm), *i.e.* by direct excitation of perylene (**2**), fluorescence was clearly detected at the membrane (Figure 5.2b). To visualize upconversion, a 630 nm continuous wave PDT laser was coupled into the microscope and set at a power of a few milliwatts, resulting in the focal spot in an intensity of ~300 W.cm^{-2}. All wavelengths other than 450 − 575 nm were strictly blocked by a combination of notch and short-pass filters (Appendix IV). High-quality images were obtained that were superimposable to the bright field images and to the fluorescence images recorded under white and violet light irradiation, respectively (Figure 5.2a-c). Control samples were prepared in which the porphyrin sensitizer **1** was omitted from the formulation (**GUV2**). Images recorded in identical conditions were black, *i.e.*, no blue emission was observed (Figure S.IV.7). **GUV12** samples prepared in absence of sulfite

oxygen scavenger and observed under air did not give any observable emission either (Figure S.IV.8). Altogether, these observations prove that the blue images recorded under 630 nm irradiation of **GUV12** samples supplemented with sulfite comes from the TTA upconversion process and are not the result of sensitizer emission (at 800 nm) or of two-photon absorption. Overall, all data conclude that both dyes **1** and **2** co-localize in the membrane and result in TTA upconversion. At this scale of observation the upconverted emission is homogeneous across the membrane and no phase separation of the lipids or dyes was observed.

Under the red-light irradiation conditions initially used in the microscopy setup (630 nm at an intensity of 320 $W.cm^{-2}$), substantial bleaching of the upconverted emission of **GUV12** samples was observed even in presence of 0.3 M of sulfite. A plot of the averaged normalized pixel values as a function of red irradiation time shows that the upconverted emission is halved after less than 3 seconds (Figure 5.3). When the light intensity was lowered 60 times (*i.e.*, down to 5.2 $W.cm^{-2}$) clear upconversion images could still be recorded. In such conditions the bleaching rate was significantly lower (Figure 5.3), and the time necessary for halving the upconverted emission intensity of a pixel increased to approximately 15 seconds. The upconversion luminescence of **LUV-12** in a spectroscopy setup could be observed for less than 8 $mW.cm^{-2}$, with linear power dependency above 60 $mW.cm^{-2}$ (Figure S.IV.4). Overall, these findings show that high power is not a requirement for the upconversion imaging of **GUV-12**.

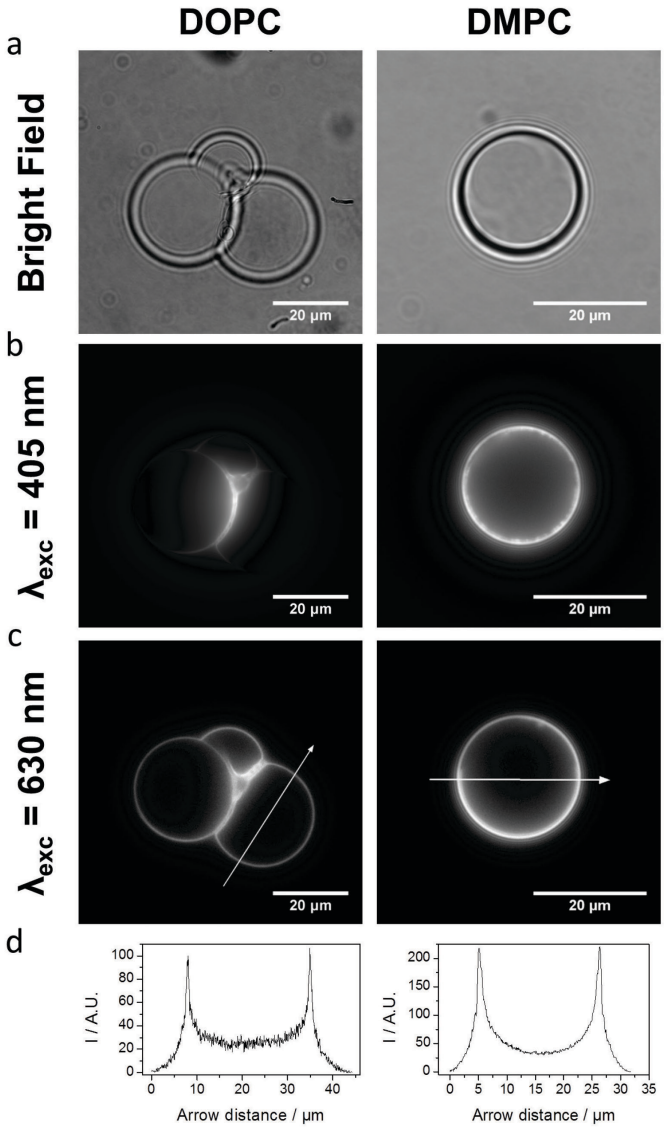

*Figure 5.2. Imaging of DOPC (left) and DMPC (right) upconverting giant vesicles (**GUV12**) with a) bright field, b) 405 nm excitation and 450-500 nm detection, and c) 630 nm excitation and 450-575 nm detection. d) Upconversion intensity profile plot following the arrows in the images directly above (c). At 630 nm: laser spot size diameter 39 µm, power 3.8 mW, intensity 320 W.cm^{-2}. At 405 nm: laser spot size diameter 22 µm (power 1 mW, intensity 60 W.cm^{-2}) for DOPC image or 39 µm (power 1 mW, intensity 300 W.cm^{-2}) for DMPC image. Images were acquired at 298 K in sulfite-supplemented (0.3 M) PBS buffer.*

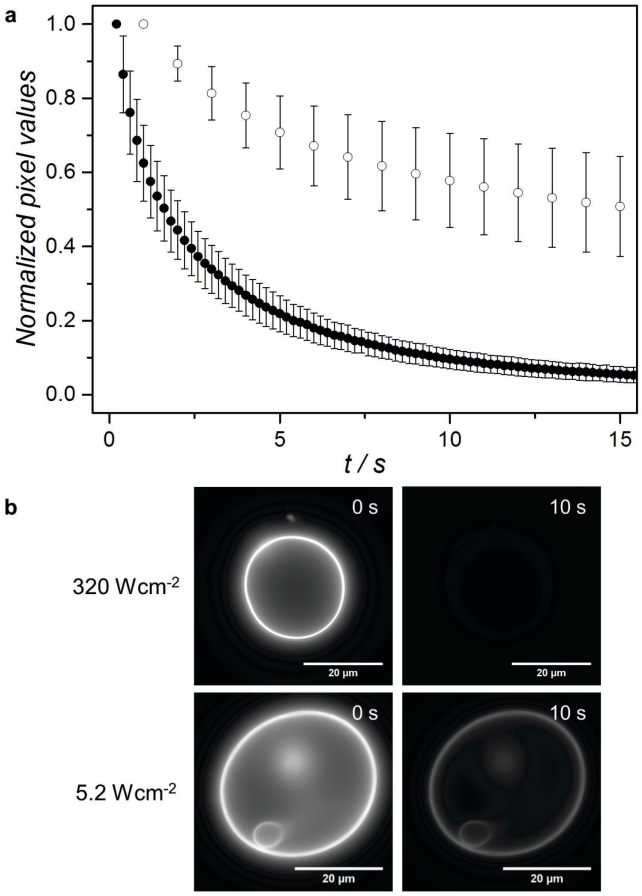

Figure 5.3 a) Averaged normalized pixel values as a function of red irradiation time during upconversion imaging of ***GUV12*** *samples in sulfite-supplemented PBS buffer (0.3 M). Conditions: 630 nm excitation at 320 W.cm^{-2} (black filled circles) or 5.2 W.cm^{-2} (empty circles), detection in the 450–575 nm region, T = 298 K. Snapshots were taken with an exposure time of 0.2 s (320 W.cm^{-2}) or 1.0 s (5.2 W.cm^{-2}). Error bars represent standard deviation based on six individual measurements. b) Upconversion emission microscopy images of* ***GUV12*** *samples at t = 0 s (left) and at t = 10 s (right) at an illumination intensity of 320 W.cm^{-2} (top) and 5.2 W.cm^{-2} (bottom). Excitation at 630 nm, detection at 450–575 nm.*

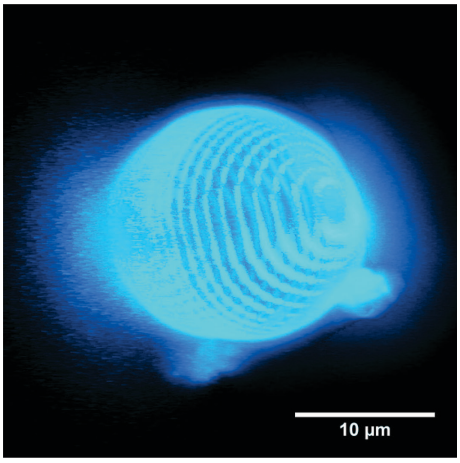

*Figure 5.4. 3D reconstructed image of a DMPC **GUV12** sample, rotated counter-clockwise by 50° about the y-axis. Each z-slice was imaged at 298 K with 630 nm excitation (320 W.cm^{-2}) and detection in the 450-575 nm region. The z-distance between slices was 1.0 µm. Video V1 (http://www.rsc.org/suppdata/c5/cc/c5cc02197a/c5cc02197a2.mpeg) exhibits a 360° rotational view of this image and of four other individual DMPC **GUV12**.*

In optimized conditions, we realized that the upconverted emission was intense enough to be utilized for reconstructing in 3D the membrane of the giant vesicles. Z-stack upconversion image acquisition was indeed performed on both DMPC and DOPC **GUV12** samples. The illumination intensity was deliberately chosen to be high (320 W.cm^{-2}) to make sure that z-stack image acquisition was short (200 ms exposure time per slice, *ca*. 45 slices per stack, total acquisition time < 10 s). In such conditions, the slight lateral motion of the GUVs did not significantly affect the imaging process. From these stacks, 3D reconstructions were made (*e.g.* Figure 5.4), of which a video was compiled (See Video V1 on-line at http://www.rsc.org/suppdata/c5/cc/c5cc02197a/c5cc02197a2.mpeg). This reconstruction demonstrates that the TTA-upconverted emission can be utilized for the three-dimensional reconstruction of an object that is 10 to 30 µm in size.

5.3 Conclusion

In conclusion, DOPC and DMPC giant vesicles capable of upconverting red light to blue light by means of triplet-triplet annihilation were prepared by lipid film hydration on a hydrogel substrate at high ionic strengths. The preparation method is facile and does not involve any specific equipment. Sodium sulfite added as an oxygen scavenger to the vesicle samples allows for observing upconversion even under air. According to optical microscopy, the upconverted emission allows for recording high quality images showing that

upconversion is homogeneously realized across the lipid bilayer. The quality and stability of the upconverted images enabled the 3D reconstruction of upconverting GUVs. These results show the great potential of TTA upconversion for imaging applications under anoxic conditions, and open a route towards cell membrane imaging with upconverted light.

5.4 Experimental section

5.4.1 General

Palladium tetraphenyltetrabenzoporphyrin (**1**) was purchased from Frontier Scientific, Inc. (Logan, Utah, USA). Perylene (**2**) was purchased from Sigma-Aldrich Chemie BV (Zwijndrecht, The Netherlands). Sodium N-(carbonyl-methoxypolyethylene glycol-2000)-1,2-distearoyl-sn-glycero-3-phospho ethanolamine (DSPE-MPEG-2000), 1,2-dioleoyl-sn-glycero-3-phosphocholine (DOPC), and 1,2-dimyristoyl-sn-glycero-3-phosphocholine (DMPC) were purchased from Lipoid GmbH (Ludwigshafen, Germany) and stored at −18 °C. Dulbecco's phosphate buffered saline (PBS) was purchased from Sigma Aldrich and had a formulation of 8 $g.L^{-1}$ NaCl, 0.2 $g.L^{-1}$ KCl, 0.2 $g.L^{-1}$ KH_2PO_4, and 1.15 $g.L^{-1}$ K_2HPO_4 with a *pH* of 7.1 − 7.5. All other chemicals were purchased from major chemical suppliers and used as received. Images and data were processed with Fiji ImageJ, Origin Pro, and Microsoft Excel software.

5.4.2 GUV preparation

All GUVs were prepared by lipid film re-hydration on dextran chemically cross-linked hydrogel substrates by a method described elsewhere.[7] The preparation of **GUV12** is described here as an example. Glass microscopy slides were first incubated with 1:1 vol MeOH : HCl (37%) for 30 min, then with 98% H_2SO_4 for 30 min, and then thiol-functionalized by incubating them for 1 h in a 2 wt.% solution of (3-mercaptopropyl)triethoxysilane in dry toluene under a nitrogen atmosphere, and washing them three times with toluene. Directly after, a homogeneous film of Dex-PEG hydrogel was formed on this surface by drop-casting 600 µL of a 1:1 volume mixture of 2 wt.% maleimide-functionalized dextran, with a substitution degree of 3 maleimide groups per 100 glucopyranose residues of dextran (synthesis and characterization detailed in ref. 2), in water and 2 wt.% α,ω-PEG dithiol (1500 $g.mol^{-1}$) in water at room temperature. A homogenous hydrogel film was formed after 30 − 45 minutes at 40 °C. Then, 10 µL of lipid mixture stock solution in chloroform, containing 20 mM DMPC or DOPC, 0.8 mM DSPE-PEG-2K, 0.1 mM perylene (**2**), and 5 µM of compound **1**, was deposited on the hydrogel surface. The organic solvent was evaporated for 30 minutes under a gentle stream of air followed by a period of at least 30 minutes in a 30 °C vacuum oven. The lipid film was then hydrated with 400 µL phosphate buffered saline (PBS) supplemented with 0.2 M sucrose, and when wanted 0.3 M sodium sulfite, for 1 - 2 hours at room temperature (ca. 293 K) in case of DOPC GUVs, or at 308 K in case of DMPC GUVs. This recipe produced a solution containing free-floating vesicles that could be directly pipetted in a fluorescence cuvette for emission spectroscopy (see section 5.4.3). Alternatively, it was further used for the preparation of a microscopy experiment (section 5.4.4).

5.4.3 Emission spectroscopy on GUVs

For upconversion emission spectroscopy, approximately 700 µL of the above-mentioned solution of free-floating vesicles in buffer was transferred to a semi-micro cuvette and used as such in the setup detailed in section 5.4.6

5.4.4 Preparation of a microscopy experiment with GUVs

For optical microscopy imaging, 300 µL of the solution containing free-floating vesicles in buffer (section 5.4.2) was transferred to an Eppendorf tube containing 700 µL phosphate buffered saline supplemented with 0.3 M sodium sulfite and 0.2 M glucose to allow the sucrose-loaded giant vesicles to sink to the bottom of the tube. After one hour, 200 µL of this GUV suspension was transferred to a visualization microscopy chamber that had previously been coated with bovine serum albumin (BSA). As a result of surface treatment with BSA and of the greater density of the sucrose-loaded vesicles, the giant vesicles were immobilized on the glass surface of the chamber, which allowed for imaging with minimal diffusion during image recording. The rest of the chamber was filled with 100 µL PBS supplemented with 0.3 M sodium sulfite and 0.2 M glucose. The vesicles were imaged within 24 hours.

5.4.5 LUV preparation and characterization

Upconverting LUVs, *i.e.* **LUV12** samples, were prepared as described before as a reference.[4f] Aliquots of chloroform stock solutions containing the liposome constituents were added together in a flask to obtain a solution with 20 µmol DMPC, 0.8 µmol DSPE-MPEG-2000, 100 nmol perylene (**2**), and 5 nmol of compound **1**. The organic solvent was removed by rotary evaporation and subsequently under high vacuum for at least 30 minutes to create a lipid film. 1.0 mL PBS buffer, optionally supplemented with 0.3 M Na_2SO_3, was added and the lipid film was hydrated by 5 cycles of freezing the flask in liquid nitrogen and thawing in warm water (50 °C). The resulting dispersion was extruded through a Whatman Nuclepore 0.2 µm polycarbonate filter at 40-50 °C at least 11 times using a mini-extruder from Avanti Polar Lipids, Inc. (Alabaster, Alabama, USA). The number of extrusions was always odd to prevent any unextruded material ending up in the final liposome sample. The extrusion filter remained colorless after extrusion, suggesting complete inclusion of the sensitizer and annihilator in the lipid bilayer. LUVs were stored in the dark at 4 °C and used within 7 days. The LUVs had an average diameter of ca. 150 nm and a polydispersity index of 0.1, as determined from dynamic light scattering measurements with a Malvern Instruments Zetasizer Nano-S machine, operating at a wavelength of 632 nm. Additionally, cryo transmission electron microscopy was performed on DMPC **LUV12** (see Figure S.IV.1) as described before.[9]

5.4.6 Upconversion emission spectroscopy

Upconversion emission spectroscopy was performed in a custom-built setup (Figure 5.5). All optical parts were connected with FC-UVxxx-2 (xxx = 200, 400, 600) optical fibers from Avantes (Apeldoorn, The Netherlands), with a diameter of 200-600 µm, respectively, and that were suitable for the UV-Vis range (200 − 800 nm). For **LUV12** samples that were deoxygenated by argon bubbling: argon was bubbled through the sample (3.0 mL) with a rate of ~2 bubbles per second for at least 30 minutes in an external ice-cooled pear-shaped flask. After this period, bubbling was stopped while maintaining the argon flow, and the sample was warmed in a water bath of approximately 40 °C for 10 minutes. Then, the sample was transferred by means of cannulation with argon pressure to a 111-OS macro fluorescence cuvette from Hellma in a CUV-UV/VIS-TC temperature-controlled cuvette holder from Avantes, while keeping the sample

under a constant flow of argon throughout the measurement. For **LUV12** samples that were deoxygenated by addition of sodium sulfite, 3.0 mL of the sample was simply transferred to the cuvette and emission spectra were recorded under air. Likewise, **GUV12** samples in sodium sulfite buffer (approximately 700 µL) were transferred to a 104F-QS or 104F-OS semi-micro cuvette from Hellma.

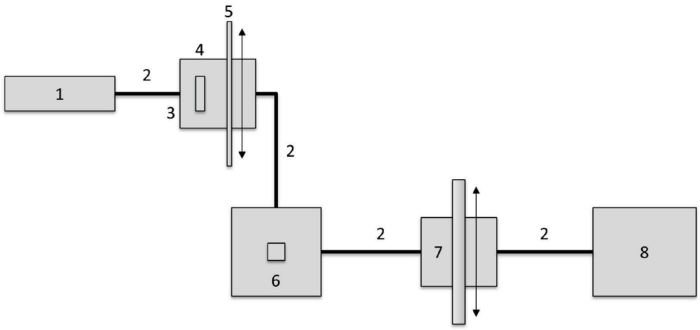

Figure 5.5. Setup used for emission measurements under red light irradiation. Legend: (1) 630 nm laser source, (2) optical fibers, (3) filter holder, (4) 630 nm band pass filter, (5) variable neutral density filter, (6) temperature controlled cuvette holder, (7) variable filter holder, and (8) CCD spectrometer.

The sample in the cuvette holder was allowed to equilibrate at 298 K for 10 minutes. The sample was irradiated from the side with a 30 mW 630 nm laser light beam from a clinical grade Diomed 630 nm PDT laser (4 mm beam, 0.24 W.cm^{-2}). The 630 nm light was filtered through an FB630-10, 630 nm band pass filter (Thorlabs, Dachau/Munich, Germany) put between the laser and the sample. The excitation power was controlled using a NDL-25C-4 variable neutral density filter (Thorlabs), and measured using a S310C thermal sensor connected to a PM100USB power meter (Thorlabs). Emission spectra were recorded at a 90° angle with respect to the excitation source using a 2048L StarLine CCD spectrometer from Avantes. To visualize the spectrum from 550 nm to 900 nm, while blocking the red excitation light, a Thorlabs NF-633 notch filter was used in a variable filter holder. To visualize the spectrum from 400 nm to 550 nm, an OD4 575 nm short pass filter (Edmund Optics, York, United Kingdom, part no. 84-709) was used. All spectra were recorded with Avasoft software from Avantes and further processed with Microsoft Office Excel 2010 and Origin Pro software. The emission spectra obtained with the two filters were stitched together at 550 nm to obtain a continuous spectrum from 400 to 900 nm. No correction was needed to seamlessly connect the spectra.

5.4.7 Power dependency measurements

Luminescence emission spectra of DMPC and DOPC **LUV-12** were recorded at various excitation powers from 1 to 40 mW so that the excitation intensity (P) was 8 to 318 mW.cm^{-2} (4 mm laser beam diameter). The samples were placed in a Hellma 101-OS macro fluorescence cuvette (2.25 mL, [lipid] = 1.0 mM) and thermally equilibrated at 298 K before measurement in the same fluorescence setup as described in Section 5.4.6. In this case, the spectrum was visualized with only a Thorlabs NF-633 notch filter in between the sample and the detector. The recorded spectra were integrated from 420 to 575 nm to obtain the integrated upconversion luminescence intensity (I_{UC}), which was then plotted in a double logarithmic plot as a function

of the excitation intensity (Figure S.IV.4). The low power (≤ 40 mW.cm^{-2}) and high power (≥ 120 mW.cm^{-2}) regimes were consistently fitted with slopes around 1 and 2, respectively, which shows the typical power dependency of TTA-UC.[1] The intersection of these straight lines represents the intensity threshold (I_{th}) at which the power dependency changes from quadratic to linear. I_{th} was found to be 50 and 59 mW.cm^{-2} for the upconversion in DMPC and DOPC **LUV-12**, respectively. Assuming no difference in power dependency between **LUV-12** and **GUV-12**, these results indicate that all microscopy images with red light excitation (P ≥ 5.2 W.cm^{-2}) were acquired in the linear power regime.

5.4.8 Microscopy imaging

Bright field and (upconversion) emission imaging was performed with a customized Zeiss Axiovert S100 TV Inverted Microscope setup (Figure 5.6), fitted with a Zeiss 100x Plan Apochromat 1.4 NA oil objective and an Orca Flash 4.0 V2 sCMOS camera from Hamamatsu, which together produced images with 65 nm pixel size. For direct perylene excitation, a CrystaLaser 50 mW 405 nm Solid State laser was used, combined with a ZT405/514/561rpc dichroic beam splitter (Chroma Technology Corporation) and ZET442/514/568m emission filter (Chroma Technology Corporation) (see Figure S.IV.5 for the transmission spectra of this set). For upconversion emission microscopy, a Diomed clinical grade 630 nm continuous wave PDT laser was used as excitation source. The light was filtered through a FB630-10 630 nm band pass filter (Thorlabs) put between the laser and the Chroma ZT405/532/635rpc dichroic beam splitter. To block everything except upconversion emission, a NF633-25 633 nm notch filter (Thorlabs) and a 575 nm short pass filter (Edmund Optics, part no. #84-709) were placed between the sample and the camera, resulting in OD >13 at 630 nm and OD>4 around 800 nm (*i.e.* at the phosphorescence emission of compound **1**). The transmission curves of the filters and dichroic mirror are displayed in Figure S.IV.5 and Figure S.IV.6. The output power of the 630 nm laser was typically 3.8 mW (39 μm spot size, 320 W.cm^{-2}) at the sample. The typical camera exposure time was 200 ms, unless otherwise specified.

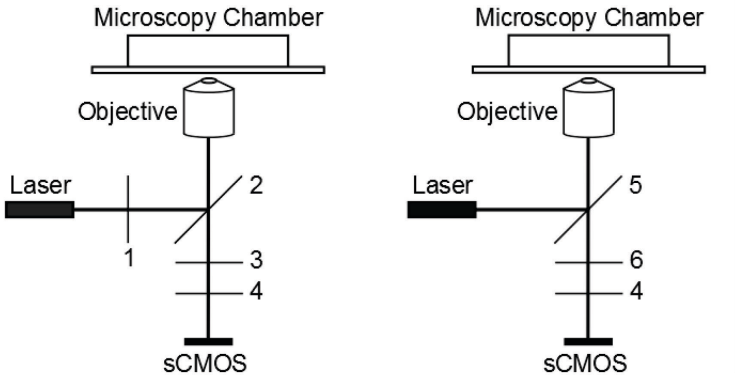

Figure 5.6. Microscopy setups used for imaging GUVs with 630 nm (left) and 405 nm (right) excitation. Legend: (1) Thorlabs FB630-10 band pass filter, (2) Chroma ZT405/532/635rpc dichroic beam splitter, (3) Edmund Optics 575 nm OD4 short pass filter, 4) Thorlabs NF633-25 notch filter, (5) Chroma ZT405/514/561rpc dichroic beam splitter, (6) Chroma ZET442/514/568 emission filter.

5.4.9 Determination of bleaching curves

Giant vesicles were first located in bright field mode and were subsequently irradiated for 60 seconds at 630 nm with either 5.2 $W.cm^{-2}$ (62 µW, laser spot size diameter 39 µm) or 320 $W.cm^{-2}$ (3.8 mW, laser spot size diameter 39 µm) illumination intensity while acquiring an image every 1.0 or 0.2 s, respectively. For each image, the pixel values (A.U.) of the brightest half of all the pixels was averaged and normalized to one. Six individual vesicles were measured per time point. The mean and standard deviation are plotted *versus* time (s) in order to obtain a bleaching curve.

5.5 References

[1] a) J. Zhou, Q. Liu, W. Feng, Y. Sun, F. Li, *Chem. Rev.* **2014**, *115*, 395-465; b) Q. Liu, W. Feng, T. Yang, T. Yi, F. Li, *Nat. Protocols* **2013**, *8*, 2033-2044.

[2] J.-H. Kim, J.-H. Kim, *J. Am. Chem. Soc.* **2012**, *134*, 17478-17481.

[3] a) T. N. Singh-Rachford, F. N. Castellano, *Coord. Chem. Rev.* **2010**, *254*, 2560-2573; b) J. Zhao, S. Ji, H. Guo, *RSC Adv.* **2011**, *1*, 937-950; c) Y. C. Simon, C. Weder, *J. Mater. Chem.* **2012**, *22*, 20817-20830; d) Y. Y. Cheng, B. Fückel, T. Khoury, R. l. G. C. R. Clady, N. J. Ekins-Daukes, M. J. Crossley, T. W. Schmidt, *J. Phys. Chem. A* **2011**, *115*, 1047-1053; e) P. Duan, N. Yanai, H. Nagatomi, N. Kimizuka, *J. Am. Chem. Soc.* **2015**, *137*, 1887-1894.

[4] a) A. Turshatov, D. Busko, S. Baluschev, T. Miteva, K. Landfester, *New J. Phys.* **2011**, *13*, 083035; b) M. Penconi, P. L. Gentili, G. Massaro, F. Elisei, F. Ortica, *Photochem. Photobiol. Sci.* **2014**, *13*, 48-61; c) Q. Liu, B. Yin, T. Yang, Y. Yang, Z. Shen, P. Yao, F. Li, *J. Am. Chem. Soc.* **2013**, *135*, 5029-5037; d) C. Wohnhaas, V. Mailänder, M. Dröge, M. A. Filatov, D. Busko, Y. Avlasevich, S. Baluschev, T. Miteva, K. Landfester, A. Turshatov, *Macromol. Biosci.* **2013**, *13*, 1422–1430; e) K. Tanaka, H. Okada, W. Ohashi, J.-H. Jeon, K. Inafuku, Y. Chujo, *Bioorg. Med. Chem.* **2013**, *21*, 2678-2681; f) S. H. C. Askes, A. Bahreman, S. Bonnet, *Angew. Chem., Int. Ed.* **2014**, *53*, 1029-1033.

[5] P. Walde, K. Cosentino, H. Engel, P. Stano, *ChemBioChem* **2010**, *11*, 848-865.

[6] H. Valkenier, N. Lopez Mora, A. Kros, A. P. Davis, *Angew. Chem., Int. Ed.* **2015**, *54*, 2137-2141.

[7] N. Lopez Mora, J. S. Hansen, Y. Gao, A. A. Ronald, R. Kieltyka, N. Malmstadt, A. Kros, *Chem. Commun.* **2014**, *50*, 1953-1955.

[8] D. Marsh, *Handbook of Lipid Bilayers*, 2nd ed., Taylor & Francis Group, LLC, Boca Raton, FL, USA, **2013**.

[9] A. Bahreman, B. Limburg, M. A. Siegler, R. Koning, A. J. Koster, S. Bonnet, *Chem. Eur. J.* **2012**, *18*, 10271-10280.

CHAPTER 6

Temperature dependence of triplet-triplet annihilation upconversion in phospholipid membranes

Understanding the temperature dependency in photon-upconverting nano-systems is important to realize optimized upconversion applications. In this chapter, the temperature dependency of red-to-blue triplet-triplet annihilation upconversion in a variety of neutral PEGylated phospholipid membranes is reported. It appears that in these systems a delicate balance between lateral diffusion rate, annihilator aggregation, and sensitizer self-quenching and thermal deactivation leads to the maximization of the upconversion intensity near the main transition temperature of the membrane.

Sven H.C. Askes, Philip Brodie, Gilles Bruylants, and Sylvestre Bonnet. Manuscript in preparation.

6.1 Introduction

Light upconversion is the generation of high-energy photons from low-energy photons, for example the conversion of red light to blue light. Generating upconverted light can be achieved through various mechanisms and in different materials, such as two-photon absorption dyes, energy upconversion processes in rare-earth doped materials or nanoparticles, and triplet-triplet annihilation (TTA-UC) in solution and solid state materials. Among these principles, TTA-UC offers many advantages: it can occur at low excitation power (in the best cases even lower than 1 $mW.cm^{-2}$), it uses sensitizers having high molar absorptivity, and the obtained upconversion quantum yields may reach up to 14% in aqueous solution.[1] Since its popularization more than a decade ago,[2] TTA-UC has been used in many applications such as photocatalysis,[3] solar energy harvesting,[4] drug delivery and activation,[5] and luminescence bio-imaging.[1a, 6]

TTA-UC is based on the photophysical interplay of photosensitizer and annihilator chromophores (see Chapter 2, Figure 2.1).[7] The photosensitizer absorbs low energy light, after which intersystem crossing leads to a long-lived triplet state. The energy of this triplet state is transferred to the annihilator upon diffusional collision by means of triplet-triplet energy transfer (TTET); a succession of TTET leads to a concentration buildup of long-lived triplet-state annihilators. Two triplet state annihilators can then perform triplet-triplet annihilation upconversion, in which one of them departs with the energy of both to reach a high-energy singlet state. Finally, this singlet excited state returns to the ground state by emission of a high-energy photon, thus realizing light upconversion. TTA-UC has been demonstrated in an extensive assortment of organic, inorganic, and/or supramolecular materials,[1c, 8] as well as in nano or micro-sized particles.[9]

Among the various applications in the field of TTA-UC, there are some that are not operated at room temperature, such as bio-imaging and phototherapy. It is thus important to understand the temperature dependency of upconversion efficiency in order to optimize the use of TTA-UC. Because TTET and TTA occur *via* molecular contact, they are highly dependent on molecular diffusion; the efficiency of TTA-UC is generally greatly influenced by the fluidity and hence thermal responsiveness of the host material.[10] For many materials, a higher temperature leads to a higher fluidity, and therefore to higher TTA-UC efficiency. For example, green-to-blue TTA-UC in a rubbery polymer matrix

was only visible above the glass transition temperature of the material, above which the matrix becomes more fluid.[11] However, diffusion is not the only important factor. First of all, temperature-dependent chemical phenomena such as dye aggregation may affect upconversion as well: counter-intuitively, it was recently shown that at lower temperatures, mixed aggregation of sensitizer and annihilator molecules in diluted conditions resulted in higher TTA-UC efficiency.[12] It has also been shown that upconversion in gel matrices decreased at higher temperatures due to temperature-dependent disassembly of the host-material.[8c] Overall, understanding the temperature-dependence of all chemical and physical properties of a given medium, is necessary for optimizing upconversion.

Our group recently demonstrated that green-to-blue and red-to-blue TTA-UC can be realized in the phospholipid membrane of neutral PEGylated liposomes composed of 1,2-dimyristoyl-sn-glycero-3-phosphocholine (DMPC). This knowledge was later used for the activation of photoactivatable chemotherapeutic agents in the photodynamic window.[5] In our initial studies it was reported that the upconversion intensity was reversibly affected by changes in temperature. [5b] Upon heating the sample from 15 to 25 °C the upconversion intensity increased significantly, which we interpreted as a consequence of the gel-to-liquid crystalline phase transition temperature (T_m) of the DMPC lipid bilayer. Upon raising the temperature above T_m the molecular diffusion of the dyes in the membrane is expected to increase greatly, which should lead to higher TTET and TTA rates, and thus higher TTA-UC efficiencies. In this work, we evaluate the general applicability of this hypothesis by systematically investigating the temperature dependency of TTA-UC in neutral PEGylated liposomes, using different lipids with different T_m.

6.2 Results and discussion

Neutral PEGylated liposome dispersions were prepared in phosphate buffered saline (PBS) by hydration and extrusion of lipid films containing five different neutral phosphatidylcholines, *i.e.* 1,2-dioleyl-*sn*-glycero-3-phosphocholine (DOPC), 1,2-dilaureyl-*sn*-glycero-3-phosphocholine (DLPC), 1,2-dimyristoyl-*sn*-glycero-3-phosphocholine (DMPC), 1,2-dipentadecanoyl-*sn*-glycero-3-phosphocholine (DPDPC), and 1,2-dipalmitoyl-*sn*-glycero-3-phosphocholine (DPPC), and in presence of 4 mol% of sodium N-(carbonyl-methoxypolyethylene glycol-2000)-1,2-distearoyl-*sn*-glycero-3-

phosphoethanolamine (DSPE-MPEG-2000, see Figure 6.1). Addition of DSPE-MPEG-2000 is a well-known strategy to prevent liposome aggregation and fusion. The lipid composition of liposome samples **O**, **L**, **M**, **PD**, and **P** is shown in Table 6.1. A well-investigated red-to-blue TTA-UC dye couple consisting of palladium tetraphenyltetrabenzoporphyrin (**1**) and perylene (**2**, see Figure 6.1) was selected for incorporation in the liposomes. Samples containing these dyes, *i.e.* **O12**, **L12**, **M12**, **PD12**, and **P12** (defined in Table 6.1), were prepared following an identical procedure. The hydrodynamic diameters (z-ave = 135 ± 5 nm) and polydispersity indices (PDI = 0.09 ± 0.02), as measured by dynamic light scattering (DLS), were found to be very similar regardless of the lipid type or dye functionalization.

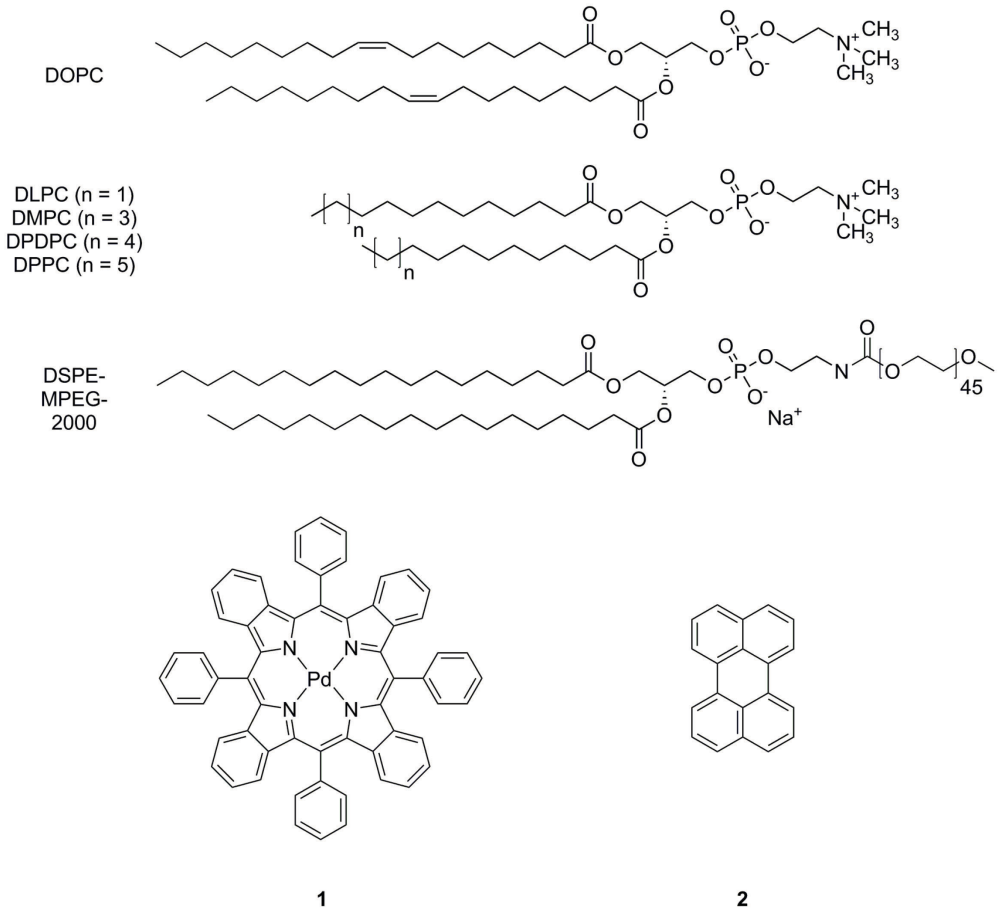

*Figure 6.1. Chemical structures of DOPC, DLPC, DMPC, DPDPC, DPPC, DSPE-MPEG-2000, palladium tetraphenyltetrabenzoporphyrin (**1**), and perylene (**2**).*

Table 6.1. Lipid formulations of the PEGylated phosphatidylcholine liposomes used in this work, and their physical characterization by dynamic light scattering (with z-ave as hydrodynamic diameter and PDI as polydispersity index) and differential scanning calorimetry. DSC measurements were performed with a scanning rate of 1 °C.min^{-1} at 3 atm. pressure.

Sample	Lipid[a]	[1] (μM)	[2] (μM)	z-ave (nm)	PDI	T_m (lit. value)[13] (°C)[b]	ΔH (lit. value)[13] (kJ.mol^{-1})[b]
O	DOPC			139	0.11	- (−18.2)	- (35.5)
O1	DOPC	2.5					
O1'	DOPC	25					
O2	DOPC		25				
O12	DOPC	2.5	25	135	0.11	-	-
L	DLPC			127	0.11	- (−2.1)	- (7.5)
L12	DLPC	2.5	25	134	0.12	-	-
M	DMPC			132	0.07	25.0 (23.9)	27.7 (29.3)
M1	DMPC	2.5					
M2	DMPC		25				
M12	DMPC	2.5	25	134	0.09	24.9	26.6
PD	DPDPC			132	0.09	34.9 (34.7)	33.6 (32.7)
PD12	DPDPC	2.5	25	140	0.07	34.6	32.0
P	DPPC			140	0.08	42.4 (41.4)	40.1 (36.8)
P12	DPPC	2.5	25	137	0.11	42.1	38.7

[a] All liposomes were prepared with 5.0 mM lipid and 0.20 mM DSPE-mPEG-2000.[b] T_m is defined as the main transition temperature of the bilayer, and ΔH as the molar enthalpy change of the phase transition (the enthalpy change of the pretransition is included, in case there is one). Literature T_m and ΔH values given for the pure phospholipids.

It is well known that phase changes of phospholipid membranes greatly influence the two-dimensional translational molecular diffusion coefficient (D_T in μm^2.s^{-1}) of membrane solutes. Therefore, the gel-to-liquid phase transition temperature (T_m) and the total enthalpy change of the phase transition (ΔH) were measured for samples based on DMPC, DPDPC, and DPPC using differential scanning calorimetry (DSC, see Table 6.1 and Figure 6.2b). T_m and ΔH for dye-free PEGylated liposomes **M**, **PD**, and **P** were found to be very close to literature values for PEG-free liposomes, *i.e.* the PEG groups do not significantly influence the phase transition at these concentrations. Upon functionalization of the PEGylated liposomes with compounds **1** and **2**, a small decrease in the main transition peak height was observed, but the main features of the thermogram remained. These results indicate that for liposome samples **M12**, **PD12**, and **P12**, compounds **1** and **2** were indeed buried in the lipid bilayer, and that their presence only minimally perturbed the physical properties of the membranes. No transitions were found between 5 and 50 °C for samples **O**, **O12**, **L**, and **L12**, because T_m for pure DOPC and DLPC are reported to be below the freezing point of water.[13]

Next, UV-vis absorption and emission spectroscopy was performed on samples **O12**, **L12**, **M12**, **PD12**, and **P12** at 20 °C in presence of 0.3 M sodium

sulfite for chemical deoxygenation, see Figure 6.2.[5a, 14] The absorption spectra show the superposition of the characteristic peaks of **1** at 440 and 630 nm and the vibronically structured band of **2** from 350 – 450 nm.[5b] Upon irradiation with 630 nm laser light (10 mW, 80 mW.cm^{-2}), phosphorescence of **1** at 800 nm and upconversion emission of **2** at 474 nm were observed for each sample. The emission stability at 20 °C was tested for each formulation by continuously irradiating for one hour and collecting emission spectra. All samples exhibited good emission stability during this period, see Figure S.V.1.

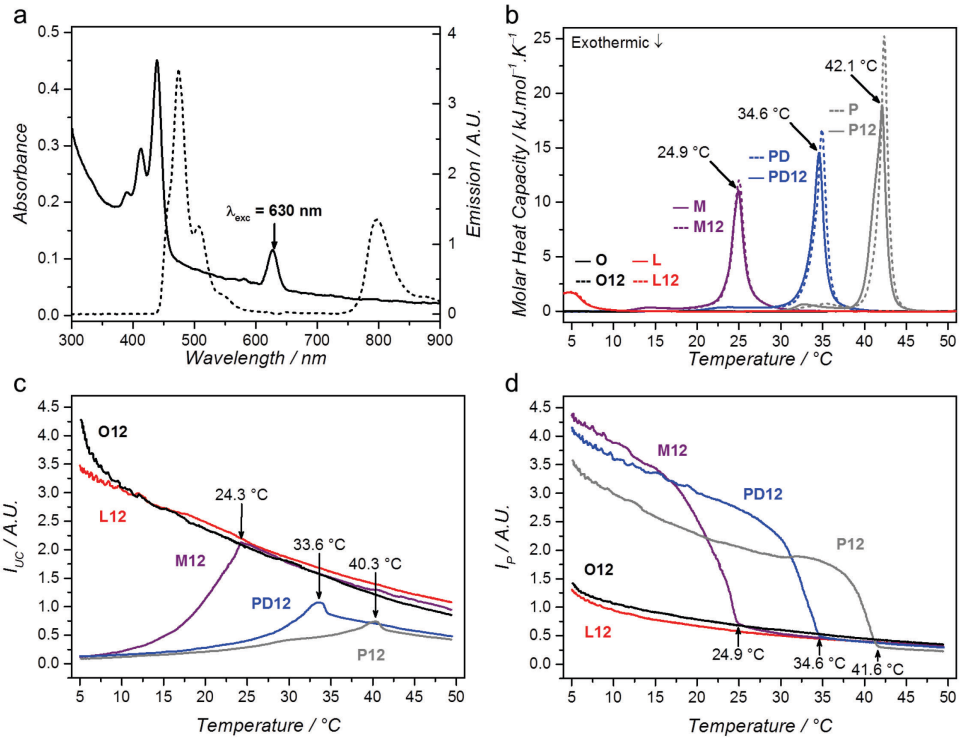

*Figure 6.2. (Photo)physical characterization of upconverting liposomes. a) Typical absorption (solid, left axis) and emission spectrum (dashed, right axis, λ_{exc} = 630 nm, intensity 80 mW.cm^{-2}) of **L12** liposomes ([DLPC] = 1.0 mM) at 20 °C in 0.3 M sodium sulfite PBS under air. b) Differential scanning calorimetry thermograms between 5 °C and 50 °C of liposomes with TTA-UC dyes (**O12**, **L12**, **M12**, **PD12**, and **P12**, solid) or without (**O**, **L**, **M**, **PD**, **P**, dashed). Arrows indicate T_m of the dyed liposomes, where applicable. Measurements were performed in heating mode with a scanning rate of 1 °C.min^{-1} at 3 atm. pressure. c & d) Temperature evolution of the upconversion intensity at 474 nm (c) and of the phosphorescence intensity (d) of **O12**, **L12**, **M12**, **PD12**, and **P12**. Samples were heated from 5 °C to 50 °C at a rate of 0.3 °C.min^{-1} while continuously irradiated with 80 mW.cm^{-2} 630 nm light.*

To investigate the temperature dependency of TTA-UC in **O12**, **L12**, **M12**, **PD12**, and **P12**, these samples were heated from 5 °C to 50 °C at a rate of 0.3

°C.min^{-1} while stirring, and upconversion spectra were continuously recorded. A submerged thermocouple registered the accurate temperature inside the solution. Figure 6.2 shows the evolution of the luminescence intensities at 800 nm (I_P) and 474 nm (I_{UC}) *vs.* temperature for each liposome formulation. For **O12** and **L12**, both phosphorescence and upconversion intensity gradually decreased with increasing temperature. For **M12**, **PD12**, and **P12**, I_{UC} increased up to 25, 35, and 42 °C, respectively, and then decreased gradually, whereas I_P decreased steeply up to 25, 35, and 42 °C, respectively, and then continued to decrease, but less steeply. When the samples were brought back from 50 °C to 5 °C, the initial emission spectra at 5 °C were obtained again in all cases except for **O12**, showing that bleaching did not occur and that the thermo-photophysical evolution is reversible (Figure S.V.2). For **O12**, we attribute this relative instability to the presence of the unsaturated bond, which might participate in undesired photochemical reactions. Interestingly, for **M12**, **PD12**, and **P12**, the temperature values at which I_{UC} maximizes and I_P kinks are very close to the phase transition temperature of the bilayer (T_m) recorded with DSC.

The increase of I_{UC} when approaching T_m is easily explained: heating the liposomes above T_m greatly increases the membrane fluidity and thus increases the lateral diffusion coefficient (D_T) of membrane dyes, which in turn causes an increase in TTA-UC efficiency. For instance, the D_T for fluorescent probes in DMPC lipid bilayers has reported to increase from 0.01 μm^2.s^{-1} at 15 °C, to 6 μm^2.s^{-1} at 30 °C to 13 μm^2.s^{-1} at 50 °C.[13, 15] It is worth mentioning that for such DMPC bilayers, the foremost change in D_T (a three-order increase in magnitude) was found between 20 and 25 °C, and so the most considerable transition in TTA-UC efficiency was expected to occur in this temperature domain. This is indeed in accordance with our data for **M12**.[15] In absence of accurate literature data of D_T in DPDPC and DPPC across the full temperature range, we assume that the same explanation holds for the results obtained with **PD12** and **P12**. However, this rationale is clearly no longer valid above T_m: although D_T continues to increase (*vide supra*), I_{UC} decreased. Furthermore, for **O12** and **L12**, in absence of a phase transition between 5 and 50 °C, I_{UC} and I_P both decrease across the whole temperature range. It is thus clear that other photophysical phenomena must play a role in the temperature dependence of TTA-UC in lipid bilayers.

Therefore, the thermo-photophysical behavior of the isolated dyes was considered in DOPC, DMPC, and in toluene (Figure 6.3). First, the fluorescence

intensity of compound **2** (λ_{exc} = 420 nm, λ_{em} = 474 nm) was found to decrease by 10% in both DOPC liposomes and toluene when heated from 5 °C to 50 °C. This is most likely explained by a slightly increased thermal deactivation. In DMPC, the fluorescence intensity increased by 25% when heated from 5 °C to 30 °C, with the most sharp increase around 25 °C, and then decreased slightly again up to 50 °C. This observation is in agreement with the work of Khan *et al.* who reported that perylene tends to form staggered aggregates in the tightly packed gel membrane below T_m, which break apart in the more loosely packed liquid-crystalline state above T_m.[16] Since the fluorescence intensity is lower in presence of such aggregates, the TTA-UC efficiency is lower below T_m. Overall, dissociation of perylene aggregates gives an additional explanation for the increase of upconversion intensity up to T_m.

Secondly, the phosphorescence intensity of **1** (λ_{exc} = 630 nm, λ_{em} = 800 nm) was investigated under deoxygenated conditions. In toluene solution, roughly 50% of the phosphorescence intensity is lost upon going from 5 °C to 50 °C due to increased thermal deactivation. When the dye was inserted into DOPC or DMPC liposomes (**O1** and **M1**, respectively) about 70% phosphorescence intensity was lost upon going from 5 °C to 50 °C; the additional 20% loss of phosphorescence intensity with respect to the toluene sample may be due to increased dynamic self-quenching, because the molecules are much more confined in the lipid bilayer. The explanation of self-quenching is supported by the fact that for **M1**, the highest loss of phosphorescence is observed around the transition temperature, at which the fluidity of the membrane increases most rapidly and diffusion-based processes such as self-quenching are expected to have an increased effect. Overall, these results explain that the decrease of TTA-UC with rising temperature is most likely due to increased thermal deactivation and self-quenching of **1**.

Based on these data, we explain the typical maximization of I_{UC} around T_m in lipid bilayers that have a transition temperature between 5 and 50 °C as follows. On the one hand, the increase in photosensitizer quenching as a function of temperature is rather linear (Figure 6.3). On the other hand, the temperature dependence of D_T has been described in literature as sigmoidal, with three-orders of magnitude increase when approaching T_m, and flattening directly after T_m.[15] In other words, upon approaching T_m the membrane becomes fluid rather quickly, but once it reaches the liquid crystalline state the fluidity changes negligibly. Therefore, above T_m the effect of the only minor increase in lateral diffusion coefficient on the upconversion efficiency is

completely outcompeted by the increased quenching of the photosensitizer. Furthermore, the dissociation of annihilator aggregates results in a rather abrupt and significant increase in fluorescence around T_m as well (Figure 6.3a). It is thus concluded that the combination of these three temperature-dependent phenomena results in the maxima that were observed in the I_{UC} *versus* temperature curve at 24, 34, and 40 °C for samples **M12**, **PD12**, and **P12**, respectively (Figure 6.2c).

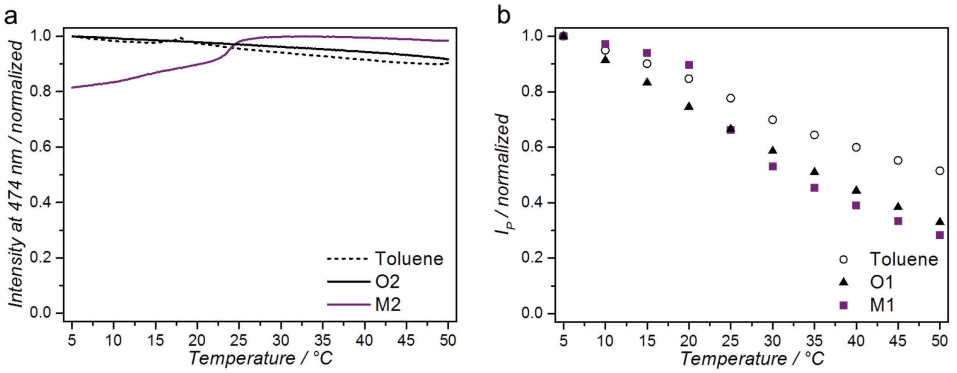

*Figure 6.3. Temperature-dependent emission spectroscopy of compounds **2** or **1** in toluene, DMPC liposomes, or DOPC liposomes. a) Normalized fluorescence intensity at 474 nm of compound **2** in toluene (dashed, 20 μM), **M2** liposomes (purple, [DMPC] = 1 mM), or **O2** liposomes (black, [DOPC] = 1 mM) as a function of temperature. λ_{exc} = 420 nm, 0.7 mW (6 mW.cm^{-2}). b) Temperature variation of the normalized phosphorescence intensity at 800 nm in 5 °C intervals for compound **1** in toluene under argon (open circles) and for liposomes **O1** (black triangles, [DOPC] = 1 mM) or **M1** (purple squares, [DMPC] = 1 mM) prepared in PBS with 0.3 M sodium sulfite. λ_{exc} = 630 nm, 10 mW (80 mW.cm^{-2}).*

Finally, for the biological application of these upconverting liposomes in bio-imaging or phototherapy, it would be beneficial to achieve the highest upconversion intensity at human body temperature (37 °C). From our results, it is evident that the systems **O12**, **L12**, and **M12** achieve identical upconversion intensities at 37 °C, while **PD12** and **P12** exhibit inferior intensities. We cannot offer any explanation why I_{UC} is lower in **PD12** and **P12**. Altogether, the results suggest that even though I_{UC} maximizes around T_m (for **M12**, **PD12**, and **P12**), choosing a lipid with a T_m near 37 °C does not result in an optimized upconverting liposome formulation. Finally, considering that little has been reported about the biocompatibility of DLPC,[I] we conclude that

[I] In preliminary experiments, A549 lung carcinoma cells were incubated with **L12** liposomes ([DLPC] = 0.5 mM) for 4 h, which resulted in 100% cell death (data not shown).

O12 and **M12** upconverting liposomes are the most promising for biological applications.

6.3 Conclusion

The temperature dependence of red-to-blue TTA-UC was studied in PEGylated liposomes with PC lipids with different lipophilic chain lengths and transition temperatures, and it was found that the upconversion intensity maximizes around T_m. Three major effects contribute to this temperature dependency: (1) an increase in lipid bilayer fluidity above T_m results in higher diffusion rates and thus higher rates of TTET and TTA, (2) dissociation of perylene aggregates when approaching T_m results in higher annihilator emission intensity, and (3) higher thermal deactivation and self-quenching rates of the photosensitizer at higher temperatures lead to a lower TTET rate and lower upconversion intensity beyond T_m. Measuring the point at which I_{UC} maximizes may be exploited for probing the transition temperature of phospholipid membranes. Furthermore, for TTA-UC applications that require high performance at elevated temperatures, the results underline the importance of selecting photosensitizers that are minimally affected by temperature. Finally, all liposome formulations were efficient in upconversion at biological temperature, which underlines that liposomes are versatile platforms for upconversion bio-imaging and photopharmaceutical applications. The phospholipid can be freely chosen to further optimize the liposomal formulation in terms of medium stability, biocompatibility, clearance from the bloodstream, and surface functionalization.

6.4 Experimental

6.4.1 General

Palladium tetraphenyltetrabenzoporphyrin (**1**) was purchased from Bio-Connect (Huissen, The Netherlands). Perylene (**2**) was purchased from Sigma-Aldrich Chemie BV (Zwijndrecht, The Netherlands). All lipids were purchased from either Lipoid GmbH (Ludwigshafen, Germany) or Avanti Polar Lipids (Alabaster, AL, USA) and stored at −18 °C. Dulbecco's phosphate buffered saline (DPBS) was purchased from Sigma Aldrich and had a formulation of 8 $g.L^{-1}$ NaCl, 0.2 $g.L^{-1}$ KCl, 0.2 $g.L^{-1}$ KH_2PO_4, and 1.15 $g.L^{-1}$ K_2HPO_4 with a *pH* of 7.1 − 7.5.

6.4.2 Liposome assembly

All liposome formulations were prepared by the classical hydration-extrusion method. As an example, the preparation of **O12** is described here. Aliquots of chloroform stock solutions containing the liposome constituents were added together in a flask to obtain a solution with 5.0 µmol DOPC, 0.20 µmol DSPE-MPEG-2000, 2.5 nmol compound **1**, and 25 nmol compound **2**. The organic solvent was removed by rotary evaporation and subsequently under high vacuum

for at least 30 minutes to create a lipid film. 1.0 mL DPBS buffer, with or without 0.3 M sodium sulfite, was added and the lipid film was hydrated by 4 cycles of freezing the flask in liquid nitrogen and thawing in warm water (50 °C). The resulting dispersion was extruded through a Whatman Nuclepore 0.2 μm polycarbonate filter at 40 − 50 °C at least 11 times using a mini-extruder from Avanti Polar Lipids, Inc. (Alabaster, Alabama, USA). The number of extrusions was always odd to prevent any unextruded material ending up in the final liposome sample. The extrusion filter remained practically colorless after extrusion, suggesting near-complete inclusion of the chromophoric compounds in the lipid bilayer. Liposomes were stored in the dark at 4 °C and used within 7 days. The average liposome size and polydispersity index were measured with a Malvern Instruments Zetasizer Nano-S machine, operating with a wavelength of 632 nm.

6.4.3 Differential Scanning Calorimetry

Differential scanning calorimetry (DSC) was performed on a TA Instruments (DE, USA) nano-DSC III instrument in the range of 5 °C to 50 °C with a scanning rate of 1 °C.min^{-1} at 3 atm. The capillary cell (V = 300 μL) was filled with the liposome solution (lipid bulk concentration of 5 mM), and the reference cell was filled with PBS buffer solution. A blank measurement was performed with PBS buffer. The liposome dispersions were degassed for 10 − 15 minutes prior to measurement on a Nalgene degassing station. For each sample, at least two cycles of heating and cooling were performed with 10 minutes of thermal equilibration between the ramps. The machine was cleaned beforehand with 50% formic acid and rinsed thoroughly with Milli-Q water. The thermograms were processed and analyzed using NanoAnalyze software from TA Instruments.

6.4.4 Absorption and emission spectroscopy

Absorption and emission spectroscopy was conducted in a custom-built setup (Figure S.V.3). All optical parts were connected with FC-UVxxx-2 (xxx = 200, 400, 600) optical fibers from Avantes (Apeldoorn, The Netherlands), with a diameter of 200-600 μm, respectively, and that were suitable for the UV-Vis range (200-800 nm). Typically, 2.25 mL of sample was placed in a 111-OS macro fluorescence cuvette from Hellma in a CUV-UV/VIS-TC temperature-controlled cuvette holder with stirring from Avantes. Deoxygenated toluene samples were prepared in a glovebox in a sealed fluorescence cuvette. The cuvette holder temperature was controlled with a TC-125 controller and T-app computer software from Quantum Northwest (Liberty Lake, WA, USA), while the sample temperature was measured with an Omega RDXL4SD thermometer with a K-type probe submerged in the sample. The sample was excited with a collimated 630 nm laser light beam (4 mm beam diameter) from a Diomed 630 nm PDT laser. The 630 nm light was filtered through a FB630-10, 630 nm band pass filter (Thorlabs, Dachau/Munich, Germany) put between the laser and the sample. The excitation power was controlled using the laser control in combination with a NDL-25C-4 variable neutral density filter (Thorlabs), and measured using a S310C thermal sensor connected to a PM100USB power meter (Thorlabs). For regular measurements, the excitation power was set at a power of 10 mW (80 mW.cm^{-2}). UV-Vis absorption spectra were measured using an Avalight-DHc halogen-deuterium lamp (Avantes) as light source and a 2048L StarLine spectrometer (Avantes) as detector, both connected to the cuvette holder at a 180° angle and both at a 90° angle with respect to the red laser irradiation direction. The filter holder between cuvette holder and detector was in a position without a filter (Figure S.V.3, item 8). Luminescence emission spectra were measured using the same detector but with the UV-Vis light source switched off. To visualize the spectrum

from 450 nm to 900 nm, while blocking the red excitation light, a Thorlabs NF-633 notch filter was used in the variable filter holder. All spectra were recorded with Avasoft software from Avantes and further processed with Microsoft Office Excel 2010 and Origin Pro software. Temperature dependent luminescence experiments were done with continuous irradiation and temperature ramping, except for phosphorescence measurements of compound **1** to prevent bleaching during the experiment. Instead, spectra were taken every 5 °C with 10 min thermal equilibration between temperature points.

6.5 References

[1] a) Q. Liu, W. Feng, T. Yang, T. Yi, F. Li, *Nat. Protocols* **2013**, *8*, 2033-2044; b) J.-H. Kim, J.-H. Kim, *J. Am. Chem. Soc.* **2012**, *134*, 17478-17481; c) P. Mahato, A. Monguzzi, N. Yanai, T. Yamada, N. Kimizuka, *Nat. Mater.* **2015**, *14*, 924-930.

[2] a) R. R. Islangulov, D. V. Kozlov, F. N. Castellano, *Chem. Commun.* **2005**, 3776-3778; b) S. Baluschev, T. Miteva, V. Yakutkin, G. Nelles, A. Yasuda, G. Wegner, *Phys. Rev. Lett.* **2006**, *97*, 143903.

[3] a) M. Majek, U. Faltermeier, B. Dick, R. Pérez-Ruiz, A. Jacobi von Wangelin, *Chem. Eur. J.* **2015**, *21*, 15496-15501; b) O. S. Kwon, J. H. Kim, J. K. Cho, J. H. Kim, *ACS Appl. Mater. Interfaces* **2015**, *7*, 318-325.

[4] a) A. Monguzzi, S. M. Borisov, J. Pedrini, I. Klimant, M. Salvalaggio, P. Biagini, F. Melchiorre, C. Lelii, F. Meinardi, *Adv. Funct. Mater.* **2015**, *25*, 5617-5624; b) A. Nattestad, C. Simpson, T. Clarke, R. W. MacQueen, Y. Y. Cheng, A. Trevitt, A. J. Mozer, P. Wagner, T. W. Schmidt, *Phys. Chem. Chem. Phys.* **2015**; c) S. P. Hill, T. Banerjee, T. Dilbeck, K. Hanson, *J. Phys. Chem. Lett.* **2015**, *6*, 4510-4517; d) A. Nattestad, Y. Y. Cheng, R. W. MacQueen, T. F. Schulze, F. W. Thompson, A. J. Mozer, B. Fückel, T. Khoury, M. J. Crossley, K. Lips, G. G. Wallace, T. W. Schmidt, *J. Phys. Chem. Lett.* **2013**, *4*, 2073-2078.

[5] a) S. H. C. Askes, M. Kloz, G. Bruylants, J. T. Kennis, S. Bonnet, *Phys. Chem. Chem. Phys.* **2015**, *17*, 27380-27390; b) S. H. C. Askes, A. Bahreman, S. Bonnet, *Angew. Chem., Int. Ed.* **2014**, *53*, 1029-1033.

[6] a) A. Nagai, J. B. Miller, P. Kos, S. Elkassih, H. Xiong, D. J. Siegwart, *ACS Biomater. Sci. Eng.* **2015**, *1*, 1206-1210; b) C. Wohnhaas, V. Mailänder, M. Dröge, M. A. Filatov, D. Busko, Y. Avlasevich, S. Baluschev, T. Miteva, K. Landfester, A. Turshatov, *Macromol. Biosci.* **2013**, *13*, 1422–1430; c) Q. Liu, B. Yin, T. Yang, Y. Yang, Z. Shen, P. Yao, F. Li, *J. Am. Chem. Soc.* **2013**, *135*, 5029-5037; d) O. S. Kwon, H. S. Song, J. Conde, H.-i. Kim, N. Artzi, J.-H. Kim, *ACS Nano* **2016**, *10*, 1512-1521.

[7] a) J. Zhou, Q. Liu, W. Feng, Y. Sun, F. Li, *Chem. Rev.* **2014**, *115*, 395-465; b) T. N. Singh-Rachford, F. N. Castellano, *Coord. Chem. Rev.* **2010**, *254*, 2560-2573.

[8] a) S. Hisamitsu, N. Yanai, N. Kimizuka, *Angew. Chem. Int. Ed.* **2015**, *54*, 11550-11554; b) S. H. Lee, D. C. Thévenaz, C. Weder, Y. C. Simon, *J. Polym. Sci., Part A: Polym. Chem.* **2015**, *53*, 1629-1639; c) P. Duan, N. Yanai, H. Nagatomi, N. Kimizuka, *J. Am. Chem. Soc.* **2015**, *137*, 1887-1894; d) P. Duan, N. Yanai, N. Kimizuka, *J. Am. Chem. Soc.* **2013**, *135*, 19056–19059; e) A. J. Svagan, D. Busko, Y. Avlasevich, G. Glasser, S. Baluschev, K. Landfester, *ACS Nano* **2014**, *8*, 8198-8207.

[9] a) J.-H. Kim, J.-H. Kim, *ACS Photonics* **2015**, *2*, 633-638; b) Z. Huang, X. Li, M. Mahboub, K. Hanson, V. Nichols, H. Le, M. L. Tang, C. J. Bardeen, *Nano Lett.* **2015**, *15*, 5552-5557.

[10] a) Y. C. Simon, C. Weder, *J. Mater. Chem.* **2012**, *22*, 20817-20830; b) A. Monguzzi, M. Mauri, A. Bianchi, M. K. Dibbanti, R. Simonutti, F. Meinardi, *J. Phys. Chem. C* **2016**, *120*, 2609-2614.

[11] T. N. Singh-Rachford, J. Lott, C. Weder, F. N. Castellano, *J. Am. Chem. Soc.* **2009**, *131*, 12007-12014.

[12] G. Massaro, J. Hernando, D. Ruiz-Molina, C. Roscini, L. Latterini, *Chem. Mater.* **2016**.

[13] D. Marsh, *Handbook of Lipid Bilayers*, 2nd ed., Taylor & Francis Group, LLC, Boca Raton, FL, USA, **2013**.
[14] a) M. Penconi, P. L. Gentili, G. Massaro, F. Elisei, F. Ortica, *Photochem. Photobiol. Sci.* **2014**, *13*, 48-61; b) S. H. C. Askes, N. Lopez Mora, R. Harkes, R. I. Koning, B. Koster, T. Schmidt, A. Kros, S. Bonnet, *Chem. Commun.* **2015**, *51*, 9137-9140.
[15] C.-H. Chang, H. Takeuchi, T. Ito, K. Machida, S.-i. Ohnishi, *J. Biochem.* **1981**, *90*, 997-1004.
[16] T. K. Khan, P. L.-G. Chong, *Biophys. J.* **2000**, *78*, 1390-1399.

CHAPTER 7

Synthesis and in-vitro application of upconverting silica-coated liposomes

Light upconversion by triplet-triplet annihilation (TTA-UC) in nanoparticles has received considerable research attention for bio-imaging and light activation of prodrugs. However, the mechanism of TTA-UC is inherently sensitive for quenching by molecular oxygen. A potential oxygen protection strategy is the coating of TTA-UC nanoparticles with a layer of oxygen impermeable material. In this work, we explore if (organo)silica can fulfill this role. Three synthesis routes are described for obtaining monodispersed (organo)silica-coated red-to-blue upconverting liposomes; their upconversion properties are investigated in solution and in A549 lung carcinoma cells. Although it was found that the silica offered no protection from oxygen in solution and after uptake in A549 cancer cells, upon drying of the silica-coated liposome dispersion in an excess of (organo)silica precursor, interesting liposome-silica nanocomposite materials were obtained that were capable of generating light upconversion in air.

Sven H. C. Askes, Vincent Leeuwenburgh, Wim Pomp, Stefania Grecea, Thomas Schmidt, and Sylvestre Bonnet. Manuscript in preparation.

7.1 Introduction

Photon upconversion is defined as the generation of high energy light (*e.g.* blue) from low energy light (*e.g.* red). Among the wide variety of applications, light upconversion has received substantial interest in upconversion bio-imaging and as method to shift the activation wavelength of photoactivatable anticancer prodrugs towards the phototherapeutic window.[1] One mechanism of light upconversion is triplet-triplet annihilation upconversion (TTA-UC), which is based on the photophysical interplay of photosensitizer and annihilator chromophores (see Chapter 2, Figure 2.1).[2] The photosensitizer absorbs low energy light, after which a long lived triplet excited state is reached *via* intersystem crossing. The energy of this triplet state is transferred to the annihilator upon diffusional collision by means of triplet-triplet energy transfer (TTET); a succession of TTET leads to a buildup of long lived triplet state annihilators. Two triplet state annihilators can then perform triplet-triplet annihilation upconversion, in which one of them departs with all the energy and reaches a high energy singlet excited state. Finally, this singlet excited state returns to the ground state by fluorescent emission of a high energy photon, realizing light upconversion. TTA-UC has been demonstrated in an extensive assortment of organic, inorganic, and/or supramolecular materials,[3] as well as in nano- or micro-sized particles,[4] and has been used for applications in photocatalysis,[5] solar energy harvesting,[6] drug delivery and activation,[1a, 1b] and bio-imaging.[7]

Evidently, for biological application of TTA-UC, supramolecular assemblies are required to co-localize photosensitizer and annihilator. Furthermore, for the biological application in anticancer applications, such an assembly is required to support efficient TTA-UC, have selective uptake in tumors, and cause minimal toxicity for healthy tissues. Meanwhile, liposomes functionalized with PEGylated lipids have emerged since decades as supramolecular tools in drug delivery. Liposomes have high biocompatibility and low toxicity, and accumulate selectively in tumors because of the enhanced permeability and retention effect (EPR).[8] Our group recently combined liposomes with TTA-UC: red-to-blue upconversion was demonstrated in the lipid bilayer of neutral PEGylated DMPC (1,2-dimyristoyl-*sn*-glycero-3-phosphocholine) liposomes.[1a, 1b] These upconverting liposomes were further functionalized with a blue-light activatable Ru(II) polypyridyl complex. Upon red light irradiation of this combined system, the upconverted light was efficiently transferred to the Ru-complex *via* FRET, which triggered the release of the photoactivated

compound. This mechanism may be exploited in photoactivated cancer therapy to release a cytotoxic compound in tumors.

However, no upconversion could be observed in air, because molecular oxygen quenches the triplet states of sensitizer and annihilator. In other words, the upconverting drug carrier did not function in oxygen-rich conditions, and the use of this system *in vitro* would lead to unreliable performance, because oxygen concentrations vary drastically in the complex microenvironment of a tumor.[9] Oxygen sensitivity can be reduced by developing upconversion systems that either (i) feature very fast TTA UC so that upconversion takes place on a shorter timescale than physical quenching by molecular oxygen, (ii) have built-in functionality for the consumption of molecular oxygen to create a locally oxygen-depleted microenvironment, or (iii) are protected by a nanoscale oxygen-impenetrable barrier. Most noteworthy examples of the latter strategy include upconverting oil-core nanocapsules embedded in an oxygen protective cellulose material or polyvinyl alcohol nanofibers,[3f, 10] and upconversion in hyperbrached unsaturated polyphosphoesters.[11] However, there are no examples yet where a nanoscale oxygen-barrier is used to protect TTA-UC in a drug delivery system. In this work, we attempt to coat upconverting liposomes with (organo)silica[I] as potential oxygen barrier and investigate the oxygen protection potential of such a silica barrier.

Using silica has several advantages. First of all, silica has been widely recognized as a chemically inert, biocompatible, *pH* insensitive, and transparent material.[12] Secondly, the silica surface can be modified to attach molecules such as PEG, biotin, or Ru(II)-complexes.[13] Finally, it has been demonstrated that nm-thick silica layers can act as an oxygen barrier in silica-coated polymer films,[14] and it has been suggested that silica protects oxygen-sensitive chromophores such as $[Ru(bpy)_3]^{2+}$ and $[Ru(phen)_3]^{2+}$ in doped silica nanoparticles.[15] Silica-coating of liposomes has been described before;[16] for example, Bégu *et al*. described the application of a silica-coating to DPPC liposomes (1,2-dipalmitoyl-*sn*-glycero-3-phosphocholine) by sequential hydrolysis and condensation of tetraethylorthosilicate (TEOS) as silica precursor.[16a, 16b, 17] It was suggested that the deposition of silica on the membrane was controlled by hydrogen-bonding interactions between the

[I] Organosilica is defined as silica containing organic groups as integral part of its structure

phosphate groups of the lipids, interfacial water, and silanol groups of the silica. Furthermore, nitrogen adsorption isotherms suggested that the dried particles were non-porous. However, most of the published articles do not explicitly discuss whether the particles are stable and monodispersed in aqueous buffer, which is a important criterion for a drug delivery device.

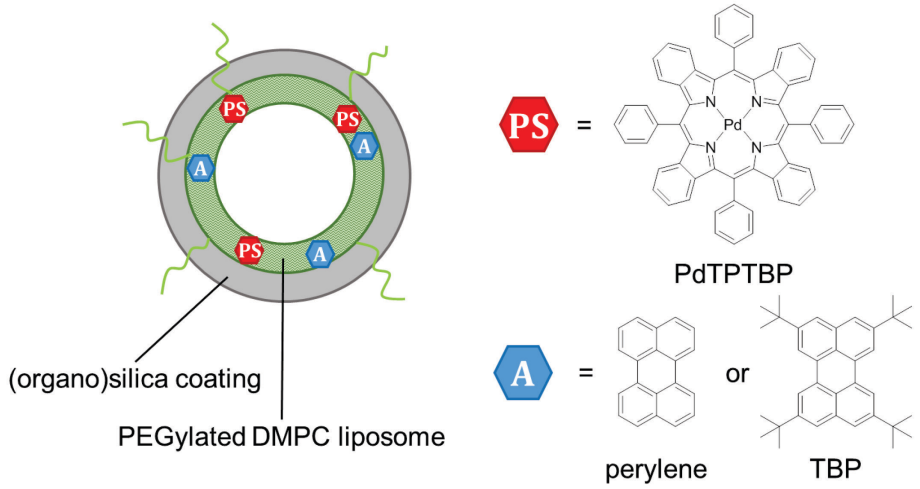

*Figure 7.1. Schematic representation of (organo)silica-coated liposomes containing photosensitizer (PS; PdTPTBP) and annihilator chromophores (A; perylene or TBP). PdTPTBP = palladium tetraphenyltetrabenzoporphyrin, TBP = 3,5,8,11-tetra(*tert*-butyl)perylene*

This chapter describes three synthetic routes for obtaining monodispersed (organo)silica-coated DMPC liposomes containing a red-to-blue upconverting couple, *i.e.* palladium tetraphenyltetrabenzoporphyrin (PdTPTBP) and perylene (Figure 7.1). In a second step, the upconverting properties of silica-coated liposomes are investigated in order to assess whether silica can act as an oxygen-barrier to allow upconversion in air. Furthermore, the uptake of these particles and their ability to perform upconversion *in vitro* will be evaluated. Finally, the silica-coated liposomes are dried in presence of an excess of (organo)silica precursor and the upconversion properties of the resulting nanocomposite materials are investigated.

7.2 Results and Discussion

7.2.1 Preparation of upconverting liposomes

Preliminary attempts to reproduce the work of Bégu *et al.*, who described the synthesis of silica-coated liposomes based on direct addition of tetraethylorthosilicate (TEOS) to non-PEGylated DPPC liposomes were

unsuccessful.[16b] In our hands, these experiments inevitably led to the formation of silica nanoparticles, gelation of the reaction mixture, and/or aggregation of the silica-coated liposomes. Also, silica-coating experiments with 1,2-dilauroyl-sn-glycero-3-phosphocholine (DLPC) liposomes were unsuccessful. Therefore, only DMPC-based liposomes were further considered for preparing silica-coated liposomes. Three synthetic routes, called methods A, B, and C, were developed to apply an (organo)silica-coating to upconverting DMPC liposomes and obtain monodispersed particles (Figure 7.2).

First of all, upconverting DMPC liposomes (from now on called **UL**) were prepared according to a literature procedure.[1a] Briefly, a mixture of 5 mM 1,2-dimyristoyl-sn-glycero-3-phosphocholine (DMPC), 4 mol% sodium N-(carbonyl-methoxypolyethylene glycol-2000)-1,2-distearoyl-*sn*-glycero-3-phosphoethanolamine (DSPE-mPEG-2000) was used to prepare liposomes *via* a hydration-extrusion method in phosphate buffered saline (PBS). A red-to-blue upconverting TTA-UC couple was selected for incorporation in the liposomes, consisting of palladium(II) tetraphenyltetrabenzoporphyrin (PdTPTBP, 0.05 mol%) and perylene (0.5 mol%). Dynamic light scattering (DLS) measurements reported a reproducible average hydrodynamic diameter (z-ave) of around 150 nm and a polydispersity index (PDI) of 0.1 (Table 7.1). The UV-vis absorption spectrum (Figure 7.3) of **UL** shows the characteristic absorption peaks of perylene (390, 414, 440 nm) and PdTPTBP (440, 630 nm). The emission spectrum (λ_{exc} = 630 nm, 80 mW.cm^{-2}) of **UL** in 50 mM sodium sulfite in PBS shows both the phosphorescence of PdTPTBP and the perylene-based emission, characteristic of upconversion with this dye couple (Figure 7.3a).[1a] In Figure 7.3b, the temperature dependence is shown of the upconversion emission and phosphorescence. The upconversion first increases up to 25 °C, and then decreases slightly, while the phosphorescence decreases steeply up to 25 °C, and then continues to decrease, but less steeply. The rise in upconversion up to 25 °C is explained by the fact that the DMPC membrane changes its phase from gel to liquid crystalline at 24 °C;[18] in the liquid crystalline phase the fluidity of the membrane is increased, and collision-dependent processes such as TTET and TTA become more efficient.[1a] A detailed discussion of this phenomenon is described in Chapter 6. Here, this thermo-photophysical phenomenon is used to verify the integrity of the lipid bilayer after silica-coating (see below).

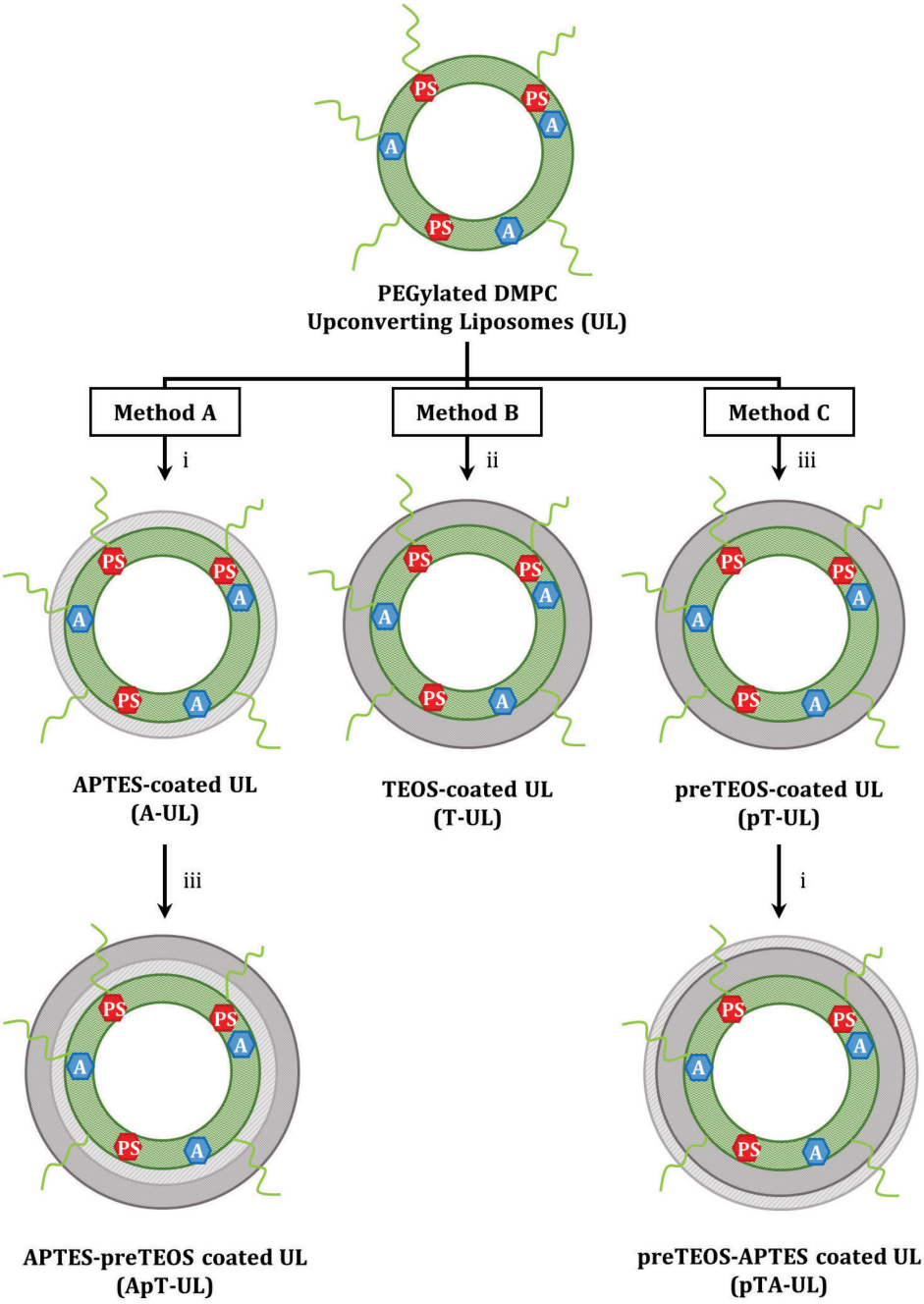

Figure 7.2. Three different synthesis methods to obtain silica-coated upconverting PEGylated liposomes. Conditions per eq. DMPC: (i) 25 eq. APTES, 16 h; (ii) 8 eq. TEOS, 1 M HCl, 30 min (iii) 8 eq. "preTEOS" (TEOS, stirred for 24 h in PBS (50 mM) at 40 °C before addition), 24 h.

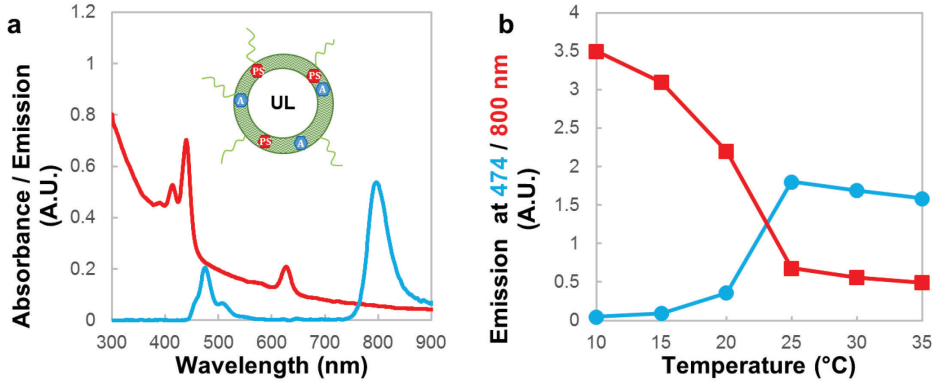

Figure 7.3. a) Absorption spectrum (red) and emission spectrum (blue) of ***UL*** *under 10 mW 630 nm irradiation (80 mW.cm^{-2}) at 20 °C in 50 mM Na_2SO_3 PBS in air. b) Temperature dependency of upconversion (at 474 nm) and phosphorescence (at 800 nm) of* ***UL*** *in 50 mM Na_2SO_3 PBS in air.*

Table 7.1. Physical characterization of liposomes ***UL*** *and (organo)silica-coated liposomes* ***A-UL****,* ***pT-UL****,* ***pTA-UL****,* ***ApT-UL*** *and* ***T-UL*** *by Dynamic Light Scattering (DLS) and zeta-potentiometry, with reported average hydrodynamic diameter (z-ave), polydispersity index (PDI) and zeta potential at the given pH.*

Sample	z-ave (nm)[a]	PDI[a]	zeta potential[b] (mV)	*pH*
UL	148 ± 4	0.09 ± 0.01	−16 ± 0	7.1
A-UL (unwashed)	171 ± 5	0.14 ± 0.02		
A-UL	128 ± 1	0.10 ± 0.02	−40 ± 5	6.8
ApT-UL	145 ± 1	0.15 ± 0.01	−20 ± 0	7.0
pT-UL			−19 ± 1	6.9
pTA-UL	167 ± 1	0.15 ± 0.01	−17 ± 1	7.2
T-UL			−33 ± 1	6.7

[a] Standard deviation based on N ≥ 3 samples. [b] Standard deviation based on 3 measurements of the same sample

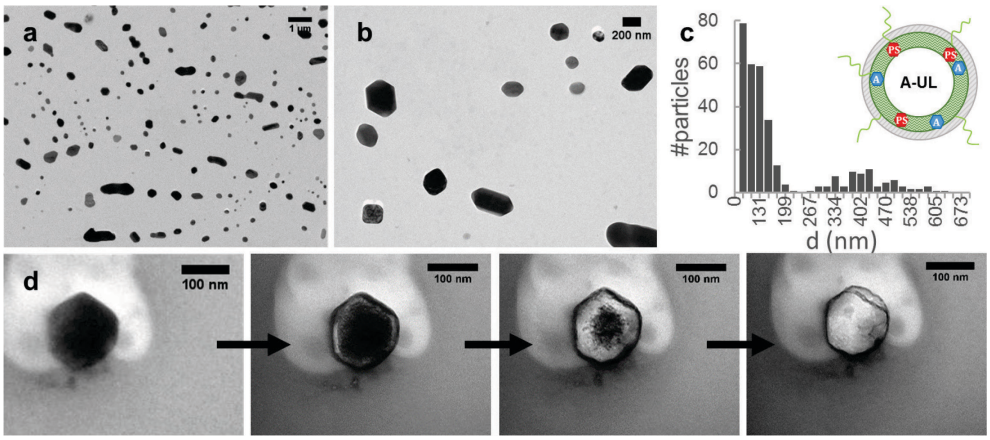

Figure 7.4. TEM micrographs (a/b) and particle diameter distribution (c, N = 324 particles) of ***A-UL****. d) An* ***A-UL*** *particle dries out over time during TEM, leaving behind an organosilica shell.*

7.2.2 Preparation of silica-coated liposomes – method A

UL were subsequently used for silica-coating experiments. In the first silica-coating method (method A), **UL** were first coated with (3-aminopropyl)triethoxysilane (APTES) to make organosilica-coated liposomes named **A-UL**, followed by additional coating with pre-hydrolyzed TEOS, making **ApT-UL**. APTES was chosen as initial layer because it has been suggested in the literature that the protonated amino group of APTES (pK_a = 10.4) associates with the negatively charged phospholipid head groups of the liposome membrane;[16d, 16e, 19] in other words, the liposome membrane acts as a template on which APTES hydrolyses and condenses. After the first reaction step and before purification, DLS measurements showed an increase of 20 nm in hydrodynamic size of **A-UL** with respect to **UL** (Table 7.1), suggesting the deposition of an organosilica layer on the membrane of about 10 nm in thickness. As a control, **UL** were kept in the same reaction conditions, without adding APTES. The DLS values of **UL** remained unchanged during these 16 h, which excludes that this change in size was caused by instability of the **UL**. Note that in absence of the liposomes, APTES is likely to form five- or six-membered organosilicate rings in aqueous solution, which suppresses nanoparticle formation.[20] Therefore, APTES alone cannot result in changes in DLS measurements.

To visually confirm the deposition of an APTES layer, **A-UL** were imaged by transmission electron microscopy (TEM), see Figure 7.4. The micrographs show individual particles in various polygonal shapes. No other nanoparticles were observed. Interestingly, when these particles were irradiated by an intense electron beam in the vacuum of the TEM, the liquid inside the particles visibly boiled and leaked out of the particles, leaving behind electron dense shells (Figure 7.4d). This observation suggested that the particles indeed consist of organosilica-coated liposomes. Surprisingly, the particles collapsed only upon high electron irradiation and the particles withstood the high vacuum of the TEM ($\sim 10^{-5}$ bar) at low irradiance, which is evidence that the organosilica layer greatly fortifies the outer shell of a liposome. The average particle diameter from TEM (176 nm, Figure 7.4c) is consistent with the hydrodynamic size observed by DLS (171 nm, Table 7.1). The observed particles with a diameter of around 400 nm are likely to have been individual particles that merged during drying of the TEM grid, because these were absent in DLS measurements. Zeta potentiometry on **A-UL** gave a zeta-potential of −30 mV at *pH* 6.8 (Table 7.1). Such a negative surface charge was

unexpected, given that the amino-groups of the organosilica layer are likely to be protonated at neutral *pH*.

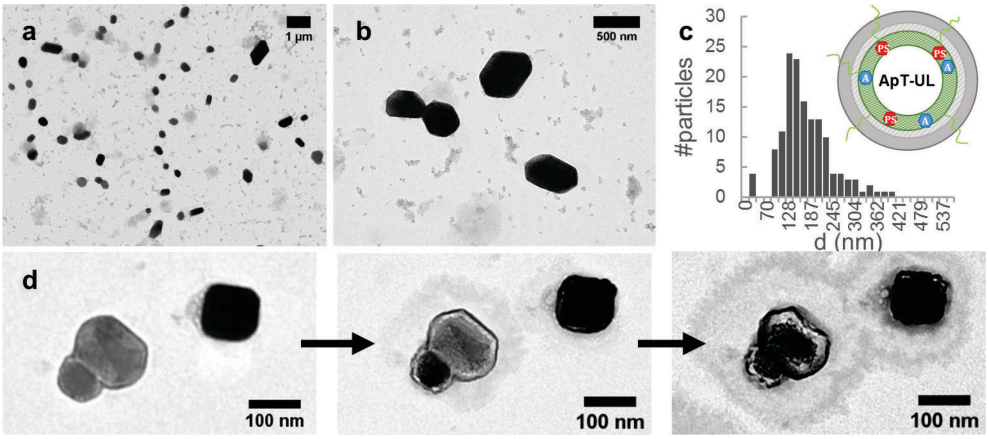

Figure 7.5. TEM micrographs (a/b) and particle diameter distribution (c, N = 142 particles) of ***ApT-UL****. d) An* ***ApT-UL*** *particle dries out over time during TEM, leaving behind an (organo)silica shell.*

The second synthesis step, to make **ApT-UL**, involved coating of **A-UL** with pre-hydrolyzed TEOS, *i.e.* TEOS that had been hydrolyzed for 24 h prior to addition.[17a] This pre-hydrolysis step was found to be essential in acquiring monodispersed silica-coated liposomes: instead of hydrophobic TEOS, that may enter the liposome membrane and disrupt its structure, hydrolyzed TEOS (*i.e.* $Si(OH)_4$ and small condensed oligomers) only condenses in solution. Without pre-hydrolysis the silica-coated liposomes aggregated quickly during the application of the coating. When TEOS was pre-hydrolyzed before addition to **A-UL**, DLS measurement of **ApT-UL** (before washing) showed that the resulting coated liposomes were monodisperse with an increase in hydrodynamic size of 17 nm with respect to the purified **A-UL** (Table 7.1), indicating that an additional layer of silica was deposited on **A-UL**. The DLS values did not change significantly for at least one week after preparation. TEM images showed single particles with an average particle diameter of 163 nm, together with smaller clustered particles, which are probably silica nanoparticles (Figure 7.5). Similar to previous observations with **A-UL**, the particles dried out under intense electron irradiation in the vacuum of the TEM (Figure 7.5d), which allowed direct visualization of the solid silica shell around the liposome. Overall, method A successfully produced (organo)silica-coated liposomes that were mono-dispersed and stable in aqueous solution.

7.2.3 Preparation of silica-coated liposomes – method B

Method B involved the silica-coating of **UL** with TEOS under acidic catalytic conditions to make **T-UL**. Similar methods have previously been used for the silica-coating of micelles.[7a, 7b] Literature suggests that the use of acid catalysis results in more extensive condensation of the silica network,[12b] which might in turn reduce the porosity of the silica layer and improve protection against oxygen. The synthesis method yielded clear solutions that did not aggregate visibly within one week, but an accurate size distribution by DLS could not be obtained (PDI = 1.00). The zeta potential of **T-UL** was found to be negative (−33.4 mV). TEM imaging showed that **T-UL** consists of single dispersed particles with a rather broad size distribution (Figure 7.6). Much smaller particles (< 10 nm) were also present, which are probably silica nanoparticles originating from TEOS condensation in solution instead of on the liposome surface. Interestingly, compared to **A-UL** and **ApT-UL** these particles show only little drying out under intense electron irradiation in the TEM. This may indicate that the silica network in these particles is indeed more condensed than in **A-UL** and **ApT-UL**. Overall, our results demonstrate that using method B resulted in successful silica-coating of liposomes, albeit with a poorly defined particle diameter and poor particle purity.

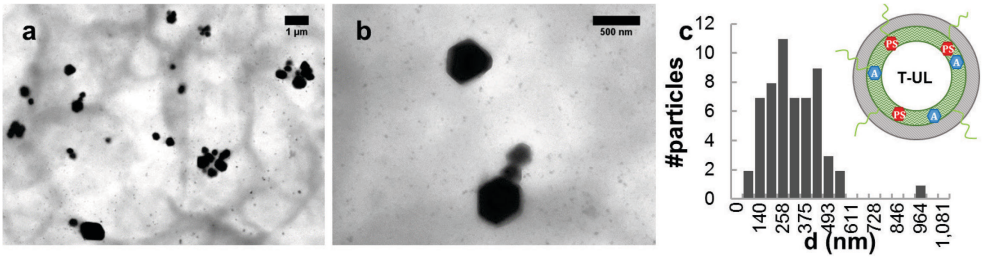

*Figure 7.6. TEM micrographs (a/b) and particle diameter distribution (c, N = 57 particles) of **T-UL**.*

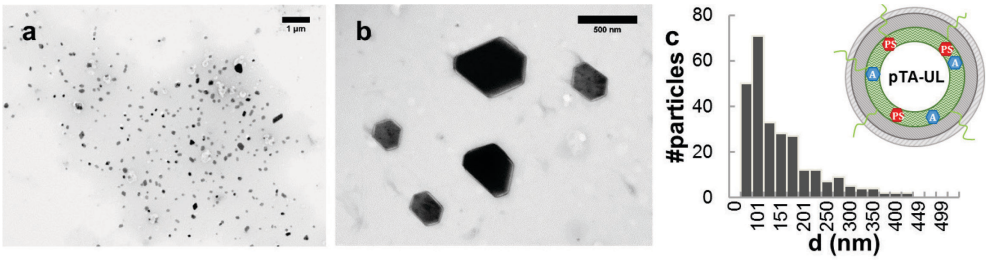

*Figure 7.7. TEM micrographs (a/b) and particle diameter distribution (c, N = 268 particles) of **pTA-UL**.*

7.2.4 Preparation of silica-coated liposomes – method C

Method C involved silica-coating of **UL** with pre-hydrolyzed TEOS to make **pT-UL**, after which the product was additionally coated with APTES to make **pTA-UL**. The zeta-potential of **pT-UL** and **pTA-UL** had similar negative values (−18.8 and −17.0 mV, respectively). Aqueous samples containing **pTA-UL** were not very stable over time; aggregated particles were observed after a few days at room temperature. Freshly prepared **pTA-UL** had an average hydrodynamic size of 167 nm. TEM imaging showed polygonal particles similar to **ApT-UL**, with an average particle diameter of 137 nm. In conclusion, although singly dispersed silica-coated liposomes were produced with method C, the particles were of lower quality than **ApT-UL** from method A in terms of aggregation over time. Overall, these results suggest that an initial APTES "template" layer, such as applied in method A, is beneficial for producing stable silica-coated liposome dispersions.

7.2.5 Spectroscopic properties of silica-coated liposomes in solution

To evaluate whether the silica-coated liposome solutions produced upconversion, samples **A-UL**, **ApT-UL**, **T-UL**, and **PtA-UL** were investigated with UV-vis absorption and emission spectroscopy (λ_{exc} = 630 nm, 10 mW, 80 mW.cm^{-2}), see Figure 7.8. All absorption spectra matched the absorption spectrum of **UL** (Figure 7.3),[1a] which means that the silica-coating did not affect the molecular dyes. Emission spectra were first taken in air, after which sodium sulfite (Na_2SO_3, 50 mM) was added to scavenge ground-state oxygen and the emission spectra were recorded again. Without sulfite, for all solutions only very weak phosphorescence of PdTPTBP (λ_{em} = 800 nm) was observed in comparison with **UL** in presence of sulfite (Figure 7.3). However, upon addition of sulfite, all samples directly exhibited much more intense phosphorescence of PdTPTBP and intense upconverted emission of perylene at 474 nm. In a second experiment, to ascertain that the silica-coating had not destroyed the lipid bilayer, the temperature dependence of phosphorescence and upconversion was recorded between 10 and 35 °C in presence of sulfite (Figure S.VI.1). If the lipid bilayer would still be intact, a steep increase in upconversion and decrease of phosphorescence around the lipid bilayer main transition temperature (T_m ≈ 25 °C) would be expected, just as was observed for **UL** (Figure 7.3). Indeed, in all cases, the thermo-photophysical behavior was similar to **UL**, confirming that the lipid bilayer was still intact. Overall, despite the lipid bilayer being intact inside the particles, it is clear that none of the (organo)silica layers around the liposomes were capable of blocking

oxygen. This must mean that the organo(silica) coating is either porous to oxygen or incomplete, because the capability of upconversion, which takes place inside the particles, is affected by the sodium sulfite added to the solution outside the particles. This result can only be explained if oxygen is able to diffuse freely across the organosilica-coating or across the patches that have remained uncoated.

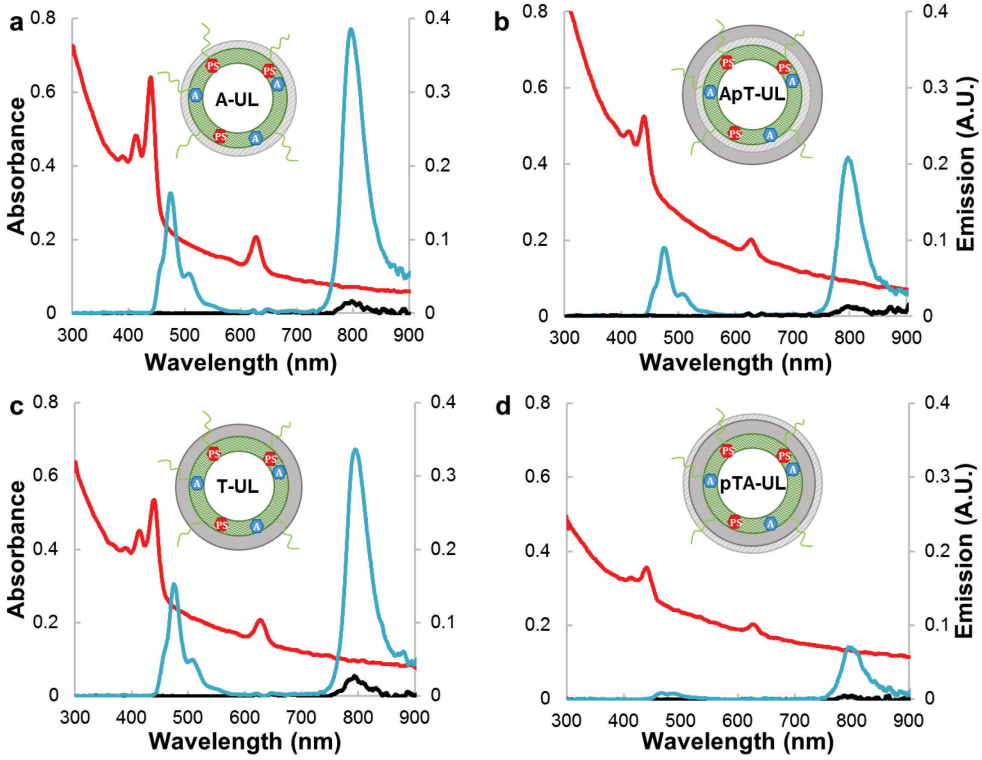

*Figure 7.8. Absorption (red, left axes), and emission spectra in air (black, right axes) and in air in 50 mM Na_2SO_3 PBS (blue, right axes) of **A-UL** (a), **ApT-UL** (b), **T-UL** (c), and **pTA-UL** (d) with 10 mW 630 nm (80 mW.cm^{-2}) at 20 °C.*

Other silica-coated hybrid systems for TTA-UC have been reported. For example, Liu *et al.* described acid-catalyzed silica-coating of TTA-UC dye-loaded Pluronic F-127 micelles with TEOS (similar to method B).[7a, 7b] They showed that the water-soluble particles performed upconversion, but did not mention oxygen quenching of the process at all. In fact, Wang and coworkers used identical particles that were functionalized with two dyes for ratiometric oxygen sensing in cells.[21] Obviously, such particles must be oxygen

permeable if they are used for oxygen sensing. Kwon *et al.* discussed the oxygen sensitivity of an upconverting oleic acid-core silica-shell nanocapsules, with a silica shell thickness of 12 – 23 nm.[5b] While the system was capable of upconversion in air, it was not the relatively thick silica shell that protected the dyes from oxygen, but the oleic acid that is able to scavenge oxygen; without oleic acid, no upconversion was observed. Thus, so far, in all TTA-UC systems with nm-thick silica shells, silica offers no protection from oxygen. Our results seem to be yet another example that nano-size silica layers, made by various methods, is not able to block the diffusion of molecular oxygen in aqueous solution.

7.2.6 Upconversion with silica-coated liposomes in cells

Although TTA-UC in liposomes or (organo)silica-coated liposomes in solution is too oxygen-sensitive, it would be incorrect to assume that they do not function in biological systems. Indeed, TTA-UC has been shown before to occur *in vitro* and *in vivo* with nanoparticle systems that are oxygen sensitive as well.[22] Up to now, a reasonable explanation has not yet been provided in the literature why such particles are able to produce upconversion in biological systems. Possibly, TTA-UC is facilitated by the presence of endogenous anti-oxidants that are able to lower the local oxygen concentration by consuming ground state oxygen or singlet oxygen (see Chapter 8 and Chapter 9). Furthermore, the silica shell may actually offer protection from oxygen in a biological situation in which oxygen is present at a lower concentration than in an aqueous dispersion. With this in mind, A549 lung carcinoma cells were treated with **UL**, **A-UL**, **ApT-UL**, or **pTA-UL** and then imaged with (upconversion) luminescence microscopy. For these experiments, perylene was substituted by 2,5,8,11-tetra(*tert*-butyl)perylene (TBP, Figure 7.1) to prevent the annihilator from escaping the liposomes, which is known to occur for perylene.[23] First of all, uptake of the particles was investigated after 24 h incubation by regular fluorescence microscopy (20x magnification) to image the emission of TBP (λ_{exc} = 377 nm), see Figure S.VI.2. For both liposomes and silica-coated liposomes, the appearance of blue fluorescence throughout the cytosol confirmed the cellular uptake of the particles. The differences in zeta-potential and the presence of the (organo)silica-coating did not seem to affect the particle uptake significantly. Furthermore, no signs of particle toxicity were observed. In a second experiment, the cells were incubated with either **UL** or **ApT-UL** for 24 h and then imaged at 100x magnification with 405 nm and 639 nm excitation under

poorly oxygenated conditions (1% O_2), see Figure 7.9. For both **UL** and **ApT-UL**, under 405 nm excitation, bright fluorescent spots were observed, marking the locations of the TBP dye. Given that the usual uptake mechanism of liposomes is endocytosis, we assign these spots to be endo- and lysosomes. Interestingly, upon 639 nm excitation and observing between 450 to 575 nm, upconverted emission was observed at the same locations as that observed for TBP fluorescence upon 405 nm excitation (Figure 7.9). Comparable upconversion was observed *in vitro* for both **UL** and **ApT-UL**. It was noticed that the upconversion intensity varied significantly from cell to cell, which possibly reflects differences in oxygenation levels and concentration of endogenous anti-oxidants. Overall, **UL** and **ApT-UL** performed upconversion in A549 cells, but silica-coating of the liposomes improved neither uptake nor upconversion luminescence intensity *in vitro*.

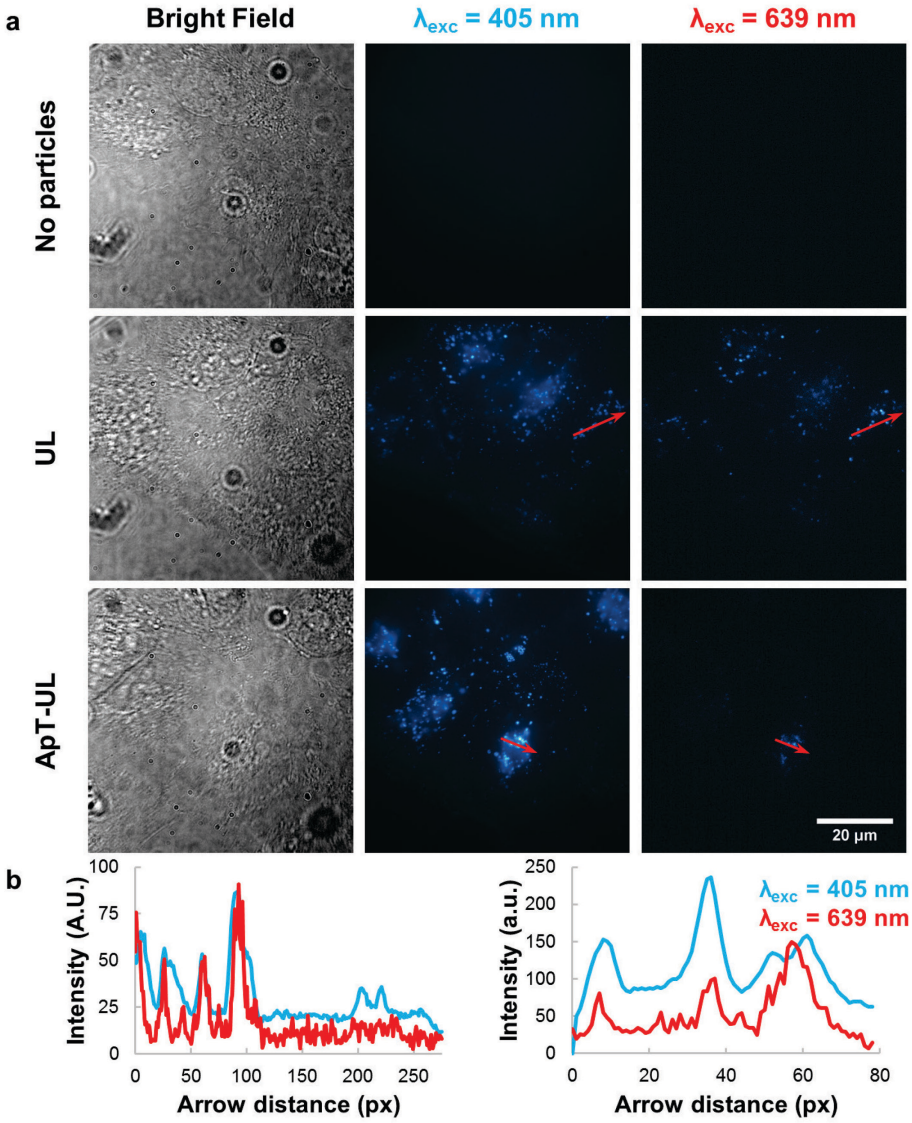

*Figure 7.9. a) Microscopy imaging in bright field mode at 100x magnification and with 405 or 639 nm (26 W.cm^{-2}) excitation of living A549 cells treated with either medium only ("no particles"), **UL**, or **ApT-UL** at 1% O_2, 7% CO_2, and 37 °C. b) Intensity profiles of luminescence observed with 405 and 639 nm along the red arrows given in (a), for samples **UL** (left) and **ApT-UL** (right).*

7.2.7 Dried upconverting silica-coated liposomes

One of the reasons why the silica-coating does not act as an oxygen barrier may be the coating thickness. How thick should the silica-coating be to become a barrier for oxygen? Attempts were undertaken to grow extra layers of silica on **ApT-UL**, but this led inevitably to aggregation of the particles in

solution. As an alternative, it was decided to prepare a solid silica-liposome composite material by drying unpurified **A-UL** and **ApT-UL** samples, *i.e.* without removing the excess of APTES or preTEOS, in an oven at 50 °C overnight. The new samples were called **A-UL-D** and **ApT-UL-D**, respectively. As silica-free control, liposomes **UL** were freeze-dried (sample **UL-F**). For **A-UL-D** and **ApT-UL-D**, heat-drying drives the condensation equilibrium of the (organo)silica network to the fully condensed species by the removal of H_2O and EtOH, making a dense silica material.

The solids were characterized with Scanning Electron Microscopy (SEM) and ^{29}Si-NMR. Figure 7.10 shows SEM images of the solids. **A-UL-D** consisted of a mesh of spherical-polygonal particles within the same size range as the water dispersed **A-UL** particles observed by TEM. The ^{29}Si-NMR spectrum (Figure S.VI.3) shows a broad peak at −68 ppm, corresponding to the fully condensed (T_3) organosilica product of APTES.[20a, 24][II] In comparison, **ApT-UL-D** had a more coarse structure, and individual particles could not be distinguished. This is consistent with the hypothesis that **ApT-UL** particles are embedded in a matrix of amorphous silica. The ^{29}Si-NMR spectrum of this material showed two peaks at −106 and −96 ppm, corresponding to the triple-condensed (Q_3) and double-condensed (Q_2) silica products of TEOS (Figure S.VI.3). Thus, the silica matrix of **ApT-UL-D** is not fully condensed. No signals originating from condensed APTES were detected, which emphasizes that the silica *vs.* organosilica ratio is very high. In contrast, SEM images of **UL-F** suggested that this sticky solid consisted of a network of broken lipid bilayers, which underlines that the silica shell around the liposomes is necessary to conserve the nanostructure of the silica-coated liposomes inside the dried composite materials.

To investigate the integrity of the liposomes inside the material, thermogravimetric analysis (TGA) was performed of all solid samples. If the liposomes would be intact, *i.e.* defined as a lipid bilayer surrounding an aqueous interior, it was expected that first water would escape from ∼100 °C onwards, followed by thermal decomposition of the phospholipids at a higher temperature. Figure 7.11 shows the TGA curves of freeze-dried liposomes **UL-F**, and heat-dried (organo)silica-coated liposomes **A-UL-D** and **ApT-UL-D**. The

[II] ^{29}Si-NMR peak designations are coded by the number of bonded oxygen atoms (T = 3, Q = 4) and by the number of siloxane (Si-O-Si) bonds (subscript 0 – 4).[20a]

mass of **UL-F** reduces by 75% between 230 and 350 °C, indicating the expected thermal decomposition of the phospholipids. The curve for **ApT-UL-D** is very similar to **UL-F**, but with a 40% mass reduction between 230 and 350 °C. The higher residual mass is attributed to the empty residual silica shells, which evidently do not decompose at this temperature. No mass decrease was observed between 30 and 230 °C, indicating the absence of water and thus the absence of intact liposomes inside this material. The TGA curve for **A-UL-D** shows a gradual mass reduction of 13% between 100 and 200 °C, and again a second mass reduction from 230 °C onwards. The mass reductions between 100 and 200 °C suggest the loss of water. However, the theoretical percentage of water mass, assuming 100% synthesis yield and 130 nm diameter liposomes, would amount to 50 – 60%. Therefore, these data indicate that only a relatively small part of **A-UL-D** consist of intact liposomes and that the (organo)silica matrix around the liposomes was not able to prevent drying out of the aqueous interior of the liposomes.

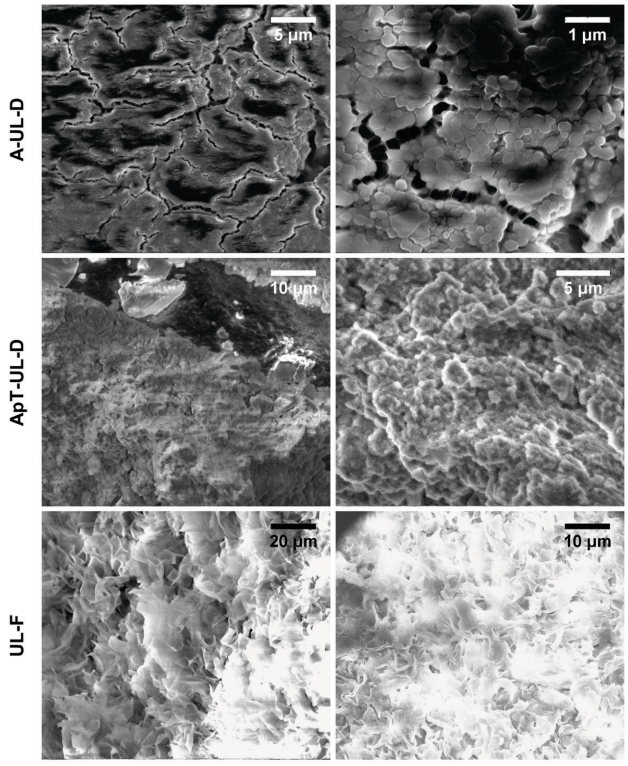

*Figure 7.10. SEM micrographs of dried (organo)silica-coated liposomes **A-UL-D** and **ApT-UL-D**, and freeze-dried liposomes **UL-F**.*

Regardless of the fact that the water inside the material is lost, the residual fragments of dye-doped lipid bilayer inside the solid may still be able to perform upconversion. As an initial test, **A-UL-D** powder was irradiated with 630 nm in air, and surprisingly, blue luminescence was clearly visible after blocking the excitation light (Figure 7.12a). Emission spectroscopy (λ_{exc} = 630 nm, 30 mW, 0.66 W.cm^{-2}) confirmed that **A-UL-D** and **ApT-UL-D** were indeed producing upconverted luminescence under red light irradiation (Figure 7.12b). In contrast, no upconversion in air was detected for freeze-dried liposomes **UL-F** (Figure S.VI.4). These results indicate that (organo)silica can indeed offer protection from oxygen in TTA-UC materials. To offer such protection, however, it is clear that a much thicker layer is necessary than the nano-thick shells applied to water-dispersible silica-coated liposomes. The upconversion emission in **A-UL-D** and **ApT-UL-D** was not very durable; bleaching occurred within minutes at 0.66 W.cm^{-2} irradiance (Figure 7.12c). Time-traces of the upconversion intensity revealed that the emission was more long-lasting for **A-UL-D**. Whereas all upconversion luminescence had bleached within 2 min for **ApT-UL-D**, 40% of the start intensity still remained for **A-UL-D**. This difference may be caused by the greater amount of primary amine groups in **A-UL-D**, which are known to chemically quench singlet oxygen. Such a chemical reaction consumes dioxygen and therefore may contribute to an oxygen-low environment inside the material upon irradiation.[25] Nonetheless, the relative instability of the upconversion emission underlines that even in such bulk materials, (organo)silica does not completely obstruct the diffusion of oxygen. Finally, it must be emphasized that these results are rather preliminary and that the preparation method for obtaining these silica-coated materials can be greatly improved. We foresee that an optimized drying procedure would yield solids with higher degree of silica condensation and in which all the water inside the liposomes remains trapped. Then, the addition of water soluble anti-oxidants to the aqueous interior of the liposomes before silicification and drying, which would end up inside the material, would greatly enhance the upconversion quantum yield and stability in air (see Chapter 8 and Chapter 9). Such highly tunable nano-composite materials, consisting of silica, phospholipids, and water, would effectively allow air-sensitive photophysical processes to take place in a solid state material.

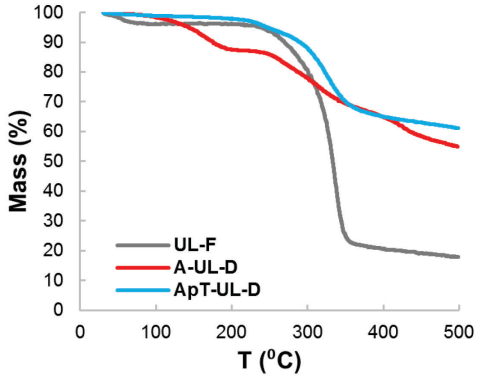

*Figure 7.11. Thermogravimetric analysis plots from 30 to 500 °C (10 °C.min^{-1} in air) of freeze-dried liposomes **UL-F**, and heat-dried (organo)silica-coated liposomes **A-UL-D** and **ApT-UL-D**.*

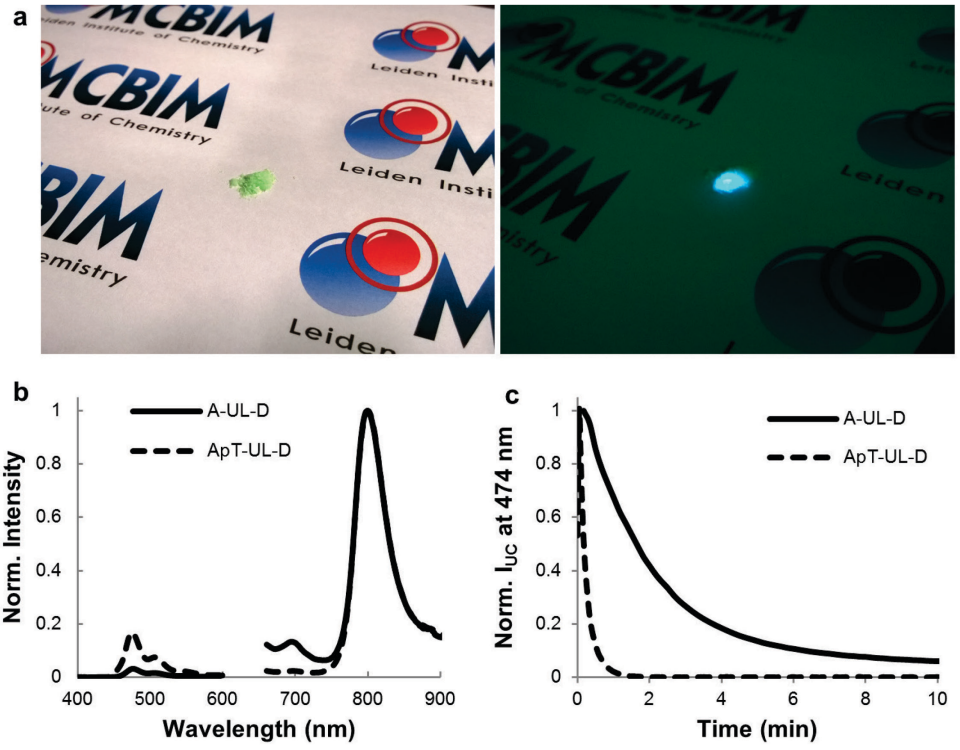

*Figure 7.12. Upconversion with heat-dried silica-coated liposomes. a) Photographs of heat-dried organosilica-coated liposomes **A-UL-D** in ambient light (left) and irradiated with red light and photographed with a 575 nm short pass filter in front of the camera (right). b) Emission spectra of **A-UL-D** (solid) and **ApT-UL-D** (dashed) under 630 nm irradiation, normalized at 800 nm. c) Typical time-traces of the normalized upconversion intensity (I_{UC}) at 474 nm of **A-UL-D** (solid) and **ApT-UL-D** (dashed) under continuous 630 nm irradiation. All experiments were performed at 20 °C with 30 mW 630 nm irradiation (0.66 W.cm^{-2}).*

7.3 Conclusion

Monodisperse (organo)silica-coated liposomes were prepared that can be used to upconvert red light to blue light by means of triplet-triplet annihilation upconversion. The silica-coating did not prevent the upconversion to be quenched by molecular oxygen in solution. Furthermore, the upconverted blue light could be imaged in living A549 cells in hypoxic conditions without causing cytotoxicity, but the luminescence was not more intense than in control cells that had been treated with uncoated upconverting liposomes. However, when the (organo)silica-coated liposomes were heat-dried in presence of excess (organo)silica precursor, solids were obtained that could perform upconversion in air. Our results suggest that the (organo)silica shell of the silica-coated liposomes in solution needs to be much thicker and/or compact to protect the upconversion from oxygen in a biological setting. This work represents noteworthy examples of the combination of phospholipids, water, and silica for the construction of tunable upconverting nanoparticles and materials. Such hybrid systems combine the favorable properties of their constituents, and may eventually be used in applications such as drug delivery, cell imaging, photocatalysis, and solar energy harvesting.

7.4 Experimental Section

7.4.1 General

1,2-dilaureyl-*sn*-glycero-3-phosphocholine (DLPC), 1,2-dimyristoyl-*sn*-glycero-3-phospho choline (DMPC), 1,2-dipalmitoyl-*sn*-glycero-3-phosphocholine (DPPC), and sodium N-(carbonyl-methoxypolyethylene glycol-2000)-1,2-distearoyl-*sn*-glycero-3-phosphoethanolamine (DSPE-mPEG-2000) were purchased from Lipoid GmbH (Ludwigshafen, Germany) and stored at −18 °C. Palladium tetraphenyltetrabenzoporphyrin (PdTPTBP) was purchased from Bio-Connect (Huissen, The Netherlands). Perylene was purchased from Sigma-Aldrich Chemie BV (Zwijndrecht, The Netherlands). The synthesis of 2,5,8,11-tetra(*tert*-butyl)perylene (TBPe) is described in Chapter 9. Dulbecco's phosphate buffered saline (DPBS) was purchased from Sigma Aldrich and had a formulation of 8 $g.L^{-1}$ NaCl, 0.2 $g.L^{-1}$ KCl, 0.2 $g.L^{-1}$ KH_2PO_4, and 1.15 $g.L^{-1}$ K_2HPO_4 with a *pH* of 7.1 − 7.5. All other chemicals were obtained from the major companies and used as received.

7.4.2 Instrumentation

Ultracentrifugation was done with a Beckman-Coulter Optima L-90K ultracentrifuge, equipped with a 70.1 Ti rotor, at 50K rpm (230,000 g) for 30 min. Freeze-dried samples were prepared with a Christ Alpha 1-2 LDPlus machine, operating at <0.03 mbar. Liposome or silica-coated liposome samples were placed in 50 mL round bottom flasks, frozen in liquid nitrogen while gently swirling, and attached to the freeze-dryer. Dynamic Light Scattering (DLS) measurements were performed on undiluted samples ([DMPC] = 10 mM) using a Zetasizer nano

S (Malvern Instruments) operating at 633 nm, with 3 measurements of 12 runs each time. Zeta-potential measurements were performed on a Zetasizer nano ZS (Malvern Instruments), at 25 °C with 3 measurements and 10 − 100 automatic runs. Samples were diluted 20x in MilliQ in a DTS1070 cell, at a known *pH*, so that [DMPC] = 0.5 mM. Fourier Transform Infrared (FT-IR) spectra were recorded on a Perkin-Elmer Paragon 1000. Transmission Electron Microscopy (TEM) imaging was performed on a JEOL 1010 TEM using accelerating voltages of 60.0 or 80.0 kV, iTEM software and a Olympus Megaview G2 camera. Samples were loaded onto Formvar-coated carbon grids (Van Loenen instruments, Netherlands) by depositing a grid on top of a sample droplet for about 30 minutes. CP-MAS ^{29}Si Nuclear Magnetic Resonance (NMR) spectroscopy was performed on a Bruker AV400 using a relaxation delay of 60 seconds and pulse duration of 3 µsec. Scanning Electron Microscopy (SEM) was performed on a Nova NanoSEM (FEI) using accelerating voltages of 15.0 kV. Powder samples were deposited on conducting tape. Thermogravimetric Analysis (TGA) measurements were performed on a Netzsch STA with a DSC/TG Al_2O_3 pan crucible, with a temperature increasing from 30 to 500 °C at 10 °C.min^{-1}, and a gas flow of 40 mL.min^{-1}.

7.4.3 Preparation of upconverting liposomes

Aliquots of stock solutions in chloroform were added together in a round bottom flask to obtain a mixture of DMPC lipid (5 mM in $CHCl_3$, 10 mL, 50 µmol), DSPE-mPEG-2000 (0.2 mM in $CHCl_3$, 10 mL, 2 µmol), PdTPTBP (10 µM in $CHCl_3$, 2.5 mL, 25 nmol) and perylene (0.2 mM in $CHCl_3$, 1.25 mL, 250 nmol). For liposomes used in cell treatment, the perylene dye was replaced by TBPe in the same amount. The solvent was removed by rotary evaporation at 50 °C under reduced pressure and then under high vacuum for at least 15 minutes. PBS buffer (5 mL) was added to the lipid film to obtain a final DMPC lipid concentration of 10 mM. The flask was then freeze-thawed using liquid nitrogen and a water bath at 50 °C for 3 cycles, and the suspension was subsequently extruded using a 200 nm Nuclepore polycarbonate filter and a mini-extruder (Avanti Polar Lipids, Inc.) at 55 °C, for at least 11 times. All dyes were incorporated into the liposomes with minimal losses, as indicated by the lack of color on the filter after the extrusion. The resulting liposome suspension was analyzed by DLS before use in further synthesis steps.

Optionally, an oxygen scavenger was added in a given concentration to the PBS buffer. After extrusion, the oxygen scavenger-loaded liposomes were purified using an Illustra NAP-25 size exclusion column with Sephadex G25 packing (GE Healthcare). Typically, liposomes were loaded on the column in 1 mL portions, and eluted with 2 mL PBS. Fractions of about 0.4 mL were collected; fractions 6 − 10 contained the liposomes as judged by the green-yellow color, fractions 12 and above contained the oxygen scavenger, as judged by the addition of 2,6-dichlorophenolindophenol (DCPIP; 1.0 mM in PBS, 200 µL, 200 nmol) to each fraction. The fractions containing the liposomes (~ 2 mL, *i.e.* [lipid] ≈ 5 mM) were combined and used for further synthesis.

7.4.4 Silica-coating of upconverting liposomes

Silica-coated liposomes were prepared according to a modified literature procedure.[16a, 17a, 17b]

Method A - APTES-preTEOS coating

(3-Aminopropyl)triethoxysilane (APTES, 293 µL, 1.25 mmol) was added to the liposome solution (section 7.4.3, 5 mL, [DMPC] ≈ 5 mM) and the mixture was stirred for 16 h. At this

point, the *pH* was 10.7. To remove unreacted and unassociated APTES, the sample was ultracentrifuged and resuspended in 5 mL PBS twice, which neutralized the *pH*. This washing procedure did not affect the particle size distribution and shape, as judged by TEM (data not shown). Meanwhile, tetraethylorthosilicate (TEOS) was pre-hydrolyzed in PBS (typically 50 mM TEOS) for 24 h at 40 °C, creating a solution of 50 mM pre-hydrolyzed TEOS called "preTEOS". Preliminary experiments determined that a pre-hydrolysis time of 24 hours was optimal for 50 mM TEOS in PBS. A longer time resulted in the formation of non-desired silica nanoparticles (observed by DLS), and a shorter time resulted in sample aggregation during liposome coating. Higher TEOS concentrations resulted in formation of silica nanoparticles as well. Thus, 8 mL preTEOS (50 mM, 400 µmol) was added to the APTES-coated liposome suspension (5 mL) and the mixture was stirred for 24 h at 20 °C. The final APTES-preTEOS coated liposomes were purified by ultracentrifugation and redispersion in 5 mL MilliQ or PBS (once).

Method B – Acid-catalyzed TEOS coating

Liposomes were prepared as mentioned in Section 7.4.3, but instead of PBS, 1 M HCl in PBS was used to hydrate the lipid film. The liposome assembly under such acidic conditions produced high quality liposomes (z-ave 134 nm, 0.1 PDI). After liposome assembly, TEOS (36 µL, 160 µmol) was added to 2 mL of the liposome solution ([DMPC] ≈ 5 mM) and stirred for 30 minutes. Then, the solution was transferred to a dialysis bag (Servapor, MW cutoff 12 – 14 KDa; SERVA Electrophoresis GmbH) and dialyzed against demineralized water (1 L) for 24 h, during which time the water was refreshed twice.

Method C – PreTEOS-APTES coating

First, TEOS was pre-hydrolyzed in PBS (typically 50 mM TEOS) for 24 hours at 40 °C, creating a solution of 50 mM pre-hydrolyzed TEOS called "preTEOS". 8 mL PreTEOS (400 µmol) was then added to the liposome suspension (Section 7.4.3, 5 mL, [DMPC] ≈ 5 mM) and stirred for 24 h at 20 °C. These TEOS-coated liposomes were ultracentrifuged and redispersed in 5 mL PBS twice to remove unreacted and unassociated TEOS. APTES (293 µL, 1.25 mmol) was added to the coated liposome solution (5 mL) and the solution was stirred overnight for 16 h. The final preTEOS-APTES coated liposomes were purified by ultracentrifugation and redispersion in 5 mL MilliQ or PBS (once).

7.4.5 Preparation of (silica-coated) liposome solids

Freeze-dried liposome solids were prepared by freeze-drying at ≤ 0.03 mbar (section 7.4.2). Oven-dried silica-coated liposome solids were prepared by depositing unpurified silica-coated liposomes **A-UL** or **ApT-UL** (*i.e.* including excess APTES and/or preTEOS) in 5 mL portions on watch glasses and drying overnight at 50 °C.

7.4.6 UV-Vis absorption and emission spectroscopy

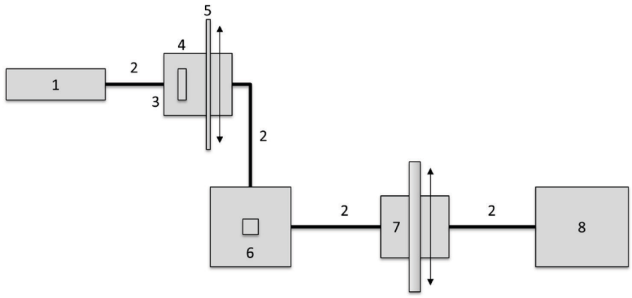

Figure 7.13 Setup used for emission spectroscopy on samples in solution using red light irradiation. Legend: (1) 630 nm laser source, (2) optical fibers, (3) filter holder, (4) 630 nm band pass filter, (5) variable neutral density filter, (6) temperature controlled cuvette holder, (7) variable filter holder with a 633 nm notch filter, and (8) CCD spectrometer.

Absorption and emission spectroscopy was performed with a custom-built setup (Figure 7.13). Typically, a 2 mL sample was transferred in a 111-OS macro fluorescence cuvette from Hellma and placed in a CUV-UV/VIS-TC temperature-controlled cuvette holder from Avantes (Apeldoorn, The Netherlands). Every time the temperature was changed, the sample was allowed to equilibrate for 5 minutes. The samples were irradiated from the side with a 10 mW 630 nm laser light beam from a clinical grade Diomed 630 nm PDT laser (4 mm beam, 80 $mW.cm^{-2}$). The 630 nm light was filtered through a FB630-10, 630 nm band pass filter (Thorlabs, Dachau/Munich, Germany) put between the laser and the sample. The excitation power was controlled using a NDL-25C-4 variable neutral density filter (Thorlabs), and measured using a S310C thermal sensor connected to a PM100USB power meter (Thorlabs). An Avantes 2048L StarLine CCD spectrometer was connected at 90° angle with respect to the excitation source. A Thorlabs NF-633 notch filter placed between the cuvette holder and the spectrometer was used to block the excitation light. To make the emission spectra of the different samples in solution comparable, the samples were diluted in PBS so that A_{630} = 0.20. Optionally, Na_2SO_3 (1 mL, 100 mM in PBS, pH = 7.4) was freshly added to 1 mL samples so that 50 mM Na_2SO_3 was present for oxygen scavenging during spectroscopy.

7.4.7 Solid state emission spectroscopy

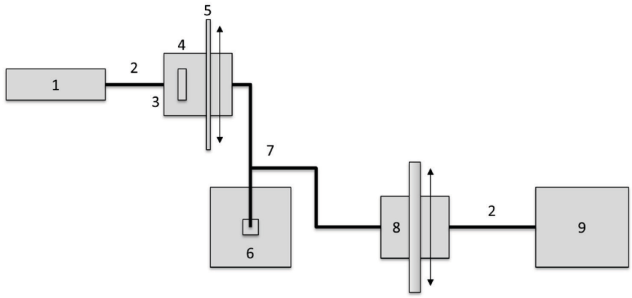

Figure 7.14. Setup used for emission spectroscopy on powders using red light irradiation. Legend: (1) 630 nm laser source, (2) optical fibers, (3) filter holder, (4) 630 nm band pass filter, (5) variable neutral density filter, (6) temperature controlled cuvette holder, (7) bifurcated optical fiber, (8) variable filter holder with a 633 nm notch filter, and (9) CCD spectrometer.

Solid state emission spectroscopy was done in a slightly different setup than for liquid samples (Figure 7.14). A bifurcated fiber (FCB UVIR 400-2, Avantes) was connected to the top of the cuvette holder, in which a lens (Avantes COL-UV/VIS lens, f = 8.7 mm) was fitted that simultaneously transmitted excitation light and captured the emission. 7.1 mg solid sample was deposited on the bottom of a semi-micro cuvette. Samples were irradiated with 30 mW 630 nm light (2.4 mm beam, 0.66 $W.cm^{-2}$).

7.4.8 General cell culturing

A549 human lung carcinoma cells were cultured in 25 cm^2 flasks in 8 mL Dulbecco's Modified Eagle Medium with phenol red (DMEM; Sigma Life Science, USA), supplemented with 8.2% v/v fetal calf serum (FCS; Hyclone), 200 $mg.L^{-1}$ penicillin and streptomycin (P/S; Duchefa), and 1.8 mM glutamine S (GM; Gibco, USA), under standard culturing conditions (humidified, 37 °C atmosphere containing 7.0% CO2). The cells were split approximately once per week upon reaching 70 − 80% confluency, using seeding densities of 2×10^5 cells, and the medium was refreshed once per week. Cells were passaged for 4 − 8 weeks.

7.4.9 Regular fluorescence microscopy

For regular fluorescence microscopy experiments, cells were seeded into 6-well plates, 200K cells per well. Meanwhile, the liposome- or silica-coated liposome-samples at a 2.5 mM lipid concentration were filtered through a 0.45 µm filter and further brought to a 1 mM final lipid concentration with OptiMEM (Life Technologies, USA), supplemented with 2.5% FCS, 200 mg/L P/S, and 1.8 mM GM ("OptiMEM complete"). 24 h after cell seeding, 3 mL of liposome mixture was added to each well, and the cells were incubated for another 24 hours. Then, the liposomes were removed and the cells were washed once with PBS and supplied with 1 mL OptiMEM. The cells were imaged in bright field mode (250 ms exposure) and with 377 nm excitation (1000 ms exposure) using a Leica SPE confocal microscope at 20x magnification and Cell^M software.

7.4.10 Upconversion luminescence microscopy

For upconversion microscopy experiments, cells were seeded at 30K on 25 mm diameter microscopy coverslips (VWR, thickness no. 1) in 6-well plates. Meanwhile, the liposome- or silica-coated liposome-samples at a 2.5 mM lipid concentration were filtered through a 0.45 µm pore filter and further brought to a 1 mM final lipid concentration with OptiMEM complete. 24 h after seeding, 3 mL liposome-medium mixture was added to each well and incubated for 24 h. Then, the liposomes were washed once with PBS and supplied with 1 mL OptiMEM. The coverslips were transferred to custom-made coverslip holders, which in turn were put in a stage-top miniature incubator (Tokai Hit, INUBG2ETFP-WSKM) fitted with a GM-8000 gas controller. The cells were incubated for 30 minutes at 1% O_2, 7% CO_2, and 37 °C before imaging. Imaging was performed with a customized Zeiss Axiovert S100 Inverted Microscope setup, fitted with a Zeiss 100x Plan Apochromat 1.4 NA oil objective, and an Orca Flash 4.0 V2 sCMOS camera from Hamamatsu, which together produced images with pixel size of 69 nm (for 100x). The typical camera exposure time was 1000 ms. Excitation at 405 nm was performed with a CrystaLaser DL405-050 diode laser, in combination with a Chroma zet442/514/568m emission filter and Chroma zt405/514/561rpc dichroic mirror. The output power of the 405 nm laser at the sample was typically 62 µW at 100 x magnification (60 µm spot diameter, intensity 2.2 $W.cm^{-2}$). Excitation at 639 nm was performed with a Power Technology 1Q1A30(639-35B)G3 diode laser, in combination with a 575 nm short pass filter (Edmund Optics, part no. #84-709) and Chroma zt405/532/635rpc dichroic mirror. The output power of the 639 nm laser at the

sample was typically 1.0 mW at 100 x magnification (70 µm spot diameter, 26 $W.cm^{-2}$ intensity).

7.5 References

[1] a) S. H. C. Askes, A. Bahreman, S. Bonnet, *Angew. Chem., Int. Ed.* **2014**, *53*, 1029-1033; b) S. H. C. Askes, M. Kloz, G. Bruylants, J. T. Kennis, S. Bonnet, *Phys. Chem. Chem. Phys.* **2015**, *17*, 27380-27390; c) Z. Chen, W. Sun, H.-J. Butt, S. Wu, *Chem. Eur. J.* **2015**, *21*, 9165-9170; d) J. Zhou, Q. Liu, W. Feng, Y. Sun, F. Li, *Chem. Rev.* **2014**, *115*, 395-465; e) L. Xia, X. Kong, X. Liu, L. Tu, Y. Zhang, Y. Chang, K. Liu, D. Shen, H. Zhao, H. Zhang, *Biomaterials* **2014**, *35*, 4146-4156; f) E. Ruggiero, J. Hernandez-Gil, J. C. Mareque-Rivas, L. Salassa, *Chem. Commun.* **2015**.

[2] a) T. N. Singh-Rachford, F. N. Castellano, *Coord. Chem. Rev.* **2010**, *254*, 2560-2573; b) T. W. Schmidt, F. N. Castellano, *J. Phys. Chem. Lett.* **2014**, *5*, 4062-4072; c) A. Monguzzi, R. Tubino, S. Hoseinkhani, M. Campione, F. Meinardi, *Phys. Chem. Chem. Phys.* **2012**, *14*, 4322-4332; d) N. Yanai, N. Kimizuka, *Chem. Commun.* **2016**, *52*, 5354-5370.

[3] a) S. Hisamitsu, N. Yanai, N. Kimizuka, *Angew. Chem. Int. Ed.* **2015**, *54*, 11550-11554; b) P. Mahato, A. Monguzzi, N. Yanai, T. Yamada, N. Kimizuka, *Nat. Mater.* **2015**, *14*, 924-930; c) S. H. Lee, D. C. Thévenaz, C. Weder, Y. C. Simon, *J. Polym. Sci., Part A: Polym. Chem.* **2015**, *53*, 1629-1639; d) P. Duan, N. Yanai, H. Nagatomi, N. Kimizuka, *J. Am. Chem. Soc.* **2015**, *137*, 1887-1894; e) P. Duan, N. Yanai, N. Kimizuka, *J. Am. Chem. Soc.* **2013**, *135*, 19056–19059; f) A. J. Svagan, D. Busko, Y. Avlasevich, G. Glasser, S. Baluschev, K. Landfester, *ACS Nano* **2014**, *8*, 8198-8207.

[4] a) J.-H. Kim, J.-H. Kim, *ACS Photonics* **2015**, *2*, 633-638; b) Z. Huang, X. Li, M. Mahboub, K. Hanson, V. Nichols, H. Le, M. L. Tang, C. J. Bardeen, *Nano Lett.* **2015**, *15*, 5552-5557.

[5] a) M. Majek, U. Faltermeier, B. Dick, R. Pérez-Ruiz, A. Jacobi von Wangelin, *Chem. Eur. J.* **2015**, *21*, 15496-15501; b) O. S. Kwon, J. H. Kim, J. K. Cho, J. H. Kim, *ACS Appl. Mater. Interfaces* **2015**, *7*, 318-325.

[6] a) A. Monguzzi, S. M. Borisov, J. Pedrini, I. Klimant, M. Salvalaggio, P. Biagini, F. Melchiorre, C. Lelii, F. Meinardi, *Adv. Funct. Mater.* **2015**, *25*, 5617-5624; b) A. Nattestad, C. Simpson, T. Clarke, R. W. MacQueen, Y. Y. Cheng, A. Trevitt, A. J. Mozer, P. Wagner, T. W. Schmidt, *Phys. Chem. Chem. Phys.* **2015**; c) S. P. Hill, T. Banerjee, T. Dilbeck, K. Hanson, *J. Phys. Chem. Lett.* **2015**, *6*, 4510-4517; d) A. Nattestad, Y. Y. Cheng, R. W. MacQueen, T. F. Schulze, F. W. Thompson, A. J. Mozer, B. Fückel, T. Khoury, M. J. Crossley, K. Lips, G. G. Wallace, T. W. Schmidt, *J. Phys. Chem. Lett.* **2013**, *4*, 2073-2078.

[7] a) Q. Liu, W. Feng, T. Yang, T. Yi, F. Li, *Nat. Protocols* **2013**, *8*, 2033-2044; b) Q. Liu, T. Yang, W. Feng, F. Li, *J. Am. Chem. Soc.* **2012**, *134*, 5390-5397; c) A. Nagai, J. B. Miller, P. Kos, S. Elkassih, H. Xiong, D. J. Siegwart, *ACS Biomater. Sci. Eng.* **2015**, *1*, 1206-1210; d) C. Wohnhaas, V. Mailänder, M. Dröge, M. A. Filatov, D. Busko, Y. Avlasevich, S. Baluschev, T. Miteva, K. Landfester, A. Turshatov, *Macromol. Biosci.* **2013**, *13*, 1422–1430; e) C. Wohnhaas, A. Turshatov, V. Mailänder, S. Lorenz, S. Baluschev, T. Miteva, K. Landfester, *Macromol. Biosci.* **2011**, *11*, 772-778; f) Q. Liu, B. Yin, T. Yang, Y. Yang, Z. Shen, P. Yao, F. Li, *J. Am. Chem. Soc.* **2013**, *135*, 5029-5037; g) O. S. Kwon, H. S. Song, J. Conde, H.-i. Kim, N. Artzi, J.-H. Kim, *ACS Nano* **2016**, *10*, 1512-1521.

[8] a) R. R. Sawant, V. P. Torchilin, *Soft Matter* **2010**, *6*, 4026-4044; b) A. S. L. Derycke, P. A. M. de Witte, *Adv. Drug Delivery Rev.* **2004**, *56*, 17-30; c) T. M. Allen, P. R. Cullis, *Adv. Drug Delivery Rev.* **2012**.

[9] a) H. J. Feldmann, M. Molls, P. Vaupel, *Strahlenther. Onkol.* **1999**, *175*, 1-9; b) P. Vaupel, F. Kallinowski, P. Okunieff, *Cancer Res.* **1989**, *49*, 6449-6465; c) E. E. Graves, M. Vilalta, I. K. Cecic, J. T. Erler, P. T. Tran, D. Felsher, L. Sayles, A. Sweet-Cordero, Q.-T. Le, A. J. Giaccia, *Clin. Cancer Res.* **2010**, *16*, 4843-4852.

[10] C. Wohnhaas, K. Friedemann, D. Busko, K. Landfester, S. Baluschev, D. Crespy, A. Turshatov, *ACS Macro Lett.* **2013**, *2*, 446-450.

[11] F. Marsico, A. Turshatov, R. Peköz, Y. Avlasevich, M. Wagner, K. Weber, D. Donadio, K. Landfester, S. Baluschev, F. R. Wurm, *J. Am. Chem. Soc.* **2014**.

[12] a) C. J. Brinker, G. W. Scherer, *Sol-Gel Science: The Physics And Chemistry Of Sol-Gel Processing*, Academic Press, Inc., **1990**; b) C. J. Brinker, *J. Non-Cryst. Solids* **1988**, *100*, 31-50; c) C. Barbe, J. Bartlett, L. G. Kong, K. Finnie, H. Q. Lin, M. Larkin, S. Calleja, A. Bush, G. Calleja, *Adv. Mater.* **2004**, *16*, 1959-1966; d) S. S. Lucky, K. S. Soo, Y. Zhang, *Chem. Rev.* **2015**.

[13] M. Frasconi, Z. C. Liu, J. Y. Lei, Y. L. Wu, E. Strekalova, D. Malin, M. W. Ambrogio, X. Q. Chen, Y. Y. Botros, V. L. Cryns, J. P. Sauvage, J. F. Stoddart, *J. Am. Chem. Soc.* **2013**, *135*, 11603-11613.

[14] Y. Leterrier, *Prog. Mater Sci.* **2003**, *48*, 1-55.

[15] a) M. Mirenda, V. Levi, M. L. Bossi, L. Bruno, A. V. Bordoni, A. E. Regazzoni, A. Wolosiuk, *J. Colloid Interface Sci.* **2013**, *392*, 96-101; b) D. Zhang, Z. Wu, J. Xu, J. Liang, J. Li, W. Yang, *Langmuir* **2010**, *26*, 6657-6662; c) L. M. Rossi, L. Shi, F. H. Quina, Z. Rosenzweig, *Langmuir* **2005**, *21*, 4277-4280.

[16] a) N. Folliet, C. Roiland, S. Bégu, A. Aubert, T. Mineva, A. Goursot, K. Selvaraj, L. Duma, F. Tielens, F. Mauri, G. Laurent, C. Bonhomme, C. Gervais, F. Babonneau, T. Azaïs, *J. Am. Chem. Soc.* **2011**, *133*, 16815-16827; b) S. Begu, R. Durand, D. A. Lerner, C. Charnay, C. Tourne-Peteilh, J. M. Devoisselle, *Chem. Commun.* **2003**, 640-641; c) D. H. W. Hubert, M. Jung, P. M. Frederik, P. H. H. Bomans, J. Meuldijk, A. L. German, *Adv. Mater.* **2000**, *12*, 1286-1290; d) N. V. Beloglazova, O. A. Goryacheva, E. S. Speranskaya, T. Aubert, P. S. Shmelin, V. R. Kurbangaleev, I. Y. Goryacheva, S. De Saeger, *Talanta* **2015**, *134*, 120-125; e) N. V. Beloglazova, I. Y. Goryacheva, P. S. Shmelin, V. Kurbangaleev, S. De Saeger, *J. Mater. Chem. B* **2015**, *3*, 180-183; f) A. Corma, U. Díaz, M. Arrica, E. Fernández, Í. Ortega, *Angew. Chem., Int. Ed.* **2009**, *48*, 6247-6250; g) S. Shen, L. Yang, Y. Lu, J.-G. Chen, S. Song, D. Hu, A. Parikh, *ACS Appl. Mater. Interfaces* **2015**.

[17] a) S. Bégu, A. A. Pouëssel, D. A. Lerner, C. Tourné-Péteilh, J. M. Devoisselle, *J. Controlled Release* **2007**, *118*, 1-6; b) S. Begu, S. Girod, D. A. Lerner, N. Jardiller, C. Tourne-Peteilh, J. M. Devoisselle, *J. Mater. Chem.* **2004**, *14*, 1316-1320; c) Y. Steinberg, A. Schroeder, Y. Talmon, J. Schmidt, R. L. Khalfin, Y. Cohen, J.-M. Devoisselle, S. Begu, D. Avnir, *Langmuir* **2007**, *23*, 12024-12031.

[18] D. Marsh, *Handbook of Lipid Bilayers*, 2nd ed., Taylor & Francis Group, LLC, Boca Raton, FL, USA, **2013**.

[19] F. Wang, S. L. Nimmo, B. Cao, C. Mao, *Chem. Sci.* **2012**, *3*, 2639-2645.

[20] a) S. Chen, S. Hayakawa, Y. Shirosaki, E. Fujii, K. Kawabata, K. Tsuru, A. Osaka, *J. Am. Ceram. Soc.* **2009**, *92*, 2074-2082; b) A. van Blaaderen, A. Vrij, *J. Colloid Interface Sci.* **1993**, *156*, 1-18.

[21] X.-d. Wang, J. A. Stolwijk, T. Lang, M. Sperber, R. J. Meier, J. Wegener, O. S. Wolfbeis, *J. Am. Chem. Soc.* **2012**, *134*, 17011-17014.

[22] a) Q. Liu, T. S. Yang, W. Feng, F. Y. Li, *J. Am. Chem. Soc.* **2012**, *134*, 5390-5397; b) C. Wohnhaas, V. Mailander, M. Droge, M. A. Filatov, D. Busko, Y. Avlasevich, S. Baluschev, T. Miteva, K. Landfester, A. Turshatov, *Macromol. Biosci.* **2013**, *13*, 1422-1430.

[23] M. Almgren, *J. Am. Chem. Soc.* **1980**, *102*, 7882-7887.

[24] S. H. Kim, O. H. Han, J. K. Kim, K. H. Lee, *Bull. Korean Chem. Soc.* **2011**, *32*, 3644-3649.

[25] a) B. Rånby, J. F. Rabek, *Singlet Oxygen Reactions with Organic Compounds & Polymers*, John Wiley & Sons, Ltd., **1978**; b) F. A. Carey, R. J. Sundberg, *Advanced Organic Chemistry*, 5 ed., Springer US, **2007**.

CHAPTER 8

Activation of liposome-bound Ru(II) prodrugs using red-to-blue triplet-triplet annihilation upconversion in a biological context

Light upconversion by means of triplet-triplet annihilation upconversion (TTA-UC) is a promising photochemical approach to shift the activation wavelength of photodissociative ruthenium(II) prodrugs to the phototherapeutic window. In this chapter, the biological application of liposomes doped with red-to-blue upconverting TTA-UC dyes and blue-light responsive Ru-prodrugs is addressed. The oxygen-sensitivity of TTA-UC in liposomes was effectively reduced by the addition of water-soluble and biocompatible anti-oxidants. This strategy also resulted in greatly enhanced upconversion emission in living cells. To demonstrate the *in vivo* applicability of upconversion mediated Ru-prodrug release, it was shown that red-to-blue TTA-UC could be generated at a depth of 12 mm in chicken and pork fillet, and that Ru prodrugs could be activated by red-to-blue TTA-UC at a depth of 7 mm in pork fillet under irradiation of a medical grade 630 nm PDT laser. Finally, the photocytotoxicity of the liposomes in combination with red light irradiation was investigated in A549, MCF7, and MRC5 cells. Unfortunately, neither irradiation of Ru-bound prodrugs with blue light (direct activation) nor with red light (mediated by TTA-UC) resulted in high toxicity compared to experiments conducted in the dark, due to the poor overall toxicity of the here-studied Ru complexes. Altogether, the results presented in this chapter provide valuable insights in which requirements need to be fulfilled in the future to achieve photoactivation of Ru-complexes by TTA-UC *in vitro.*

Sven H. C. Askes, Michael S. Meijer, Lucien N. Lameijer, Wim Pomp, Samantha L. Hopkins, Marlize van Breugel, Iris Landman, Tessel Bouwens, Thomas Schmidt, and Sylvestre Bonnet.

8.1 Introduction

Light-activatable ruthenium polypyridyl complexes have received considerable attention as promising anticancer pro-drugs in photoactivated chemotherapy (PACT).[1] It is proposed that upon excitation with visible light, they are transformed from the non-toxic "caged" compound to the cytotoxic species. With such compounds, undesired side-effects for patients can be greatly reduced by the excellent spatio-temporal control over activation. Also, the toxicity does not depend on the presence of oxygen, as opposed to photodynamic therapy (PDT) that functions by generating highly reactive oxygen species (ROS). Thus, using light-activatable Ru-complexes may be suitable for hypoxic tumor tissues for which PDT is not effective. Furthermore, non-covalent binding of ruthenium polypyridyl complexes to PEGylated liposomes by means of a lipophilic anchor-ligand may help targeting these compounds towards tumor tissues by making use of the leaky vasculature of tumors, i.e. the enhanced permeability and retention effect .[2]

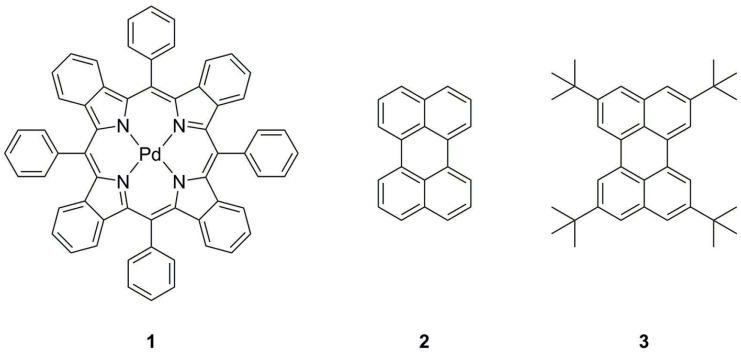

*Figure 8.1. Chemical structures of palladium(II) tetraphenyltetrabenzoporphyrin (**1**), perylene (**2**), and 2,5,8,11-tetra(tert-butyl)perylene (**3**).*

However, most Ru-complexes are only activatable with blue or green light, while those wavelengths do not penetrate human tissue very well. Shifting the excitation wavelength of ruthenium complexes to the phototherapeutic window (600 – 950 nm) by molecular design remains very challenging.[3] To circumvent this problem, upconversion of light can be used to locally "upgrade" red to near-infrared photons to blue or green photons, with which the pro-drug can be activated. Especially the combination of red-to-blue triplet-triplet annihilation upconversion (TTA-UC) and light-sensitive ruthenium complexes on liposomal drug carriers is very promising, as demonstrated in Chapter 3 and Chapter 4.[4] A red-to-blue TTA-UC dye couple

consisting of palladium(II) tetraphenyltetrabenzoporphyrin (**1**) and perylene (**2**, see Figure 8.1) was doped in PEGylated liposomes and used for effectively triggering the photodissociation reaction of [Ru(tpy)(bpy)(thioether-cholesterol)]$^{2+}$ ($\mathbf{4}^{2+}$, see Figure 8.2) to [Ru(tpy)(bpy)(H_2O)]$^{2+}$ ($\mathbf{8}^{2+}$). In further experiments (Chapter 4), lifetime and steady-state spectroscopy experiments revealed that the upconverted blue light of **2** was transferred with ~90% efficiency to $\mathbf{4}^{2+}$ via a Förster resonance energy-transfer (FRET) mechanism when all three molecules were doped in the same liposome membrane.

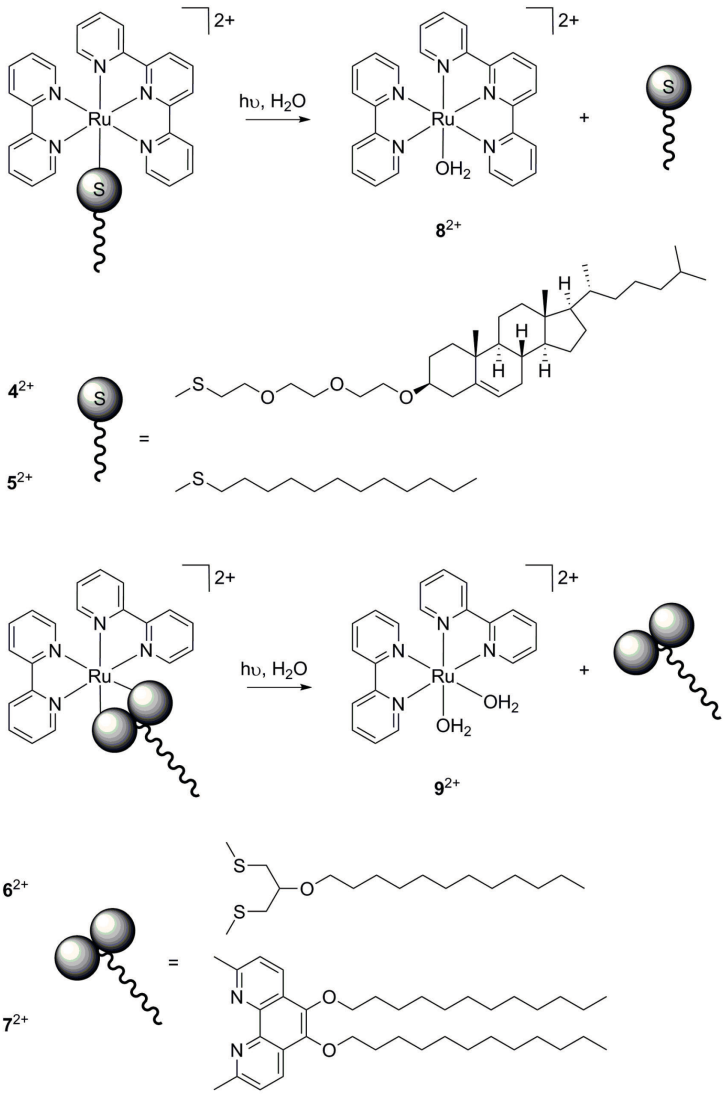

Figure 8.2. Chemical structures of ruthenium polypyridyl complexes $\mathbf{4}^{2+}$, $\mathbf{5}^{2+}$, $\mathbf{6}^{2+}$, and $\mathbf{7}^{2+}$ and their photochemical reaction to the aquated species $\mathbf{8}^{2+}$ or $\mathbf{9}^{2+}$.

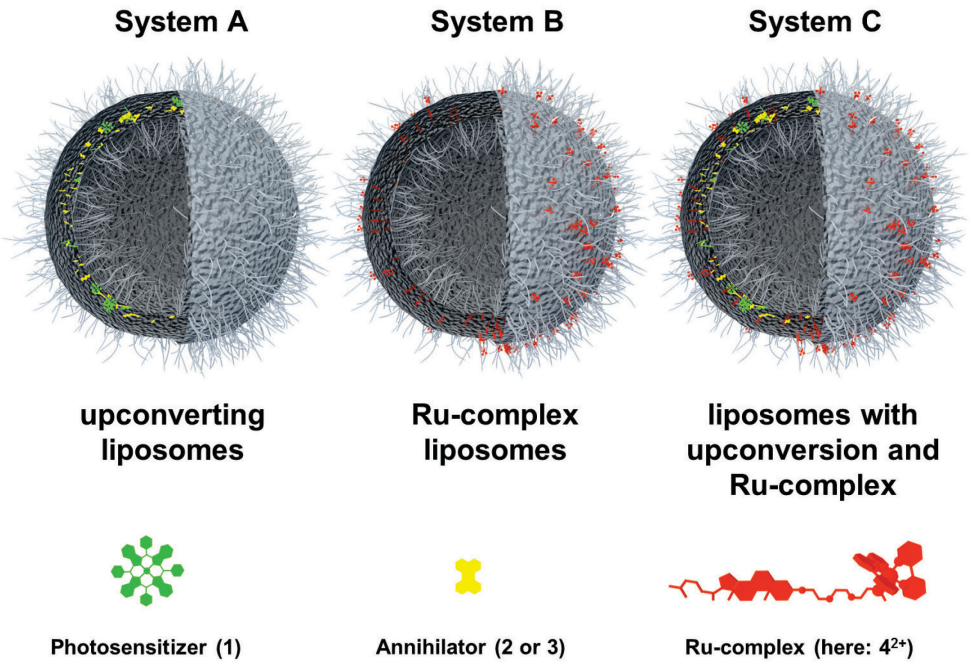

Figure 8.3. Schematic representation of the three liposome systems (System A, B, and C) studied in this chapter. Compound $\mathbf{4}^{2+}$ *features as an example of a Ru-complex which can be anchored to liposome membrane.*

However, the biological application of these upconverting liposomes doped with Ru-prodrugs is not straightforward. Especially the biocompatibility and toxicity of the system, the oxygen sensitivity of the TTA-UC mechanism, and the photoactivation with red light in biological systems have not been addressed so far. Moreover, the (photo)cytotoxicity of Ru-prodrug doped liposomes with blue light irradiation (*i.e.* without upconversion) has not yet been investigated as well. In this chapter, three major types of liposomes will be prepared, called System A, B, and C (Figure 8.3), and their photochemical properties and (photo)cytotoxicity will be evaluated. System A consists of liposomes doped with upconverting dyes **1** and **2** or **1** and **3**; System B consists of liposomes doped with only Ru-complex $\mathbf{4}^{2+}$, $\mathbf{5}^{2+}$, $\mathbf{6}^{2+}$, or $\mathbf{7}^{2+}$; System C consists of liposomes doped with upconverting dyes **1** and **3** and Ru-complex $\mathbf{6}^{2+}$. The following research questions will be addressed:

i. Are red-to-blue upconverting liposomes able to produce upconversion *in vitro* and can the oxygen sensitivity of TTA-UC in cells be reduced? (System A)

ii. Are upconverting liposomes cytotoxic in the dark and what becomes their cytotoxicity under red-light irradiation? (System A)
iii. How are upconverting liposomes digested after uptake? (System A)
iv. Up to which depth can TTA-UC with red-to-blue upconverting liposomes be generated in a model of healthy human tissue? (System A)
v. Is it really advantageous to use red light instead of blue light? Does the greater penetration depth of red light with respect to blue light result in a greater degree of prodrug activation? (System C)
vi. Are liposomes doped with ruthenium complexes (photo)cytotoxic under dark and blue light irradiated conditions? (System B)
vii. Can ruthenium prodrugs on liposomes be activated by red-to-blue TTA-UC *in vitro* in hypoxic conditions? (System C)

8.2 Results and discussion

8.2.1 Liposome preparation

Neutral PEGylated liposomes were prepared by a standard hydration-extrusion protocol in phosphate buffered saline (PBS) as described before (Chapter 3 – Chapter 7). Where applicable, before addition to the lipid film, PBS was supplemented with a known concentration of L-ascorbic acid (L-Asc) and/or glutathione (GSH), and neutralized to *pH* 7.0 – 7.6 with NaOH. The major component of all liposomes was a neutral phospholipid, *i.e.* either 1,2-dilauroyl-*sn*-glycero-3-phosphocholine (DLPC, liposomes denoted with L in Table 8.1) or 1,2-dimyristoyl-*sn*-glycero-3-phosphocholine was used (DMPC, liposomes denoted with M). The liposomes were PEGylated with 4 mol% sodium N-(carbonyl-methoxy polyethyleneglycol-2000)-1,2-distearoyl-*sn*-glycero-3-phospho ethanolamine (DSPE-mPEG-2000), which is known to prevent aggregation and prolong the blood-circulation lifetime of liposomes.[2] Finally, the liposomes were doped with either the TTA-UC dye couple (System A; 0.05 mol% **1**, 0.5 mol% **2** or **3**), or Ru-complex (System B; 4 mol% $\mathbf{4}^{2+}$, $\mathbf{5}^{2+}$, $\mathbf{6}^{2+}$, or $\mathbf{7}^{2+}$), or all three components (System C; 0.05 mol% **1**, 1 mol% **3**, and 4 mol% $\mathbf{6}^{2+}$); see Figure 8.3 for a schematic representation of systems A, B, and C and Table 8.1 for the exact liposome formulations and the codes used to name all liposomes. Incorporation of all dopants in the final samples was complete, as the extrusion filter during liposome preparation remained almost colorless. Dynamic light scattering (DLS) experiments revealed that the

hydrodynamic size (z-ave) of all liposomes varied from 130 – 170 nm with an average polydispersity index (PDI) of 0.1.

Table 8.1. Summary of liposome formulations used in this chapter. Liposomes with designation L or M are made with DLPC or DMPC as main lipid, respectively.

System	Code	[DMPC] mM	[DLPC] mM	[PEG][a] mM	[**1**] µM	[**2**] µM	[**3**] µM	[$\mathbf{4}^{2+}$] µM	[$\mathbf{5}^{2+}$] µM	[$\mathbf{6}^{2+}$] µM	[$\mathbf{7}^{2+}$] µM
A	**L1-2**		5.0	0.20	2.5	25					
	M1	5.0		0.20	2.5						
	M2	5.0		0.20		25					
	M3	5.0		0.20			25				
	M1-3	5.0		0.20	2.5		25				
B	**M4**	5.0		0.20				200			
	M5	5.0		0.20					200		
	M6	5.0		0.20						200	
	M7	5.0		0.20							200
C	**L1-3-6**		5.0	0.20	2.5		50			200	
	M1-3-6	5.0		0.20	2.5		50			200	
	M3-6	5.0		0.20			50			200	

[a] PEG = DSPE-mPEG-2000

8.2.2 Anti-oxidants protect TTA-UC in DLPC liposomes in air in solution

One strategy of reducing the oxygen-sensitivity of TTA-UC in liposomes is the addition of water soluble anti-oxidants that react with ground state or singlet state oxygen to chemically deoxygenate the solution. To evaluate the influence of water-soluble anti-oxidants on TTA-UC, red-to-blue upconverting PEGylated DLPC liposomes (**L1-2**) were mixed with various amounts of L-Asc or GSH. Here, DLPC was used as main lipid, because red-to-blue TTA-UC was found to be much more efficient at room temperature in DLPC than DMPC liposomes (Chapter 6). The UV-vis absorbance spectrum of **L1-2** in presence of 5 mM L-Asc shows the typical absorption peaks of **2** between 375 and 450 nm, and the absorption peaks of **1** at 440 and 630 nm (Figure 8.4a). A small band below 400 nm was attributed to absorption of L-Asc and oxidized ascorbate products. When the sample was irradiated with 10 mW 630 nm light (80 mW.cm^{-2}), emission spectra (recorded every 3 s) after switching on the laser initially showed only weak phosphorescence of **1** at 800 nm and no upconversion emission (Figure 8.4a, inset). However, after 1 min of red light irradiation, the phosphorescence at 800 nm suddenly intensified and intense upconversion emission at 474 nm was observed. We define the progressed time until this time-point as the "lag-time" (see Figure 8.4a, inset). After 2 min, the emission spectrum had stabilized in time and it was identical to that observed under deoxygenated conditions (see Chapter 6, Figure 6.2). No upconversion was observed in air in absence of L-Asc (data not shown). To explain this observation, it was hypothesized that upon irradiation compound

1 first reacted with ground-state oxygen to make singlet oxygen, that in turn reacted with L-Asc. This photoreaction was repeated until all ground-state oxygen present in the irradiated solution was depleted. When the oxygen concentration becomes low enough, triplet-state photosensitizer and annihilator are no longer quenched, leading to efficient TTA-UC and increased phosphorescence of **1**.

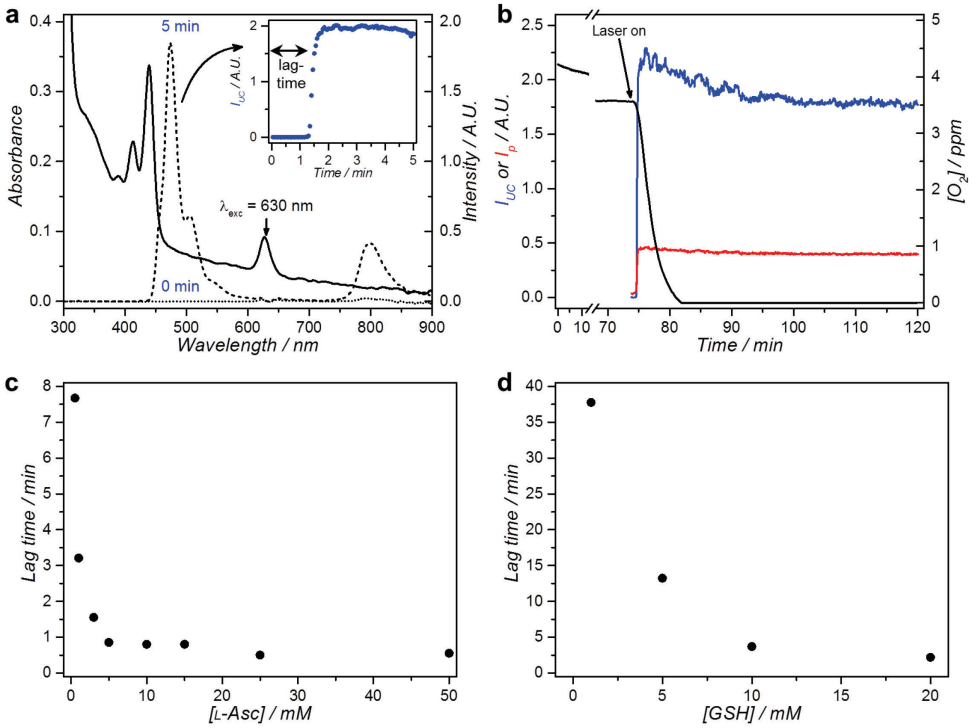

*Figure 8.4. Emission spectroscopy in air of **L1-2** liposomes PBS supplemented with L-Asc or GSH. a) Absorption (solid) and emission spectra (dotted: t = 0; dashed: t = 5 min) of **L1-2** liposomes in PBS supplemented with 5 mM L-Asc. Inset shows the upconversion intensity (I_{UC} at 474 nm) for the first 5 min of irradiation with 3 s intervals. b) Time trace of the upconversion intensity (I_{UC} at 474 nm, blue), phosphorescence intensity (I_p at 800 nm, red), and dissolved oxygen concentration (black) during red light irradiation of **L1-2** liposomes in PBS supplemented with 5 mM L-Asc. The laser was turned on after 74 min in the dark, as indicated by the arrow. c/d) Lag-time as a function of [L-Asc] (c) or [GSH] (d). Exp. conditions: [DLPC] = 1 mM, [**1**] = 0.5 μM, [**2**] = 5 μM, 2.25 mL sample, T = 20 °C 10 mW 630 nm laser excitation (80 mW.cm^{-2}) with approximately 8% of the volume simultaneously irradiated, pH 7.0 – 7.6.*

To confirm this hypothesis, the experiment was repeated while measuring the dissolved oxygen concentration using a NeoFox oxygen probe dipped in the solution (Figure 8.4b). In the first 74 min the sample was left in the dark and the oxygen concentration remained close to the initial value, showing that

ground state O_2 quenching is very slow with L-Asc. When the laser was turned on however, rapid consumption of all the oxygen in the cuvette was observed within 5 min while intense upconversion emission was observed after 1 min of continuous irradiation. The upconversion was stable for the next 45 min after which the experiment was stopped. Overall, these results demonstrate that the addition of L-Asc to a dispersion of upconverting liposomes allows efficient and stable upconversion to occur in air due to singlet-oxygen consumption upon irradiation.

To study whether the lag-time varies with anti-oxidant concentration, the experiment was repeated with [L-Asc] ranging from 0.25 to 50 mM and the lag-time was measured in each situation (Figure 8.4c). Noteworthy a concentration of 0.25 mM did not give rise to any upconversion, presumably because the concentration of oxygen in air-equilibrated water has about the same value (9 ppm; ~0.25 mM). Upon increasing [L-Asc] from 0.5 mM to 5.0 mM, the lag-time strongly decreased from 8 min to 1 min and had a value of ca. 0.5 min at a concentration of 50 mM. The same experiments were performed with GSH as anti-oxidant at 1 – 20 mM concentrations (Figure 8.4d), which is close to physiological concentrations of this biological anti-oxidant (0.5 – 10 mM).[5] For all concentrations, intense upconversion was also observed after a certain lag-time, but the lag-times were significantly longer than with L-Asc. Finally, a combination of 1 mM L-Asc and 5 mM GSH was used as anti-oxidant "cocktail". Stable upconversion was observed after 1.1 min, which is significantly faster than either of the anti-oxidants alone (3.2 min for [L-Asc] at 1 mM; 13 min for [GSH] at 5 mM). This result suggests that using a combination of L-Asc and GSH synergistically minimizes the lag-time. For this reason, in further experiments a combination of these two anti-oxidants was used. In conclusion, it was demonstrated that the addition of biologically relevant concentrations of biological anti-oxidants to upconverting liposomes results in stable TTA-UC in air-equilibrated solutions. Unfortunately, **L1-2** liposomes were found to be unsuitable for *in-vitro* experiments, due to high cytotoxicity of the PEGylated DLPC liposomes in preliminary experiments: when A549 lung carcinoma cells were incubated with **L1-2** liposomes ([DLPC] = 0.5 mM) for 4 h, 100% cell death was observed (data not shown). In contrast, DMPC liposomes were much less toxic and selected for the *in vitro* experiments (see below).

8.2.3 Anti-oxidants protect TTA-UC for DMPC liposomes *in vitro*

To investigate whether the addition of anti-oxidants would also enhance TTA-UC in cells, A549 lung carcinoma cells were grown *in vitro* and incubated with upconverting DMPC liposomes **M1-3** for 24 h with or without an anti-oxidant "cocktail" composed of 2 mM L-Asc and 2 mM GSH. Perylene (compound **2**) was replaced by 2,5,8,11-tetra(*tert*-butyl)perylene (compound **3**) to avoid partitioning of the annihilator to the water phase, which is known to occur for normal perylene.[6] Indeed, it was found that tert-butylation prevented liposomal escape of **3** (see Appendix VII for data and discussion). These experiments also confirmed that compound **1** does not escape from liposomes. After 24 h incubation and removing the excess of liposomes, the cells were imaged in bright field mode, with 405 nm, and with 639 nm excitation (2.7 and 26 $W.cm^{-2}$ intensity, respectively). Additionally, a 1% oxygen atmosphere was used to mimic median tumor oxygen partial pressures, which generally range from 0.5% to 4% (pO_2 = 5 – 30 mm Hg).[7] Using 405 nm excitation compound **3** was excited directly, leading to normal fluorescence. In this mode numerous fluorescent spots were observed throughout the cell cytoplasm, indicating that the liposomes had been successfully taken up. The presence of anti-oxidants did not influence the uptake of the vesicles. In absence of anti-oxidants, 639 nm excitation did not lead to significant upconversion luminescence, indicating that the liposomes were not capable of producing upconversion. However, when the cells were co-incubated with the anti-oxidant cocktail, bright upconversion was observed at the same sites as that of the fluorescence observed under 405 nm excitation. This result indicates that at these locations, both dyes were present simultaneously, thus suggesting that the liposomes were intact and functional. Note that under these conditions the upconversion luminescence was not very stable: it quickly faded and disappeared within a few seconds. Overall, these results demonstrate that co-treatment of cells with biologically relevant amounts of anti-oxidants can significantly boost upconversion of **M1-3** liposomes *in vitro*.

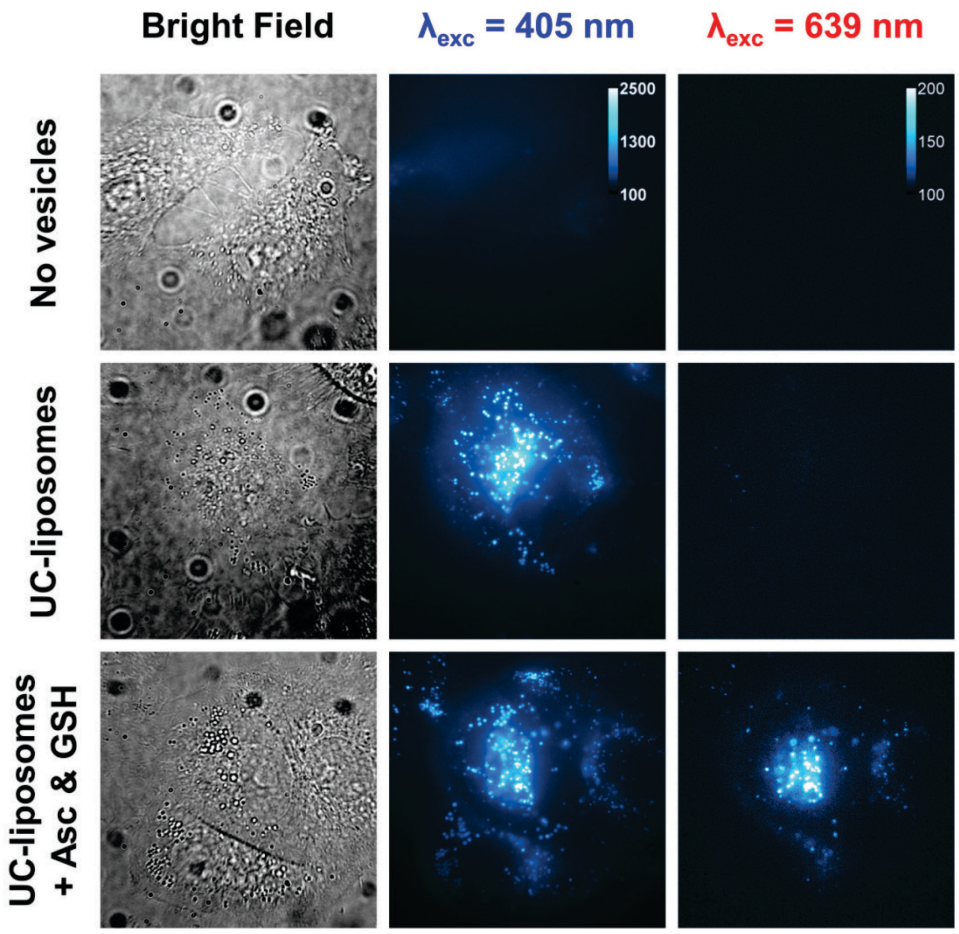

*Figure 8.5. In vitro upconversion imaging of **M1-3** upconverting liposomes in living A549 lung carcinoma cells in bright field mode (left column), with λ_{exc} = 405 nm and λ_{em} = 450 – 525 nm (middle column), and with λ_{exc} = 635 nm and λ_{em} = 450 – 525 nm (right column) at 100x magnification. Cells were incubated for 24 h with medium only (top row), with **M1-3** liposomes (middle row, [DMPC] = 1 mM), or **M1-3** liposomes with addition of 2 mM L-Asc and 2 mM GSH (bottom row, [DMPC] = 1 mM). Imaging conditions: T = 37 °C, 7.0% CO_2, 1.0% O_2, 75 µW 405 nm laser power (60 µm spot diameter, 2.7 W.cm^{-2} intensity), 1.0 mW 639 nm laser power (70 µm spot diameter, 26 W.cm^{-2} intensity). For comparability, the images are identically colored for λ_{exc} = 405 nm from 100 – 2500 pixel values (black → blue → white) , and for λ_{exc} = 635 nm from 100 – 200 pixel values (black → blue → white), as indicated by the calibration bars in the top row.*

To investigate the exact location of **M1-3** liposomes, the cells were additionally stained with LysoTracker Red DND-99 to label acidic organelles such as late endosomes and lysosomes. This probe is not excited with either 405 or 639 nm (Figure S.VII.2), and therefore does not interfere with the

fluorescence and upconversion luminescence imaging. Although live-cell colocalization was challenging due to the rapid movement of some of the fluorescent sites, images were successfully acquired in bright field mode, and with 405, 561, and 639 nm excitation when excitation sources were quickly changed (Figure 8.6). It was found that prompt fluorescence of compound **3** (λ_{exc} = 405 nm), upconversion luminescence (λ_{exc} = 639 nm), and LysoTracker Red fluorescence (λ_{exc} = 561 nm) all co-localized centrally in the cytosol. This colocalization indicates that the upconverting liposomes are present in acidic vesicles inside the cell. Therefore, **M1-3** liposomes are probably taken up by endocytosis and accumulate in late endosomes and lysosomes.

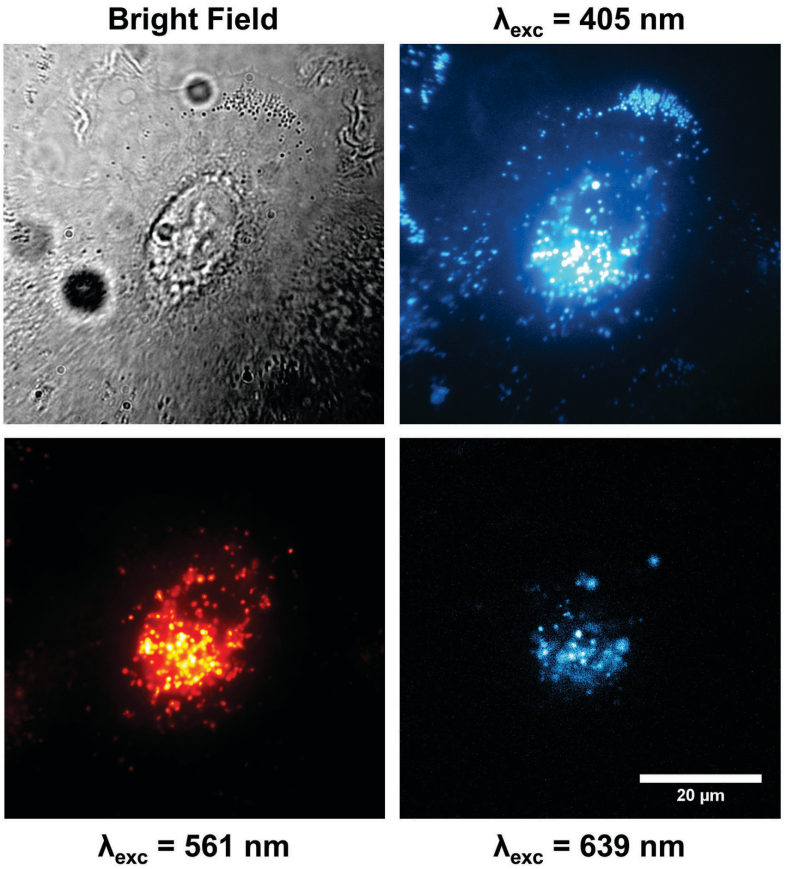

*Figure 8.6. In vitro imaging of **M1-3** liposomes in living A549 cells that were additionally stained with LysoTracker Red DND 99 in bright field mode, with λ_{exc} = 405 nm (to excite compound **3**), with λ_{exc} = 561 nm (to excite LysoTracker), and with λ_{exc} = 639 nm to generate TTA-UC (λ_{em} = 450 – 525 nm) at 1 % O_2. The cells had been incubated for 24 h with **M1-3** and anti-oxidants prior to imaging ([DMPC] = 1 mM, [L-ascorbate] =[GSH] = 5 mM). Same imaging conditions as in Figure 8.5.*

Curiously, upconversion was not observed at all locations where fluorescence of compound **3** was observed (Figure 8.5 and Figure 8.6). Whereas upconversion luminescence was especially located around the nucleus, the peripheral sites showing fluorescence of **3** did not produce any detectable upconversion. The peripheral fluorescence sites were found to be strongly clustered, strongly contrasting in bright-field mode, and not stained by LysoTracker Red (Figure 8.6). Furthermore, their size and location closely resemble that of lipid droplets[I] in HeLa and A549 cells.[8] We thus propose that compound **3** accumulates in lipid droplets after the digestion of the liposomes in lysosomes. The fact that the lipid droplets do not produce upconversion may be due to separation of **1** and **3** after liposome digestion, or because the local oxygen concentration in the lipid droplets is higher compared to endo- and lysosomes and TTA-UC is quenched. To investigate the latter hypothesis, cells were first treated with liposomes in absence of anti-oxidants. Then, instead of using singlet-oxygen scavengers, the cells were imaged in presence of 100 mM sodium sulfite (neutralized to *pH* 7) as ground-state oxygen to effectively deoxygenate the entire medium. Although many cells did not survive this treatment because of the dramatic increase in osmotic pressure, some cells could be successfully imaged before their death (Figure 8.7). The images strongly resemble the situation where the cells were co-treated with L-Asc and GSH: both the acidic organelles and the lipid droplets exhibit fluorescence of **3** (λ_{exc} = 405 nm), but upconverted emission (λ_{exc} = 639 nm) was only observed centrally in the cell. This result indicates that upconversion cannot be realized at any oxygenation level in the lipid droplets, and that compounds **1** and **3** must be physically separated and/or that compound **1** is degraded during digestion of the liposomes.

[I] Lipid droplets are the cell's organelles for lipid storage and metabolism.

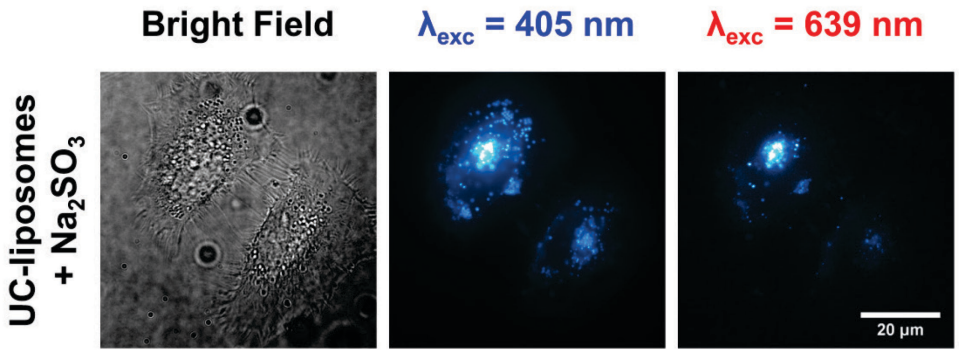

*Figure 8.7. In vitro imaging of **M1-3** liposomes in living A549 cells in bright field mode (left), with λ_{exc} = 405 (middle), and with λ_{exc} = 639 nm (right). After 24 h incubation with **M1-3** liposomes, the medium was refreshed, and the cells were imaged at 37 °C, 20% O_2 and 7% CO_2. Just before recording these images, 100 mM Na_2SO_3 in PBS (pH 7) was added to deoxygenate the medium. Other imaging conditions as in Figure 8.5.*

8.2.4 Cytotoxicity of upconverting DMPC liposomes with red light irradiation

It has been reported that photosensitizer **1** generates singlet oxygen upon red-light irradiation,[9] which is a highly cytotoxic species. In fact, singlet-oxygen generating photosensitizers are frequently used in photodynamic therapy (PDT) type II to kill cancer cells. Thus, it was anticipated that irradiation of **M1-3** liposomes inside living cells may lead to cell death. Therefore, the toxicity of upconverting DMPC liposomes was evaluated in the dark and upon red-light irradiation by treating three cell lines with **M1-3** liposomes according to a recently published (photo)cytotoxicity protocol developed in our group.[10] The cell lines used for this study were A549 (human lung carcinoma), MCF7 (human breast adenocarcinoma) and MRC5 (normal human lung) cells. As controls, **M1** (doped with only the photosensitizer) and **M3** (doped with only the annihilator) liposomes were used. In short, the photocytotoxicity protocol involved incubation of the cells with the liposomes for 24 h, after which the medium was refreshed and the cells were either irradiated in normoxic conditions (7% CO_2, 20% O_2, 37 °C) with high-power red light (628 nm, 23.0 ± 1.5 mW, 15 min, 20.7 J.cm^{-2}) or kept in the dark in otherwise identical conditions. The viability of the cells 48 h after irradiation was quantified with a sulforhodamine B staining assay. Prior to these experiments, the uptake of **M3** and **M1-3** liposomes after 24 h incubation was verified by imaging the fluorescence of **3** in the cells by fluorescence microscopy (λ_{exc} = 377 nm, Figure S.VII.3 and Figure S.VII.4). Because compound **1** is not emissive under these conditions, the uptake of **M1**

liposomes could not be visualized and we assumed that the uptake of **M1** is similar to the uptake of **M3**.

Figure 8.8 shows the evolution of cell viability as a function of the liposome concentration, expressed as the bulk concentration of DMPC (in mM) or compound **1** (in nM). In dark conditions, the data showed a limited decrease in cell viability of A549 and MCF7 cells treated with increasing liposome concentration, while the MRC5 cells were unaffected at any liposome concentration tested. This dark cytotoxicity can be explained by a lipid overdose at higher concentrations (> 100 μM). However, such high liposome concentrations are probably not clinically relevant[II] and it can thus be concluded that upconverting liposomes **M1-3** are non-toxic in the dark. Following red light irradiation, the dose-response curves were found to be very similar to those obtained in dark conditions. This result is surprising, as the experiments were carried out in a 20% O_2 atmosphere where PDT effects were expected. Apparently, the amount of singlet oxygen generated is too low to induce a cytotoxic effect. We attribute the low amount of singlet oxygen generation to the much lower photosensitizer dye doping (~0.05 mol% with respect to the lipid) compared to published liposomal PDT studies. For instance, one study reports M5076 ovarian sarcoma cells incubated with photofrin-loaded liposomes (8 mol% photofrin with respect to lipid) for 1 h[III] and exposed to 2 J.cm^{-2} 630 nm light;[13] this treatment caused approximately 50% cell death at a photofrin bulk concentration of 9 nM. Other explanations for the absent PDT effect may be: (i) the amount of endocytosed liposomes is too low to import enough photosensitizer; (ii) singlet oxygen that is generated in endo- and lysosomes may be less harmful compared to other cellular targets such as the mitochondria;[14] (iii) or the photosensitizer may be bleached before a significant amount of singlet oxygen is produced. Overall, our results clearly show that **M1-3** liposomes are not (photo)cytotoxic below

[II] Two clinically used liposomal anti-cancer drug formulations are Lipoplatin™ (9:91 w/w% cisplatin/lipid) and Doxil (11:89 w/w% doxorubicin/lipid).[11] The recommended dose of Lipoplatin™ is 200 mg.m^{-2} body surface area per 14 days. Given an average human body surface of 1.7 m^2, this leads to a dose of 309 mg lipids. At about 5 L of blood volume, the lipid in blood concentration would be 62 mg.L^{-1} (~ 85 μM). The recommended dose of Doxil is 50 mg/m^2 doxorubicin. Using the same figures, the lipid in blood concentration directly after administration would be 0.17 mM. These calculations suggest that lipid concentrations higher than ~0.1 mM, for which **M1-3** starts to become toxic, are probably not relevant for clinical application. Furthermore, liposome uptake studies in mice from the late 1980s and early 1990s report concentrations of 0.1 – 0.7 mM (in blood circulation directly after injection).[12]

[III] The authors do not mention refreshment of the medium before irradiation.

0.1 mM [DMPC] in the dark and under a high dose of red-light irradiation (20.7 J.cm^{-2}) in both cancer cells and healthy cells.

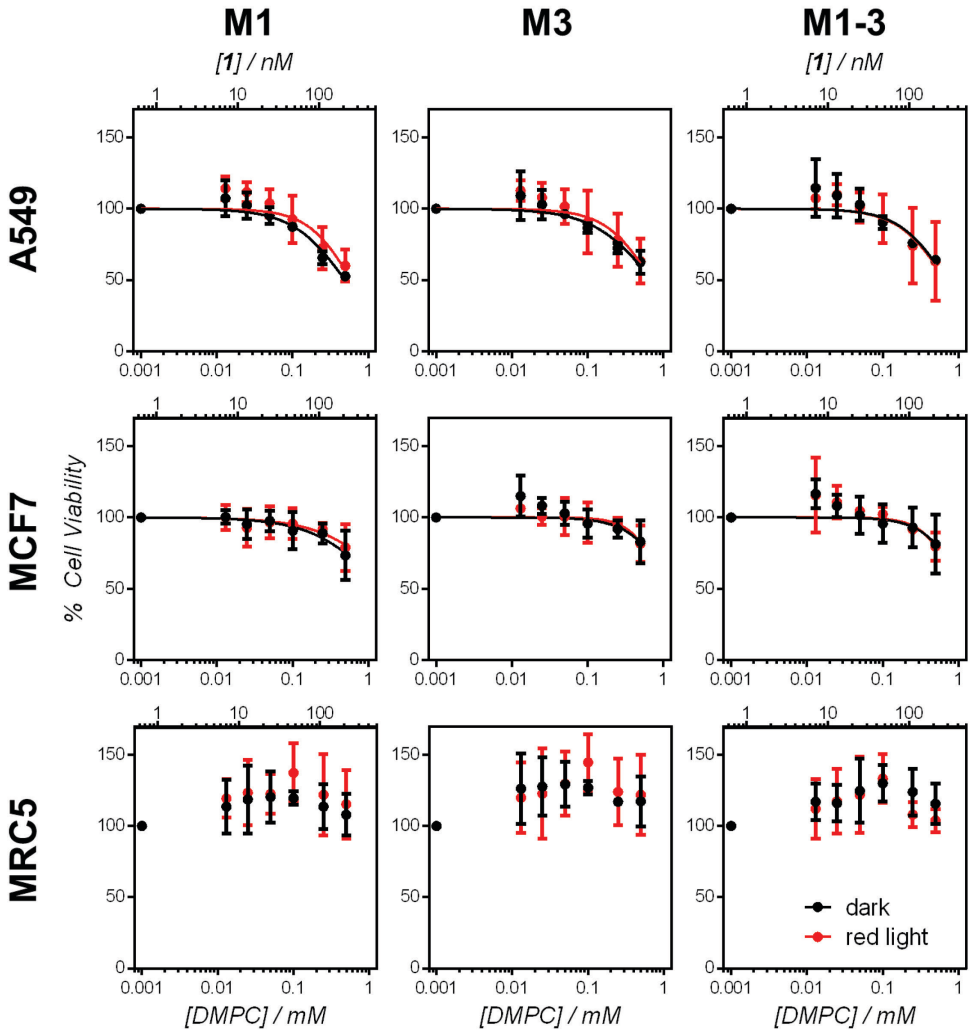

*Figure 8.8. Cell viability of A549 (top row), MCF7 (middle row) and MRC5 cells (bottom row) treated with **M1** (left column), **M3** (middle column), or **M1-3** liposomes (right column) and left in the dark (black data points) or irradiated for 15 min with 628 nm light (red data points, 20.7 J.cm^{-2} light dose) as a function of [DMPC] (bottom axes) or [**1**] (top axes). Solid lines represent Hill-slope fit curves to the same color data points. Error bars represent the standard deviation of the mean cell viability value from three individual biological experiments.*

8.2.5 Anchoring amphiphilic Ru-complexes to DMPC liposomes

After establishing the photophysical properties and low cytotoxicity of the upconverting liposomes (System A), the photocytotoxicity of Ru-complex

functionalized liposomes (System B) irradiated with blue light in absence of upconversion was considered. Four Ru-complexes were investigated for use in System B: compounds $\mathbf{4}^{2+}$, $\mathbf{5}^{2+}$, $\mathbf{6}^{2+}$, and $\mathbf{7}^{2+}$ (Figure 8.2). These compounds all dissolve poorly in water, and feature a cationic Ru^{2+} compound functionalized with a lipophilic ligand (cholesterol-thioether in $\mathbf{4}^{2+}$, alkyl-thioether in $\mathbf{5}^{2+}$ and $\mathbf{6}^{2+}$, and double alkyl-tailed neocuproine in $\mathbf{7}^{2+}$). Each of these compounds is non-emissive (Φ_{em} << 1%) and photodissociative: upon blue-light irradiation in water, compounds $\mathbf{4}^{2+}$ and $\mathbf{5}^{2+}$ react to mono-aqua product $[Ru(tpy)(bpy)(H_2O)]^{2+}$ (compound $\mathbf{8}^{2+}$),[15] and compounds $\mathbf{6}^{2+}$ and $\mathbf{7}^{2+}$ react to bis-aqua product $[Ru(bpy)_2(H_2O)_2]^{2+}$ (compound $\mathbf{9}^{2+}$; see Figure S.VII.6 to Figure S.VII.8). In presence of liposomes, these compounds insert in the membrane and upon blue-light irradiation the photoproduct dissociates from the membrane as illustrated in Figure 8.9a.[16] Thus, PEGylated DMPC liposomes were functionalized with 4 mol% $\mathbf{4}^{2+}$, $\mathbf{5}^{2+}$, $\mathbf{6}^{2+}$, or $\mathbf{7}^{2+}$ (**M4**, **M5**, **M6**, and **M7** respectively). In spite of the lipophilic anchor ligands it was initially uncertain whether the Ru complexes were adequately anchored and would not escape the membrane over time in the dark. In an *in vivo* situation, such "hopping" would mean that in the dark the Ru-complex would escape the liposome drug carrier and insert in biological membranes, *i.e.* before the tumor site is reached, leading to poor selectivity and to potential side-effects.

To investigate whether or not hopping of the complexes from one membrane to another occurs, a simple but effective assay was developed, illustrated in Figure 8.9b. In short, **M4**, **M5**, **M6**, or **M7** liposomes were added to a stirred solution of **M3** liposomes while measuring the fluorescence intensity of **3** (λ_{exc} = 420 nm, λ_{em} = 486 nm). As discussed in Appendix VII, **3** does not hop from membrane to membrane. Compounds $\mathbf{4}^{2+}$, $\mathbf{5}^{2+}$, $\mathbf{6}^{2+}$, and $\mathbf{7}^{2+}$ all have substantial absorbance overlap with the emission of **3** (Figure S.VII.5), so that FRET occurs if the Ru complexes come in close proximity of **3**, as was reported in Chapter 4.[4b] Also, fusion of the liposomes does not spontaneously occur (no changes in DLS were observed upon mixing), and close liposomal proximity is prevented because both liposome samples are sterically hindered with PEG groups.

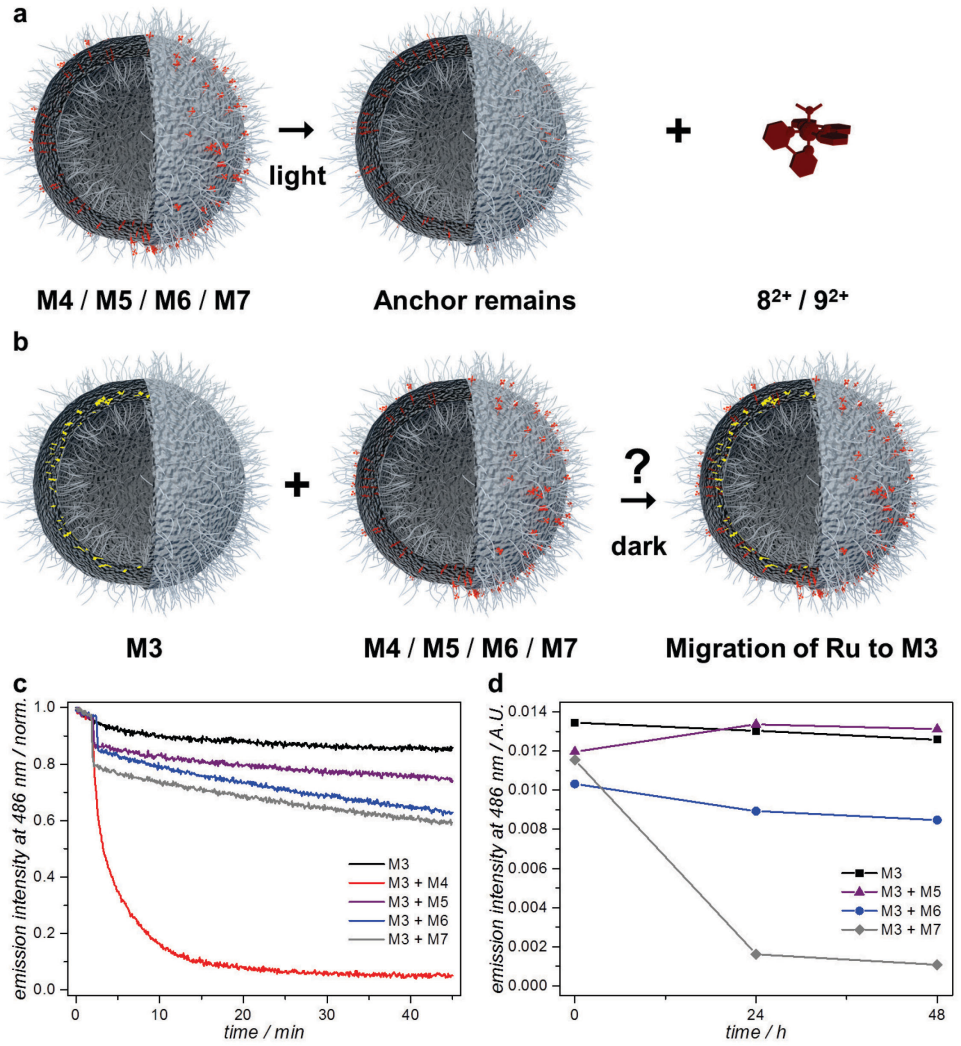

Figure 8.9. Fluorescence assay to determine "hopping" of Ru-complexes ***4***$^{2+}$, ***5***$^{2+}$, ***6***$^{2+}$, *and* ***7***$^{2+}$ *from liposome to liposome. a) Cartoon illustrating the photodissociation reaction of a Ru complex that is anchored to a liposome with a lipophilic ligand: upon irradiation the photoproduct dissociates while the anchor remains (here* ***4***$^{2+}$ *reacts to* ***8***$^{2+}$*). b) Cartoon of the hopping process. c/d) Fluorescence emission intensity of* ***3*** *at 486 nm (*λ_{exc} *= 420 nm, 240 µW.cm*$^{-2}$ *intensity) as a function of time after mixing liposomes* ***M3*** *with* ***M4***, ***M5***, ***M6***, *or* ***M7*** *for the first 45 min (c) and for 24 h and 48 h after mixing (d). In part (c), the Ru-doped liposomes were added at t = 2 min. Conditions: 2 mL volume in a stirred macro cuvette at 20 °C, [DMPC] = 50 µM of each liposome formulation,* ***[3]*** *= 0.25 µM.*

In Figure 8.9 the fluorescence intensity of **3** as a function of time after mixing is shown. While the fluorescence intensity in the mixtures of **M3** and **M5**, **M3** and **M6**, or **M3** and **M7** stayed relatively stable with time, the fluorescence

intensity of **3** in the mixture of **M3** and **M4** rapidly decreased within the first 20 minutes after mixing and was quenched by 95% after 45 min. Negligible reduction in fluorescence was observed for **M3** without any addition. It is thus very clear that $\mathbf{4}^{2+}$ is inadequately trapped in **M4** liposomes and readily equilibrates with the membrane of **M3** within the first 45 minutes of mixing. The other Ru complexes seem to be tightly anchored to the liposomes, at least during the first 45 min. In a further experiment, the fluorescence of **3** in these mixtures was measured 24 and 48 h after mixing (Figure 8.9b). The fluorescence intensity of **3** in the mixtures of **M3** and **M5**, and **M3** and **M6** was again very stable, but it decreased greatly for the mixture of **M3** and **M7** (~90% quenching after 48 h). Thus, $\mathbf{7}^{2+}$ also hops from membrane to membrane, but slower than $\mathbf{4}^{2+}$. These results imply that it is not straightforward to synthesize a lipophilic anchor to trap an inorganic Ru-complex to a liposome. For $\mathbf{3}^{2+}$ we attribute the escape to the PEG_3-cholesterol moiety of $\mathbf{3}^{2+}$ being not lipophilic enough. However, it was surprising to find that a double-tail alkyl ligand ($\mathbf{7}^{2+}$) is not a strong anchor, while a single-tail alkyl ligand is. Overall, it was found that under these conditions, complexes $\mathbf{5}^{2+}$ and $\mathbf{6}^{2+}$ are well-trapped in the lipid bilayer of **M5** and **M6**, so that these complexes were considered as suitable candidates for further biological experiments. Complexes $\mathbf{4}^{2+}$ and $\mathbf{7}^{2+}$ were excluded from biological experiments.

8.2.6 Photo(cytotoxicity) of Ru-complex doped liposomes under blue light irradiation

As introduced earlier, the purpose of Ru-complex doped liposomes (System B) is to transport the Ru-complex inside the cell, after which the complex can be activated with blue light to produce a toxic aqua species (complex $\mathbf{8}^{2+}$ or $\mathbf{9}^{2+}$, see Figure 8.2). To test this hypothesis, the (photo)cytotoxicity of **M5** and **M6** liposomes was evaluated in A549, MCF7, and MRC5 cells according to the same protocol that was used before for **M1-3** liposomes (Section 8.2.4). However, instead of using red light the cells were this time irradiated for 10 minutes with a 454 nm LED-array (7.0 ± 0.8 $mW.cm^{-2}$ intensity, 4.2 $J.cm^{-2}$ dose) under 7% CO_2 and 20% O_2. It was previously found that a longer irradiation time may cause significant cell death.[17] As complexes $\mathbf{5}^{2+}$ and $\mathbf{6}^{2+}$ are not emissive the uptake of the liposomes could not be confirmed by fluorescence microscopy. Furthermore, the activation half-time to convert $\mathbf{5}^{2+}$ to $\mathbf{8}^{2+}$ and $\mathbf{6}^{2+}$ to $\mathbf{9}^{2+}$ was estimated to be 3 min (see Appendix VII for calculation), so that in such conditions it was anticipated that 10 min

irradiation would nearly convert all of the complex to the aqua species. The evolution of cell viability as a function of concentration is shown in Figure 8.10, and the 50% effective concentration values (EC_{50}) and photo-indices (PI, calculated by $PI = EC_{50}^{dark} / EC_{50}^{light}$) are reported in Table 8.2.

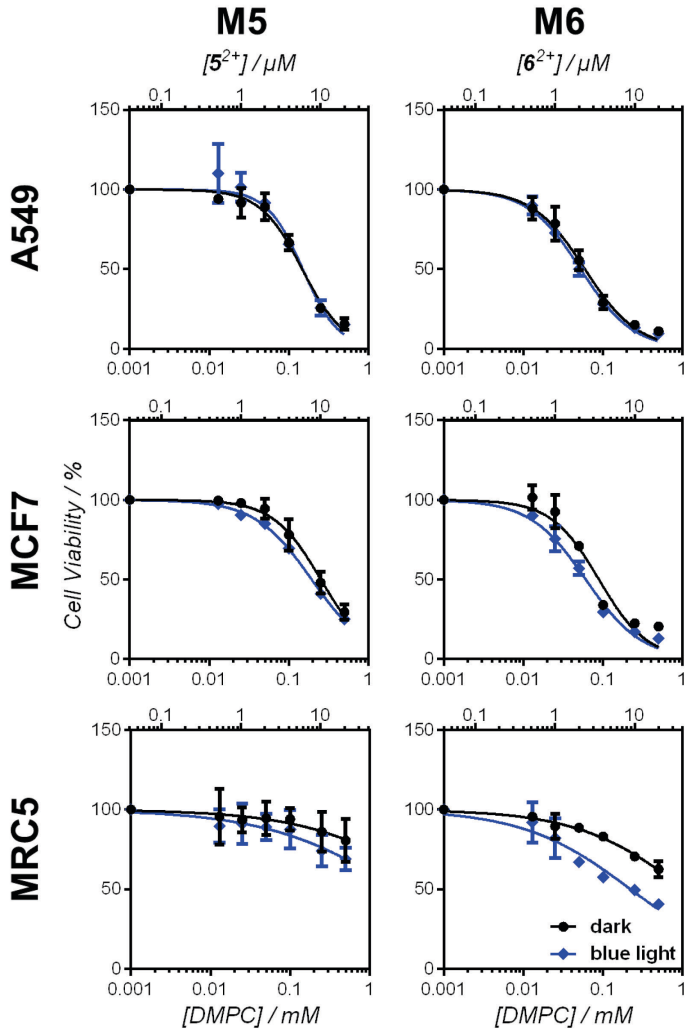

*Figure 8.10. Cell viability of A549 (top row), MCF7 (middle row) and MRC5 cells (bottom row) treated with **M5** (left column), or **M6** (right column) liposomes and left in the dark (black circles) or irradiated for 10 min with 454 nm light (blue diamonds, 4.2 J.cm⁻² light dose) as a function of [DMPC] (bottom axes) or [Ru] (top axes). Solid lines represent Hill-slope fit curves to the same color data points. Error bars represent the standard deviation of the mean cell viability value from three individual biological experiments.*

*Table 8.2. EC_{50} values (expressed in μM [Ru]; [Ru] = 0.04 × [DMPC]) and photo-indices (PI) of **M5** and **M6** liposomes after irradiation with 454 nm light (10 min, 7.0 ± 0.8 mW.cm^{-2} intensity, 4.2 J.cm^{-2}) and in the dark in A549, MCF7 and MRC5 cells. Confidence intervals (CI) are given in μM.*

Cell line	Light	**M5**				**M6**			
		EC_{50} (μM)	CI (μM) -	CI (μM) +	*PI*	EC_{50}	CI (μM) -	CI (μM) +	*PI*
A549	+	6.0	1.1	1.4	1.0	2.1	0.2	0.2	1.1
	-	5.9	0.8	0.9		2.4	0.3	0.4	
MCF7	+	7.8	0.6	0.6	1.3	2.4	0.3	0.4	1.5
	-	10	1.3	1.5		3.6	0.8	1.0	
MRC5	+	93	76	410	3.0	8.9	2.8	4.0	4.8
	-	270	270	15E3		43	13	20	

The data show that both **M5** and **M6** liposomes are toxic for A549 cells in the dark with EC_{50} values of 5.9 and 2.4 μM [Ru], respectively. In both cases irradiation with blue light marginally affected the values. In MCF7 cells, **M5** and **M6** had EC_{50} values of 10 and 3.6 μM [Ru]; light irradiation slightly lowered these values to 7.8 and 2.4 μM [Ru], respectively. Finally, in MRC5 cells, **M5** and **M6** liposomes had EC_{50} values of 270 and 43 mM [Ru], respectively, which shows that the liposomes barely affect MRC5 cells in the dark. However, light irradiation lowered the EC_{50} values to 93 and 8.9 μM [Ru], respectively, which is statistically significant. Unfortunately the photo-indices of both liposome-bound complexes were rather low. Overall, the data show that **M5** and **M6** are more toxic in the dark than **M1-3** liposomes (compare Figure 8.10 to Figure 8.8), clearly indicating that **5**$^{2+}$ and **6**$^{2+}$ are toxic in the dark. What is the origin of this toxicity? Since the surface of the liposomes is sterically hindered with PEG groups, the interaction of the membrane-bound complex with biomolecules of the cell is hindered. Another possibility is that toxic interactions arise after digestion of the liposomes, after which **5**$^{2+}$ or **6**$^{2+}$ is liberated. In such a scenario, even though **5**$^{2+}$ and **6**$^{2+}$ are not photoactivated, their amphiphilicity may in fact cause significant toxicity. For instance, it has recently been shown that complex **4**$^{2+}$ in absence of liposomes and in the dark is significantly toxic in A549 and MCF7 cells with a EC_{50} value of 5 μM, comparable to the data of **M5** and **M6**.[18] If liposome digestion is indeed the cause of the dark toxicity, drug carriers with higher resistance towards digestion may be needed to lower the dark toxicity. Interestingly, the data also show that **M5** and **M6** are more toxic for cancerous cells (A549 and MCF7) than for healthy cells (MRC5). This observation may indicate a selectivity of liposome-bound complexes **5**$^{2+}$ and **6**$^{2+}$ for cancer cell lines. Thus,

blue light irradiation can generally cause more cell death, but that this effect is highly cell-dependent. In the rest of this chapter, complex $\mathbf{6}^{2+}$ is used as Ru prodrug, because it exhibits the greatest photo-index.

8.2.7 Activation of a photodissociative ruthenium complex using upconverting DMPC liposomes in air

As introduced earlier, the photoreaction of $\mathbf{6}^{2+}$ can only be executed efficiently using blue light. In Chapter 4 it was demonstrated that in liposomes that were doped with compounds **1**, **2**, and $\mathbf{4}^{2+}$, the upconverted light was efficiently transferred to the ruthenium complex via FRET and triggered the photodissociation of the complex. However, those experiments were performed under deoxygenated conditions (by bubbling the solution with argon) and the red light activation did not work in air, which clearly limited the biological applicability of System C liposomes. On the other hand, as demonstrated in sections 8.2.2 and 8.2.3, anti-oxidants such as L-Asc and GSH protect TTA-UC against oxygen. An obvious step forward was thus to add anti-oxidants to System C liposomes in order to protect TTA-UC and trigger the photodissociation with red light in air. In such a mixture of anti-oxidants and TTA-UC-Ru liposomes, it is important to consider that the anti-oxidants may in fact interfere with the photosubstitution reaction of $\mathbf{6}^{2+}$ to $\mathbf{9}^{2+}$: for instance, anti-oxidants may react with ground or excited-state $\mathbf{6}^{2+}$ and cause unwanted side-reactions, or the thiol of GSH may substitute water in $\mathbf{9}^{2+}$ to form a GSH-Ru adduct. Thus, the influence of anti-oxidants on a TTA-UC-photodissociation reaction cascade had to be evaluated.

For this purpose, **M1-3-6** liposomes were prepared at 1 mM [DMPC] that contained red-to-blue TTA-UC compounds **1** and **3** and photodissociative Ru-compound $\mathbf{6}^{2+}$. The photodissociation reaction with red light irradiation was performed in either deoxygenated conditions by bubbling argon for 30 min, or in air-equilibrated conditions and in presence of 10 mM L-Asc and 10 mM GSH. Both samples were irradiated at human body temperature (37 °C) with 630 nm light (150 mW, 1.2 W.cm^{-2}) for 2.5 h while recording UV-vis absorbance (Figure 8.11a and b) and emission spectra every 15 min. The UV-vis spectrum at t = 0 shows the characteristic absorption bands of **1** at 440 and 630 nm, of **3** between 375 and 450 nm, while the absorbance of $\mathbf{6}^{2+}$ (Figure S.VII.7) is hidden under the bands of **1** and **3**. Under argon, in absence of anti-oxidants, the absorption band of the photoproduct $\mathbf{9}^{2+}$ evolves to completion in the first hour of irradiation, just as observed for complex $\mathbf{6}^{2+}$ in water upon blue light irradiation (Figure S.VII.7). By plotting the absorbance at 490 nm *versus* time

(Figure 8.11c), it is clear that the photoreaction was completed after about 45 min of irradiation. While the photoreaction was progressing, the upconversion emission at 486 nm increased (Figure 8.11d), because complex $\mathbf{9}^{2+}$ dissociates into solution and no longer quenches the emission of **3** via FRET (see Chapter 4). After 60 – 90 min of irradiation, both the absorption and emission spectra completely stabilized. When the experiment was conducted in air and in presence of anti-oxidants, the same absorption band between 460 and 600 nm appeared in the first 30 min of irradiation (Figure 8.11b), which strongly resembled the absorption band of $\mathbf{9}^{2+}$. After that time-point, this absorption band slowly disappeared, indicating that the photoproduct was not stable upon prolonged irradiation or further reacts with L-Asc and/or GSH. Also the upconversion emission intensity increased in the first two hours of irradiation, similar to the previous experiment. As control, the irradiation experiment under argon was repeated with **M3-6** liposomes, which did not contain photosensitizer **1** and hence could not produce TTA-UC. A slow evolution of the absorbance at 490 was observed, which is attributed to direct absorption of the red light by $\mathbf{6}^{2+}$. These results demonstrate that TTA-UC greatly amplified the rate of photodissociation upon red light irradiation. At these irradiation conditions, 45 min were necessary to activate 40 µmol ruthenium prodrug.

Is the same photoproduct obtained under argon and in air in presence of anti-oxidants? To answer this question, the irradiation experiments were repeated, but stopped after 60 min; the liposomes were removed from the solution using a centrifugal filtration, and UV-vis absorption spectra of the filtrates were recorded. In case of irradiation under argon, the UV-vis absorption spectrum of the filtrate was identical to the absorption spectrum of $\mathbf{9}^{2+}$ (Figure S.VII.7 and Figure S.VII.9), thereby confirming the photodissociation reaction of $\mathbf{6}^{2+}$ to $\mathbf{9}^{2+}$. In the presence of anti-oxidants, the resulting absorption spectrum was very similar, suggesting that the same (or a similar) Ru-complex had been formed. As control, no absorption was detected for filtered solutions of non-irradiated **M1-3-6** liposomes under argon or in presence of anti-oxidants. Finally, the same irradiation experiments were repeated at higher concentration (20 mM DMPC), and mass spectra were recorded after centrifugal filtration, lyophilisation of the filtrate, and redissolving the residue in acetone (Figure S.VII.10). In case of irradiation under argon, the mass spectrum confirmed that $\mathbf{9}^{2+}$ had indeed formed during irradiation (main peaks 490.1 and 507.1 m/z belonging to $[Ru(bpy)_2(OH_2)(OH)]^+$(MeCN) and

$[Ru(bpy)_2(OH_2)(OH)]^+$(acetone), respectively). In case of irradiation in air in presence of anti-oxidants, the sample only dissolved in methanol, which suggests that another Ru-complex had been formed. The mass spectrum showed 481.1 and 490.0 m/z, belonging to $[Ru(bpy)_2(OH_2)_2]^{2+}(MeO^-)$ and $[Ru(bpy)_2(OH_2)(OH)]^+(MeCN)$, see Figure S.VII.11. Although no signals were detected from a GSH complex, for example expected at m/z 738.1 for $[Ru(bpy)_2(GS)(H_2O)]^+$, it is still plausible that compound **9**$^{2+}$ and products such as GSH adducts co-exist in the reaction mixture. Overall, the results demonstrate that GSH and L-Asc facilitated the photoactivation cascade of TTA-UC, FRET, and Ru-photodissociation in air while minimally interfering with the photochemistry. These findings may thus be used to investigate Ru-prodrug activation using TTA-UC *in vitro*.

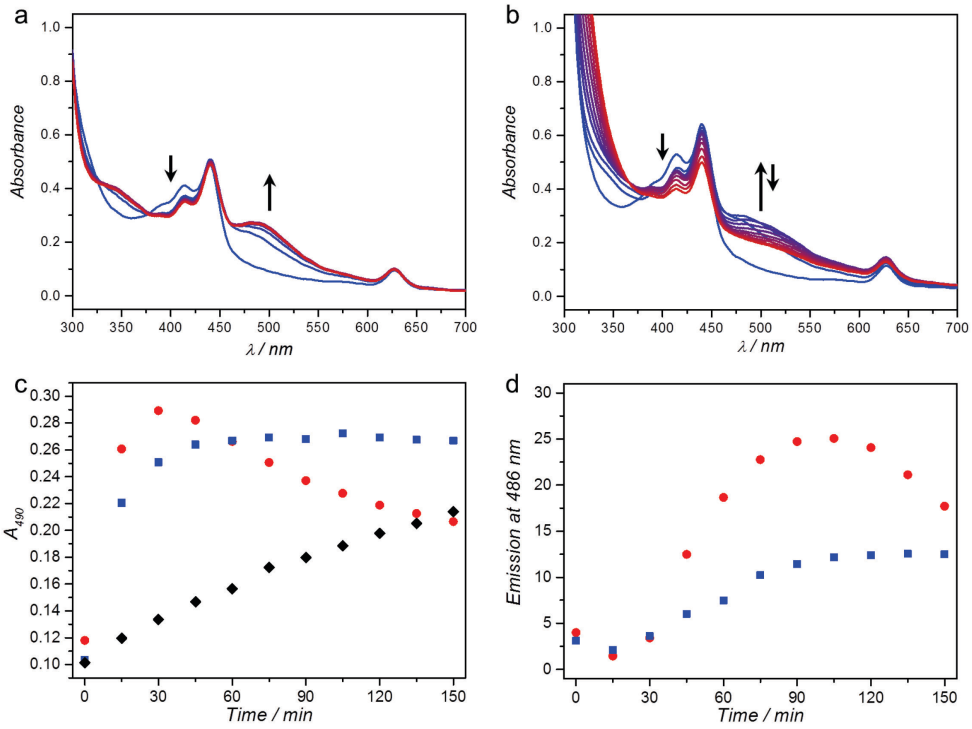

*Figure 8.11. a/b) UV-vis absorption spectroscopy in 15 min intervals (blue to red gradient) during red-light irradiation of **M1-3-6** liposomes under argon (a) and in air in presence of 10 mM L-Asc and GSH (b). c/d) Absorbance at 490 nm (c) and upconversion emission at 486 nm (d) as a function of time for the experiment under argon (blue squares) and in air in presence of anti-oxidants (red circles). As control, **M3-6** liposomes were irradiated under the same conditions under argon (c, black diamonds). Conditions: 2 mL sample with 1 mM DMPC, irradiated at 37 °C with 150 mW 630 nm light (1.2 W.cm^{-2}).*

8.2.8 Inducing TTA-UC and drug activation through meat with DLPC liposomes

The main reason to use red-to-blue light upconversion in PACT is the increased excitation penetration depth of red light in tissues. To study the activation of a ruthenium prodrug using red-to-blue TTA-UC in liposomes, a two-fold investigation was performed. First, the depth at which TTA-UC can be generated through biological tissues was measured for **L1-2** liposomes by placing layers of fresh meat (chicken or pig) between the excitation source and the sample. Secondly, the photodissociation of $\mathbf{6}^{2+}$ to $\mathbf{9}^{2+}$ with red light and **L1-3-6** liposomes was attempted through a layer of pork to simulate operation conditions.

In order to measure the depth at which red-to-blue upconversion can be generated through biological tissues, first an upconverting gel was prepared by mixing **L1-2** liposomes ([DLPC] = 10 mM) with 0.5 wt.% agarose and 5 mM L-Asc and GSH in PBS and was deposited as a thin disk between two microscopy slide. The gel was then covered with a variable stack of meat slices, a 630 nm laser beam (0.57 W.cm^{-2}) was directed through the meat at the upconverting gel, and the emission spectrum was measured of the sample in a custom-made cage spectroscopy setup (see experimental section, Figure 8.16). Raw chicken breast fillet and pork fillet were selected to mimic human tissue of different color and structure, and were thinly sliced with 1 – 2 mm thickness.

The emission spectra for both meat types showed the typical phosphorescence of **1** at 800 nm and upconversion emission of **2** at 474 nm identical to the emission spectra shown in section 8.2.2 (Figure 8.12a and c). As could be expected, the intensity of the entire spectrum decreased as a function of meat thickness due to filtering and scattering of the excitation source by the meat. In a typical experiment, upconversion was still observable for 12.8 mm thick chicken and for 11.6 mm thick pork. Figure 8.12c and d show the upconversion intensity (I_{UC}), the phosphorescence of **1** (I_p), and their ratio as a function of meat thickness. It can be clearly seen that from the third meat layer onwards, I_{UC} decreases relatively faster than I_p; *i.e.* I_{UC}/I_p decreases. This can be rationalized by the fact that TTA-UC is quadratically dependent on the excitation intensity below the intensity threshold for efficient upconversion (I_{th}), while the phosphorescence is linearly dependent. I_{th} was previously determined to be 0.05 W.cm^{-2} for very similar red-to-blue TTA-UC in DOPC liposomes (Chapter 5). Considering that I_{UC}/I_p changes for the first

time after 3 layers of meat, this must mean that the excitation intensity after 3 layers of meat has decreased from 0.57 W.cm^{-2} to approximately 0.05 W.cm^{-2}). Overall, the results show that upconversion was generated even beyond 1 cm penetration depth, but that beyond 5 to 6 mm meat depth the TTA-UC efficiency decreased quickly. Naturally, the depth at which the excitation intensity equals I_{th} depends on the initial excitation intensity, so it was decided that a higher irradiance was needed to activate Ru-prodrugs through meat (see below). Finally, the results also suggest that upconverting drug carriers should have a low I_{th} value, so that their performance would be minimally dependent on the excitation intensity.

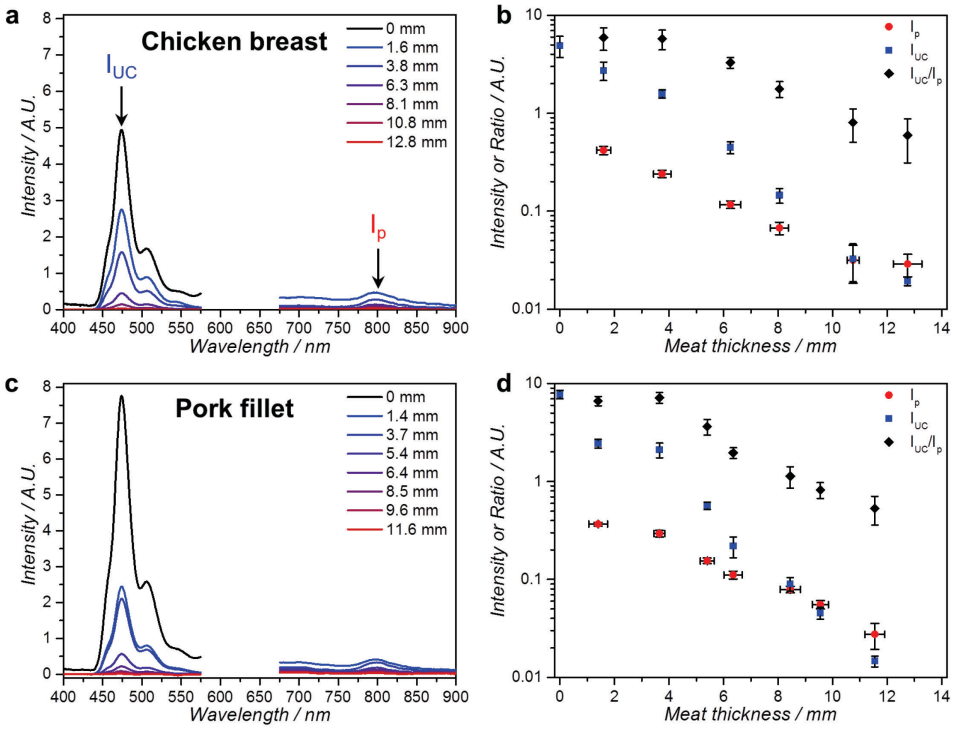

*Figure 8.12. Emission spectroscopy of an upconverting liposome gel through layers of chicken breast or pork fillet. a/c) Emission spectra of gellified **L1-2** liposomes through layers of meat at room temperature as a function of chicken breast (a) or pork fillet thickness (c). b/d) Upconversion intensity (I_{UC}, at 474 nm), phosphorescence intensity of compound **1** (I_p) and the ratio of I_{UC} and I_p as a function of chicken breast (b) or pork fillet (d) thickness. Conditions: 20 µL sample in a 25 µm × 25 mm diameter disk of **L1-2** liposomes ([DLPC] = 10 mM) in 0.5% wt.% agarose gel, 5 mM L-Asc, and 5 mM GSH in PBS at room temperature, irradiated with 30 mW (3 mm spot, 0.57 W.cm^{-2}) 630 nm light through a variable number of meat slices. The spectra are cut off between 575 nm and 675 nm to omit the large excitation scatter peak.*

The second set of experiments involved Ru-complex activation through a layer of meat. For this, a 2 mm thick cuvette was filled with 400 µL **L1-3-6** liposomes ([DLPC] = 10 mM) in anti-oxidant PBS (10 mM L-Asc and GSH), buried under a layer of pork fillet (7 ± 0.5 mm), and irradiated from the top with either red or blue light for 2 h, as shown in Figure 8.13a. The light dose was equal for both experiments (110 mW laser light, 3 mm spot size, 1.6 W.cm^{-2}, 11.2 kJ.cm^{-2}); higher intensity blue light could not be realized in our experimental setup. The UV-vis absorption spectrum of the cuvette (without meat) was measured before and after irradiation (Figure 8.13b). The absorption band that appeared between 460 and 600 nm indicated the formation of a small quantity of the aqua species **9**$^{2+}$ (compare Figure 8.11a and Figure 8.13b). The amount of activated Ru-complex was similar for both excitation wavelengths.

This result can be interpreted by considering the two different photochemical pathways of activation. In the case of blue light, the light does not penetrate the meat far, but the photons that do reach the sample have a high chance of being absorbed due to the high absorbance of **6**$^{2+}$ at 450 nm (ε_{450} ≈ 6000 M^{-1}.cm^{-1}, [**6**$^{2+}$] = 0.40 mM; $A_{450}^{\mathbf{6}^{2+}}$≈ 0.5 for 2 mm path length). Upon blue light absorption, the complex is directly activated without intervention of the TTA-UC process, i.e. the chance is high that a blue photon causes photodissociation of **6**$^{2+}$. In the case of red light, the light penetrates much further, *i.e.* more light reaches the cuvette, but the overall activation efficiency is the product of upconversion quantum yield (Φ_{UC}), energy transfer efficiency from annihilator **3** to Ru-complex **6**$^{2+}$ (E_{ET}), and photodissociation quantum yield (Φ_{Ru}; see Chapter 4),[4b] leading to a ~20 times lower overall activation efficiency. Also, the absorbance of compound **1** at 630 nm was comparatively low ($A_{630}^{\mathbf{1}}$ = 0.15), leading to less use of the light that permeates through the meat. Finally, at 1.6 W.cm^{-2} 630 nm excitation intensity, it is likely that Φ_{UC} is lower than its maximum value, because the excitation intensity likely drops to I_{th} or below (~0.05 W.cm^{-2}). Thus, even though **L1-3-6** liposomes are clearly more responsive to blue light, the data show that the overall activation with red light was approximately just as efficient as with blue light. Improvements in red-light absorbance and upconversion efficiency may eventually lead to a better performance with red light compared to blue light at this meat thickness.

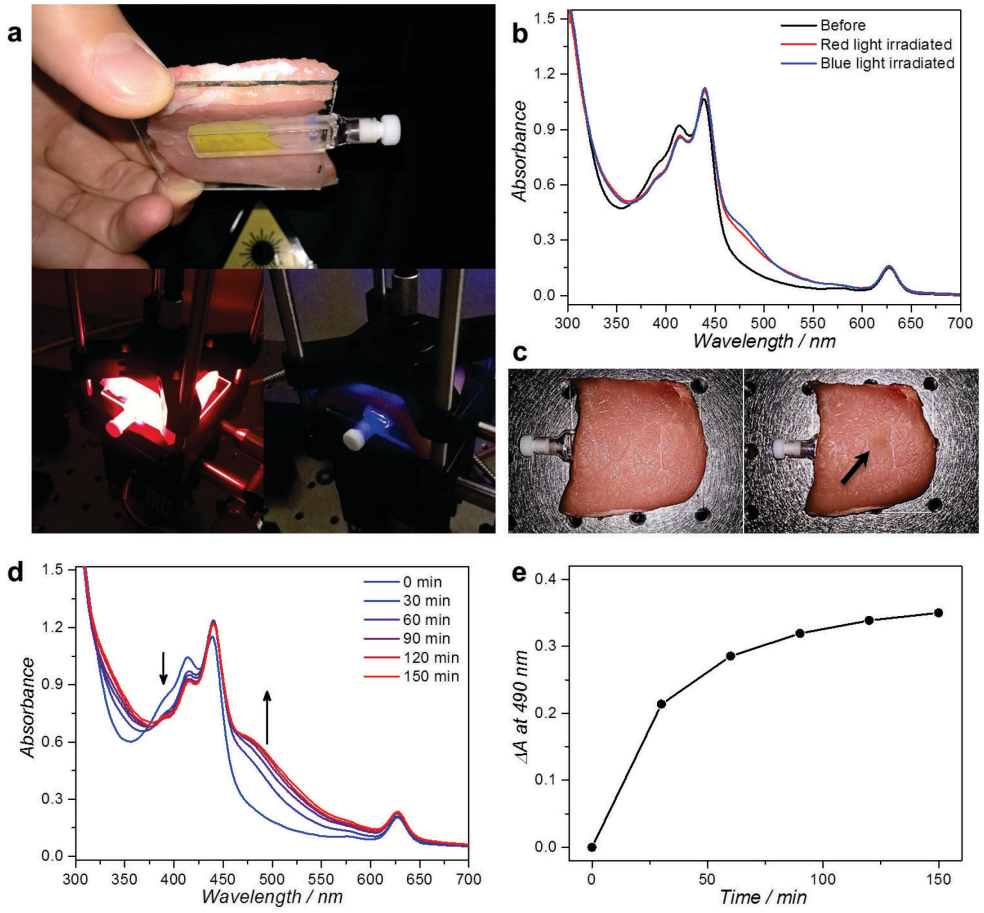

*Figure 8.13. Irradiation of **L1-3-6** liposomes through a thick slice of pork fillet. a) Photographs of the experimental setup used for red and blue light irradiation. The 2 mm cuvette holding 400 µL **L1-3-6** ([DLPC] = 10 mM) is covered with 7 mm pork fillet and irradiated for 2 h from above with a collimated 110 mW 630 or 450 nm beam (3 mm spot size, 1.6 W.cm^{-2} intensity, 11.2 kJ.cm^{-2} light dose). b) UV-vis absorbance spectra of the sample before (black) and after irradiation with 450 nm (blue) or 630 nm light (red). c) Photographs of the pork fillet after red (left) or blue light irradiation (right). Upon blue light irradiation, a clear "burn mark" was observed, as indicated with the arrow. d/e) UV-vis absorbance spectra (d) and the absorbance difference at 490 nm (e) as a function of irradiation time for **L1-3-6** liposomes irradiated through 7 mm pork fillet with 300 mW.cm^{-2} 630 nm light (4.2 W.cm^{-2}).*

Apart from investigating the sample after irradiation, the meat was also visually inspected after the 2 h irradiation. While red light had caused no damage at all, blue light had burned the meat considerably at the irradiation spot (Figure 8.13c). This result is consistent with data of our group that blue light is much more harmful for cells than green or red light.[10] Red light is thus much more favorable for drug activation than blue light. Tissue ablation is also

a great issue in the biological application of lanthanoid-based upconversion nanoparticles (UCNPs): for instance, it has been shown by Wu *et al.* that irradiation of chicken meat with 980 nm laser light for 20 min at ≥ 5 W.cm^{-2} intensity causes significant burn marks. In the case of red-to-blue TTA-UC, our data show that upconversion-mediated drug activation is possible at relatively low power without any tissue ablation.

Finally, the irradiation experiment was repeated with higher intensity red light (300 mW, 4.2 W.cm^{-2} intensity) and the absorption spectrum was measured every 30 min (Figure 8.13d and e). The evolution of the absorption band of **9**$^{2+}$ between 460 and 600 nm reached completion after approximately 2 h of irradiation, which indicates that a higher irradiation intensity indeed leads to more activation. Again, no visible signs of irradiation damage of the tissue were observed. In conclusion, the data show that activation of complex **6**$^{2+}$ by red light in combination with red-to-blue TTA-UC could be realized through a 7 mm thick slice of pork fillet. Furthermore, the results demonstrate that TTA-UC mediated photoactivation of photo-pharmacological compounds such as Ru-compounds is a promising and feasible strategy that may lead to treatment of tumors without tissue ablation.

8.2.9 Testing *in vitro* toxicity of M1-3-6 liposomes in hypoxic conditions with red light irradiation

The photocytotoxicity under high power red light was evaluated of **M1-3-6** liposomes that contained TTA-UC dyes **1** and **3**, and Ru-complex **6**$^{2+}$ in A549 and MRC5 cells. The same experimental protocol was used as in Section 8.2.6, but with a few important adaptations. The liposomes were tested only at 0.1 mM concentration, because **M1-3** liposomes were not toxic at this concentration. To enhance the amount of upconverted photons, (i) the cells were co-treated with 5 mM L-Asc and GSH, (ii) the irradiation was performed with a much higher light intensity and dose than before (1.1 W.cm^{-2} intensity, 5 min irradiation, 320 J.cm^{-2} dose), (iii) the irradiation was performed under hypoxic conditions (1% O_2), and (iv) another plate design was used (Figure 8.18). As controls, liposomes were used that contained only the TTA-UC dyes (**M1-3**), and liposomes deprived of photosensitizer (**M3-6**). As always, all experiments were also performed without irradiation in the dark. In order to reach the higher light intensity, instead of using LED arrays, which cannot reach such intensities, a PDT laser with collimating lens was fitted underneath the plate. As a consequence, not all wells could be irradiated at the same time,

the irradiation time per well needed to be short, the total irradiation time was higher (2 h in total), and the statistical error on the data was higher.

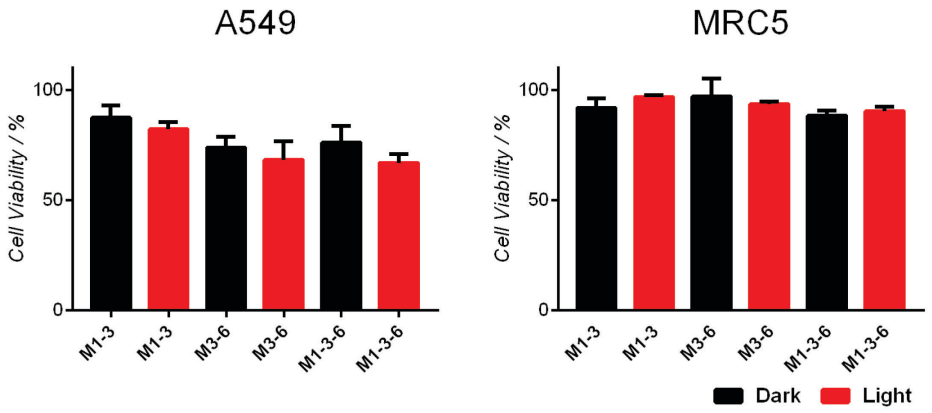

*Figure 8.14. Cell viability of A549 (left) and MRC5 cells (right) that were treated with **M1-3**, **M3-6**, and **M1-3-6** liposomes ([DMPC] = 0.1 mM), co-treated with 5 mM L-Asc and GSH, and irradiated with 1.1 W.cm^{-2} 630 nm light for 5 min (320 J.cm^{-2}) at 1% O_2 (red) or left in the dark under the same conditions (black). Error bars represent standard deviation of three individual wells. The experiment was conducted once.*

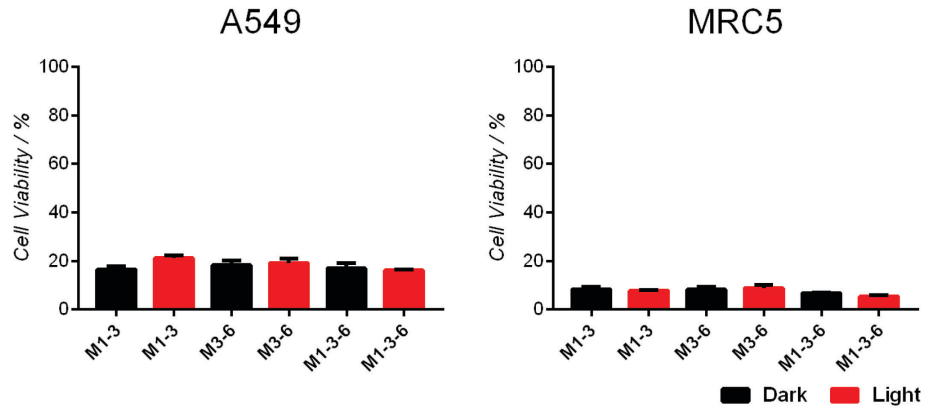

*Figure 8.15. Cell viability of A549 (left) and MRC5 cells (right) that were treated with **M1-3**, **M3-6**, and **M1-3-6** liposomes ([DMPC] = 0.1 mM), co-treated with 5 mM L-Asc and GSH, and irradiated with 1.1 W.cm^{-2} 630 nm light for 5 min (320 J.cm^{-2}) at 1% O_2 (red) or left in the dark under the same conditions (black). In this experiment, the medium was not refreshed either before or after irradiation, so that the liposomes and anti-oxidants were present during the last 72 h of the treatment. Error bars represent standard deviation of three individual wells. The experiment was conducted once.*

In Figure 8.14, the cell viability of A549 and MRC5 cells is reported after treatment with **M1-3**, **M3-6**, and **M1-3-6** liposomes that were irradiated or left in the dark. For both cell lines, **M1-3** liposomes were not found to be significantly toxic in dark and light conditions, consistent with the results discussed in Section 8.2.4. In dark conditions, **M3-6** liposomes were found to be more toxic in A549 cells than **M1-3** liposomes, but were not toxic in MRC5 cells. Red-light irradiation did not significantly influence the toxicity. Finally, in dark conditions, **M1-3-6** liposomes were found to be equally toxic as **M3-6** liposomes in both cell lines. Again, irradiation did not significantly influence the toxicity. To summarize: MRC5 cells were unaffected by any treatment, while a mild toxicity regardless of irradiation was observed for **M3-6** or **M1-3-6** liposomes in A549 cells. Because the toxicity of **M3-6** and **M1-3-6** liposomes is equal, the toxicity is most probably caused by the dark toxicity of compound $\mathbf{6}^{2+}$ (see Section 8.2.6). Furthermore, the result that light irradiation did not change the toxicity of **M1-3-6** liposomes in A549 cells was expected based on the results of **M6** liposomes (Section 8.2.6), which showed that the conversion of $\mathbf{6}^{2+}$ to $\mathbf{9}^{2+}$ upon irradiation does not cause more toxicity in A549 cells. In contrast, blue light irradiation of **M6** in MRC5 cells caused a decrease in cell viability at 0.1 mM from 82% in the dark to 55% in light conditions (Figure 8.10). Thus, the fact that **M1-3-6** liposomes are not toxic in MRC5 cells upon 5 min red light irradiation may indicate that upconversion was not effective in triggering the photodissociation reaction of $\mathbf{6}^{2+}$ to $\mathbf{9}^{2+}$. Most probably, 5 min of red light irradiation is simply not enough to release enough toxic $\mathbf{9}^{2+}$. For instance, in the preceding experiments discussed in Section 8.2.7, conducted in ideal, deoxygenated conditions, 30 – 60 min was needed to convert all $\mathbf{6}^{2+}$ to $\mathbf{9}^{2+}$ at similar light intensity. Furthermore, it is uncertain to what extent the toxicity of $\mathbf{9}^{2+}$ is affected by the presence of L-Asc and GSH, as it is known for example that GSH greatly decreases the toxicity of metallodrugs such as cisplatin.[19]

As a final experiment the cell treatment was repeated without removing the liposomes and anti-oxidants from the cell medium; the liposomes and anti-oxidants were present during the last 72 h of the photocytotoxicity assay. During irradiation stable upconversion emission was detected in the whole well volume when the plate was viewed with red-light blocking laser goggles. The cell viability of the A549 and MRC5 cells after treatment is plotted in Figure 8.15. Apart from the great decrease in viability in all wells, attributed to the continuous presence of liposomes and anti-oxidants, only minor

differences in cytotoxicity were observed in A549 cells that had been treated with **M1-3**, **M3-6**, or **M1-3-6** liposomes. Thus, under these conditions the toxicity of red-light irradiated **M1-3-6** liposomes is not substantial. Much further work is necessary to elucidate the conditions at which the activation of Ru-prodrugs using TTA-UC causes significant photocytotoxicity in cancer cells. For instance, Ru-complexes with a better photo-index are needed so that the upconversion strategy may be better tested *in vitro*. Also, longer irradiation times are required to release enough Ru-complex to induce a potentially toxic effect.

8.3 Conclusion

In this chapter, the biological applicability of three liposome systems was addressed: upconverting liposomes (System A), Ru-prodrug doped liposomes (System B), and liposomes doped with both upconverting dyes and Ru-prodrugs (System C). First of all, it was found that the biocompatible anti-oxidants L-Asc and GSH at biologically relevant concentrations greatly enhanced TTA-UC for **L1-2** liposomes in solution and in **M1-3** liposomes in cancer cells (System A). Then, it was established that **M1-3** liposomes are not (photo)cytotoxic in A549, MCF7, and MRC5 cell lines in the dark in and in red-light irradiated conditions; no PDT effect was observed, even at relatively high red light dose. Photocytotoxicity studies with Ru-prodrug functionalized liposomes **M5** and **M6** (System B) showed that both liposome formulations were considerably toxic in the dark, and that blue light irradiation enhanced their toxicity only slightly. Furthermore, it was demonstrated that photoactivation of Ru-prodrugs in liposomes mediated by red-to-blue TTA-UC (System C) could be obtained in air by adding biologically relevant concentrations of L-Asc and GSH. The same reaction could be triggered when a thick slice of pork fillet was placed between the laser and the sample, which illustrates the practical applicability of upconverting liposomes. Finally, the photocytotoxicity of **M1-3-6** liposomes was investigated under high power red light irradiation. Unfortunately, no significant cytotoxic effect was observed, which may be due to a low overall activation efficiency or to the poor cytotoxicity of the activated Ru-drug $\mathbf{9}^{2+}$. Overall, our results pave the way for photoactivation of Ru-complexes by TTA-UC *in vitro*, and give important insights in what requirements need to be fulfilled in order to make the activation-by-upconversion strategy perform well in a biological context: important optimization parameters that need to be considered include nanoparticle design, excitation wavelength and intensity, local oxygen

concentration and presence of anti-oxidants, TTA-UC emission stability, light dose, tissue thickness, and photo-index of Ru-prodrugs.

8.4 Experimental section

8.4.1 General

Palladium tetraphenyltetrabenzoporphyrin (**1**) was purchased from Frontier Scientific, Inc. (Logan, Utah, USA). Perylene (**2**) was purchased from Sigma-Aldrich Chemie BV (Zwijndrecht, The Netherlands). The synthesis of 2,5,8,11-tetra(*tert*-butyl)perylene (compound **3**) is described in Chapter 9. The synthesis of **4**$(PF_6)_2$ is described in section 3.4.2. The synthesis of [Ru(tpy)(bpy)(Cl)](Cl) is described elsewhere.[20] Compounds **5**$(PF_6)_2$ was synthesized by Lucien Lameijer. Compounds **10**, **11**, **12**, **6**$(PF_6)_2$, and **7**$(PF_6)_2$ were synthesized by Michael Meijer. Sodium N-(carbonyl-methoxypolyethylene glycol-2000)-1,2-distearoyl-sn-glycero-3-phospho ethanolamine (DSPE-mPEG-2000), 1,2-dilauroyl-sn-glycero-3-phosphocholine (DLPC), and 1,2-dimyristoyl-sn-glycero-3-phosphocholine (DMPC) were purchased from Lipoid GmbH (Ludwigshafen, Germany) and stored at −18 °C. Dulbecco's phosphate buffered saline (PBS) was purchased from Sigma Aldrich and had a formulation of 8 $g.L^{-1}$ NaCl, 0.2 $g.L^{-1}$ KCl, 0.2 $g.L^{-1}$ KH_2PO_4, and 1.15 $g.L^{-1}$ K_2HPO_4 with a *pH* of 7.1 – 7.5. Anti-oxidant supplemented PBS was prepared by dissolving L-ascorbic acid and/or glutathione in PBS and neutralizing with sodium hydroxide to *pH* 7.0 − 7.6. Other chemicals were purchased from major chemical suppliers and used as received. Images and data were processed with Fiji ImageJ, Origin Pro, and Microsoft Excel software. Emission and absorption spectroscopy, and photodissociation experiments using red light were performed in experimental setups reported in other chapters (see Sections 4.4.5 and 6.4.4). Photodissociation experiments using blue light were recorded in a Cary 50 Varian spectrometer equipped with a Cary Single Cell Peltier for temperature control.

8.4.2 Synthesis of 5$(PF_6)_2$

To a suspension of [Ru(tpy)(bpy)Cl]Cl (202 mg, 0.360 mmol) in acetone/H_2O (9:1, 40 mL) were added dodecyl(methyl)sulfide (1.17 g, 5.41 mmol) and $AgPF_6$ (200 mg, 0.791 mmol). This mixture was heated at 55° C for 24 hours under argon, after which the solvent was removed by rotary evaporation. The residue was dissolved in a minimal amount of acetone and precipitated by the addition of Et_2O. Collection by filtration and washing with Et_2O (3×) afforded [Ru(tpy)(bpy)(dodecyl(methyl)sulfide)]$(PF_6)_2$ (compound **5**$(PF_6)_2$) as a red-brown precipitate (250 mg, 0.251 mmol, 70%). TLC: R_f = 0.64 (100/10/2 acetone/water/sat. KPF_6). ^{1}H NMR (400 MHz, CD_3OD) δ = 9.79 (d, J = 6.3 Hz, 1H, H_a), 8.82 (d, J = 7.7 Hz, 1H, H_A), 8.78 (d, J = 8.2 Hz, 2H, H_D+H_G), 8.63 (d, J = 8.0 Hz, 2H, H_E+H_H), 8.59 (d, J = 7.0 Hz, 1H, H_K), 8.40 (t, J = 8.0 Hz, 2H, H_B+H_F), 8.15 – 8.00 (m, 4H, H_I+H_J+H_b)), 7.92 (t, J = 7.8 Hz, 1H, H_c), 7.81 (d, J = 6.4 Hz, 2H, H_d+H_e), 7.50 – 7.39 (m, 2H, H_C+H_f), 7.28 (d, J = 5.0 Hz, 1H, H_h), 7.27 – 7.18 (m, 1H, H_g), 1.65 (dd, J = 8.4, 6.5 Hz, 2H, H_2), 1.36 (s, 3H, H_1), 1.34 – 1.11 (m, 16H, H_3 – H_{10}), 1.09 – 1.00 (m, 4H, H_{11}+H_{12}), 0.93 – 0.84 (m, 3H, H_{13}). ^{13}C NMR (100 MHz, CD_3OD) δ = 158.1 (Quat. Arom.), 157.4 (Quat. Arom.), 156.7 (Quat. Arom.), 153.0 (C_d+C_e), 151.83 (Quat. Arom.), 151.7 (C_a), 151.6 (Quat. Arom.), 149.4 (C_h), 138.8 (C_I+C_J), 138.2 (C_c), 138.0 (C_B), 136.9 (C_F), 128.4 (C_C+C_f), 127.8 (C_b), 127.1 (C_h), 124.9 (C_E+C_H), 124.6 (C_K), 124.1 (C_D+C_G) 123.8 (C_A), 33.5 (C_2), 31.7 (C_{10}), 29.4 (C_9), 29.3 (C_8), 29.1 (C_7), 28.6 (C_6), 28.0 (C_5), 26.4 (C_4), 22.4 (C_3), 19.0 (C_2), 13.2 (C_1+C_{13}). ESI-MS m/z exp. (calcd.): 261.7 (261.5, $[M\text{-}2PF_6\text{-}H_2O\text{+}MeOH]^{2+}$); 353.5 (353.6, $[M\text{-}2PF_6]^{2+}$); 522.0 (522.1, $[M\text{-}2PF_6\text{-}H_2O\text{+}MeO]^{+}$);

852.2 (852.2, $[M\text{-}PF_6]^+$). UV-Vis: λ_{max} in H_2O: 452 nm (ε = 6300 $M^{-1}.cm^{-1}$). Photosubstitution quantum yield = 0.0070 in H_2O (λ_{exc} = 452 nm), as determined with a literature procedure.[21]

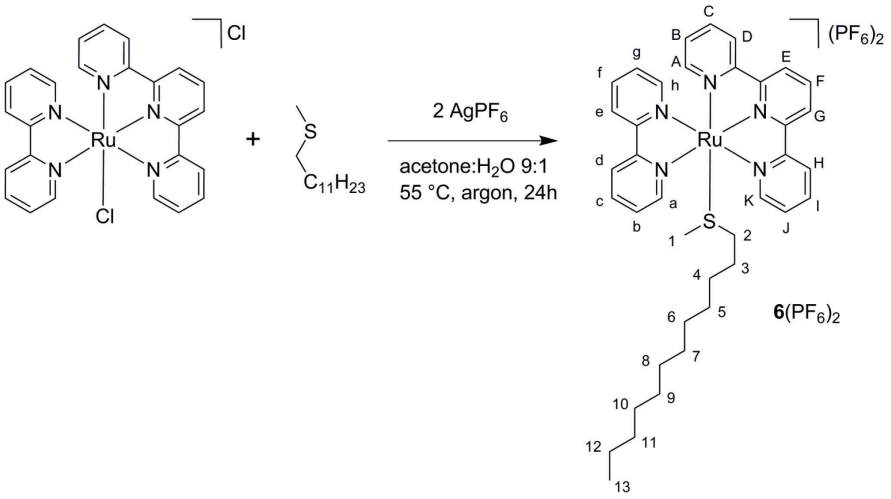

*Scheme 8.1. Synthesis of compound **5**$(PF_6)_2$ from [Ru(tpy)(bpy)Cl]Cl and dodecyl(methyl)sulfide.*

8.4.3 Synthesis of 1,3-bis(methylthio)-2-dodecyloxypropane – compound 10

To a stirred suspension of NaH (222 mg, 5.55 mmol) in dry and deoxygenated THF (5 mL) under Ar atmosphere was added 1,3-bis(methylthio)-2-propanol (0.25 mL, 1.85 mmol). The mixture was stirred at RT for 10 min, after which 1-bromododecane (0.5 mL, 2.13 mmol) was added dropwise, resulting in a light-brown suspension. The reaction mixture was heated to reflux for 20 h. Hereafter, the mixture was concentrated to 1 – 2 mL, Et_2O (40 mL) was added, and the resulting mixture was washed with brine (40 mL), 1 M aq. NH_4Cl (2 × 40 mL) and brine (40 mL). The organic layer was dried with $MgSO_4$ and the solvent was removed by rotary evaporation. After column chromatography (SiO_2, petroleum ether 40-60: DCM (2:1) to neat DCM) the title compound was obtained as a light-yellow oil (250 mg, 0.78 mmol, 42%). TLC: R_f = 0.9 (DCM). ^1H NMR (300 MHz, δ in $CDCl_3$): 3.58 (p, J = 5.8 Hz, 1H, H3), 3.51 (t, J = 6.6 Hz, 2H, H1'), 2.74 (ddd, J = 18.9, 13.6, 5.8 Hz, 4H, H2+H4), 2.16 (s, 6H, H1+H5), 1.65 – 1.51 (m, 2H, H2'), 1.42 – 1.18 (m, 18H, H3'-H11'), 0.88 (t, J = 6.5 Hz, 3H, H12'); ^{13}C NMR (75 MHz, δ in $CDCl_3$): 79.3, 70.3, 37.7, 32.1, 30.2, 29.8, 29.8, 29.8, 29.7, 29.6, 29.5, 26.3, 22.8, 16.9, 14.3; ESI-MS m/z exp. (calcd.): 135.1 (135.0, $[M\text{-}C_{12}H_{25}O]^+$), 208.0 (208.2, $[C_{12}H_{25}O+Na]^+$), 321.2 (321.2, $[M+H]^+$).

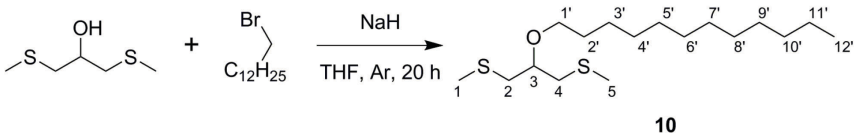

*Scheme 8.2. Synthesis of compound **10** from 1,3-bis(methylthio)-2-propanol and 1-bromododecane.*

8.4.4 Synthesis of $6(PF_6)_2$

A mixture of compound **10** (66 mg, 0.206 mmol) and *cis-Λ/Δ*-$[Ru(bpy)_2Cl_2]$ (50 mg, 0.103 mmol) under Ar atmosphere was dissolved in a 1:1 mixture of EtOH and H_2O (10 mL) and heated to reflux in the dark for 20 h. Hereafter, the reaction mixture was cooled to room

temperature, and the solvent was removed *in vacuo.* The reaction mixture was poured onto 30 mL of sat. aq. KPF_6, extracted with DCM (4 × 20 mL), and concentrated by rotary evaporation. Removal of the excess ligand was done by centrifugal washing with diethyl ether (2 × 12 mL, 2800 g). *cis-Λ/Δ*-[Ru(bpy)$_2$(**10**)](PF6)$_2$ (compound **6**$(PF_6)_2$) was obtained as an orange powder in 45% yield (47 mg, 0.046 mmol). ^{1}H NMR (400 MHz, δ in CD_3CN): 9.62 (d, J = 5.3 Hz, 1H, H_H), 9.17 (d, J = 5.3 Hz, 1H, H_h), 8.52 (t, J = 8.7 Hz, 2H, H_e+H_E), 8.38 (dd, J = 8.2, 2.8 Hz, 2H, H_d+H_D), 8.33 – 8.24 (m, 2H, H_f+H_F), 8.03 – 7.96 (m, 2H, H_c+H_C), 7.93 – 7.85 (m, 2H, H_g+H_G), 7.49 (d, J = 5.1 Hz, 1H, H_A), 7.43 (d, J = 5.1 Hz, 1H, H_a), 7.36 – 7.26 (m, 2H, H_b+H_B), 4.37 (s, 1H, H3), 3.67 (dt, J = 9.2, 6.5 Hz, 1H, H1'), 3.49 (dt, J = 9.2, 6.5 Hz, 1H, H1'), 3.20 (dd, J = 13.2, 6.2 Hz, 1H, H4), 3.12 (dd, J = 13.9, 2.7 Hz, 1H, H2), 2.95 (s, 1H, H2), 2.61 (dd, J = 13.1, 1.6 Hz, 1H, H4), 1.66 – 1.54 (m, 2H, H2'), 1.43 (s, 3H, H1), 1.40 – 1.21 (m, 18H, H3'-11'), 1.08 (s, 3H, H5), 0.88 (d, J = 6.8 Hz, 3H, H12'); ^{13}C NMR (100 MHz, δ in CD_3CN): 158.6 (C_q), 158.5 (C_q), 157.3 (C_q), 157.2 (C_q), 154.6 (C_h), 153.9 (C_H), 152.2 (C_a), 151.9 (C_A), 139.8 (C_c+C_C+C_f+C_F), 129.7 (C_g), 128.7 (C_b+C_B), 128.6 (C_G), 125.9 (C_e), 125.8 (C_E), 125.2 (C_d), 125.1 (C_D), 74.2 (C3), 70.4 (C1'), 38.0 (C4), 37.2 (C2), 32.6, 30.5, 30.3, 30.3, 30.0, 26.8, 23.4, 20.9 (all C2'-11'), 18.5 (C1), 16.0 (C5), 14.4 (C12'); HR-MS m/z exp. (calcd.): 367.1310 (367.1312, $[M\text{-}2PF_6]^{2+}$); UV-Vis: λ_{max} (ε in $L.mol^{-1}.cm^{-1}$) in CH_3CN: 415 nm (6172); Elemental analysis for $C_{37}H_{52}F_{12}N_4OP_2RuS_2$: (calcd.): C, 43.40; H, 5.12; N, 5.47; (exp.): C, 43.38; H, 5.15; N, 5.49.

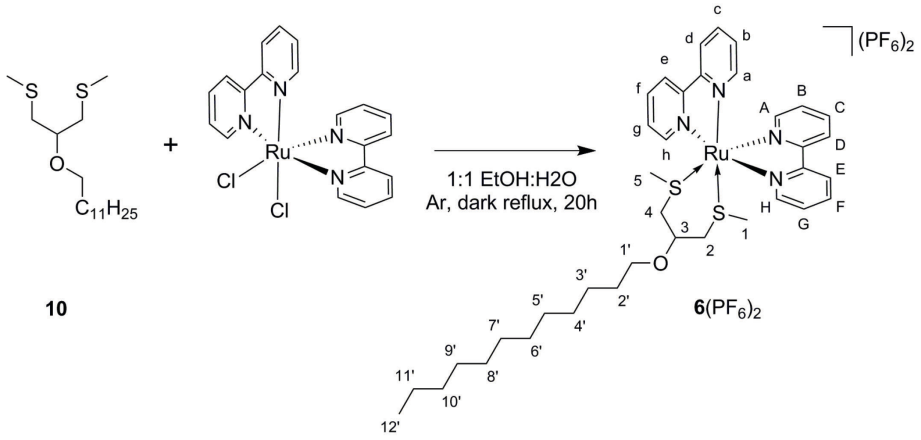

Scheme 8.3. Synthesis of ***6****$(PF_6)_2$ from compound* ***10*** *and cis-Λ/Δ-[Ru(bpy)$_2$Cl$_2$].*

8.4.5 Synthesis of 2,9-dimethyl-1,10-phenanthroline-5,6-dione – compound 11

According to literature procedure.[22] **11** was obtained as ocher yellow needles in 59% yield (2.03 g, 8.53 mmol). ^{1}H NMR (300 MHz, δ in $CDCl_3$): 8.38 (d, J = 8.0 Hz, 2H, H4+H7), 7.42 (d, J = 8.0 Hz, 2H, H3+H8), 2.86 (s, 6H, H2+H9); Spectrum matches literature data.[22] ESI-MS m/z exp. (calcd.): 239.1 (239.1, $[M+H]^+$), 261.1 (261.1, $[M+Na]^+$).

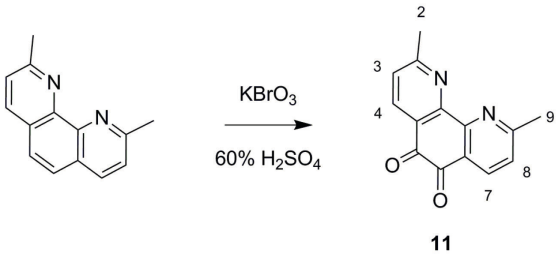

*Scheme 8.4. Synthesis of compound **11**.*

8.4.6 Synthesis of 5,6-bis(dodecyloxy)-2,9-dimethyl-1,10-phenanthroline – compound 12

Compound **11** (500 mg, 2.10 mmol) was dissolved in a 1:1 mixture of H_2O and THF (20 mL), and placed under Ar atmosphere, followed by the addition of tetrabutylammonium bromide (451 mg, 1.40 mmol), sodium dithionite (2.19 g, 12.6 mmol) and 1-bromododecane (1.66 mL, 6.93 mmol). To the resulting yellow suspension was slowly added a solution of KOH (1.77 g, 31.5 mmol) in H_2O (10 mL), leading to a dark brown suspension. The reaction mixture was stirred at 40 °C for 3 days, during which the color lightened to yellow-brown. After dilution with H_2O (50 mL), the mixture was extracted with EtOAc (3 x 75 mL). The combined organic layers were washed with H_2O (100 mL), dried over $MgSO_4$ and the solvent was removed by rotary evaporation. Column chromatography (SiO_2, EtOAc) yielded the title compound in 59% yield as a beige powder (720 mg, 1.25 mmol). TLC: R_f = 0.8 (EtOAc). ^{1}H NMR (300 MHz, δ in $CDCl_3$): 8.45 (d, J = 8.4 Hz, 2H, H4+H7), 7.49 (d, J = 8.4 Hz, 2H, H3+H8), 4.21 (t, J = 6.7 Hz, 4H, H1'), 2.93 (s, 6H, H2+H9), 1.88 (p, J = 6.7 Hz, 4H, H2'), 1.61 – 1.48 (m, 4H, H3'), 1.45 – 1.20 (m, 32H, H4'-H11'), 0.88 (t, J = 6.9 Hz, 6H, H12'); ^{13}C NMR (75 MHz, δ in $CDCl_3$): 158.2, 141.9, 131.0, 124.4, 123.7, 74.1, 32.1, 30.6, 29.8, 29.8, 29.7, 29.5, 26.4, 25.7, 22.9, 14.3; HR-MS m/z exp. (calcd.): 577.4721 (577.4728, $[M+H]^+$).

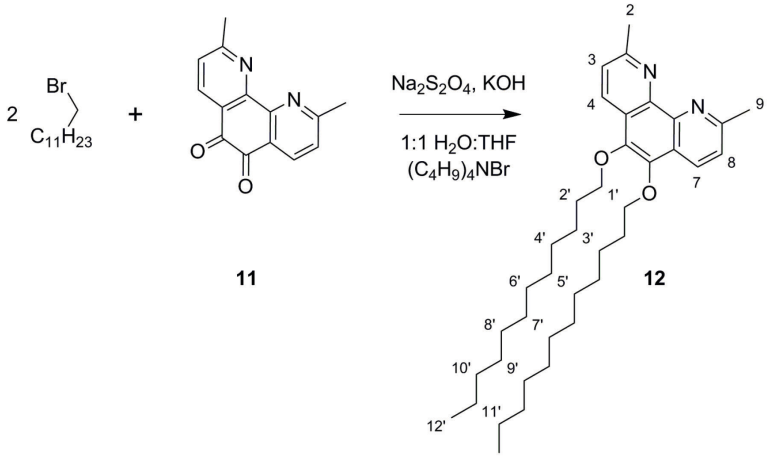

*Scheme 8.5. Synthesis of compound **12** from 1-bromododecane and compound **11**.*

8.4.7 Synthesis of 7$(PF_6)_2$

A mixture of **12** (100 mg, 0.172 mmol) and *cis*-*Λ*/*Δ*-[Ru(bpy)$_2$Cl$_2$] (100 mg, 0.206 mmol) was placed in a 25-mL Teflon-lined stainless steel reaction vessel. Ethylene glycol (8 mL) was added, and the closed vessel was heated to 200 °C for 6 h. The red solution obtained was poured onto

water (50 mL) and an orange precipitate was produced by adding sat. aq. KPF_6 (5 mL). After cooling the mixture to 4 °C, the precipitate was collected by filtration, washed with cold water and cold Et_2O, and purified by column chromatography (SiO_2, acetone to acetone:H_2O:sat. aq. KPF_6 (100:10:2)). Further purification using size exclusion chromatography (Sephadex LH20, acetone) yielded *cis-Λ/Δ*-[Ru(bpy)$_2$(**12**)]$(PF_6)_2$ (compound **7**$(PF_6)_2$) as a red powder (29 mg, 0.023 mmol, 13%). ^{1}H NMR (300 MHz, δ in CD_3CN): 8.63 (d, J = 8.5 Hz, 2H, H4+H7), 8.49 (d, J = 8.1 Hz, 2H, H_e), 8.43 (d, J = 8.1 Hz, 2H, H_d), 8.02 (td, J = 8.0, 1.5 Hz, 2H, H_f), 7.97 (td, J = 8.0, 1.5 Hz, 2H, H_c), 7.68 (d, J = 5.3 Hz, 2H, H_a), 7.61 (d, J = 5.1 Hz, 2H, H_h), 7.56 (d, J = 8.5 Hz, 2H, H3+H8), 7.27 (dd, J = 5.7, 1.0 Hz, 2H, H_g), 7.23 (dd, J = 5.7, 1.1 Hz, 2H, H_b), 4.38 – 4.18 (m, 4H, H1'), 1.91 – 1.83 (m, 10H, H2+H9+H2'), 1.54 (p, J = 7.1 Hz, 4H, H3'), 1.41 – 1.21 (m, 32H, H4'-H11'), 0.88 (t, J = 6.5 Hz, 6H, H12'); ^{13}C NMR (75 MHz, δ in CD_3CN): 166.6, 153.8 (C_h), 152.9 (C_a), 138.8 (C_c), 138.6 (C_f), 133.1 (C4+C7), 128.3 (C3+C8+C_b+C_g), 125.4 (C_d+C_e), 75.4 (C1'), 32.7 (C2'), 30.8, 30.4, 30.3, 30.1, 26.8 (all C3'-C10'), 26.0 (C2+C9), 23.4 (C11'), 14.4 (C12'); HR-MS m/z exp. (calcd.): 495.2534 (495.2539, $[M\text{-}2PF_6]^{2+}$); UV-Vis: λ_{max} (ε in L.mol^{-1}.cm^{-1}) in CH_3CN: 452 nm (13730); Elemental analysis for $C_{58}H_{76}F_{12}N_6O_2P_2Ru$: (calcd.): C, 54.41; H, 5.98; N, 6.56; (exp.): C, 54.94; H, 5.23; N, 6.58.

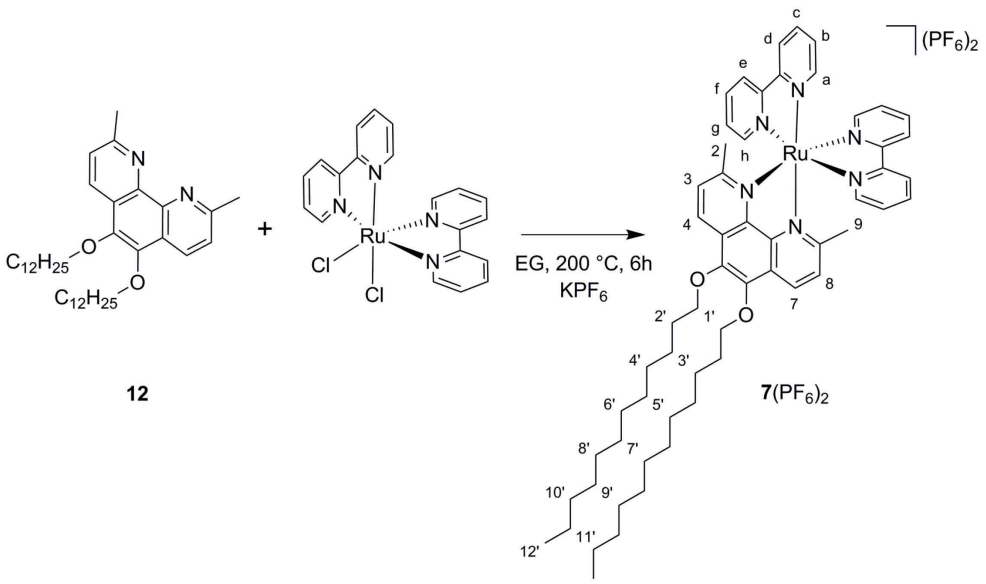

*Scheme 8.6. Synthesis of compound **7**$(PF_6)_2$ from cis-Λ/Δ-[Ru(bpy)$_2$Cl$_2$] and compound **12**.*

8.4.8 Liposome preparation

All liposome formulations were prepared by the classical hydration-extrusion method. As an example, the preparation of **M1-3-6** is described here. Aliquots of chloroform stock solutions containing the liposome constituents were added together in a flask to obtain a solution with 5.0 µmol DMPC, 0.20 µmol DSPE-mPEG-2000, 2.5 nmol **1**, 25 nmol **3**, and 0.20 µmol **6**$[PF_6]_2$. The organic solvent was removed by rotary evaporation and subsequently under high vacuum for at least 30 minutes to create a lipid film. 1.0 mL PBS buffer (with or without L-ascorbic acid and/or glutathione) was added and the lipid film was hydrated by 4 cycles of freezing the flask in liquid nitrogen and thawing in warm water (50 °C). The resulting dispersion was extruded through a Whatman Nuclepore 0.2 µm polycarbonate filter at 40-50 °C at least 11 times using a mini-

extruder from Avanti Polar Lipids, Inc. (Alabaster, Alabama, USA). The number of extrusions was always odd to prevent any unextruded material ending up in the final liposome sample. The extrusion filter remained practically colorless after extrusion, suggesting near-complete inclusion of the chromophoric compounds in the lipid bilayer. Liposomes were stored in the dark at 4 °C and used within 7 days. The average hydrodynamic liposome size and polydispersity index (PDI) were measured with a Malvern Instruments Zetasizer Nano-S machine, operating with a wavelength of 632 nm. The size and PDI were typically 130 – 170 nm and 0.1, respectively.

8.4.9 Upconversion emission spectroscopy with L1-2 liposomes and meat

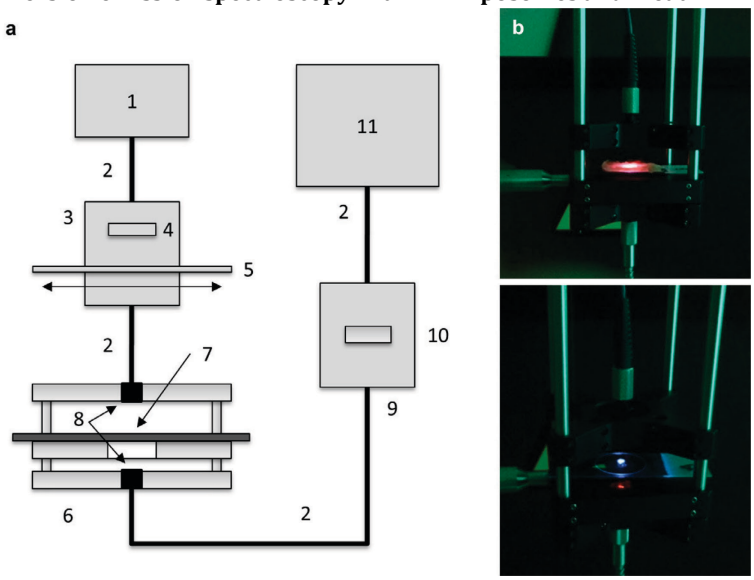

Figure 8.16. Experimental setup used for spectroscopy through meat. a) Schematic representation of the setup: 630 nm laser (1); optical fibers (2); filter holder (3) for 630 nm band pass filter (4) and variable neutral density filter (5); cage system (6) with two oppositely facing cage plates, both fitted with a collimating lens (8), and a central sample-holding plate; microscopy slide holding the liposome gel and meat on top (7); filter holder (9) for a 630 nm notch filter (10) for blocking the excitation source; spectrometer (11). b) Photographs of the cage system with the upconverting liposome gel only (bottom) and with 1 layer of pork fillet on top (top). Both photographs were taken with a 575 nm OD 4 short pass filter in front of the camera to block the excitation source.

L1-2 liposomes were prepared according to Section 8.4.8 ([DLPC] = 20.0 mM). To prepare a liposome hydrogel and to allow upconversion in air, this solution was heated to 55 °C and 1:1 v/v mixed with a solution at 55 °C containing 1 wt.% agarose, 10 mM sodium L-ascorbate and 10 mM sodium glutathionate (*pH* 7.3). 20 µL of this mixture was pipetted with a warm pipet on a warm 1 mm thick microscopy slide (Menzel-Gläser Superfrost, 76 x 26 mm) and immediately covered with a round 25 mm diameter microscopy coverslip (VWR, thickness no. 1). Upon cooling to room temperature, this procedure produced a thin gel slice with ~25 µm thickness. On top of the coverslips, thin slices of chicken breast fillet or pork fillet were layered (1 – 2 mm thick each, measured for each slice with a caliper) up to ~13 mm thick. The entire sample construct was allowed to reach room temperature (20 °C) before measurement in a custom-build spectroscopy setup (Figure 8.16). A cage with an open sample space was constructed with

single collimating lenses (Avantes COL-UV/VIS) on both sides for excitation (from the top) and detection (from the bottom) connected with FC-UVxxx-2 (xxx = 400, 600) optical fibers (Avantes). The excitation lens was connected to a clinical grade Diomed 630 nm PDT laser set to 30 mW (3 mm beam, 0.42 $W.cm^{-2}$) using a PM100 USB power meter and S310C detector (Thorlabs). Between the laser and the excitation lens, a filter holder was placed with a FB630-10 band pass filter and a NDL-25C-4 variable neutral density filter (Thorlabs). The detection lens was connected to a 2048L StarLine spectrometer (Avantes); between the spectrometer and detection lens, a filter holder with a NF-633 notch filter was placed. For each meat layer thickness, the spectrum was taken at 5 different sample locations, and the spectrum was averaged. Then, a new layer of meat was carefully placed on top and the measurements were repeated until a thickness of ~13 mm was achieved.

8.4.10 Photodissociation experiments with meat

For photodissociation experiments with **L1-3-6** liposomes and meat, the sample was prepared as described in Section 8.4.8 ([DLPC] = 10 mM). 400 µL sample was placed in a 2 mm thick cuvette and sandwiched between a 5 × 5 cm glass plate and a 5 × 5 cm slice of pork fillet (Albert Heijn; "AH Filetlapjes à la minute naturel"), 7 ± 0.5 mm thick. This meat-sample construct was placed in the same cage setup as described in Section 8.4.9, but the laser was now directly coupled to the excitation lens and the FB630-10 band pass filter was now placed directly between the excitation lens and the sample (see Figure 8.13). The detection lens and spectrometer were left out. To compare blue and light irradiation, the meat-sample construct was irradiated from the top with either 110 mW 450 nm or 630 nm laser light in a 3 mm collimated beam (1.6 $W.cm^{-2}$). Also, the experiment was repeated with 300 mW 630 nm light (4.2 $W.cm^{-2}$).

8.4.11 General cell culturing

A549 human lung carcinoma cells were cultured in 25 cm^2 flasks in 8 mL Dulbecco's Modified Eagle Medium with phenol red (DMEM; Sigma Life Science, USA), supplemented with 8.2% v/v fetal calf serum (FCS; Hyclone), 200 $mg.L^{-1}$ penicillin and streptomycin (P/S; Duchefa), and 1.8 mM glutamine-S (GM; Gibco, USA), under standard culturing conditions (humidified, 37 °C atmosphere containing 7.0% CO_2). The cells were split approximately once per week upon reaching 70 − 80% confluency, using seeding densities of 2 × 10^5 cells, and the medium was refreshed once per week. Cells were passaged for 4 − 8 weeks.

8.4.12 Live cell imaging with M1-3 liposomes - preparation

After cell splitting, the cells were suspended in OptiMEM (Life Technologies, USA), supplemented with 2.5% FCS, 200 mg/L P/S, and 1.8 mM GM at 3 × 10^5 cells per mL. 100 µL of this suspension was placed in a droplet on round 25 mm diameter microscopy coverslips (VWR, thickness no. 1) in a 6-well plate. After 5 min of sedimentation, 3 mL OptiMEM was carefully added to each well, and the cells were incubated for 24 h. Meanwhile, **M1-3** liposome samples were prepared as before ([DMPC] = 2.5 mM, 2 mL volume). Optionally, this solution contained 5 mM sodium L-ascorbate and 5 mM sodium glutathionate. The solution was sterilized with a 0.2 µm filter and from this a 3:5 v/v liposomes/Opti-MEM solution was prepared ([DMPC] = 1 mM). 3 mL of this solution was added to the desired wells, and the cells were incubated for 24 h. Then, the cells were washed once with PBS, and resupplied with 1 mL Opti-MEM before imaging. Optionally, the cells were incubated with 50 nM LysoTracker Red DND-99 in Opti-MEM for 30 min, after which the cells were washed once with PBS, and resupplied with 1 mL Opti-

MEM before imaging. Finally, the coverslips were transferred to a custom-made sample holder for round 25 mm coverslips, and supplied with 500 µL Opti-MEM.

8.4.13 Live cell imaging with M1-3 liposomes - microscopy

Bright field and (upconversion) emission imaging was performed with a customized Zeiss Axiovert S100 Inverted Microscope setup, fitted with a Zeiss 100× Plan Apochromat 1.4 NA oil objective, and an Orca Flash 4.0 V2 sCMOS camera from Hamamatsu, which together produced 4.2 megapixel images with pixel size of 69 nm. The typical camera exposure time was 1000 ms. Samples were loaded in a temperature and atmosphere controlled stage-top mini-incubator (Tokai Hit, Japan) set at 37 °C with 1% O_2 and 7% CO_2 in which samples were incubated for 30 min before imaging. For direct excitation and fluorescence imaging of **2**, a CrystaLaser DL-405-050 405 nm solid state laser was used, combined with a ZT405/514/561rpc dichroic beam splitter (Chroma Technology Corporation) and ZET442/514/568m emission filter (Chroma Technology Corporation). The output power of the 405 nm laser at the sample was typically 75 µW (60 µm spot diameter, intensity 2.7 W.cm^{-2}). For upconversion emission microscopy, a Power Technology 1Q1A30(639-35B)G3 639 nm diode laser was used as excitation source, combined with a Chroma ZT405/532/635rpc dichroic beam splitter. To block everything except upconversion emission, a 575 nm short pass filter (Edmund Optics, part no. #84-709) was placed between the sample and the camera, resulting in OD > 5 at 639 nm and 800 nm (*i.e.* the excitation source and the phosphorescence of **1** were completely blocked). The output power of the 639 nm laser at the sample was typically 1.0 mW (70 µm spot diameter, intensity 26 W.cm^{-2}). All laser beam spots had a Gaussian intensity profile; spot diameters are reported as Full Width at Half Maximum (FWHM) values.

8.4.14 Photocytotoxicity assay of liposomes with red and blue light

The phototoxicity of upconverting liposomes and liposomes doped with Ru-complexes was determined according to a photocytotoxicity protocol that was recently developed in our group.[10] MCF7, A549, or MRC5 cells were seeded in the central 60 wells of a 96 well plate at 8 K, 5 K, and 6 K cells respectively in 100 µL Opti-MEM. 100 µL Opti-MEM was added to the outer wells. The plate was incubated for 24 h. Meanwhile, liposomes were prepared as before ([DMPC] = 5.0 mM) and sterilized by extruding through a 0.2 µm filter. This procedure did not change the DLS values of the liposomes. The sterilized solution was used to prepare a dilution series of liposomes in 8-chamber reservoirs, and 100 µL of each diluted mixture was added to the wells according to the plate-design, see Figure 8.18a. The outer wells and control wells were mock-treated with 100 µL Opti-MEM only. The plates were incubated for 24 h, after which the cells were washed once with 200 µL Opti-MEM and resupplied with 200 µL Opti-MEM. The well-plate was placed in a temperature and atmosphere controlled stage-top mini-incubator (Tokai Hit, Japan) set at 37 °C, 20% O_2, and 7% CO_2 in which samples were incubated for 10 min before irradiation. Then, the plate was irradiated with either 15 min of 628 nm light (23.0 ± 1.5 mW.cm^{-2} intensity, 20.7 J.cm^{-2} dose) or 10 min of 454 nm light (7.0 ± 0.8 mW.cm^{-2} intensity, 4.2 J.cm^{-2} dose) using a custom-build array of 96 LED lights that fitted exactly on top of the mini-incubator, which have been characterized by our group recently.[10] The irradiation intensities were determined with a custom build spectroscopy setup, detailed in Section 8.4.15. Control plates were treated in the same way, but not irradiated. After irradiation, the plate was incubated for 48 h at 37 °C, 7% CO_2 and 20% O_2. Then, the cells were fixed by adding 100 µL 10% w/w trichloroacetic acid (TCA) in H_2O to each well and the plate was placed in a refrigerator at 4 °C for 60 h. The TCA was removed by rinsing the plate gently with H_2O five

times and the plate was dried overnight. Then, the inner 60 wells of the plate were stained with 100 µL sulforhodamine B (SRB, 0.6 w% in 1 v% acetic acid) for 30 min, after which the plate was washed five times in 1 v% acetic acid. Once the plate was dry (± 3 h), the SRB stain was dissolved in 200 µL 10 mM tris-base solution and the plate was placed on an orbital shaker for 30 min. Finally, the absorbance at 510 nm was measured with a plate reader (Tecan Infinite M1000 Pro) and the absorbance was converted to relative cell-viabilities using Microsoft Excel 2010 and GraphPad Prism 7 software. In case of **M1-3**, **M1**, and **M3** liposomes, the experiment was performed three times (three biological replicates); in case of **M5** and **M6**, the experiment was performed twice (two biological replicates).

8.4.15 Characterization of red and blue LED arrays in mini-incubator irradiation setup

The light power density of the LED arrays was measured using a custom-built spectroscopy setup consisting of an integrating sphere, which was positioned underneath the 96-well plate to simulate the irradiation conditions during cell experiments (Figure 8.17). The integrating sphere was mounted in a custom-made holder that mimicked the height of the mini-incubator while allowing the integrating sphere to be aligned exactly with a single 6 mm diameter well of a 96-well plate. On top of the holder, the lid of the mini-incubator was positioned, and on top of that, the LED array just like during cell irradiation. The integrating sphere position was diagonally adjustable over ten wells in order to individually measure a representative set of wells (B2, C3, C7, D4, D8, E5, E9, F6, F10, and G11). The integrating sphere was connected via an optical fiber to an Avantes CCD spectrometer, which were together spectrally calibrated just before measurement using a NIST-traceable calibration lamp (Avantes) to report the spectrum in spectral irradiance units ($\mu W.cm^{-2}.nm^{-1}$), where the surface here refers to that of the aperture of the integrating sphere. The light averaged intensity at the bottom of each well in $mW.cm^{-2}$ was then determined by spectrally integrating the spectrum for each well with OriginPro software and averaging these values over the different wells. Analysis of the spectrum also provided the intensity maximum and full-width-half-maximum (FWHM) bandwidth of each LED array. For the 454 nm LED array had a FWHM of 23 nm and an intensity of 7.0 ± 0.8 $mW.cm^{-2}$. The 628 nm LED array had a FWHM of 19 nm and an intensity of 23.0 ± 1.5 $mW.cm^{-2}$.

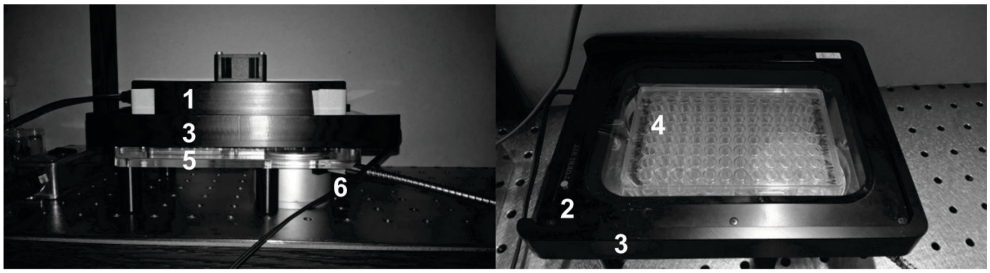

Figure 8.17. Photographs of the setup used for characterization of LED arrays, consisting of (from top to bottom) 96-LED array (1), mini-incubator lid (2), mini-incubator mimicking plate holder (3), 96-well plate (4), bottom of the plate holder (5), and integrating sphere fitting directly underneath the 96-well plate (6).

8.4.16 Photocytotoxicity assay of liposomes with high intensity red light

For photocytotoxicity assays using high intensity red light, a different procedure was followed; the differences are reported here. Instead of using all 60 central wells of a 96 well plate, only 24

of them were used according to the plate design in Figure 8.18b. Wells between the test-wells were intentionally left empty to avoid unintentional irradiation of neighboring wells. For this experiment, the diluted liposome solution (0.20 mM DMPC in Opti-MEM) was mixed 1:1 v/v with 10 mM sodium L-ascorbate and sodium glutathionate in PBS to make a 100 µM DMPC and 5 mM anti-oxidant solution. Additionally, the experiment was performed under hypoxic conditions by adjusting the O_2 level in the mini-incubator to 1%. Single wells were irradiated for 5 min with a 630 nm Diomed 630 PDT laser, fiber-coupled with a 600 µm fiber (Avantes) to a collimating lens (Omicron Laserprodukte GmbH, DE) fitted underneath the well plate (Figure 8.19). Together, these produced a 6 mm collimated beam (300 mW power, 1.1 $W.cm^{-2}$ intensity, 320 $J.cm^{-2}$ dose for 5 min irradiation) that illuminated an entire well surface area exactly. In these experiments, the well plate was moved every 5 min with an automated stage (MLS203-1, Thorlabs) so that each well was irradiated consecutively (2 h total irradiation time). This experiment was performed only once.

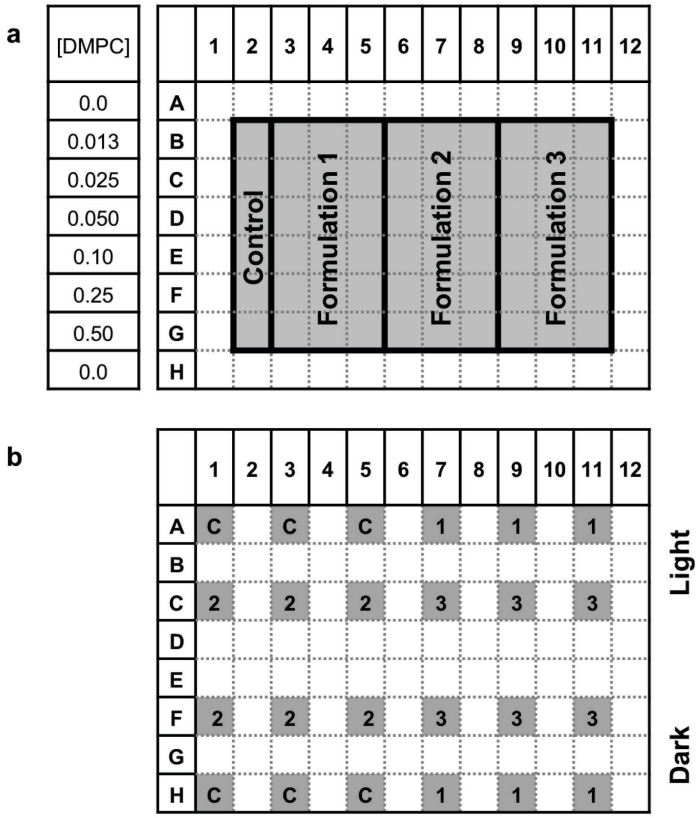

Figure 8.18. Plate design for photocytotoxicity assays. a) Plate design for an experiment using the inner 60 wells with a control column and three liposome formulations.[10] Each liposome formulation at each concentration is added to three different wells (technical triplicate). b) Plate design for an experiment using high intensity red light irradiation with three control wells (C) and three liposome formulations (indicated with 1, 2, and 3). The white wells have been left empty to avoid unintentional irradiation of neighboring wells. Only the top half of the wells was irradiated (12 wells in total).

Figure 8.19. Photographs of setup used for irradiation experiments with high intensity red light, consisting of a mini-incubator (1; for clarity here without 96-well plate), motorized XY-translation stage (2), and collimating lens fitted underneath the mini-incubator (3), connected to a fiber-coupled laser (not shown).

8.5 References

[1] a) R. E. Goldbach, I. Rodriguez-Garcia, J. H. van Lenthe, M. A. Siegler, S. Bonnet, *Chem. Eur. J.* **2011**, *17*, 9924-9929; b) B. S. Howerton, D. K. Heidary, E. C. Glazer, *J. Am. Chem. Soc.* **2012**, *134*, 8324-8327; c) L. M. Loftus, J. K. White, B. A. Albani, L. Kohler, J. J. Kodanko, R. P. Thummel, K. R. Dunbar, C. Turro, *Chem. Eur. J.* **2016**, *22*, 3704-3708; d) K. Arora, J. K. White, R. Sharma, S. Mazumder, P. D. Martin, H. B. Schlegel, C. Turro, J. J. Kodanko, *Inorg. Chem.* **2016**.

[2] a) M. Ferrari, *Nat. Rev. Cancer* **2005**, *5*, 161-171; b) Y. Matsumura, H. Maeda, *Cancer Res.* **1986**, *46*, 6387-6392.

[3] a) P. S. Wagenknecht, P. C. Ford, *Coord. Chem. Rev.* **2011**, *255*, 591-616; b) A. Bahreman, J.-A. Cuello-Garibo, S. Bonnet, *Dalton Trans.* **2014**, *43*, 4494-4505; c) S. L. H. Higgins, K. J. Brewer, *Angew. Chem., Int. Ed.* **2012**, *51*, 11420–11422.

[4] a) S. H. C. Askes, A. Bahreman, S. Bonnet, *Angew. Chem., Int. Ed.* **2014**, *53*, 1029-1033; b) S. H. C. Askes, M. Kloz, G. Bruylants, J. T. Kennis, S. Bonnet, *Phys. Chem. Chem. Phys.* **2015**, *17*, 27380-27390.

[5] A. Meister, M. E. Anderson, *Annu. Rev. Biochem.* **1983**, *52*, 711-760.

[6] M. Almgren, *J. Am. Chem. Soc.* **1980**, *102*, 7882-7887.

[7] a) H. J. Feldmann, M. Molls, P. Vaupel, *Strahlenther. Onkol.* **1999**, *175*, 1-9; b) P. Vaupel, F. Kallinowski, P. Okunieff, *Cancer Res.* **1989**, *49*, 6449-6465; c) E. E. Graves, M. Vilalta, I. K. Cecic, J. T. Erler, P. T. Tran, D. Felsher, L. Sayles, A. Sweet-Cordero, Q.-T. Le, A. J. Giaccia, *Clin. Cancer Res.* **2010**, *16*, 4843-4852.

[8] a) H.-J. Yang, C.-L. Hsu, J.-Y. Yang, W. Y. Yang, *PLoS One* **2012**, *7*, e32693; b) A. L. Magra, P. S. Mertz, J. S. Torday, C. Londos, *J. Lipid Res.* **2006**, *47*, 2367-2373; c) R. Chowdhury, M. A. Amin, K. Bhattacharyya, *J. Phys. Chem. B* **2015**, *119*, 10868-10875.

[9] S. A. Vinogradov, D. F. Wilson, *Journal of the Chemical Society, Perkin Transactions 2* **1995**, *0*, 103-111.

[10] S. L. H. Hopkins, B. Siewert, S. H. C. Askes, P. van Veldhuizen, R. Zwier, M. Heger, S. Bonnet, *Photochem. Photobiol. Sci.* **2016**, *15*, 644-653.

[11] a) Summary of Lipoplatin product characteristics, *http://lipoplatin.com/info_sop.php*, accessed on **13 July 2016**; b) Doxil prescribing information, *https://www.doxil.com/shared/product/doxil/doxil-prescribing-information.pdf*, accessed on **15 July 2016**

[12] a) T. M. Allen, A. Chonn, *FEBS Lett.* **1987**, *223*, 42-46; b) A. Gabizon, D. Papahadjopoulos, *Proceedings of the National Academy of Sciences* **1988**, *85*, 6949-6953; c) D. Liu, A. Mori, L. Huang, *Biochim. Biophys. Acta, Biomembr.* **1991**, *1066*, 159-165; d) A. L. Klibanov, K. Maruyama, V. P. Torchilin, L. Huang, *FEBS Lett.* **1990**, *268*, 235-237.

[13] Y. Sadzuka, K. Tokutomi, F. Iwasaki, I. Sugiyama, T. Hirano, H. Konno, N. Oku, T. Sonobe, *Cancer Letters* **2006**, *241*, 42-48.

[14] R. Weijer, M. Broekgaarden, M. Kos, R. van Vught, E. A. J. Rauws, E. Breukink, T. M. van Gulik, G. Storm, M. Heger, *Journal of Photochemistry and Photobiology C: Photochemistry Reviews* **2015**, *23*, 103-131.
[15] A. Bahreman, M. Rabe, A. Kros, G. Bruylants, S. Bonnet, *Chem. Eur. J.* **2014**, *20*, 7429-7438.
[16] S. Bonnet, B. Limburg, J. D. Meeldijk, R. J. M. Klein Gebbink, J. A. Killian, *J. Am. Chem. Soc.* **2010**, *133*, 252-261.
[17] S. L. H. Hopkins, B. Siewert, S. H. C. Askes, P. van Veldhuizen, R. Zwier, M. Heger, S. Bonnet, *Photochem. Photobiol. Sci.* **2016**.
[18] B. Siewert, V. H. S. van Rixel, E. J. van Rooden, S. L. Hopkins, M. J. B. Moester, F. Ariese, M. A. Siegler, S. Bonnet, *Chem. Eur. J.* **2016**, n/a-n/a.
[19] J. Reedijk, *Chem. Rev.* **1999**, *99*, 2499-2510.
[20] K. J. Takeuchi, M. S. Thompson, D. W. Pipes, T. J. Meyer, *Inorg. Chem.* **1984**, *23*, 1845-1851.
[21] A. Bahreman, B. Limburg, M. A. Siegler, E. Bouwman, S. Bonnet, *Inorg. Chem.* **2013**, *52*, 9456-9469.
[22] R. H. Zheng, H. C. Guo, H. J. Jiang, K. H. Xu, B. B. Liu, W. L. Sun, Z. Q. Shen, *Chin. Chem. Lett.* **2010**, *21*, 1270-1272.

CHAPTER 9

Imaging upconverting polymersomes in cancer cells: biocompatible anti-oxidants brighten triplet-triplet annihilation upconversion

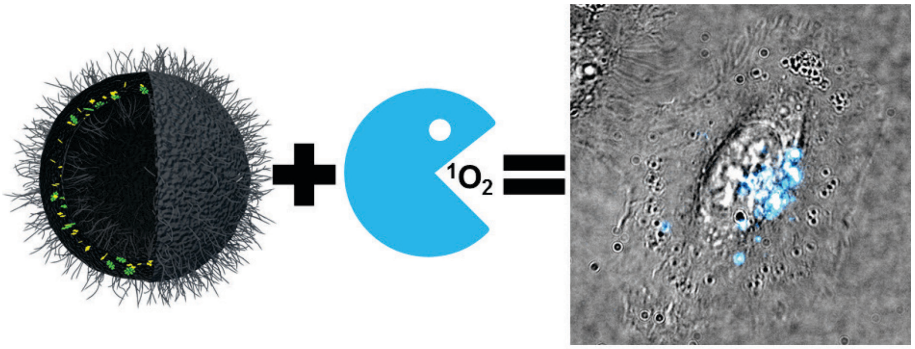

Light upconversion is a powerful tool in bio-imaging as it can abolish autofluorescence, increase imaging contrast, reduce irradiation damage, and increase excitation penetration depth in vivo. Among the various principles of light upconversion, triplet-triplet annihilation upconversion (TTA-UC) in nanoparticles holds great promise, due to the high efficiency at low excitation power. However, the TTA UC mechanism is inherently obstructed by molecular oxygen, leading to drug delivery systems and nano devices that do not function in air. In this work, we demonstrate that sacrificial anti-oxidants can be used to protect TTA-UC in polymersomes by photochemically depleting the local oxygen concentration. Red-to-blue upconverting polymersomes were prepared, which did not upconvert significantly in air, but did produce bright upconversion upon addition of 10 mM of L-ascorbate, glutathionate, L-histidine, sulfite, or trolox. Most importantly, this strategy also succeeded in living cells: A549 lung cancer cells were co-treated with upconverting polymersomes and 5 mM L-ascorbate and glutathionate, resulting in an order of magnitude brighter upconversion than without anti-oxidants. These results demonstrate a simple chemical solution to the issue of oxygen sensitivity of TTA-UC, which is of paramount importance for the technological advancement of this technique in biology.

This chapter was published as a full article: Sven H.C. Askes, Wim Pomp, Samantha L. Hopkins, Alexander Kros, Si Wu, Thomas Schmidt, and Sylvestre Bonnet, *Small*, **2016**

9.1 Introduction

Upconversion of light is the generation of high-energy photons from low-energy photons, for example the conversion of red light to blue light. In biological systems, upconversion imaging is characterized by negligible auto-fluorescence, increased imaging contrast, reduced irradiation damage, and increased excitation penetration depth *in vivo*. Because of these advantages, lanthanoid-based upconverting nanoparticles (UCNPs), for example, have attracted extensive interest.[1] However, UCNPs suffer from several disadvantages, such as the need for high excitation intensities or the low upconversion efficiencies observed in aqueous solution (typically ≤ 0.5%), which results from the low absorption cross section of lanthanoid ions and luminescence quenching by water at their surface.[2] In contrast, triplet-triplet annihilation upconversion (TTA-UC) requires low excitation intensity (down to 1 $mW.cm^{-2}$), employs sensitizers having high molar absorptivity in the phototherapeutic window, resulting in upconversion quantum yields up to 14% in aqueous solution.[2-3] TTA-UC is based on the photophysical interplay of photosensitizer and annihilator chromophores (see Chapter 2, Figure 2.1).[1b, 4] The photosensitizer absorbs low energy light, after which intersystem crossing leads to a long-lived triplet state. This triplet state is transferred to the annihilator upon diffusional collision by means of triplet-triplet energy transfer (TTET); a succession of TTET leads to a concentration buildup of long-lived triplet state annihilators molecules. Two triplet state annihilator molecules interact resulting in triplet-triplet annihilation upconversion, in which one of them departs with all the energy of the pair, thus reaching a high-energy singlet excited state. Finally, this singlet excited state returns to the ground state by fluorescent emission of a high-energy photon, thereby realizing upconversion. TTA-UC has been demonstrated in an extensive assortment of organic, inorganic, and/or supramolecular materials,[3b, 5] as well as in nano- or micro-sized particles.[6] It has been used for applications in photocatalysis,[7] solar energy harvesting,[8] drug delivery and drug activation,[9] or bio-imaging. In particular bio-imaging using TTA-UC has been demonstrated, often in fixed cells, using silica-coated micelles,[2, 10] dye-modified cellulose templates,[11] PMMA nanocapsules,[12] or soybean oil or oleic acid core nanocapsules.[13]

Although many published studies focusing on biological application of TTA-UC avoid discussing the sensitivity of their system to oxygen, TTA-UC inherently suffers from physical quenching of the sensitizer and/or annihilator triplet

excited states by O_2. Such quenching leads to the formation of undesirable, cytotoxic singlet oxygen and concomitant loss of upconversion in the nano-devices. For example, the TTA-UC liposome system initially described by our group for the activation of a blue-light sensitive prodrug[9] functioned only under inert atmosphere. Other groups showed that TTA-UC bio-imaging of PMMA nanocapsules in HeLa cells also suffered from oxygen sensitivity; upconversion was shown to be enhanced upon addition of valinomycin, which stimulates mitochondrial oxygen consumption.[12a] Here we argue that addressing the issue of oxygen sensitivity is of paramount importance for the technological advancement of TTA-UC in biology. Using TTA-UC polymersomes we demonstrate that it is possible to dramatically reduce the oxygen sensitivity of TTA-UC nano-sized systems by the addition of antioxidants thereby creating a locally oxygen-depleted environment. Interestingly, this strategy can be applied to cell cultures as exemplified by the imaging of TTA-UC polymersomes inside living cancer cells.

The polymersomes used in this study belong to a large family of vesicles that have attracted significant attention in the fields of drug delivery and bio-imaging research.[14] Polymersomes are typically composed of synthetic amphiphilic block copolymers that, similar to liposomes, self-assemble into spherical bilayer membranes surrounding an aqueous interior. Analogous to liposomes, the hydrophobic membrane of polymersomes can be doped with hydrophobic dyes such as palladium(II) tetraphenyl tetrabenzoporphyrin (**1**) and 2,5,8,11-tetra(*tert*-butyl)perylene (**2**, see Figure 9.1). When combined these dyes form a TTA-UC couple that is capable of upconverting red light into blue light. Polymersomes have many advantages compared to lipid-based liposomes. Notably, the membrane thickness, rigidity, fluidity, plasticity, permeability, and surface functionalization, can be tuned by choosing the appropriate copolymer. In addition, polymersomes typically feature high retention of encapsulates, high stability in aqueous media, and can be very cheap to make.[14a-d] In this study poly-isobutylene (PiB, $M_w \sim 1.0$ kg.mol^{-1}) and poly-ethylene glycol (PEG, $M_W \sim 0.35$ or 0.75 kg.mol^{-1}) were chosen here as the hydrophobic and hydrophilic polymer blocks respectively.[15] PiB is a well-known polymer with low permeability to small molecules such as dioxygen; it has a high chemical and thermal resistance and a high biocompatibility.[16] PEG is a biocompatible polymer that has become an established standard for the surface functionalization of drug delivery and bio-imaging systems. In this article we describe the synthesis and

characterization of upconverting PiB-PEG polymersomes, study the stability of red-to-blue TTA-UC in aqueous solution in presence of a range of biocompatible antioxidants, and demonstrate the enhanced TTA-UC imaging of these vesicles in living human cancer cells in presence of biocompatible antioxidants.

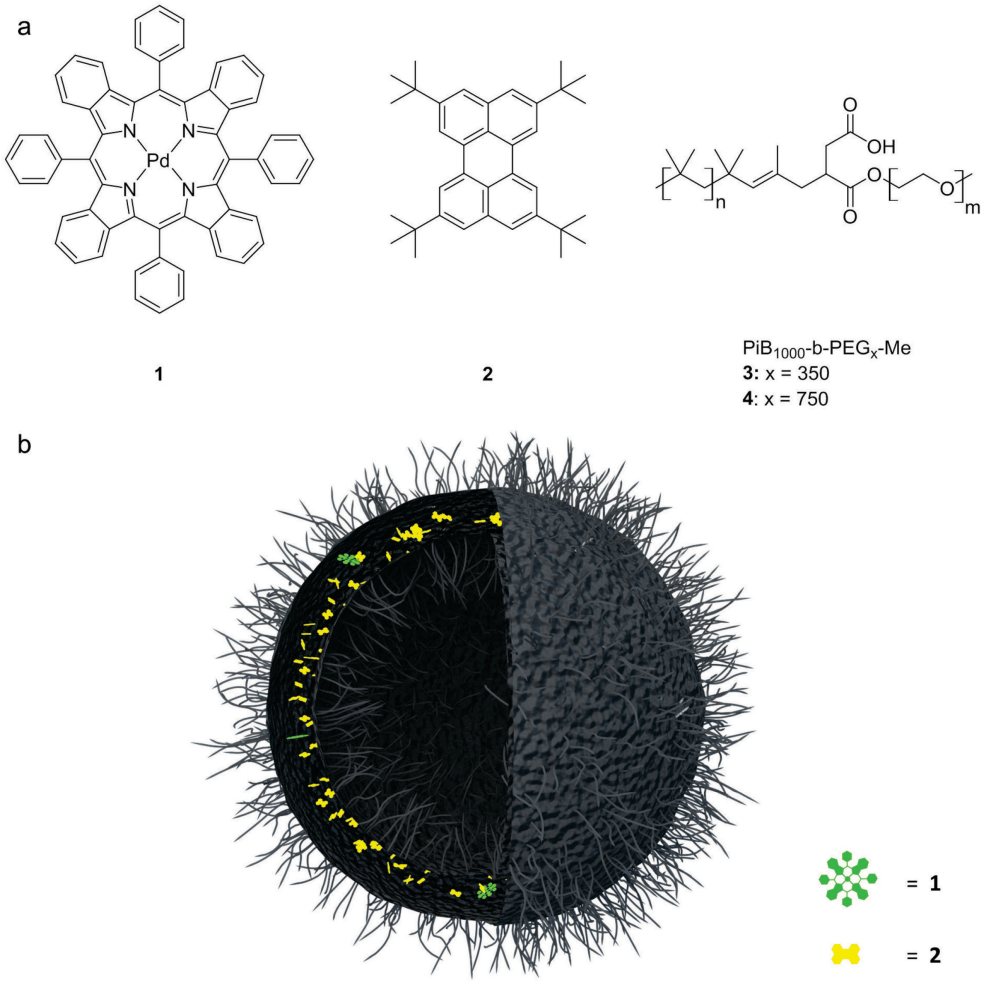

*Figure 9.1. a) Chemical structures of the red photosensitizer palladium(II) tetraphenyl tetrabenzoporphyrin (**1**), of the blue emitter 2,5,8,11-tetra(*tert*-butyl)perylene (**2**), and of the polyisobutylene-block-monomethyl polyethylene glycol (PiB_{1000}-b-PEG_x-Me, x = 350 or 750) amphiphilic block copolymers used in this study, with PiB molecular weight of 1.0 kg.mol^{-1} and PEG block molecular weights of 0.35 kg.mol^{-1} (**3**) and 0.75 kg.mol^{-1} (**4**). b) Schematic illustration of a polymersome composed of **3** or **4**, and doped with compounds **1** and **2**.*

9.2 Results and discussion

9.2.1 Synthesis and characterization of TTA-upconverting polymersomes

In order to acquire a vesicle morphology, an amphiphilic block copolymer needs to have a hydrophilic block volume fraction of 0.25 to 0.45.[14b] Hence, two amphiphilic block copolymers (compounds **3** and **4**) were synthesized by condensation of polyisobutylene succinic anhydride (PiB-SA, $M_W \sim 1.0$ kg.mol^{-1}) and mono-methoxy polyethylene glycol ($M_W \sim 0.35$ kg.mol^{-1} for **3** and 0.75 kg.mol^{-1} for **4**).[17] The products were characterized using NMR spectroscopy, IR spectroscopy, and gel-permeation chromatography (see experimental section and Appendix VIII). Nanoparticle dispersions called **P3** and **P4** were produced with polymers **3** and **4**, respectively, using a freeze-thaw-extrusion protocol in phosphate buffered saline at a concentration of 10 mg/mL polymer. **P3** and **P4** were clear solutions that exhibited a typical nanoparticle scatter (Figure S.VIII.10). Sample **P3** was more opaque than **P4**, indicating a larger particle size. The hydrodynamic diameter (z-average) and polydispersity index (PDI) of the particles was measured using dynamic light scattering (DLS), revealing typical particle diameters of ~150 and 80 nm for **P3** and **P4**, respectively, and PDI's ranging from 0.1 to 0.3 (Table 9.1). The nanoparticle dispersions were stable over time and the hydrodynamic radius did not change over a period of at least two months. The ζ-potentials were found to be −42.0 and −24.0 mV for **P3** and **P4**, respectively. The negative surface charge originates from the carboxylic acid groups in the polymer junction, which are deprotonated at neutral *pH*. The less negative charge of **P4** can be explained by the larger PEG-brush on its surface, which is known to decrease the observed surface charge due to an increased hydrodynamic drag.[18]

To examine the particle morphology and measure the particle diameter distribution, the samples were examined with transmission electron microscopy (TEM, see Figure 9.2). The micrographs show that **P3** and **P4** consisted of particles of 156 ± 90 nm (bimodal distribution) and 95 ± 49 nm (unimodal distribution), respectively. The size populations as determined with TEM were in good agreement with the DLS values. For both **P3** and **P4**, upon high-intensity exposure to the electron beam of the TEM microscope, the particle shell collapsed, liquid visibly leaked from the interior, and the particles became more and more translucent for electrons. After this transformation was complete, only an empty collapsed shell remained (Figure

S.VIII.7). Surprisingly, the particles did not burst at low electron beam exposures, indicating that the shell successfully tolerated the high vacuum in the TEM chamber. Overall, these observations are consistent with vesicular nanoparticles composed of rubbery membranes surrounding an aqueous interior, *i.e.* polymersomes.

Table 9.1. Sample composition of all studied polymersome samples, and their typical particle sizes and surface charges; hydrodynamic particle diameters (z-average), polydispersity index (PDI), ζ-potential, and particle diameters from transmission electron microscopy (TEM). ζ-potentials were measured in 1:9 PBS:H_2O at pH 7.1. All measurements were done at 20 °C.

Sample	[3] (mg/mL)	[4] (mg/mL)	[1] (μM)	[2] (μM)	z-average (nm)	PDI	ζ-potential (mV)	TEM size (nm)
P3	10	-	-	-	149	0.120	−42.0 ± 7.5	156 ± 90
P3-1	10	-	10	-	152	0.136		
P3-2	10	-	-	200	154	0.154		
P3-1-2	10	-	10	200	146	0.189		
P4	-	10	-	-	83	0.263	−24.0 ± 10.7	95 ± 49
P4-1	-	10	10		83	0.277		
P4-2	-	10	-	200	86	0.267		
P4-1-2	-	10	10	200	77	0.263		

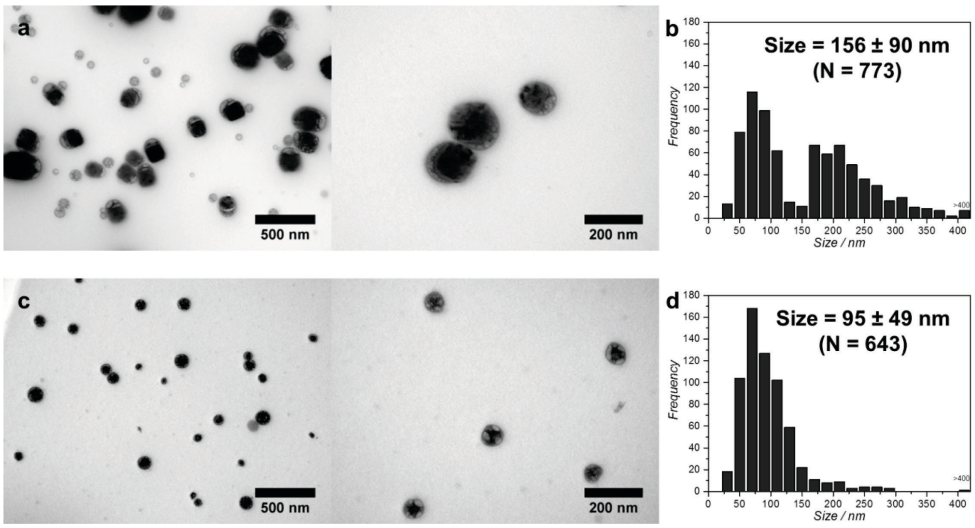

*Figure 9.2. Transmission electron micrographs of **P3** (a) and **P4** (c) vesicles and their respective measured particle diameter distributions (b and d). The mean diameters and standard deviations were determined from a population (N) of 773 and 643 individual particles for **P3** and **P4**, respectively.*

The TTA-UC dyes that were selected for incorporation in the polymersome membrane were palladium(II) tetraphenyl tetrabenzoporphyrin (**1**) as the red light-absorbing photosensitizer, and 2,5,8,11-tetra(*tert*-butyl)perylene (**2**) as

the blue light-emitting annihilator. Instead of using perylene, the benchmark annihilator in many TTA-UC systems,[1b] four-fold *tert*-butylated perylene was used to prevent aromatic stacking and thereby enhance solubility of the molecule in the hydrophobic environment of the membrane.[19] Preliminary experiments indeed indicated that the greater lipophilicity of **2** prevented the molecule from partitioning with the water phase in amphiphilic dispersions, whereas unsubstituted perylene shuttles between different membranes (data not shown).[20] With respect to perylene, the fluorescence maximum of **2** is reported to be bathochromically shifted by only about 15 nm while the fluorescence lifetime and quantum yield are very similar.[19, 21] Indeed this tetrasubstitution of perylene did not significantly alter the ability of this blue emitter to serve as an annihilator for red-to-blue TTA-UC. Bright red-to-blue TTA-UC was achieved in air by dissolving **1** and **2** in a 3:1 mixture of chloroform and oleic acid and illuminating with 50 mW 630 nm excitation (0.4 $W.cm^{-2}$), without deoxygenation (Figure S.VIII.8). Next, **1** and/or **2** were incorporated in polymersomes **P3** and **P4** resulting in dye-loaded polymersomes, denoted as **P3-1, P3-2, P3-1-2, P4-1, P4-2**, and **P4-1-2** (see Table 9.1 for the membrane composition, and Figure 9.3 and Figure S.VIII.10 for photographs of the samples). Both dyes were incorporated quantitatively in the vesicle membrane, and dye doping had no effect on particle size or stability (Table 9.1 and Figure 9.2). UV-Vis absorption and emission spectroscopy on **P3-1, P3-2, P4-1,** and **P4-2** confirmed that both dyes were incorporated, with the dye absorbance and emission spectra being identical to those of the isotropic chloroform solutions (compare Figure S.VIII.9 with Figure S.VIII.10).

To demonstrate TTA-UC, polymersomes **P3-1-2** and **P4-1-2** were first examined using UV-Vis absorption and emission spectroscopy under aerobic conditions in the presence of 50 to 75 mM sodium sulfite (Figure 9.3). Sulfite is a known scavenger of ground-state molecular oxygen.[9a, 22] The UV-Vis absorption spectrum shows the characteristic absorption bands of **1** (around 630 nm) and **2** (350 – 450 nm). At 20 °C and under red light excitation (at 630 nm, 50 mW, 0.4 $W.cm^{-2}$) the emission spectrum of both samples showed the typical phosphorescence band of **1** at 800 nm and the structured emission band of **2** at 460 nm (Figure 9.3c). These results represent the first example of TTA-UC in polymersomes. The upconversion emission was intense and could easily be viewed by the naked eye when the red excitation source was blocked with a 575 nm short-pass filter (Figure 9.3b). To study the location of TTA-UC,

giant polymersomes **GP3-1-2** with a diameter of 5 – 10 µm diameter were assembled using the same constituents as in **P3-1-2**. Imaging using an optical microscope setup with 635 nm excitation and visualized from 450 to 575 nm confirmed that TTA-UC was indeed located in the polymer membrane (Figure S.VIII.12). The absolute quantum yield of upconversion (Φ_{UC}) in the polymersomes, measured using an integrating sphere setup (see experimental section), amounted to 0.002 at 20 °C for both **P3-1-2** and **P4-1-2** (see Table 9.2).

To investigate TTA-UC at human body temperature (37 °C), upconversion and phosphorescence were measured as a function of temperature between 5 and 50 °C (Figure S.VIII.13). Upon elevating the temperature, the upconversion emission gradually intensified (Φ_{UC} at 37 °C = 0.005) while the phosphorescence intensity decreased. This trend is beneficial for bio-imaging at 37 °C. We attribute the higher TTA-UC efficiency at higher temperatures to the higher mobility of **1** and **2** in the PiB membrane, as the translational diffusion rate of polyaromatic hydrocarbons in polyisobutylene materials is usually positively correlated to temperature.[23] The upconversion efficiency of **P3-1-2** and **P4-1-2** are in the same order of magnitude compared to red-to-blue TTA-UC in phospholipid-based liposomes measured in similar conditions (Φ_{UC} at 37 °C = 0.015% using perylene as annihilator).[9a] Finally, the intensity threshold (I_{th}) at which the power dependency of upconversion changes from quadratic to linear was determined, as it is regarded as a benchmark parameter for the efficiency of TTA-UC.[3b, 24] The red laser excitation power was varied between 16 and 510 mW.cm^{-2} while measuring the upconversion intensity at both 20 and 37 °C (Figure S.VIII.14). From the double logarithmic plot of upconversion intensity (I_{UC}) *vs*. excitation intensity (P), a value of *ca*. 200 mW.cm^{-2} was determined for I_{th} (Table 9.2). At 37 °C, I_{th} decreased down to 20 – 50 mW.cm^{-2}, owing to the greater TTA-UC efficiency at this temperature. Note that excitation intensities above 200 mW.cm^{-2} can easily be reached in common laser microscopy setups. In summary, TTA-UC in polymersomes was established for the first time, and the photophysical characteristics were found compatible with biological imaging applications.

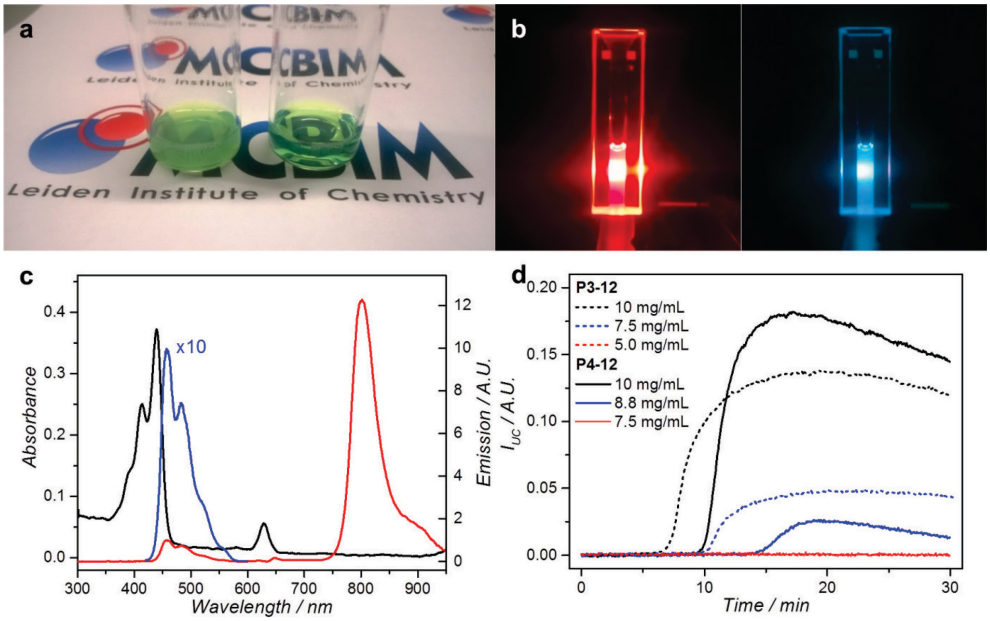

*Figure 9.3. Visual and photophysical characterization of TTA-UC in **P3-1-2** and **P4-1-2**. a) Photographs of 10 mg/mL dispersions of **P3-1-2** (left) and **P4-1-2** (right). b) Photographs of a 7.5 mg/mL **P3-1-2** dispersion irradiated with a 50 mW 4 mm diameter red laser beam from the left side in presence of 75 mM sodium sulfite. In the right picture, the excitation source is blocked with a 575 nm short pass filter. c) UV-Vis absorbance (black) and emission (red/blue) spectroscopy of **P4-1-2** vesicles (0.5 mg/mL compound 4) at 20 °C. Emission spectrum taken under red light irradiation (630 nm, 50 mW, 0.4 W.cm^{-2}) in presence of 50 mM sodium sulfite. For clarity, the blue curve is the red curve multiplied by 10. d) I_{UC} at 486 nm under red light irradiation (630 nm, 50 mW, 0.4 W.cm^{-2}, 4 mm excitation path length) of samples **P3-1-2** and **P4-1-2**. **[3]** = 10, 7.5, and 5.0 mg/mL (dashed black, blue, and red, respectively), and **[4]** = 10, 8.8, and 7.5 mg/mL (solid black, blue, and red, respectively). Conditions: 600 µL sample in a non-stirred semi-micro cuvette at 20 °C. No oxygen scavenger was added here.*

*Table 9.2. Photophysical characteristics of **P3-1-2** and **P4-1-2** in presence of 50 mM sodium sulfite: absolute quantum yield of upconversion (Φ_{UC}) at 20 °C, ratio of upconversion emission intensity at 37 °C and 20 °C, estimation of Φ_{UC} at 37 °C calculated from multiplying the intensity ratio $I_{UC,37°C}/I_{UC,20°C}$ with Φ_{UC} at 20 °C, and the intensity threshold (I_{th}) for efficient TTA-UC at 20 °C and 37 °C.*

Sample	Φ_{UC} at 20 °C (%)	$\frac{I_{UC37°C}}{I_{UC20°C}}$	Est. Φ_{UC} at 37 °C (%)	I_{th} at 20 °C (mW.cm^{-2})	I_{th} at 37 °C (mW.cm^{-2})
P3-1-2	0.20	2.7	0.54	256	204
P4-1-2	0.21	2.4	0.50	220	197

9.2.2 Do these polymersome dispersions produce upconversion in air?

In phospholipid-based liposomes TTA-UC is inhibited by the presence of molecular oxygen, which physically quenches triplet excited states and results in the photocatalytic production of singlet oxygen. To investigate whether **P3-1-2** and **P4-1-2** were capable of producing upconversion under aerobic

conditions polymersome samples were prepared without the oxygen scavenger sulfite at different copolymer bulk concentrations, and irradiated for 30 minutes while monitoring I_{UC} (Figure 9.3d, see Figure S.VIII.15 and Figure S.VIII.17 for full datasets). At a concentration of 10 mg/mL polymer **3**, no upconversion was observed at t = 0, but after 7 minutes of red light irradiation the band of upconverted blue light appeared and I_{UC} reached a maximum after ~15 minutes irradiation. Comparison of the UV-Vis absorbance spectra before and after irradiation showed significant bleaching of both dyes **1** and **2** (Figure S.VIII.15). No difference in DLS values were found before and after the experiment, indicating that red light irradiation did not damage the polymersomes' integrity. At a concentration of 7.5 mg/mL polymer **3**, qualitatively identical observations were made but I_{UC} maximized at a lower value, whereas at 5 mg/mL no upconversion was observed at all after 30 min irradiation. As a control, a 7.5 mg/mL **P3-1-2** sample prepared in presence of 75 mM sodium sulfite exhibited a 1000-fold more intense upconversion band that was very stable over 30 min (Figure S.VIII.16). The results with **P4-1-2** vesicles were very similar: upconversion did not occur at polymer concentrations lower than 8.8 mg/mL. These results clearly indicated that in air TTA-UC in polymersomes is concentration-dependent. We interpret this result by the fact that the block-copolymers contain a C=C double bond that is known to be able to chemically quench singlet oxygen *via* a perepoxide mechanism.[25] We hypothesize that such chemical quenching results in the local consumption of oxygen during initial red light irradiation, up to the point where the oxygen concentration is low enough to allow TTA-UC to occur. Similar observations have been reported by Kim *et al.*, who have used polyisobutylene as the liquid core in TTA-UC nanocapsules.[3a, 26] At lower polymer concentrations, oxygen diffusion outcompeted its photochemical consumption, so that no upconversion was observed. To confirm this hypothesis, we repeated the experiment in a stirred macro cuvette with an oxygen sensor probing the oxygen concentration in solution (Figure S.VIII.18; [**3**] = [**4**] = 10 mg/mL). During red light irradiation a gradual decrease in dissolved oxygen was indeed observed while upconversion first appeared after 15 min for **P3-1-2** and after 60 min for **P4-1-2**, *i.e.*, when the bulk oxygen concentration was below 1–2 ppm. Overall, these results show that upconversion in polymersomes can indeed occur in air and in absence of sulfite, most likely due to singlet oxygen scavenging by the unsaturated polymer itself. However, under diluted conditions and thus reduced singlet

oxygen scavenging capacity, upconversion in air does not occur anymore unless sulfite is added.

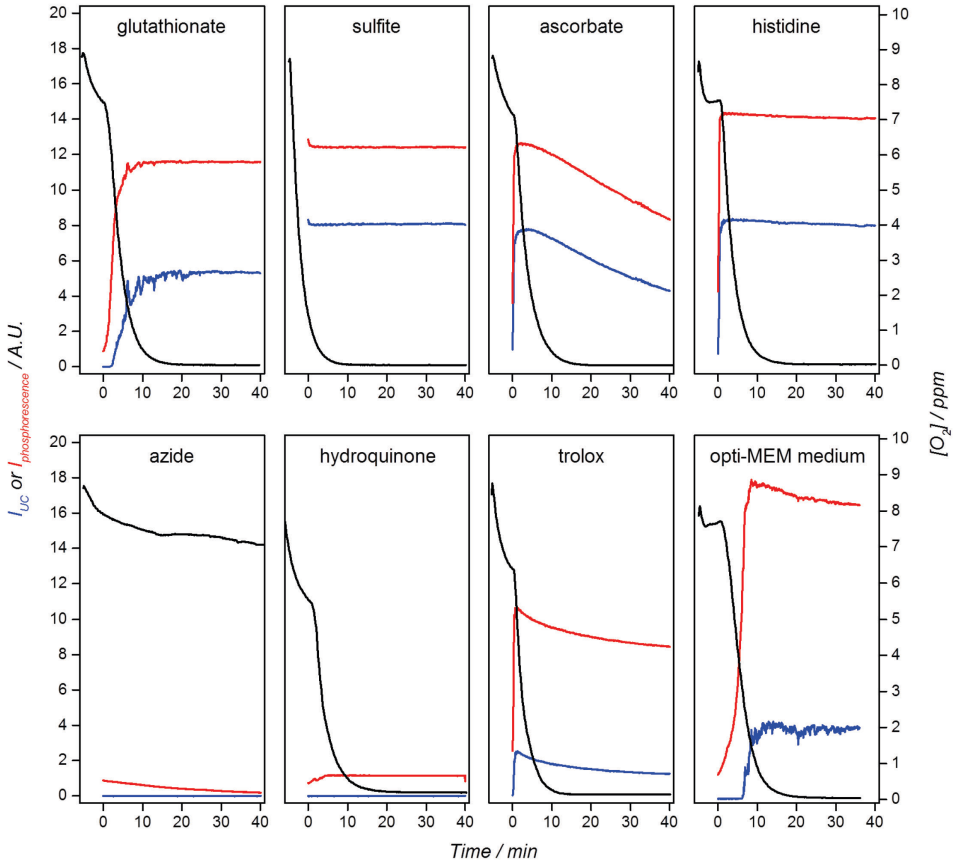

*Figure 9.4. Emission (red/blue) and oxygen concentration (black) time traces of polymersome **P4-1-2** samples in air under red light irradiation (630 nm, 50 mW, 0.4 W.cm^{-2}) irradiation with addition of 10 mM sodium glutathionate, sodium sulfite, sodium L-ascorbate, L-histidine, sodium azide, hydroquinone, trolox, or 1:19 v/v mixed with opti-MEM cell culture medium (see formulation in exp. section). Red and blue line represent $I_{phosphorescence}$ (at 800 nm) and I_{UC} (at 486 nm, multiplied by 10 for clarity), respectively. Conditions: [**4**] = 0.5 mg/mL, [**1**] = 0.5 µM, [**2**] = 10 µM, T = 20 °C, pH = 7.0-7.3 (pH for the trolox experiment was 7.6 to dissolve the compound completely), with a 2 mL sample volume in a stirred macro cuvette. Laser was turned on at t = 0.*

9.2.3 Addition of other water-soluble oxygen scavengers to P4-1-2

Encouraged by these results, and realizing that TTA-UC in air can occur by chemical scavenging of ground state oxygen (sulfite) or singlet oxygen (copolymer alkene function), **P4-1-2** vesicles were mixed with a selection of known anti-oxidants and irradiated with red light while continuously measuring oxygen concentration, the phosphorescence intensity $I_{phosphorescence}$

(at 800 nm), and the upconversion intensity I_{UC} (at 486 nm, see Figure 9.4). The bulk copolymer concentration was fixed at 0.5 mg.ml^{-1}, so that there would be no TTA-UC in air without anti-oxidants (see previous section). The anti-oxidants chosen were sodium sulfite, sodium L-ascorbate, sodium glutathionate, L-histidine, hydroquinone, and trolox, *i.e.*, the water-soluble derivative of vitamin E. The anti-oxidant concentration was kept constant (10 mM at *pH* 7.0 – 7.6) to mimic cellular concentrations of glutathione (0.5 – 10 mM)[27] and so that there was an excess of the anti-oxidants with respect to the dissolved oxygen concentration in an air-saturated aqueous solution at room temperature (~9 ppm; 2.5 mM). In each of these experiments, as soon as the laser was switched on, a clear consumption of oxygen was observed, which decreased from ~8 to 0 ppm in 15 – 25 min. In all cases, except for L-histidine, oxygen was already consumed in the dark, but illumination clearly accelerated the process, probably due to the higher redox potential of the $^1O_2/O_2^{\bullet-}$ couple (E^0 = +0.65 V at *pH* 7) compared to the $^3O_2/O_2^{\bullet-}$ couple (E^0 = −0.33 V at *pH* 7).[28] More importantly, the time evolution of emission showed a steep rise both for I_{UC} and $I_{phosphorescence}$, signifying the stabilization of the triplet excited states at sufficiently low oxygen concentrations. Strong TTA-UC was observed instantaneously (within 30 seconds) for sodium sulfite, sodium L-ascorbate, L-histidine, and trolox. For sodium glutathionate, upconversion was first observed after 2 min. Upconversion was not observed in mixtures with hydroquinone, even at 0 ppm oxygen concentrations. We explain this result by the fact that the reaction of hydroquinone and oxygen produces benzoquinone, which is known to quench the triplet excited states of aromatic hydrocarbons due to charge-transfer interactions.[29] As control experiments, irradiation at identical conditions was repeated without oxygen scavengers, and without oxygen scavengers in the dark (Figure S.VIII.19). As expected, no oxygen consumption or upconversion were observed. Additionally, a physical quencher of singlet oxygen, *i.e.*, sodium azide,[30] was tested as well. In presence of 10 mM NaN_3 however (Figure 9.4), no UC and only weak phosphorescence were observed, which confirmed that chemical quenching is required for obtaining TTA-UC, rather than physical quenching. Finally, upconversion in **P4-1-2** vesicles was also tested in a 1:19 v/v mixture of vesicles and opti-MEM cell medium, which also contains biocompatible anti-oxidants (see formulation in experimental section). Upconversion was first detected after 6 min irradiation and dissolved oxygen was depleted within 20 min irradiation, which confirmed the presence of chemical quenchers of singlet oxygen in the medium (probably sodium pyruvate and bovine serum

albumin from fetal calf serum).[31] Overall, these results clearly demonstrate that the addition of a biologically realistic concentration of anti-oxidants is a potent strategy to obtain TTA-UC in air. The local O_2 concentration is depleted by chemically consuming either ground-state oxygen (sulfite) or the photocatalytically generated singlet oxygen (histidine, *etc.*), until an oxygen concentration threshold is reached where TTA-UC becomes possible.

9.2.4 Anti-oxidants brighten TTA-UC in cancer cell cultures

To see whether our concept is also valid in cell culture conditions using live cells, human lung carcinoma A549 cells were incubated with **P4-1-2** for 4 h, in the absence or presence of a mixture of 5 mM sodium L-ascorbate and sodium glutathionate as anti-oxidant "cocktail". After refreshing the medium and staining the nuclei with Hoechst 33342, the cells were visualized with optical microscopy at 37 °C, 7% CO_2, and 1% O_2 (Figure 9.5). An atmosphere with a low oxygen concentration was chosen to mimic median tumor oxygen partial pressures, which generally range from 0.5% to 4% (pO_2 = 5 − 30 mm Hg).[32] In absence of anti-oxidants and under 405 nm excitation, fluorescent spots were detected in the cytosol that correspond to singlet emission of **2** in the polymersomes. Under the hypothesis that nanoparticles are usually endocytosed,[33] we tentatively assigned these spots to be endosomes, lysosomes, and/or multi-vesicular bodies containing the polymersomes. Attempts were undertaken to demonstrate the co-localization of these spots and endo- or lysosomes using LysoTracker Red, but the rapid motion of these fluorescent spots during imaging prevented a conclusive outcome. Under 635 nm excitation, upconverted emission was detected in locations that closely matched the emission detected under 405 nm irradiation (Figure S.VIII.20). Considering that upconversion only occurs when **1** and **2** are co-located in the same membrane, this observation indicates that the polymersomes were still intact and located where upconversion was detected. However, the upconversion emission intensity was rather weak and sometimes difficult to detect at all.

In contrast, when the cells where incubated with the anti-oxidants cocktail described above, very similar images for the bright field and 405 nm excitation were obtained. However, a much brighter image was obtained upon 635 nm excitation. Imaging was also performed at 19% O_2 and 7% CO_2 (*i.e.* pO_2 far exceeding any *in vivo* tissue oxygenation level), but no upconversion emission was detected at all under these conditions (data not shown). To quantify the emission at 1% O_2, 30 individual image sets with 40x

magnification were acquired in the presence and absence of anti-oxidants (10 – 20 cells per image, see experimental section and Figure S.VIII.21), and the emission was quantified by calculating the mean pixel value of each image (Figure 9.6). While the emission intensity with λ_{exc} = 405 nm, and thus the uptake of polymersomes, was not influenced by the addition of anti-oxidants, the upconversion emission (λ_{exc} = 635 nm) was found to be an order of magnitude more intense in presence of the anti-oxidant cocktail. The mean signal to background ratio (S/B, see experimental section for definition) increased from 0.2 (without anti-oxidant) to 2.6 (with antioxidant, see Figure 9.6b). By contrast, the S/B ratio for λ_{exc} = 405 nm remained low (~1) due to substantial autofluorescence of the cells, and it was not influenced by the presence of the antioxidant cocktail (Figure 9.6a). These exciting results demonstrate the potential of TTA-UC polymersomes in bio-imaging applications. Indeed, the *in vitro* data mirror the data obtained in homogeneous solution, demonstrating that co-treatment with cell-compatible anti-oxidants, at oxygen concentration that are realistic for tumor environments, brighten TTA-UC in living human cancer cells.

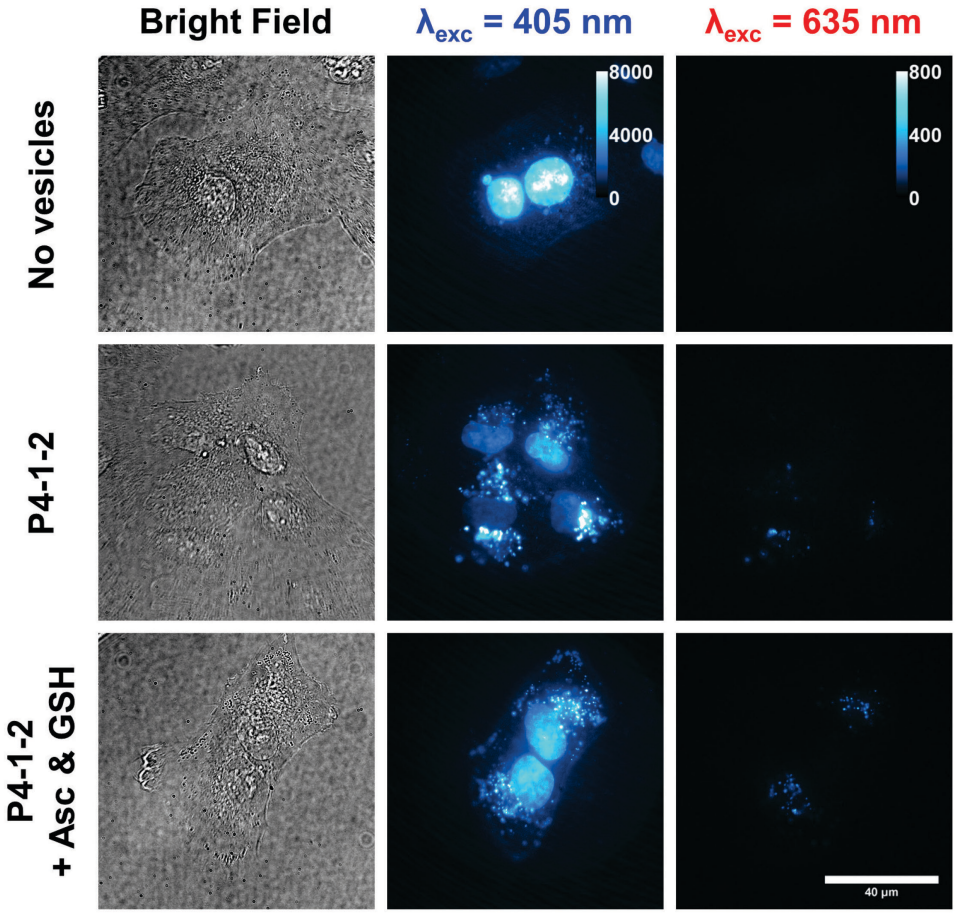

*Figure 9.5. In vitro upconversion imaging of **P4-1-2** upconverting polymersomes in living A549 lung carcinoma cells in bright field mode (left column), with λ_{exc} = 405 nm (middle column), and with λ_{exc} = 635 nm (right column) with 100x magnification. Cells were incubated for 4 h with Opti-MEM only (top row),with 1:1 v/v mixture of Opti-MEM and **P4-1-2** vesicles (middle row, [**4**] = 0.5 mg/mL), or with 1:1 v/v mixture of Opti-MEM and **P4-1-2** vesicles ([**4**] = 0.5 mg/mL) and addition of 5 mM sodium L-ascorbate and 5 mM sodium glutathionate (bottom row). The cell nuclei were stained with Hoechst 33342 prior to imaging. Imaging conditions: T = 37 °C, 7.0% CO_2, 1.0% O_2, 62 µW 405 nm laser power (60 µm spot diameter, 2.2 W.cm^{-2} intensity), 13 mW 635 nm laser power (50 µm spot diameter, 640 W.cm^{-2} intensity). For comparison, the image histograms for λ_{exc} = 405 nm are scaled from 0 – 8000 pixel values, and for λ_{exc} = 635 nm are scaled from 0 – 800 pixel values, as indicated by the calibration bars in the top row.*

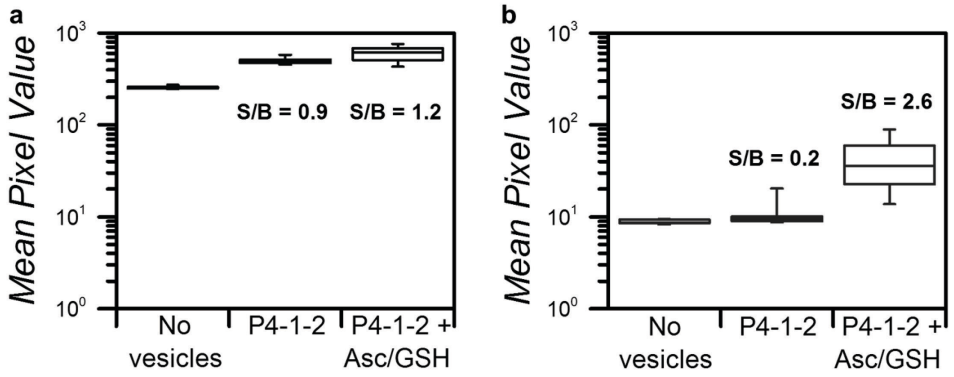

Figure 9.6. Quantified fluorescence emission under 405 nm (a) and 635 nm (b) excitation. The emission was quantified as the mean pixel value, based on 30 individual images at 40x magnification for each experiment, without nuclear stain, see experimental section and Figure S.VIII.21. Mean signal to background ratios (S/B) are given for both 405 and 635 nm excitation as the ratio of the mean luminescence intensity and the mean background intensity (i.e. the "No vesicles" dataset).

9.3 Conclusion

TTA-UC polymersomes were constructed in aqueous buffers by self-assembly of polyisobutylene-b-monomethoxy polyethylene glycol block-copolymers (PiB-b-PEG-Me, **3** or **4**), a red-light absorbing porphyrin photosensitizer **1**, and a blue-light emitting tert-butylated perylene annihilator **2**. Only weak red-to-blue upconversion was observed in concentrated dispersions in air, and dilution completely abolished upconversion emission. However, upon the addition of chemical antioxidants such as sulfite, L-ascorbate, glutathionate, L-histidine, or trolox, intense and stable upconversion was observed in air (21% O_2). Scavenging of reactive oxygen species by the sacrificial anti-oxidant led to an oxygen-depleted environment in the illuminated area where TTA-UC can occur efficiently. The biocompatibility of this strategy was demonstrated by incubating these polymersomes *in vitro* in the absence or presence of a mixture of L-ascorbate and glutathionate. The upconversion luminescence was an order of magnitude more intense when the cells were co-treated with the anti-oxidants cocktail. These results clearly demonstrate that biocompatible anti-oxidants brighten TTA-UC in aqueous solution but also in living cancer cells. These results reinforce the applicability of TTA-UC nanoparticles in bio-imaging and may open new routes towards the application of TTA-UC for phototherapy.

9.4 Experimental

9.4.1 General

Polyisobutylene succinic anhydride (PiB_{1000}-SA, Dovermulse H1000) with a saponification number of 58.1 mg KOH/g was kindly provided by DoverChem (Dover, OH, USA) and was purified by silica flash chromatography in pure DCM before use. Palladium tetraphenyltetrabenzoporphyrin (**1**) was purchased from Bio-Connect (Huissen, The Netherlands). Dulbecco's phosphate buffered saline (DPBS) was purchased from Sigma Aldrich and had a formulation of 8 $g.L^{-1}$ NaCl, 0.2 $g.L^{-1}$ KCl, 0.2 $g.L^{-1}$ KH_2PO_4, and 1.15 $g.L^{-1}$ K_2HPO_4 with a *pH* of 7.1 − 7.5. All other chemicals were purchased from major chemical suppliers and used as received.

The average polymersome diameter, polydispersity index, and zeta-potential were measured using a Malvern Instruments Zetasizer Nano-S machine, operating with a wavelength of 632 nm. The zeta-potential measurement was carried out in a DTS1070 folded capillary cell. Transmission electron microscopy was done on a Jeol 1010 with an acceleration voltage of 80 kV. Images were collected with an Olympus Megaview G2 camera, and Olympus iTEM software. Samples were loaded on Formvar/Carbon film on Copper 400 mesh TEM grids (FC400Cu100; van Loenen Instruments, Zaandam, The Netherlands). Oxygen measurements were done with an Ocean Optics NeoFox Foxy oxygen probe that was calibrated with 1 M Na_2SO_3 as the zero-oxygen point. Images and data were processed using Fiji ImageJ,[34] Origin Pro, and/or Microsoft Excel software.

9.4.2 Synthesis of 2,5,8,11-tetra(*tert*-butyl)perylene (compound 2)

Adapted from literature procedures.[35] Perylene (0.50 g, 1.98 mmol) was added to 50 mL dry *tert*-butyl chloride under Schlenck conditions. Anhydrous aluminium trichloride (1.0 g, 7.5 mmol) was added and the mixture was refluxed for 6 h, after which an additional 30 mL *tert*-butyl chloride was added and the mixture was further refluxed overnight. Then, 20 mL *tert*-butyl chloride and 1.0 g anhydrous aluminium trichloride were added and reflux was continued for another 24 h. The mixture was allowed to cool to room temperature and extracted with 100 mL brine in a separatory funnel. The aqueous layer was separated and extracted with three 50 mL portions of DCM. The DCM fractions were combined with the previously obtained organic fraction and dried with anhydrous sodium sulfate. The dried organic layer was filtered and rotary-evaporated at 80 °C until a concentrate remained, which was baked in a petri-dish on a hot plate at 170 °C for 30 h, at which point smoke ceased to evolve. The remaining dark brown solid was dissolved in a 2:1 mixture of petroleum ether and chloroform and purified with silica column chromatography (gradient of pure PE to 2:1 PE:$CHCl_3$ mixture, R_f = 0.93 in PE:$CHCl_3$) to afford 0.72 g of orange crystalline product (1.51 mmol, 76%). An aliquot of the product was recrystallized from 50:50 DCM:MeOH for use in photophysical experiments. ^{1}H NMR (300 MHz, $CDCl_3$) δ (ppm) 8.24 (d, J = 1.7 Hz, 4 H), 7.63 (d, J = 1.6 Hz, 4 H), 1.50 (s, 36 H). ^{13}C NMR (75 MHz, $CDCl_3$) δ (ppm) 148.8, 135.0, 130.9, 125.9, 123.4, 117.8, 35.0, 31.5. NMR spectra match literature data.[36]

9.4.3 Synthesis of PiB_{1000}-b-PEG_{350}-Me (compound 3)

Adapted from literature procedure, see Scheme S.VIII.1.[17] 3.66 g PiB_{1000}-SA (3.79 mmol) and 1.32 g mono-methoxy PEG_{350} (3.77 mmol) were heated to 80 °C, blanketed with argon by three cycles of evacuation and argon purging, and then stirred overnight at 110 − 120 °C. The mixture

was allowed to cool to room temperature, after which it was purified by silica column chromatography (DCM:MeOH gradient from 99:1 to 95:5; R_f = 0.37 for 95:5 DCM:MeOH) to yield 2.89 g of product (2.08 mmol, 55%). ^{1}H NMR (400 MHz, $CDCl_3$) δ (ppm) 4.9 – 4.8 (1 H, C=C of PiB), 4.3 – 4.1 (2 H, alpha protons of the ester), 3.8 – 3.5 (30 H, PEG) 3.4 (3 H, O-CH_3 of PEG-Me), 3.1 – 2.9; 2.8 – 2.4; 2.3 – 2.1; 2.1 – 0.8 (111 H, methyl and methylene of PiB). IR spectroscopy (cm^{-1}): 3467 (OH), 2949, 2883 (C-H), 1734 (C=O), 1638 (C=C), 1470, 1389, 1366, 1231 (PiB skeleton), and 1104 (C-O of PEG). NMR and IR spectra given in Figure S.VIII.3 and Figure S.VIII.5, respectively, both corresponding to literature data.[17] Gel permeation chromatogram given in Figure S.VIII.1. MALDI-TOF mass spectrometry did not yield a usable spectrum.

9.4.4 Synthesis of PiB_{1000}-b-PEG_{750}-Me (compound 4)

Identical procedure as for PiB_{1000}-PEG_{350}-Me. Used 1.87 g PiB_{1000}-SA (1.81 mmol) and 1.29 g mono-methoxy PEG_{750} (1.72 mmol). 1.79 g product obtained (1.00 mmol, 59%). R_f = 0.29 for 95:5 DCM:MeOH. ^{1}H NMR (400 MHz, $CDCl_3$) δ (ppm) 4.9 – 4.8 (1 H, C=C of PiB), 4.3 – 4.1 (2 H, alpha protons of the ester), 3.8 – 3.5 (71 H, PEG) 3.4 (3 H, O-CH_3 of PEG-Me), 3.1 – 2.9; 2.8 – 2.4; 2.3 – 2.1; 2.1 – 0.8 (169 H, methyl and methylene of PiB). IR spectroscopy (cm^{-1}): 3487 (OH), 2949, 2878 (C-H), 1737 (C=O), 1636 (C=C), 1470, 1388, 1366, 1230 (PiB skeleton), and 1107 (C-O of PEG). NMR and IR spectra given in Figure S.VIII.4 and Figure S.VIII.6, respectively, both corresponding to literature data.[17] Gel permeation chromatogram given in Figure S.VIII.2. MALDI-TOF mass spectrometry did not yield a usable spectrum.

9.4.5 Preparation of upconverting polymersomes

Polymersomes and dye-doped polymersomes were prepared according to a hydration-extrusion protocol. As an example, the preparation of **P4-1-2** is described here. Aliquots of chloroform stock solutions containing the polymersome constituents were added together in a glass tube to obtain a solution with 10 mg PiB_{1000}-PEG_{750}-Me, 10 nmol palladium tetraphenyltetrabenzoporphyrin (**1**), and 200 nmol 2,5,8,11-tetra(*tert*-butyl)perylene (**2**). The organic solvent was removed by rotary evaporation and subsequently under high vacuum for at least 15 minutes to create a polymer film. 1.0 mL DPBS buffer was added and the polymer film was hydrated by 3 cycles of freezing the flask in liquid nitrogen and thawing in warm water (50 °C). The resulting dispersion was extruded through a Whatman Nuclepore 0.1 µm polycarbonate filter at room temperature at least 11 times using a mini-extruder from Avanti Polar Lipids, Inc. (Alabaster, Alabama, USA). The number of extrusions was always odd to prevent any unextruded material ending up in the final liposome sample. The extrusion filter remained completely colorless after extrusion, suggesting full inclusion of the chromophoric compounds in the polymer membrane. Polymersomes were stored at room temperature and were typically used for further experiments within 24 h. The polymersomes were characterized with dynamic light scattering (DLS), zeta potentiometry, and (cryo) transmission electron microscopy.

9.4.6 Preparation of giant polymersomes

All giant polymersomes were prepared by lipid film re-hydration on dextran chemically cross-linked hydrogel substrates by a method described elsewhere.[22a, 37] The preparation of **GP3-1-2** is described here as an example. Glass microscopy slides were first incubated with 1:1 vol MeOH:HCl (37%) for 30 min, then with 98% H_2SO_4 for 30 min, and then thiol-functionalized by incubating them for 1 h in a 2 wt% solution of (3-mercaptopropyl)triethoxysilane in dry toluene under a nitrogen atmosphere, and washing them three times with toluene. Directly

after, a homogeneous film of Dex-PEG hydrogel was formed on this surface by drop-casting 600 µL of a 1:1 volume mixture of 2 wt.% maleimide-functionalized dextran, with a substitution degree of 3 maleimide groups per 100 glucopyranose residues of dextran (synthesis and characterization detailed in ref. 2), in water and 2 wt.% α,ω-PEG dithiol (1500 $g.mol^{-1}$) in water at room temperature. A homogenous hydrogel film was formed after 30 − 45 min at 40 °C. Then, 10 µL of polymer mixture stock solution in chloroform, containing 10 mg/mL **3**, 0.8 mM DSPE-PEG-2K, 0.20 mM **2**, and 10 µM **1**, was deposited on the hydrogel surface. The organic solvent dried within 1 min, after which the slide was dried further for at least 20 min under vacuum at room temperature. The polymer film was then hydrated with 400 µL 0.2 M sucrose in phosphate buffered saline for 1 h at 50 °C, creating a buffered solution containing free-floating vesicles. For optical microscopy imaging, 300 µL of this solution was transferred to an Eppendorf tube containing 700 µL 0.2 M glucose in PBS to allow the sucrose-loaded giant vesicles to sink to the bottom of the tube. After one hour, 300 µL of this GUV sediment was transferred to a visualization microscopy chamber, and the rest of the chamber was filled with 100 µL 0.2 M glucose PBS. Finally, to chemically deoxygenate the chamber, 100 µL 0.5 M sodium sulfite in PBS was added. The vesicles were imaged within 24 hours with a modified epifluorescence microscope setup, see below.

9.4.7 Emission spectroscopy

Emission spectroscopy was conducted in a custom-built setup (Figure S.VIII.22). All optical parts were connected with FC-UVxxx-2 (xxx = 200, 400, 600) optical fibers from Avantes (Apeldoorn, The Netherlands), with a diameter of 200 − 600 µm, respectively, and that were suitable for the UV-Vis range (200 − 800 nm). Typically, 2.0 mL of sample was placed in a 111-OS macro fluorescence cuvette from Hellma in a CUV-UV/VIS-TC temperature-controlled cuvette holder with stirring from Avantes. The cuvette holder temperature was controlled with a TC-125 controller and T-app computer software from Quantum Northwest (Liberty Lake, WA, USA), while the sample temperature was measured with an Omega RDXL4SD thermometer with a K-type probe submerged in the sample. The sample was excited with a collimated 630 nm laser light beam (4 mm beam diameter) from a clinical grade Diomed 630 nm PDT laser. The 630 nm light was filtered through a FB630-10, 630 nm band pass filter (Thorlabs, Dachau/Munich, Germany) put between the laser and the sample. The excitation power was controlled using the laser control in combination with a NDL-25C-4 variable neutral density filter (Thorlabs), and measured using a S310C thermal sensor connected to a PM100USB power meter (Thorlabs). For regular measurements, the excitation power was set at a power of 50 mW (0.4 $W.cm^{-2}$). UV-Vis absorption spectra were measured using an Avalight-DHc halogen-deuterium lamp (Avantes) as light source and a 2048L StarLine spectrometer (Avantes) as detector, both connected to the cuvette holder at a 180° angle and both at a 90° angle with respect to the red laser irradiation direction. The filter holder between cuvette holder and detector was in a position without a filter (Figure S.VIII.22, item 8). Luminescence emission spectra were measured using the same detector but with the UV-Vis light source switched off. To visualize the spectrum from 550 nm to 900 nm, while blocking the red excitation light, a Thorlabs NF-633 notch filter was used in the variable filter holder. To visualize the spectrum from 400 nm to 550 nm, an OD4 575 nm short pass filter (Edmund Optics, York, United Kingdom, part no. 84-709) was used. All spectra were recorded with Avasoft software from Avantes and further processed with Microsoft Office Excel 2010 and Origin Pro software. The emission spectra obtained from the two filters were stitched together

at 550 nm to obtain a continuous spectrum from 400 to 900 nm. No correction was needed to seamlessly connect the spectra.

9.4.8 Determination of the quantum yield of upconversion

The quantum yield of upconversion was determined absolutely by means of an integrating sphere setup. The setup and measurement procedure are discussed in depth in Appendix I.

9.4.9 General cell culturing

A549 human lung carcinoma cells were cultured in 25 cm^2 flasks in 8 mL Dulbecco's Modified Eagle Medium with phenol red (DMEM; Sigma Life Science, USA), supplemented with 8.2% v/v fetal calf serum (FCS; Hyclone), 200 $mg.L^{-1}$ penicillin and streptomycin (P/S; Duchefa), and 1.8 mM glutamine-S (GM; Gibco, USA), under standard culturing conditions (humidified, 37 °C atmosphere containing 7.0% CO_2). The cells were split approximately once per week upon reaching 70 – 80% confluency, using seeding densities of 2×10^5 cells, and the medium was refreshed once per week. Cells were passaged for 4 – 8 weeks.

9.4.10 Cell imaging preparation

After cell splitting, the cells were suspended in OptiMEM (Life Technologies, USA), supplemented with 2.5% FCS, 200 mg/L P/S, and 1.8 mM GM at 3×10^5 cells per mL. For imaging at 100× magnification, 100 µL of this suspension was placed in a droplet on round 25 mm diameter microscopy coverslips (VWR, thickness no. 1) in a 6-well plate. After 5 min of sedimentation, 3 mL OptiMEM was carefully added to each well, and the cells were incubated for 24 h. For imaging at 40× magnification, cells were seeded in a glass-bottom 24-well plate (Greiner Bio-One International, Germany, item no. 662892) at 50k cells per well and incubated for 24 h. Meanwhile, **P4-1-2** polymersome samples were prepared as before ([**4**] = 10 mg/mL, 1 mL volume), and then purified by size exclusion chromatography (NAP-25 columns from GE healthcare, PBS as eluens) by collecting only the green eluting band (~ 2 mL), and diluting this elute further to a volume of 10.0 mL with PBS. Optionally, this final PBS solution contained 20 mM sodium L-ascorbate and 20 mM sodium glutathionate. Then, the solution was sterilized with a 0.2 µm filter and diluted with 10 mL Opti-MEM ([**4**] = 0.5 mg/mL). 3 mL of this solution was added to each well of the 6-well plate, and the cells were incubated for 4 h. Then, the cells were washed once with PBS, and resupplied with 1 mL Opti-MEM before imaging. Optionally, the cells were incubated with 1 µg/mL Hoechst 33342 in PBS for 20 min at 37 °C to stain the cell nuclei.

9.4.11 Cell and giant polymersome imaging

Bright field and (upconversion) emission imaging was performed with a customized Zeiss Axiovert S100 Inverted Microscope setup, fitted with a Zeiss 100× Plan Apochromat 1.4 NA oil objective or a Zeiss 40× EC Plan Neofluar 1.3 NA oil objective, and an Orca Flash 4.0 V2 sCMOS camera from Hamamatsu, which together produced 4.2 megapixel images with pixel size of 69 nm (for 100x) or 173 nm (for 40x). The typical camera exposure time was 1000 ms. Samples were loaded in a temperature and atmosphere controlled stage-top mini-incubator (Tokai Hit, Japan) set at 37 °C with 1% O_2 and 7% CO_2 in which samples were incubated for 30 min before imaging. For imaging at 100× magnification, a custom-made sample holder for round 25 mm cover slips was used. For direct excitation and fluorescence imaging of **2**, a CrystaLaser DL-405-050 405 nm solid state laser was used, combined with a ZT405/514/561rpc dichroic beam splitter (Chroma Technology Corporation) and ZET442/514/568m emission filter

(Chroma Technology Corporation). The output power of the 405 nm laser at the sample was typically 62 μW at 100× magnification (60 μm spot diameter, intensity 2.2 W.cm^{-2}) and 76 μW at 40× magnification (150 μm spot diameter, intensity 0.44 W.cm^{-2}). For upconversion emission microscopy, a LRD-0635-PFR-00200-01 LabSpec 635 nm Collimated Diode Laser (Laserglow Technologies, Toronto, Canada) was used as excitation source, combined with a Chroma ZT405/532/635rpc dichroic beam splitter. To block everything except upconversion emission, a 575 nm short pass filter (Edmund Optics, part no. #84-709) was placed between the sample and the camera, resulting in OD > 5 at 635 nm and 800 nm (*i.e.* the excitation source and the phosphorescence of **1** were completely blocked). The output power of the 635 nm laser at the sample was typically 12.6 mW at 100× magnification (50 μm spot diameter, intensity 640 W.cm^{-2}) and 13.1 mW at 40× magnification (131 μm spot diameter, intensity 97 W.cm^{-2}). All laser beam spots had a Gaussian intensity profile; spot diameters are reported as Full Width at Half Maximum (FWHM) values.

9.4.12 Quantification of luminescence

The mean total signal (S_T) of the images was defined as

$$S_T = BG + L \qquad \textit{Equation 9.1}$$

where BG is the mean background signal and L is the mean luminescence signal. BG was measured in absence of **P4-12** (*i.e.* L = 0). S_T was calculated in mean pixel value by taking the sum of all pixel values (V) in the region of interest (ROI), containing a certain amount of pixels (px), and dividing by the ROI area (A_{ROI}, in px):

$$S_T = \frac{\sum_{px \in ROI} V_{px}}{A_{ROI}} \qquad \textit{Equation 9.2}$$

The same ROI was used for all images with a 1200 px diameter, closely encircling the illumination spot, see Figure S.VIII.21. The cell confluency in the illumination spot was always 70 – 100%, amounting to 10 – 20 cells located in the ROI. S_T was calculated for 30 individual images of each experiment (300 to 600 individual cells) by measuring the mean pixel value within the ROI with Fiji ImageJ software.[34] The mean signal to background ratio (S/B) was then calculated from the S_T and BG values:

$$S/B = \frac{L}{BG} = \frac{S_T - BG}{BG} \qquad \textit{Equation 9.3}$$

9.5 Acknowledgements

Prof. Dr. Elisabeth Bouwman is kindly acknowledged for the support and scientific discussion. Bart Jan van Kolck is kindly acknowledged for the supply of hydrogel slides for the giant vesicle

experiments. NWO (The Netherlands Organization for Scientific Research) is acknowledged for a VIDI grant to S.B. The European Research Council is acknowledged for an ERC starting grant to S.B.

9.6 References

[1] a) J. Shen, L. Zhao, G. Han, *Adv. Drug Delivery Rev.* **2012**; b) J. Zhou, Q. Liu, W. Feng, Y. Sun, F. Li, *Chem. Rev.* **2014**, *115*, 395-465; c) Z. Chen, W. Sun, H.-J. Butt, S. Wu, *Chem. Eur. J.* **2015**, *21*, 9165-9170; d) K. Liu, Y. Wang, X. Kong, X. Liu, Y. Zhang, L. Tu, Y. Ding, M. C. G. Aalders, W. J. Buma, H. Zhang, *Nanoscale* **2014**, *6*, 9257-9263; e) H. Shi, T. Fang, Y. Tian, H. Huang, Y. Liu, *J. Mater. Chem. B* **2016**.

[2] Q. Liu, W. Feng, T. Yang, T. Yi, F. Li, *Nat. Protocols* **2013**, *8*, 2033-2044.

[3] a) J.-H. Kim, J.-H. Kim, *J. Am. Chem. Soc.* **2012**, *134*, 17478-17481; b) P. Mahato, A. Monguzzi, N. Yanai, T. Yamada, N. Kimizuka, *Nat. Mater.* **2015**, *14*, 924-930.

[4] T. N. Singh-Rachford, F. N. Castellano, *Coord. Chem. Rev.* **2010**, *254*, 2560-2573.

[5] a) S. Hisamitsu, N. Yanai, N. Kimizuka, *Angew. Chem. Int. Ed.* **2015**, *54*, 11550-11554; b) S. H. Lee, D. C. Thévenaz, C. Weder, Y. C. Simon, *J. Polym. Sci., Part A: Polym. Chem.* **2015**, *53*, 1629-1639; c) P. Duan, N. Yanai, H. Nagatomi, N. Kimizuka, *J. Am. Chem. Soc.* **2015**, *137*, 1887-1894; d) P. Duan, N. Yanai, N. Kimizuka, *J. Am. Chem. Soc.* **2013**, *135*, 19056–19059; e) A. J. Svagan, D. Busko, Y. Avlasevich, G. Glasser, S. Baluschev, K. Landfester, *ACS Nano* **2014**, *8*, 8198-8207.

[6] a) J.-H. Kim, J.-H. Kim, *ACS Photonics* **2015**, *2*, 633-638; b) Z. Huang, X. Li, M. Mahboub, K. Hanson, V. Nichols, H. Le, M. L. Tang, C. J. Bardeen, *Nano Lett.* **2015**, *15*, 5552-5557.

[7] a) M. Majek, U. Faltermeier, B. Dick, R. Pérez-Ruiz, A. Jacobi von Wangelin, *Chem. Eur. J.* **2015**, *21*, 15496-15501; b) O. S. Kwon, J. H. Kim, J. K. Cho, J. H. Kim, *ACS Appl. Mater. Interfaces* **2015**, *7*, 318-325.

[8] a) A. Monguzzi, S. M. Borisov, J. Pedrini, I. Klimant, M. Salvalaggio, P. Biagini, F. Melchiorre, C. Lelii, F. Meinardi, *Adv. Funct. Mater.* **2015**, *25*, 5617-5624; b) A. Nattestad, C. Simpson, T. Clarke, R. W. MacQueen, Y. Y. Cheng, A. Trevitt, A. J. Mozer, P. Wagner, T. W. Schmidt, *Phys. Chem. Chem. Phys.* **2015**, *17*, 24826-24830; c) S. P. Hill, T. Banerjee, T. Dilbeck, K. Hanson, *J. Phys. Chem. Lett.* **2015**, *6*, 4510-4517; d) A. Nattestad, Y. Y. Cheng, R. W. MacQueen, T. F. Schulze, F. W. Thompson, A. J. Mozer, B. Fückel, T. Khoury, M. J. Crossley, K. Lips, G. G. Wallace, T. W. Schmidt, *J. Phys. Chem. Lett.* **2013**, *4*, 2073-2078.

[9] a) S. H. C. Askes, M. Kloz, G. Bruylants, J. T. Kennis, S. Bonnet, *Phys. Chem. Chem. Phys.* **2015**, *17*, 27380-27390; b) S. H. C. Askes, A. Bahreman, S. Bonnet, *Angew. Chem., Int. Ed.* **2014**, *53*, 1029-1033.

[10] Q. Liu, T. Yang, W. Feng, F. Li, *J. Am. Chem. Soc.* **2012**, *134*, 5390-5397.

[11] A. Nagai, J. B. Miller, P. Kos, S. Elkassih, H. Xiong, D. J. Siegwart, *ACS Biomater. Sci. Eng.* **2015**, *1*, 1206-1210.

[12] a) C. Wohnhaas, V. Mailänder, M. Dröge, M. A. Filatov, D. Busko, Y. Avlasevich, S. Baluschev, T. Miteva, K. Landfester, A. Turshatov, *Macromol. Biosci.* **2013**, *13*, 1422–1430; b) C. Wohnhaas, A. Turshatov, V. Mailänder, S. Lorenz, S. Baluschev, T. Miteva, K. Landfester, *Macromol. Biosci.* **2011**, *11*, 772-778.

[13] a) Q. Liu, B. Yin, T. Yang, Y. Yang, Z. Shen, P. Yao, F. Li, *J. Am. Chem. Soc.* **2013**, *135*, 5029-5037; b) O. S. Kwon, H. S. Song, J. Conde, H.-i. Kim, N. Artzi, J.-H. Kim, *ACS Nano* **2016**, *10*, 1512-1521.

[14] a) C. LoPresti, H. Lomas, M. Massignani, T. Smart, G. Battaglia, *J. Mater. Chem.* **2009**, *19*, 3576-3590; b) D. E. Discher, A. Eisenberg, *Science* **2002**, *297*, 967-973; c) J. P. Jain, W. Y. Ayen, N. Kumar, *Curr. Pharm. Des.* **2011**, *17*, 65-79; d) D. E. Discher, F. Ahmed, *Annu. Rev. Biomed. Eng.* **2006**, *8*, 323-341; e) R. J. R. W. Peters, M. Marguet, S. Marais, M. W. Fraaije, J. C. M. van Hest, S. Lecommandoux, *Angew. Chem., Int. Ed.* **2014**, *53*, 146-150; f) S. Cavalli, F. Albericio, A. Kros, *Chem. Soc. Rev.* **2010**, *39*, 241-263; g) J. V. Georgieva,

R. P. Brinkhuis, K. Stojanov, C. A. G. M. Weijers, H. Zuilhof, F. P. J. T. Rutjes, D. Hoekstra, J. C. M. van Hest, I. S. Zuhorn, *Angew. Chem., Int. Ed.* **2012**, *51*, 8339-8342.

[15] a) W. H. Binder, R. Sachsenhofer, *Macromol. Rapid Commun.* **2008**, *29*, 1097-1103; b) M. Noor, T. Dworeck, A. Schenk, P. Shinde, M. Fioroni, U. Schwaneberg, *J. Biotechnol.* **2012**, *157*, 31-37.

[16] J. E. Puskas, Y. Chen, Y. Dahman, D. Padavan, *J. Polym. Sci., Part A: Polym. Chem.* **2004**, *42*, 3091-3109.

[17] U. Karl, C. Sierakowski, M. Darijo, M. Haberer, H. Hartl, Use Of Amphiphilic Block Copolymers For Producing Polymer Blends, **2008**, 20080293886

[18] a) M. C. Woodle, M. S. Newman, J. A. Cohen, *J. Drug Targeting* **1994**, *2*, 397-403; b) M. C. Woodle, L. R. Collins, E. Sponsler, N. Kossovsky, D. Papahadjopoulos, F. J. Martin, *Biophys. J.* **1992**, *61*, 902-910.

[19] B. X. Mi, Z. Q. Gao, C. S. Lee, S. T. Lee, H. L. Kwong, N. B. Wong, *Appl. Phys. Lett.* **1999**, *75*, 4055-4057.

[20] M. Almgren, *J. Am. Chem. Soc.* **1980**, *102*, 7882-7887.

[21] B. Kalman, N. Clarke, L. B. A. Johansson, *J. Phys. Chem.* **1989**, *93*, 4608-4615.

[22] a) S. H. C. Askes, N. Lopez Mora, R. Harkes, R. I. Koning, B. Koster, T. Schmidt, A. Kros, S. Bonnet, *Chem. Commun.* **2015**, *51*, 9137-9140; b) M. Penconi, P. L. Gentili, G. Massaro, F. Elisei, F. Ortica, *Photochem. Photobiol. Sci.* **2014**, *13*, 48-61.

[23] D. Bainbridge, M. Ediger, *Rheol. Acta* **1997**, *36*, 209-216.

[24] A. Monguzzi, R. Tubino, F. Meinardi, *Phys. Rev. B* **2008**, *77*, 155122.

[25] a) F. A. Carey, R. J. Sundberg, *Advanced Organic Chemistry*, 5 ed., Springer US, **2007**; b) B. Rånby, J. F. Rabek, *Singlet Oxygen Reactions with Organic Compounds & Polymers*, John Wiley & Sons, Ltd., **1978**.

[26] J.-H. Kim, F. Deng, F. N. Castellano, J.-H. Kim, *ACS Photonics* **2014**, *1*, 382-388.

[27] A. Meister, M. E. Anderson, *Annu. Rev. Biochem.* **1983**, *52*, 711-760.

[28] G. R. Buettner, *Arch. Biochem. Biophys.* **1993**, *300*, 535-543.

[29] F. Wilkinson, J. Schroeder, *J. Chem. Soc. Faraday Trans. 2* **1979**, *75*, 441-450.

[30] M. Y. Li, C. S. Cline, E. B. Koker, H. H. Carmichael, C. F. Chignell, P. Bilski, *Photochem. Photobiol.* **2001**, *74*, 760-764.

[31] M. Roche, P. Rondeau, N. R. Singh, E. Tarnus, E. Bourdon, *FEBS Lett.* **2008**, *582*, 1783-1787.

[32] a) H. J. Feldmann, M. Molls, P. Vaupel, *Strahlenther. Onkol.* **1999**, *175*, 1-9; b) P. Vaupel, F. Kallinowski, P. Okunieff, *Cancer Res.* **1989**, *49*, 6449-6465; c) E. E. Graves, M. Vilalta, I. K. Cecic, J. T. Erler, P. T. Tran, D. Felsher, L. Sayles, A. Sweet-Cordero, Q.-T. Le, A. J. Giaccia, *Clin. Cancer Res.* **2010**, *16*, 4843-4852.

[33] a) S. Zhang, H. Gao, G. Bao, *ACS Nano* **2015**, *9*, 8655-8671; b) G. Sahay, D. Y. Alakhova, A. V. Kabanov, *J. Controlled Release* **2010**, *145*, 182-195; c) N. Oh, J.-H. Park, *Int. J. Nanomedicine* **2014**, *9*, 51-63.

[34] J. Schindelin, I. Arganda-Carreras, E. Frise, V. Kaynig, M. Longair, T. Pietzsch, S. Preibisch, C. Rueden, S. Saalfeld, B. Schmid, J.-Y. Tinevez, D. J. White, V. Hartenstein, K. Eliceiri, P. Tomancak, A. Cardona, *Nat. Methods* **2012**, *9*, 676-682.

[35] a) L. B. A. Johansson, Y. G. Molotkovskii, L. D. Bergel'son, *J. Am. Chem. Soc.* **1987**, *109*, 7374-7381; b) R. O. Al-Kaysi, T. Sang Ahn, A. M. Muller, C. J. Bardeen, *Phys. Chem. Chem. Phys.* **2006**, *8*, 3453-3459.

[36] A. Minsky, A. Y. Meyer, M. Rabinovitz, *J. Am. Chem. Soc.* **1982**, *104*, 2475-2482.

[37] N. Lopez Mora, J. S. Hansen, Y. Gao, A. A. Ronald, R. Kieltyka, N. Malmstadt, A. Kros, *Chem. Commun.* **2014**, *50*, 1953-1955.

CHAPTER 10

SUMMARY, CONCLUSIONS, AND OUTLOOK

10.1 TTA-UC nanovesicles in solution and in living cells

As described in Chapter 3, PEGylated DMPC liposomes were successfully prepared that were capable of generating blue photons by triplet-triplet annihilation upconversion of either green or red light with two distinct molecular chromophore pairs (Figure 10.1). The upconversion intensity in liposomes was found to be comparable to that in toluene solution at 20 °C and was linearly dependent on excitation intensity above only 0.05 $W.cm^{-2}$ (Chapter 5). To investigate the location where upconversion took place, red-to-blue upconverting giant vesicles (GUVs) were prepared and imaged with upconversion luminescence microscopy, as reported in Chapter 5. The results demonstrated that TTA-UC was occurring in the lipid bilayer of the giant vesicles, and the high quality and stability of the upconverted images enabled the 3D reconstruction of upconverting GUVs. Because TTA-UC in liposomes would have to be performed at human body temperature (37 °C), the temperature dependency of TTA-UC was investigated in a series of neutral PEGylated phospholipid liposomes, of which the results are reported in Chapter 6. It was found that for phospholipids with a gel-to-liquid phase transition, the TTA-UC intensity maximized near the main transition temperature (T_m). This result was explained by the fact that molecular diffusion of dyes, and thus TTA-UC efficiency, increases towards T_m, while thermal quenching of the photosensitizer as a function of temperature decreases the TTA-UC efficiency above T_m. The TTA-UC efficiency in DOPC, DLPC, and DMPC liposomes were very similar at 37 °C. Thus, TTA-UC in liposomes can be generally realized and the phospholipid can be freely chosen to further optimize the liposomal formulation in terms of medium stability, biocompatibility, clearance from the bloodstream, and surface functionalization.

Building further on these results, it was important to establish whether TTA-UC upconversion in vesicles can take place in living cells. Indeed, in Chapter 7 and Chapter 8 it is described that upconverting liposomes were endocytosed

by cancer cells and that the red-to-blue upconversion luminescence could be imaged under hypoxic conditions. The liposomes were localized in endosomes and lysosomes, and were degraded by the cells within 24 h after uptake. However, the upconversion luminescence bleached rapidly (within a couple of seconds) and the intensity was rather low due to quenching by molecular oxygen in the cells. As described in Chapter 8, the oxygen sensitivity was improved by co-treating the cells with a biologically relevant concentration of glutathione and L-ascorbic acid, which greatly improved the upconversion luminescence inside the cells. Furthermore, the upconverting liposomes were found to be non-cytotoxic in the dark and under high-power red light irradiation; no PDT effect was observed, probably because of the low photosensitizer concentration in the membrane that results in very low singlet oxygen production.

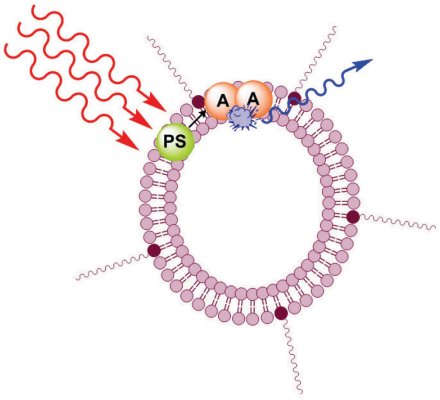

Figure 10.1. Red-to-blue TTA-UC in nanovesicles with a photosensitizer (PS) and annihilator (A) dye.

Besides liposomes, red-to-blue TTA-UC was also realized in the membrane of polymersomes, which were self-assembled from polyisobutylene-polyethylene glycol block copolymers, as described in Chapter 9. Although red-to-blue upconversion was somewhat less efficient in polymersomes than in liposomes, the polymersomes were much more quickly internalized by living cells. The upconverting polymersomes were then successfully imaged in living cells, while the addition of glutathione and L-ascorbic acid greatly boosted their performance *in vitro*. Compared to liposomes, the strong rubbery membrane of polymersomes may be more resistant towards digestion in cells or in the digestive tract of mammals, which opens up possibilities in drug delivery. Altogether, TTA-UC in liposomes and polymersomes represents exciting opportunities for luminescence bio-

imaging, because auto-fluorescence and irradiation damage to the cells or tissue are effectively eliminated.

10.2 Overcoming the oxygen sensitivity of TTA-UC

The TTA-UC mechanism relies heavily on triplet-state chromophores, which are readily quenched by molecular oxygen. This quenching event usually leads to severely compromised TTA-UC efficiencies in air; an issue that is poorly resolved in literature. Indeed, in the initial work described in Chapter 3 it was realized that the upconversion was only observed when the liposome solutions were deoxygenated by bubbling with argon. To counter the issue of oxygen sensitivity in TTA-UC nanosystems, three strategies were pursued in this research (Figure 10.2). The first strategy was applying a potentially oxygen-impermeable coating to the nanoparticle. Chapter 7 describes how a nanometer-thick (organo)silica coating was applied to upconverting DMPC liposomes. Although these nanocomposites were readily taken up by cancer cells, unfortunately the silica coating did not decrease the quenching by oxygen (neither in solution nor in cells), most probably because of the porosity of the silica coating. However, upon drying of the silica-coated liposome dispersion in an excess of (organo)silica precursor, interesting lipid-silica nanocomposite materials were obtained that were capable of TTA-UC in air, thereby confirming that in certain conditions (organo)silica can act as oxygen barrier for TTA-UC systems. These results represent intriguing examples of the combination of phospholipids, water, and silica for the construction of tunable upconverting nanoparticles and materials.

In a second approach, it was realized that physical deoxygenation methods such as bubbling with argon could be replaced by adding a ground-state molecular oxygen scavenger to the liposomes, such as sodium sulfite, as described in Chapter 5. Sulfite depletes the oxygen dissolved in solution, thereby allowing efficient and stable TTA-UC to occur in air (Figure 10.2b). However, many ground-state oxygen scavengers are incompatible with biological systems (*e.g.* hydrazine), and they slowly deplete over time when oxygen leaks into the sample. To improve on this approach, the third strategy (Chapter 8) involved addition of a singlet-oxygen scavenger ("anti-oxidants") such as L-ascorbic acid or glutathione. Instead of reacting with ground state oxygen, such anti-oxidants only react with excited-state singlet oxygen: Upon continuous irradiation of the TTA-UC system, the photosensitizer produces singlet oxygen, which is then scavenged by the anti-oxidant until all oxygen is

consumed (Figure 10.2c). This strategy was very efficient in allowing intense and stable TTA-UC in air (>80% stability during the first hour of continuous irradiation). As described in Chapter 9, the role of anti-oxidant can also be fulfilled by histidine, trolox, or the anti-oxidants present in cell medium (e.g. bovine serum albumin or pyruvate). Thus, the anti-oxidant approach is a rather general and powerful strategy that can be applied to virtually any existing TTA-UC system.

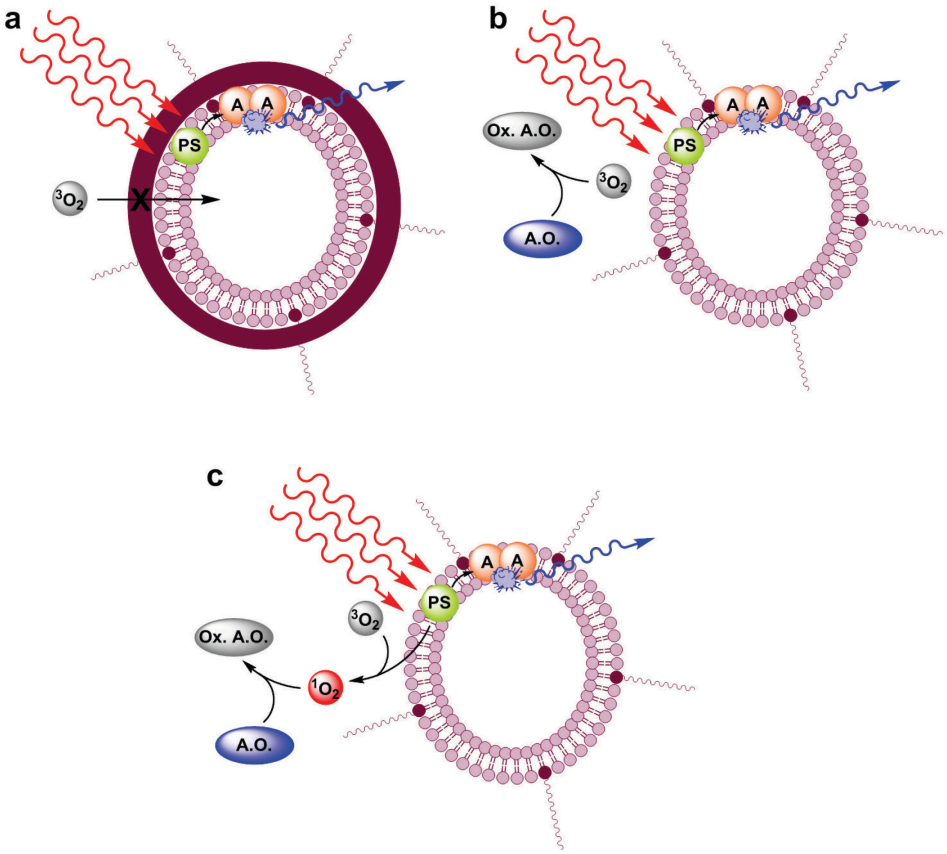

Figure 10.2. Cartoon illustrating the three different oxygen protection strategies pursued in this thesis. a) Coating the upconverting liposomes with an oxygen impermeable barrier. b) Chemical deoxygenation with a ground-state oxygen scavenger, i.e. anti-oxidant (A.O.), leading to an oxidized anti-oxidant (Ox. A.O.). c) Singlet-state oxygen scavenging: upon irradiation, the photosensitizer generates singlet oxygen, which then reacts with an anti-oxidant to form the oxidized anti-oxidant, thereby lowering the local oxygen concentration.

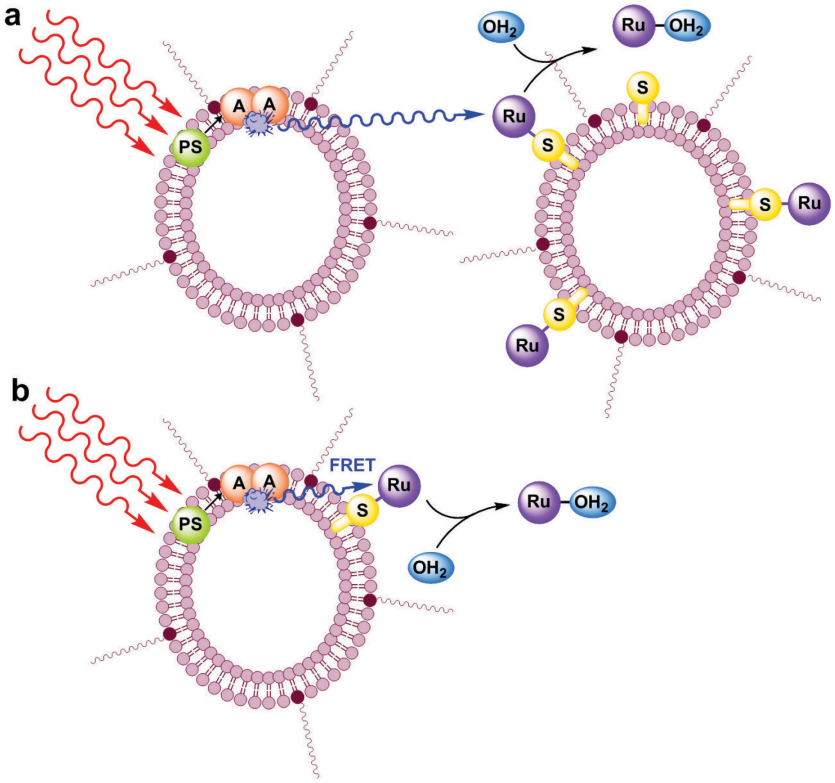

Figure 10.3. Cartoon illustrating the combination of TTA-UC in liposomes and light-activatable, membrane-anchored Ru-polypyridyl complexes. a) TTA-UC and Ru complex are physically separated on two different liposomes: the generated blue light from TTA-UC is transferred to the Ru complex via radiative energy transfer (Chapter 3). b) TTA-UC and Ru complex are located on the same liposome: the generated blue light from TTA-UC is transferred to the Ru complex via FRET (Chapter 4), after which the activated Ru-aqua complex dissociates from the membrane. PS: photosensitizer; A: annihilator; FRET: Förster Resonance Energy Transfer.

10.3 Activation of Ru(II) prodrugs by TTA-UC

The aim of this thesis was to activate Ru(II) prodrugs with red light by means of an upconverting drug carrier. This goal was first met in Chapter 3, where it was described how the photodissociation reaction of a Ru(II) polypyridyl complex from liposomes could be triggered by upconverting liposomes in a physical mixture of red-to-blue upconverting liposomes and Ru complex-doped liposomes. In this initial work, the blue upconverted light was transferred to the Ru-complex by radiative energy transfer, i.e. by emission of blue light and reabsorption of this light by the Ru-complex. When the upconverting dyes and the Ru-complex were doped in the same liposome membrane, as described in Chapter 4, it was found that the upconverted light

was transferred to the Ru-complex by Förster Resonance Energy Transfer (FRET) with more than 85% efficiency for moderate Ru-complex molar doping amounts (4 mol% with respect to the phospholipids). These studies supported the potential of Ru-prodrug activation by red-to-blue TTA-UC, but unfortunately the experiments did not succeed yet in air due to quenching of TTA-UC by oxygen. To allow the system to function in air, the photoreaction was successfully performed in presence of L-ascorbate and glutathione, as described in Chapter 8. It was also attempted to test liposomes doped with TTA-UC dyes and Ru-prodrugs *in vitro*. However, the Ru-complexes that were used exhibited high cytotoxicity without irradiation as well, and did not become significantly more toxic upon irradiation; for these reasons, activation by red-to-blue TTA-UC did not lead to a pronounced photochemotherapeutic effect, and the feasibility of the approach remains uncertain. At this point, more research efforts are necessary for the design of membrane-anchored Ru-prodrugs with high photo-indices and low toxicity in the dark before the feasibility of the activation-by-upconversion approach can be validated in biological systems.

10.4 General remarks

The results described in this thesis provide valuable insights for developing biological applications of TTA-UC. Liposomes and polymersomes were successfully used as multifunctional red-to-blue TTA-UC platform for bio-imaging and activation of light-activatable Ru prodrugs. It is clearly demonstrated that blue-light sensitive Ru-polypyridyl complexes, that normally do not respond well to light in the phototherapeutic window, can be activated by red light by means of TTA-UC. The biological evaluation of this activation-by-upconversion strategy requires more research attention to elucidate which parameters need optimization, such as nanoparticle design, TTA-UC stability, oxygen sensitivity and presence of anti-oxidants, light dose, amount of nanoparticle dopants (dyes and drug), and photo-index of the Ru prodrugs. We expect that the results of this thesis will lead to exciting applications in photoactivation chemotherapy that provide an alternative for photodynamic therapy in hypoxic tumors.

The red-to-blue upconversion quantum yield was found to be high at human body temperature (1.5% at 37 °C) and maximized at much lower excitation intensities (~0.1 $W.cm^{-2}$) compared to lanthanoid-based upconversion nanoparticles (UCNPs), which typically achieve upconversion quantum yields

in water much lower than 0.5% at much greater excitation intensities (>1 $W.cm^{-2}$). In contrast to TTA-UC nanovesicles, UCNPs also suffer from low absorption, poorly reproducible synthesis routes and poor stability in aqueous solution, cell growing medium, or serum. Naturally, TTA-UC systems also have disadvantages, such as the oxygen sensitivity and photostability. However, in recent years, it has been successfully shown that oxygen sensitivity is a hurdle that can be overcome with creative approaches and continuous research efforts.[1] As a contribution to this, in this thesis it was successfully demonstrated that the oxygen sensitivity of TTA-UC nanovesicles can be greatly reduced (even *in vitro*!) when biocompatible anti-oxidants were added. Of course, still much work is required in designing and synthesizing new types of TTA-UC nanoparticle systems with much lower intrinsic oxygen sensitivity, higher temporal stability *in vitro*, higher upconversion efficiencies, while maximizing biocompatibility and biostability. Overall, in our opinion TTA-UC nanoparticles outperform UCNPs in many ways. Yet curiously, the field of biological TTA-UC research receives much less attention than the field of UCNPs: a quick search on SciFinder (August 2016) with keywords "triplet-triplet annihilation upconversion" produces 365 results (of which ~10 are biology-oriented), while "upconversion nanoparticles" produces 2318 results, of which most are aimed towards biological application of UCNPs. We expect that the results described in this thesis reinforce the applicability of TTA-UC nanoparticles in biology and hope that they will convince the scientific community that this research field deserves more attention.

10.5 Outlook

10.5.1 Oxygen sensitivity

Although substantial work in this thesis was dedicated towards the reduction of the oxygen sensitivity of TTA-UC nanoparticle systems in combination with PACT, a number of improvements can be made. In the future design and preparation of TTA-UC nanoparticle systems, the oxygen sensitivity must first be minimized in the design, and then characterized in air-equilibrated solutions and in biological systems. As outlined in this thesis, it has become apparent that oxygen sensitivity can be minimized by using anti-oxidants that scavenge ground state or singlet state oxygen. It may be also possible to use nanoparticles with built-in anti-oxidants. For example, in a vesicle design the aqueous interior may be filled with a high concentration of water-soluble anti-oxidants; alternatively the membrane can be functionalized with oxygen-

scavenging moieties such as unsaturated carbon-carbon bonds or lipophilic anti-oxidants such as β-carotenes (Figure 10.4). Regardless of which anti-oxidant is used and at which location, it is important to evaluate their toxicity. It may also be important to separate anti-oxidants from TTA-UC dyes and Ru prodrugs, because:

i. Some anti-oxidants or anti-oxidant products quench triplet state dyes, for example α-tocopherol or hydroquinone.[2]
ii. Anti-oxidants such as glutathione may cause photo-reduction of dyes and/or Ru prodrugs
iii. An anti-oxidant such as glutathione or histidine may coordinate to heavy metal photosensitizers or to the activated Ru complex.
iv. Oxidized anti-oxidant products may react further with upconversion dyes and degrade them, such as in the case of peroxidized carbon-carbon bonds.

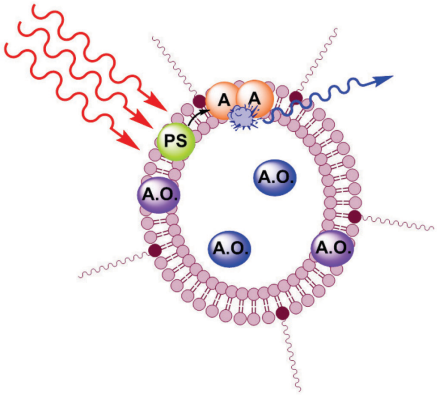

Figure 10.4. Upconversion polymersomes with built-in anti-oxidants, either in the hydrophilic interior or inside the hydrophobic membrane.

To illustrate this built-in anti-oxidant strategy, during the work described in this thesis a red-to-blue upconverting polymersome formulation was prepared with a polybutadiene-polyethylene glycol block copolymer (kindly provided by Prof. dr. Jan van Hest, Radboud University, Figure 10.5a) and investigated with emission spectroscopy without any further addition of anti-oxidants (Figure 10.5c). The polymer and TTA-UC dyes concentration (5 mg/mL, 5 μM PdTPTBP, 100 μM 2,5,8,11-tetra(*t*-butyl)perylene), and irradiation conditions (0.4 $W.cm^{-2}$ 630 nm excitation) were identical to those used for Figure 9.3d (Chapter 9). In this case the upconversion was observed

instantaneously and at lower polymer concentration (still observable at 1.6 mg/mL polymer), suggesting that the unsaturated bonds of polybutadiene were more effective in scavenging singlet oxygen than polyisobutylene. Curiously, in a preliminary experiment upconversion could not yet be realized in living cells.

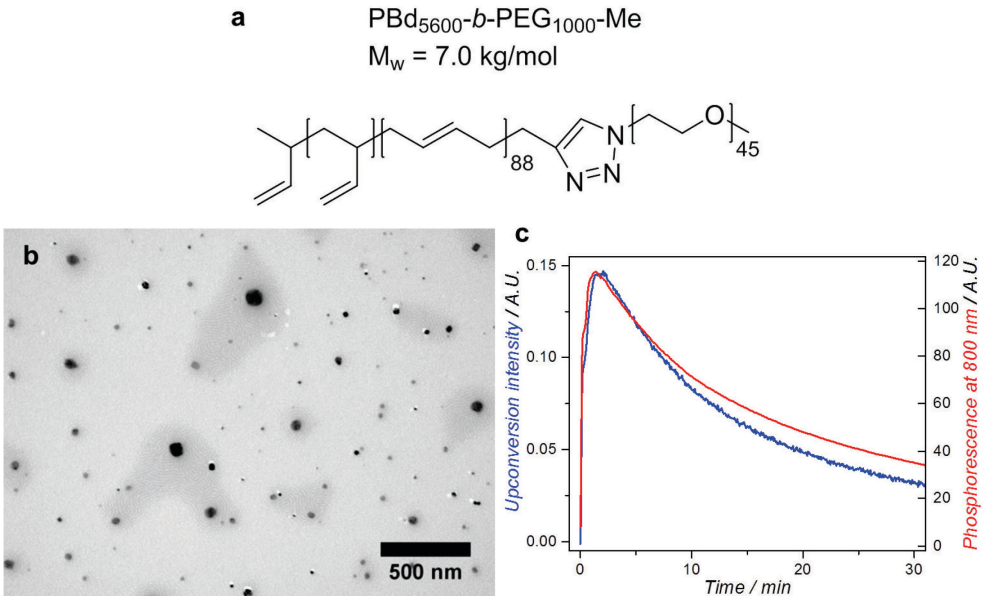

Figure 10.5. Upconverting polymersomes based on polybutadiene-block-monomethylpolyethylene glycol copolymer (PBd-b-PEG-Me), prepared according to Georgieva et al.[3] with [PBd-b-PEG-Me] = 9.8 mg/mL, [PdTPTBP] = 10 µM, and [2,5,8,11-tetra(t-butyl)perylene] = 0.20 mM. a) Molecular structure of PBd_{5600}-b-PEG_{1000}-Me block copolymer with PBd M_W ~5600 g/mol and PEG M_W 1000 g/mol, received from Prof. dr. Jan van Hest (Radboud University). b) TEM micrographs of the polymersomes. Hydrodynamic particle size according to DLS: 120 nm, 0.1 polydispersity index. c) Time traces of upconversion emission at 486 nm (blue, left axis) and phosphorescence of PdTPTBP at 800 nm (red, right axis) during 630 nm irradiation (50 mW, 0.4 W.cm^{-2}, 4 mm excitation path length) of upconverting PBd-b-PEG-Me polymersomes at 4.9 mg.mL^{-1} concentration. Conditions: 600 µL sample in a non-stirred semi-micro cuvette at 20 °C. No oxygen scavenger was added. Directly comparable with data from Chapter 9, see Figure 9.3d.

An alternative strategy to improve the oxygen sensitivity of TTA-UC is the design of supramolecular assemblies that feature tight networks of annihilator molecules. Such networks support fast diffusion of triplet excitons and greatly enhance the rates of TTET and TTA. In this way, TTA-UC is competitive with quenching by molecular oxygen and becomes appreciably efficient in air. A number of studies by the group of Kimizuka represent sophisticated examples of this strategy, which are expected to greatly impact the field of TTA-UC and might lead to highly efficient, oxygen-independent TTA-UC nanoparticles.[4]

10.5.2 Biocompatibility of TTA-UC dyes

In the research described in Chapter 8, it was found that the annihilator dye, 2,5,8,11-tetra(*t*-butyl)perylene, accumulated in lipid droplets in A549 cells after digestion of the liposomes by the cell. This suggested that this dye could not be digested by the cell, and it raises concern on the long-term toxicity and mutagenicity. Thus, for real-world biological TTA-UC applications it is necessary to evaluate the mutagenicity and carcinogenicity of TTA-UC dyes.

10.5.3 Shifting the activation wavelength further to the NIR

In this thesis it was chosen to use red-to-blue TTA-UC to shift the prodrug activation wavelength into the phototherapeutic window (630 nm). However, the highest tissue transparency while minimizing absorption by water is achieved in the NIR region between 700 and 900 nm.[5] In order to further shift the wavelength from 630 nm towards this region, other photosensitizer-annihilator pairs may be used that can be excited with 700 – 850 nm and emit in the green, yellow, or red.[6] Since it was already demonstrated in Chapter 3 that liposomes can accommodate a diverse selection of lipophilic TTA-UC dyes, we expect that incorporation of a NIR sensitive photosensitizer and visible-range emitting annihilator in the liposomes is straightforward. However, it must be kept in mind that in order to further use the upconversion emission to achieve prodrug activation, the emission wavelength must overlap well with the prodrug absorption. Therefore, in the case of Ru polypyridyl complexes, NIR-to-green TTA-UC would be best suited for this approach.[6e]

10.5.4 Nanoparticle-bound Ru-prodrugs

More research is necessary for the design of nanoparticle-anchored photoactivatable Ru prodrugs with high toxicity when irradiated and low toxicity in the dark. In the research described in Chapter 8, it was found that irradiation did not affect the cytotoxicity of certain Ru-prodrugs anchored to DMPC liposomes, while a relatively high toxicity was found in the dark. It was hypothesized that the degradation of Ru-doped liposomes was the cause of the observed dark toxicity. Thus, two key steps are needed to find a good PACT candidate to combine with a TTA-UC activation route: (i) it must be established that the activated complex is toxic once it is released inside the cell, and (ii) it is important to affirm that the complex is anchored and remains anchored to the nanoparticle throughout the entire treatment procedure. In this context, it may be beneficial if Ru-complexes are doped in more rigid nanoparticles such as polymersomes or silica nanoparticles. However, our

results are rather preliminary, and substantially more research must be performed in this area.

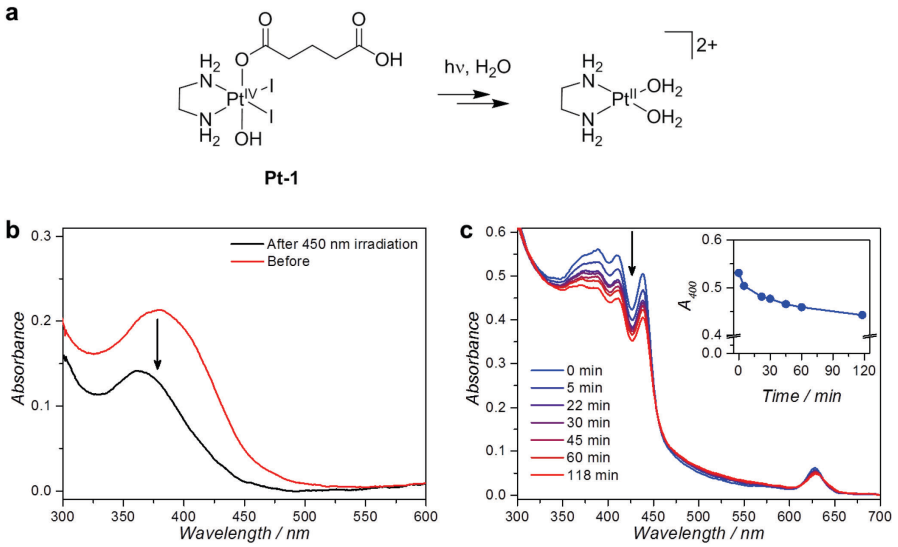

*Figure 10.6. Photoactivation of Pt(IV) prodrugs with upconverting liposomes. a) Molecular structure of complex **Pt-1**, received from Prof. dr. Bednarski (Universität Greifswald) and the proposed conversion to the aquated Pt(II) species upon irradiation in water.[7] b) Absorption spectroscopy before and after irradiation of **Pt-1** in PBS (0.13 mM) with 450 nm (arbitrary power). c) Absorption spectroscopy during red light irradiation (120 mW 630 nm; 1 W.cm^{-2} intensity) of a mixture of **Pt-1** (0.25 mM) and upconverting liposomes (1.25 mM DMPC, 0.25 mM DSPE-mPEG-2000, 0.6 μM PdTPTBP, 6 μM perylene) at 37 °C; the inset shows the absorbance at 400 nm as a function of irradiation time. The sample was deoxygenated prior to irradiation by bubbling argon for 30 min.*

10.5.5 Activation-by-upconversion of other prodrugs

The general applicability of TTA-UC for the activation of other prodrugs than Ru-compounds deserves more attention in future work. During the work described in this thesis an experiment was conducted in collaboration with Prof. dr. Bednarski (Universität Greifswald) to examine whether compound **Pt-1** could be activated with red-to-blue upconverting liposomes (Figure 10.6). In water, in absence of upconverting liposomes, it is proposed that upon UV to blue light irradiation **Pt-1** converts to the aquated Pt(II) species,[7] which can be observed by UV-vis absorption spectroscopy as a decrease of the LMCT absorption band (Figure 10.6b). Upon 630 nm irradiation of a mixture of upconverting liposomes and **Pt-1**, the same decrease in LMCT band was observed, suggesting successful conversion of **Pt-1** to the aquated Pt(II) species. Thus, upconverting liposomes may also be suitable for red-light

activation of Pt(IV) compounds. This preliminary experiment demonstrates that the strategy of combining PACT drugs with TTA-UC in nanoparticles can be easily extended to other (inorganic) prodrugs such as Pt(IV) compounds, CO or NO releasing molecules, and photocleavable coumarin derivatives.

10.6 References

[1] a) Q. Liu, B. Yin, T. Yang, Y. Yang, Z. Shen, P. Yao, F. Li, *J. Am. Chem. Soc.* **2013**, *135*, 5029-5037; b) A. J. Svagan, D. Busko, Y. Avlasevich, G. Glasser, S. Baluschev, K. Landfester, *ACS Nano* **2014**, *8*, 8198-8207; c) J.-H. Kim, J.-H. Kim, *ACS Photonics* **2015**, *2*, 633-638.

[2] a) F. Wilkinson, J. Schroeder, *J. Chem. Soc. Faraday Trans. 2* **1979**, *75*, 441-450; b) D. R. Cardoso, K. Olsen, L. H. Skibsted, *J. Agric. Food Chem.* **2007**, *55*, 6285-6291.

[3] J. V. Georgieva, R. P. Brinkhuis, K. Stojanov, C. A. G. M. Weijers, H. Zuilhof, F. P. J. T. Rutjes, D. Hoekstra, J. C. M. van Hest, I. S. Zuhorn, *Angew. Chem., Int. Ed.* **2012**, *51*, 8339-8342.

[4] a) P. Mahato, A. Monguzzi, N. Yanai, T. Yamada, N. Kimizuka, *Nat. Mater.* **2015**, *14*, 924-930; b) S. Hisamitsu, N. Yanai, N. Kimizuka, *Angew. Chem. Int. Ed.* **2015**, *54*, 11550-11554; c) N. Yanai, N. Kimizuka, *Chem. Commun.* **2016**, *52*, 5354-5370; d) P. Duan, N. Yanai, H. Nagatomi, N. Kimizuka, *J. Am. Chem. Soc.* **2015**, *137*, 1887-1894.

[5] K. R. Byrnes, R. W. Waynant, I. K. Ilev, X. Wu, L. Barna, K. Smith, R. Heckert, H. Gerst, J. J. Anders, *Lasers in Surgery and Medicine* **2005**, *36*, 171-185.

[6] a) T. N. Singh-Rachford, F. N. Castellano, *J. Phys. Chem. A* **2008**, *112*, 3550-3556; b) T. N. Singh-Rachford, A. Nayak, M. L. Muro-Small, S. Goeb, M. J. Therien, F. N. Castellano, *J. Am. Chem. Soc.* **2010**, *132*, 14203-14211; c) F. Deng, W. Sun, F. N. Castellano, *Photochem. Photobiol. Sci.* **2014**, *13*, 813-819; d) S. Amemori, N. Yanai, N. Kimizuka, *Phys. Chem. Chem. Phys.* **2015**, *17*, 22557-22560; e) S. Baluschev, V. Yakutkin, T. Miteva, Y. Avlasevich, S. Chernov, S. Aleshchenkov, G. Nelles, A. Cheprakov, A. Yasuda, K. Müllen, G. Wegner, *Angew. Chem., Int. Ed.* **2007**, *46*, 7693-7696; f) A. Nagai, J. B. Miller, P. Kos, S. Elkassih, H. Xiong, D. J. Siegwart, *ACS Biomater. Sci. Eng.* **2015**, *1*, 1206-1210.

[7] S. Perfahl, M. M. Natile, H. S. Mohamad, C. A. Helm, C. Schulzke, G. Natile, P. J. Bednarski, *Mol. Pharm.* **2016**, *13*, 2346-2362.

APPENDIX I: DETERMINATION OF QUANTUM YIELD OF UPCONVERSION

I.1. Experimental setup

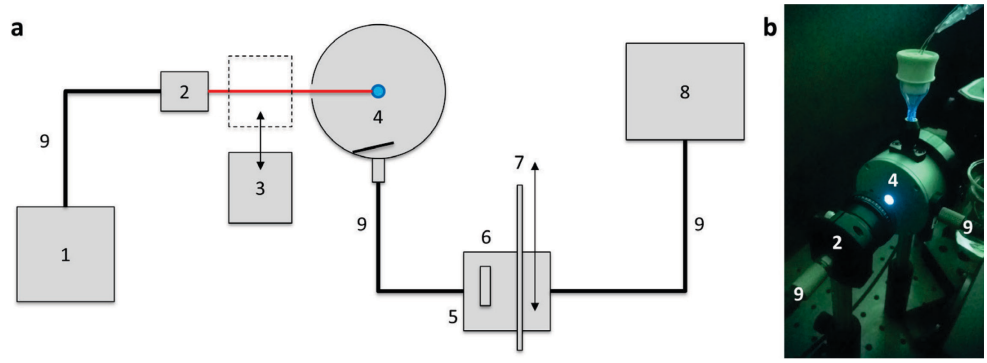

Figure S.I.1. Setup used for absolute quantum yield measurements. a) Schematic representation; (1) 532 nm or 630 nm laser source, (2) collimating lens, 630 nm band pass filter, and mechanical iris – these parts were only used in case of 630 nm excitation (3) power meter adjustable in position, (4) integrating sphere with sample tube in the center, (5) filter holder, (6) notch filter or short pass filter that can be installed or removed, (7) variable neutral density filter that can be installed or removed, (8) CCD spectrometer, (9) optical fibers. b) Picture of the integrating sphere while irradiating a red-to-blue upconverting sample with 630 nm light. A 630 nm notch filter was held in front of the camera to block the red-light scatter. The blue light originates from the upconversion in the sample.

An integrating sphere setup was used for determining the quantum yield of upconversion (Figure S.I.1). For green-to-blue upconversion quantum yield determinations, the excitation source was a 532 nm continuous wave Aries 150 portable DPSS laser from LaserGlow (Toronto, ON, Canada) with a beam diameter of 1.5 mm. For red-to-blue upconversion, the excitation source was a fiber-coupled clinical grade Diomed 630 nm PDT laser. The optical fiber was connected to a collimating lens, after which the light passed a 630 nm band pass filter (Thorlabs, Dachau/Munich, Germany, part no. FB630-10) and a mechanical iris to produce a ca. 2 mm beam. The excitation power was measured using a S310C thermal sensor connected to a PM100USB power meter (Thorlabs). An AvaSphere-30-IRRAD integrating sphere, customized with a sample holder and an extra aperture, and an AvaSpec-ULS2048L StarLine CCD spectrometer were purchased from Avantes (Apeldoorn, The Netherlands). The integrating sphere and spectrometer were calibrated together using a Avalight-HAL-CAL-ISP30 NIST traceable calibration lamp

from Avantes, so that the observed intensities are expressed with the dimension of a photon flux (mol of photons.s^{-1}.nm^{-1}). The filter holder was fabricated by our own mechanical department, and held a NDL-25C-4 variable neutral density filter (Thorlabs), or a NF533-17 notch filter (Thorlabs) in case of excitation with 532 nm light, or an OD4 575 nm short pass filter (Edmund Optics, York, United Kingdom, part no. 84-709) in case of excitation with 630 nm light. The FC-UVxxx-2 (xxx = 200, 400, 600) optical fibers with 200-600 µm diameter were purchased from Avantes and were suitable for the UV-Vis range (200-800 nm). Spectra were recorded with Avasoft software from Avantes and further processed with Microsoft Office Excel 2010 and Origin Pro software.

I.2. Procedure for determining the quantum yield of upconversion

The quantum yield of upconversion (Φ_{uc}) is defined by Equation S.I.1:

$$\Phi_{UC} = \frac{number\ of\ upconverted\ photons}{number\ of\ low\text{-}energy\ photons\ absorbed} = \frac{q_{p-em}}{q_{p-abs}} \qquad \textit{Equation S.I.1}$$

where $q_{p\text{-}em}$ is the emission photon flux of the singlet annihilator species (in photons.s^{-1}) and $q_{p\text{-}abs}$ is the photon flux absorbed by the sensitizer species (in photons.s^{-1}).

Note that for TTA-UC quantum yields, it is common to multiply Φ_{uc} by 2, because TTA-UC intrinsically has a maximum quantum yield of 50% and thus must be scaled to attain a maximum value of 100%. This was only applied in Chapter 3, as it was later realized that this factor is rather confusing.

Φ_{uc} can be calculated by Equation S.I.2:

$$\Phi_{UC} = \frac{\int_{\lambda_1}^{\lambda_2} I_{annihilator}(\lambda)d\lambda}{q_{p-abs}} \qquad \textit{Equation S.I.2}$$

where $I_{annihilator}(\lambda)$ is the spectral luminescence intensity (in photons.s^{-1}.nm^{-1}) of the annihilator species, λ_1 and λ_2 are the low- and high-wavelength

boundaries, respectively, of the upconverted annihilator emission spectrum. $q_{p\text{-}abs}$ is determined by subtracting the spectral light intensity of the excitation source that has passed through the sample ($I_{exc\text{-}sample}$, in photons.s^{-1}.nm^{-1}) from the spectral light intensity of the excitation source that has passed through a blank sample ($I_{exc\text{-}blank}$, in photons.s^{-1}.nm^{-1}), and by integrating over the excitation wavelength range λ_3 to λ_4, see Equation S.I.3. The blank sample resembled the upconverting sample in all ways, except that it did not contain any sensitizer, and thus did not absorb at the excitation wavelength.

$$q_{p-abs} = \int_{\lambda_3}^{\lambda_4} (I_{exc-blank}(\lambda) - I_{exc-sample}(\lambda))d\lambda \qquad \textit{Equation S.I.3}$$

Equation S.I.2 can then be expressed as Equation S.I.4:

$$\Phi_{UC} = \frac{\int_{\lambda_1}^{\lambda_2} I_{annihilator}(\lambda)d\lambda}{\int_{\lambda_3}^{\lambda_4} (I_{exc-blank}(\lambda) - I_{exc-sample}(\lambda))d\lambda} \qquad \textit{Equation S.I.4}$$

The spectrometer and the integrating sphere were calibrated so that the observed intensities are directly proportional to the photon flux, *i.e.* $I(\lambda) \propto [mol\ of\ photons.s^{-1}.nm^{-1}]$. Therefore, integrating these values over the relevant wavelength regions gave directly the flux of photons arriving at the spectrometer.

Because the intensity of the upconverted light is relatively low compared to that of the exciting laser source the absorption and emission of the sample cannot be measured at the same time. In other words, the laser light saturates the spectrometer, which prevents upconversion to be measured. To circumvent this problem, the absorption was measured using a variable neutral density filter with known attenuation (typically $F_{attn} \approx 0.01$, *i.e.*, ~99% attenuation). This filter was placed between the integrating sphere and the spectrometer to measure the absorbed photon flux, whereas it was replaced for the measurement of the upconverted emission by a notch (533 nm) or by an OD4 short pass filter (< 575 nm) to remove the excitation wavelength. Thus, Equation S.I.4 was changed into Equation S.I.5. The attenuation factor F_{attn} was averaged over the wavelength range of the laser (520 – 540 nm or 615 – 645 nm).

Additionally, during the research described in Chapter 4 and Chapter 9 it was realized a correction was necessary for $I_{annihilator}$ to account for the secondary inner-filter effect, *i.e.* reabsorption of the upconverted light. This reabsorption occurred because the samples were relatively concentrated so that enough excitation light was absorbed to have an accurate value of $q_{p\text{-}abs}$. To this end, the upconversion emission spectrum was recorded under highly diluted conditions in the temperature controlled cuvette holder setup (*e.g.* section 4.4.5) and this spectrum was scaled at the second emission peak of the annihilator (*i.e.* 474 nm for perylene and 486 nm for 2,5,8,11-tetra(*tert*-butyl)perylene), which cannot be reabsorbed, to match the photon flux value at 474 nm / 486 nm of $I_{annihilator}$. This corrected spectrum was called $I_{annihilator\text{-}corr}$. *Note that this correction has not been applied for the quantum yield determination in Chapter 3, i.e. for those calculations* $I_{annihilator\text{-}corr} = I_{annihilator}$.

Finally, although at first the notch or short pass filter was assumed to only block the laser signal from reaching the spectrometer, in reality there was a small reduction of transmission for wavelengths situated in the upconversion range as well. This filtering can be corrected when calculating Φ_{uc} by dividing the upconversion luminescence intensity by the transmission curve $T(\lambda)$ of the notch or short pass filter in the wavelength range of the upconverted light. The corrected equation for Φ_{uc} became Equation S.I.5:

$$\Phi_{UC} = \frac{\int_{\lambda_1}^{\lambda_2} \left(\frac{I_{annihilator-corr}(\lambda)}{T(\lambda)} \right) d\lambda}{\int_{\lambda_3}^{\lambda_4} \frac{I_{exc-blank}(\lambda) - I_{exc-sample}(\lambda)}{F_{attn}} d\lambda} \equiv \frac{q_{p-em}}{q_{p-abs}} \qquad \textit{Equation S.I.5}$$

The boundary wavelengths that were used for determining Φ_{uc}, as well as the measured values for $q_{p\text{-}em}$ and $q_{p\text{-}abs}$ at 293 K, are given in Table S.I.1.

Because the integrating sphere setup did not feature temperature control, Φ_{UC} at 310 K was estimated from measuring the upconversion emission under highly diluted conditions in the temperature controlled cuvette holder setup at 293 K and at 310 K (*e.g.* Section 4.4.5) and scaling Φ_{UC} at 293 K with the ratio of the upconversion emission at 293 K and 310 K by using Equation S.I.6:

$$\Phi_{UC}^{310\,K} = \Phi_{UC}^{293\,K} * \frac{\int_{\lambda_1}^{\lambda_2} I_{annihilator}^{310\,K}(\lambda)d\lambda}{\int_{\lambda_1}^{\lambda_2} I_{annihilator}^{293\,K}(\lambda)d\lambda} \qquad \textit{Equation S.I.6}$$

Table S.I.1. Values used throughout this thesis for Φ_{uc} determination at 293 K. See each chapter for the exact sample formulations.

Chapter	Sample	λ_1 (nm)	λ_2 (nm)	λ_3 (nm)	λ_4 (nm)	$q_{p\text{-}em}$ (nmol photon s.s^{-1})	$q_{p\text{-}abs}$ (nmol photon s.s^{-1})	Φ_{uc}
Chapter 3	**L1-2**	390	525	520	545	0.0384	3.32	0.023
	PtOEP & DPA in toluene[a]	390	525	520	545	0.124	4.81	0.051
	L3-4	400	575	615	645	0.0306	11.4	0.0054
	PdTPTBP & perylene in toluene[b]	400	600	615	645	0.0420	7.13	0.012
Chapter 4	**L12**	400	575	615	645	0.705	30.0	0.024
Chapter 9	**P3-1-2**	400	575	615	645	0.0925	45.3	0.0020
	P4-1-2	400	575	615	645	0.103	49.7	0.0021

[a] [PtOEP] = 3.5 µM, [DPA] = 100 µM. [b] [PdTPTBP] = 2.5 µM, [perylene] = 50 µM. PtOEP = platinum(II) octaethylporphyrin, DPA = 9,10-diphenylanthracene, PdTPTBP = palladium (II) tetraphenyltetrabenzoporphyrin

For each measurement, two liposome or polymersome samples were prepared: one blank sample, containing only the annihilator but deprived of sensitizer. Since the concentration of the sensitizer is very small compared to the other sample constituents ([sensitizer] ≤ 0.05 mol%), we assume that removal of the sensitizer from the lipid or polymer mixture did not influence the physical properties of the vesicles (membrane fluidity, scattering properties of the sample, or others). The upconverting sample or the blank sample was loaded into specially designed measurement tubes that were made of a quartz EPR-tube bottom (± 7 cm length) fused to a NS-14 glass connector (± 2 cm length), at the top of which a septum was adapted. The tube fit precisely a hole made in the integrating sphere, and reached the center of the sphere, where it was hit by the excitation laser beam.

In Chapter 3 and Chapter 4, deoxygenation of the sample was performed in a separate ice-cooled, pear-shaped flask, by bubbling the sample with argon for at least 30 minutes with a rate of 1 − 2 mL per second. The degassed sample was then transferred to the measurement tube by cannulation in the strict

absence of oxygen. Degassing in the tube was found to be impossible due to foam formation. In Chapter 9, the samples were 1:1 v/v mixed with a 50 mM Na_2SO_3 solution in PBS to chemically deoxygenate the samples and allow measurements to conveniently take place in air. For these measurements, the final concentrations were [PiB-PEG-Me polymer] = 5.0 mg/mL, [sensitizer] = 5 μM, and [annihilator] = 100 μM.

APPENDIX II: SUPPORTING INFORMATION FOR CHAPTER 3

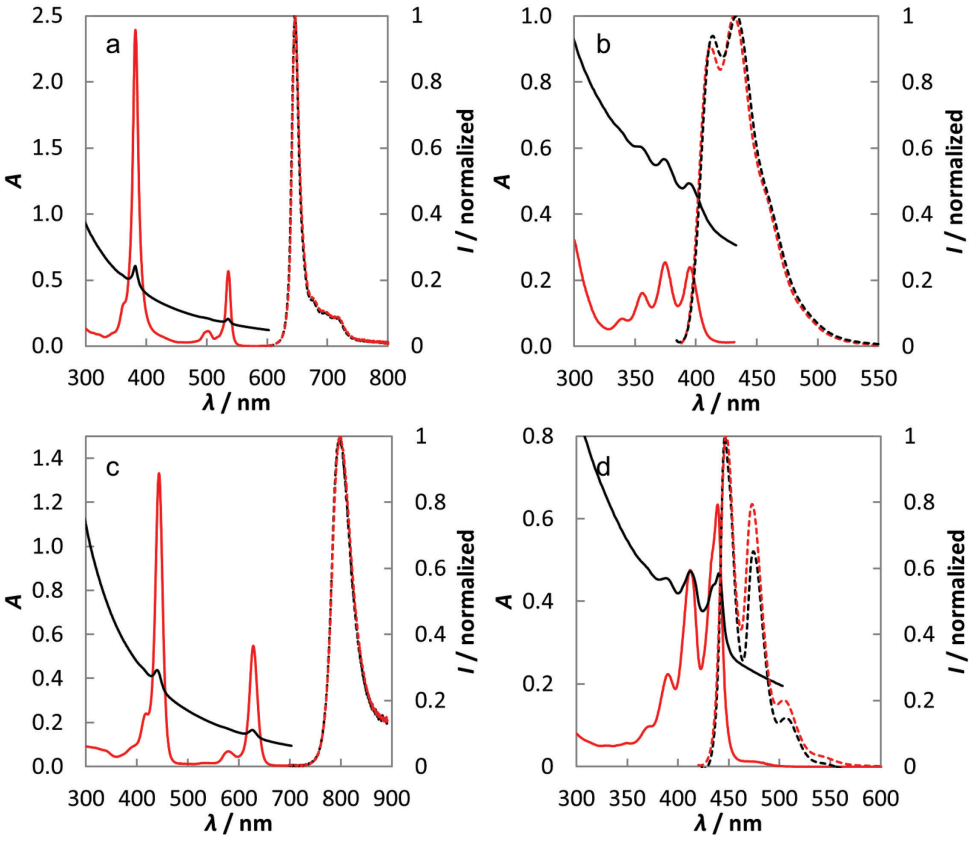

*Figure S.II.1. Absorbance (left axes, solid lines) and normalized emission (right axes, dashed lines) spectra of compounds **1-4** in toluene solution (red) and in liposome samples (black). Liposome samples were diluted 12 times with respect to the formulation given in Table 3.1, to keep absorbance values low enough. Absorbance spectra of liposome samples are uncorrected for scattering. Samples containing compound **1** or **3** were deoxygenated thoroughly before measurement by bubbling the sample with argon for 30 min with a rate of ~2 bubbles per second. All spectra were taken at room temperature. (a) Sample **L1** ([**1**] = 0.3 μM) and **1** in toluene (7 μM). For emission, λ_{exc} = 532 nm. (b) Sample **L2** ([**2**] = 8 μM) and **2** in toluene (20 μM). For emission λ_{exc} = 378 nm. (c) Sample **L3** ([**3**] = 0.2 μM) and **3** in toluene (5 μM). For emission λ_{exc} = 630 nm. (d) Sample **L4** ([**4**] = 4 μM) and **4** in toluene (20 μM). For emission, λ_{exc} = 416 nm.*

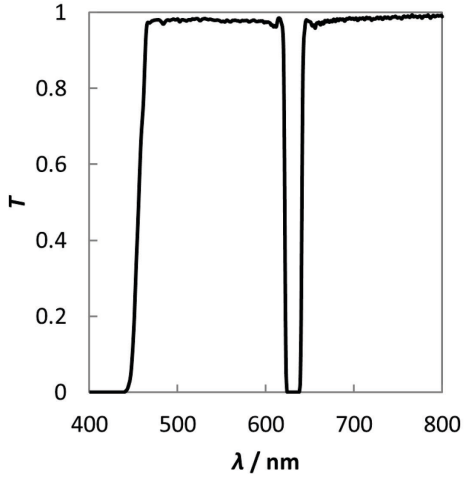

Figure S.II.2. Transmission curve of the 633 nm notch filter used in this work (Thorlabs part no. NF633-25). The low transmission for λ ≤ 450 nm explains the difference between the emission of ***4*** *in Figure S.II.1d and the upconverted emission of* ***4*** *as observed in spectra acquired in upconversion experiments using the 633 nm notch filter (Figure 3.3).*

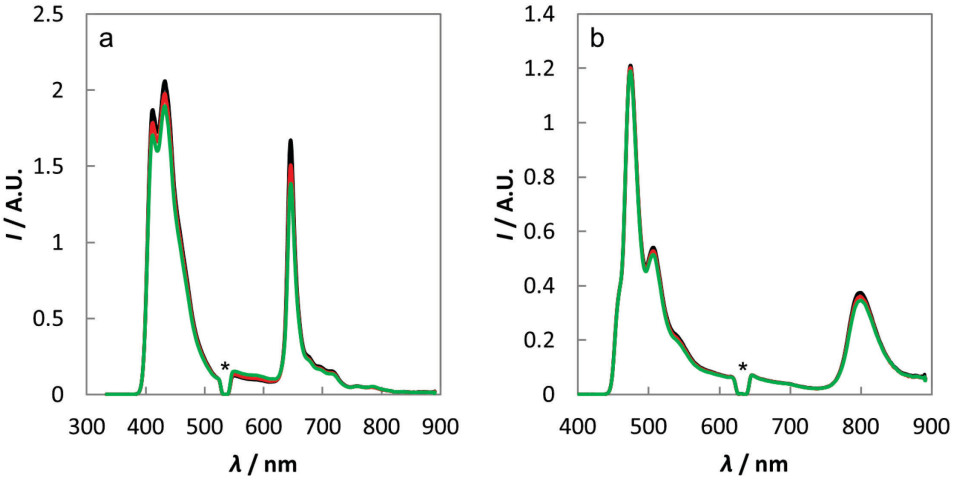

Figure S.II.3. (a) Emission spectra of couple ***1-2*** *([****1****] = 3.5 µM, [****2****] = 100 µM) in toluene at 288 K (black line), 293 K (red line), and 298 K (green line). (b) Emission spectra of couple* ***3-4*** *([****3****] = 2.5 µM, [****4****] = 50 µM) in toluene at 288 K (black line), 293 K (red line), and 298 K (green line). Asterisks indicate excitation wavelength: couple* ***1-2*** *and couple* ***3-4*** *were excited at 532 nm and 630 nm, respectively. Samples were thoroughly deoxygenated before measurement. The excitation power for both samples was 27 mW in a 2.6 mm diameter beam (light intensity: 0.51 W.cm^{-2}).*

APPENDIX III: SUPPORTING INFORMATION FOR CHAPTER 4

III.1. Ru concentration in liposome samples by inductively coupled plasma optical emission spectroscopy

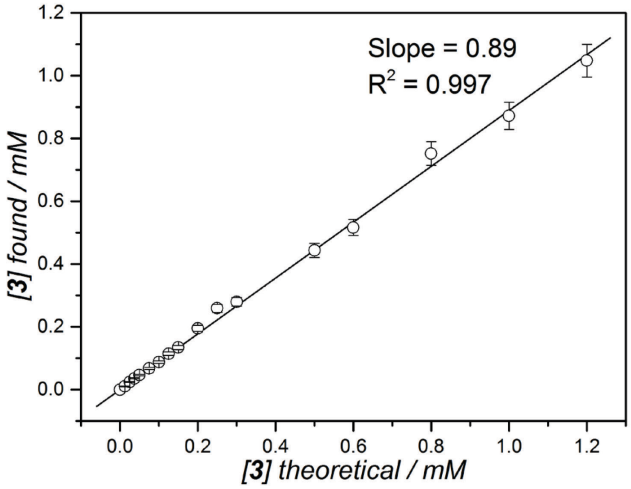

Figure S.III.1. Bulk concentrations of $\mathbf{3}^{2+}$ *experimentally found in PEGylated DMPC liposome samples, determined by inductively coupled plasma optical emission spectroscopy, versus theoretical concentrations. As best fit, a straight line was plotted through the origin with a slope of 0.89 (*R^2 *= 0.997). Error bars represent 5% instrumental error.*

The bulk concentration of $\mathbf{3}^{2+}$ in liposome samples was measured with inductively coupled plasma optical emission spectroscopy (ICP-OES), see Figure S.III.1. From the slope of a linear fit of the measured values plotted *versus* theoretical values it was determined that on average, 89% of the theoretical concentration $\mathbf{3}^{2+}$ was experimentally found. In all experiments when the determined value was too low with respect to the threshold of the ICP-OES machine, an extrapolated value was used from the theoretical concentration multiplied by 0.89.

III.2. Differential scanning calorimetry

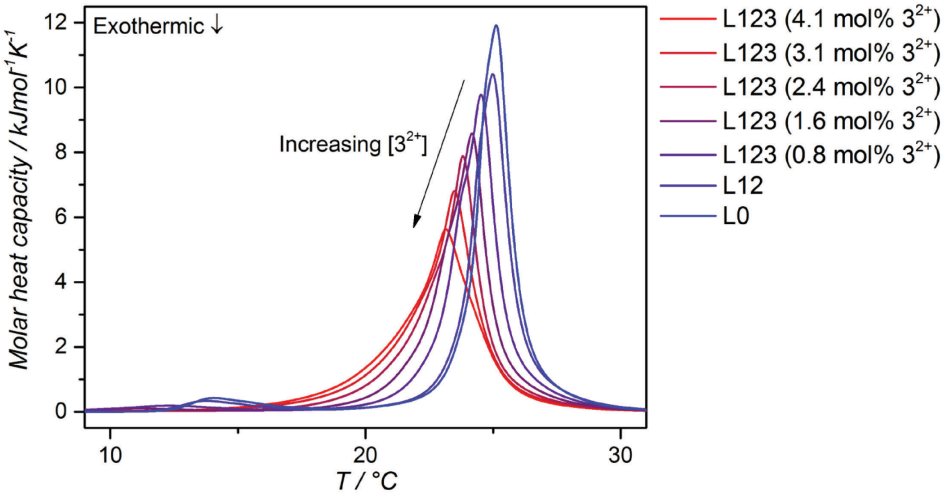

*Figure S.III.2. Differential scanning calorimetry thermograms (in heating mode) for PEGylated (4 mol%) DMPC liposomes without any chromophores (**L0**), with the TTA-UC dye couple (**L12**), and with the TTA-UC dye couple and various amounts of **3**$^{2+}$ added (**L123**). Reported molar percentages of **3**$^{2+}$ are based on ICP-OES measurements (see Chapter 4). Measurements were performed with a scanning rate of 1 K.min^{-1} at 3 atm. pressure.*

*Table S.III.1. Differential scanning calorimetry data for PEGylated (4 mol%) DMPC liposomes without any chromophores (**L0**), with the TTA-UC dye couple (**L12**), and with the TTA-UC dye couple and various amounts of **3**$^{2+}$ added (**L123**) , with T_m (in °C) as the main transition temperature and ΔH (in kJ.mol^{-1}) as the molar change in enthalpy when heating from 10 to 35 °C. Reported molar percentages of **3**$^{2+}$ are based on ICP-OES measurements (see Chapter 4). Measurements were performed with a scanning rate of 1 K.min^{-1} at 3 atm. pressure.*

Sample	**3^{2+} molar percentage**	***T*$_m$ (°C)**	**Δ*H* (kJ.mol^{-1})**
L0		25.1	25.1
L12		25.0	23.1
L123	0.8	24.5	23.8
L123	1.6	24.2	22.4
L123	2.4	23.8	21.6
L123	3.1	23.5	21.7
L123	4.1	23.2	21.1

III.3. Photodissociation experiments using red light

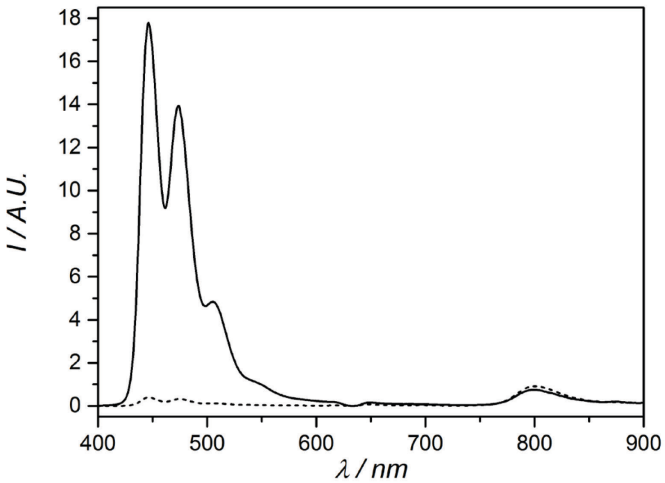

*Figure S.III.3. Luminescence emission spectrum of **L12** (black) and **L123** with 3.3 mol% **3**$^{2+}$ at t = 0 of the irradiation experiment using red light (dashed). λ_{exc} = 630 nm. Irradiation conditions: power 120 mW, beam diameter 4 mm, intensity 0.95 W.cm^{-2}, T = 310 K, sample volume 1.5 ml. The liposome dispersion was diluted prior to measurement so that [**2**] = 2.5 µM and [**1**] = 0.25 µM, and in the case of **L123**, the concentration of **3**$^{2+}$ = 18 µM.*

III.4. Lifetime studies with time-correlated single photon counting and transient absorption spectroscopy

III.4.1. Analysis of time-correlated single photon counting data

Fluorescence lifetime measurements were performed using time-correlated single photon counting (TCSPC). The obtained histograms were fitted with Origin Pro software as the sum of single exponential decays, as described by Equation S.III.1:

$$I(t) = \sum_i A_i e^{\frac{t}{\tau_i}} \qquad \textit{Equation S.III.1}$$

where t is time, *I(t)* is the time-dependent observed emission intensity (photon counts), A_i is the decay amplitude, and τ_i is the decay constant. For each sample, fitting with a single exponential decay curve did not give satisfactory fits. In the case of liposomes **L2**, this is attributed to the molecules being dissolved in a heterogeneous system (*e.g.* liposomes), and a small degree of self-energy transfer (homo-transfer) due to clustering of **2** in the membrane.[1] In the case of **L23** or **L123**, the occurrence of energy transfer results in a multitude of donor excited state lifetimes, *i.e.* multi-exponential decays. To achieve a single lifetime value, required for further data processing, it was therefore necessary to use amplitude weighted average lifetimes (τ), as calculated by Equation S.III.2:

$$\tau = \frac{\sum_i A_i \tau_i}{\sum_i A_i} \qquad \textit{Equation S.III.2}$$

III.4.2. Time-correlated single photon counting data

*Table S.III.2. Fitting parameters to various decay functions for the fluorescence lifetime (in ns) of compound 2, as measured with TCSPC at 293 K (λ_{exc} = 440 nm, and λ_{em} = 474 nm), in PEGylated DMPC liposomes with a fixed amount (0.5 mol%) of **2** while varying the molar percentage of **3**$^{2+}$ from 0 to 6%, as well as the calculated parameters τ as the amplitude averaged lifetime calculated from τ_1, A_1, τ_2, A_2, τ_3, and A_3 by Equation S.III.2, and E_{ET} as the efficiency of energy transfer calculated from Equation S.III.6. Goodness of fit expressed as R^2 values. The bulk concentration of 3^{2+} was determined by ICP-OES. Bulk concentration of DMPC, DSPE-PEG-2000, and compound **2** were 0.20 mM, 8 µM, and 1 µM, respectively.*

Decay function	**Concentration of 3^{2+} in the membrane in mol%**					
	0.0%	0.2%	0.5%	0.7%	0.9%	1.7%
Multi-exponential						
τ_1 (A_1 in %)	6.49 ± 0.01 (93%)	5.82 ± 0.01 (77%)	5.37 ± 0.01 (83%)	5.10 ± 0.13 (44%)	4.56 ± 0.08 (36%)	2.43 ± 0.03 (37%)
τ_2 (A_2 in %)	1.58 ± 0.06 (7%)	1.64 ± 0.02 (23%)	1.30 ± 0.02 (17%)	2.09 ± 0.16 (38%)	1.79 ± 0.08 (42%)	0.79 ± 0.05 (40%)
τ_3 (A_3 in %)				0.63 ± 0.04 (19%)	0.54 ± 0.03 (23%)	0.30 ± 0.03 (23%)
τ	6.17 ± 0.01	4.85 ± 0.01	4.67 ± 0.01	3.14 ± 0.08	2.50 ± 0.05	1.29 ± 0.02
R^2	0.9997	0.9996	0.9996	0.9996	0.9995	0.9994
E_{ET}	0%	21%	24%	49%	60%	79%
Förster 3D model						
γ	0.00 ± 0.00	0.23 ± 0.00	0.28 ± 0.00	0.74 ± 0.01	1.044 ± 0.01	1.82 ± 0.01
R^2	0.9995	0.9996	0.9996	0.9995	0.9995	0.999

Decay function	**Concentration of 3^{2+} in the membrane in mol%**				
	2.1%	2.4%	3.5%	5.0%	5.6%
Multi-exponential					
τ_1 (A_1 in %)	2.85 ± 0.08 (21%)	3.35 ± 0.19 (18%)	2.12 ± 0.18 (19%)		
τ_2 (A_2 in %)	0.98 ± 0.06 (42%)	1.21 ± 0.08 (41%)	0.85 ± 0.14 (33%)	1.20 ± 0.01 (24%)	0.96 ± 0.01 (41%)
τ_3 (A_3 in %)	0.32 ± 0.02 (36%)	0.37 ± 0.01 (41%)	0.33 ± 0.02 (48%)	0.31 ± 0.00 (76%)	0.29 ± 0.01 (59%)
τ	1.14 ± 0.03	1.25 ± 0.05	0.85 ± 0.06	0.53 ± 0.00	0.57 ± 0.01
R^2	0.9992	0.9993	0.9992	0.9991	0.9992
E_{ET}	82%	80%	86%	91%	91%
Förster 3D model					
γ	2.04 ± 0.01	1.93 ± 0.01	2.67 ± 0.02	3.99 ± 0.08	3.84 ± 0.08
R^2	0.9992	0.9993	0.9991	0.9991	0.9991

*Table S.III.3. Fitting parameters to various decay functions for the fluorescence lifetime (in ns) of compound **2**, as measured with TCSPC at 310 K (λ_{exc} = 440 nm, and λ_{em} = 474 nm), in PEGylated DMPC liposomes with a fixed amount (0.5 mol%) of **2** while varying the molar percentage of **3**$^{2+}$ from 0 to 6%, as well as the calculated parameters τ as the amplitude averaged lifetime calculated from τ_1, A_1, τ_2, A_2, τ_3, and A_3 by Equation S.III.2, and E_{ET} as the efficiency of energy transfer calculated from Equation S.III.6. Goodness of fit expressed as R^2 values. The bulk concentration of **3**$^{2+}$ was determined by ICP-OES. Bulk concentration of DMPC, DSPE-PEG-2000, and compound **2** were 0.20 mM, 8 µM, and 1 µM, respectively.*

Decay function	**Concentration of 3^{2+} in the membrane in mol%**					
	0.0%	0.2%	0.5%	0.7%	0.9%	1.7%
Multi-exponential						
τ_1 (A_1 in %)	5.94 ± 0.01 (94%)	5.33 ± 0.01 (80%)	4.79 ± 0.01 (77%)	4.01 ± 0.03 (63%)	4.06 ± 0.11 (36%)	
τ_2 (A_2 in %)	2.01 ± 0.10 (6%)	1.72 ± 0.03 (20%)	1.35 ± 0.02 (23%)	1.38 ± 0.10 (29%)	1.86 ± 0.13 (41%)	1.85 ± 0.01 (45%)
τ_3 (A_3 in %)				0.49 ± 0.09 (9%)	0.64 ± 0.03 (23%)	0.54 ± 0.00 (55%)
τ	5.69 ± 0.01	4.60 ± 0.01	4.00 ± 0.01	2.96 ± 0.03	2.37 ± 0.07	1.14 ± 0.00
R^2	0.9997	0.9997	0.9996	0.9996	0.9996	0.9995
E_{ET}	0%	19%	30%	52%	58%	80%
Förster 3D model						
γ	0.00 ± 0.01	0.22 ± 0.00	0.36 ± 0.00	0.74 ± 0.01	1.15 ± 0.01	2.25 ± 0.02
R^2	0.9996	0.9997	0.9996	0.9996	0.9996	0.9994

Decay function	**Concentration of 3^{2+} in the membrane in mol%**				
	2.1%	2.4%	3.5%	5.0%	5.6%
Multi-exponential					
τ_1 (A_1 in %)	2.61 ± 0.20 (7%)				
τ_2 (A_2 in %)	1.07 ± 0.08 (32%)	1.53 ± 0.01 (38%)	0.84 ± 0.01 (29%)	0.66 ± 0.01 (13%)	0.72 ± 0.01 (17%)
τ_3 (A_3 in %)	0.40 ± 0.02 (61%)	0.43 ± 0.00 (62%)	0.30 ± 0.00 (71%)	0.23 ± 0.00 (87%)	0.26 ± 0.00 (83%)
τ	0.77 ± 0.03	0.84 ± 0.00	0.45 ± 0.00	0.29 ± 0.00	0.34 ± 0.00
R^2	0.9993	0.9993	0.9994	0.9985	0.9990
E_{ET}	87%	85%	92%	95%	94%
Förster 3D model					
γ	2.86 ± 0.02	2.75 ± 0.01	5.49 ± 0.09	8.46 ± 0.19	7.25 ± 0.14
R^2	0.9993	0.9992	0.9993	0.9982	0.9989

III.4.3. Analysis of transient absorption data

Data from transient absorption (TA) spectroscopy was fitted using the software package Glotaran, with which the user can conveniently analyze TA data and correct for experimental artefacts. The software features global fitting, with which different components that contribute to the data can be untangled and represented as separate datasets.[2] Each component i in the observed time-dependent transient absorption spectrum $\Delta OD(t,\lambda)$ is described with a non-normalized Decay-Associated transient absorption Spectrum $DAS_i(\lambda)$ and a single exponential decay function with decay constant τ_i, see Equation S.III.3:

$$\Delta OD(t,\lambda) = \sum_i DAS_i(\lambda) * e^{\frac{t}{\tau_i}} \qquad \textit{Equation S.III.3}$$

In the case of multi-exponential behavior of one of the species (*i.e.* **2** in presence of $\mathbf{3}^{2+}$), multiple components were identified with different τ_i, but with identical $DAS_i(\lambda)$. The amplitude averaged lifetime (τ) was then calculated using Equation S.III.4:

$$\tau = \frac{\sum_i B_i \tau_i}{\sum_i B_i} \qquad \textit{Equation S.III.4}$$

in which B_i represents the relative amplitude of DAS_i. For measurements on liposomes **L2** and **L23**, *i.e.* experiments that were meant to probe the lifetime of **2**, B_i was calculated from the average *DAS* value at 695 − 705 nm, at which **2** has a very strong transient peak, while the influence of $\mathbf{3}^{2+}$ is negligible (see below). For measurements on liposomes with only $\mathbf{3}^{2+}$ (*i.e.* **L3** liposomes), A_i was calculated from the average *DAS* value from 445 − 455 nm, where the transient absorption of $\mathbf{3}^{2+}$ is strongest (see below).

III.4.4. Transient absorption data

*Table S.III.4. Fitting parameters to various decay functions for the excited state lifetime (in ns) of compound **2**, as measured with TA spectroscopy at 293 K (λ_{exc} = 400 nm), in PEGylated DMPC liposomes with a fixed amount (0.5 mol%) of **2** while varying the molar percentage of **3**$^{2+}$ from 0 to 3%, as well as the calculated parameters τ as the amplitude averaged lifetime calculated from τ_3, B_3, τ_4, and B_4 by Equation S.III.4, and E_{ET} as the efficiency of energy transfer calculated from Equation S.III.6. Goodness of fit expressed as R^2 values. Bulk concentration of DMPC, DSPE-PEG-2000, and compound **2** were 20 mM, 0.8 mM, and 0.1 mM, respectively. All experimental details can be found in the experimental section.*

Kinetic model	**Concentration of 3^{2+} in the membrane in mol%**					
	0	0.4%	0.8%	1.7%	2.5%	3.3%
Multi-exponential (GLOTARAN)						
τ_1	0.10E−3 ± 0.00E−3	0.01E−3 ± 0.00E−3	0.11E−3 ± 0.00E−3	0.02E−3 ± 0.00E−3	0.09E−3 ± 0.00E−3	0.07E−3 ± 0.00E−3
τ_2	8.3E−3 ± 0.1E−3	8.9E−3 ± 0.09E−3	9.2E−3 ± 0.13E−3	9.1E−3 ± 0.14E−3	9.9E−3 ± 0.17E−3	5.5E−3 ± 0.11E−3
τ_3 (B_3 in %)	2.30 ± 0.12 (22.1%)	0.45 ± 0.00 (27.0%)	0.26 ± 0.00 (41.7%)	0.19 ± 0.00 (49.1%)	0.11 ± 0.00 (57.6%)	0.07 ± 0.00 (55.3%)
τ_4 (B_4 in %)	7.05 ± 0.12 (77.9%)	3.99 ± 0.02 (73.0%)	2.43 ± 0.01 (58.3%)	1.85 ± 0.01 (50.1%)	0.79 ± 0.01 (42.4%)	0.56 ± 0.00 (44.7%)
τ_5	118 ± 34	629 ± 78	916 ± 161	6380 ± 4160	1850 ± 359	613 ± 79
τ	6.00 ± 0.10	3.03 ± 0.02	1.52 ± 0.01	1.04 ± 0.01	0.40 ± 0.00	0.29 ± 0.00
E_{ET}	0%	49.5%	74.7%	82.7%	93.3%	95.1%
Förster 3D model						
γ	0.02 ± 0.02	0.43 ± 0.02	1.00 ± 0.06	1.35 ± 0.05	2.43 ± 0.07	2.99 ± 0.09
R^2	0.9974	0.9991	0.9959	0.9975	0.9968	0.9969

III.4.5. Transient absorption in liposomes L2

The transient absorption spectrum of PEGylated DMPC liposomes bearing 0.5 mol% **2** (liposomes **L2**), 1.0 ns after a 400 nm excitation pulse, is displayed in Figure S.III.4. The spectrum closely matches literature reports for perylene in cyclohexane, and features negative signals from 430 to 550 nm, due to ground state bleach and stimulated emission, and a strong positive band centered at 700 nm, due to excited state absorption as the result of an S_1-S_n transition.[3] The transient absorption data was analyzed with Glotaran and was best-fitted using 5 single-exponential decay functions (Table S.III.4). The fastest decay component (τ_1 = 0.1 ps) is attributed to coherent artefacts due to spatial and temporal overlap of the pump and probe pulses around t = 0. The second decay component (τ_2 = 8.3 ps) is attributed to vibrational relaxation of compound **2** and/or solvent relaxation of the phospholipid matrix. A component with a very long lifetime (τ_5 > 100 ns) and almost negligible amplitude is attributed to either triplet state and/or excimer absorption. The nanosecond scale components with τ_3 = 2.3 and τ_4 = 7.1 ns have identical

spectra, which indicates that they originate from the same species. In this case, τ_1, τ_2, and τ_5 were not taken into account for calculating τ by Equation S.III.4, so that $\tau = \tau_{34}$ = 6.00 ± 0.10 ns, which corresponds to literature values of the excited state lifetime of **2**.[1, 3]

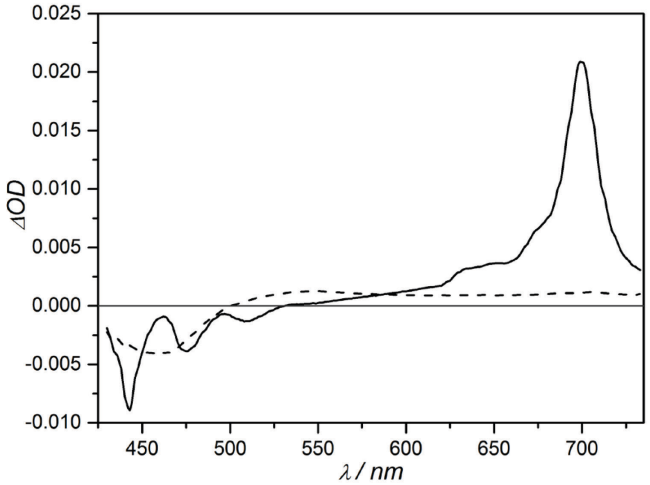

*Figure S.III.4. Transient absorption spectra at 293 K of PEGylated DMPC liposomes with either 0.5 mol% 2 (liposomes **L2**, solid line), 1.0 ns after the excitation pulse, and 3.3 mol% 3^{2+} (liposomes **L3**, dashed line), 1.0 ps after the excitation pulse. Both samples were excited with 400 nm light (20-60 nJ/pulse, 1 kHz repetition rate). Bulk DMPC concentration: 20 mM.*

III.4.6. Transient absorption in liposomes L3

Next, the transient absorption of liposomes with 3.3 mol% of $\mathbf{3}^{2+}$ (liposomes **L3**) was evaluated. It was confirmed with UV-VIS spectroscopy before and after the experiment that negligible photodissociation occurred during the time-resolved spectroscopic analysis. The maximum amount of photodissociation, expressed as the total amount of mol $\mathbf{4}^{2+}$, can be estimated from the photon flux at 400 nm (Φ_{400} = 30 µW, *i.e.* = 1.0 x 10^{-10} einstein.s^{-1}), measurement time (≤ 7200 s), quantum yield of photodissociation (0.52%),[4] and chance of absorption (A_{400} ≤ 0.60), see Equation S.III.5:

$$n_{\mathbf{4}} = (1 - 10^{-A})\Phi_{400}\Phi_{Ru}t \qquad \textit{Equation S.III.5}$$

The value of n_4 for these experiments is ≤ 2.8 x 10^{-9} mol. With a sample volume of 200 µL and a $\mathbf{3}^{2+}$ concentration of 0.71 mM (as determined by ICP-OES),

n_3 = 1.4 x 10^{-7} mol. The maximum amount of photodissociation reaction triggered during the measurement is therefore 2%.

Figure S.III.4 shows the transient absorption spectrum of liposomes **L3** 1.0 ps after the excitation pulse at 400 nm. A negative band ranging from 400 to 500 nm and a weaker positive band from 500 nm onwards are observed. The negative band from 400 to 500 nm coincides with the region of the MLCT absorption band in the steady state absorption spectrum (Figure 1c). Thus this band can be attributed to ground-state bleaching of the ruthenium complex. The broad positive band for λ > 500 nm are attributed to the ^{3}MLCT excited state absorption, as the ^{1}MLCT to ^{3}MLCT intersystem crossing is known to be extremely fast (300 fs time scale).[5] The time evolution of the transient spectrum was best fitted with Glotaran using a model with two exponential decay curves using Glotaran. Two DAS were identified with identical spectra and with lifetimes of 0.17 (53%) and 0.92 ns (47%), hence the average ^{3}MLCT lifetime τ_{Ru} has a value of 0.52 ns.

III.4.7. Transient absorption in liposomes L23

For liposomes **L23**, *i.e.* samples containing both **2** and a varying amount of $\mathbf{3}^{2+}$, the time-dependent absorption data was consistently fitted using 5 single exponential decays, similar to as discussed above (Table S.III.4). Each time, it was most satisfactory to fit the decays in the nanosecond regime with a bi-exponential decay. The decay associated spectra for these two components consistently featured the transient spectral characteristics of compound **2**. For calculation of τ with Equation S.III.4, τ_1, τ_2, and τ_5 were irrelevant, so that the reported τ for liposomes **L23** is each time the average of τ_3 and τ_4, *i.e.* $\tau = \tau_{34}$. The results of these experiments are discussed in the main text.

III.5. Analysis and quantification of non-radiative energy transfer

III.5.1. Calculation of energy transfer efficiency E_{ET}

For liposomes **L23**, the energy transfer efficiency (E_{ET}) values were calculated by Equation S.III.6:

$$E_{ET} = 1 - \frac{\tau}{\tau_0} = 1 - \frac{I}{I_0}$$ *Equation S.III.6*

where τ and τ_0 are the amplitude-weighted averages of the excited state lifetime of compound **2** in presence and absence of $\mathbf{3}^{2+}$, respectively, and I and I_0 are the integrated fluorescence intensity of compound **2** in presence and absence of $\mathbf{3}^{2+}$, respectively.[6] Stern-Volmer kinetics are generally applied to photochemical quenching based on collisional quenching, but are to known to may be applicable to FRET systems as well.[7] By rewriting the classical Stern-Volmer equation, see Equation S.III.7,

$$\frac{\tau_0}{\tau} = 1 + K_{SV}[\mathbf{3}] = 1 + k_{SV}\tau_0[\mathbf{3}]$$ *Equation S.III.7*

an expression for E_{ET} is obtained, see Equation S.III.8:

$$E_{ET} = 1 - \frac{1}{1 + K_{SV}[\mathbf{3}]} = \frac{K_{SV}[\mathbf{3}]}{1 + K_{SV}[\mathbf{3}]}$$ *Equation S.III.8*

where K_{SV} is the Stern-Volmer quenching constant (in $L.mol^{-1}$), k_{SV} is the Stern-Volmer rate of quenching ($L.mol^{-1}.s^{-1}$), τ_0 is the lifetime of the energy donor without any quencher present, and [**3**] is the bulk concentration of $\mathbf{3}^{2+}$. However, the volume in which the quenching occurs is much smaller than the sample volume, because both compound **2** and $\mathbf{3}^{2+}$ are only located within the membrane. Therefore, [**3**] was substituted with $[\mathbf{3}]_{local}$, *i.e.* the local concentration of $\mathbf{3}^{2+}$ at the membrane, which is defined by Equation S.III.9:

$$[\mathbf{3}]_{local} = \frac{n_3}{n_{DMPC}V_M} = \frac{x_3}{V_M}$$ *Equation S.III.9*

where n_3 is the number of mol $\mathbf{3}^{2+}$, as calculated by ICP-OES, n_{DMPC} is the number of mol DMPC, V_M is the molar volume of DMPC in lipid bilayers at 293 K (V_M = 0.637 $L.mol^{-1}$),[8] and x_3 is the mol fraction of $\mathbf{3}^{2+}$ in the lipid bilayer. To simplify, we did not account for the volume of DSPE-PEG-2000, **2**, and $\mathbf{3}^{2+}$, because no data was available, and we did not account for the fact that $\mathbf{3}^{2+}$ occupies a volume outside the lipid bilayer as well. Under these assumptions,

K_{SV} was found to be 0.32 L.mol^{-1}. With τ_0 = 6.2 ns, the value of k_{SV} is 5.2 x 10^7 L.mol^{-1}.s^{-1}.

III.5.2. Calculating the theoretical R_0 distance

One of the prerequisites for FRET is to have a good spectral overlap between the donor emission spectrum and acceptor absorption spectrum, as given by the overlap integral J_{DA} (in M^{-1}.cm^{-1}.nm^4) in Equation S.III.10,

$$J_{DA} = \int_0^\infty F_D(\lambda)\varepsilon_A(\lambda)\lambda^4 d\lambda \qquad \textit{Equation S.III.10}$$

where $F_D(\lambda)$ is the area-normalized donor emission spectrum and $\varepsilon_A(\lambda)$ is the molar absorption spectrum of the acceptor (in L.mol^{-1}.cm^{-1}). J_{DA} = 2.8 x 10^{14} nm^4.M^{-1}.cm^{-1} for **2** as FRET-donor and **3**$^{2+}$ as FRET-acceptor (see Figure 1c). From J_{DA}, the relative orientation factor κ, the refractive index of the medium n (1.334 for PBS buffer), and the fluorescence quantum yield of the donor φ_D, the Förster distance R_0 (in Å) can be calculated, for which half the donor molecules decay by FRET, according to Equation S.III.11 below.[6] Assuming $\kappa^2 = 2/3$ and using φ_D = 0.94 in cyclohexane,[9] R_0 was predicted to be 41 Å.

$$R_0 = 0.211 \times (\kappa^2 n^{-4} \phi_D J_{DA})^{\frac{1}{6}} \qquad \textit{Equation S.III.11}$$

III.5.3. Fitting lifetime data with a Förster decay model

Besides the use of multi-exponential decays to calculate FRET efficiencies and Stern-Volmer parameters, the time-correlated single photon counting data and transient absorption spectroscopy data were also analyzed using a Förster decay model to derive different system parameters. This model has been used before for the analysis of energy transfer from perylene to various transition metal ions in DPPC vesicles.[1, 10] For TCSPC data, Equation S.III.12 was used:

$$I(t) = I_0 e^{-\frac{t}{\tau_0} - 2\gamma\left(\frac{t}{\tau_0}\right)^{1/d}}$$ *Equation S.III.12*

where $I(t)$ is the time-dependent fluorescence intensity, I_0 is the fluorescence intensity directly after excitation, τ_0 is the FRET donor lifetime in absence [1, 10]of the FRET acceptor, d is the dimensionality of the system (d = 2 and d = 3 for quenching in two and three dimensions, respectively), and γ is defined as $[\mathbf{3}]/C_0$, with [**3**] the bulk concentration $\mathbf{3}^{2+}$ (in M) and C_0 the critical acceptor concentration for energy transfer (in M), which is the acceptor concentration needed for 72% energy transfer.[6] In this work, the lifetime data acquired from TCSPC were indeed fitted using the Förster decay model, see Table S.III.2-Table S.III.3. For the fitting, τ_0 was fixed at 6.2 ns. Figure S.III.5 shows a fit of the three-dimensional model (d = 3) on lifetime decay data from TCSPC at 293 K acquired from a liposome sample (**L23**) with 0.5 mol% **2** and 0.9 mol% $\mathbf{3}^{2+}$.

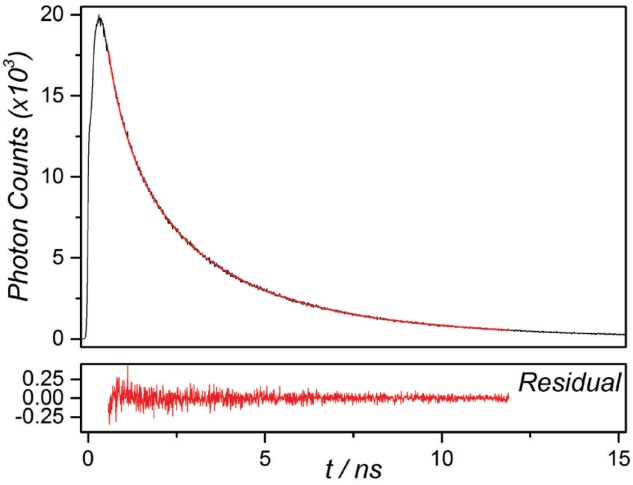

*Figure S.III.5. Time-correlated single photon counting decay curve (black) of PEGylated (4 mol%) DMPC liposomes **L23**, ([DMPC] = 0.2 mM) at 293 K with 0.5 mol% **2** and 0.9 mol% $\mathbf{3}^{2+}$ upon excitation with 440 nm (6 µW laser power, 0.6 pJ/pulse) and collecting emission at 474 nm. The red curve (top) represents a fit of the data according to a 3D FRET model (Equation S.III.12) with d = 3, τ = 6.2 ns, γ = 1.04, with the corresponding residual plot (bottom). The fit has an R^2 value of 0.9995.*

In the case of TA spectroscopy data, Equation S.III.12 was modified to Equation S.III.13:

$$\Delta OD(t,\lambda) = \Delta OD(\lambda)_0 \times e^{-\frac{t}{\tau_0} - 2\gamma\left(\frac{t}{\tau_0}\right)^{1/d}} \qquad \textit{Equation S.III.13}$$

where $\Delta OD(t,\lambda)$ is the observed time-dependent transient absorption spectrum and $\Delta OD(\lambda)_0$ is the transient absorption spectrum at t = 0. It was most convenient to use a kinetic trace at a particular wavelength to fit the data. Preliminary experiments with TA spectroscopy on **L2** and **L3** alone showed that 400 nm light excites both molecules, but that at 700 nm compound **2** has a major transient absorption peak while there is negligible signal of $\mathbf{3}^{2+}$ (see above). Therefore the kinetic trace at 700 nm was therefore selected for fitting with Equation S.III.13, *i.e.* λ = 700 nm. Similar to the fitting of TCSPC data, the TA data was indeed fitted using the model (Table S.III.4). Figure S.III.6 shows a fit of the three-dimensional model (d = 3) on lifetime decay data from TA at 293 K acquired from a liposome sample **L23** with 0.5 mol% **2** and 0.8 mol% $\mathbf{3}^{2+}$.

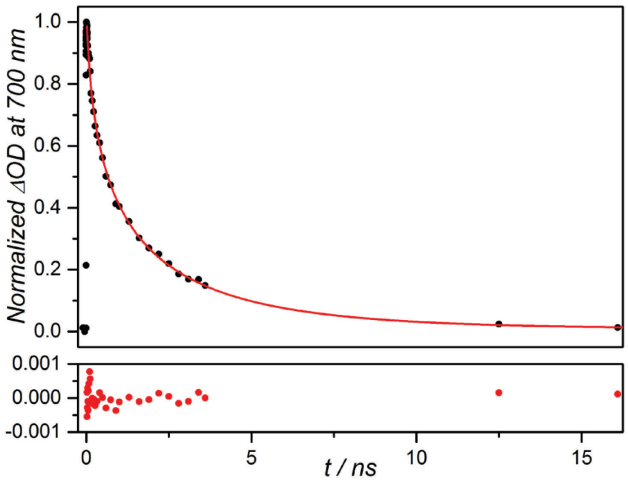

*Figure S.III.6. Transient absorption decay curve at 700 nm (black) of PEGylated (4 mol%) DMPC liposomes **L23** ([DMPC] = 20 mM) at 293 K with 0.5 mol% **2** and 0.8 mol% $\mathbf{3}^{2+}$ upon excitation with 400 nm (20-60 nJ/pulse, 1 KHz repetition rate). The red curve (top) represents a fit of the data according to a 3D FRET model (Equation S.III.12) with d = 3, τ = 6.0 ns, γ = 0.99, with the corresponding residual plot (bottom). The fit has a R^2 value of 0.997.*

The fitting parameters of the Förster three-dimensional decay model for both TCSPC and TA data, listed in Table S.III.2-Table S.III.4, show that for greater concentration of $\mathbf{3}^{2+}$, higher values of γ are obtained. In general, a three-dimensional model fitted the data better than a two-dimensional model, as the

3D model produced fits with X^2 values closer to 1. This agrees with the work of Holmes *et al.*[1, 10]

III.5.4. Calculating the experimental R_0 distance

The critical acceptor concentration C_0 (in M) is related to R_0 (in dm) by Equation S.III.14:

$$C_0 = \frac{3}{2\pi^{\frac{3}{2}} N_A R_0^3} \qquad \textit{Equation S.III.14}$$

so that a plot of γ *versus* [**3**] provided a straight line, of which the slope $1/C_0$ was used to evaluate R_0 (in dm), see Figure S.III.7. Again, [**3**] was substituted with $[\mathbf{3}]_{local}$ (see Equation S.III.9). In such conditions, R_0 was calculated to be 29 Å.

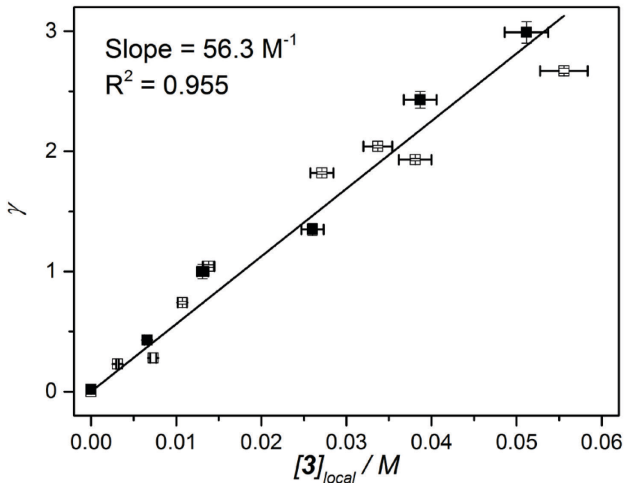

Figure S.III.7. Plot of γ at 293 K, as determined from transient absorption data (black filled squares) or from time-correlated single photon counting data (empty squares), as a function of the local concentration of $\mathbf{3}^{2+}$*, as defined by Equation S.III.9, in the lipid bilayer of PEGylated DMPC liposomes as determined by ICP-OES. Horizontal error bars represent 5% instrumental error from ICP-OES. Vertical error bars represent the fitting error of Equation S.III.12 on the data. The black line represents the best linear fit from the origin through the two combined data sets, and has a slope of 56.3* M^{-1} *with* $R^2 = 0.955$.

III.6. Photodissociation experiments using red light

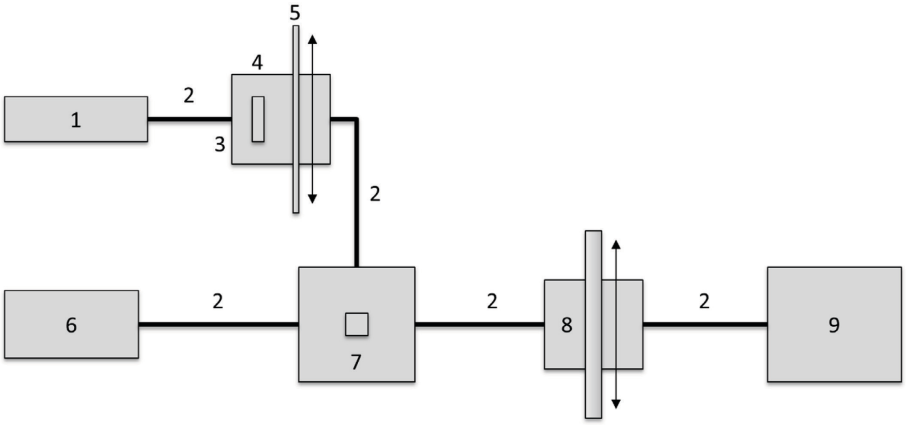

Figure S.III.8. Setup used for photosubstitution experiments using red light. Legend: (1) 630 nm laser source, (2) optical fibers, (3) filter holder, (4) 630 nm band pass filter, (5) variable neutral density filter that can be installed or removed, (6) halogen-deuterium light source for UV-Vis absorption spectroscopy, (7) temperature controlled cuvette holder, (8) variable filter holder, and (9) CCD spectrometer.

III.7. Definition and calculation of the total efficiency of TTA-UC, FRET and photodissociation

When TTA-UC and FRET are combined within the same membrane to realize the photochemical conversion of $\mathbf{3}^{2+}$ to $\mathbf{4}^{2+}$, the relevant photophysical and photochemical steps are

$$^1PS \xrightarrow{h\nu} {}^1PS^*$$

$$^1PS^* \xrightarrow{k_{ISC}} {}^3PS^*$$

$$^3PS^* + {}^1A \xrightarrow{k_{TTET}} {}^1PS + {}^3A^*$$

$$2\ {}^3A^* \xrightarrow{k_{TTA}} {}^1A + {}^1A^*$$

$$^1A^* + {}^1\mathbf{3}^{2+} \xrightarrow{k_{ET}} {}^1A + {}^1\mathbf{3}^{2+*}$$

$$^1\mathbf{3}^{2+*} \xrightarrow{k_{photosubstitution}} {}^1\mathbf{4}^{2+}$$

where for clarity purposes PS is the photosensitizer (**1**), and A is the annihilator (**2**), ISC means intersystem crossing, TTET means triplet-triplet energy transfer, TTA means triplet-triplet annihilation, and ET means non-radiative energy transfer. The rate of reaction is then defined by Equation S.III.15,

$$r = -\frac{dn_{\mathbf{3}^{2+}}}{dt} = \left|\frac{dn\,{}^{1}_{PS}}{dt}\right|_{created} \phi_{ISC}\phi_{TETT}\phi_{TTA}E_{ET}\phi_{Ru} \qquad \textit{Equation S.III.15}$$

where $\left|\frac{dn\,{}^{1}_{PS}}{dt}\right|_{created}$ is the rate of singlet state photosensitizer generated, φ_{ISC} is the QY of ISC of the photosensitizer, φ_{TETT} is the QY of TTET, φ_{TTA} is the QY of TTA, E_{ET} is the energy transfer efficiency as defined in Equation S.III.8, and φ_{Ru} is the quantum yield of photosubstitution in absence of **1** and **2**, measured under blue light irradiation. The rate of singlet state photosensitizer generated is further defined by Equation S.III.16:

$$\left|\frac{dn\,{}^{1}_{PS}}{dt}\right|_{created} = \Phi_{630}(1 - 10^{-A_{630}}) \qquad \textit{Equation S.III.16}$$

where Φ_{630} is the photon flux at 630 nm (einstein.s^{-1}) and A_{630} is the absorbance of the photosensitizer at 630 nm. In addition, similarly to Equation S.III.8, the efficiency of non-radiative energy transfer, E_{ET}, is given by Equation S.III.17:

$$E_{ET} = 1 - \frac{1}{1 + K_{SV} * [\mathbf{3}]_{local}} = \frac{K_{SV}[\mathbf{3}]_{local}}{1 + K_{SV}[\mathbf{3}]_{local}} \qquad \textit{Equation S.III.17}$$

where $[\mathbf{3}]_{\text{local}}$ is the local concentration of $\mathbf{3}^{2+}$ in the membrane, defined by Equation S.III.9 ($[\mathbf{3}]_{local} = \frac{n_{\mathbf{3}}}{n_{DMPC}V_M}$), and K_{SV} is the Stern-Volmer constant (L.mol^{-1}) for the quenching of ^{1}A* by $\mathbf{3}^{2+}$ in the lipid membrane. The quantum yield of TTA-UC is given by Equation S.III.18:

$$\phi_{ISC}\phi_{TETT}\phi_{TTA} = \phi_{TTA-UC} \qquad \textit{Equation S.III.18}$$

Thus Equation S.III.15 becomes Equation S.III.19:

$$r = -\frac{dn_{\mathbf{3}}}{dt} = \Phi_{630}(1 - 10^{-A_{630}})\phi_{TTA-UC}\frac{K_{SV}[\mathbf{3}]_{local}}{1 + K_{SV}[\mathbf{3}]_{local}}\phi_{Ru} \qquad \textit{Equation S.III.19}$$

Equation S.III.19 shows that the rate of the photosubstitution reaction depends on the local concentration of $\mathbf{3}^{2+}$ and a non-zero order reaction rate can be expected. Realizing that $K_{SV}[\mathbf{3}]_{\text{local}} << 1$, and that therefore E_{ET} can be approximated with $K_{SV}[\mathbf{3}]_{local} \equiv K_{SV}\frac{n_{\mathbf{3}}}{n_{DMPC}V_M}$, Equation S.III.19 simplifies to Equation S.III.20:

$$r = -\frac{dn_3}{dt} = \Phi_{630}(1 - 10^{-A_{630}})\phi_{TTA-UC}K_{SV}\frac{n_{\mathbf{3}}}{n_{DMPC}V_M}\phi_{Ru} \qquad \textit{Equation S.III.20}$$

Integrating Equation S.III.20 yields a first-order expression for $n_{\mathbf{3}}(t)$:

$$n_{\mathbf{3}}(t) = n_{\mathbf{3}}(0) * e^{-kt} \qquad \textit{Equation S.III.21}$$

where k is given by Equation S.III.22:

$$k = \frac{\Phi_{630}}{n_{DMPC}V_M}(1 - 10^{-A_{630}})\phi_{TTA-UC}K_{SV}\phi_{Ru} \qquad \textit{Equation S.III.22}$$

The total efficiency of TTA-UC, FRET, and photodissociation of $\mathbf{3}^{2+}$ in liposomes **L123** is defined by Equation S.III.23:

$$E_{total} = \phi_{TTA-UC}E_{ET}\phi_{Ru} \approx \phi_{TTA-UC}K_{SV}\frac{n_{\mathbf{3}}}{n_{DMPC}V_M}\phi_{Ru} \qquad \textit{Equation S.III.23}$$

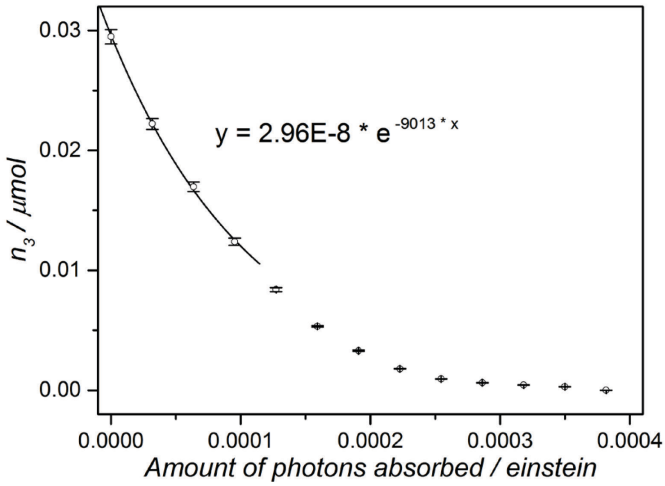

*Figure S.III.9. Plot of n_3 as a function of the amount of photons absorbed during the photodissociation experiment with red light of **L123**. The black line represents a single exponential fit for the first 45 min of irradiation.*

For t = 0 – 45 min, *i.e.* when E_{ET} is more or less constant, E_{total} can be experimentally determined from a plot of the amount of mol of $\mathbf{3}^{2+}$ as a function of the amount of absorbed photons, *i.e.*$\Phi_{630} * (1 - 10^{-A_{630}}) * t$, see Figure S.III.9. Φ_{630} was estimated from measuring the optical power (120 mW at 630 nm, *i.e.* 0.632 µeinstein.s^{-1}) and A_{630} was 0.025. Note that at t = 0, mostly **1** absorbs at 630 nm. Some bleaching of **1** was observed during the reaction (Figure 4.3b), but it was neglected in this calculation. Therefore, the amount of absorbed photons per unit time was considered to be constant. E_{total} at t = 0 can be evaluated from the slope at t = 0 of the single exponential fit curve of the evolution of n_3 *versus* the amount of red photons absorbed since t = 0 (see Figure S.III.9). From this, a value of 0.027% was determined.

The amount of mol $\mathbf{3}^{2+}$ was determined from the UV-VIS absorbance data at 490 nm by accounting for the contributions of both $\mathbf{3}^{2+}$ and $\mathbf{4}^{2+}$ to the absorption at this wavelength, as explained here. The total absorbance at 490 nm is given by Equation S.III.24:

$$A^{490} = \varepsilon_{\mathbf{3}}^{490} \times l \times [\mathbf{3}] + \varepsilon_{\mathbf{4}}^{490} \times l \times [\mathbf{4}] \qquad \textit{Equation S.III.24}$$

where $\varepsilon_{\mathbf{3}}^{490}$ is the molar absorption coefficient of $\mathbf{3}^{2+}$ at 490 nm (3760 M^{-1}.cm^{-1} in $CHCl_3$), [**3**] is the bulk concentration of $\mathbf{3}^{2+}$, $\varepsilon_{\mathbf{4}}^{490}$ is the molar absorption

coefficient of $\mathbf{4}^{2+}$ at 490 nm (8690 $M^{-1}.cm^{-1}$ in H_2O), [**4**] is the bulk concentration of $\mathbf{4}^{2+}$, and l is the cuvette path length (*i.e.* 1 cm). At $t = \infty$, the photoreaction is complete and no more $\mathbf{3}^{2+}$ is present, which means that

$$A_{\infty}^{490} = \varepsilon_{\mathbf{4}}^{490} \times l \times [\mathbf{3}]_0 \qquad \textit{Equation S.III.25}$$

By replacing [**4**] with $[\mathbf{3}]_0 - [\mathbf{3}]$ in Equation S.III.24, [**3**] can be expressed as a function of A^{490} in Equation S.III.26:

$$[\mathbf{3}] = \frac{A^{490} - A_{\infty}^{490}}{\varepsilon_{\mathbf{3}}^{490} \times l - \varepsilon_{\mathbf{4}}^{490} \times l} \qquad \textit{Equation S.III.26}$$

Finally, the amount of mol $\mathbf{3}^{2+}$ is obtained by multiplying with the volume in the cuvette (*V*, *i.e.* 1.5 ml), see Equation S.III.27:

$$n_{\mathbf{3}} = V * \frac{A^{490} - A_{\infty}^{490}}{\varepsilon_{\mathbf{3}}^{490} - \varepsilon_{\mathbf{4}}^{490}} \qquad \textit{Equation S.III.27}$$

At $t = 0$, the value for n_3 ($2.95 \times 10^{-8} \pm 0.06 \times 10^{-8}$ mol) was very comparable with the value for n_3 determined by ICP-OES ($2.82 \times 10^{-8} \pm 0.01 \times 10^{-8}$) , which confirms the validity of this approach.

III.8. Photodissociation experiments with lower red-light intensities

Irradiation experiments on liposomes **L123** were repeated with three different red light intensities of 30, 60, and 120 mW (0.24, 0.48, and 0.95 $W.cm^{-2}$, respectively). The course of the reaction was monitored by UV-Vis absorption spectroscopy following the absorbance of the aqua photoproduct at 490 nm (Figure S.III.10). As expected, a decrease in reaction rate was observed for lower irradiation intensities (Figure S.III.10d). To determine the total efficiency of the system (E_{total}, see Equation S.III.23), the amount of ruthenium (n_3) was plotted *versus* the amount Q of photons absorbed since $t = 0$ (Figure S.III.11). E_{total} was calculated from the exponential fit of the data by multiplying the exponent with the amplitude, yielding values of 0.026% for 0.24 $W.cm^{-2}$, 0.024% for 0.48 $W.cm^{-2}$, and 0.019% for 0.95 $W.cm^{-2}$. The

somewhat lower quantum yield for the experiment using 0.95 W.cm^{-2} irradiation is attributed to some bleaching of the photosensitizer (**1**) in this particular experiment (compare A_{630} at t = 180 between the three individual experiments in Figure S.III.10). The real amount of photons absorbed by **1** is therefore lower (*i.e.* the real quantum yield is higher), but the data is not corrected for this effect. Overall, all three efficiencies values E_{total} were found very similar to that given in the main text (0.027% for 0.95 W.cm^{-2} red light irradiation), so it can be concluded that the quantum efficiency of red light-induced photosubstitution in **L123** is unaffected by light intensity and this range of intensities.

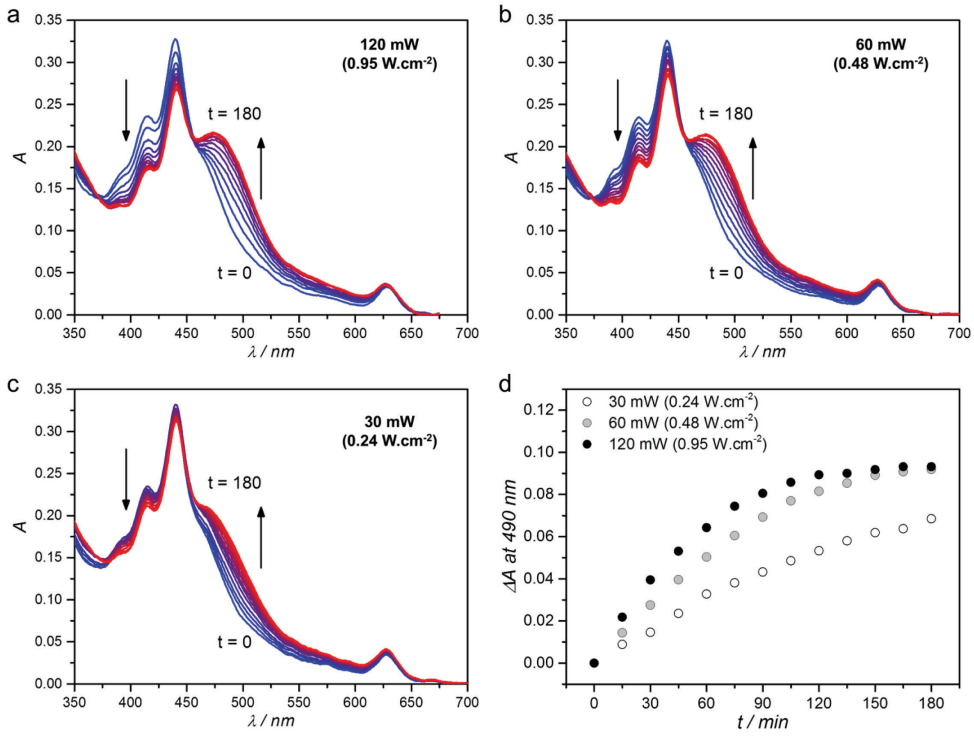

*Figure S.III.10. Absorption spectra of liposomes **L123** during red light irradiation (630 nm) with (a) 30 mW (0.24 W.cm^{-2}), (b) 60 mW (0.48 W.cm^{-2}), and (c) 120 mW (0.95 W.cm^{-2}). Blue line: spectrum at t = 0; red line: spectrum at t = 180 minutes; other spectra measured every 15 minutes. d) Difference in absorbance at 490 nm, after baseline correction, during red-light irradiation of **L123** with 30 mW (white), 60 mW (grey), or 120 mW (black). T = 310 K, sample volume 1.5 ml, 8% of sample volume simultaneously irradiated. A single **L123** liposome stock dispersion was used in these experiments and diluted with PBS buffer prior to measurement so that every time [**1**] = 0.25 μM, and [**2**] = 2.5 μM.*

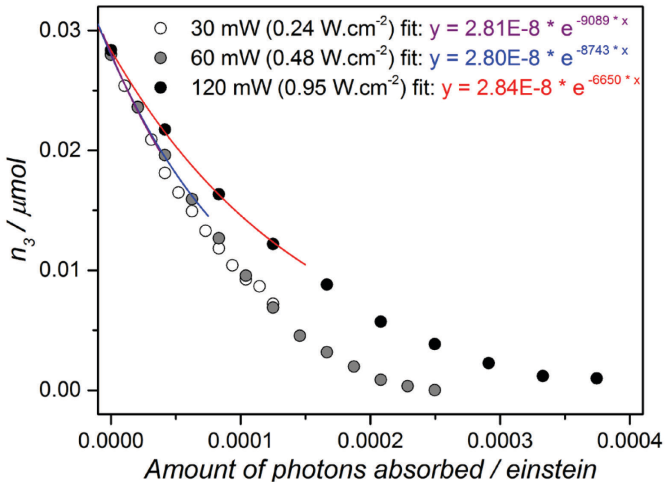

Figure S.III.11. Evolution of the number of mol of $\mathbf{3}^{2+}$ *(*n_3*) as a function of the amount of red photons absorbed since t = 0 for liposome sample* ***L123*** *irradiated with 30 mW (0.24 W.cm*$^{-2}$ *white circles, purple fit curve), 60 mW (0.48 W.cm*$^{-2}$*, grey circles, blue fit curve), or 120 mW (0.95 W.cm*$^{-2}$*, black circles, red fit curve). The fit lines represent single exponential fits for the first 45 min of irradiation for each dataset. The lower slope for the 120 mW experiment is attributed to more bleaching of the photosensitizer during irradiation.*

III.9. References

[1] A. S. Holmes, D. J. S. Birch, T. Salthammer, *J. Fluoresc.* **1993**, *3*, 77-84.
[2] S. L. Joris J. Snellenburg, Ralf Seger, Katharine M. Mullen, Ivo H. M. van Stokkum, *J. Stat. Softw.* **2012**, *49*, 1-22.
[3] Y. H. Meyer, P. Plaza, *Chem. Phys.* **1995**, *200*, 235-243.
[4] S. Bonnet, B. Limburg, J. D. Meeldijk, R. J. M. Klein Gebbink, J. A. Killian, *J. Am. Chem. Soc.* **2010**, *133*, 252-261.
[5] N. H. Damrauer, G. Cerullo, A. Yeh, T. R. Boussie, C. V. Shank, J. K. McCusker, *Science* **1997**, *275*, 54-57.
[6] J. R. Lakowicz, *Principles of Fluorescence Spectroscopy*, 3rd ed., Springer Science+Business Media, LLC, New York, NY, USA, **2006**.
[7] J. T. Buboltz, C. Bwalya, S. Reyes, D. Kamburov, *J. Chem. Phys.* **2007**, *127*, 215101.
[8] D. Marsh, *Handbook of Lipid Bilayers*, 2nd ed., Taylor & Francis Group, LLC, Boca Raton, FL, USA, **2013**.
[9] I. B. Berlman, *Handbook of fluorescence spectra of aromatic molecules*, 2nd ed., Academic Press, New York, NY, USA, **1971**.
[10] A. S. Holmes, K. Suhling, D. J. S. Birch, *Biophys. Chem.* **1993**, *48*, 193-204.

APPENDIX IV: SUPPORTING INFORMATION FOR CHAPTER 5

IV.1. Cryo transmission electron microscopy

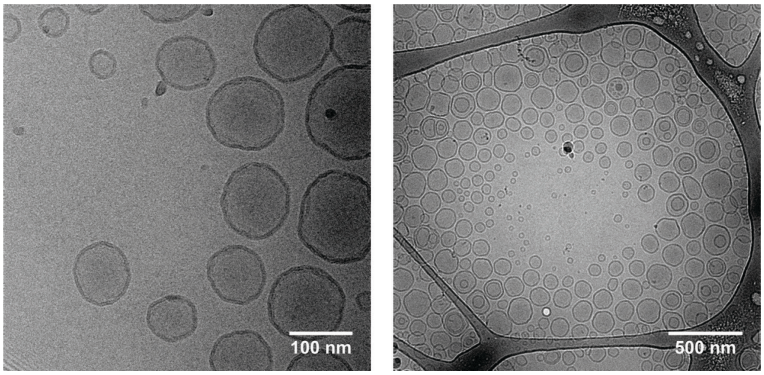

*Figure S.IV.1. Cryo transmission electron micrographs of DMPC **LUV12**.*

IV.2. Emission spectroscopy on LUVs

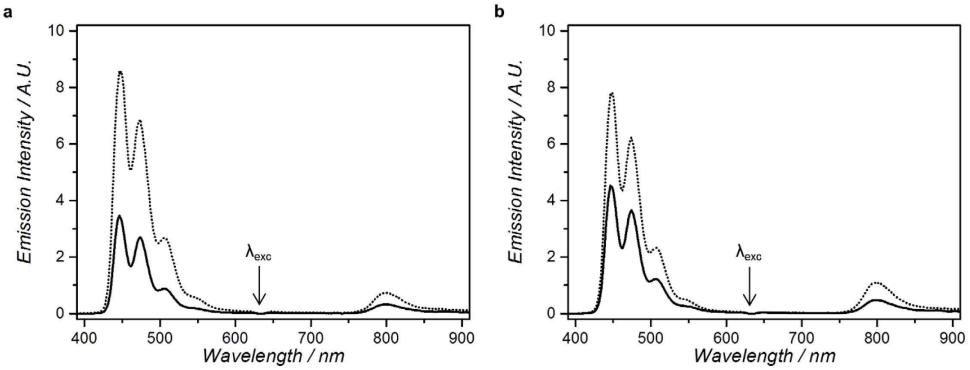

*Figure S.IV.2. Emission spectra of DOPC (a) and DMPC (b) **LUV12** samples ([lipid] = 1 mM, [DSPE-PEG-2000] = 0.04 mM, [**2**] = 5 μM, [**1**] = 0.25 μM) under 630 nm excitation at 298 K. The samples were either deoxygenated by bubbling argon for 30 min prior to measurement (solid curves) or by addition of sodium sulfite at a concentration of 0.3 M to the buffer (dotted curves). Irradiation conditions: 3.0 mL sample volume in a macro fluorescence cuvette, with 30 mW 630 nm irradiation power (4 mm beam diameter, intensity 0.24 W.cm^{-2}). Bubbling of argon through the sample inevitably results in the formation of small bubbles on the walls of the measurement cuvette, resulting in scattering of light in both the excitation and the detection pathway. These bubbles are absent in the case of deoxygenation using the sodium sulfite oxygen scavenger, which explains why the observed intensities are higher for samples deoxygenated with sulfite.*

IV.3. Emission spectroscopy on GUVs

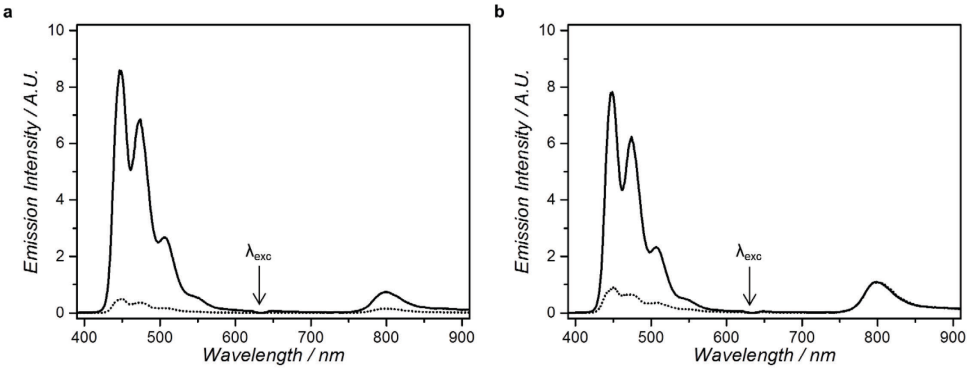

Figure S.IV.3. Emission spectra of DOPC (a) and DMPC (b) ***LUV12*** *(solid curves) and* ***GUV12*** *(dotted curves) with 30 mW 630 nm excitation (0.24 W.cm² intensity) at 298 K. In the case of LUVs, [DMPC] = 1 mM, [DSPE-PEG-2000] = 0.04 mM, [**2**] = 5 µM, [**1**] = 0.25 µM, whereas in the case of GUVs, the lipid concentration was not known, but the components in the membrane were introduced in the same molar ratio as for the LUV samples. In all cases, the buffer was deoxygenated by addition of sodium sulfite (0.3 M) and the spectra were measured under air.*

IV.4. Power dependency measurements

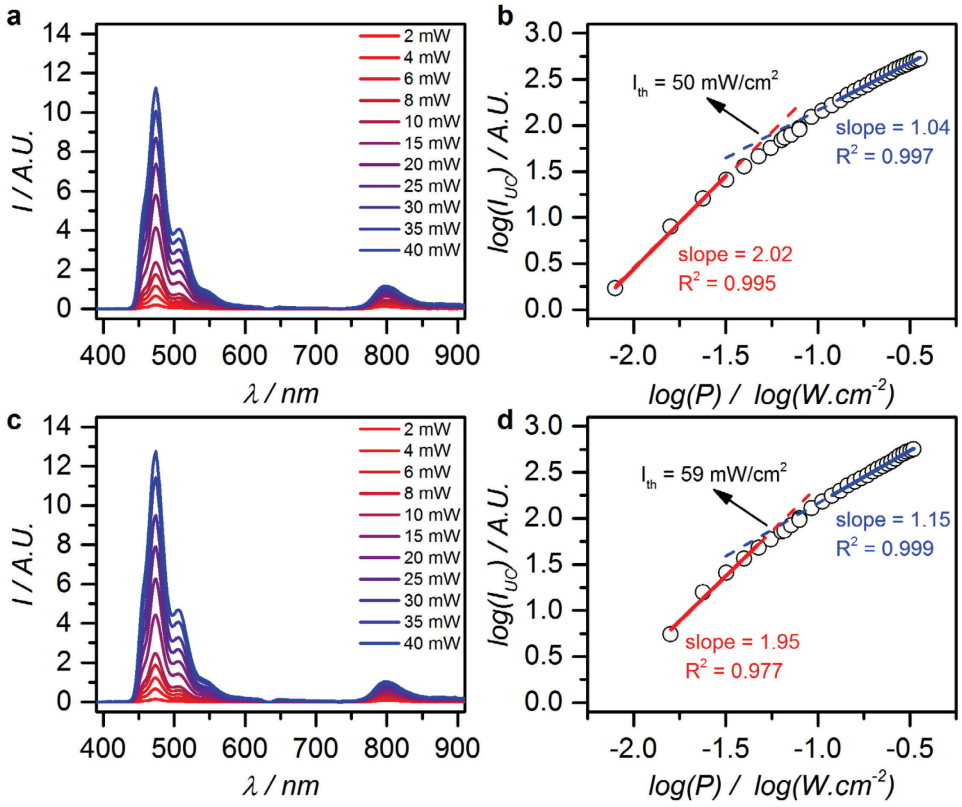

*Figure S.IV.4. Luminescence emission spectra of DMPC **LUV-12** (a) and DOPC **LUV-12** (c) at various excitation intensities. Double logarithmic plot of the upconversion luminescence intensity (I_{UC}) of DMPC **LUV-12** (b) and DOPC **LUV-12** (d), integrated from 420 to 575 nm, as a function of the excitation intensity P (in W.cm^{-2}). The low power regime was fitted with straight lines with slopes 2.02 (R^2 = 0.995) and 1.95 (R^2 = 0.977) for DMPC and DOPC **LUV-12**, respectively (red solid lines), and the high power regime was fitted with straight lines with slopes 1.04 (R^2 = 0.997) and 1.15 for DMPC and DOPC **LUV-12**, respectively (blue solid lines). From the intersection of the extrapolated fits (red and blue dashed lines), the intensity threshold (I_{th}) was found to be 50 mW.cm^{-2} for DMPC **LUV-12** and 59 mW.cm^{-2} for DOPC **LUV-12**. Irradiation conditions: [lipid] = 1.0 mM, T = 298 K, laser beam diameter 4 mM.*

IV.5. Microscopy imaging

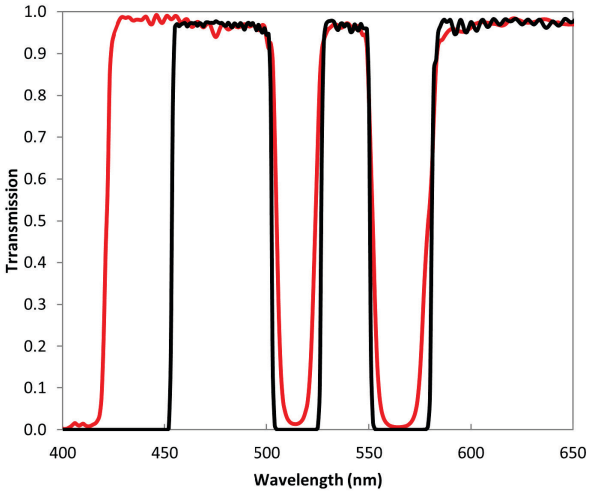

Figure S.IV.5. Transmission curves of the filter and dichroic beam splitter that were used for emission microscopy with violet light (405 nm), consisting of a Chroma ZT405/514/561rpc dichroic beam splitter (red) and a Chroma ZET442/514/568m emission filter (black).

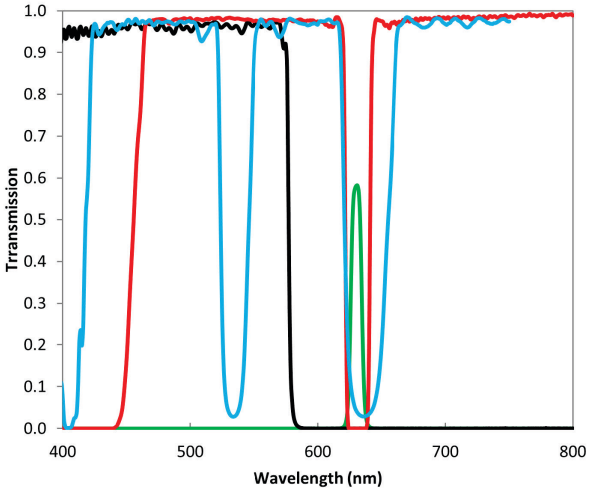

Figure S.IV.6. Transmission curves of the filters and dichroic beam splitter that were used for emission microscopy with red light (630 nm), consisting of a Thorlabs NF633-25 notch filter (red) and an Edmund Optics 575 nm OD4 short pass filter (black), a Thorlabs FB630-10 band pass filter (green), and a Chroma ZT405/532/635rpc dichroic mirror (blue).

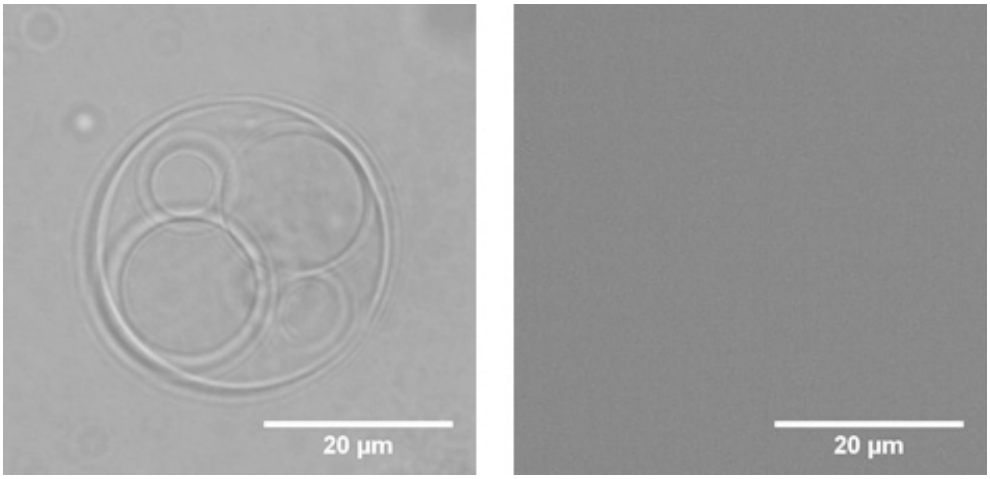

*Figure S.IV.7. Bright field (left) and upconversion emission (right) photographs of DOPC **GUV2**, i.e. GUVs similar to **GUV12** but deprived of the photosensitizer 1, in buffer without sodium sulfite and under air atmosphere.*

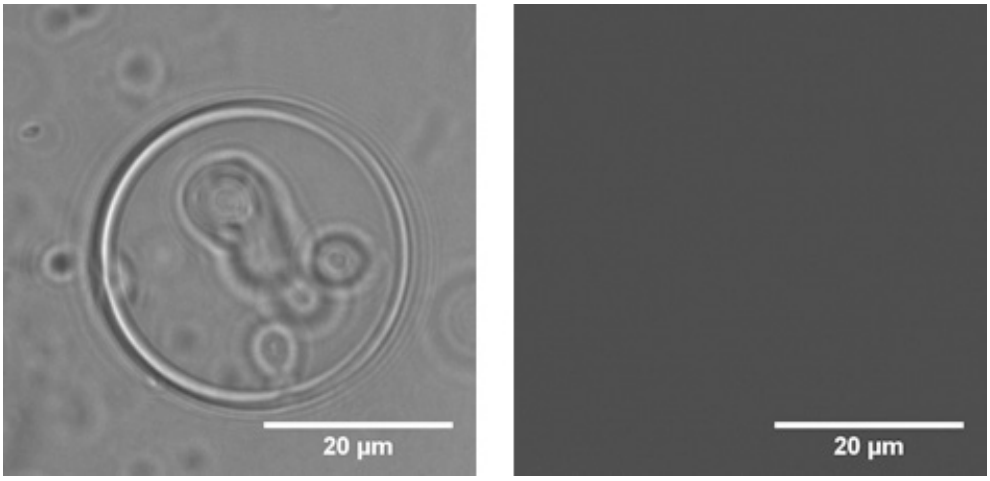

*Figure S.IV.8. Bright field (left) and upconversion emission (right) photographs of DOPC **GUV12** in air atmosphere in buffer without sodium sulfite.*

APPENDIX V: SUPPORTING INFORMATION FOR CHAPTER 6

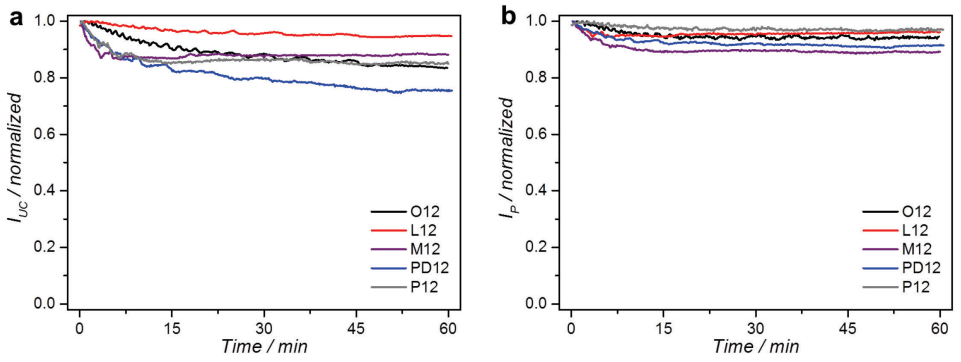

*Figure S.V.1. Time dependence of I_{UC} and I_P at 20 °C of samples **O12**, **L12**, **M12**, **PD12**, and **P12**. All samples show an initial drop in phosphorescence, followed by stabilization. Considering that trace amounts of oxygen are still present at t = 0, we attribute this to the generation of singlet oxygen by the photosensitizer upon light excitation and reaction of singlet oxygen with the photosensitizer and/or annihilator.*

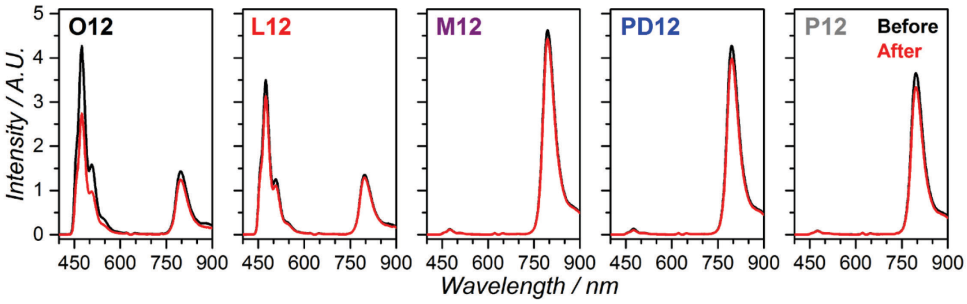

*Figure S.V.2. Luminescence spectra of samples **O12**, **L12**, **M12**, **PD12**, and **P12** at 5°C before (black) and after (red) heating from 5 °C to 50 °C and continuous red light irradiation. Spectra taken with 10 mW (80 mW.cm^{-2}) 630 nm excitation. Only **O12** shows significant bleach.*

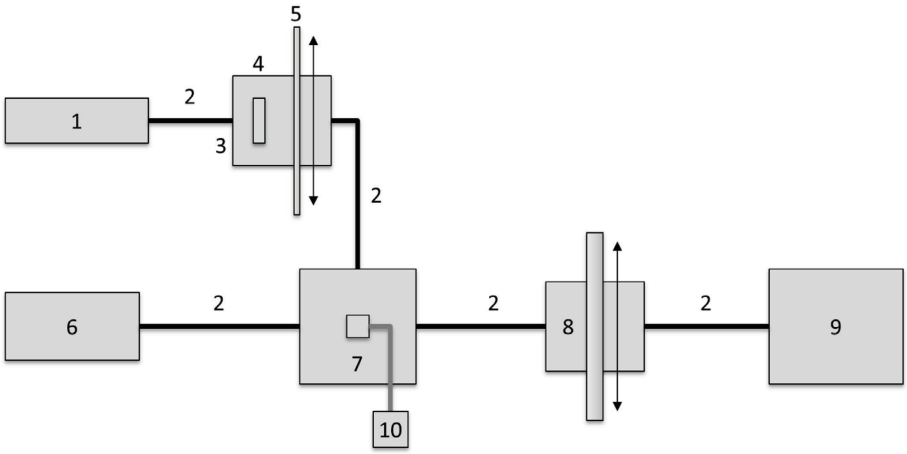

Figure S.V.3. Setup used for emission spectroscopy. Legend: (1) 630 nm laser source, (2) optical fibers, (3) filter holder, (4) 630 nm band pass filter, (5) variable neutral density filter that can be installed or removed, (6) halogen-deuterium light source for UV-Vis absorption spectroscopy, (7) temperature controlled cuvette holder, (8) variable filter holder, (9) CCD spectrometer, and (10) temperature probe submerged in the sample.

APPENDIX VI: SUPPORTING INFORMATION FOR CHAPTER 7

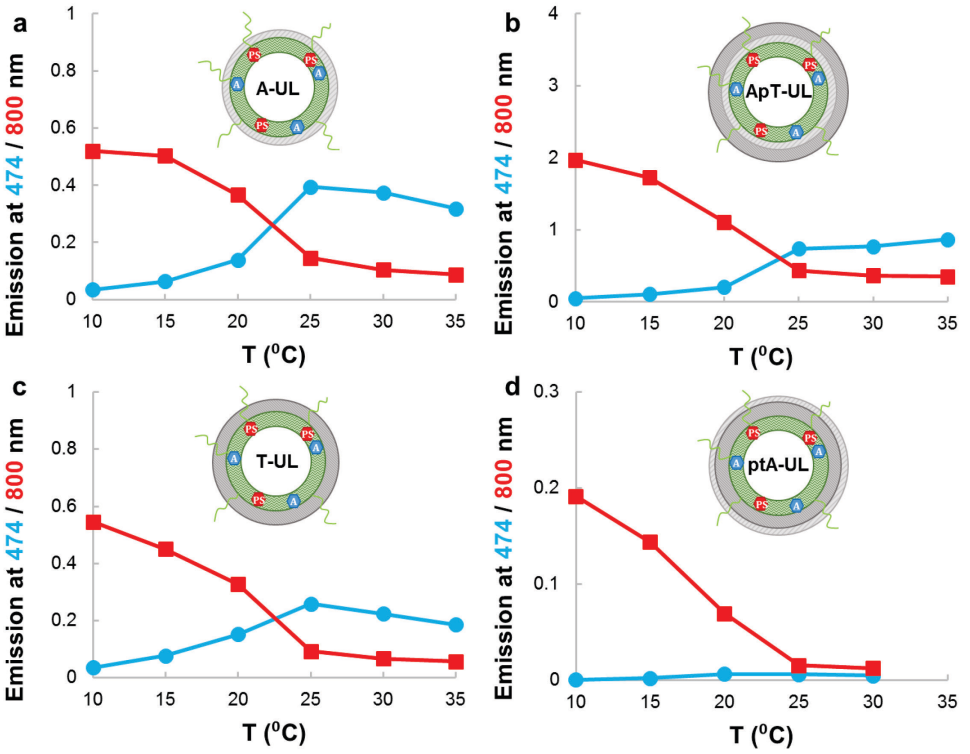

*Figure S.VI.1. Temperature dependencies of upconversion (at 475 nm, blue circles) and phosphorescence (at 800 nm, red squares) for **A-UL** (a), **ApT-UL** (b), **T-UL** (c), and **pTA-UL** (d) in 50 mM Na_2SO_3 PBS with 30 mW 630 nm (240 mW.cm^{-2}).*

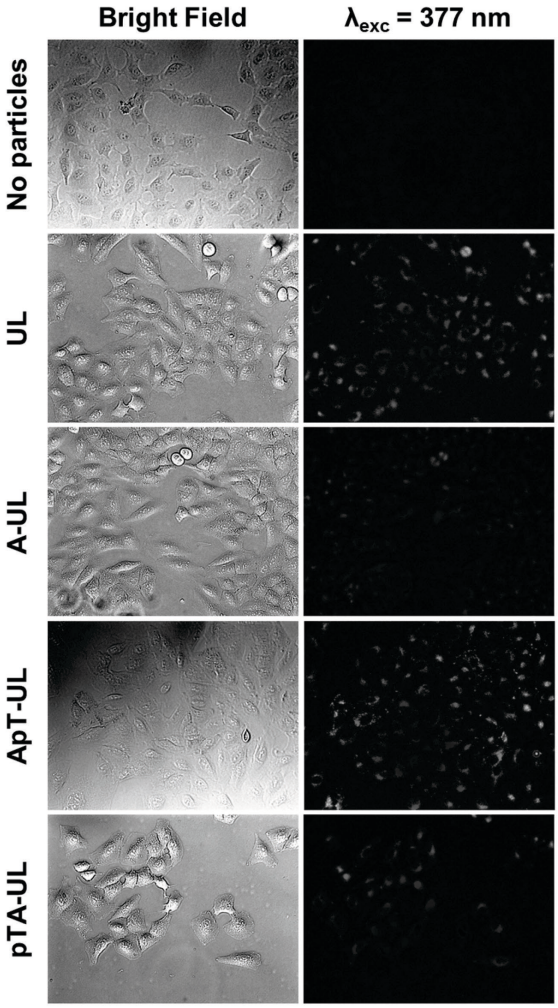

*Figure S.VI.2. Microscopy imaging in bright field mode (left column) and with 377 nm excitation (right column) of A549 cells treated with either **UL**, **A-UL**, **ApT-UL**, **pTA-UL**, or no particles as control.*

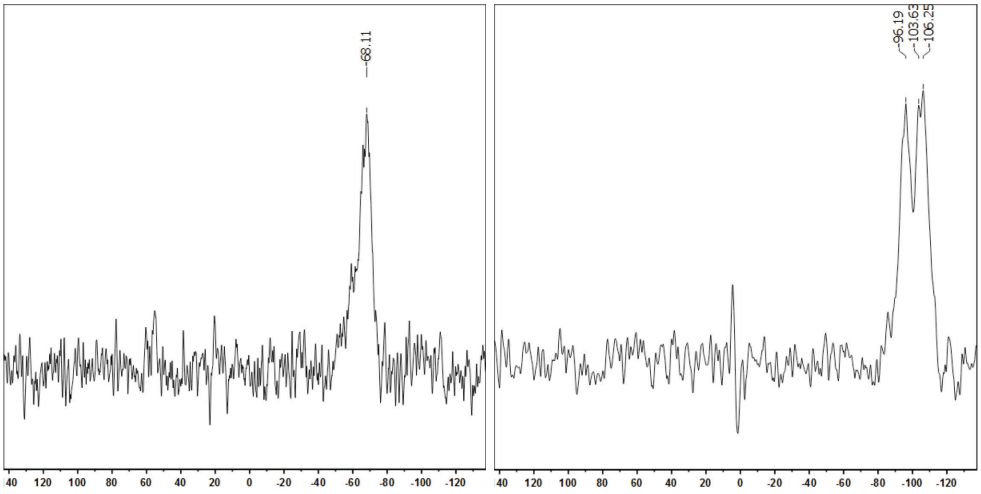

*Figure S.VI.3. ^{29}Si-NMR spectra of samples **A-UL-D** (left) and **ApT-UL-D** (right).*

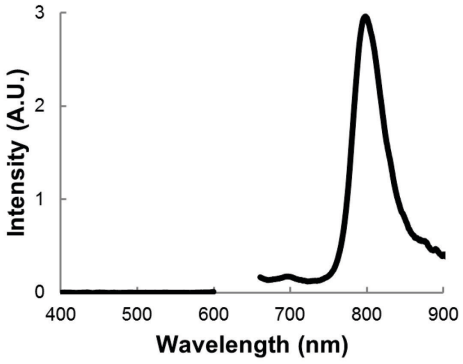

*Figure S.VI.4. Emission spectrum of freeze-dried upconverting liposomes (**UL-F**) under 30 mW 630 nm excitation (0.66 W.cm^{-2}) at 20 °C.*

APPENDIX VII: SUPPORTING INFORMATION FOR CHAPTER 8

VII.1. Hopping of perylene (compound 2) *versus* 2,5,8,11-tetra(*tert*-butyl)perylene (compound 3)

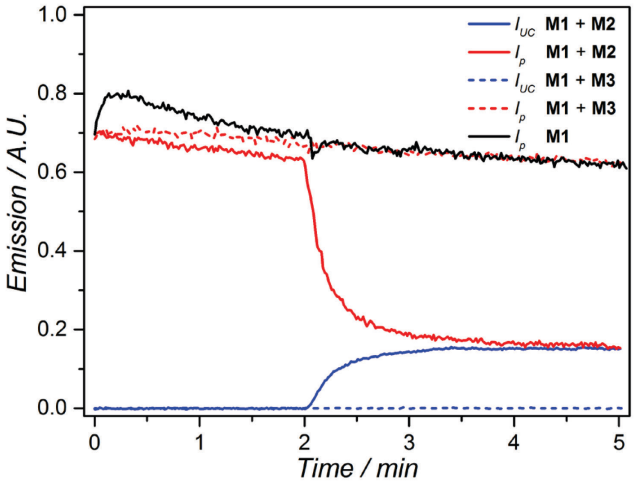

*Figure S.VII.1. Hopping of compound **2** versus compound **3** by monitoring TTA-UC upon mixing **M1** with either **M2** or **M3**. A diluted sample of **M1** liposomes (0.25 mM DMPC) in 0.1 M Na_2SO_3 in PBS was placed in a stirred macro cuvette at 25 °C and the emission spectrum was acquired for 2 min with 10 mW 630 nm (80 mW.cm^{-2}). At t = 2 min, 1 equivalent of either **M2**, **M3**, or only PBS (all containing 0.1 M Na_2SO_3) was added and spectra were continuously acquired. The upconversion intensity (I_{UC}) at 474 nm (**2**) or 486 nm (**3**), and the phosphorescence intensity (I_P) at 800 nm (**1**) are plotted versus time.*

It is known in the literature that perylene (compound **2**) partitions with the aqueous phase when dissolved in the lipid bilayer of liposomes.[1] To prevent perylene from escaping the vesicles, 2,5,8,11-tetra(*tert*-butyl)perylene (compound **3**) was synthesized (see Chapter 9, section 9.4.2). In order to investigate whether tert-butylation made the compound more membrane-bound, a "hopping" experiment was conducted as follows. Three different PEGylated DMPC liposome samples were prepared in 0.1 M Na_2SO_3 in PBS: one containing only photosensitizer **1** (**M1**), one containing only perylene **2** (**M2**), and one containing only tert-butylated perylene **3** (**M3**). Then, **M1** was placed in a stirred cuvette at 25 °C and the emission spectrum was continuously acquired under 10 mW 630 nm irradiation (80 mW.cm^{-2}). After

2 min, **M2** was added and the emission spectrum was acquired for 3 more min. The same experiment was also performed with using **M3** instead of **M2**. As a control, the emission of **M1** was monitored for 5 min without further liposome addition. In Figure S.VII.1, the upconversion intensity (I_{UC}) and phosphorescence intensity of **1** (I_p) are plotted versus time. Upon addition of **M2** to **M1**, upconversion was instantaneously observed and stabilized 1 min after mixing, while the phosphorescence was quenched and also stabilized after 1 min after mixing. Note that TTA-UC requires molecular contact, and that the liposomes do not fuse or come in close proximity of each other due their PEGylated surface. Thus, under the assumption that **1** does not hop, these results indicate that compound **2** had hopped from **M2** to **M1** within this time, which is consistent with the observations of Almgren.[1] For the mixture of **M1** and **M3**, no phosphorescence quenching was observed and no upconversion was observed throughout the experiment. From this, it can be concluded that neither compound **3** nor compound **1** escapes DMPC membranes. Overall, these results demonstrate that four-fold *t*-butylation of perylene indeed prevents liposomal escape.

VII.2. Fluorescence spectrum of LysoTracker Red

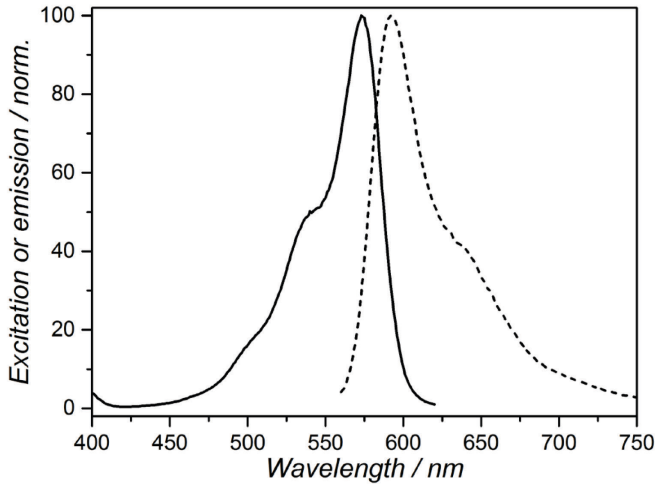

Figure S.VII.2. Normalized excitation (solid) and emission spectrum (dashed) of LysoTracker Red DND-99. Data acquired from manufacturer ThermoFisher Scientific.

VII.3. Uptake of M1, M3, and M1-3 liposomes in cells

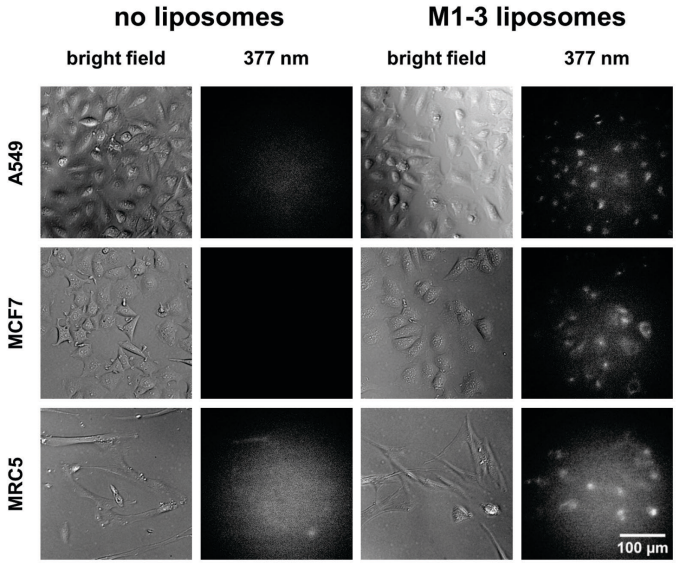

*Figure S.VII.3. Bright field and fluorescence micrographs (λ_{exc} = 377 nm) at 20x magnification of A549 (top row), MCF7 (middle row), and MRC5 cells (bottom row) that were incubated with no liposomes (left side) and **M1-3** liposomes (right side) for 24h.*

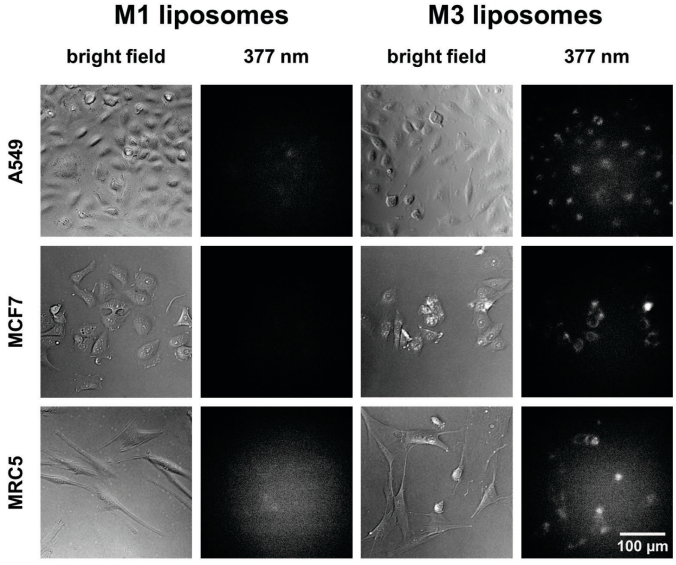

*Figure S.VII.4. Bright field and fluorescence micrographs (λ_{exc} = 377 nm) at 20x magnification of A549 (top row), MCF7 (middle row), and MRC5 cells (bottom row) that were incubated with **M1** liposomes (left side) and **M3** liposomes (right side) for 24h. Note that **M1** liposomes are not fluorescent and only autofluorescence is observed.*

VII.4. Overlap between absorption of Ru-complexes 5^{2+}, 6^{2+}, 7^{2+} and 8^{2+} and emission of compound 3

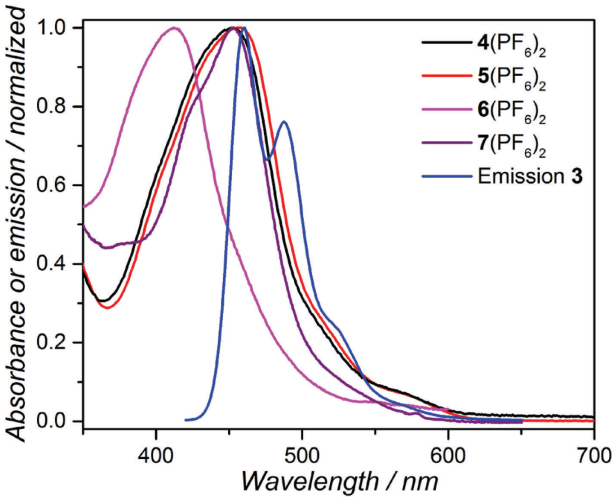

*Figure S.VII.5. Overlap between normalized absorption spectra of Ru-complexes **5**$^{2+}$, **6**$^{2+}$, **7**$^{2+}$ and **8**$^{2+}$ and the normalized emission spectrum of compound **3**.*

VII.5. Photosubstitution of Ru-complexes 5^{2+}, 6^{2+}, and 7^{2+} with blue light

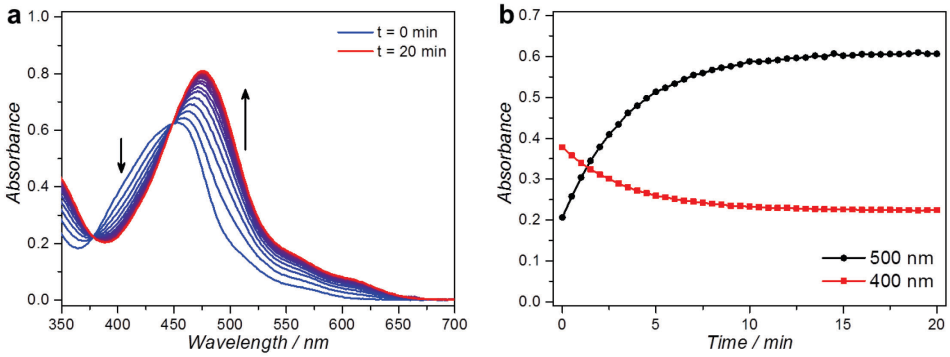

*Figure S.VII.6. Time-dependent UV-vis absorption spectroscopy of complex **5**$^{2+}$ (0.1 mM) during blue light irradiation (450 nm, photon flux 0.17 µEinstein.s^{-1}) in water at 25 °C. a) Absorption spectra, recorded every 1 min (blue to red evolution). b) Evolution of the absorbance at 400 nm (red squares) and 500 nm (black circles). The water was deoxygenated for 10 min by bubbling with argon and the solution was kept under an argon atmosphere during spectroscopy. The quantum yield of photosubstitution of converting **5**$^{2+}$ to **8**$^{2+}$ was calculated to be 0.70% according to a previously published method.[2]*

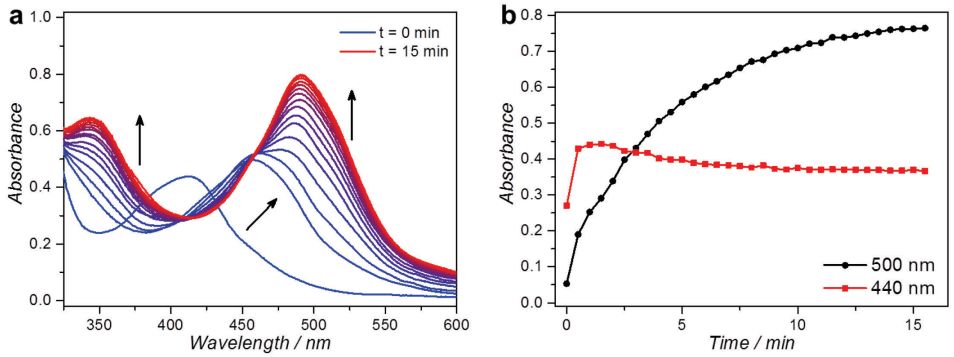

Figure S.VII.7. Time-dependent UV-vis absorption spectroscopy of complex $\mathbf{6}^{2+}$ *(0.07 mM) during blue light irradiation (450 nm, photon flux 0.17 µEinstein.s*$^{-1}$*) in water at 25 °C. a) Absorption spectra, recorded every 1 min (blue to red evolution). b) Evolution of the absorbance at 440 nm (red squares) and 500 nm (black circles). The water was deoxygenated for 10 min by bubbling with argon and the solution was kept under an argon atmosphere during spectroscopy. The spectral evolution upon reaction of* $\mathbf{6}^{2+}$ *to* $\mathbf{9}^{2+}$ *shows that the photoreaction proceeds via two distinct steps: it is proposed that the first step is fast and involves the release of one of the thioether-ruthenium bonds (see how the spectrum changes in the first minute), and the second step is slower and involves the release of the other thioether-ruthenium bond.*

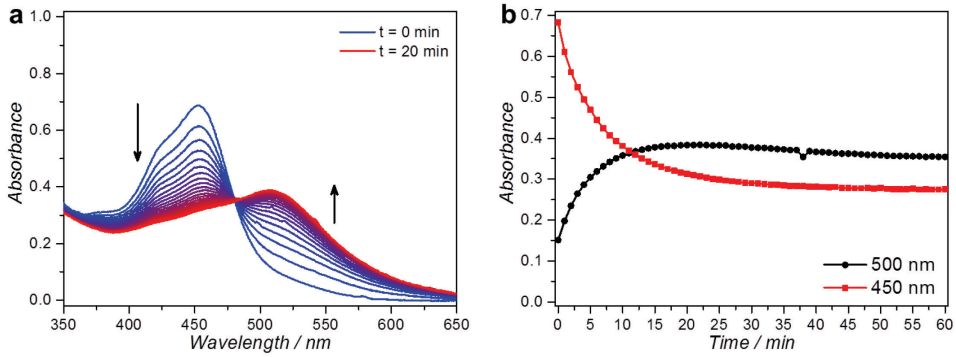

Figure S.VII.8. Time-dependent UV-vis absorption spectroscopy of complex $\mathbf{7}^{2+}$ *(0.070 mM) during blue light irradiation (450 nm, photon flux 0.17 µEinstein.s*$^{-1}$*) in 9:1 v/v acetone:*H_2O *at 25 °C. a) Absorption spectra, recorded every 1 min (blue to red evolution). b) Evolution of the absorbance at 450 nm (red squares) and 500 nm (black circles). The water was deoxygenated for 10 min by bubbling with argon and the solution was kept under an argon atmosphere during spectroscopy.*

VII.6. Photosubstitution of Ru-complexes with blue light: estimation of reaction half-time

Because the amount of [Ru] inside the cells was unknown, an estimation was based on a 10 µM aqueous solution. The reaction half-time for a prototypical Ru-complex photosubstitution ([Ru-L] + hν → [Ru-H_2O] + L) was estimated using the following set of equations.

$$\frac{dn_{RuOH_2}}{dt} = k \times n_{RuL} \qquad \textit{Equation S VII.1}$$

where n_{RuOH_2} is the amount of Ru-H_2O molecules (mol), n_{RuL} is the amount of Ru-L molecules (mol), and k is the photosubstitution rate, defined by Equation S VII.2:

$$k = W \times \varphi_{454} \times (1 - 10^{-A_{454}}) \times \left(\frac{\varepsilon_{454} \times l}{A_{454} \times V}\right) \times \Phi_{Ru} \qquad \textit{Equation S VII.2}$$

in which W is the surface area of a 96 well-plate well (0.3 cm^2), φ_{454} is the photon flux at 454 nm (7.0 $mW.cm^{-2}$, *i.e.* 2.7 × 10^{-8} $mol.s^{-1}.cm^{-2}$), A_{454} is the absorbance at 454 nm (0.042 for a complex with a molar absorption coefficient (ε_{454}) of 6000 $M^{-1}cm^{-1}$), l is the light path length for a 200 µL work volume (V) in a 96 well-plate well (l = 0.7 cm), and Φ_{Ru} is the photosubstitution quantum yield (usually around 0.01 for such complexes).[3] Under these assumptions, k at t = 0 was estimated to be 3.6 × 10^{-3} s^{-1}. Then, the half time ($t_{1/2}$) of the reaction is given by Equation S VII.3:

$$t_{1/2} = \frac{\ln(2)}{k} \qquad \textit{Equation S VII.3}$$

The value of $t_{1/2}$ was estimated to be 192 s (~ 3 min).

VII.7. UV-vis spectroscopy and mass spectrometry after red-light irradiation of M1-3-6 liposomes

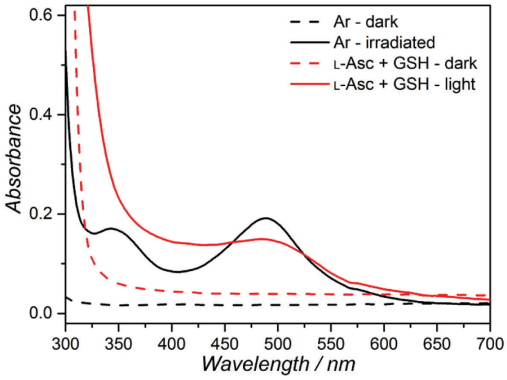

Figure S.VII.9. UV-vis absorption spectra of filtered solutions of red-light irradiated ***M1-3-6*** *liposomes ([DMPC] = 1 mM) under argon (solid black) and in air in presence of 10 mM L-Asc and GSH (solid red). Irradiation was done for 60 min with 2 mL sample volume, 150 mW 630 nm light (1.2 W.cm^{-2} intensity, 4.3 kJ.cm^{-2}), and at 37 °C, and then the solution was filtered with a centrifuge filter (MWCO = 100,000 Da); the UV-vis absorption spectrum of the filtrate is shown here. As controls, samples were kept in the dark and filtered in the same way (dashed lines): these spectra show neither absorption of the upconversion compounds* ***1*** *and* ***3****, nor that of the Ru-complex* ***6***$^{2+}$*, which indicates that no Ru photosubstitution has taken place and that the liposomes remain in the filter.*

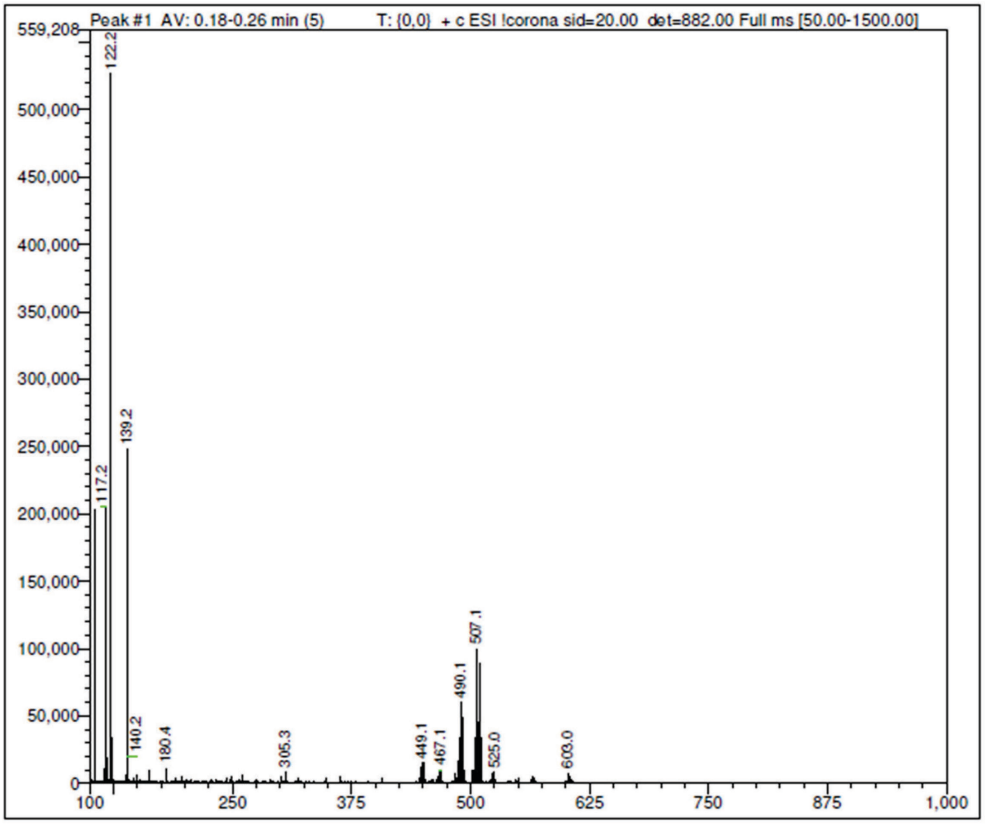

*Figure S.VII.10. Mass spectrometry after red light irradiation of **M1-3-6** liposomes (DMPC = 20 mM). After 60 min irradiation with 150 mW 630 nm light (1.2 W.cm⁻²) at 37 °C under argon, the liposome solution was filtered with a centrifuge filter (MWCO = 100,000 Da), the filtrate was lyophilized and redissolved in a minimal amount of acetone. Attribution of main peaks in m/z (calculated): 449.1 $[Ru(bpy)_2Cl]^+$ (449.0); 467.1 $[Ru(bpy)_2Cl(OH_2)]^+$ (467.0); 490.1 $[Ru(bpy)_2(OH_2)(OH)]^+$(MeCN) (490.1); 507.1 $[Ru(bpy)_2(acetone)Cl]^+$ (507.1) or $[Ru(bpy)_2(OH_2)(OH)]^+$(acetone) (507.1).*

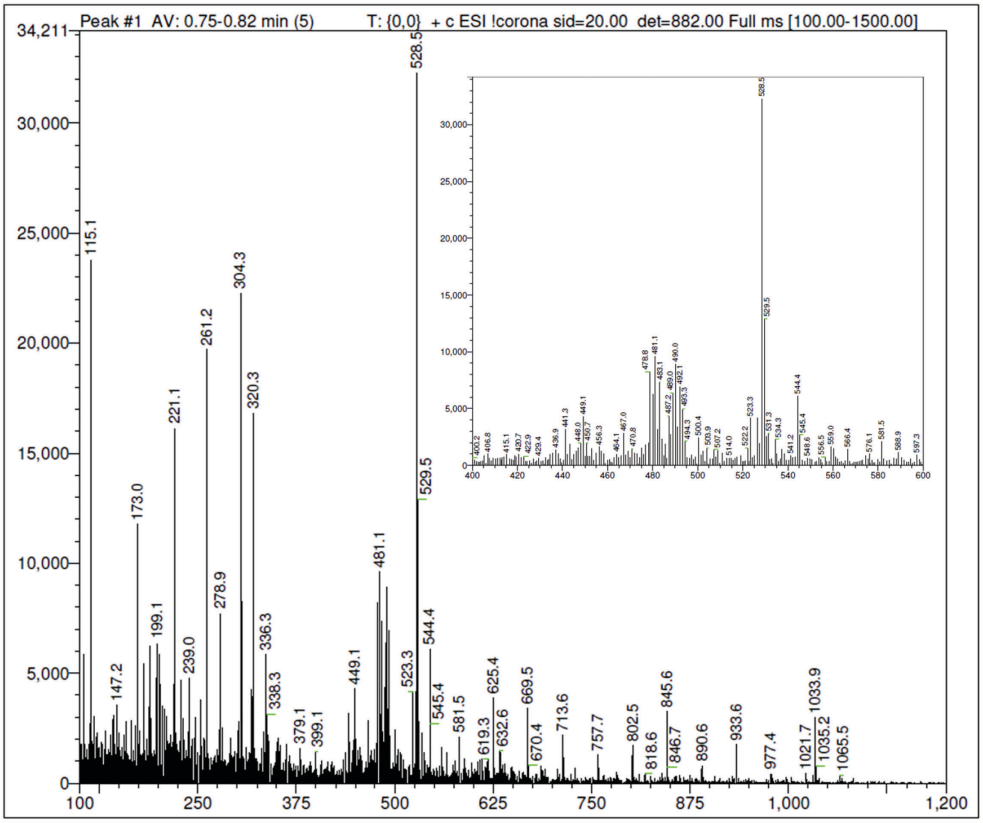

*Figure S.VII.11. Mass spectrometry after red light irradiation of **M1-3-6** liposomes (DMPC = 20 mM) in presence of 10 mM L-Asc and GSH. After 60 min irradiation with 150 mW 630 nm light (1.2 W.cm^{-2}) at 37 °C under argon, the liposome solution was filtered with a centrifuge filter (MWCO = 100,000 Da), the filtrate was lyophilized and redissolved in a minimal amount of methanol. Attribution of main peaks in m/z (calculated): 481.1 [Ru(bpy)$_2$(MeOH)Cl]$^+$ (481.0) or [Ru(bpy)$_2$(OH$_2$)$_2$]$^{2+}$(MeO$^-$) (481.1); 490.0 [Ru(bpy)$_2$(OH$_2$)(OH)]$^+$(MeCN) (490.1). The rest of the signals do not contain a ruthenium isotope pattern.*

VII.8. References

[1] M. Almgren, *J. Am. Chem. Soc.* **1980**, *102*, 7882-7887.

[2] A. Bahreman, B. Limburg, M. A. Siegler, E. Bouwman, S. Bonnet, *Inorg. Chem.* **2013**, *52*, 9456-9469.

[3] A. Bahreman, J.-A. Cuello-Garibo, S. Bonnet, *Dalton Trans.* **2014**, *43*, 4494-4505.

APPENDIX VIII: SUPPORTING INFORMATION FOR CHAPTER 9

VIII.1. Synthesis and characterization of PiB-PEG-Me block copolymers

VIII.1.1. Synthesis

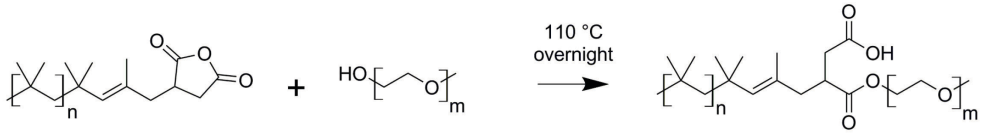

PiB_{1000}-SA PEG_x-Me PiB_{1000}-PEG_x-Me
3: x = 350
4: x = 750

Scheme S.VIII.1. Synthesis of PiB-b-PEG-Me block copolymers 3 and 4 from polyisobutylene succinic anhydride (PiB_{1000}-SA) and mono-methoxy ethylene glycol (PEG_{350}-Me or PEG_{750}-Me).

VIII.1.2. Molecular weights

*Table S.VIII.1. Molecular weights of PiB_{1000}-SA, PEG_{350}-Me, PEG_{750}-Me, and compounds **3** and **4** in weight averaged molecular weight (M_w) and number averaged molecular weight (M_n), according to the manufacturer, gel permeation chromatography (GPC), and NMR, see sections VIII.1.3 and VIII.1.4. Gel permeation chromatography was done in THF with molecular weights reported relative to polybutadiene standards.*

Polymer	**Manufacturer**	**GPC**		**^{1}H NMR**
	M_n (kg.mol^{-1})	M_n (kg.mol^{-1})	PDI (M_w/M_n)	M_n (kg.mol^{-1})
PiB_{1000}-SA	1.05	0.95	1.71	1.11[a]
PEG_{350}-Me	0.35	N/A	N/A	0.36[b]
PEG_{750}-Me	0.75	N/A	N/A	0.80[b]
3	-	1.32	1.50	1.25[b]
4	-	1.18	1.54	2.11[b]

[a] Based on normalization of the alkene signal at 4.6 – 5.3 ppm as 1 proton. [b] Based on normalization of the terminal methyl peak at 3.2 ppm as 3 protons.

For the GPC results, we expected M_n of **4** to have a value in the range of 1.50 to 2.00 kg/mol, but found a value of 1.18 kg/mol. We attribute this to the greater molecular weight of the hydrophilic fraction.

VIII.1.3. Gel Permeation Chromatography (GPC)

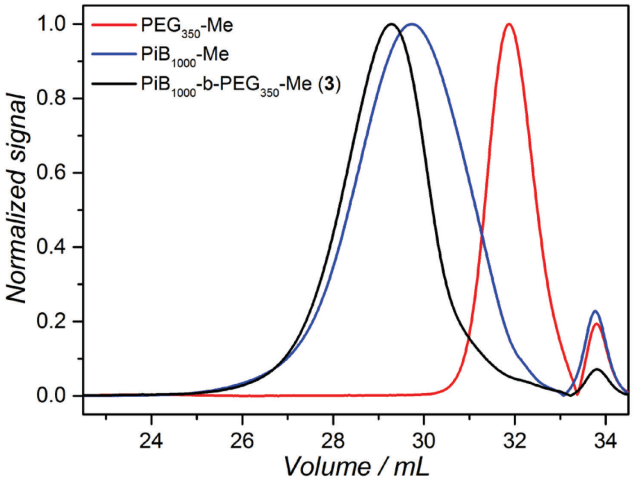

*Figure S.VIII.1. Elugram of monomethyl polyethylene glycol (PEG_{350}-Me, red), polyisobutylene-succinic anhydride (PiB_{1000}-SA, blue), and compound **3** (black).*

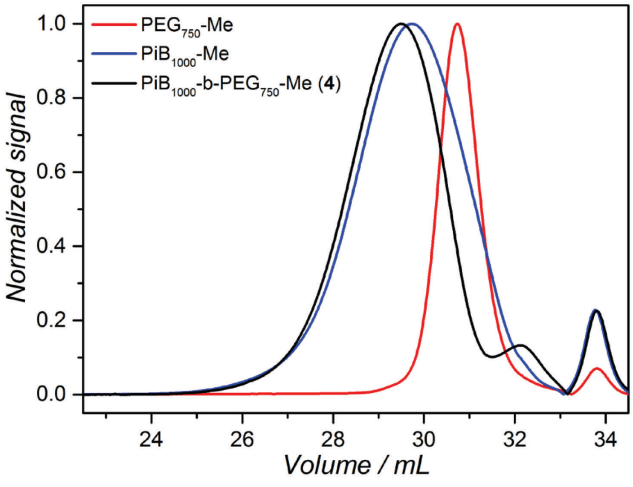

*Figure S.VIII.2. Elugram of monomethyl polyethylene glycol (PEG_{750}-Me, red), polyisobutylene-succinic anhydride (PiB_{1000}-SA, blue), and compound **4** (black).*

VIII.1.4. NMR Spectroscopy

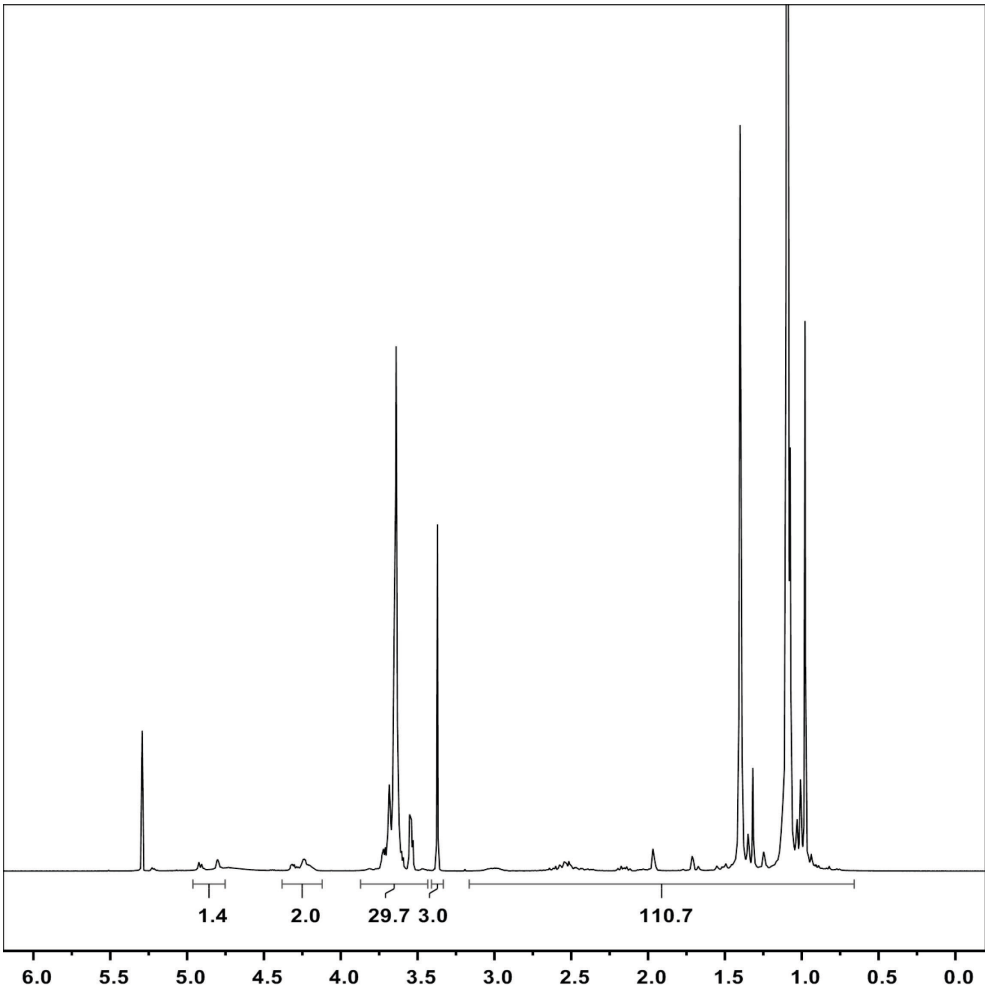

*Figure S.VIII.3. ^{1}H NMR spectrum of compound **3** (PiB_{1000}-b-PEG_{350}-Me) in $CDCl_3$. Attribution: δ (ppm) 4.9 – 4.8 (1 H, C=C of PiB), 4.3 – 4.1 (2 H, alpha protons of the ester), 3.8 – 3.5 (30 H, PEG) 3.4 (3 H, O-CH_3 of PEG-Me), 3.1 – 2.9; 2.8 – 2.4; 2.3 – 2.1; 2.1 – 0.8 (111 H, methyl and methylene of PiB). The spectrum corresponds to literature data.[1]*

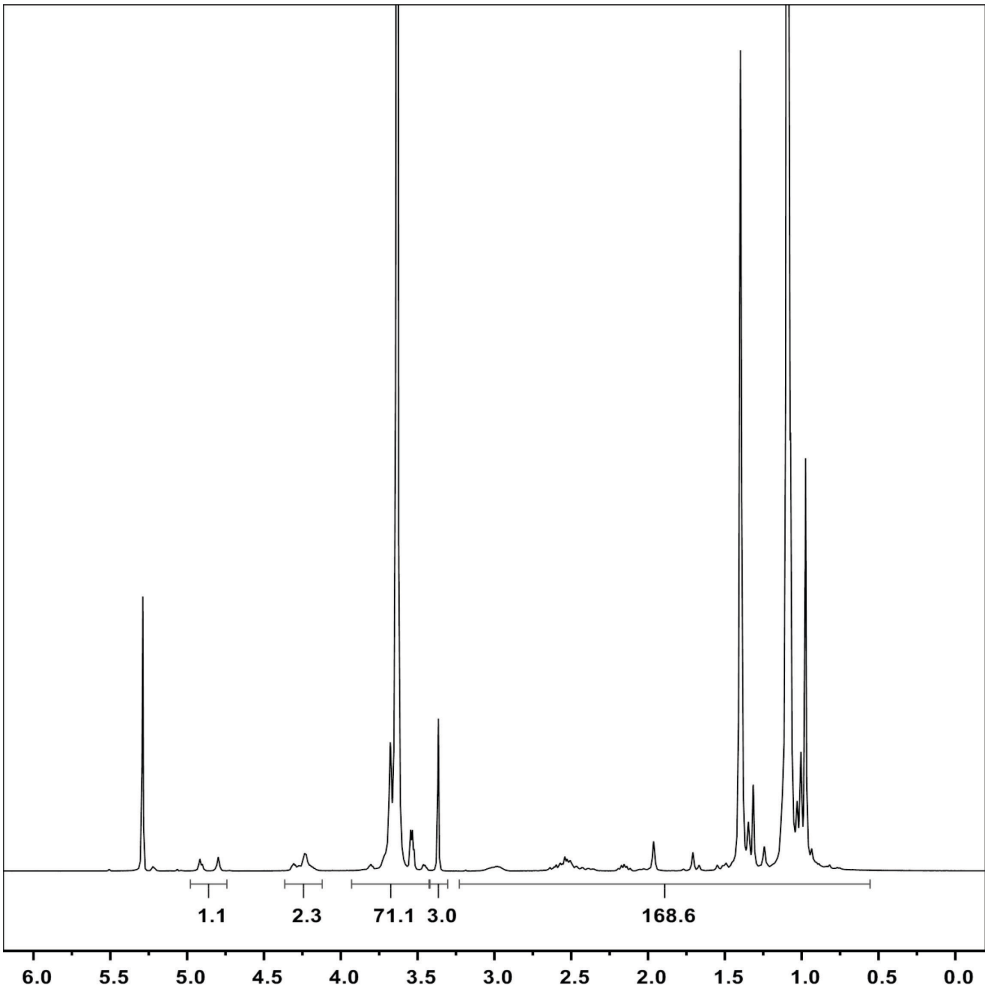

*Figure S.VIII.4. ^{1}H NMR spectrum of compound **4** (PiB_{1000}-b-PEG_{750}-Me) in $CDCl_3$. Attribution: δ (ppm) 4.9 – 4.8 (1 H, C=C of PiB), 4.3 – 4.1 (2 H, alpha protons of the ester), 3.8 – 3.5 (71 H, PEG) 3.4 (3 H, O-CH_3 of PEG-Me), 3.1 – 2.9; 2.8 – 2.4; 2.3 – 2.1; 2.1 – 0.8 (169 H, methyl and methylene of PiB). The spectrum corresponds to literature data.[1]*

VIII.1.5. IR Spectroscopy

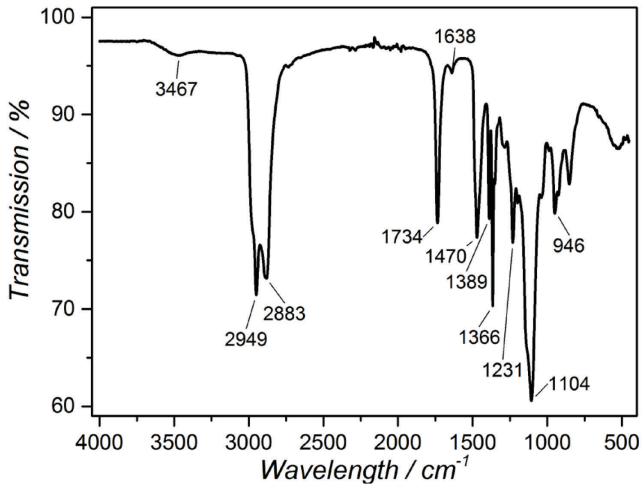

*Figure S.VIII.5. Infrared spectrum of **3** (PiB_{1000}-b-PEG_{350}-Me). Peak assignment (cm^{-1}): 3467 (OH), 2949, 2883 (C-H), 1734 (C=O), 1638 (C=C), 1470, 1389, 1366, 1231 (PiB skeleton), and 1104 (C-O of PEG). The spectrum corresponds to literature data.[1]*

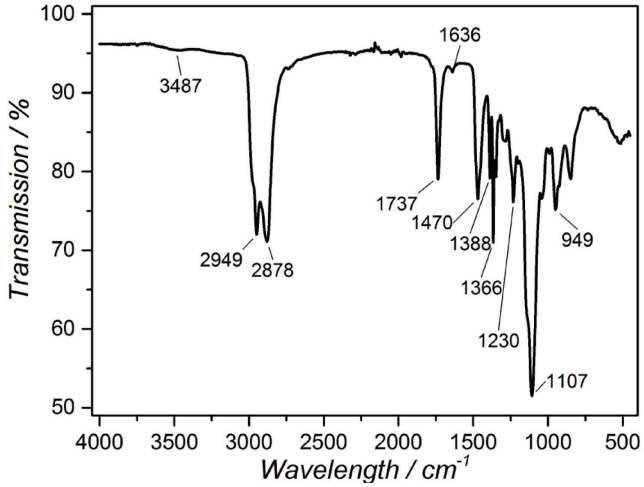

*Figure S.VIII.6. Infrared spectrum of **4** (PiB_{1000}-b-PEG_{750}-Me). Peak assignment (cm^{-1}): 3487 (OH), 2949, 2878 (C-H), 1737 (C=O), 1636 (C=C), 1470, 1388, 1366, 1230 (PiB skeleton), and 1107 (C-O of PEG). The spectrum corresponds to literature data.[1]*

VIII.2. Transmission electron microscopy images of vesicles

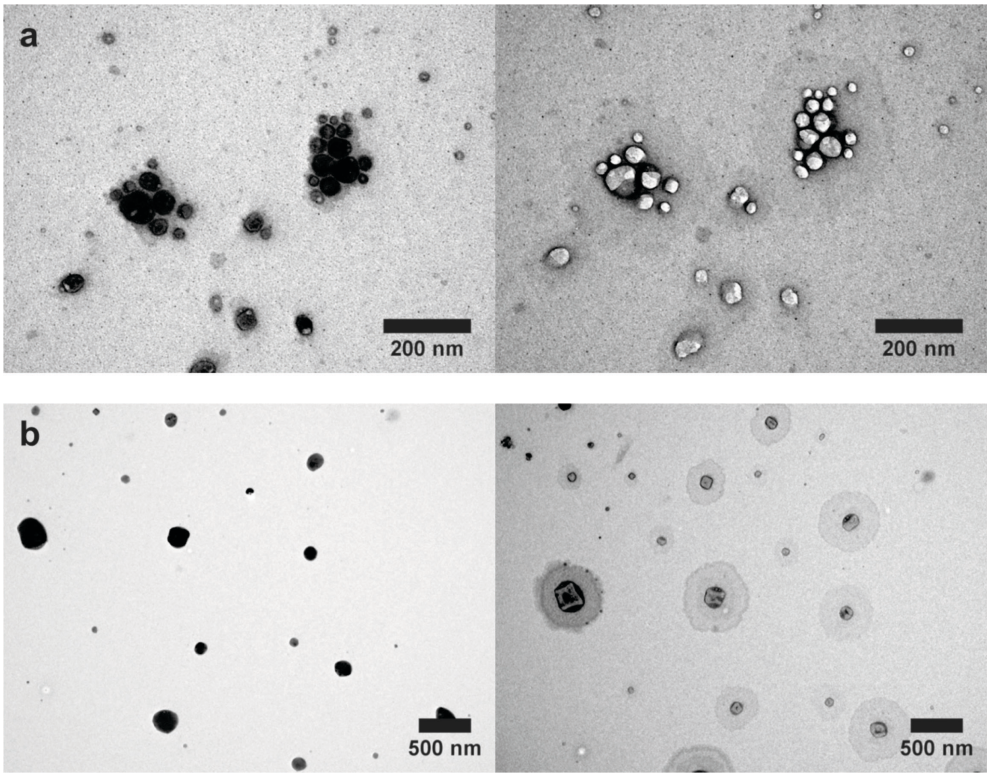

*Figure S.VIII.7. TEM micrographs of **P3** (a) and **P4** (b) vesicles in intact state (left) and after 2 minutes when the vesicles had collapsed and dried out under influence of the electron beam in the transmission electron microscope (right). Note the ring of salt around the vesicles after drying out, indicating the escape of salty water from the vesicles' interior. No TEM-stain was needed to visualize the vesicles.*

VIII.3. Upconversion with 1 and 2 in organic solvent

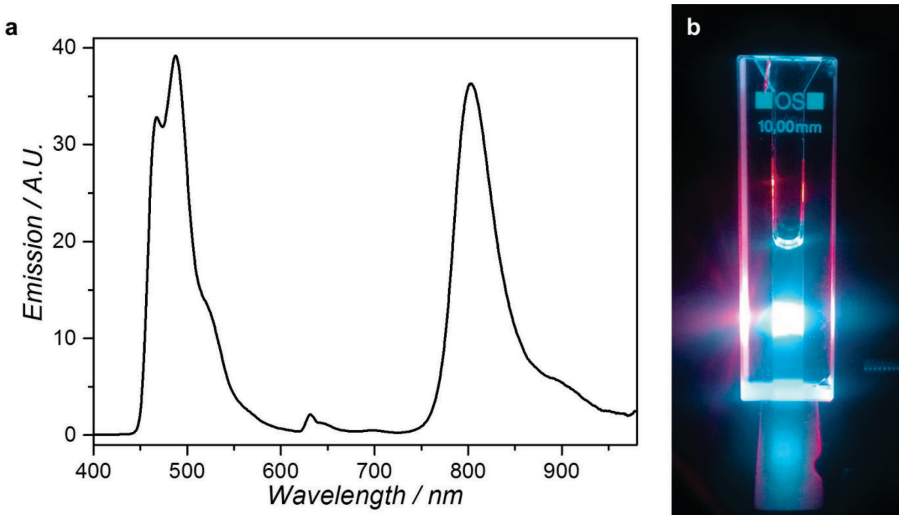

*Figure S.VIII.8. a) Emission spectroscopy of **1** and **2** in a 3:1 v/v chloroform/oleic acid mixture ([**1**] = 7.5 μM, [**2**] = 150 μM) in air, irradiated with 50 mW 630 nm laser light (4 mm beam diameter, 0.4 W.cm^{-2}) in a macro cuvette at 20 °C. No emission filters were used. b) Photograph of the same solution in a semi-micro cuvette, irradiated with a 50 mW 630 nm laser beam (4 mm beam diameter, 0.4 W.cm^{-2}) from the left side. The photograph was taken without filtering the excitation source.*

VIII.4. Compounds 1 and 2 in organic solvent

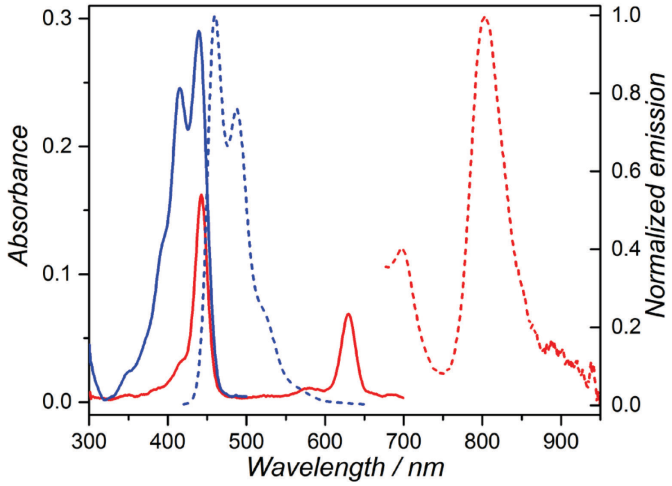

*Figure S.VIII.9. UV-Vis absorbance (solid lines) and emission (dashed lines) spectroscopy of **1** and **2** in chloroform. [**1**] = 0.5 μM, [**2**] = 10 μM. λ_{exc} = 405 nm for compound **2** and λ_{exc} = 630 nm for compound **1**.*

VIII.5. Compounds 1 and 2 in polymersomes

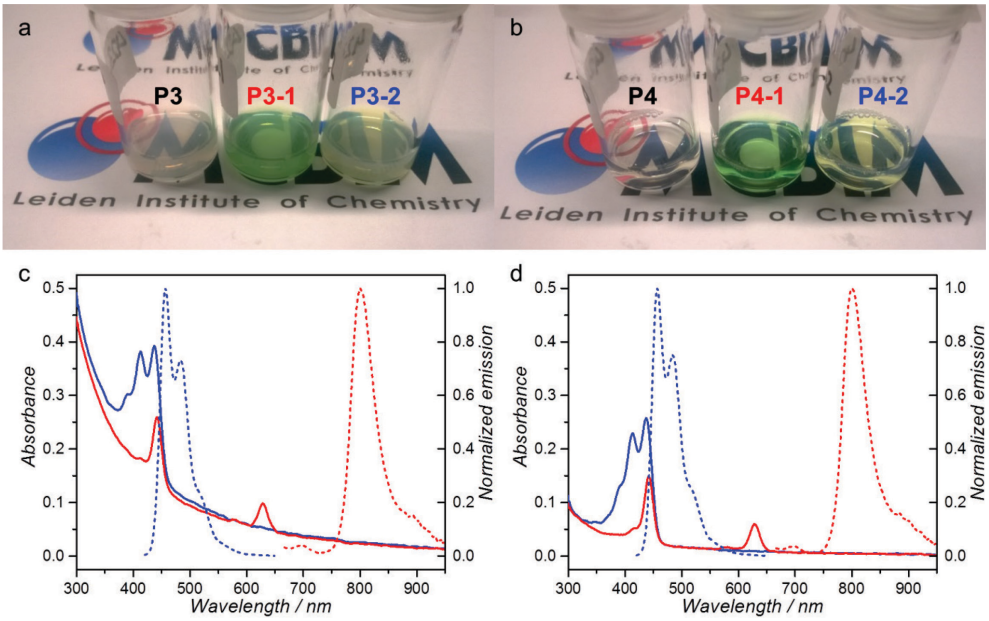

*Figure S.VIII.10. a) Photograph of samples **P3**, **P3-1**, and **P3-2**. b) Photograph of samples **P4**, **P4-1**, and **P4-2**. c) UV-Vis absorbance (solid lines) and normalized emission (dashed lines) of samples **P3-1** (red) and **P3-2** (blue). d) UV-Vis absorbance (solid lines) and normalized emission (dashed lines) of samples **P4-1** (red) and **P4-2** (blue). Conditions: [**3**] = [**4**] = 0.5 mg/mL, [**1**] = 0.5 μM, [**2**] = 10 μM, T = 20 °C, λ_{exc} = 405 nm for **P3-2** and **P4-2** and λ_{exc} = 630 nm for **P3-1** and **P4-1**. Spectra taken in air without anti-oxidants.*

VIII.6. Giant vesicles

To investigate whether TTA-UC truly occurs in the polymer membrane, giant polymersomes with polymer **3** were prepared by following a procedure for self-assembly of phospholipid giant vesicles to make giant polymersomes **GP3-1-2**,[2] and imaged by bright field and emission spectroscopy. First, the vesicles were imaged in a regular fluorescence microscope at 20x magnification and λ_{exc} = 377 nm (Figure S.VIII.11). The bright field images showed microscale spherical vesicles. When excited at 377 nm (*i.e.* direct excitation of **2**), bright fluorescence was observed from the membrane, which proves that **2** was indeed located inside the membrane. Then, the vesicles were imaged with a laser microscopy setup (see experimental section) with 405 and 635 nm excitation in presence of 0.1 M sodium sulfite (Figure S.VIII.12). The addition of the sulfite after GUV preparation caused the vesicles to shrink significantly (compare Figure S.VIII.11 with Figure S.VIII.12), but they could be imaged nonetheless. Again, bright fluorescence was observed

from the membrane when **2** was excited directly (λ_{exc} = 405 nm). The giant vesicles were also illuminated with 635 nm laser light, while selectively imaging between 450 – 575 nm: upconversion emission was indeed detected in the membrane, completely superimposable with the bright field and 405 nm excitation images and ultimately proving that **1** and **2** were co-localized in the polymer membrane. In control experiments, in which **2** was omitted from the formulation (**GP3-1**), only very weak luminescence with 405 nm excitation was observed, due to phosphorescence of **1** at 800 nm that is not entirely blocked with the dichroic mirror and emission filter used for 405 nm excitation. However, no emission was observed with 635 nm excitation, due to strict blocking of everything but 450 – 575 nm. This confirmed that our microscopy setup was indeed selectively imaging upconversion emission under 635 nm excitation.

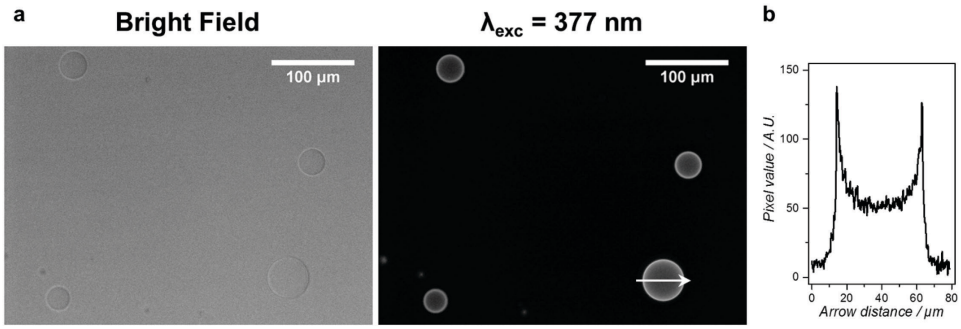

*Figure S.VIII.11. a) Bright field (left) and emission spectroscopy (right, λ_{exc} = 377 nm) of giant polymersomes **GP3-1-2**. The profile plot of the white arrow is given in (b).*

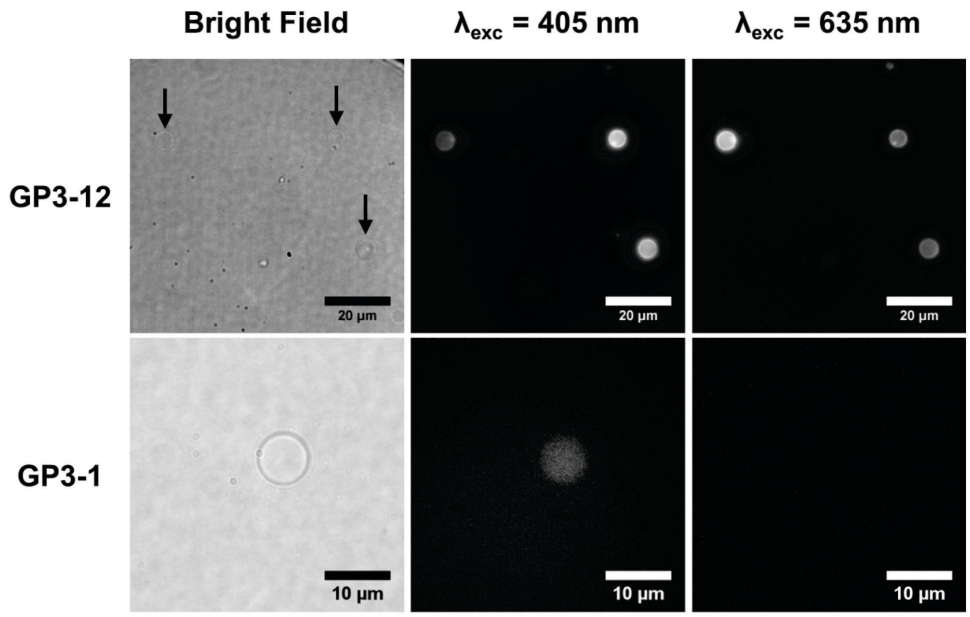

Figure S.VIII.12. Bright field and emission microscopy images of giant polymersomes ***GP3-1-2*** *(top) and* ***GP3-1*** *(bottom). Left: Bright field image. The vesicles are indicated with arrows. Middle: fluorescence microscopy by directly exciting compound* ***2*** *with 405 nm light (6.7 µW, 60 µm spot size, intensity 0.24 W.cm^{-2}). Right: upconversion microscopy by exciting compound* ***1*** *with 635 nm light (13 mW, 50 µm spot size, intensity 640 W.cm^{-2}) and imaging from 450 to 575 nm. The images were acquired in air in presence of 0.1 M Na_2SO_3.*

VIII.7. Temperature dependency of TTA-UC in polymersomes

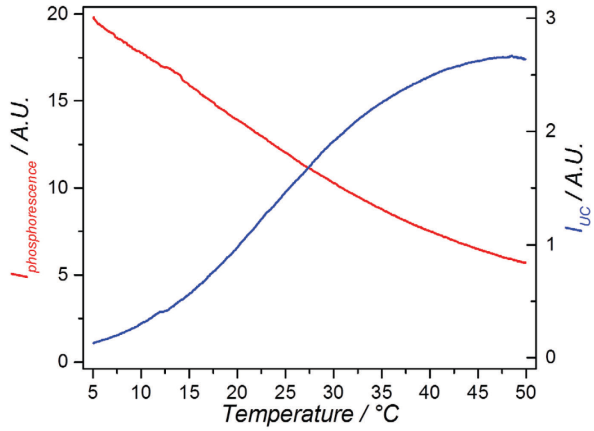

*Figure S.VIII.13. Temperature dependency of phosphorescence (red) and upconversion emission (blue) in **P4-1-2** vesicles (0.5 mg/mL compound **4**) irradiated with 50 mW 630 nm (4 mm diameter, 0.4 W.cm^{-2}) in presence of 50 mM sodium sulfite. Experiment with **P3-1-2** vesicles yielded very similar results.*

VIII.8. Power dependency of TTA-UC in polymersomes

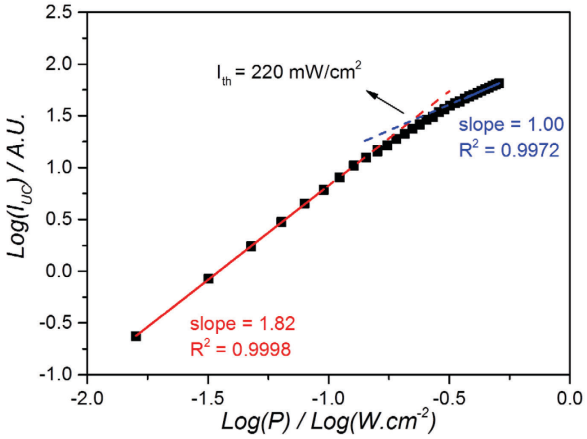

*Figure S.VIII.14. Power dependency of upconversion emission in **P4-1-2** vesicles (0.5 mg/mL compound **4**) at 20 °C. The red and blue lines are straight fit curves through the first and last data points, respectively, where the intersection of the two lines represent the intensity threshold (I_{th}). Experiment with **P4-1-2** at 37 °C, and experiments with **P3-1-2** at 20 °C and 37 °C yielded very similar results.*

VIII.9. Time evolution of upconversion with P3-1-2 and P4-1-2 in air and dye bleaching

VIII.9.1. P3-1-2 vesicles

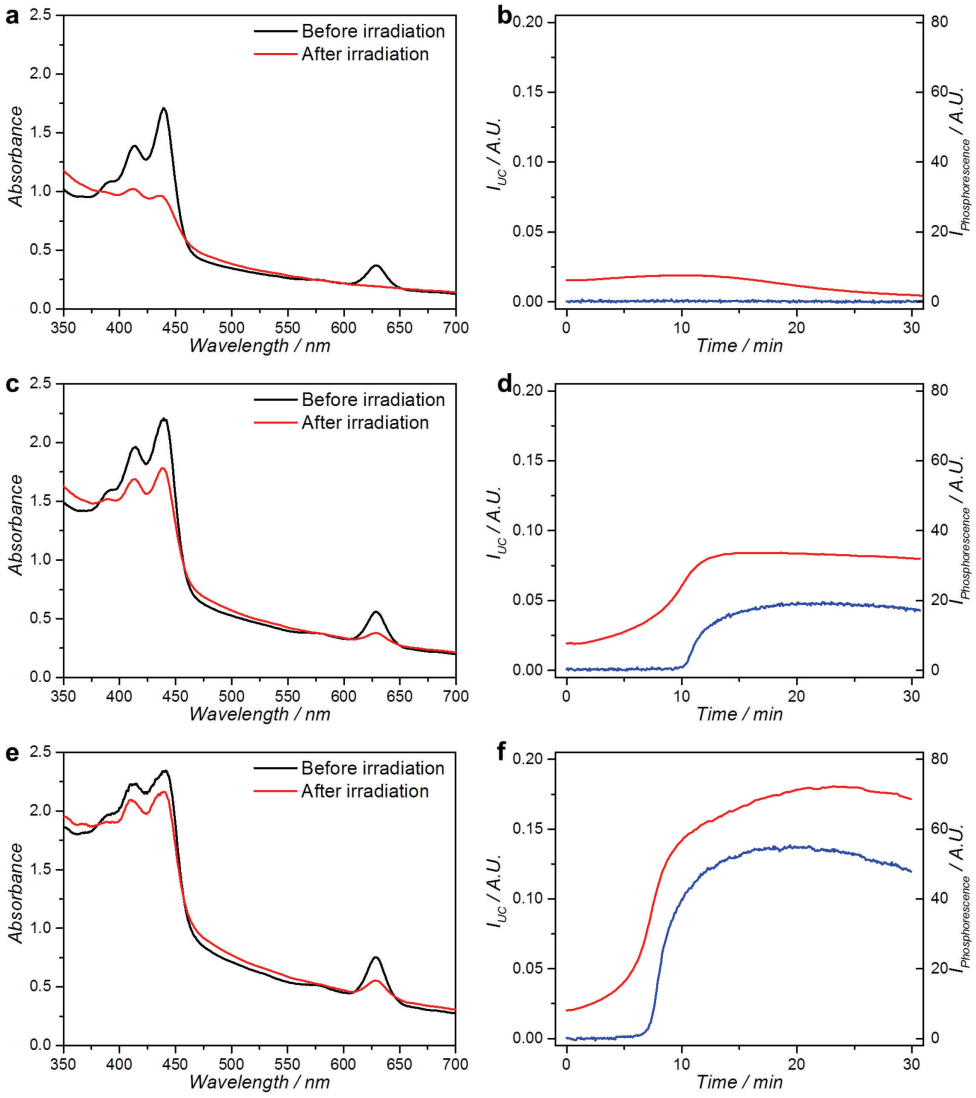

*Figure S.VIII.15. Red-light irradiation of **P3-1-2** vesicles at 5.0 (a, b), 7.5 (c, d), and 10 mg/mL (e, f) in air and in absence of added oxygen-scavenger. UV-Vis absorption spectra (a, c, e, 4 mm path length) before (black) and after (red) 30 min 630 nm irradiation (50 mW, 0.4 W.cm^{-2}, 4 mm path length) showing dye bleaching. Emission time traces (b, d, f) during the irradiation experiment, showing I_{UC} (blue, left axis) and $I_{phosphorescence}$ (red, right axis). Conditions: 600 µL sample in a semi-micro cuvette at 20 °C.*

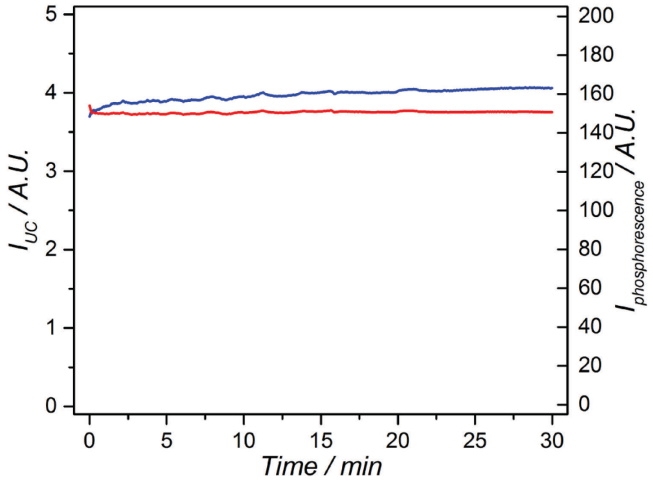

Figure S.VIII.16. Emission time traces of a 7.5 mg/mL ***P3-1-2*** *sample with addition of 75 mM* Na_2SO_3 *as oxygen scavenger, showing* I_{UC} *(blue, left axis) and* $I_{phosphorescence}$ *(red, right axis), during 50 mW 630 nm (0.4 W.cm*$^{-2}$*, 4 mm path length) irradiation.*

VIII.9.2. P4-1-2 vesicles

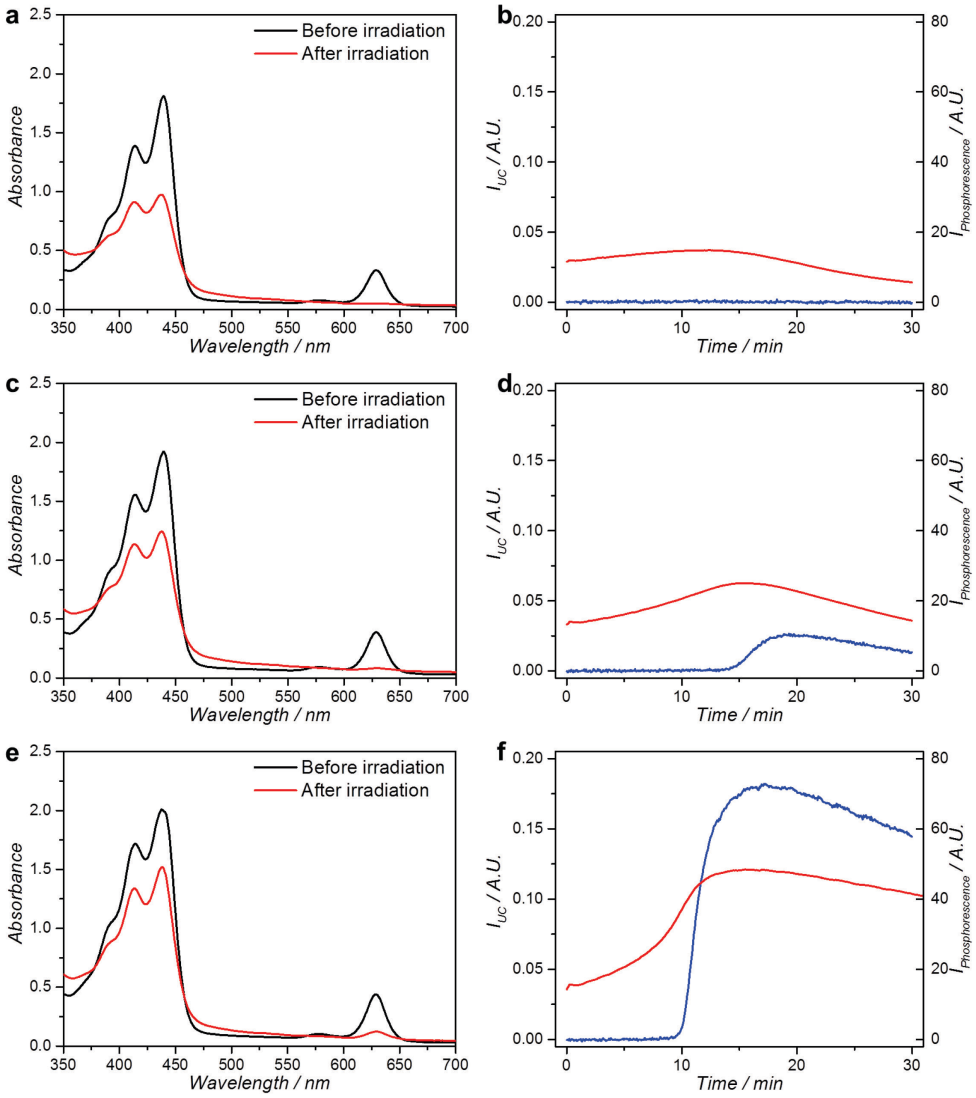

*Figure S.VIII.17. Red light irradiation experiments with **P4-1-2** vesicles at 7.5 (a, b), 8.8 (c, d), and 10 mg/mL (e, f) in air without added anti-oxidants. UV-Vis absorption spectra (a, c, e, 4 mm path length) before (black) and after (red) 30 min 630 nm irradiation (50 mW, 0.4 W.cm^{-2}, 4 mm path length) showing bleaching. Emission time traces (b, d, f) during the irradiation experiment, showing I_{UC} (blue, left axis) and $I_{phosphorescence}$ (red, right axis). Conditions: 600 µL sample in a semi-micro cuvette at 20 °C.*

VIII.10. Oxygen consumption during red light irradiation of P3-1-2 and P4-1-2 in air

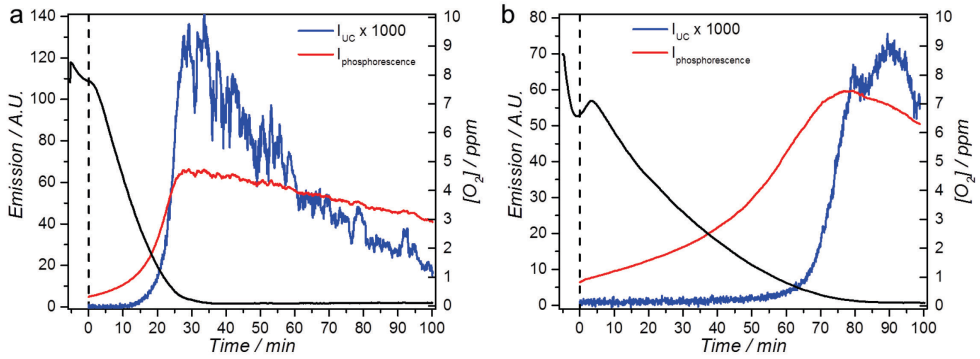

*Figure S.VIII.18. Upconversion intensity I_{UC} (blue, data multiplied by 1000 for clarity, left axis), phosphorescence intensity $I_{phosphorescence}$ (red, left axis), and dissolved oxygen concentration (black, right axis, measured using a submerged oxygen probe) during 50 mW 630 nm light irradiation (10 mm path length, 4 mm beam diameter, 0.4 W.cm^{-2}) of 2.0 mL samples of **P3-1-2** (a) or **P4-1-2** (b) at 10 mg/mL polymer concentration in a stirred macro cuvette at 20 °C. Laser was turned on at t = 0, as indicated by the dashed line, and I_{UC} and $I_{phosphorescence}$ were recorded at 486 and 800 nm, respectively.*

VIII.11. Oxygen and emission time traces of diluted samples of P4-1-2 without addition of oxygen scavengers

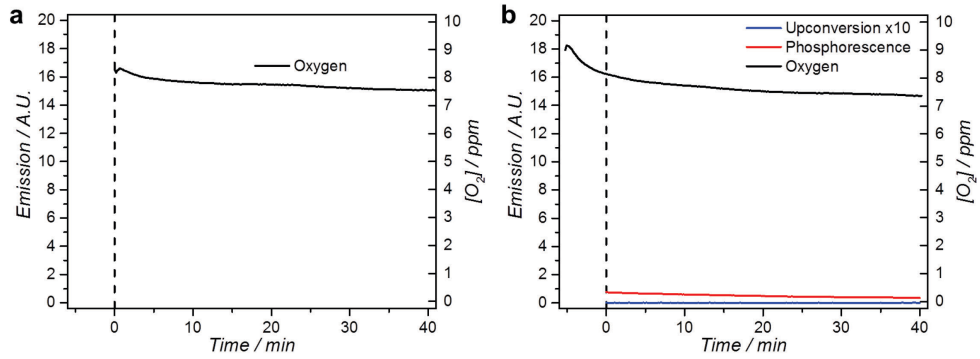

*Figure S.VIII.19. Oxygen measurement of a **P4-1-2** sample without the addition of oxygen scavengers in the dark (left) and during 50 mW 630 nm (0.4 W.cm^{-2}) excitation (right). Red and blue line represent photosensitizer phosphorescence at 800 nm and upconversion emission at 486 nm, respectively. **[4]** = 0.5 mg/mL, **[1]** = 0.5 µM, **[2]** = 10 µM, T = 20 °C, 2 mL sample volume in a stirred macro cuvette. Laser was turned on at t = 0, as indicated by the dashed line.*

VIII.12. Cell imaging with upconverting polymersomes

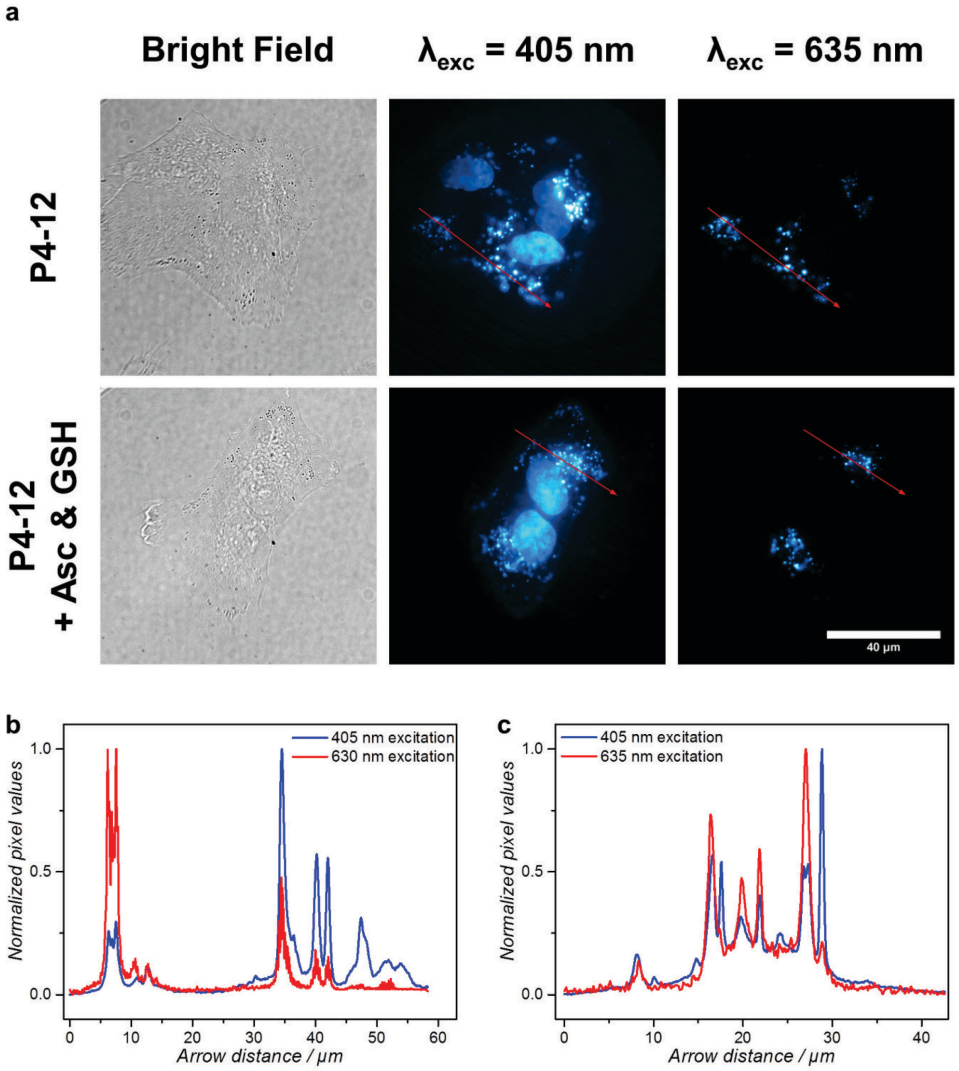

*Figure S.VIII.20. a) Imaging of **P4-1-2** upconverting polymersomes in A549 lung carcinoma cells in bright field mode (left column), with λ_{exc} = 405 nm (middle column), and with λ_{exc} = 635 nm (right column). Cells were incubated for 4 h with 1:1 v/v mixture of Opti-MEM and **P4-1-2** vesicles (top row, [**4**] = 0.5 mg/mL), or with 1:1 v/v mixture of Opti-MEM and **P4-1-2** vesicles ([**4**] = 0.5 mg/mL) and addition of 5 mM sodium L-ascorbate and 5 mM sodium glutathionate (bottom row). The cell nuclei were stained with Hoechst 33342 prior to imaging (1 µg/mL in PBS, incubated for 20 min). Imaging conditions: T = 37 °C, 7.0% CO_2, 1.0% O_2, 62 µW 405 nm laser power (60 µm spot diameter, 2.2 W.cm^{-2} intensity), 13 mW 635 nm laser power (50 µm spot diameter, 640 W.cm^{-2} intensity), cells were allowed to equilibrate for 30 min before imaging. b/c) Profile plots of the red arrows in panel [a] in absence (b) or presence (c) of sodium L-ascorbate and sodium glutathionate, with 405 nm (blue line) or 635 nm excitation (red line).*

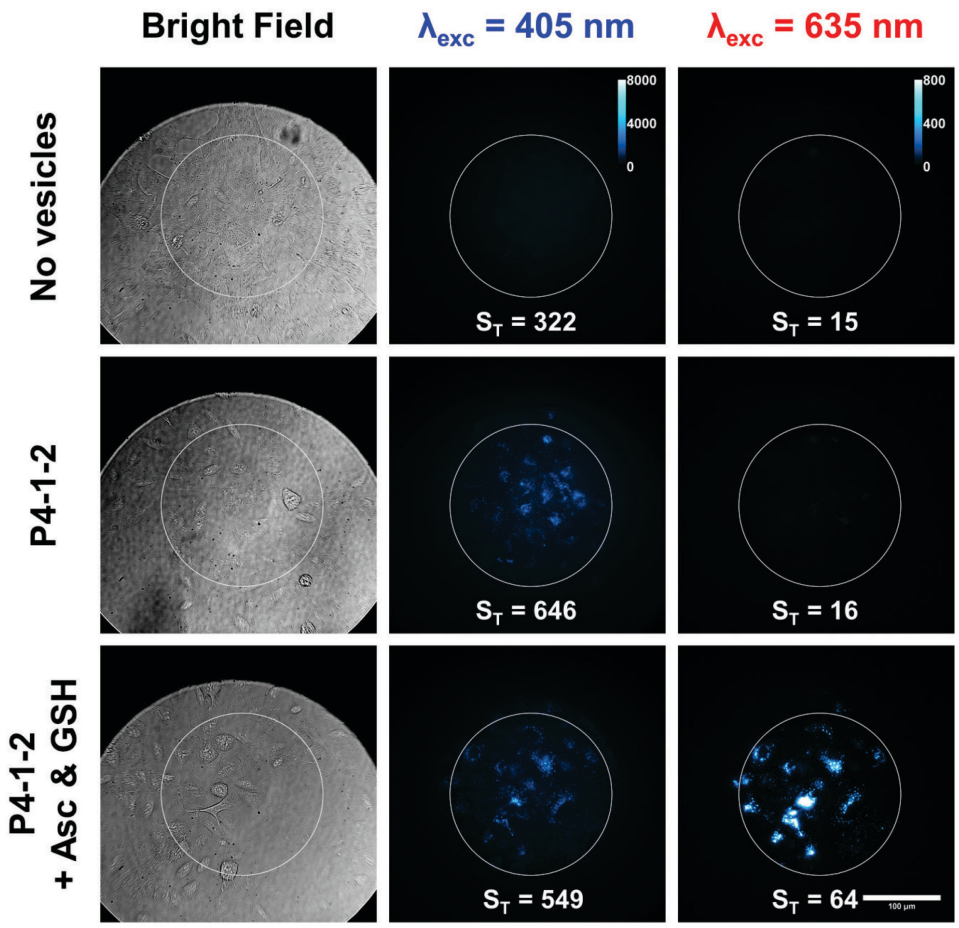

Figure S.VIII.21. Example images used for quantification of in vitro upconversion luminescence. Imaging of ***P4-1-2*** *upconverting polymersomes in A549 lung carcinoma cells in bright field mode (left column), with* λ_{exc} *= 405 nm (middle column), and with* λ_{exc} *= 635 nm (right column) with 40x magnification. Cells were incubated for 4 h with Opti-MEM only (top row),with 1:1 v/v mixture of Opti-MEM and* ***P4-1-2*** *vesicles (middle row, [4] = 0.5 mg/mL), or with 1:1 v/v mixture of Opti-MEM and* ***P4-1-2*** *vesicles ([****4****] = 0.5 mg/mL) and addition of 5 mM sodium L-ascorbate and 5 mM sodium glutathionate (bottom row). Imaging conditions: T = 37 °C, 7.0%* CO_2*, 1.0%* O_2*, 76 µW 405 nm laser power (150 µm spot diameter, 0.44* $W.cm^{-2}$ *intensity), 13 mW 635 nm laser power (131 µm spot diameter, 97* $W.cm^{-2}$ *intensity), cells were allowed to equilibrate for 30 min before imaging. For comparison, the image histograms for* λ_{exc} *= 405 nm are scaled from 0 – 8000 pixel values, and for* λ_{exc} *= 635 nm are scaled from 0 – 800 pixel values, as given by the calibration bars in the top row. In each image, the region of interest (ROI) is indicated with a white circle, and the total signal* S_T *(in mean pixel value) within the ROI is given.*

VIII.13. Emission spectroscopy setup

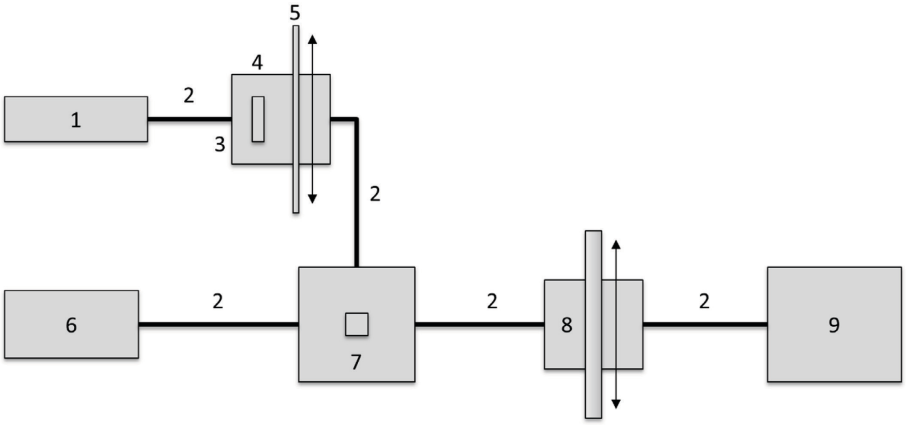

Figure S.VIII.22. Setup used for photosubstitution experiments using red light. Legend: (1) 630 nm laser source, (2) optical fibers, (3) filter holder, (4) 630 nm band pass filter, (5) variable neutral density filter that can be installed or removed, (6) halogen-deuterium light source for UV-Vis absorption spectroscopy, (7) temperature controlled cuvette holder, (8) variable filter holder, and (9) CCD spectrometer.

VIII.14. References

[1] U. Karl, C. Sierakowski, M. Darijo, M. Haberer, H. Hartl, Use Of Amphiphilic Block Copolymers For Producing Polymer Blends, **2008**, 20080293886

[2] a) S. H. C. Askes, N. Lopez Mora, R. Harkes, R. I. Koning, B. Koster, T. Schmidt, A. Kros, S. Bonnet, *Chem. Commun.* **2015**, *51*, 9137-9140; b) N. Lopez Mora, J. S. Hansen, Y. Gao, A. A. Ronald, R. Kieltyka, N. Malmstadt, A. Kros, *Chem. Commun.* **2014**, *50*, 1953-1955.

Inleiding

Chemotherapie is een van de voornaamste therapieën om kanker te genezen. De huidige chemotherapeutische geneesmiddelen die goedgekeurd zijn voor klinische toepassing veroorzaken echter ernstige bijwerkingen in patiënten omdat de drugs systemisch actief zijn in het lichaam en daardoor ook gezond weefsel aantasten. Een veelbelovende manier om het probleem van systemische giftigheid te omzeilen is het gebruik van lichtactiveerbare "prodrugs" in een therapie genaamd lichtgeactiveerde chemotherapie (PACT): een inactieve voorloper van het geneesmiddel wordt in het lichaam geïntroduceerd en wordt alleen in de tumor omgezet naar de giftige vorm van het geneesmiddel door het kankerweefsel te bestralen met zichtbaar licht. Op deze manier kan het gebruik van licht zorgen voor een uitstekende controle over waar en wanneer de prodrug geactiveerd wordt. Veelbelovende moleculen voor toepassing in PACT zijn lichtgevoelige ruthenium(II)-polypyridylcomplexen met een ligand dat met licht afgesplitst kan worden (Hoofdstuk 1). Wanneer zulke verbindingen worden bestraald met licht, wordt het lichtafsplitsbare ligand vervangen door een zwakgebonden watermolecuul. Vervolgens kan het geactiveerde complex interactie aangaan met diverse biomoleculen aanwezig in het menselijk lichaam door het vervangen van het waterligand met stikstof of zwavelrijke liganden, zoals DNA-baseparen of cysteïneresiduen in eiwitten, wat uiteindelijk kan leiden tot celdood. Het grote voordeel van dit soort verbindingen is dat de giftigheid niet afhangt van de aanwezigheid van zuurstof, in tegenstelling tot fotodynamische therapie (PDT) wat werkt door reactieve zuurstofdeeltjes (ROS) te genereren. Het gebruik van lichtactiveerbare Ru complexen kan dus geschikt zijn voor het behandelen van tumorweefsel waarvoor PDT niet effectief is.

De meeste Ru(II)-polypyridylcomplexen absorberen echter alleen blauw tot groen licht, wat slechts tot ongeveer een millimeter in menselijk weefsel doordringt. Idealiter gebruikt men rood tot nabij-infrarood licht, wat tot wel een centimeter doordringt: daardoor wordt dit deel van het lichtspectrum ook wel het "fototherapeutische venster" genoemd. Om de activatiegolflengte van Ru(II)-polypyridylcomplexen naar het fototherapeutische venster te verschuiven, wordt in dit proefschrift voorgesteld om "lichtopwaardering" te

gebruiken om laag-energetisch licht, zoals rood of nabij-infrarood licht, om te zetten naar hoog-energetisch licht, zoals blauw licht. Praktisch gezien betekent dit dat de tumor wordt bestraald met rood tot nabij-infrarood licht, wat lokaal wordt opgewaardeerd naar blauw licht, waarmee de prodrug kan worden geactiveerd. Onder de verscheidene vormen van lichtopwaardering is "triplet-triplet annihilatie upconversie" (TTA-UC) verkozen als meest veelbelovende methode omdat het gerealiseerd kan worden bij lage bestralingsintensiteit en met hoge efficiëntie.

TTA-UC is gebaseerd op het samenspel van fotosensibilisator en annihilator kleurstoffen, zoals als volgt beschreven (zie ook Hoofdstuk 2). De fotosensibilisator absorbeert het laag-energetische licht, waarna intersysteemkruising leidt tot het molecuul in een langlevende triplet-toestand. Wanneer deze triplet-fotosensibilisator botst met een annihilatormolecuul, wordt de triplet-toestand overgedragen aan de annihilator door middel van triplet-triplet energie overdracht (TTET); een opeenvolging van dit TTET proces zorgt voor een concentratieopbouw van langlevende triplet-toestand annihilatormoleculen. De botsing van twee triplet-toestand annihilatormoleculen resulteert vervolgens in triplet-triplet annihilatie (TTA), waarbij één van de annihilatormoleculen vertrekt met de gecombineerde energie van beide triplet-toestanden en een hoog-energetische aangeslagen singlet-toestand bereikt. Deze singlet-toestand annihilator keert vervolgens terug naar de grondtoestand door uitstraling van een hoog-energetisch foton, waarbij de licht opwaardering tot stand is gebracht. In dit proefschrift wordt voorgesteld om rood-naar-blauw TTA-UC te gebruiken om een licht-gevoelig Ru(II)-polypyridylcomplex te activeren door de fotosensibilisator, annihilator, en Ru(II)-complex gezamenlijk te doteren in een nano-geneesmiddelafgiftesysteem zoals liposomen of polymeersomen. Dit heeft twee belangrijke voordelen: aan de ene kant zorgt deze supramoleculaire benadering voor een hogere selectiviteit voor tumoren door gebruik te maken van het feit dat het vaatstelsel van tumoren van nature meer doordringbaar is dan normale bloedvaten en tumoren geen lymfesysteem heeft (EPR effect). Aan de andere kant garandeert het gebruik van een nanodeeltje dat de lichtopwaardering plaatsvindt in nabijheid van de Ru(II)-prodrug.

TTA-UC in liposomen en polymeersomen

Zoals beschreven in Hoofdstuk 3 zijn met succes liposomen vervaardigd die in staat zijn blauwe fotonen te genereren uit groen of rood licht door middel van TTA-UC met twee verschillende kleurstofparen (Figuur S.1). De lichtopwaarderingsefficiëntie in liposomen was hoog en zeer vergelijkbaar met dat in organisch oplosmiddel. Om te onderzoeken waar de lichtopwaardering plaatsvond, werden rood-naar-blauw opwaarderende "giant vesicles" (GUVs) vervaardigd en gefotografeerd door middel van lichtopwaardering luminescentie microscopie, zoals beschreven in Hoofdstuk 5. De resultaten laten zien dat TTA-UC plaatsvond in de lipide dubbellaag van de GUVs en de hoge kwaliteit en stabiliteit van de afbeeldingen gaf gelegenheid tot het 3D-reconstrueren van de lichtopwaarderende GUVs. Omdat uiteindelijk de liposomen functioneel behoren te zijn bij menselijke lichaamstemperatuur (37 °C), werd de temperatuur-afhankelijkheid van TTA-UC in liposomen getest in een reeks van neutrale fosfolipide liposomen, waarvan de resultaten beschreven zijn in Hoofstuk 6. Er werd vastgesteld dat de TTA-UC-intensiteit rond de hoofdtransitietemperatuur (T_m) maximaliseerde. Dit werd verklaard door het feit dat de moleculaire bewegingsvrijheid van de TTA-UC-kleurstoffen toeneemt met hogere temperatuur tot T_m, en daarmee TTA-UC-efficiëntie, terwijl bij nog hogere temperatuur het uitdoven van de fotosensibilisator resulteerde in een afname van TTA-UC-intensiteit boven T_m. De TTA-UC-efficiëntie bij 37 °C in DOPC, DLPC en DMPC liposomen was zeer vergelijkbaar. TTA-UC kan dus in het algemeen gerealiseerd worden in liposomen en de fosfolipide kan vrij worden gekozen om de liposoomformulering te optimaliseren wat betreft stabiliteit in medium, biologische compatibiliteit, verwijdering uit de bloedbaan en functionalisatie van het deeltjesoppervlakte.

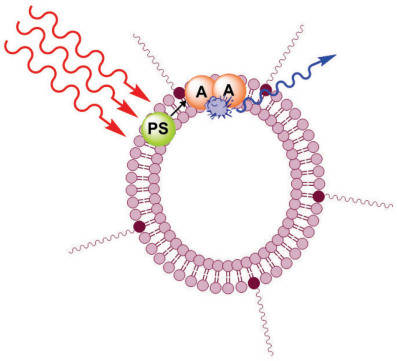

Figuur S.1. TTA-UC in liposomen met een fotosensibilisator (PS) en annihilator-kleurstof (A).

Om op deze resultaten voort te bouwen was het belangrijk om vast te stellen of TTA-UC kon plaatsvinden in levende cellen. Inderdaad is vastgesteld dat lichtopwaarderende liposomen door kankercellen werden opgenomen en dat de rood-naar-blauwe opwaardering kon worden waargenomen en gefotografeerd onder zuurstofarme condities, zoals beschreven in Hoofdstuk 7 en 8. De liposomen waren gelokaliseerd in endosomen en lysosomen en werden binnen 24 uur na opname door de cellen afgebroken. De lichtopwaardering verbleekte echter binnen een aantal seconden en de intensiteit was erg laag door uitdoving door de aanwezigheid van zuurstof in de cellen. Zoals beschreven in Hoofstuk 8 werd deze zuurstofgevoeligheid verminderd door de cellen ook te behandelen met een biologisch relevante hoeveelheid glutathion en L-ascorbinezuur waardoor de TTA-UC-intensiteit sterk verhoogd werd. Daarnaast werd vastgesteld dat de lichtopwaarderende liposomen niet toxisch waren in het donker en onder bestraling met rood licht; er werd geen PDT effect waargenomen ten gevolge van de singlet-toestand zuurstof die werd gegenereerd door de fotosensibilisator.

Afgezien van liposomen werd rood-naar-blauw TTA-UC ook gerealiseerd in het membraan van polymeersomen, die zelf-geassembleerd waren uit polyisobutyleen-polyethyleenglycol blokcopolymeren, zoals beschreven in Hoofdstuk 9. Alhoewel de rood-naar-blauw opwaardering enigszins minder efficiënt was dan in liposomen, werden de polymeersomen sneller opgenomen door levende cellen. Vervolgens konden de lichtopwaarderende polymeersomen gefotografeerd worden in de levende cellen, terwijl de toevoeging van glutathion en L-ascorbinezuur de *in vitro* prestaties sterk verbeterde. In vergelijking met liposomen kan het sterke rubberachtige membraan van polymeersomen beter bestendig zijn tegen afbraak door cellen of in het spijsverteringskanaal van zoogdieren, wat diverse mogelijkheden biedt voor toepassingen zoals medicijnafgifte. Alles samengenomen vertegenwoordigt TTA-UC in liposomen en polymeersomen interessante mogelijkheden in luminescentie biofotografie, omdat auto-fluorescentie en lichtbeschadiging van cellen en weefsel effectief worden voorkomen.

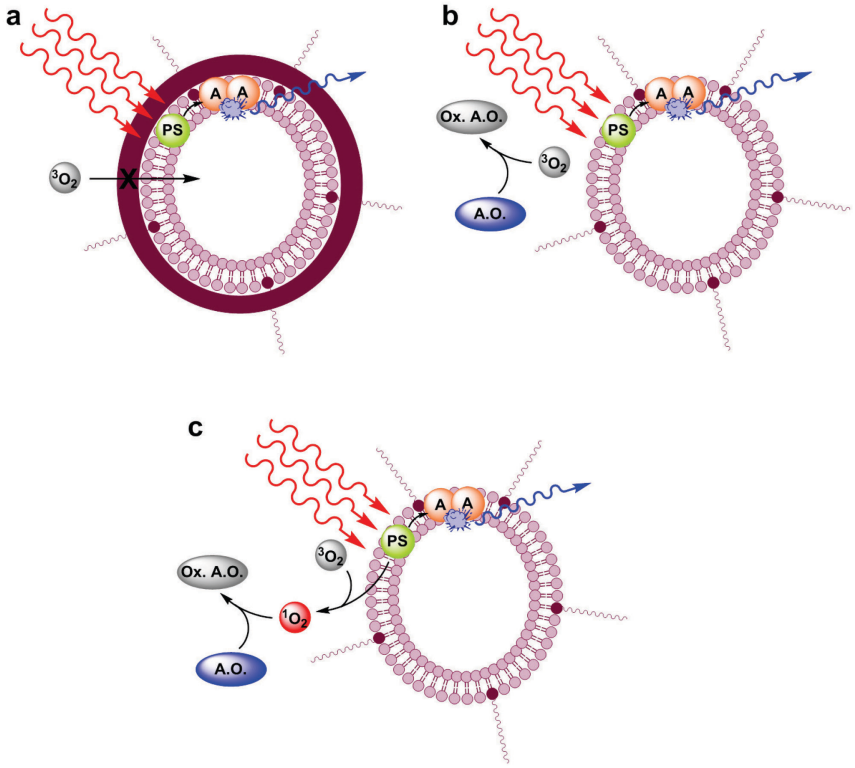

Figuur S.2.Cartoon ter illustratie van de drie verschillende strategieën die zijn nagestreefd in dit proefschrift om de zuurstofgevoeligheid van TTA-UC in nanodeeltjes te verlagen. a) Coating van het nanodeeltje met een materiaal als barrière voor zuurstof. b) Toevoeging van een antioxidant (A.O.) die reageert met grondtoestand zuurstof, wat leidt tot een geoxideerde antioxidant (Ox. A.O.). c) Toevoeging van een antioxidant die reageert met aangeslagen singlet-toestand zuurstof: wanneer de fotosensibilisator aangeslagen wordt ontstaat singlet-zuurstof, wat reageert met de antioxidant en leidt tot een zuurstofarme omgeving.

Zuurstofgevoeligheid van TTA-UC

Het mechanisme van TTA-UC hangt sterk af van langlevende triplet-toestand moleculen, die sterk kunnen worden uitgedoofd door zuurstof. Deze uitdoving leidt tot zeer lage TTA-UC-efficiëntie in aanwezigheid van zuurstof; in de literatuur zijn er tot op heden nog maar nauwelijks manieren gerapporteerd om dit probleem te verhelpen. Inderdaad werd tijdens het eerste werk voor Hoofdstuk 3 gerealiseerd dat TTA-UC in liposomen alleen goed werkte wanneer de oplossingen strikt zuurstofvrij waren gemaakt door een argonstroom door de oplossing te borrelen. Om dit grote nadeel tegen te gaan werden in opvolgende experimenten drie strategieën nagestreefd om de zuurstofgevoeligheid van TTA-UC in nanodeeltjes te verlagen (Figuur S.2). De eerste strategie was het aanbrengen van een zuurstof-ondoordringbare laag

rondom liposomen (Figuur S.2a). In Hoofdstuk 7 wordt beschreven hoe een nanometer-dikke (organo)silica-coating werd aangebracht rondom lichtopwaarderende liposomen. Alhoewel de resulterende nanodeeltjes gemakkelijk werden opgenomen in kankercellen zonder celdood te veroorzaken, zorgde de silica-coating helaas niet voor de beoogde zuurstofbescherming (noch in oplossing, noch in cellen), hoogstwaarschijnlijk door de porositeit van de silica-coating. Wanneer de silica-gecoate deeltjes werden gedroogd in een overmaat (organo)silica precursor werden echter interessante nano-composietmaterialen verkregen waarmee TTA-UC in lucht mogelijk was. Deze resultaten bevestigden dat (organo)silica onder bepaalde omstandigheden inderdaad TTA-UC materialen kan beschermen tegen zuurstof. Dit werk vertegenwoordigt een interessant voorbeeld van de combinatie van fosfolipiden, water, en silica voor het vervaardigen van lichtopwaarderende nanodeeltjes en materialen die eenvoudig kunnen worden afgestemd op de toepassing.

In een tweede benadering werd gerealiseerd dat het verwijderen van zuurstof uit de oplossing door middel van een fysieke methode (bubbelen van argon) kon worden vervangen door het toevoegen van een antioxidant die reageert met grondtoestand zuurstof, zoals natriumsulfiet (Figuur S.2b). Sulfiet zorgt voor een sterke afname van opgeloste zuurstof, waardoor stabiele en efficiënte TTA-UC in oplossing kan plaatsvinden. Veel antioxidanten die met grondtoestand zuurstof kunnen reageren zijn echter niet compatibel met biologische systemen (bijv. hydrazine) en ze putten langzaam uit wanneer zuurstof in de samples lekt. Om deze benadering te verbeteren werd een derde benadering nagestreefd met antioxidanten die alleen met aangeslagen singlet-toestand zuurstof kunnen reageren, zoals ascorbinezuur of glutathion (Hoofdstuk 8). Dit werkt als volgt: wanneer het TTA-UC systeem continu wordt bestraald, produceert de fotosensibilisator aangeslagen singlet-toestand zuurstof dat vervolgens reageert met de antioxidant totdat alle zuurstof in het monster is geconsumeerd. Deze strategie leidde tot zeer efficiënte en stabiele TTA-UC in lucht (> 80% stabiliteit gedurende het eerste uur bestraling). Zoals beschreven wordt in Hoofdstuk 9 kan de rol van antioxidant ook vervuld worden door histidine, trolox, of de antioxidanten die aanwezig zijn in celgroeimedium (bijv. bovien serum albumine of pyruvaat). Het gebruik van antioxidanten is dus een zeer algemene en krachtige strategie om de zuurstofgevoeligheid van vrijwel elk TTA-UC systeem te verminderen.

Activering van Ru prodrugs door middel van TTA-UC

Het doel van dit proefschrift was de activering van Ru(II)-prodrugs met rood licht door middel van lichtopwaardering in een geneesmiddelafgiftesysteem. Dit doel werd voor het eerst behaald in Hoofdstuk 3, waarin wordt beschreven hoe de fotochemische afsplitsing van een Ru(II)-polypyridylcomplex van liposomen werd getriggerd door lichtopwaarderende liposomen in een mengsel van rood-naar-blauw opwaarderende liposomen en Ru-complex gedoteerde liposomen (Figuur S.3a). In dit eerste werk werd het blauwe opgewaardeerde licht naar het Ru-complex overgebracht door middel van radiatieve energieoverdracht, d.w.z. door tussenkomst van een foton. Wanneer het Ru-complex in hetzelfde membraan werd gedoteerd als de lichtopwaarderende kleurstoffen, werd de energie door middel van Förster resonantie-energieoverdracht (FRET) overgebracht met meer dan 85% efficiënte bij relatief lage Ru-complex hoeveelheden (4 mol% met betrekking tot de fosfolipiden), zoals beschreven in Hoofdstuk 4 en Figuur S.3b. Deze studies lieten zien dat Ru-prodrug activering door rood-naar-blauw TTA-UC veelbelovend is, maar werkte helaas nog niet in lucht vanwege het uitdoven van TTA-UC door zuurstof. Om het systeem in lucht te laten functioneren werd de fotoreactie succesvol uitgevoerd in aanwezigheid van ascorbinezuur en glutathion, zoals beschreven in Hoofdstuk 8. Er is ook geprobeerd om de liposomen met Ru-complex en TTA-UC-kleurstoffen te testen in cellen. De Ru complexen die werden gebruikt waren echter ook zeer giftig in het donker, en werden niet significant meer giftig onder bestraling van licht. Vanwege deze redenen kon de activatie door rood-naar-blauw TTA-UC in liposomen niet leiden tot een uitgesproken fotochemotherapeutisch effect, en de haalbaarheid van deze aanpak blijft dus nog onzeker. Op dit moment is meer onderzoek nodig naar het ontwerp van membraangebonden Ru-prodrugs met hoge giftigheid na bestraling en lage giftigheid in het donker om de activering-door-lichtopwaardering benadering te valideren in biologische systemen.

Algemene opmerkingen

De resultaten beschreven in dit proefschrift verschaffen waardevolle inzichten voor het ontwikkelen van biologische TTA-UC toepassingen. Liposomen en polymeersomen werden succesvol gebruikt als multifunctionele rood-naar-blauw opwaarderend platform voor biofotografie en activering van lichtgevoelige Ru-prodrugs. Het is duidelijk gedemonstreerd dat blauw-licht gevoelige Ru-polypyridylcomplexen, die normaal gesproken niet gevoelig zijn voor licht in het fototherapeutische venster, kunnen worden geactiveerd door

rood licht door middel van TTA-UC. De biologische evaluatie van deze activering-door-lichtopwaardering strategie vereist meer wetenschappelijke aandacht om te achterhalen welke parameters optimalisatie nodig hebben, zoals het ontwerp van het nanodeeltje, stabiliteit van TTA-UC, zuurstofgevoeligheid en aanwezigheid van antioxidanten, lichtdosis, doteringshoeveelheid van kleurstoffen en prodrugs in het nanodeeltje, en de foto-index van de Ru-prodrugs. We verwachten dat de resultaten van dit proefschrift zullen leiden tot interessante toepassingen in fotogeactiveerde chemotherapie dat een alternatief biedt voor fotodynamische therapie in zuurstofarme tumoren.

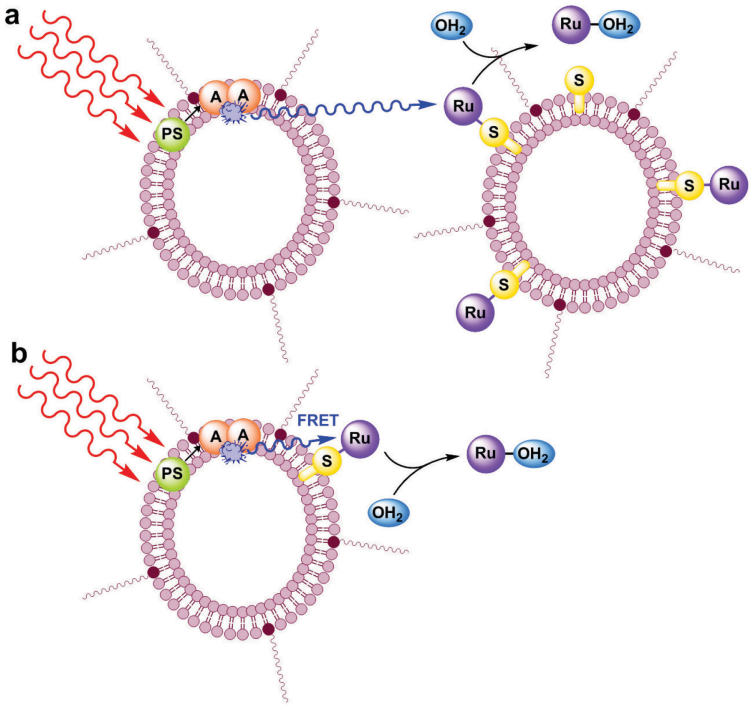

Figuur S.3. Cartoon ter illustratie van de combinatie van TTA-UC in liposomen en lichtactiveerbare, membraangebonden Ru-polypyridylcomplexen. a) TTA-UC en Ru-complex zijn fysiek gescheiden op twee verschillende liposomen: het blauwe licht wat door TTA-UC wordt gegenereerd wordt aan het Ru-complex overgedragen door radiatieve energieoverdracht (Hoofdstuk 3), waarna het geactiveerde Ru-aqua complex vertrekt van het membraan. b) TTA-UC en Ru complex zijn gelokaliseerd op hetzelfde liposoom: het blauwe licht wat door TTA-UC wordt gegenereerd wordt via FRET aan het Ru complex overgedragen (Hoofdstuk 4). PS: fotosensibilisator; A: annihilator; FRET: Förster Resonance Energy Transfer.

Curriculum Vitae

Sven Askes was born in Culemborg, The Netherlands on 31 May 1989. In 2007, he graduated from Christelijke Scholengemeenschap Walcheren High School in Middelburg. In 2010, he received his Bachelor of Science degree in Molecular Science and Technology of Leiden University and Technical University Delft. During the BSc program he visited Radford University (VA, USA) for a one-semester minor in business administration. His bachelor thesis was titled "*β-enaminoketonato and β-diketiminato ligands and lanthanide (Eu, Tb) complexes thereof*". In 2012, he received his Master of Science degree *cum laude* in Chemistry with a specialization in "Science Based Business" at Leiden University. His scientific thesis was titled "*Luminescent properties of lanthanide coordination compounds with 2-hydroxy-isophthalate ligands*" and his business thesis was titled "*Working safely with production chemicals at Heineken International*". His scientific master thesis was awarded with the Unilever Research Prize in 2012.

In October 2012, he started his PhD research under supervision of Sylvestre Bonnet and Elisabeth Bouwman at the "Metals in Catalysis, Biomimetics and Inorganic Materials" (MCBIM) research group of the Leiden Institute of Chemistry, Leiden University. During his PhD studies, he collaborated with Prof. Dr. A. Kros (Leiden University), Prof. Dr. T. Schmidt (Leiden University), Dr. J. Kennis (Vrije University Amsterdam), Dr. Gilles Bruylants (Université Libre de Bruxelles), Dr. S. Wu (Max Planck Institute Mainz), Prof. Dr. B. Koster (Leiden University Medical Center), Prof. Dr. D. Heinrich (Leiden University), Prof. Dr. P. Bednarski (Universität Greifswald), Prof. Dr. A. Schiller (Friedrich-Schiller Universität Jena), Dr. S. Dembski (Fraunhofer Institute Würzburg), and Prof. J. van Hest (Radboud Universitity Nijmegen). In total, he supervised two BSc and four MSc students during the PhD research, and he frequently supervised the first year practical courses. He was awarded with a poster prize at the International Symposium on the Photochemistry and Photophysics of Coordination Compounds (ISPPCC) in Krakow, Poland (2015), and he was nominated as Discoverer of the Year 2014 of the Faculty of Science, Leiden University. He presented the research described in this thesis at the following meetings and conferences:

- NWO "Protein research, Nucleic acids and Lipids & Biomembranes" meeting, 2013 (Oral presentation)
- COST 1105 Whole Action Meeting in Zürich, Switzerland, 2014 (Oral presentation)
- Biomembranes meeting of Utrecht University, 2014 (Oral presentation)
- Cell Observatory Lecture, Leiden University, 2013 (Oral presentation)
- Chemical Biology Lecture, Leiden University, 2015 (Oral presentation)
- International Symposium on the Photochemistry and Photophysics of Coordination Compounds, Krákow, Poland, 2015 (Poster)
- Holland Research School of Molecular Chemistry (HRSMC) Symposium 2014 (Poster)
- CHAINS 2014 and 2015 (Poster)
- Reedijk symposium 2014 (Poster)

During the PhD research, he participated in the following courses:

- HRSMC Physical Methods in Inorganic Chemistry
- HRSMC Photophysics, Photochemistry, and Photobiology
- Metals and Life (Leiden University)
- Spin and Photochemistry (Leiden University)
- Graduate School courses of Leiden University: "Time management", "On being a scientist", "Communication in Science", "Effective Communication", and "Negotiation"

List of publications

J. H. Adriaanse, **S. H. C. Askes**, Y. van Bree, S. van Oudheusden, E. D. van den Bos, E. Günay, I. Mutikainen, U. Turpeinen, G. A. van Albeda, J. G. Haasnoot, J. Reedijk. "*Coordination chemistry of 5,6,7-trimethyl-[1,2,4]triazolo[1,5-a]pyrimidine with first-row transition-metal salts: Synthesis, spectroscopy and single-crystal structures, with counter-anion dependence of the structures.*" Polyhedron, **2009**, 28, 3143

S. H. C. Askes, A. Bahreman, and S. Bonnet. "*Activation of a Photodissociative Ruthenium Complex by Triplet–Triplet Annihilation Upconversion in Liposomes.*" Angew. Chem., Int. Ed., **2014**, 53, 1029.

S. H. C. Askes and S. Bonnet. "*Upconverting Vesicles and Uses*" International Patent Application, **2015**, WO/2015/059180.

S. H. C. Askes, N. López Mora, R. Harkes, R. I. Koning, B. Koster, T. Schmidt, A. Kros, and S. Bonnet. "*Imaging the lipid bilayer of giant unilamellar vesicles using red-to-blue light upconversion.*" Chem. Commun., **2015**, 51, 9137.

S. H. C. Askes, M. Kloz, G. Bruylants, J. T. Kennis, and S. Bonnet. "*Triplet-triplet annihilation upconversion followed by FRET for the red light activation of a photodissociative ruthenium complex in liposomes.*" Phys. Chem. Chem. Phys., **2015**, 17, 27380.

X. Liu, S. Akerboom, **S. H. C. Askes**, I. Mutikainen, and E. Bouwman. "*A novel coordination network of Tb(III) with 2-hydroxy-trimesic acid showing very intense photoluminescence.*" Inorg. Chem. Commun., **2015**, 61, 60.

L. Kong, **S. H. C. Askes**, S. Bonnet, A. Kros, and F. Campbell. (2016). "*Temporal Control of Membrane Fusion through Photolabile PEGylation of Liposome Membranes.*" Angew. Chem., Int. Ed., **2016**, 55, 1396.

S. L. Hopkins, B. Siewert, **S. H. C. Askes**, P. van Veldhuizen, R. Zwier, M. Heger, and S. Bonnet. "*In vitro cell irradiation protocol for testing photopharmaceuticals and the effect of blue, green, and red light on human cancer cell lines.*" Photochem. Photobiol. Sci., **2016**, 15, 644.

V. H. S. van Rixel, B. Siewert, S. L. Hopkins, **S. H. C. Askes**, A. Busemann, M. A. Siegler, and S. Bonnet. "*Green light-induced apoptosis in cancer cells by a tetrapyridyl ruthenium prodrug offering two trans coordination sites.*" Chem. Sci., **2016**, 7, 4922.

J. A. Göttle, F. Alary, M. Boggio-Pasqua, I. M. Dixon, J.-L. Heully, A. Bahreman, **S. H. C. Askes**, and S. Bonnet. "*Pivotal Role of a Pentacoordinate 3MC State on the Photocleavage Efficiency of a Thioether Ligand in Ruthenium(II) Complexes: A Theoretical Mechanistic Study*." Inorg. Chem., **2016**, 55, 4448.

S. H. C. Askes, W. Pomp, S. L. Hopkins, A. Kros, S. Wu, T. Schmidt, and S. Bonnet. "*Imaging upconverting polymersomes in cancer cells: biocompatible anti-oxidants brighten triplet-triplet annihilation upconversion.*" Small, **2016**, DOI: 10.1002/smll.201601708.

L. N. Lameijer, S. L. Hopkins, T. G. Brevé, **S. H. C. Askes**, and S. Bonnet. "*L-versus D-glucose conjugation: Mitochondrial targeting of a light-activated dual-mode of action ruthenium-based anticancer prodrug.*" Chem. Eur. J., **2016**, in press.

S. H. C. Askes, P. Brodie, G. Bruylants, and S. Bonnet. "*Temperature dependence of triplet-triplet annihilation upconversion in phospholipid membranes*." **2016**, to be submitted.

S. H. C. Askes, M. S. Meijer, T. Bouwens, I. Landman, and S. Bonnet. "*Photochemical activation of Ru(II) polypyridyl prodrugs through meat using triplet-triplet annihilation upconversion*." **2016**, to be submitted.

S. H. C. Askes, V. Leeuwenburgh, W. Pomp, S. Grecea, T. Schmidt, and S. Bonnet. "*Silica-coating of upconverting liposomes for protection against quenching by oxygen.*" **2016**, to be submitted.

S. H. C. Askes, M. S. Meijer, L. N. Lameijer, and S. Bonnet. "*Escape of membrane-anchored chromophores from liposomes.*" **2016**, to be submitted.

S. H. C. Askes, and S. Bonnet. "*Light upconversion using triplet-triplet annihilation for application in biology*." **2016**, to be submitted.

Acknowledgements

COST action CM1005 (Supramolecular Chemistry in Water) is acknowledged for financial support for a short term scientific mission to Brussels. Dr. Gilles Bruylants is thanked for his hospitality and supervision in Brussels during differential scanning calorimetry experiments. Prof. Dr. A. Kros is acknowledged for stimulating discussion and collaboration on giant vesicle research described in Chapter 5 and Chapter 9. Prof. Dr. T. Schmidt is acknowledged for fruitful collaborations on several microscopy projects, included in Chapter 5 to Chapter 9. Dr. J. Kennis is acknowledged for collaboration on time-dependent fluorescence and transient absorption projects, included in Chapter 4. Prof. Dr. Bram Koster and Dr. Roman Koning are acknowledged for providing cryo-TEM images of upconverting liposomes, reported in Chapter 5. Dr. Stefania Grecea is acknowledged for TGA measurements of silica-coated liposome samples described in Chapter 7. Dr. Si Wu is acknowledged for gel permeation chromatography and MALDI-TOF MS measurements reported in Chapter 9. Azadeh Bahreman, Miroslav Kloz, Nestor Lopez Mora, Rolf Harkes, Wim Pomp, Lucien N. Lameijer, Michael S. Meijer, and Samantha L. Hopkins are gratefully acknowledged for shared learning experiences, stimulating discussion, and use of chemicals or equipment. Supervised students, namely Selwyn Hanselman, Philip Brodie (Chapter 6), Vincent Leeuwenburgh (Chapter 7), Tessel Bouwens (Chapter 8), Iris Landman (Chapter 8), and Marlize van Breugel (Chapter 8), are kindly acknowledged for their contributions to this thesis. Parts of the research described in Chapter 8 were performed as “short-rotation” internships of the Holland Research School for Molecular Chemistry (HRSMC).